

AD-A273 666
403



1



12th International Corrosion Congress

PRECEEDINGS

DTIC
ELECTE
DEC 09 1993
S A

September 19-24, 1993
Volume 5A
Houston, Texas USA

This document has been approved
for public release and sale; its
distribution is unlimited.

CORROSION: GENERAL ISSUES

NACE
International

CORROSION CONTROL FOR LOW-COST RELIABILITY



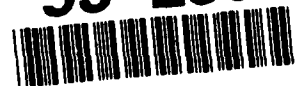
**12th
International
Corrosion
Congress**

PRECEEDINGS

VOLUME 5A

CORROSION: GENERAL ISSUES

93-29515



93 12 27 1 0 2

The manuscripts in this volume have been printed from camera-ready copy and have been accepted without editing by NACE International.

Neither NACE International, its officers, directors, members thereof, nor instructors accept any responsibility for the use of the methods and materials discussed herein.

Any goods, products, and/or services mentioned are mentioned as items of information only. Such mention does not constitute an endorsement by NACE International.

The information is advisory only, and use of the materials and methods is solely at the risk of the user.

Printed in the USA. All rights reserved. This book, or parts thereof, may not be reproduced in any form without permission of the copyright owners.

Copyright, NACE International, 1993

ISBN: 1-877914-65-7

Published by

NACE International
P.O. Box 218340
Houston, TX 77218-8340

| | | |
|---------------|-----------------------|---|
| Accession For | | |
| NTIS | CRA&I | ✓ |
| DTIC | TAB | ☐ |
| Unannounced | | ☐ |
| Justification | | ☐ |
| By | Vol. 5A - \$142 | |
| Distrib | St. 5400 | |
| Availability | | |
| Dist | Avail. and/or special | |
| A-1 | 21 | |

NACE
International

DTIC QUALITY INSPECTED 3

PRECEEDINGS CONTENTS

Paper # Page # Paper # Page #

VOLUME 1

PLENARY LECTURES

- Corrosion: Its Effect on Society
N. Hackerman Plenary 1
- Low-Cost Corrosion Engineering and Risk Potential, Operational and Environmental Safety - nad Irreconcilable Antagonism in the Chemical Process Industry
H. Spahn Plenary 4
- Methodology of Predicting Materials Failures in Advance Nuclear Systems
T. Kondo Plenary 20
- Corrosion Control by Transferring Knowledge
R. Parkins Plenary 43

COATINGS ON STEEL

- 514 Advancements in Automotive Corrosion Resistance
M. Ostermiller, L. Lee-Piepho, and L. Singer 1
- 268 Automotive Phosphating Technology 1975 - 1995
R. Miller, M. Petschel Jr., and R. Hart 16
- 400 Hydrothermal Properties of Protective Polymer Coatings on Steel
R. Granata and K. Kovaleski 24
- 293 Corrosion Behavior of Oxide Coated Cold-Rolled and Electrogalvanized Sheet Steel
W. Nowak, H. Townsend, and L. Li 42
- 039 Electrodeposition of Zn-Fe Alloy at High Current Densities
L. Yanping and W. Jixun 53A
- 569 Study of Enameling Properties on the Hot-Rolled Ti-Containing Steel Sheets
X. Xiaolian, Z. Kegang, and L. Ri 54

COATINGS

- 025 Study of Anticorrosion Properties of Metal Arc-Sprayed Coatings on a Carbon Steel for use in Petro Products
A. Groysman and V. Belashchenko 63
- 266 A Discussion on the Role of Cations in Enhancing Internally Coated Metal Container Corrosion Failure
W. Tait and K. Handrich 77
- 085 The Detrimental Effect of Water-soluble Contaminants at the Steel/Paint Interface
M. Morcillo 87

- 106 Anticorrosive Coatings Based on Phase Decomposed Polymer Blends
V. Verkholtantsev and M. Flavian 99
- 097 Application of Electrochemical Impedance Spectroscopy to Study the Efficiency of Anti-Corrosive Pigments in and Epoxy Resin
A. Amirovudin, C. Barreau, and D. Thierry 114
- 046 Determination of Protective Properties of Polymer Coatings from High-Frequency Impedance Data
F. Mansfield and C. Tsai 128
- 156 Long-Term Electrochemical Characterizations of MIL-P-24441 Epoxy Coated Steel Using Electrochemical Impedance Spectroscopy (EIS)
J. Murray and H. Hack 151
- 073 Electrochemical Methods to Monitor Degradation of Organic and Metallic Coatings
T. Simpson 157
- 096 Determination of Coating Delamination & Underfilm Corrosion during Atmospheric Exposure by Means of Electrochemical Impedance Spectroscopy
A. Amirudin, P. Jernberg, and D. Thierry 171
- 486 Characterization of Corrosion under Marine Coating by Electrochemical Noise Methods
D. Mills, G. Bierwagen, D. Tallman, and B. Skerry 182
- 066 New Accelerated Test Simulating the Atmospheric Undercoat Corrosion
A. Martello 195
- 044 Compatibility of Organic Coatings with Flame Spraying Zn, Al and Zn-Al Alloy Coatings
Z. Zhaoqing 204

METALLIC COATING AND SURFACE TREATMENTS

- 036 Surface Modification by Chemical and Electrochemical Processes
F. Mansfield, V. Wang, S. Lin, and L. Kwiatkowski 219
- 180 Laser Melting of Plasma Sprayed Alumina Coatings
M. Escudero, V. Lopez, A. Jimenez-Morales, E. Vida, and J. Galvan 240
- 244 Corrosion and Oxidation Behavior of Ti-Al Surface Alloys Formed Using Laser Irradiation
A. Khanna, V. Desai, and G. Goswami 250
- 254 Corrosion and Heat Resistance of Alumina Coated Iron to Alkali Carbonate at 700°C
M. Okuyama, T. Noshiro, and S. Kambe 259

| Paper # | | Page # |
|---------|--------------------------------------------------------------------------------------------------------------------------------------------------------------------------------------------------------------|--------|
| 319 | Corrosion Resistance of Amorphous Plasma Sprayed Coatings <i>N. Bacha and C. Roy</i> | 271 |
| 350 | Formation of Protective Wearresistant Oxide Coatings of Aluminum Alloys by the Microplasma Methods from Aqueous Electrolyte Solutions <i>A. Timoshenko, B. Opara, and Y. Magurova</i> | 280 |
| 356 | Superior Corrosion Resistance by Niobium Coating <i>S. Ylassaari, M. Turkia, and O. Forsen</i> | 294 |
| 394 | Effects of Laser Transformation Hardening on the Corrosion Resistance of AISI ₀₁ Tool Steel <i>L. Yang, S. Jana, S. Tam, L. Lim, and M. Lau</i> | 307 |
| 423 | A Comparison of the Corrosion Properties of Thick Layers of Chromium and its Alloys with Nickel Deposited from Chromium (III) Electrolytes <i>M. El-Sharif, A. Watson, X. Wang, and C. Chisholm</i> | 315 |
| 424 | Studies of Chemical Conversion Treatments of Electrodeposited Zinc-Chromium and Zinc-Nickel-Chromium Alloys <i>M. El-Sharif, Y. Su, A. Watson, and C. Chisholm</i> | 329 |
| 461 | Study of Corrosion Resistance of Electroless Ni-P Platings <i>L. Yi</i> | 341 |
| 472 | Resistance to Aqueous Corrosion of Steels Protected by a Cr-Si Diffusion Coating <i>X. Wan, G. Wang, and R. Rapp</i> | 353 |

NON-METALLIC COATINGS ON STEEL SUBSTRATES

| | | |
|-----|----------------------------------------------------------------------------------------------------------------------------------------------------------------------|-----|
| 150 | Flourescent Materials as Corrosion Sensors for Coatings <i>R. Johnson and V. Agarwala</i> | 370 |
| 175 | The Investigation of a New Autodeposition Coating System <i>Z. Pan, D. Qiu, Z. You, and Y. Zhao</i> | 379 |
| 213 | The Influence of Absorbed Layers of Silane Coupling Agents on Protective Properties of Polymer Coatings <i>M. Petrunin, A. Nazarov, and N. Mikhailovski</i> | 386 |
| 309 | Research of Weather Resistant Bridge Paint and Wear Resistant Primer and Finish for Bridge Cover Plates <i>Y. Shaoyu</i> | 398 |
| 290 | Determination of Water Transport Properties of Organic Coatings with EIS <i>L. Nicodemo, F. Monetta, and F. Bellucci</i> | 406 |
| 324 | Characterization of Organic Coatings with Impedance Spectroscopy <i>J. de Wit</i> | 420 |
| 331 | Substrate Effects on the Corrosion Performance of Coated Steels under Immersed Conditions <i>J. Costa, S. Faidi, and J. Scantlebury</i> | 437 |
| 333 | Why the Best Performance of Phosphoric Acid Pretreatments when Activated with Aluminium Hydroxide <i>E. Almeida and D. Pereira</i> | 449 |
| 007 | A Unique Plasma Spray Process to Create Corrosion Control Surfaces <i>G. Sweet and W. Bristowe</i> | 460 |

| Paper # | | Page # |
|---------|------------------------------------------------------------------------------------------------------------------------------------------|--------|
| 193 | Evaluation of Corrosion Resistant Coating for Mild Steel <i>M. Trivedi, H. Mandalia, and C. Mital</i> | 473 |
| 332 | Electrocorrosion-inhibiting Behaviour of Flame Retarding PVC Pressure-sensitive Adhesive Tape <i>W. Tao, H. Ge, and Y. Qing</i> | 484 |

VOLUME 2

ATMOSPHERIC CORROSION

| | | |
|------|---------------------------------------------------------------------------------------------------------------------------------------------------------------------------------------------------------------------------------------------------------------|-----|
| 335 | Materials Damage Caused by Acidifying Air Pollutants - 4 Year Results from an International Exposure Program within UN ECE <i>V. Kucera, A. Coote, J. Henriksen, D. Knotkove, C. Leygraf, and B. Stockle</i> | 494 |
| 145 | Worldwide Data on the Atmospheric Corrosion Resistance of Weathering Steels <i>M. Komp, S. Coburn, and S. Lore</i> | 509 |
| 040 | The Effects of Acid Deposition on the Atmospheric Corrosion Behavior of Structural Materials in California <i>F. Mansfeld, H. Xiao, and R. Henry</i> | 529 |
| 584 | The Influence of Environmental Acidification on the Atmospheric Corrosion of Zinc <i>E. Johansson and M. Linder</i> | 549 |
| 042 | Atmospheric Corrosivity Classification Results of the International Testing Program ISOCORRAG <i>D. Knotkova</i> | 561 |
| 230 | Techniques Applied to the Analysis of the Atmospheric Corrosion of Low Carbon Steel, Zinc, Copper, and Aluminum <i>A. Fernandez, M. Leiro, B. Rosales, E. Ayllon, F. Varela, C. Gervasi, and J. Vilche</i> | 574 |
| 530 | Indoor Gaseous Sulfide and Chloride Pollutants and Their Reaction with Silver <i>L. Volpe and P. Peterson</i> | 590 |
| 222 | Field Exposure Studies of Corrosion Products on Metals <i>C. Leygraf, I. Odnevall, D. Persson, and J. Tidblad</i> | 600 |
| 437B | Protective Rust Layer Formed on Weathering Steel by Atmospheric Corrosion for a Quarter of a Century <i>T. Misawa, M. Yamashita, H. Miyukii, and H. Nagano</i> | 612 |
| 005 | Structure of Rust on Weathering Steel in Rural and Industrial Environments <i>H. Townsend, T. Simpson, and G. Johnson</i> | 624 |
| 351 | Effects of Seasalt on Corrosion Attacks at 8 Years Exposure of Metals in a Small Geographical Area of the Swedish West Coast <i>J. Gullman</i> | 642 |
| 305 | Chemical Characterization of the Corrosion Products Formed on Plain C Steel, Zinc, Copper, and Aluminum <i>S. Granese, A. Fernandez, and B. Rosales</i> | 652 |
| 294 | Initial Stages of SO ₂ Induced Atmospheric Corrosion of Zinc Investigated by In-Situ IR Spectroscopy and Time Resolved Trace Gas Analysis; Synergistic Effects of NO ₂ and O ₃ <i>J. Svensson and L. Johannsson</i> | 662 |

| Paper # | Page # |
|------------------------------------------------------------------------------------------------------------------------------------------------------------------------|--------|
| 377 Galvanic Corrosion of Zinc/Steel Under Thin Layer Electrolytes <i>X. Zhang and E. Valeriotte</i> | 676 |
| 416 Experimental Approaches to the Study of Corrosion in Thin Water Layers <i>V. Brusic, G. Frankel, T. Peterson, and S. Huang</i> | 687 |
| 420 Simulation of the Degradation of Limestone and Dolomitic Sandstone under Dry Deposition Conditions <i>S. Haneef, J. Johnson, G. Thompson, and G. Wood</i> | 700 |
| 308 Dissolution and Precipitation Phenomena in Atmospheric Corrosion <i>T. Graedel</i> | 711 |
| 439 Atmospheric Corrosion Model for Zinc and Copper <i>S. Cramer, L. McDonald, and J. Spence</i> | 722 |
| 043 Defects of Steel Structures Caused by Atmospheric Corrosion <i>D. Knotkova, J. Vlckova, and L. Rozlivka</i> | 734 |
| 382 Environmental Effects in the Atmospheric Corrosion of Zinc: An Immersion - Drying Study <i>A. Valencia, R. Perez, C. Arroyave, and S. Mesa</i> | 748 |
| 463 Estimate of Economic Damage of large Industrial Cities Infrastructure from Corrosion Caused by Pollutions into Environments <i>A. Lyagh</i> | 761B |

CHEMICAL PROCESS INDUSTRY WORKSHOP

| | |
|-----------------------------------------------------------------------------------------------------------------------------------------------------------------------|-----|
| 092 The Mechanism and Control of Stress Corrosion Cracking of Zirconium in Sulfuric Acid <i>B. Fitzgerald and T. Yau</i> | 762 |
| 035 What Has Happened to SA-516-70? <i>T. Phillips and D. Kloss</i> | 778 |
| 028 Corrosion of Weld Zone of Stainless Steels in Industrial Urea Media <i>H. Xizhang, R. Xiaoshan, C. Xiaojun, H. Wenan, and Z. Feng</i> | 784 |
| 105 The Fractality of Corroding Metallic Surfaces <i>K. Trethewey, J. Keenan, D. Sargeant, S. Haines, and P. Roberge</i> | 795 |
| 379 Methods to Combat Liquid Metal Embrittlement in Cryogenic Aluminum Heat Exchangers <i>S. Wilhelm, R. Kane, and A. McArthur</i> | 807 |
| 132 Prevention of Localized Corrosion Caused by Thiosulphate in Paper Mill Environments <i>V. Marichev, T. Saario, and V. Molokanov</i> | 826 |
| 253 Corrosion of Stainless Steels in Kraft Process Liquors <i>A. Klarin, J. Westermarck, S. Ylasaari, J. Aromaa, and O. Forsen</i> | 834 |
| 004 The Electrochemical Protection of Nickel in an NaOH + NaCl Solution <i>R. Juchniewicz, W. Sokolski, J. Walaszowski, P. Domzalcki, and B. Picrozynski</i> | 849 |
| 435 Proactive Corrosion Program Improves Process Heater Reliability <i>K. Baumert, B. Heft, and S. Dean</i> | 855 |

| Paper # | Page # |
|----------------------------------------------------------------------------------------------------------------------------------------------------------------|--------|
| 102 Plant Measurement Cell for Carrying Out Electrochemical Corrosion Investigations on the Plant <i>G. Wagner and R. Munster</i> | 862 |
| 061 Experience with Neutron Activation for Real-time Corrosion Monitoring in a Urea Plant <i>G. Notten, J. Thoelen, H. Verhoef, and R. Van Sluijs</i> | 869 |
| 330 Corrosion Upsets are Probably More Costly Than You Know <i>A. Perkins</i> | 882 |
| 378 Automated Ultrasonic Corrosion Mapping <i>C. Sinclair</i> | 891 |
| 104 Autoadaptive Email Test AZ 90 for Corrosion Monitoring of Glass Lined Reactors <i>J. Hamert</i> | 906 |

HIGH TEMPERATURE CORROSION

| | |
|---------------------------------------------------------------------------------------------------------------------------------------------------------------------------------------------------------------------------------------------------------------------------------------------|------|
| 345 Rare Earth Element Effect on Oxidation Behavior of Chromia Forming Alloys <i>L. Ramanathan</i> | 914 |
| 018 A Study of the Metal-Oxide Diffusion Barrier Coating, <i>G. Hengrong, S. Xiaofeng, and S. Biwu</i> | 923 |
| 082 High-Temperature Sulfidation Properties and Demixing Process of Sulfide Scale of Fe-25Cr-9Mn Ternary Alloy <i>H. Qi, R. Zhu, and Y. He</i> | 934 |
| 214 Influence of Nd on Oxidation of Ti-5621S Alloy and Adherence of Oxide Scales <i>L. Meishuan and L. Tiefan</i> | 943 |
| 113 High Temperature Corrosion Behavior of Fe-Cr-Al Alloys with and without Y Addition in Pure S _{o2} Gas Atmosphere <i>Y. Zhang</i> | 951B |
| 468 Rupture in a Steam Boiler Tube <i>B. Rezgui and M. Larbi</i> | 963 |
| 069 Na ₂ SO ₄ Deposits Induced Hot Corrosion of Iron Based Alloys at Intermediate Temperatures <i>Y. Zhang, L. Shi, and S. Shih</i> | 971 |
| 391 Electrochemical Noise Measurement of Iron in Equimolar NaNO ₃ -KNO ₃ Melt at Various Temperatures <i>I. Singh, G. Venkatachari, and K. Balakrishnan</i> | 979 |
| 114 Corrosion Kinetic Study at High Temperature of the In 657 Super-alloy after Laser Surface Treatment in Contact with the Eutectic Melt 82% K ₂ S ₂ O ₇ - 18% V ₂ O ₅ <i>A. Pardo, E. Otero, F. Perez, and J. Alvarez</i> | 987 |
| 316 Performance of Cr-Al Coating on Carbon Steel to Control High Temperature Corrosion due to Ash Deposit <i>G. Navas, C. Leal, E. Baron, and O. Rincon</i> | 999 |
| 409 High Temperature Sulfidation of CO-CR Binary Alloys in H ₂ /H ₂ S Mixture in Co ₃ S ₈ Stability Region <i>Z. Zurek, M. Zilik, and A. Szuryn</i> | 1008 |

PLANT MATERIALS

317 Failure of Alloy 800 Steam Super Heating Coils in Refinery Hydrocracker
M. Islam and H. Shalaby 1022

216 The Effect of Blaze on the Mechanical and Corrosion Properties of Isfahan Refinery Distillation Unit Towers
A. Saatchi and A. Pishnamazi 1032

367 New Alloys for High Temperature Applications in Incineration Plants
H. Martinz and W. Kock 1039

260 Corrosion Evaluation of Materials in Sulfur Compound Environments
M. Teng and I. Yang 1056

447 Materials Selection Considerations for Vapor Collection Systems at Marine Tanker Facilities
T. Dunford, K. Lewis, and D. Rein 1064

169 Cracking of Weldments in Feed Water Deaerator Systems
T. Gooch, D. Noble, and R. Walker 1076

410 Using Fuel Oils with Different Sulphur Content and Treatment of Waste Waters Polluted with Heavy Metals in Thermoelectric Power Plants
L. Dukic 1090B

492 Case Study of a Service Water System Piping Corrosion Assessment
R. Tatara, K. Rhoades, and H. Olstowski 1091

VOLUME 3A

CORROSION: MATERIALS PERFORMANCE

210 Corrosion-Resistant Amorphous Chromium-Valve Metal Alloys
K. Hashimoto, J. Kim, E. Akiyama, H. Habazaki, A. Kawashima, and K. Asami 1102

089 A New Ni-Mo Alloy with Improved Thermal Stability
D. Klarstrom 1111

277 Corrosion Behaviour of Stainless Maraging Steel in Acidic Chloride Solutions
M. Viswanathan and K. Balakrishnan 1124

372 Electrochemical Characterization of Ni-Based Soft Magnetic Alloys
G. Ball and J. Payer 1132

413 Evaluation and Application of the EPR-double Loop Test to Assess the Degree of Sensitisation in Stainless Steels
R. Jargelius-Pettersson and P. Szakalos 1143

406 Corrosion Behaviour of Sintered Austenitic Stainless Steels in Sulphate and Chloride Media
E. Angelini, P. Bianco, F. Rosalbino, M. Rosso, and G. Scavino 1154

125 Advances in Technology Produce New Materials for Challenging Applications
N. Schmidt and T. DeBold 1170

512 Passive Behavior of Niobium and Niobium-Titanium Alloys in Sulfuric Acid Solutions
L. Bulhoes and D. Rehfeld 1183

464 The Effects of Microstructure (Cast versus Wrought) on the Wear and Corrosion Properties of a Cobalt-based Alloy
T. Meyer and P. Crook 1191

184 Effect of Aging Treatments on the Intergranular Corrosion of 22Cr-5Ni Duplex Stainless Steel
K. Ravindranath, S. N. Malhotra 1202

120 Optimized Lean-Pd Titanium Alloys for Aggressive Reducing Acid and Halide Service Environments
R. Schutz and M. Xiao 1213

049 Corrosion Characteristics and Applications of Newer High and Low Nickel Containing Ni-Cr-Mo Alloys
D. Agarwal, U. Heubner, and W. Herda 1226

178 Duplex Stainless Steels for Demanding Applications
J. Nicholls 1237

CORROSION: MODES AND BEHAVIOR

100 Investigation of Modified Schiff Bases for High Temperature Applications in the Area of Tribology
K. Rajan, P. Sen, A. Snelson, V. Agarwala, and A. Conte Jr. 1252

255 Corrosion Inhibition of Calcium Chloride Brines
K. Sotoudeh and P. Cote 1262

313 The Effect of Temperature and Chloride Concentration on Stainless Steels in Ammonium Chloride Solutions
O. Forsen, J. Virtanen, J. Aromaa, and M. Tavi 1278

109 Rest Potential Measurements for Stainless and Low-Alloy Steels in High Temperature Water
A. Charles and J. Congleton 1287

215 Managing Galvanic Corrosion in Waters
A. Tuthill 1300

119 Combination of Acoustic Emission & Electrochemical Techniques in Erosion-Corrosion Studies of Passive Stainless Steels in Acidic Media
L. Renaud, B. Chapey, and R. Oltra 1315

188 Accelerated Corrosion Testing of CrNi Stainless Steels in Nitric Acid by Electrochemical Methods
G. Schanz and S. Leistikow 1327

288 Tunneling Corrosion Mechanism of the Hot Forged Austenitic Stainless Steel in Highly Oxidizing Nitric Acid
H. Nagano and H. Kajimura 1341

440 Corrosion and Wear in White Cast Iron
S. Watson, S. Cramer, and B. Madsen 1353

ELECTROCHEMICAL TECHNIQUES

055 Scanning Microelectrochemical Methods to Study the Corrosion Behavior of Metals
T. Suter and H. Bohni 1367

496 PVC Film-Modified Electrodes Studied by EHD Impedance
C. Sousa da Silva, O. Barcia, O. Mattes, and C. Deslouis .. 1378

533 Electrochemical Noise Analysis of Iron Exposed to NaCl Solution of Different Corrosivity
F. Mansfeld and H. Xiao 1388

139 Characteristics of Electrochemical Noise Generation During Pitting Corrosion
S. Muralidharan, G. Venkatachari, and K. Balakrishnan 1403

573 Electrochemical Noise as the Basis of Corrosion Monitoring
A. Legat 1410

506 Electrochemical Relaxation Techniques for the Measurement of Instantaneous Corrosion Rates
V. Lakshminarayanan and S. Rajagopalan 1420

111 Rapid Evaluation of Corrosion Behavior by Using Random Potential Pulse Method
Y. Sugie and S. Fujii 1430

070 Application of Modern Electronic Technique in Corrosion
F. Qiu 1445

094 Improvement of Mansfelds Method for Computing Electrochemical Parameters from Polarization Data
G. Rocchini 1450

532 Assessment of Corrosion of Laser Surface Alloyed Aluminum & Steel by Electrochemical Technology
R. Li, M. Ferreira, A. Almeida, R. Vilar, K. Watkins, and W. Steen 1460

067 Marine Corrosion Resistance of Aluminum and Aluminum-Lithium Alloys
P. Roberge and D. Lenard 1466

209 Measuring Corrosion Resistance of Stainless Steels Using the 'Avesta Cell' - Experiences and New Applications
P. Arnvig and R. Davison 1477

226 Corrosion Resistance and Behavior of Construction Materials Exposed to Dilute Sulfuric Acid at Elevated Temperatures Under Static Conditions
D. Nguyen and R. Daniels 1491

ENVIRONMENTAL CRACKING

241 Crack Initiation and Growth of Sensitized Type 304 Stainless Steel in NaF Solution
T. Shibata, T. Oki, and T. Haruna 1509

211 Localized Corrosion Problems in Austenitic Stainless Steel Feed-water Heater Tubing
G. Wood 1523

063 Stress Corrosion Cracking of Sensitized Type 316 Austenitic Stainless Steel in Pure Sulfuric Acid Solution
R. Nishimura and A. Sulaiman 1532

117 The Influence of H⁺ and Cl⁻ Ions on SCC of Austenitic 304SS in Acidic Chloride Solutions at Ambient Temperature
Z. Fang, R. Zhu, and Y. Wu 1542

296 Differentiation Between Sulphide Stress Corrosion Cracking in 13% Cr and Duplex Stainless Steels
J. Barker, J. Yu, and R. Brook 1549

118 Stress Corrosion Cracking of 321 Austenitic Stainless Steel Single Crystal Under Mode II Loading
L. Qiao, D. She, W. Chu, and C. Hsiao 1560

010 Effect of Heat Treatment on SCC Behavior of 40 CrMnSiMo A Steel
S. Jin, S. Li, and X. Liu 1564

425 Corrosion Kinetics within Pits or Stress Corrosion
Y. Liu, Y. Cen, and J. Zuo 1572

497 Investigation of Mechanical & Environmental Effects on the Occluded Cell withing Stress Corrosion Cracks of 1Cr13 Martensitic Stainless Steel
Y. Liu, Y. Cen, and J. Zuo 1580

596 A Fully-Plastic Micro-Cracking Model for T-SCC in Planar-Slip Materials
W. Flanagan, M. Wang, M. Zhu, and B. Lichter 1588

509 Improved Stress Corrosion Performance for Alloy 718 via Melt Practice and Heat Treatment Variation
M. Miglin, J. Monter, C. Wade, J. Nelson 1600

485 Competition between Anodic Dissolution and Hydrogen Effects During Stress Corrosion Cracking of a 7150 Aluminum Alloy
D. Najjar, O. Moriau, R. Chieraqatti, T. Magnin, and T. Warner 1613

112 The Peculiarities of Electrochemical Behaviour and Stress Corrosion for Aluminium Alloys with Lithium Additives
V. Sinyavsky 1623

122 Cathodic Corrosion and Hydrogen Effect in TiAl & Effects of Hydrogen
W. Chu, K. Gao, J. Jin, and L. Qiao 1637

380 Using Real-Time Holography to Monitor Stress Corrosion Cracking Initiation
V. Desai, E. Principe, L. Quian-Falzone, and F. Moslehy ... 1649

564 Pre-Crack Fatigue Damage and Crack Initiation under Corrosion Fatigue Conditions
J. Seidel and D. Duquette 1658

327 Corrosion Fatigue of Marine Structural Steels in Saline Environments
M. Kermani and F. Abbassian 1671

297 Corrosion Fatigue Propagation of Higher Yield Strength Offshore Structural Steel in Artificial Seawater
J. Yu, R. Brook, I. Cole, D. Morahito, and G. Demofonti ... 1692

002 Corrosion Fatigue in Fossil-Fueled Boilers
G. Ogundele, E. Ho, and D. Sidey 1702

484 Influence of Surface Microcracks on the Corrosion Fatigue Mechanisms of Ferritic and Austenitic Stainless Steels
T. Magnin 1720

| Paper # | Page # |
|---------|------------------------------------------------------------------------------------------------------------------------------------------------------|
| 448 | Influence of Applied Potential on Corrosion Fatigue Life and Crack Chemistry of Low Carbon Steel <i>H. En-Hou, H. Yuma, and K. Wei</i> 1727 |

VOLUME 3B

INHIBITORS

| | |
|-----|-------------------------------------------------------------------------------------------------------------------------------------------------------------------------------------------------------------------|
| 020 | Corrosion in Heavy Duty Diesel Engine Cooling Systems <i>B. Salas</i> 1736 |
| 053 | Synthesis and Study of Different Thioamides as Corrosion Inhibitors <i>K. Ahmed, S. Oun, and M. Shariff</i> 1743 |
| 058 | Corrosion Resistance of Copper and Copper Alloys Surface Treated with a Benzotriazole Derivative in Sodium Chloride Solutions <i>F. Zucchi, G. Brunoro, C. Monticelli, and G. Trabanelli</i> 1758 |
| 078 | Study of the Effect of Inhibitors on the Removal of Scale from Mild Steel Surface During Pickling <i>G. Banerjee and S. Malhotra</i> 1766 |
| 088 | Theoretical Calculation and Experimental Verification of Critical Passivation Concentration of Oxidizing Inhibitors in Acid Solutions <i>M. Zhao</i> 1773 |
| 144 | Chemical Composition and Structure of Surface Layer Forming in Solutions of Chromate-ions and Corrosion Behaviour of Carbon Steel <i>E. Enikceev, M. Panov, I. Krashennikova, and A. Feoktistov</i> 1784 |
| 149 | A Quantum Chemical Study of Inhibition Effect of Isoquinoline Derivatives <i>L. Yao, M. Lou, P. Kong, E. Kung, and C. Yao</i> 1794 |
| 200 | A Spectroscopic Investigation on Inhibition Mechanism of Dibenzyl Sulfoxide for Iron Corrosion in a Hydrochloric Acid Solution <i>K. Aramaki, N. Ohno, and H. Nishihara</i> 1804 |
| 287 | The Study on Synergistic Effect of corrosion Inhibitor <i>E. Kalman</i> 1814 |
| 411 | Effect of Some Organic Inhibitors on Corrosion of Stainless Steel in Hydrochloric Acid <i>A. Ismail and S. Sanad</i> 1826 |
| 508 | Corrosion Inhibition Study of Different Azoles on Copper Using Carbon-Paste Electrodes <i>V. Lakshminarayanan, R. Kannan, and S. Rajagopalan</i> 1854 |
| 605 | Inhibition of the Corrosion of Carbon Steel in Hydrochloric Acid by Phosphonium Species <i>B. Barker, I. Beech, and F. Walsh</i> 1864 |

| Paper # | Page # |
|---------|--------|
|---------|--------|

LOCALIZED CORROSION/CREVICES

| | |
|-----|--------------------------------------------------------------------------------------------------------------------------------------------------------------------------------------------------------------------|
| 225 | Prediction of Crevice Corrosion Resistance of Stainless Steels in Aqueous Environments: A Corrosion Engineering Guide <i>J. Oldfield, and R. Kain</i> 1876 |
| 347 | Seawater Testing to Assess the Crevice Corrosion Resistance of Stainless Steels and Related Alloys <i>R. Kain</i> 1889 |
| 246 | Modelling Crevice Corrosion of Fe-Cr-Ni-Mo Alloys in Chloride Solution <i>P. Gartland</i> 1901 |
| 284 | Crevice Corrosion of a Ni-Based Superalloy in Natural and Chlorinated Seawater <i>B. Shaw, P. Moran, and P. Gartland</i> 1915 |
| 300 | The IR Mechanism of Localized Corrosion <i>H. Pickering</i> 1929 |
| 446 | Corrosion Behavior of High Nitrogen Stainless Steels for Biomedical Applications <i>A. Cigada, G. Rondelli, B. Vicentini, and G. Dallaspesza</i> ... 1938 |
| 470 | Nitrogen Bearing Austenitic Stainless Steels - A Promising Replacement for Currently Used 316L Stainless Steel Orthopaedic Implant Material <i>M. Sivakumar, U. Kamachi-Mudali, and S. Rajeswari</i> 1942 |
| 471 | Pit-induced Corrosion Failures in Stainless Steel Orthopaedic Implant Devices <i>M. Sivakumar, U. Kamachi-Mudali, and S. Rajeswari</i> 1949 |
| 376 | Studies on the Environmental Degradation of Metal Matrix Composite Materials <i>A. Rawat, V. Desai, P. Ramakrishnan, and R. Prasad</i> 1960 |
| 346 | Corrosion Behavior of Alumina/Al and SiC/Al Metal Matrix Composites <i>P. Nunes and L. Ramanathan</i> 1974 |
| 252 | Effect of Cold-Working on the Crevice Corrosion of Austenitic Stainless Steels <i>T. Handa, Y. Miyata, and H. Takazawa</i> 1986 |

LOCALIZED CORROSION/PITTING

| | |
|-----|-------------------------------------------------------------------------------------------------------------------------------------------------------------------------------------------|
| 500 | Application of In-Situ Scanning X-ray Fluorescence to Study the Concentration of Metal Ions in Simulated Pits <i>H. Isaacs, J. Cho, A. Davenport, M. Rivers, and S. Sutton</i> .. 1997 |
| 599 | Pitting Conditions Evolution of 316L Stainless Steels During Aging in Sea Water: A Statistical Approach <i>M. Ghiazza, D. Festy, J. Leonard, and C. Lemaître</i> 2005 |
| 179 | Pitting Behaviour of UNS N08904 Stainless Steel in Salt Solutions <i>V. Gouda and W. Abd-El Meguid</i> 2011 |
| 086 | Corrosion Monitoring of Aluminum Easy-Open Ends by Area Polarization Technique <i>O. Sciri, K. Furuma, and Y. Matsumura</i> 2022 |
| 565 | Passivity and Passivity Breakdown in Sputtered Aluminum and Iron Alloys <i>Z. Szklarska-Smialowska and R. Inturi</i> 2030 |

| Paper # | | Page # |
|---------|----------------------------------------------------------------------------------------------------------------------------------------------------------------|--------|
| 059 | Localized Corrosion Phenomena Study in 304L and 316L Stainless Steel Prepared by Power Metallurgy <i>E. Otero, A. Pardo, V. Utrilla, and E. Saenz</i> | 2037 |
| 087 | In-Situ Measurement of the $C1^-$ Concentration Distribution in Two Dimensions of Metal Surface <i>C. Lin</i> | 2045 |

PASSIVITY AND BREAKDOWN

| | | |
|------|------------------------------------------------------------------------------------------------------------------------------------------------------------------------------------|------|
| 024 | Influence of Anions on the Surface Enhanced Raman Spectre of Passive Films Formed on Iron <i>T. Devine and J. Gui</i> | 2052 |
| 262 | Vacancy Condensation as the Precursor to Passivity <i>D. MacDonald</i> | 2065 |
| 323 | Passivity of FeCr Alloys <i>J. de Wit</i> | 2077 |
| 340A | Passive Oxide Films on Well-Defined Nickel Surfaces: An Examination of Film Growth on Ni(100) with Ex-Situ Scanning Tunneling Microscopy <i>C. Vitus and A. Davenport</i> | 2091 |
| 371A | Passivity and Pitting Corrosion <i>M. Ives</i> | 2096 |
| 398 | Atomic Structure of Passive Films on Nickel <i>P. Marcus, H. Talah, and V. Maurice</i> | 2105 |
| 453 | The Effect of Temperature on the Passive $Ni(OH)_2$ Growth on Nickel in 1M NaOH Using Rehopping Motion Model <i>C. D'Alkain and H. Mascaró</i> | 2112 |
| 071 | XPS Study of Passive Films on Stainless Steels in Neutral Solutions <i>A. Rossi, and B. Elsener</i> | 2120 |
| 567 | Passivity of Carbon Steel in Organic Solutions <i>D. Schifler, P. Moran, and J. Kruger</i> | 2131 |
| 568 | In-situ STM Characterization of Passivity and it's Breakdown on Stainless Steels <i>S. Virtanen, A. Schreyer, and H. Bohni</i> | 2142 |
| 015 | An Investigation of the Stability of Transpassivated Film on 304 Stainless Steel <i>G. Song, C. Cao, and H. Lin</i> | 2155 |
| 130 | Photoelectrochemical Studies of the Passive Films on Copper and Brass <i>G. Rajagopal, S. Sathiyarayanan, and K. Balakrishnan</i> ... | 2162 |
| 212 | The Ion-Exchange Behaviour of the Corrodible Metal Surfaces <i>A. Nazarov and M. Petrunin</i> | 2175 |
| 283 | Non-Equilibrium Aluminum Alloys: Effects on Passivity in Chloride Environments <i>E. Principe</i> | 2187 |
| 315 | The Effect of Ion Implantation on the Passivation Behavior of Pure Copper <i>E. Wright, V. Ashworth, B. Procter, and W. Grant</i> | 2207 |

| Paper # | | Page # |
|---------|--------------------------------------------------------------------------------------------------------------------------------------------------------------------------------------------|--------|
| 392 | Effect of Oxygen-Containing Oxidizers on Fe, Cu, and Sn Dissolution Rates in Acidic Sulphate Electrolytes <i>N. Chebotaryova, A. Marshakov, V. Ignatenko, and Y. Mikhailovsky</i> | 2223 |
| 451 | Kinetic Study of the $PbSO_4$ Reduction on Lead Using Rehopping Motion Model <i>C. D'Alkain and H. Mascaró</i> | 2232 |
| 452 | Variation of the Dielectric Constant and Resistivity During the Anodic Growth of $Ni(OH)_2$ <i>C. D'Alkain and H. Mascaró</i> | 2240 |
| 454 | The Oxidation/Reduction Reaction of Zinc at the Zn/ZnO Interface <i>C. D'Alkain and H. Mascaró</i> | 2248 |
| 488 | Electrochemical and Corrosion Behaviour of Passive Film on Stainless Steels After Gamma-Ray Irradiation <i>G. Capobianco, A. Glisenti, T. Monetta, and F. Bellucci</i> ... | 2255 |

VOLUME 4

CATHODIC PROTECTION

| | | |
|-----|------------------------------------------------------------------------------------------------------------------------------------------------------------------------|------|
| 001 | Stray Current Interaction in the System of Two Extensive Underground Conductors <i>W. Machczynski</i> | 2268 |
| 041 | An Initial Investigation of Calcareous Deposits Upon Cathodically Polarized Steel in Brazilian Deep Water <i>R. Vianna and G. Pimenta</i> | 2278 |
| 161 | The Isolator/Surge Protector: A Superior Alternative to Polarization Cells <i>T. Scharf</i> | 2285 |
| 223 | Laboratory Evaluation of the Effectiveness of Cathodic Protection in the Presence of Iron Bacteria <i>K. Okamura, Y. Koyama, F. Kajiyama, and K. Kasahara</i> | 2293 |
| 580 | Modification of the Corrosion Environment beneath Disbonded Coatings by Cathodic Protection <i>K. Fink and J. Payer</i> | 2302 |
| 598 | Pipeline Inspection and Rehabilitation - An Overview <i>G. Matocha</i> | 2311 |
| 607 | Prediction of Dynamic Current Density on Cathodically Protected Steel in Seawater at Different Depths <i>R. Griffin, J. Yan, R. White</i> | 2324 |

HYDROGEN EFFECTS

| | | |
|-----|--------------------------------------------------------------------------------------------------------------------------------------------------------------------------|------|
| 524 | Hydrogen Embrittlement in Steels: Mechanical Aspects <i>R. Magdowski</i> | 2332 |
| 238 | Hydrogen Embrittlement in Steels: Metallurgical Aspects <i>M. Speidel</i> | 2339 |
| 299 | Electrochemical Aspects of Hydrogen Embrittlement in Steels: (i) IPZ Model of Hydrogen Permeation (ii) IR Voltage-Induced Hydrogen Charging <i>H. Pickering</i> | 2346 |

| Paper # | Page # | Paper # | Page # |
|---------|--------------------------------------------------------------------------------------------------------------------------------------------------------------------------------------------------------------------|---------|-------------------------------------------------------------------------------------------------------------------------------------------------------------|
| 147 | Predicting the Susceptibility to Hydrogen Embrittlement <i>B. Pound</i> | 570 | Use of Composite Materials on Offshore Platforms <i>O. Sætre</i> |
| | 2356 | | 2529 |
| 322 | Evaluation of Three Different Surface Modification Techniques for Resisting Hydrogen Embrittlement in Steel <i>S. L. Ho, C. Ho, and J. Lin</i> | 014 | Corrosion Performance and Application Limits of Materials in Oil Fields <i>A. Miyasaka and H. Ogaloa</i> |
| | 2367 | | 2537 |
| 602 | Modeling of Nonsteady State Hydrogen Permeation <i>P. Janavicius, S. Amey, J. Payer, and G. Michal</i> | 093 | Corrosion Resistant Alloys UNS NO9925 and NO7725 for Oil Field and Other Applications <i>E. Hibner and R. Moeller</i> |
| | 2377 | | 2548 |
| 011 | A Sensor for Measuring the Permeation Rate of Atomic Hydrogen and its Applications in HIC Inspection <i>Y. Du</i> | 207 | Stress Corrosion Cracking Behavior of Austenitic and Duplex Stainless Steels in Simulated Sour Environments <i>K. Saarinen</i> |
| | 2383 | | 2566 |
| 393 | The Mechanism of the Effect of Oxygen-Containing Oxidizers on the Rate of Hydrogen Cathodic Evolution and Hydrogen Permeation into Metal <i>L. Maksiava, A. Marshakov, Y. Mikhailovsky, and V. Popova</i> | 427 | Role of Expert Systems in Technology Transfer of Materials for Petroleum Applications <i>S. Srinivasan</i> |
| | 2395 | | 2574 |
| 342 | On Mechanism of Hydrogen Embrittlement of Metals and Alloys <i>Y. Archakov</i> | 528 | The Effect of Certain Compositional Aspects on the Behavior of Tank and Pipe Linings Under Laboratory and Field Conditions <i>M. Winkler</i> |
| | 2405 | | 2585 |
| 121 | Effect of Composition on Hydrogen Induced Ductile Loss and K_{IH} in Ni-Fe FCC Alloys <i>W. Hu, Y. Wang, W. Chu, and C. Hsiao</i> | 549 | Methods to Develop a Performance Envelope for Internal Linings in Oilfield Production Environments <i>G. Ruschau, L. Bone III, and O. Moghissi</i> |
| | 2411 | | 2601 |

OIL AND GAS PRODUCTION AND REFINING WORKSHOP

| | | | |
|-----|-----------------------------------------------------------------------------------------------------------------------------------------------------------------------------------------------------------------------------------|-----|-----------------------------------------------------------------------------------------------------------------------------------------------------------------------------------------|
| 490 | Corrosion Management <i>D. Milliams</i> | 090 | Oxidation of Carburised and Coked Heat-Resistant Steels <i>D. Young, D. Mitchell, and W. Kleeman</i> |
| | 2420 | | 2625 |
| 586 | Development of Super _{13Cr} Stainless Steel for CO ₂ Environment Containing Small Amounts of H ₂ S <i>T. Okazawa, T. Kobayashi, and M. Veds</i> | 203 | The Effect of Environmental Variables on Crack Propagation of Carbon Steels in Sour Media <i>M. Kermani, R. MacCuish, J. Smith, R. Case, and J. Vera</i> .. |
| | 2425 | | 2639 |
| 587 | Corrosion Resistance of 13 and 15% Martensitic Stainless Steels in Oil and Gas Wells <i>O. Hashizume, Y. Miname, and Y. Ishizawa</i> | 133 | Sulfide Scales for the Protection of Steels in H ₂ S-Containing Atmospheres <i>M. Schulte and M. Schutze</i> |
| | 2439 | | 2650 |
| 588 | Development of Safe Use Limits for Martensitic and Duplex Stainless Steels <i>R. Kane and S. Srinivasan</i> | 194 | Wall Shear Stress & Flow Accelerated Corrosion of Carbon Steel in Sweet Production <i>K. Eifird, E. Wright, J. Boros, and T. Hailey</i> |
| | 2451 | | 2662 |
| 585 | Effect of Flow Velocity on CO ₂ Corrosion Performance of 13Cr, Super 13Cr, and A-Y Duplex Phase Stainless Steels <i>A. Ikeda, M. Ueda, J. Vera, A. Vilorio, and J. Morales</i> | 307 | Effect of Flow Velocity on Carbon Steel CO ₂ Corrosion and Surface Films using a Dynamic Field Tester <i>J. Vera, J. Morales, A. Vilorio, A. Ikeda, and M. Ueda</i> |
| | 2464 | | 2695 |
| 590 | The Effect of Temperature on Sulphide Stress Corrosion Cracking Resistance of Martensitic Stainless Steels used in Oil & Gas Industry <i>T. Cheldi, A. Kopliku, A. Cigada, M. Cabrini, G. Rondelli, and B. Vicentini</i> | 385 | A Proposed Mechanism for Corrosion in Slightly Sour Oil and Gas Productions <i>S. Smith</i> |
| | 2482 | | 2695 |
| 278 | Environment Sensitive Cracking of Titanium Alloys in Offshore Equipment <i>I. Azkarate, H. Flower, I. Aho-Mentila, and L. Lunde</i> | 511 | Rotating Cylinder Electrode (RCE) Simulation of Flow Accelerated Corrosion in Sweet Production <i>K. Eifird, E. Wright, J. Boros, and T. Hailey</i> |
| | 2492 | | 2707 |
| 478 | Stress Cracking & Crevice Corrosion Resistance of Pd-enhanced Ti-38644 Titanium Alloy Products in Deep Sour Gas Well Environment <i>R. Shutz, M. Xiao, and J. Skogsberg</i> | 606 | Inhibitor Performance in Annular Mist Flow <i>H. Grøtseten and A. Visser</i> |
| | 2506 | | 2726 |
| 099 | Study of Oil Aluminium Alloy Pipes With Improved Corrosion Resistance <i>V. Kuznetsova</i> | 552 | Evaluation of Magnetic Flux Leakage (MFL) Intelligent Pigging Results from Recurring Arctic Pipeline Inspections <i>G. Williamson</i> |
| | 2520 | | 2734 |
| | | 325 | Practical Approach to Evaluating a Corrosion and Scale Inhibitor Program in a Gathering System <i>R. Bess, D. Monical, and E. Yanto</i> |
| | | | 2749 |

| Paper # | | Page # |
|---------|----------------------------------------------------------------------------------------------------------------------------------------------------------|--------|
| 579 | The Importance of Wettability in Oil and Gas System Corrosion <i>J. Smart III</i> | 2758 |
| 594 | Corrosion Inhibition in Wet Gas Pipelines <i>J. Palmer, J. Dawson, K. Lawson, J. Palmer, and L. Fonczek</i> | 2768 |
| 574 | Behavior of Corrosion Resistant Alloys in Stimulation Acids, Completion Fluids, and Injected Waters <i>R. Kain</i> | 2780 |
| 553 | Effects of Acidizing on High Alloy Springs After H ₂ S Exposure <i>B. Bailey</i> | 2795 |
| 038 | Study of Corrosion Inhibitors in Waste Water Reuse System in the Oilfield <i>L. Zhu</i> | 2803B |
| 258 | The Preparation of Corrosion Inhibitor for Water Flooding in the Oil-field and Mechanism Evaluation <i>L. Zhu, H. Guangtuan, and Y. Wenjuan</i> | 2804 |
| 343 | Low Cost Material Selection for Produced Water Tank <i>T. Havn</i> | 2814 |

PIPELINE CORROSION

| | | |
|-----|----------------------------------------------------------------------------------------------------------------------------------------------------------------------------|------|
| 551 | Corrosion Prevention on the Iroquois Gas Transmission System by a Reliability Based Design Philosophy <i>T. Hamilton</i> | 2823 |
| 566 | Pitting Corrosion Behaviour of Pipeline Steel in Solutions with Coating Disbonded Area Chemistry and in Bicarbonate Solutions <i>X. Liu, X. Mao, and R. Revie</i> | 2831 |
| 510 | Prediction of Microstructural Effect on Corrosion of Linepipe Steels in CO ₂ - Brine Solution <i>B. Mishra, D. Olson, and M. Salama</i> | 2840 |
| 250 | The Effects of Latex Additions on Centrifugally Cast Concrete for Internal Pipeline Protection <i>R. Buchheit, T. Hinkelbein, P. Hlava, and D. Melton</i> | 2854 |
| 256 | A New Process for Internal Welding Joint Corrosion Protection of a Pipeline with Cement Liners <i>L. Fa and C. Jimin</i> | 2865 |
| 563 | Progress Toward a Modified B31G Criterion <i>P. Vieth and J. Kiefner</i> | 2869 |

RELIABILITY AND CORROSION CONTROL OF WELDMENTS/CORROSION RESISTANT ALLOYS

| | | |
|-----|---------------------------------------------------------------------------------------------------------------------------------|------|
| 538 | Welding of UNS S32654 - Corrosion Properties and Metallurgical Aspects <i>M. Liljas and P. Stenvall</i> | 2882 |
| 358 | Pitting Resistance of Autogenous Welds in UNS S31254 High Alloy Austenitic Stainless Steel <i>B. Ginn and T. Gooch</i> | 2895 |
| 541 | Localized Corrosion of the Unmixed Zone in Nickel-Base Alloy Weldments <i>L. Flasche and H. Ahluwalia</i> | 2907 |

| Paper # | | Page # |
|---------|-------------------------------------------------------------------------------------------------------------------------------------------------------------------------------------------------------|--------|
| 536 | Corrosion and Behaviour of SAW Stainless Steel Filler Metals with N ₂ and Mn <i>A. Gil-Negrete</i> | 2925 |
| 539 | Beneficial Effects of Nitrogen Additions on the Micro & Structure Stability & Corrosion S2N & Super Duplex Stainless Steel <i>Charles</i> | 2926 |
| 537 | Corrosion Properties of Duplex and Super Duplex Stainless Weld Metals after Isothermal Aging <i>L. Karlsson and S. Pak</i> | 2944 |
| 459 | Corrosion Characteristics of Plasma Weld Surfacing with the Duplex Materials, X2 CrNiMo22 53 and X2 CrNiMoN 257 4 <i>U. Draugelates, B. Bouaifi, A. Stark, I. Garz, and S. Schulze</i> | 2959 |
| 535 | Alloy 625 Weld Overlays for Offshore and Onshore Projects <i>D. Capitanescu</i> | 2973 |
| 458 | Characterization of the Corrosion Behaviour of Surface Welded Protective Claddings of Nickel and Titanium Alloys <i>B. Bouaifi, U. Draugelates, H. Steinberg, J. Gollner, and A. Burkert</i> | 2987 |
| 540 | Some More About Electrochemical Tests to be Performed on the Field as Non-Destructive Quality Control Inspection <i>M. Verneau, F. Dupoiron, and J. Charles</i> | 2996 |

VOLUME 5A

AIRCRAFT

| | | |
|-----|----------------------------------------------------------------------------------------------------------------------------------------------------------|------|
| 605 | The Role of Corrosion in Aging Aircraft <i>G. Koch and T. Bieri</i> | 3007 |
| 151 | Hidden Corrosion - Needs and Requirements <i>P. Bhagat and G. Hardy</i> | 3018 |
| 196 | The Corrosion Prevention & Control Program of the German Air Force for the PA200 Tornado Aircraft <i>J. Fuhr</i> | 3033 |
| 403 | Corrosion Control as a Necessary Treatment Following the Requirements of Aircraft and Environment Safety <i>E. Durig</i> | 3043 |
| 152 | A New Eddy Current Inspection System for Quantitative Corrosion Depth Measurement on AC Wing Skins <i>H. Grauvogl, F. Regler, and H. Thomas</i> | 3058 |
| 608 | Computer Assisted Aircraft Paint Stripping Technology <i>R. Carnes</i> | 3069 |
| 185 | Accelerating Factors in Galvanically Induced Polyimide Degradation <i>M. Rommel, A. Postyn, and T. Dyer</i> | 3077 |
| 141 | Reducing Aircraft Corrosion with Desiccant Dehumidifiers <i>D. McCarthy, D. Kosar, and S. Cameron</i> | 3086 |
| 137 | Corrosion Contribution to Environmental Cracking Failures of Critical Aircraft Parts <i>J. DeLuca</i> | 3099 |

| Paper # | | Page # |
|---------|-------------------------------------------------------------------------------------------------------------------------------|--------|
| 474 | Use of VCI's (Volatile Corrosion Inhibitors) for Aircraft Protection <i>A. Eydelnant, B. Miksic, and S. Russell</i> | 3109 |
| 359 | Designing Metallic Surface Coatings for Improved Corrosion Resistance <i>R. Narayan</i> | 3118 |
| 336 | Corrosion Behavior of W Implanted Aluminum <i>J. Fernandes and M. Ferreira</i> | 3130 |
| 428 | Development of Chromium Based Composite Coatings for Tribological Applications <i>R. Narayan</i> | 3139 |
| 168 | Evaluation of Chromate Free Corrosion Inhibited Primers for Airbus Aircrafts <i>C. Matz</i> | 3149 |
| 204 | Development of a Non-Cyanide Cadmium Pulse Plating Process <i>J. Steppan, D. Rocca, J. Carraway, and V. Agarwala</i> | 3156 |

AUTOMOTIVE/ACCELERATED TESTING

| | | |
|-----|--------------------------------------------------------------------------------------------------------------------------------------------------------------------------------------------------------|------|
| 030 | Effect of Surface Impurities on the Corrosion Behavior of Type 434 Stainless Steel <i>R. Baboian</i> | 3179 |
| 153 | Optimization of Corrosion and Wear Properties of Steel Component Surfaces by Controlled Gas Nitriding <i>M. Biestek, A. Czelusniak, J. Iwanow, M. Korwin, W. Liliental, and J. Tacikowski</i> | 3188 |
| 581 | In-Situ Analysis of Corrosion in the Crevice of Automotive Body by A.C. Impedance Measurement <i>S. Fujita and K. Matsamura</i> | 3200 |

CORROSION IN CONCRETE

| | | |
|-----|---------------------------------------------------------------------------------------------------------------------------------------------------------------------------------------------------------------------------------------------|------|
| 388 | Designing a Reinforced Concrete Against Corrosion in Chloride Containing Environments: Choosing the Cement by Applying a Diffusion Model and Using Electrochemical Methods <i>E. Triki, L. Dhouibi-Hachani, and A. Raharinaivo</i> | 3207 |
| 337 | A Current-Based Criterion for Cathodic Protection of Reinforced Concrete Structures <i>J. Bennett</i> | 3220 |
| 076 | Carbonation of Flyash-Containing Concrete Electrochemical Studies <i>M. Montemor, A. Simoes, M. Ferreira, and M. Salta</i> | 3235 |
| 301 | Performance of Concrete with Microsilica in Chemical Environments <i>N. Berke, T. Durning, and M. Hicks</i> | 3242 |
| 072 | Inspection and Monitoring of Reinforced Concrete Structures - Electrochemical Methods to Detect Corrosion <i>B. Elsner, H. Wojtas, and H. Bohni</i> | 3260 |
| 302 | Evaluation of Concrete Corrosion Inhibitors <i>N. Berke, M. Hicks, and P. Tournay</i> | 3271 |
| 115 | Cathodic Protection of New Steel Reinforced Concrete Structure <i>A. Tvarusko</i> | 3287 |

| Paper # | | Page # |
|---------|----------------------------------------------------------------------------------------------------------------------------------------------------------------------------------------------------------------------|--------|
| 507 | Measurement of Corrosion Rate of Reinforcing Steel and Electrical Resistivity of Concrete using Galvanostatic Steady State Polarisation Technique <i>V. Lakshminarayanan, P. Ramesh, and S. Rajagopalan</i> | 3295 |
| 057 | Corrosion and Prevention of Ferrocement Roofing Slabs in Electrical Furnace Processing Workshop <i>H. Sun, M. Chou, and Y. Yong Yang</i> | 3308 |
| 700 | Management of Corrosion Control of Reinforced Concrete in the Channel Tunnel <i>A. Pourbaix</i> | 3314 |

ELECTRONICS

| | | |
|-----|-----------------------------------------------------------------------------------------------------------------------------------------------------------|------|
| 098 | Reliability and Corrosion Testing of Electronic Components and Assemblies <i>J. Sinclair, R. Frankenthal, and D. Siconolfi</i> | 3332 |
| 131 | In-Situ Investigation of the Initial Stages of the Electrochemical Deposition of Metals by Contact Electric Resistance Method <i>V. Marichev</i> | 3344 |
| 142 | Corrosion Study of Polymer-on-Metal Systems Modified by Processing Conditions <i>K. Nenov, P. Nagarkar, D. Mitton, and R. Latanision</i> | 3355 |
| 157 | Quantitative Corrosion Testing of EMI Materials for Aerospace Applications <i>P. Lessner</i> | 3366 |
| 183 | Corrosion of Electronics: Effect of Ionic Particulates <i>R. Frankenthal, R. Lobnig, D. Siconolfi, and J. Sinclair</i> | 3378 |
| 234 | Accelerated Gaseous Corrosion Testing <i>R. Schubert</i> | 3385 |

EXPERT SYSTEMS

| | | |
|------|----------------------------------------------------------------------------------------------------------------------------------------------------------|------|
| 289B | How to Formulate Corrosion Knowledge for Expert Systems <i>T. Hakkarainen, and T. Hakkarainen</i> | 3396 |
| 236 | Transforming Computerized Information for its Integration into a Hyper Tutorial Environment <i>P. Roberge</i> | 3404 |
| 206 | Integrated Diagnostic System for Intelligent Processing of Field Inspection Data for Transmission Line Structures <i>P. Mayer and S. Moracs</i> | 3413 |
| 123 | Data Acquisition Update <i>R. Eberlein</i> | 3424 |
| 048 | Corrosion Prediction from Laboratory Tests Using Artificial Neural Networks <i>D. Silverman</i> | 3430 |

LIFE PREDICTION

037 The Deterministic Prediction of Failure of Low Pressure Steam Turbine Disks
D. Macdonald and C. Liu 3446

228 Prediction of Pitting Damage Functions for Condensing Heat Exchangers
C. Liu, M. Urquidi-Macdonald, and D. Macdonald 3460

279 An Estimation of Maintenance Costs Related to Corrosion in Brazilian Electric Power System
A. Marinho Jr. 3477

312 Numeric Model for Hydrogen Embrittlement Prediction for Structures Cathodically Protected in Marine Environments
J. Regnier and D. Festy 3484

318 Use of Fuzzy Logic as a Decision Making Tool in the Rehabilitation of Concrete Bridge Structures
M. Islam and P. Simon 3489

320 The System Analysis of a National Scale Refining Equipment Corrosion Database
Y. Luo 3503

455 Interpretation of Electrochemical Impedance Data for Damaged Automotive Paint Films
C. Diaz, M. Urquidi-Macdonald, D. Macdonald, A. Ramamurthy, W. Van Ooij, A. Sabata, M. Strom, and G. Strom 3508

456 A Test of the Reliability of Mathematical Modeling of Corrosion
P. Ault Jr. and J. Meany Jr. 3519

VOLUME 5B

460 Degradation by Ripple-Load Effect - Impact on Life Prediction
P. Pao, R. Bayles, D. Meyn, and G. Voder 3531

465 Some Through Life Risk/Reliability Considerations for Components Subject to Corrosion - A Safety Assessors View
R. Crombie 3540

466 Management of Corrosion in the Power Industry
H. Flitt 3551

469 Prediction of Corrosion Rate and Probability on Underground Pipes
Y. Katano, T. Kubo, and Y. Igawa 3561

477 A Dominant Flaw Probability Model for Corrosion and Corrosion Fatigue
D. Harlow and R. Wroblewski 3573

MARINE

074 The Effects of Complexing Agents on the Corrosion of Copper/Nickel Alloys in Sulfide Polluted Seawater under Impingement Attack
M. Reda and J. Alhajji 3587

079 A Study of Flow Dependent Corrosion of Nodular Cast Iron in Arabian Gulf Seawater
A. Al-Hasham, H. Shalaby, and V. Gouda 3600

138 Effect of Sulfide Ions on the Corrosion Behavior of Aluminum Alloy (H2O) Synthetic Sea Water
M. Valliappan, M. Natesa, G. Venkatachari, and K. Balakrishnan 3613

220 Corrosion Protection of Submerged Steel Structures by the Combined Use of Protective Coatings and Impressed Current Cathodic Protection
M. Arponen 3617

237 On the Influence of Hydrostatic Pressure on the Corrosion Behavior of 42CD4 Steel in Natural Seawater: A Mossbauer & X-Ray Study
J. Le Breton, J. Teillet, and D. Festy 3634

421 Corrosion Characterization of Explosively Bonded Materials in Marine Environment
N. Lindsey 3645

432 Corrosion and Stress Corrosion Cracking of a Marine Steel in Artificial and Natural Sea Water
M. Golozar and A. Saatchi 3660

441 Environmental Degradation of Polymer Matrix Composite Exposed to Seawater
V. Stolarski, A. Letton, W. Bradley, and R. Cornwell 3671

MICROBIOLOGICALLY INDUCED CORROSION

136 The Impact of Alloying Elements on Microbiologically Influenced Corrosion - A Review
B. Little, P. Wagner, M. McNeil, and F. Mansfeld 3680

554 Early Stages of Bacterial Biofilm and Cathodic Protection Interactions in Marine Environments
H. Videla, S. Gomez de Saravia, and M. de Mele 3687

479 Factors Contributing to Ennoblement of Passive Metals Due to Biofilms in Seawater
P. Chandrasekaran and S. Dexter 3696

189 Ennoblement of Stainless Alloys by Marine Biofilms: An Alternative Mechanism
M. Eashwar, S. Maruthamuthu, S. Sathyanarayanan, and K. Balakrishnan 3708

249 Characterization of the Bio-Film Formed on a Steel Electrode in Seawater by Analyzing the Mass Transport of Oxygen
D. Festy, F. Mazeas, M. El-Rhazi, and B. Tribollet 3717

158 Microfouling Induced Corrosion of Alloys
Z. Ying and W. Qiu 3726

555 Microbiological Aspects of the Low Water Corrosion of Carbon Steel
I. Beech, S. Campbell, and F. Walsh 3735

190 Anaerobic Corrosion of Steel by Phototrophic Sulfur Bacteria
M. Eashwar, S. Maruthamuthu, S. Sebastian-Raja, and S. Venkatakrishna-Iyer 3747

| Paper # | Page # | Paper # | Page # |
|---------|--------------------------------------------------------------------------------------------------------------------------------------------------------------------------------------------------------------------|---------|----------------------------------------------------------------------------------------------------------------------------------------------------------------------------------------------------------|
| 482 | Effect of Biofilms on Crevice Corrosion of Stainless Alloys in Coastal Seawater <i>H. Zhang and S. Dexter</i> 3761 | 401 | Comparative Analysis by AES and XPS of Passive Films on Fe-25Cr-X Model Alloys Formed in Chloride and in Sulfate Solution <i>C. Hubschmid, H. Mathieu, and D. Landolt</i> 3913 |
| 304 | Role of Metal Uptake by the Mycelium of the Fungus <i>Hormoconis resiniae</i> in the MIC of Al Alloys <i>B. Rosales, A. Puebla, and D. Cabral</i> 3773 | 340B | In-Situ Studies of Passive Film Chemistry Using X-ray Absorption Spectroscopy <i>A. Davenport, J. Bardwell, H. Isaacs, and B. MacDougall</i> .. 3921 |
| 217 | Electrochemical Noise Analysis as an Indicator of Microbiologically Induced Corrosion <i>A. Saatchi, T. Pyle, and A. Barton</i> 3786 | 027 | Laser Spot Imaging of Passive Films on Stainless Steels <i>P. Schmuki and H. Bohni</i> 3929 |
| 480 | Use of Nucleic Acid Probes in Assessing the Community Structure of Sulfate Reducing Bacteria in Western Canadian Oil Field Fluids <i>D. Westlake, J. Foght, P. Fedcrak, G. Voordouw, and T. Jack</i> 3794 | 232 | Effect of Rinsing on Analytical Results for Passivity of Amorphous Iron-Chromium-Metalloid Alloys <i>K. Hashimoto, S. Kato, B. Im, E. Akiyama, H. Habakazi, A. Kawashima, and K. Asami</i> 3940 |
| 481 | Control of Microbial Biofilm by Electrically-Enhanced Biocide Treatment <i>W. Costerton</i> 3803 | 384 | Surface Analytical and Electrochemical Examination of Passive Layers on Cu/Ni Alloys <i>P. Druska and H. Strehlow</i> 3951 |
| 483 | Use of a Biofilm Electrochemical Monitoring Device for an Automatic Application of Antifouling Procedures in Seawater <i>A. Mollica and G. Ventura</i> 3807 | 126 | Laser Raman and X-Ray Scattering Studies of Corrosion Films on Metals <i>C. Melendres</i> 3973 |
| 557 | Results of Electrochemical Monitoring of Microbiological Activity <i>G. Nekoksa and G. Licina</i> 3812B | 544 | Studies by Scanning Auger Microscopy of Electrochemical Corrosion: Serendipity and the SAM <i>J. Castle</i> 3982 |
| 271 | Evaluation of Materials and Coatings for use in Wastewater Lift Stations Subjected to Biologically Induced Corrosion <i>H. Saricimen, M. Shamim, and M. Maslehuddin</i> 3813 | 545 | Alloy Oxidation: Who is in Control as Studied by XPS <i>D. Cocke</i> 3991 |

SURFACE ANALYSIS TECHNIQUES

| | |
|-----|--------------------------------------------------------------------------------------------------------------------------------------------------------------------|
| 363 | An ¹⁸ O/SIMS Study of Oxygen Transport in Thermal Oxide Films Formed on Silicon <i>R. Hussey, G. Sproule, D. Mitchell, and M. Graham</i> 3831 |
| 054 | SNMS Studies on the Oxidation Behaviour of Titanium Aluminides <i>W. Quadackers, A. Elschner, N. Zheng, and H. Nickel</i> 3842 |
| 543 | Growth Mechanism of Alumina Scales on FeCrAl Alloys <i>M. Boualam, G. Beranger, M. Lambertin, E. Sciora, R. Hussey, D. Mitchell, and M. Graham</i> 3863 |
| 548 | Passive Film Studies using Neutron Reflectivity <i>L. Krebs, J. Kruger, G. Long, D. Wiesler, J. Ankner, C. Majczak, and S. Satija</i> 3863 |
| 199 | Corrosion of Iron in Electrolytic Anhydrous Methanol Solutions with and without Complexing Agents <i>K. Aramaki, M. Sakakibara, and H. Nishihara</i> 3868 |
| 135 | In-Situ Gravimetry of Corrosion of Iron Thin Films Combined with Surface Analytical Techniques <i>M. Seo and K. Yoshida</i> 3878 |
| 445 | Passivation of High Alloyed Stainless Steel in HCl at 22°C and 65°C <i>L. Wegrelius and I. Olefjord</i> 3887 |
| 505 | XPS and Electrochemical Studies of the Dissolution and Passivation of Molybdenum-implanted Austenitic Stainless Steels <i>E. De Vito</i> 3898 |

NUCLEAR ENERGY AND WASTE STORAGE

| | |
|-----|-------------------------------------------------------------------------------------------------------------------------------------------------------------------------------------|
| 282 | The Effect of Surface Conditions on the Localized Corrosion of a Candidate High-Level Waste Container <i>D. Dunn, N. Sridhar, and G. Cragolino</i> 4021 |
| 303 | The Influence of Long-Term Low Temperature Aging on the Performance of Candidate High-Nickel Alloys for the Nuclear Waste Repository <i>F. Hodge and H. Ahluwalia</i> 4031 |
| 295 | On-Line Monitoring of Corrosion in Field Pipe Gathering Systems <i>K. Lawson, A. Rothwell, L. Fronczek, C. Lange</i> 4046 |
| 518 | Corrosion Potential Monitoring and Its Simulation in BWR Conditions <i>M. Sakai, N. Ohnaka, and K. Ohsumi</i> 4060 |

WATER

583 Twenty Years of Experience of Dezincification Resistant Brasses in Swedish Tap Water Systems
M. Linder 4069

243 Corrosion Protection due to Deaeration using a Hollow Fiber Membrane for Water Distribution Systems in Buildings
T. Fujii, Y. Ochi, Y. Ukena, and Y. Tobisaka 4080

609 The Impact of Environmental Consideration on Corrosion Control Economic and Technology
T. Laronge 4088

VOLUME 6

ELECTRIC POWER INDUSTRY WORKSHOP

341 Cutting the Cost of Corrosion and Fouling by Real-time Performance Monitoring
P. Stokes, W. Cox, M. Winters, and P. Zuniga 4093

418 Service Water Electrochemical Monitoring Development at Ontario Hydro
A. Brennenstuhl 4102

517 Monitoring of Corrosion in a Spray Dryer Absorption FEG Plant
N. Henriksen and J. Kristgeirson 4121

476 On Line Monitoring of Fireside Corrosion in Power Plant
D. Farrell 4131

521 FSM - A New and Unique Method for Monitoring of Corrosion and Cracking Internally in Piping Systems and Vessels
R. Strommen, H. Horn, and K. Wold 4141

582 Experience with Neutron Activation for a Real-time Corrosion Monitoring in a Urea Plant
G. Notten, J. Thoelen, H. Verhoef, and R. van Sluijs 4154

311 Monitoring of Microbiological Activity in Power Plants
G. Nekoksa and G. Licina 4166

021 Electrochemical Monitoring of Erosion-Corrosion in Multiphase Flows
I. Ehmann, E. Heitz, K. Miers, A. Schnitzler, K. Schroeder, and X. Shimeng 4176

419 Monitoring and Prediction of Environmentally Assisted Crack Growth in Stainless Steel Piping
S. Ranganath, T. Diaz, F. Ford, R. Pathania, A. Pickett, S. Ranganath, G. Stevens and D. Weinstein 4185

429 Corrosion Monitoring Using Harmonic Impedance Spectroscopy
N. Thompson and B. Syrett 4200

576 Electrochemical Noise Methods as a Possible In-Situ Corrosion Sensing Technique
G. Bierwagen, D. Mills, and D. Tallman 4208

516 Simultaneous Rig Investigations of Electrochemical and Chemical Corrosion of Low Carbon Steel in Feedwater with Oxygen and Ammonia
A. Sirota, V. Latunin, and V. Donnikow 4219

251 Electrochemical Sensors for Application to Boiling Water Reactors
M. Indig 4224

321 Electrochemical Potential Monitoring in the Feedwater at the St. Lucie 2 PWR
W. Kassen, J. Seager, and K. Beichel 4237

407 On-line Chemistry Control in EDF Nuclear Power Plants
J. Doyen 4259

436 Potential Transients, Transmission and Electrochemical Corrosion Detection
H. Isaacs and J. Cho 4267

261 Development of Sensors for In-Situ Monitoring of Corrosion and Water Chemistry Parameters for the Electric Power Utility Industry
D. Macdonald, J. Pang, C. Liu, E. Medina, J. Villa, and J. Bueno 4274

270 An Electrochemical Sensor for Oxygen and pH in Aqueous Systems
C. Alcock, L. Wang, B. Li, and N. Bakshi 4286

310 On-Line Particulate Iron and Sulfur X-Ray Monitor
D. Connolly 4295

520 On-Line Dissolution and Analysis of Corrosion Products
M. Robles 4305

437A Remote Monitoring of Corrosion Chemicals via Fiber Optic Raman Spectroscopy
L. Jeffers and J. Berthold 4313

575 Surface Enhanced Raman Scattering as an In-Reactor Monitor of Phenomena of Interest to the Nuclear Power Industry
T. Devine 4321

134 A New Contact Electric Resistance Technique for In-situ Measurement of the Electric Resistance of Surface Films on Metals in Electrolytes at High Temperatures and Pressures
T. Saario and V. Marichev 4325

The Role Of Corrosion In Aging Aircraft

Gerhardus H. Koch
CC Technologies, Inc.
2704 Sawbury Boulevard
Columbus, Ohio 43235

Timothy H. Bieri
CC Technologies, Inc.
2704 Sawbury Boulevard
Columbus, Ohio 43235

Abstract

A review is presented on the impact of corrosion on the structural integrity of aging aircraft. Although corrosion has been recognized as a significant detriment to aircraft structures, corrosion can also have a more insidious effect by interacting with and promoting fatigue crack initiation and propagation in certain aluminum alloys. A possible mechanism of fatigue cracking in corroded aluminum structure is discussed. An argument is made for hydrogen embrittlement to be the controlling mechanism of corrosion fatigue interaction in certain aluminum alloys.

Key words: Corrosion, fatigue, cracking, initiation, propagation, aging, aircraft.

Introduction

A significant part of the commercial and military aircraft fleet has reached or exceeded its original design life. Corrosion of primary and secondary components has become a major factor in determining the structural integrity and life expectancy of these components. As traditional corrosion inhibiting chemicals are phased out because of their hazardous effects on the environment, corrosion will become even more significant. For example, it is anticipated that the military KC-135 transport fleet will not reach its fatigue limit, but rather corrosion will limit the life of the fleet. In the civilian sector, the effect of corrosion was evident from the post-accident investigation of the Aloha Airlines Boeing 737 fuselage structure, following the incident of April 1988. Certain fuselage lap splices, including the one where a 20 foot long fracture occurred during flight, were found with severe corrosion.

Corrosion affects the structural integrity of aircraft in three ways. First, corrosion has a direct effect on aircraft structures by metal loss which affects the strength and fracture toughness of the material, thereby reducing the structural integrity of a component. Secondly, corrosion can act simultaneously with mechanical loading resulting in cracking phenomena such as stress-corrosion cracking and corrosion fatigue. Thirdly, a phenomena that has been recognized only recently is that of the interaction between

preexisting corrosion and fatigue cracking. This paper will discuss each of these effects of corrosion on the structural integrity of aircraft.

Direct Effects Of Corrosion

Corrosion in aircraft manifests itself in several different forms.¹ Pitting and crevice corrosion are the most common forms of corrosion in the 2000 and 7000 series aluminum alloys which are the principle materials of construction. These forms of localized corrosion can be very destructive by themselves, but also act as stress risers from which stress-corrosion and fatigue cracks can initiate. Another common form of corrosion is exfoliation corrosion. Exfoliation corrosion is a form of intergranular corrosion where corrosion occurs along the grain boundaries of elongated grains and it often initiates at unprotected end grains, such as fastener holes and plate edges. Unlike pitting and crevice corrosion, susceptibility to exfoliation corrosion depends on alloy type, heat treatment, and grain orientation. Fretting corrosion often occurs when two surfaces rub at high frequency and low amplitude in the presence of a corrosive environment. This form of corrosion is for example observed in fastener holes where there is minute friction between the fastener and the wall of the fastener hole. The resulting damage often acts as initiation site for stress corrosion or fatigue cracking. Finally, galvanic corrosion is a common form of corrosion in aircraft structures, where dissimilar metals such as aluminum and steel are in direct contact. This form of corrosion can easily be prevented by isolating the different metals which can be accomplished by proper design and assembly.

There are many contributing causes to corrosion of aircraft. The first cause lies in the design of the aircraft and its components. Often, insufficient attention has been paid to the basic principles of corrosion-conscious design such as the selection of corrosion resistant materials, and the avoidance of dissimilar metal contact, crevices, stresses, and poor drainage. In addition, the selection of the finish and sealant system is an important part of corrosion-conscious design. For example, in recent years the use of corrosion inhibiting primers and corrosion inhibiting sealants in fastener holes and on faying surfaces has become a more common practice. The elimination of crevices is now required by faying surface sealing of all joints that are known to be prone to corrosion, with corrosion inhibited sealants such as chromated polysulfate sealant. Corrosion inhibiting compounds are now commonly applied in the final assembly of many aircraft components, such as inside the fuselage crown and lower lobe, pressure bulkheads, pressure deck, under lavatories and galleys, wheel wells, wing-empennage cove areas, dry bays, empennage torque box interiors, and under fairings.

Furthermore, the post-accident investigation of the April 1988 accident with the Aloha Airlines Boeing 737 indicated that cold bonded lap joints could not prevent penetration of moisture. The moisture in the lap joint resulted in disbanding of the joint, which lead to loss in load carrying capacity of the joint and eventually to multiple site fatigue cracking

from the fastener holes. The lesson learned from this investigation was that only high temperature cured adhesives should be specified for bonding structural components.

Faulty manufacturing is another source of corrosion. Specifically, the assembly and finishing processes can determine whether a specific component will be subject to premature corrosion. For example, of particular importance is the proper surface pretreatment and application of protective coatings or sealants, which must offer long term durability in order to provide adequate corrosion protection.

Finally, operating conditions can be an important contributor to corrosion of aircraft components. Operational environments such as marine, tropical, high humidity, and industrial can be very corrosive to the outside of an aircraft. Moreover, during operation, the protective surface finish can deteriorate by chipping, scratching, breaking around fasteners, abrasion and aging. Environmental conditions inside an airplane can even be more damaging. For example, lavatory spillage, galley spillage, chemical spills, condensation, animal waste, microbial growth, fire residue, and corrosive cargo such as fish can create extremely corrosive conditions inside an airplane, and become a detriment to the structural integrity of the airplane.

Environmentally Induced Cracking

The two main modes of environmentally induced cracking are stress-corrosion cracking and corrosion fatigue. Stress-corrosion cracking of aluminum alloys results from a combination of susceptibility of the alloy, grain orientation, and applied stress. When an aluminum alloy is susceptible to intergranular stress corrosion cracking and the grain orientation is such that the grain boundaries are perpendicular to the applied stress, cracking will occur along the grain boundaries.

Particularly, the 2000 and 7000 series alloys in peak hardness heat treat condition are susceptible to intergranular stress-corrosion cracking. Burleigh² concluded, in an extensive review, that most researchers in the last decade consider stress corrosion cracking of 7000 series alloys to be caused by a hydrogen embrittlement mechanism. Gruhl³ correlated the solubility of hydrogen at the grain boundaries with the concentration of zinc in solid solution. He found a linear relationship between zinc in solid solution and time to failure. Thus, it is not surprising that stress-corrosion cracking of 2000 series alloys, which do not contain zinc, is not considered to be caused by hydrogen induced cracking, but rather to anodic dissolution of the solute-depleted zone along the grain boundary, the grain boundary itself or the precipitates along the grain boundary.

Corrosion fatigue is the most common failure mode encountered in cyclically loaded structures in aircraft. Much work has been conducted on the mechanism of this failure mode. Like stress corrosion cracking, corrosion fatigue of the 7000 series alloys is thought to be the result of hydrogen embrittlement. Duquette and coworkers⁴⁻⁶ have

conducted extensive research to demonstrate this mechanism. They studied the effect of cathodic polarization and catalyst poisoning of the hydrogen recombination reaction, and based on results such as shown in Figures 1 and 2, they concluded that hydrogen is indeed responsible for the reduction of fatigue strength of 7000 series alloys. Figure 4 shows that cathodic polarization of the aluminum alloy during fatigue cracking in an NaCl solution significantly lowers the fatigue strength. At these cathodic potentials, hydrogen ion reduction is the cathodic reaction and the hydrogen generated in that reaction can be readily absorbed by the aluminum matrix. Moreover, when during fatigue cracking arsenic (As) is added to the NaCl solution, the hydrogen re-combination reaction to form H_2 is inhibited, again facilitating hydrogen absorption into the aluminum matrix.⁵ Fractography of specimens which are fatigue fractured under cathodic polarization further showed that the initial fracture mode was intergranular, but that at longer crack lengths, the fracture mode became transgranular with a significant amount of cleavage or quasi-cleavage which is characteristic of hydrogen induced cracking.

Effect of Preexisting Corrosion on Fatigue Cracking

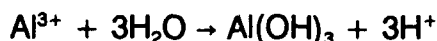
Damage tolerance requirements implemented about a decade ago state that cracks in an airframe structure are permissible. Cracks may impair the strength of a structure, but safety of the aircraft is ensured if the cracks are detected and repaired before reaching the largest permissible size. This approach requires regular inspection based on crack initiation and propagation data developed for new materials. Although the new material based damage tolerance approach is accurate for new aircraft, this approach may be questionable for older aircraft which have been exposed to corrosive environments. The presence of corrosive environments has been typically dealt with by studying the direct interaction between environment and fatigue cracking corrosion fatigue.

However, little work has been done on fatigue crack initiation and propagation in aged or corroded airframe structures. Work by Chubb et al.⁷ indicated that the effect of a corroded area on a propagating fatigue crack is unpredictable. Depending on the alloy type and heat treatment, a crack propagating through a corroded area could be accelerated considerably. The acceleration will have a significant impact on the damage tolerance approach, as is illustrated in Figure 3. Both the detectable and the permissible crack length could occur in much shorter time, so that earlier detection and smaller detection intervals may be required.

Preexisting corrosion can affect fatigue crack initiation as well as propagation. Each of these interactions will be discussed separately in the following sections.

Fatigue Crack Initiation

Fatigue crack initiation can be promoted by corrosion which creates a stress concentration or an aggressive local environment. Aluminum alloys are subject to different forms of localized corrosion depending on microstructure, heat treatment, grain orientation and applied stress. These are pitting, crevice corrosion, exfoliation corrosion and stress corrosion cracking. One of the most common forms of localized corrosion in aluminum alloys is pitting corrosion, which is caused by localized breakdown of the passive film. These pits can act as fatigue crack initiation sites by creating stress concentrations and by creating an acidic environment inside the pit. Regardless of the acidity (pH) of the bulk environment, the pH in the pit is determined by an hydrolysis reaction:



The pH values in the pit are generally between 3 and 4 when the aluminum alloy is actively corroding in the cavity. Lower pH values can be found if the concentration of the aluminum chloride that forms inside the pit increases as indicated in Figure 4⁸.



The aggressive nature of pit environments will promote fatigue crack initiation by either the anodic dissolution mechanism or by the hydrogen embrittlement mechanism. If the hydrogen ion is reduced to an hydrogen atom, it can either adsorb to the alloy surface or form hydrogen gas. The nature of the oxide film in the pit may be a critical factor in this process. Chemical or mechanical damage to the oxide film caused by corrosion and stress allows hydrogen ingress. Because of the high hydrogen fugacity inside the pit, hydrogen will be likely be absorbed by the susceptible alloy. Duquette⁹ explained that second phase particles in 7000 series aluminum alloys may act as sinks for dislocation transported hydrogen. In light of the kinetic model of hydrogen transportation by dislocations, first suggested in 1951 by Bastien and Azou¹⁰, and in 1975 proposed by Tien et al.¹¹ and Donovan¹², cyclic loading will certainly enhance hydrogen entry into the aluminum matrix. Smith et al.⁴ demonstrated that corrosion fatigue of a high purity Al-Zn-Mg-Cu alloy resulted in intergranular crack initiation with a shift to transgranular cracking as the crack propagated. The intergranular crack morphology is similar to that observed in stress-corrosion cracking.

Fatigue Crack Propagation

Little work has been done on fatigue cracking in aluminum alloys with preexisting corrosion. Early work by Person¹³ showed that pitting significantly reduced the fatigue strength of aluminum alloy 7075-T6. Chubb et al.⁷ who studied the crack propagation behavior of 7000 and 2000 series aluminum alloys through areas with exfoliation

corrosion, found that cracks propagating in 7000 series alloys accelerated considerably when reaching an exfoliated area, see Figure 5A. Fatigue crack growth data of a 2000 series alloy, however, indicated no significant effect of the exfoliated areas on the crack propagation, see Figure 5B. These observations indicate that the mechanism of crack propagation in precorroded components may be different for different alloys.

There is some indication in the literature that fatigue crack propagation in precorroded 7000 series aluminum alloys is caused by hydrogen embrittlement. However, other factors such as increased stress because of metal thinning may also play a role in the increase in crack propagation rate, and may in fact be the predominant mechanism of interaction between corrosion and fatigue cracking in other aluminum alloys such as the 2000 series aluminum alloys. In support of an hydrogen embrittlement mechanism for 7000 series aluminum alloys, Smith et al.⁶ demonstrated that the fatigue strength of aluminum alloy 7075-T6 in air decreased significantly as a result of precorrosion in a NaCl solution. Figure 6 shows the S-N curves for the aluminum alloy in air, in 0.5 NaCl, precorroded in the NaCl solution and fatigue stressed in air and, precorroded heat treated and fatigue stressed in air. The re-heat treating resulted in a partial recovery of the fatigue strength, indicating that the lowering of the fatigue strength caused by precorrosion is a reversible process. This behavior strongly suggests that fatigue cracking in precorroded 7000 series aluminum alloys is predominantly a hydrogen embrittlement process.

The mechanism of interaction between preexisting corrosion and fatigue crack propagation in these alloys can be explained in terms of moving dislocations ahead of the propagating fatigue crack. Once hydrogen atoms have formed at a localized corrosion site, they can diffuse into the lattice and be trapped by inclusions such as Al-Zn precipitates at the grain boundaries, or at stationary dislocations. When dislocations become mobile and move along with a propagating fatigue crack, they strip hydrogen atoms from the traps and transport them in a solute atmosphere. The velocity of a dislocation transporting a hydrogen cloud was estimated by Tien¹¹ to be:

$$\bar{v} = M \cdot F,$$

where M is the mobility of the hydrogen cloud and F is the force driving a dislocation.

This equation can further be developed to express the critical velocity above which the dislocation will leave the hydrogen cloud behind. This critical velocity is then expressed as:

$$\bar{v}_c = \frac{D_H \cdot E_B}{KT \cdot 30b}$$

where D_H is the hydrogen diffusion coefficient, E_B is the binding energy and b is the

Burgers vector.

When comparing the time derivative of the critical velocity, or maximum diffusion distance

$$\bar{x}_c = \frac{D_H E_B}{KT \cdot 30b} t_D$$

with the diffusion distance due to random walk diffusion

$$\bar{x}_D = 4 \sqrt{D_H t_D}$$

it can be seen that moving dislocations can effectively transport hydrogen over a much larger distance than the diffusion distance by random walk diffusion.

Thus, when dislocations move at velocities less than \bar{x}_c , the hydrogen will move with the dislocations. The aluminum alloy can be locally enriched in hydrogen when the dislocation loses its hydrogen cloud. This occurs when, for example, the dislocation speeds up and exceeds the critical velocity, or when the dislocation is annihilated or reaches a stationary sink. In this manner high concentrations of hydrogen can build up in the region ahead of the crack tip, causing the crack to accelerate by a hydrogen embrittlement mechanism.

Conclusions

Based on discussions in this paper, it can be concluded that the effect of corrosion of the structural integrity of aircraft component can be significant. The most common forms of corrosion in aircraft are pitting, crevice corrosion, exfoliation corrosion, galvanic corrosion, stress-corrosion cracking and corrosion fatigue. These forms of corrosion, which can be extremely detrimental to the structural integrity of aircraft, can be controlled by proper design, manufacturing processes, and operation and maintenance procedures.

In addition to having a direct effect on the structural integrity by means of metal loss and cracking, corrosion also plays a more insidious role by promoting fatigue crack initiation and propagation in some aluminum alloys. Specifically, it has been demonstrated that in 7000 series aluminum alloys, fatigue cracks are accelerated when they propagate through a corroded region. It was shown that the effect of corrosion on fatigue crack initiation and propagation of these alloys was likely controlled by a hydrogen embrittlement mechanism. Hydrogen atoms that form at a localized corrosion site are absorbed into the metal lattice and transported by mobile dislocations to the region ahead of the crack tip, where they alter the microstructure causing the propagating fatigue crack to accelerate. Finally, there is indication that this hydrogen embrittlement mechanism may not apply to other aluminum alloys such as the 2000 series alloys.

Further experimental work is recommended to confirm the mechanism of interaction between corrosion and fatigue cracking in aged or corroded aircraft components. The understanding of the interaction between preexisting corrosion and fatigue cracking is necessary to develop better predictive capabilities on the fatigue life of corroded airframe structures. Only then can a reliable damage tolerance program be developed for these structures.

References

1. N. L. Bauccio, "Corrosion in the Aircraft Industry" Metals Handbook, Ninth Edition, Volume 13. Corrosion, p. 1019. ASM International, 1987.
2. T. D. Burleigh, "The Postulated Mechanisms for Stress-corrosion Cracking of Aluminum Alloys - A Review of the Literature 1980 - 1989" Corrosion Volume 47, no. 2, February 1991, p. 89.
3. W. Gruhl, Z. Metallkunde, Volume 75, No. 11, 1984, p. 819.
4. E. F. Smith III, R. Jacko and D. J. Duquette, "Hydrogen Assisted Fatigue Cracking of High Strength Aluminum Alloys." Technical Report to the Office of Naval Research, Contract No. N00014-67-A-0117-0012 No N000014-75-C-0466, NR036-093, August, 1975 (NTIS-AD-A014 477).
5. R. J. Jacko and D. J. Duquette. "Hydrogen Embrittlement of a Cyclically Deformed High Strength Aluminum Alloy" Metallurgical Transactions A, Volume 8A, November, 1977, p. 1821.
6. E. F. Smith III and D. J. Duquette, "The Corrosion Fatigue Behavior of a High Purity Al-Zn-Mg-Cu Alloy" Technical Report to the Office of Naval Research Project No. N00014-75-C-0466, November, 1979, (NTIS-AD-A077-461).
7. J. P. Chubb, T. A. Morad, B. S. Hockenhuil and J. W. Bristow, "The Effect of Exfoliation Corrosion on the Fatigue Behavior of Structural Aluminum Alloys" Structural Integrity of Aging Airplanes Ed. S. N. Atluri, S. G. Sampath and P. Tong. Atlanta, Georgia, 1990 p. 87.
8. A. Turnbull, "Chemistry Within Localized Corrosion Cavities" Advanced Localized Corrosion NACE-9 Ed. H. Issacs, U. Bertocci, J. Kruger and S. Smialowski. Orlando, Florida, 1987, p. 359.
9. D. J. Duquette "Mechanisms of Corrosion Fatigue of Aluminum Alloys" RPI, Troy, New York, April, 1981, p. 15 (NTIS-AD-A09712).
10. P. Bastien and P. Azou, "Proceeding of First World Metallurgical Congress" ASM Cleveland, Ohio, 1951, p. 535.

11. J. K. Tien, A. W. Thompson, I. M. Bernstein and R. J. Richards, "Hydrogen Transport by Dislocations" Metallurgical Transactions A, Volume 7A, June, 1976, p. 28.
12. J. A. Donovan, "Accelerated Evolution of Hydrogen from metals During Plastic Deformation" Metallurgical Transactions A. Volume 7A, November, 1976, p. 1677.
13. N. L. Person, "Fatigue Properties of Prior-Corroded Aluminum Sheet Alloys" Materials Performance, December, 1975, p. 22.

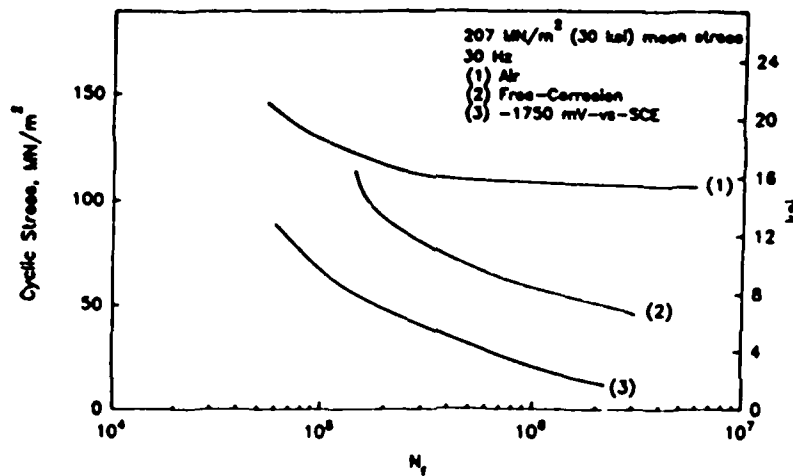


Figure 1 Fatigue behavior of Al-5.5 Zn-2.5 Mg-1.5 Cu in 0.5 M NaCl at room temperature cathodically polarized to -1750 mV vs. SCE compared to fatigue behavior air and under free corrosion conditions in 0.5 M NaCl⁴

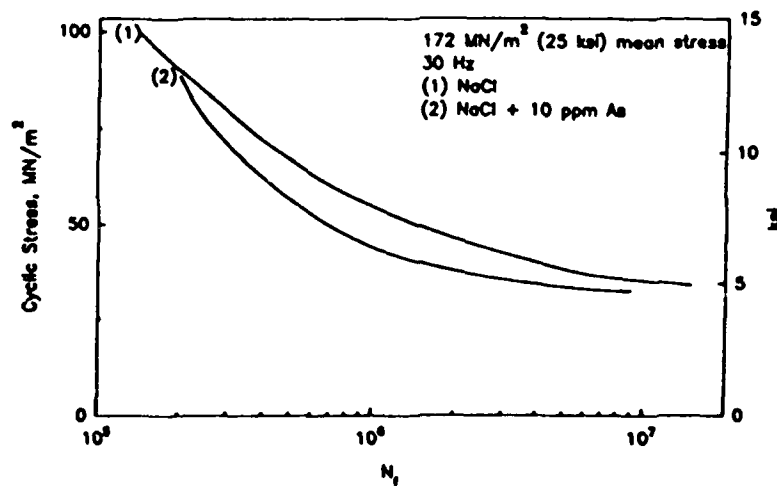


Figure 2 Fatigue behavior of 7075-T6 in 0.5N NaCl + 10 As ppm compared to fatigue behavior under free corrosion conditions in 0.5N NaCl⁵.

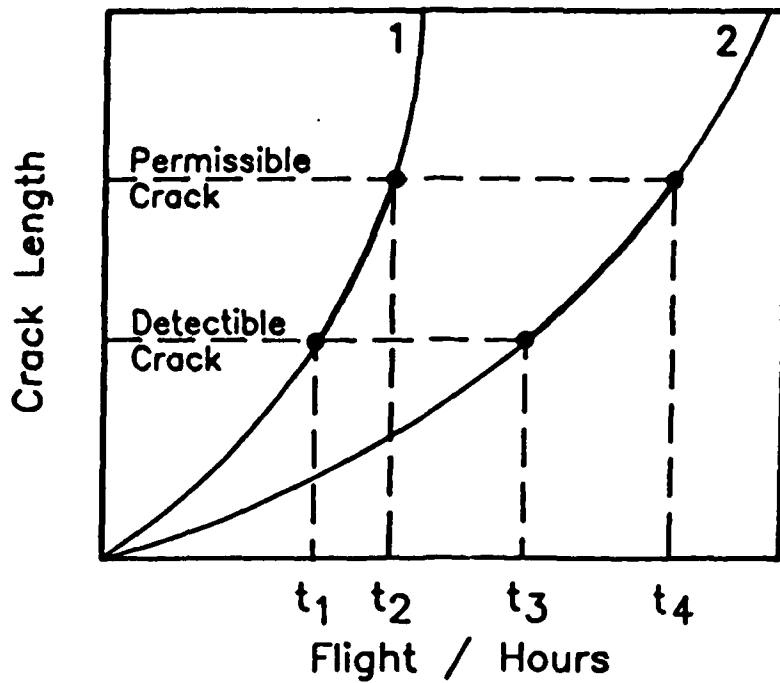


Figure 3 The effect of corrosion on structural crack growth life prediction. Curves 1 and 2 show the crack life in corroded and uncorroded structures, respectively.

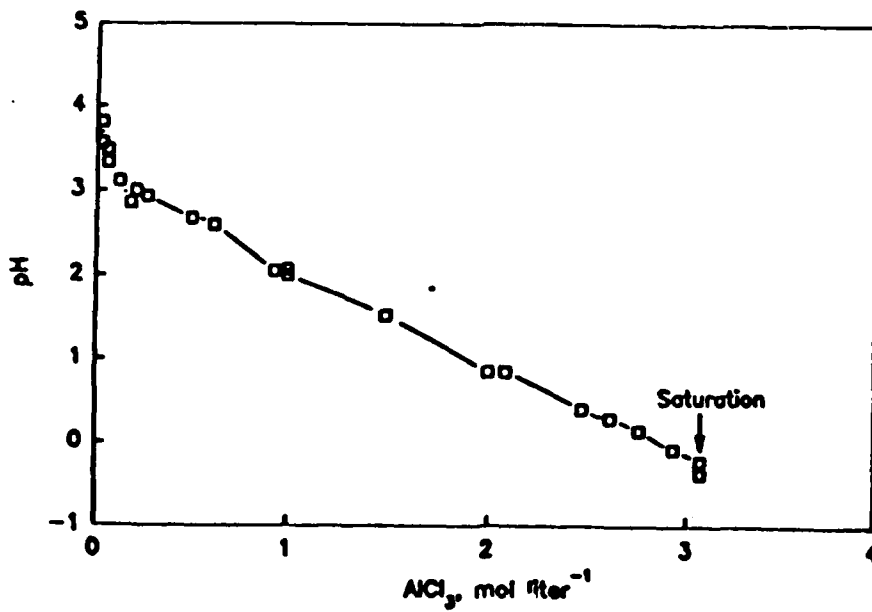


Figure 4 pH of solutions containing dissolved aluminum chloride⁹

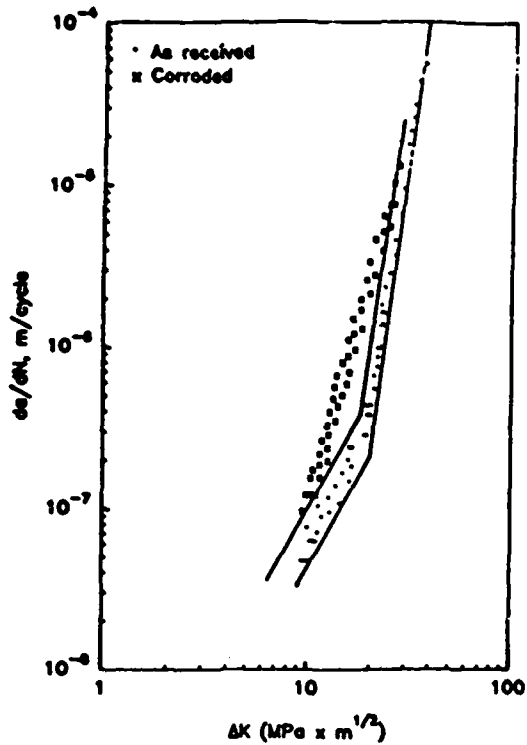


Figure 5a. Fatigue crack growth data for corroded 7178-T6 compared with as-received 7178-T6 tested in dry air [(after Chubb (1))].

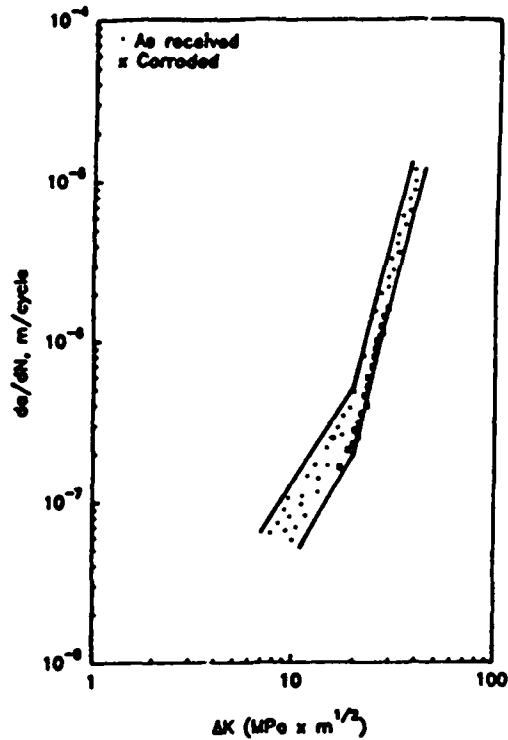


Figure 5b. Fatigue crack growth data for corroded 2024-T351 compared with as-received 2024-T351 tested in dry air [(after Chubb (1))].

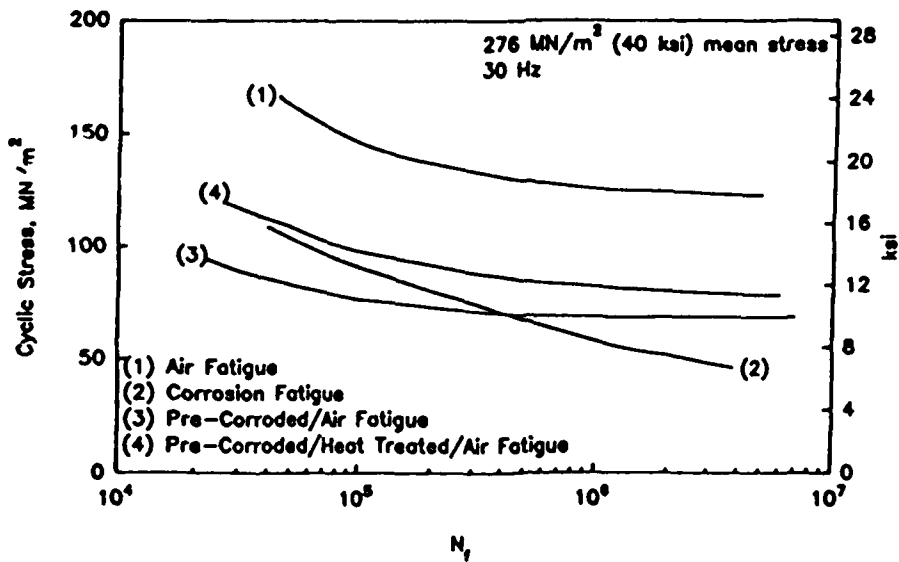


Figure 6 Fatigue behavior of 7075-T6 Al in air (1) in 0.5N NaCl (2) at room temperature precorroded in 0.5N NaCl and at room temperature and tested in air (3), and precorroded, resolutionized (3 hours at 860°C) and tested in air (4)⁶.

Hidden Corrosion - Needs & Requirements

P. K. Bhagat And G. L. Hardy
Materials Directorate
Wright Patterson AFB, OH

Abstract

Due to budget constraints, the Air Force will be operating its current aircraft for ever-longer periods of time. Recent studies have shown that corrosion related maintenance actions are costing the Air Force over \$700M annually. The Air Force identified the need for hidden corrosion detection, prevention, and control through the Logistics Need process in 1979. This report summarizes the findings of Air Force research and development efforts since that time and presents an approach to more aggressively address corrosion detection and control. Current Air Force efforts are being focused on a two-pronged attack. The Logistics community is conducting an assessment of current methods of corrosion detection and the Wright Laboratory is aggressively pursuing any available new exploratory and advanced development approaches for hidden corrosion detection.

Key terms: corrosion, hidden, detection, prevention

Introduction

It is well known that military as well as civilian aircraft operators use a significant portion of their repair and maintenance budget on corrosion related issues. These include costs attributed to corrosion detection, prevention, repair, and control at both depot and field levels. A recent AF sponsored study has concluded that approximately \$718M per year can be attributed directly to corrosion related issues on the current inventory of operating military aircraft [1]. 82% of these costs are for repair purposes. It is interesting to note that the oldest aircraft KC-135, C-130, B-52, F-111, and C-141 account for approximately half of the total cost. Numerous DoD sponsored research and development programs dealing with inspection, control, and prevention of corrosion have led to the availability of a wide variety of newer materials and alloys, corrosion protection schemes, and repair and maintenance methodologies.

During the period of expanding defense budgets with new systems entering at the operational levels in a defined time frame the harmful effects of corrosion could be managed without hampering the fleet readiness. As the current fleet ages, without newer aircraft entering the inventory, the deleterious effects of corrosion become more severe in terms of readiness and quick response. This is due to the fact that corrosion is a more severe problem for older aircraft. Preventive maintenance and repair actions require the affected system to be removed from service for long periods of time. In most cases removal of skin is required, which is an expensive and time consuming proposition. Thus, the attendant cost of maintaining older aircraft is substantially higher and increases dramatically with age. Further, corrosion degrades the fatigue life of airframes and, therefore, has implications related to life extension issues.

There has been significant amount of research on stress corrosion cracking and corrosion fatigue. Implications of corrosion thus enter into life cycle issues since fatigue is accelerated by corrosion. As a result environment related issues enter into fatigue life computations. Even the use of advanced materials, such as graphite composites, to replace metallic structures does not alleviate environmental impacts on the aircraft. Concerns about polyamide degradations due to galvanic corrosion effects on structures have recently been raised [2]. In case of these advanced materials, damage detection and reliability assessment techniques are in a preliminary developmental stage. This aspect related to advanced material inspection can become a

significant factor as today's newer planes age and get corroded. From the foregoing it should be apparent that the importance of early detection, quantification, and prevention of corrosion can not be overemphasized.

In the current era of reduced military budgets along with increased environmental constraints affecting chemicals currently in use for corrosion protection and control it is desirable that a fresh assessment of corrosion related issues be undertaken. It is, therefore, imperative that an intense effort encompassing basic and applied research as well as technology and methodology development be undertaken in order to contain corrosion costs and maintain continued airworthiness of our aging fleet. As stated earlier these efforts should be directed towards early detection, localization, and quantification of corrosion.

One of the most vexing problems in the corrosion arena is that of the detection and quantification of hidden corrosion. As understood by the depot and field personnel this refers to corrosion occurring in regions inaccessible due to structural design constraints as well as that occurring beneath the visible layer of aircraft skin. This problem, identified in the Air Force as LN 79003, "Detection of corrosion in hidden/inaccessible regions", has been a major driver in the AF Materials Directorate(WL/ML) contracted research efforts since 1979 [3]. Programs instituted since 1979 have dealt with corrosion inspection accuracy, repeatability, and identifiability issues. One of the most likely areas for hidden corrosion to occur is around fasteners due to damage to the protective coating. Current requirements to eliminate the wet(coating with primer) installation of fasteners will tend to exacerbate this problem.

Current NDE methods are poor sensors for corrosion, since they are based on the ability to detect area or volumetric flaws that have significant dimensions in one or more directions. In addition, most if not all of the current NDE technologies are man-hour intensive. As a result hidden corrosion detection at field level is a difficult and expensive proposition.

It is well known that the most reliable technique for detection of surface corrosion is the venerable visual inspection. However, visual inspections are difficult to implement for corrosion that is hidden from view. The need to detect hidden corrosion and the inability to quantify visual inspection have led to a host of technologies which are instrument-based and include eddy current, ultrasonic, and radiographic inspections.

These techniques require loss of material to be effective and are somewhat quantifiable and are an improvement over visual methods for corrosion beneath material surface. In spite of the availability of a wide choice of NDE technologies questions regarding the accuracy and reliability of these techniques to detect and quantify hidden corrosion remain. Efforts within the Air Force to assess the applicability of these techniques as well as those designed towards further development of promising scientific ideas are detailed under ' Current Efforts '.

I. Historical Background

Corrosion detection, prevention, and control issues have historically been ignored in weapon systems development. The older systems were manufactured with little or no concerns for corrosion. Material selection was primarily predicated upon reduced weight and improved mechanical properties and scant attention was paid to the possibility of galvanic effects due to proximity of dissimilar materials. Also airframe designs often provided locations that entrapped corroding agents including moisture. In addition these designs often precluded access to corrosion prone areas. As a final blow, in the past, corrosion related issues garnered lower priority than acquisition costs, weight, appearance, operational readiness, and safety of flight.

II. Past Programs

The brief review here is concerned only with efforts related to hidden corrosion detection and control since 1980. References are mainly to programs developed and monitored by Materials Directorate personnel. The initial response to LN 79003 was the release of an RFP for a comprehensive exploratory development program to address the problem of the detection of hidden corrosion. Because the problem was described in broad general terms, the responses to the RFP were found to be lacking in defining a reasonable research effort. To more precisely define the problem the Materials Directorate in 1983 held a workshop on corrosion research and development. This DoD wide workshop was designed to draw together key industry and government experts to assess the status of the field. One of the key issues that emerged was that detection of corrosion in actual aircraft structures is complicated by geometrical constraints. Much of previous efforts in this arena have, therefore, been directed at matching specific inspection techniques to specific structural geometries. It was also reported that current methods of inspection for an operational aircraft in Air Force inventory require over 1000 hours of disassembly, inspection, and

reassembly for areas which can not be inspected in-situ. In addition, significant damage was a necessary prerequisite for reliable detection. It is also significant to note that from the proceedings no single catastrophic accident can be attributed to corrosion damage except where corrosion led to further cracking of the material [10]. Detection and quantification of corrosion without disassembly was listed as a high priority research and development issue. The hidden corrosion inspection issue was further divided as corrosion under paint, and inspection of inaccessible areas. Use of indirect means of measuring corrosion damage such as, paint property alteration, coating integrity assessment, paint formulation, automated rapid inspection, field usability, and quantification were reported as areas ripe for further research and development funding. Lack of funding as well as other priorities have precluded a substantial effort to address all the needs and requirements raised by this workshop.

A Material Directorate program, "Corrosion Maintenance and Experimental Design", was directed at assessing the impact of corrosion related programs and to highlight the needed support areas[8]. The major goals of this funded effort were to evaluate corrosion inhibition effectiveness of aircraft rinsing and corrosion prediction in an airworthiness model. The report points out that benefits of aircraft rinsing/washing using corrosion inhibitors have not been scientifically established. It is suggested that a comprehensive airworthiness maintenance model be developed which would include features of fatigue-life prediction, NDE technology, reliability centered management, and corrosion prediction capability. Corrosion prediction is not readily embraced by field inspection personnel due to procedural difficulties and the general inability to verify environmental assumptions which greatly influence corrosion of an aircraft. While corrosion initiation locations are randomly distributed based on material and operational environment, its progress follows well established laws of chemical kinetics. A theoretical model is reported which can statistically predict the number of aircraft in a fleet reaching a specified damage level due to corrosion. The report recommends further development and verification of this model in conjunction with ASIP.

Another Materials Directorate sponsored program, "Corrosion Detection System Design", addresses the development of NDE techniques for locating and characterizing hidden corrosion in aluminum alloy airframe structures. The techniques evaluated were, real time x-ray, real time neutron radiography, and low frequency eddy current. All these techniques were found to be applicable in the detection of corrosion damage in the laboratory

as well as on C-130 outer wing structure specimens. The report concludes that real time x-radiography affords the best combination of corrosion detection sensitivity and cost effectiveness.

Beissner and Birring have recently carried out a state of the art review of NDE methods for characterization of corrosion [9]. This report concludes that methods for detection of hidden corrosion are not yet fully developed. These authors' also point out the need for research to develop methods to measure material degradation due to corrosion, and to quantify corrosion severity.

As a result of the Air Force Corrosion Tiger Team activities, a broader perspective was gained on hidden corrosion [4]. The Team developed the finding that some improvements in inspections for hidden corrosion, in the near term, probably can be achieved without the development of new NDE technology. The Team recommendation was that the most promising approach is to more precisely define the inspection requirements, as is currently done in fracture control programs for our weapon systems. To demonstrate the viability of this approach, each ALC was tasked by the Tiger Team to pick at least one corrosion problem on a system that they manage and focus the efforts of the local Corrosion Control and NDI groups to arrive at a solution. In response to Tiger Team recommendation, a new 6.3 program, "Quantitative Requirements for Corrosion NDE," was proposed by ML that would take a system-wide view of the same approach on approximately six weapon systems and eventually generate a fleet management practice for corrosion detection/ control patterned after our current fracture control procedures. This is a much broader effort than just NDE, involving a range of applicable, available technologies. There is no current 6.3 funding for this near-term effort, but ML is aggressively pursuing every avenue to develop funds. Availability of future funding is unknown. It is currently planned to conduct this effort as part of the FY95 program if no earlier funding becomes available.

III. CURRENT EFFORTS

Current efforts in the Air Force for assessment of aspects of hidden/inaccessible corrosion are summarized below:

1. A program at OC-ALC(Don Neiser, Program Monitor) with the major aim of disassembling an old KC-135 airplane to provide realistic corrosion samples [5]. Industry and other government agencies have been invited to employ existing

technologies to detect and verify hidden corrosion. To date over 50 organizations utilizing NDE technologies ranging from eddy current, ultrasonic, radiographic, and infra-red(IR) thermography have voluntarily accepted this task at no cost to the government. Major benefit to accrue from this program is that the effectiveness and applicability of current NDE equipment to detect and quantify corrosion on real aircraft samples can be assessed in a controlled environment. Boeing is the prime contractor for the disassembly effort which has the goal of identifying all areas of complete corrosion and uninspected damage locations addressed during Periodic Depot Maintenance(PDM). ARINC is the prime contractor for NDE experimentation effort which will try to identify appropriate NDI technology using the disassembled C/KC-135 parts and geometries.

Among the other anticipated benefits of the program is the possible availability of data, relating to crack growth rates and effects of corrosion on airframe fatigue life on KC-135. This data, can be extremely valuable for updating inspection intervals defined under Aircraft Structural Integrity Program(ASIP). It may be possible to develop maintenance actions/modifications, based on results of this experiment, which may extend fleet life to 2040. Other related goals of this program are to provide a database for the development of corrosion control program, define allowable corrosion damage tolerance limits, predict remaining structural life of C/KC-135 aircraft.

It is generally known that results from cut-up of a KC-135 and its inspection will not provide generic data for corrosion control and prevention. In addition, the Air Force Corrosion Program Office firmly states that prevention of corrosion will lead to substantial savings. Current corrosion control programs during PDM involve rework or replacement of corrode structure and re-application of corrosion prevention materials. Early detection and quantification thus may have substantial impact on PDM funding and manpower requirements.

2. The Materials Directorate is actively pursuing generic NDE technology science base programs which have the potential to improve the capability for earlier detection of corrosion. This implies detection of corrosion with no significant loss of material. It cannot be overemphasized that all of the current known methods for detecting hidden corrosion require substantial material loss to occur before reliable detection can take place. In this vein an (6.2 FY92) effort between Air Force and Navy (Naval Air Warfare Center and AF Materials Directorate) has been cooperatively funded to address

one fundamental aspect of corrosion. This effort, "Hidden Corrosion Characterization," will seek to develop practical sensors for detection of corrosion in aircraft[6]. The program envisions development of chemical sensors which can be applied to aircraft structure via a paint based system. As corrosion proceeds the optical characteristic of the sensor get altered, thus identifying corrosion location in a visual manner. This program also envisions development of micro-sensors that can exploit the galvanic potentials generated as a result of corrosion for remote assessment. This funded effort has shown good promise in laboratory studies. The miniature moisture sensitive sensors are envisioned for use in inaccessible regions. The paint based system that displays altered optical characteristics in presence of corrosion products is envisioned as a visual inspection enhancer. It will allow the inspector to quickly identify corrosion susceptible regions at an early stage. Another funded (6.2 FY92) effort (Applied Physics Laboratory) seeks to exploit InfraRed Thermal Wave imaging technology for rapid assessment of corroded samples via exploitation of thermal diffusivity mismatch [5]. If successful this technology will provide rapid inspection capability inherent in IR methods for wide area inspection in a nonintrusive manner. This method is an outgrowth of AF(WL/MLLP) sponsored research in this technology area funded over a number of years dedicated to developing technology base.

Both of these approaches under Advanced NDE Technology Program are grossly underfunded due to budgetary constraints and other pressing issues in NDE research and development.

IV. PLANNED PROGRAMS

Several programs have been proposed in the near future towards developing technology base in hidden corrosion detection and characterization.

A new 6.2 FY93 effort will attempt to develop techniques and methodologies for understanding and characterizing the effectiveness of corrosion prevention/ protection systems with time. For example a laboratory based study is envisioned where controlled environmental parameters with respect to their effects on integrity of coating protection systems will be documented.

A PRDA approach is planned for another 6.2 FY93 program to assess the availability of applicable new and novel techniques for characterization of hidden corrosion. A follow-on 6.3 program, "Corrosion Detection System Dev/Demo," for the detection of

hidden corrosion is planned for an FY95 start. This program is based on the anticipated results to be accrued from the fundamental science based efforts under 6.2 funding and related generic programs.

Based on the results of a highly successful program in solid-state x-ray detection, a 6.3 program was initiated in FY93 to scale up this technology to provide an 8in X 8in view. The semi-automated prototype is geared towards depot/field assessment of airframe structure, and engine components degradation caused by corrosion. Some of the anticipated highlights of this program are spatial resolution approaching 20 lp/mm, dynamic range exceeding 3000:1, and wide operating energy range.

Another 6.2 program in FY93 is to assess the applicability of backscattered tomography(BIT) to corrosion detection and quantification. This technology addresses the issue of structural inspection in areas of limited access, single side access. This program draws upon the results of technology development establishing the feasibility of BIT for NDE of structures.

There are several other technology programs such as laser generated ultrasound, and eddy current technology for cracks under fasteners(CUFS) that may have impacts on the corrosion issue. A roadmap detailing these programs with timeliness is shown in figure 1.

What is needed in the near term is a program to provide realistic data related to managing the corrosion related maintenance and repair issues of aging aircraft. This program should address four basic needs in order to define the base line for further research efforts. These are: where, when, how often, and how well. Defining the most occurring sites on aircraft structure for corrosion initiation should be done based on analysis of available database related to service inspection of aircraft. This database exists already for various aircraft in the Air Force inventory. These defined locations then can be inspected in a cost and time effective manner. The issue of when to inspect the aircraft relates to aspects of coating protection breakdown, corrosion initiation and growth rates related to aircraft structure. Based on the above parameters the issue of how often to inspect the aircraft can readily be addressed. Growth rates and present inspection capability related to specific aircraft type could provide important information in this regard. Accuracy of a particular NDE technique to quantify corrosion needs to be compared against cost and man hour

requirements. This data can provide a basis for future programs in corrosion detection, prevention, and control.

V. HIDDEN CORROSION PROGRAM; NEEDS AND REQUIREMENTS

It is apparent from the foregoing that efforts in detection, prevention, and control have been inadequately funded and coordinated across the Air Force. In addition there has been little or no coordination between various units within the Air Force on issues related to science base technology development and its eventual transition to field use.

The issues in development of a comprehensive program in corrosion detection, prevention, and control are:

- A. Organizational
- B. Research and Development Plan
- C. Prevention and Control Program

Each of the above is discussed in the following:

A. Organizational

A centralized working group with technical representation from corrosion, structures, and NDE areas and responsibility for coordinating research and development efforts should be established. This group should include representatives from the Air Force corrosion control, and the NDE program office as well. Membership in this organization should also include Air Force Office of Scientific Research(AFOSR), Air Force Materials Directorate, Air Force Flight Dynamics Directorate, Air Logistics Commands, the operating commands, depot and field level personnel representative. In addition mechanism for interfacing with other government agencies such as, Army, Navy, FAA, and NASA should be available so that corrosion funds can be maximized for effective use. An interface with commercial aviation industry, possibly via FAA could provide a powerful organizational structure to effectively manage corrosion related programs.

B. Research and Development Plan

Figure 2 shows a comprehensive research and development program which addresses all issues related to hidden corrosion detection, prevention and control.

1. Corrosion Science. Corrosion basic research related to corrosion under skin surface funded perhaps via AFOSR should

corrosion under skin surface funded perhaps via AFOSR should address the science base issue of providing further understanding in the technological developments needed for corrosion prevention and control. Analytical and quantitative corrosion investigation encompassing both basic and applied research should be initiated. These will address issues such as mechanisms responsible for corrosion and its quantification. Research in the development of corrosion resistant materials is an important issue. Corrosion assessment for the advanced material in aircraft structures should also be studied with a view to developing measures for corrosion prevention. Ability to predict rate of corrosion progression and its validation is another important research area with important implications on aircraft service life. Development of environmentally safe paint and paint stripping systems is an important subject related to future maintenance and cost containment of operational aircraft.

New materials such as layered organic composites which are quite sensitive to environmental and service factors need to be studied for corrosion related issues. The major issue in this instance is to establish structural reliability under corrosive damage and stress. Structural defects and in-service degradation of such materials are difficult to detect and monitor with conventional NDE technology.

Quantification of effects of corrosion on electronic components and systems as a result of various chemicals being used for corrosion control is another important area of concern with aircraft in-service. Environmental aspects related to corrosion should be documented from readily available research data and publications. Corrosion standard samples should be developed so that accurate assessment of developed NDE technologies for detection and quantification of hidden corrosion can be undertaken.

2. NDE Science. Conduct basic and applied research related to hidden corrosion identification, and quantification in both laboratory samples as well as actual structures. NDE technology development geared to reduction in the cost of inspection and man-hour requirements can also be undertaken. Assessment of repair viability via NDE technology is another important area of concern. Reliability and accuracy of quantification of corrosion damage needs to be established.

Research in established NDE technology for assessment and quantification of hidden corrosion should strengthen current programs in the areas of radiography both x-ray as well as

neutron radiography. Real time radiography has the potential to reduce the time required for inspection and evaluation significantly. In addition the development of film free radiography and the possibility of digital image acquisition may provide a quantum leap in further usability of this technology. Research in issues related to further enhancing the capabilities of neutron radiography in terms of source flux and subsequent detection may yield dividends in this hydrogen specific detection and quantification process. Further research is needed in the establishment of IR based methods for rapid assessment of corrosion infested areas on aircraft structures. All these technologies require development of image and signal interpretation capabilities to unambiguously define corrosion related damage in structures.

Further research is needed in the development of chemical and electrochemical sensors which are specific to corrosion and their eventual implementation in operational fleet. These sensors are envisioned for use in coatings and hidden/inaccessible areas of structures for in-situ detection and monitoring of material damage due to corrosion.

Integrity assessment of coating and paints used for corrosion retardation and control is another area where research and development techniques are needed.

3. Structural and Fatigue Mechanics. Documentation and further research in structural and fatigue aspects of material degradation with emphasis on corrosion need to be undertaken. Research and development issues in this area are: Stress corrosion propagation rates, environmental aspects, corrosion and structural strength, fatigue life cycle analysis. Studies of damage assessment in advanced materials and its correlation with corrosion should enhance the understanding and implications in this technology area.

While aluminum dominates the aging aircraft structures, studies related to hidden corrosion should encompass all types of material structure and components such as: Aluminum and magnesium structure, honeycomb and composite structure, engine and electric/ electronic component.

Trade off studies of various structural alloy systems relating specific modulus and strength to corrosion resistance should provide important information relating to life extension issues in replacing corroded/degraded components.

4. Corrosion Prevention and Control. A systematic attempt at reducing the costly and man-hour intensive corrosion related damage should have corrosion prevention and control as a major factor. In this vein studies related to efficacy of preventive measures such as the use of corrosion prevention chemicals, identification of corrosion susceptible regions on aircraft structures, material selection and fabrication related to corrosion resistance are important parameters. Degradation of preventive coating systems through environmental and service related causes needs to be quantified.

Another important aspect to managing and extending aging aircraft service life is the development of aircraft specific corrosion data base. This should include development of a corrosion documentation system obtained from aircraft invasive disassembly and analysis. In addition 'corrosion lesson learned' should be an important parameter in studies related to aircraft life extension analysis.

VI. Summary

In summary, the Air Force research and development community is directly involved in understanding and developing new approaches to detect and control hidden corrosion. Early identification of the deleterious effects and cost of corrosion, and the extreme difficulty of detection before significant materials loss occurs led to a variety of developmental efforts. The current logistics and research and development approaches being pursued by the Air Force will have to be enhanced if significant inroads can be hoped for in reducing the overall extremely high cost of corrosion to the Air Force. The plan presented here is a starting point for further action in this important area.

VII. References

1. Annual cost of direct corrosion maintenance on united states air force(USAF) weapon systems and equipment, Study funded by WR-ALC Corrosion Program Office.
2. V. S. Agarwala, " Electrochemical Concepts for BMI Degradation", Proceedings 1992 Tri-Service Conference, May 1992, Plymouth, MA.
3. Log Need 79003, Detection of Corrosion in Hidden/ Inaccessible Regions Wright Patterson Air Force Base, OH

4. Air Force Tiger Team activities 7 june 1990 and September 1990. Originator: USAFE/LG OPR:AFLC/XR OCR:AFSC/XTH
5. Don Neiser, C/KC-135 Disassembly and Hidden Corrosion Detection System, Minutes of the 'Nondestructive Inspection Technique to find hidden corrosion' working group, Mar 92, AF wide NDI conference, San Antonio, Tx.
6. FY 92 Advanced NDE technology program, WL/MLLP, WPAFB, OH
7. The AFWAL/ML workshop on nondestructive evaluation of aircraft corrosion: Requirements and opportunities for research and development, Proceedings, 24-25 May 1983, Dayton, OH.
8. R. Summitt, "Corrosion maintenance and experimental design", AFWAL-TR-86-4074, 1987
9. R. E. Beissner and A. S. Birring, "Nondestructive Evaluation methods for Characterization of Corrosion- State of the art Review", NTIAC-88-1, 1988
10. Page 12, Reference 7 op cit

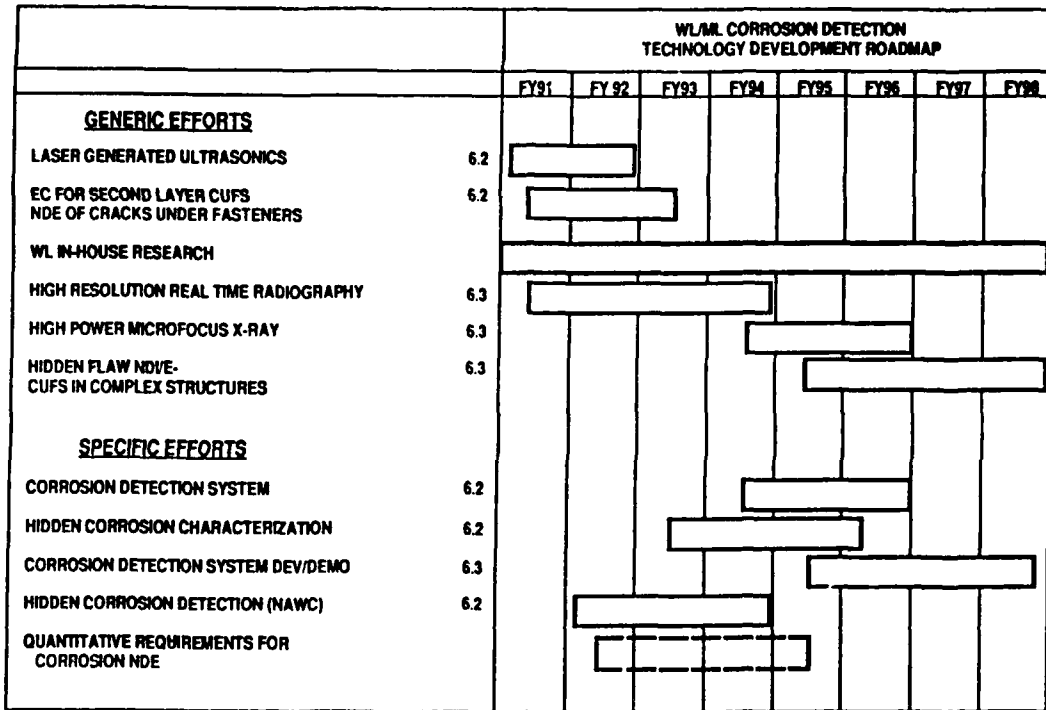


Figure 1. Corrosion Detection Technology

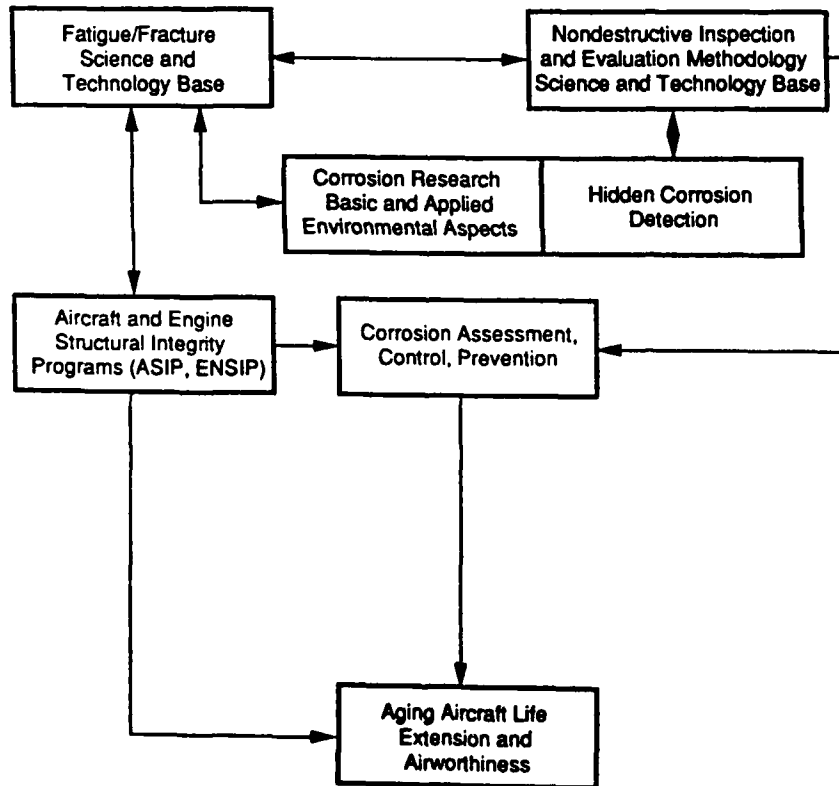


Figure 2. Corrosion Detection, Control, Prevention Model

The Corrosion Prevention & Control Program of the German Air Force for the PA 200 TORNADO aircraft

Jochen Fuhr
1st Lieutenant, Dipl.-Ing.
Luftwaffenwerft 13
Landshuter Straße 70
8058 Erding
Germany

Abstract

In 1991 the German Air Force (GAF) Corrosion Control Group was founded. This urgent step was taken due to the appearance of serious damage caused by corrosion. The Corrosion Control Group's task is to liaise between civilian companies and the military on corrosion related matters and therefore to discover corrosion prevention measures and further more. Through the issue of the Corrosion Prevention & Control Program - TORNADO (CPCP-T) in 1993 the first task the setting up of corrosion protective measures was done. The way to find these corrosion measures and the most important corrosion-protective measures are in this paper.

1. Introduction, History

During the year 1985 the GAF had the first corrosion on the TORNADO aircraft. At this time it was less of a problem and handled like an single case. So nobody really took any notice of this up and coming major problem.

In 1989 the GAF had the first really critical case. A whole wing had to be removed, because it couldn't run the air worthiness requirements without a comprehensive repair. It was decided to exchange the wing for a completely new one to have as short a ground time as possible at the maintenance facility.

Although some months later the damaged wing could be repaired by a Repair Scheme, it was a comprehensive deterioration of the situation. It was the **first time** a Repair Scheme was used, which contained the measure of **applying a patch** on the lower skin panel trailing edge of the wing box to meet the structural requirements again.

After this event the Luftwaffenwerft 13, the depot maintenance centre for the TORNADO aircraft (a/c), was ordered to think about possible solutions.

2. Organisational structure

The creation of a framework for a working group was the first step. After some initial meetings and long negotiations the project could be started, for which the concept was created for. Headquarters agreed with this plans and so the framework and working program was issued with all the different tasks for Corrosion Control on the TORNADO aircraft.

The order to start with this program came in July 1991.

2.1. Framework of Corrosion Control TORNADO

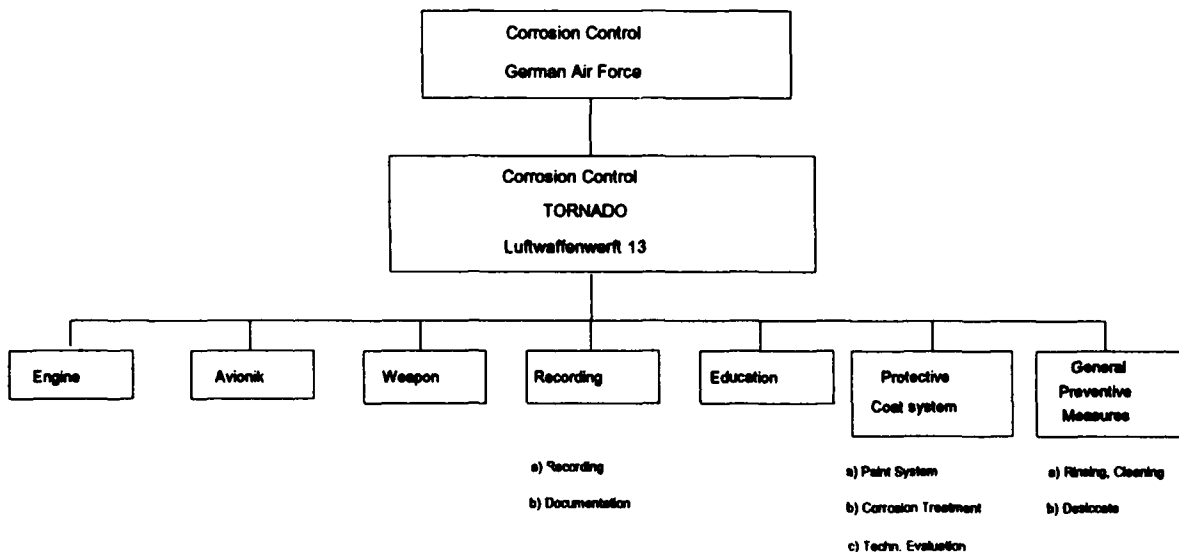


Figure 1. Structure

The framework of the working group (Figure 1) was chosen in such a way that the TORNADO a/c was split into logical sections. This is to prevent work being carried out by one group being duplicated by another.

After the first three working groups engines, avionics and weapons were set up, it was discovered that there were specific problems of corrosion protection that the three existing groups could not deal with. These specific corrosion problems, Recording, Education, Protective Coat System and General preventive Measures are treated in the following four working groups.

The major problem is the frame of the aircraft.

3. Major Problems; significant Corrosion items

3.1. Paint system

A general problem regarding the Corrosion Prevention is the protective effectiveness of the paint system. After some years the ageing process makes the paint stiff and inflexible. That, together with the stress the structure is exposed to, leads to little cracks in the paint covering all over the aircraft. However the **biggest deterioration is focused around the fasteners** supported by the production process which used no sealants between different metals.

Due to the world-wide knowledge, a paint systems like on our aircraft under the environmental conditions the TORNADO a/c performs, **protects for some 4 to 6 years**. After this time the paint system should be changed. Only with this procedure is ongoing protection guaranteed.

Based on this awareness the GAF planed to exchange the paint system on all TORNADO aircrafts by a procedure called "Dry-Stripping" in the future.

However the time between exchange is not been determined yet.

3.2. Wing

The major corrosion problem for the TORNADO a/c is the corrosion on the lower skin panel of the wing. The corrosion in this area has progressed so that several Repair Schemes were designed to meet the strength requirements of the wing again.

The corrosion in this area is mainly caused by the ageing paint systems and the declining protective effectiveness. This ageing process leads to cracks around nearly all fastener. These fasteners are not placed with a sealant to prevent direct contact between the different materials of the rivets and the panel. These cracks are starting points for the corrosion process.

At Present the problem is solved with a modification, which seems to be successful.

With this modification and with help of the Dry-Stripping-Process the coating system can be removed. The next step is to eradicate any corrosion found and to repaint the wing.

3.3. Fuel cell cavities

A further problem is the corrosion in the fuel cell cavities. Depending on the vent system you need, if you use flexible rubber tanks, together with changing temperature from below 0°C up to nearly 100°C, there is always some kind of humidity in the tank compartments. This leads to the known corrosion problems.

To tackle this problem a Modification was issued. However, further inspections to evaluate the effectiveness of this modification show, that the application of the used sealing compound PR 1422 wasn't as successful as it should be.

The proposal is based on the technique of desiccating the fuel cell compartment. This will be managed by exchanging the Rohacell 31 inlays, which are used at present, with a supplementary structure.

The Rohacell 31 inlays are foam materials, which absorb liquids and so strengthens corrosion on the surface.

The exchange gives the possibility to bring dried air between the rubber tank itself and the aircrafts structure and so to decrease the humidity too less than 50% relative humidity.

3.4. Other problems

Beside this, there are other known corrosion problems.

For example:

Air intake

Airbag compartment

But none of these problems is that important to require special programs to combat the corrosion.

4. Program and solutions

4.1. Corrosion Prevention & Control Program, CPCP-T

The aim of the Corrosion Control on the TORNADO a/c is not to prevent all corrosion perfect. The task is to prevent and control the corrosion damage in such a way that the a/c will fulfil the requirements of the next 40 years without expensive repairs.

For the choice of the corrosion prevention measures two criteria's were considered:

- first the assessment of possible measures under cost & profit

This means that towards the end of the a/c life corrosion damage is expected to increase, if this is nearly as long as it stays within the permissible level of damage.

- second the use of environmentally friendly and long lasting solutions

The problem is that we have to spend money today to prevent more serious corrosion problems in the future.

An overview of the development of corrosion damage with and without corrosion protection measures clarified on 'Figure 2'.

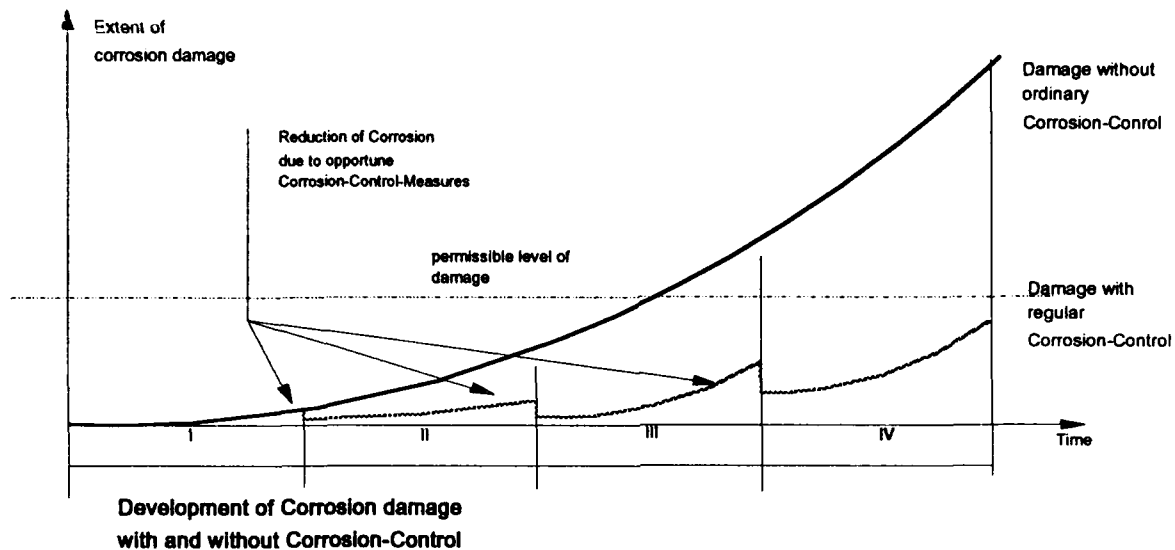


Figure 2. Development of Corrosion Damage

Figure 2 shows the running of corrosion damage with and without protection measures within fictitious inspection periods. It is important to note that the target for corrosion protection is different at the end of a/c life from the beginning.

It would be impossible to expect the same levels of corrosion on an in use a/c than those of a new a/c and therefore as long as the corrosion stays below the permissible level of damage the corrosion level is acceptable.

The development of the costs are shown in 'Figure 3'. The cost of repair using Corrosion Control compared to no control is more expensive, however by the IV period the costs of Repair without Corrosion Control is far greater than that with regular Corrosion Control.

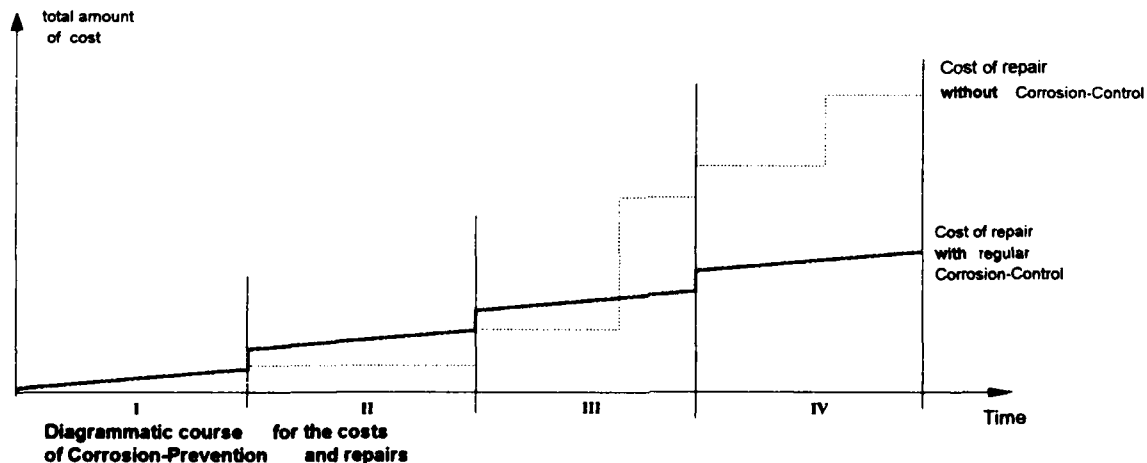


Figure 3. Development of Costs

The schematic on 'Figure 4' shows how the introduction of newer measures have been integrated into the protection and regular maintenance procedures. The abbreviation CCR in the computer symbol on the right side stands for the Corrosion Control Register. The main part of the CCR is a personal-computer-software for saving and evaluation of corrosion defects (Chapter 4.3.).

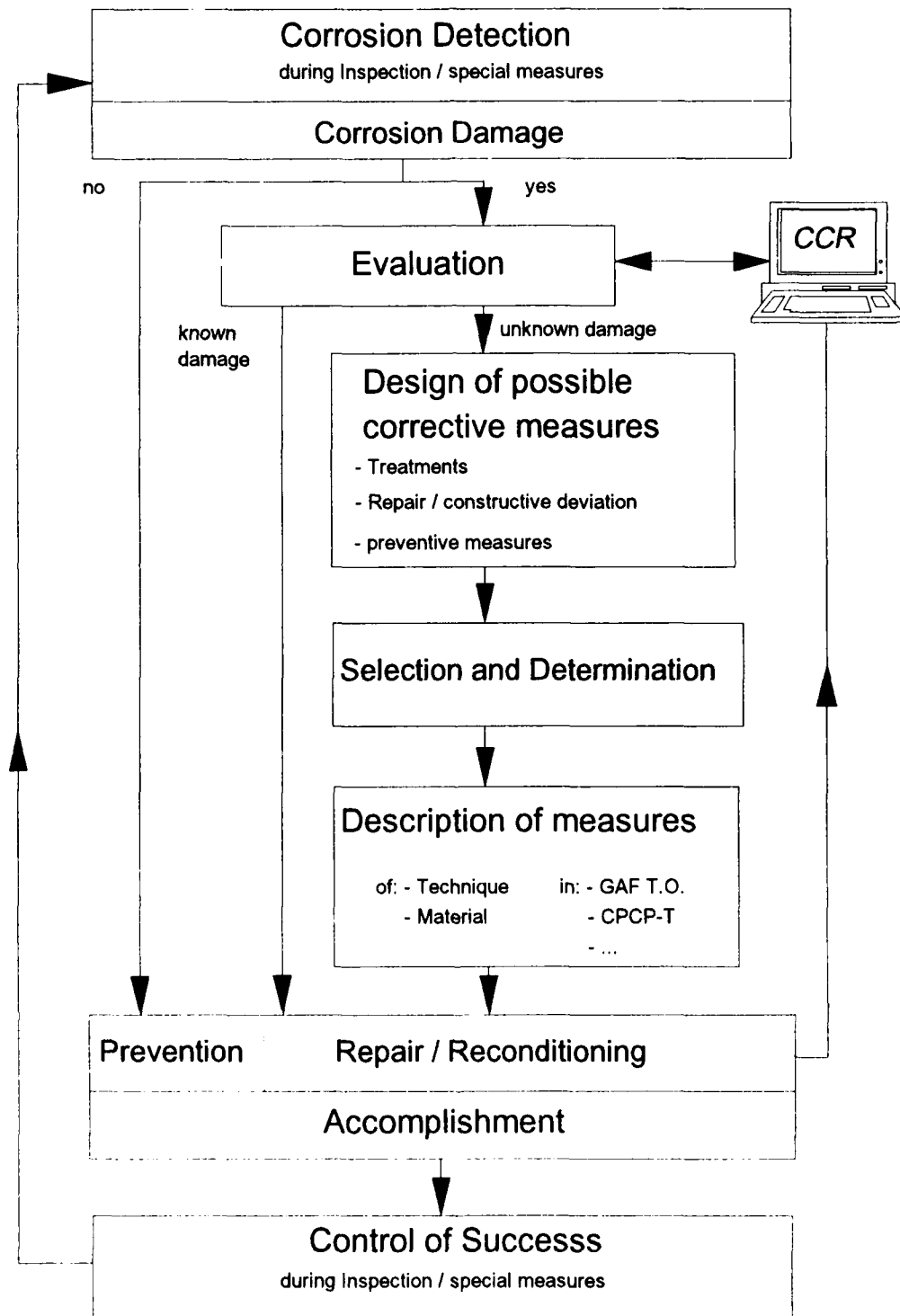


Figure 4, CPCP-T

4.2 Corrosion prevention measures

The corrosion protection measures used for the TORNADO a/c are divided into two groups:

- > Measures included in a minor services (maintenance carried out on the flying station)
- > Measures included in a major servicing (Deep maintenance carried out either at the Maintenance Depot or by civilian industry)

Within the frame of minor service the following corrosion protection methods are carried out:

- Rinsing
Rinsing the a/c with fresh water without mechanical help, to remove the salt concentration from upper surfaces;
- Desiccate
Partial drying of critical areas with dried air when standing in the Shelter;
- Preservation
Preserving with wax- respectively oilbased substances **only** in areas where no renewing of the paint system is possible;
- Cleaning
Regular cleaning of the a/c with specialist cleaning substances and mechanical aid;
- Minor maintenance of corrosion damage
Within the frame of major service the following corrosion protection methods are carried out:
 - periodical renewing of the paint system
Removal of the old paint system through Dry-Stripping and replace by a new up-to-date paint system;
 - Major/Depot maintenance of corrosion damage

4.3. Corrosion Control Register - TORNADO, CCR-T

One of the main parts of the CPCP-T is the Corrosion Control Register-TORNADO

The aims of the CCR-T are:

- > Detection of corrosion damage
- > Recognition of main-corrosion-items
- > Introduction of effective (preventive) measures
- > Checking the success of correctional measures

The schematic on 'Figure 5' shows the regular procedure of the CCR-T.

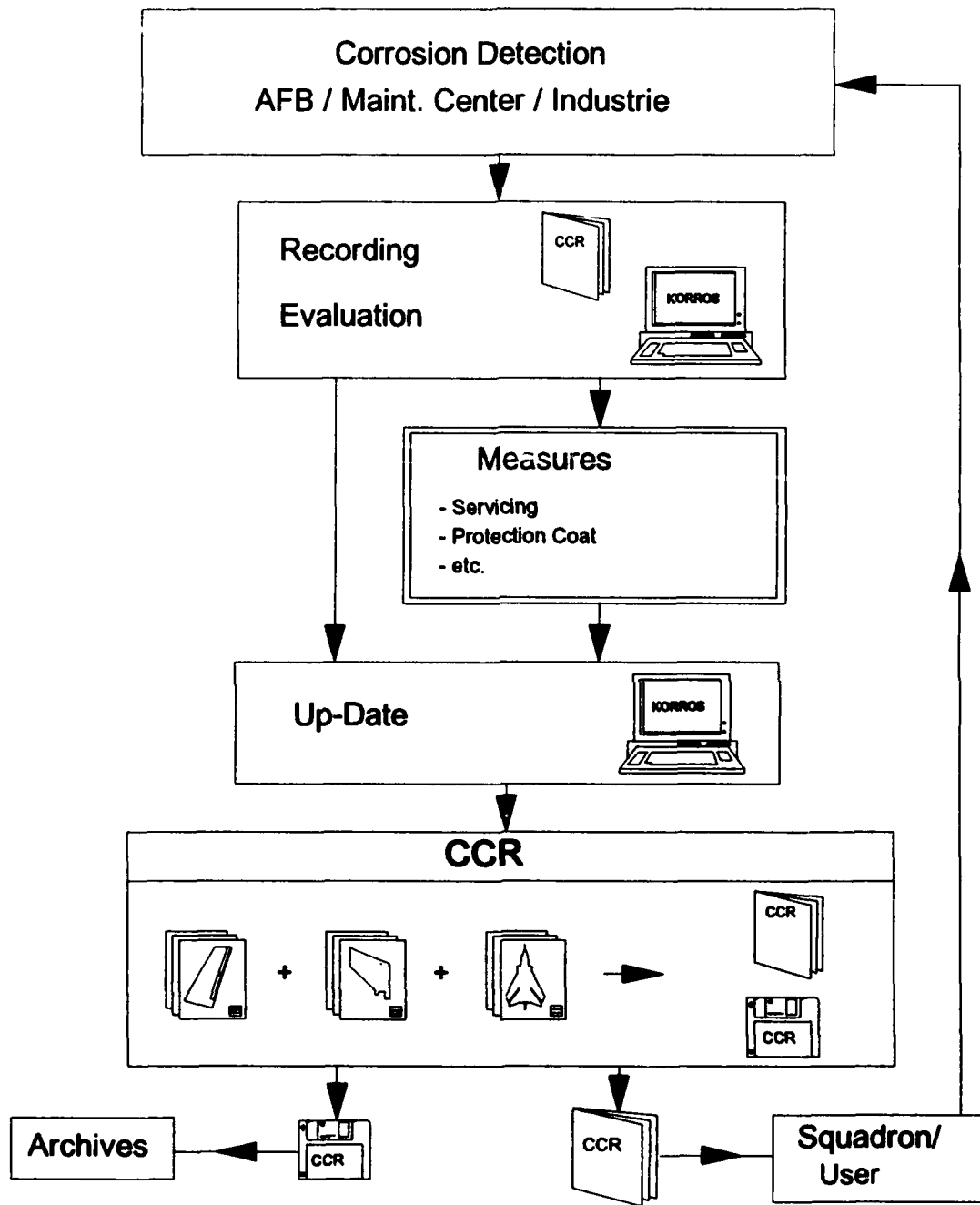


Figure 5, CCR-T

The most important part of the CCR-T is the program KORROS. This program gives the possibility to save and to evaluate all corrosion defects of the whole fleet in a lot of different ways. Another advantage is that all records of all a/c are at one place. This gives at the one hand the chance of an overlook about all corrosion defects of the whole fleet and on the other hand the specific look at one small problem area.

4.3.1. Dry-Stripping TORNADO

Another main component of the CPCP-T is the process of removing the coating system through Dry-Stripping.

The Dry-Stripping was developed by the Deutsche Aerospace AG (DASA) previously Messerschmitt Bölkow Blohm (MBB) and has been used in the GAF since 1986.

Dry-Stripping is the only practical paint stripping process that is not dangerous to the environment. As a result of the process only dry waste is produced and this although the a/c is stripped to the bare metal.

The principle of Dry-Stripping is, that the paint system is stripped by plastic-granules being blasted at an specified angle of attack under high pressure and speed, which is similar to Plastic-Media-Blasting (PMB).

The differences between PMB and Dry-Stripping are the ability to alter the strength of flow parameters depending on the thickness and kind of material. The changes parameters are spray-pressure, media flow, the angle of attack and the distance of the nozzle to the upper surfaces. Through this process sensitive a/c upper surfaces can be stripped

Before using the Dry-Stripping process on the TORNADO a/c the material- and masking plan must be adhered.

In the material plan the upper surfaces materials and thicknesses of the a/c are given. This information is used to produce the blasting parameters.

The masking plan is necessary in order to define the protected areas and the plan help to ensure, that the granules do not penetrate into the body of the a/c.

Reasons for the introduction of Dry-Stripping as a paint removing process:

- > Removal of the aged paint system from the surfaces
- > Inspection possibilities of the bare material surfaces
- > Meeting the requirements of environmental protection, health and safety in the work place and economic pressures

After the Stripping of approximately 100 a/c by DASA and more than 1000 a/c in the USA, by using the plastic media stripping method, it can be confirmed that using that method cost-savings up to 50% are possible.

The disposal-cost only of removing the paint system by chemical methods is approximately DM 15.000,- per a/c. Although Dry-Stripping takes the same length of time it only costs DM 150,-.

Based on the results by the GAF, decision was made to strip all their a/c only using the Dry-Stripping process in the future.

5. Conclusion

The CPCP-T consists of a package of measures, which further the aims to keep corrosion level to an acceptable condition.

Also in the future there will be corrosion damage, that the corrosion process cannot be stopped but only hindered. All things be checked to ensure, the damage will not escalate. Through the frame of the program and consequent control, all corrosion damage is not as grave a problem in the area of the lower skin panel of the wing as in other areas.

To conclude, the issue of the CPCP-TORNADO is a important exercise in the frame work of material maintenance.

If a corrosion protection program had been introduced at the beginning of the TORNADO a/c working life's instead of introducing when it the corrosion problem occurred, we would have saved a lot of money.

On the introduction of a new weapon-system our experiences with corrosion protection should be taken into a consideration.

**Corrosion Control as a necessary treatment
following the requirements of aircraft and environment safety**

Eberhard Dürig
Surface Treatment
Deutsche Aerospace AG
Military Aircraft
Rechliner Straße
85077 Manching

Abstract

Corrosion as an unavoidable fact requires cost effective control measures. By these control measures aircraft life will be much higher in comparison all the precaution done during the manufacturing of a/c. The main philosophy gained by the experiences of maintaining more than 5000 a/c is determined by: detection and removal of corrosion and the followed renewal of the protective coating in the very early stages of corrosion. It has to be repeated in determined intervalls, based on the lessons learned over the years. A steady development of new coating systems: the elimination of toxic/hazardous, chemicals; slower aging of the organic protective coatings; the problem of how to get the higher chemical and mechanical resistant coatings removed; and the goal to collect all divergant properties under cost effective measuring are the guidelines for new developments in the maintenance area regarding human and environmental protection.

Introduction

DASA-Manching, formerly MBB-Manching, has maintained more than 5000 a/c in the past. Most of them military a/c with a planned service time of up to 40 years. Therefore structural condition is one of the most essential requirements for their airworthiness. Depending on such an extremely long service time the protective treatments of a new a/c have to be controlled constantly. This includes the surface inspections in order to assess corrosion condition and coating aging. The increase of environmental influences requires non interrupted detection regarding the material and structural properties. Observing the surface of protected areas does not reveal problems beneath the protective layers. Based on that fact, a corrosion control concept is required.

I. Corrosion Control Concept

- Non Destructive inspections
- Visual inspections on bare metal substrates
- Corrosion removal
- Renewing the protective layers completely

Fig. 1 Shows the difference amongst the corrosion growth the normal corrosion progress, and the essential corrosion velocity caused by a consequently carried out corrosion control treatment program. Normal corrosion, untreated, will progress by an exponential term up to that damage level where structural part's, class 1, airworthiness can not be guaranteed.

Dividing the progress time into determined intervals, at which a corrosion control treatment has to be performed, the new corrosion progress time starts after corrosion removal from a much lower level. The structural condition remains in a essential better condition. Comparing the amount of corrosion damage, on the term, the difference between the treated and non treated vector locations are obvious.

Fig. 2 Essential for effective corrosion control treatment is the detectability of small corrosion spots as a just starting corrosion. Prone to corrosion are areas of production failures where poor or no adhesion occurs. Organic coatings are not closed for gas diffusion. Water in the gas phase may diffuse the coating system and condensation in the adhesion poor area is possible. Together with CO and other environmental chemicals, an electrolyte may be created. Corrosion is programmed.

Under a topcoat, primer cracks are not detectable. Such cracks are equal to poor adhesion areas. System cracks are visible, but a repair by overspraying only closes the upper surface and will leave a cave where no adhesion occurs. In such cases, the whole coating system must be renewed

The general aging of organic coatings systems causes a steadily growing embrittlement of the paint. Especially in areas where high movement/vibration works on fasteners and lapjoints cracks become visible around fasteners and at edges. These are main areas prone to corrosion. Another doubtless fact is that corrosion, which blister through the whole coating system, evolves to a damage level, where a repair is necessary in most cases.

Fig. 3 Shows a primer crack.

Fig. 4 Shows a coating system crack.

Fig. 5 Shows typical corrosion around the fasteners and metal edges.

Fig. 6 Shows corrosion which was detected much too late.
A panel 8 mm thick is corroded through its entirety.

Fig. 7 Shows the interior surface of a Tornado air intake before stripping. The corroded areas are marked.

Fig. 8 Shows much more corrosion than were found before stripping
(There is no additional comment necessary.)

II. Coating Systems

In order to reduce corrosion progress protective coatings of different types are used. Today's general coating systems are based on a chemical pretreatment followed by a 2 component primer with active corrosion protective pigments and a 2 component topcoat. Required features are: mechanical and chemical corrosion resistance, and additionally there is a long list of other essential properties. The aging component is close to the environmental conditions and is nearly not predictable. No laboratory investigations are able to forecast the change of features depending on the situation which cannot be simulated completely.

Fig. 9 Shows the rear bottom side of a F4 a/c with loose rivets. The dust from the dry stripping makes all the leaking oil visible. The picture may explain the importance of a high elasticity and, on the other hand, the reason why so many cracks occur around fasteners.

Fig. 10 Shows a riveted lap joint where the rivet is wet assembled but without corrosion protection between the panels. Residues of Alodine without complete chemical reaction create corrosion in this case.

If during overhaul renewing of the complete coating system is required, we prefer a wash primer application.

This philosophy includes all components which may have gaps and overlappings.

Certain chemical liquids with capillary flowing action/power pose problems to certain parts in that they tend to get into inaccessible areas where there is no way of removal.

Another decision was made to use chromostopherous primer. Depending on the cancerogenety of those pigments, if inhaled, they have been eliminated and substituted by chromate free primers. Interior surfaces are already coated with primers containing chromate, because most of those areas are inaccessible and a renewing of the aged coatings is impossible over the whole service life.

III. Paint Removal

1. By Chemical (Wet) Strippers

Human and environmental problems using phenols and formicacid strippers have caused the elimination of these toxic materials. By the introduction of the Dry Stripping process, the chemical stripping activities at Manching plant dropped down to less than 2 %. The new generation of chemical strippers needs higher temperatures of more than 40 °C. Therefore these higher temperature problems have to be solved.

2. By Dry Stripping (Plastic Media Blasting)

After thorough investigation and testing program which covered the influence of the fatigue to the surface condition after 10 times stripping under worst conditions we have designed a process package.

This was done by joint development. The responsibility was shared by an aerospace specific party and to a machine specific party. **DASA-Military Aircraft Group & Schlick-Roto-Jet** blasting machine manufacturer still works together especially to adapt the process to wide body a/c. Main steps of the development have been:

- The electronically controlled blasting machines.
- The measuring method for the quality assurance.
- The calibration possibility of the blasting parameters.
- The recovery system.
- The media cleaning.
- Dust collection.
- Local evacuation for media and dust.

Using those parameter combinations like

- media type
- nozzle diameter
- pressure
- media flow
- angle of attack and distance

will meet determined saturation points for the compression stress.

This means a non restricted repetition of paint removal independent to the dwelltime.

Fig. 11 Shows the correlation between the different hardness of media and substrat regarding to the created compression stress.

Fig. 12 Was part of the laboratory-tests regarding alluminum alloy 2034 T3 with specified pressure and media flow.

All that assumes the availability of precisely controlled blasting equipment. Another assumption is the knowledge of the substrate material and its thickness.

Fig. 13 Shows a substrat plan, where these details are color marked. Beside the process and equipment, a/c sealing will be as important as the paint removal avoided. Cleaning later will be very costly. By using hot glue, special masking tape and special covers, that problem was solved.

Fig. 14 Shows part of sealed a/c fuselage. Hot glue frames can be removed easily, because adhesion of the hot glue to a metal surface is good enough for blasting protection but not as strong as on other material surfaces. The Dry-Stripping facility was based on the trial results of 30 a/c stripped with test equipment. Prerequisites for the new facility were.

Fig. 15 - Hangar size 25 x 25 x 8 m

Fig. 16 - Hangar view exterior

Fig. 17 - Hangar view interior

Fig. 18 - Hangar ventilation with air exchange of 25 times p.h.

Fig. 19 - local evacuation with exhausting performance

Fig. 20 - floor recovery system vact duct (SCHLICK)

Fig. 21 - cyclon as pre dust selectors

- ° media cleaning and separating system
- ° dust filters meeting the requirements environmental
- ° 4 electronically controlled pressure blasting machines
- ° media hopper and refillstation
- ° dust collection system

The hangar size allows a/c up to a size of A 10 a/c and comparable. Depending on economic and convenience of the operator the lay-out for a basic ventilation system was determined .

In order to keep media flowing in the recovery circuit on air flow of 20 m/sec. had to be installed. Volume and pressure of the air was adapted to the drag of the local evacuation devices.

The goal of that installation was to get 80 - 90 % of the blasting media directly picked up at the local blasting area. Together with the floor recovery system, 100 % collection of media will be performed.

The floor recovery system works like vacuum cleaner having arms which move in a floor channel. The working area is controllable between two chosen points in order to avoid cleaning, in areas where no blasting operations are done.

Media and paint dust pass cyclons filters and the cleaning system where very high separation is attained.

Cleaning blown out air is done by fine dust filters. Media and paint dust separated and collected in plastic bags, with given to a special waste deposite. A comparison of the disposal cost shows:

DM 150,-- for dust deposit of 1 a/c dry stripped

DM 15.000,-- for deposit of the waste water of 1 a/c chemically stripped.

In the future the increase of chemical disposal costs will have grown to an uneconomical level. The chromate dust, as part of the primer, is cancerogne if inhaled, not if touched. Health requirements predicts:

- a) the general elimination of any cancerogene materials
- b) If it is impossible to reduce the concentration to a dust level of 0.025 mg/m³, personal protection is required.
- c) "b" will be allowed only as long as no alternative with lower danger exists.

The concentration level of point "a" is lower than required at Manching Plant.

We have stripped more than 100 c/c without problem. Oldtimer-autos and an oldtimer a/c (JU 52) have been stripped successfully too.

IV. Corrosion Treatment

After stripping and corrosion detection, corrosion removal is carried out. The detection is done visually and by marking the corrosion spots. Small corrosion will be removed by glass bead blasting, in other cases sanding, milling and small nozzle blasting with aluminium oxide. A chemical corrosion treatment will create further corrosion, therefore this method is not allowed for the GAF:

V. Intermediate Coating

After paint removal some bare metal areas such as fasteners etc. are prone to corrosion during the overhaul time of the a/c. Therefore as a temporary measure we protect such areas with acrylic laquer in aerosol spray form, which can be removed before paint renewing by acetone, thinner or degreasing solvent.

Protecting the bare surface can be avoided if a/c are not placed outdoors and will be painted before next flight.

VI. Final Coating

With the development of new high-resistant coatings and specific top coats, other problems such as filiform corrosion was born. If on military a/c no Skydrol hydraulic fluid is used and resistance against chemical warfare agents is not required. Acrylic topcoats will have many advantages. The corrosion resistance is better in combination with a 2 component EP-primer.

Removal and repairability during service on airfields are easier to do.

VII. Final Thoughts

The problem we have in the general are that introduced systems are without any doubt and an exchange to other (better) systems are nearly impossible. Now and again we should put some question marks on our basic knowledge.

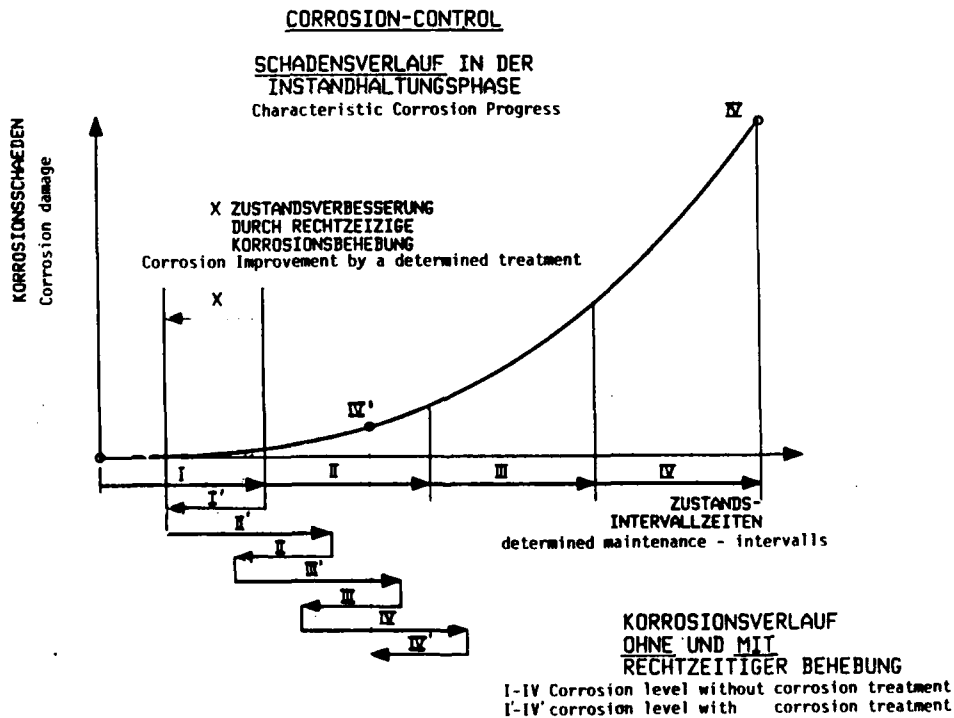


Figure 1

Corrosion detectability.

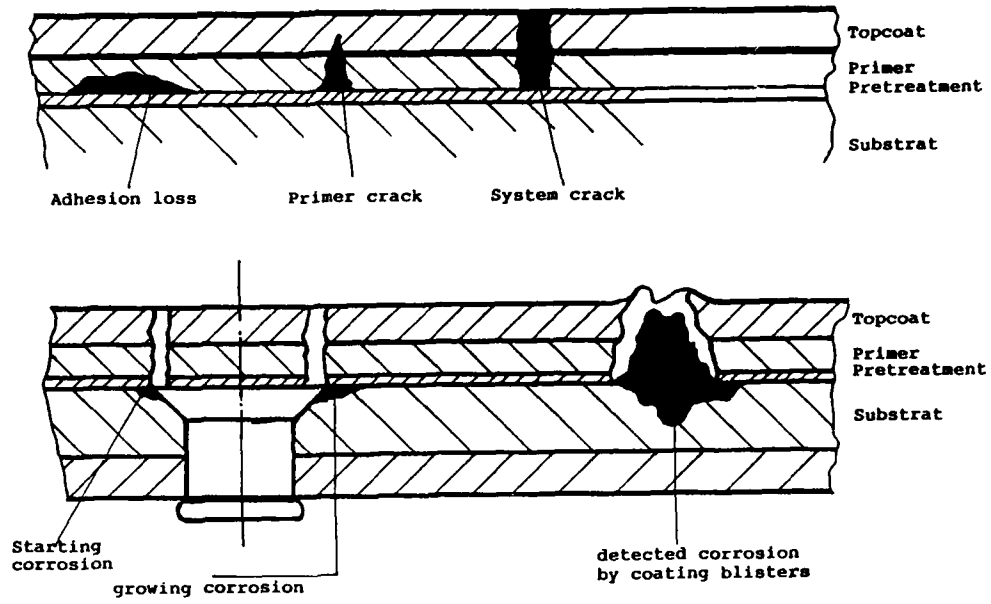


Figure 2

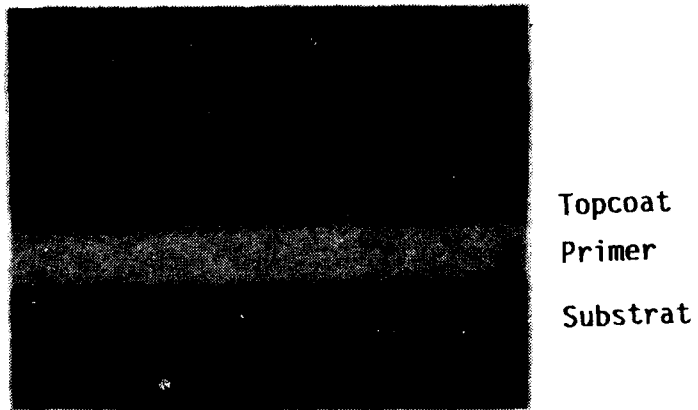


Figure 3 PRIMER - CRACKS

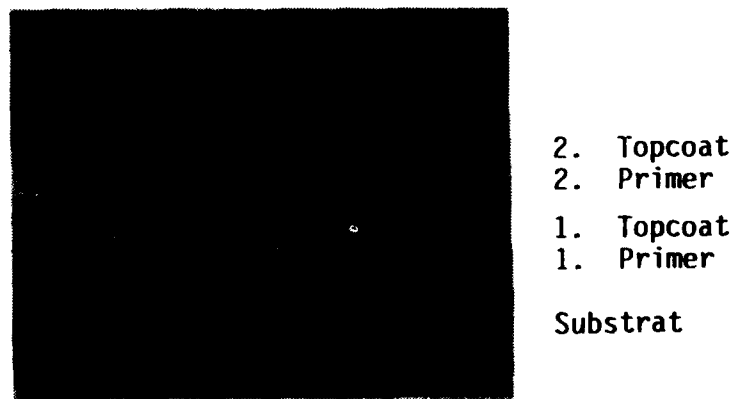


Figure 4 COATING - SYSTEM - CRACK



Figure 5

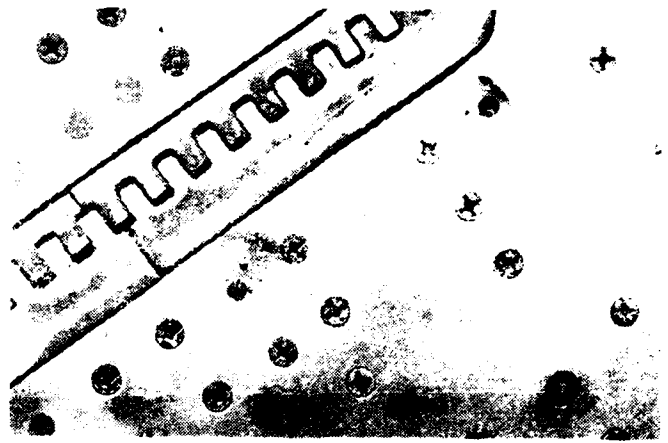


Figure 6

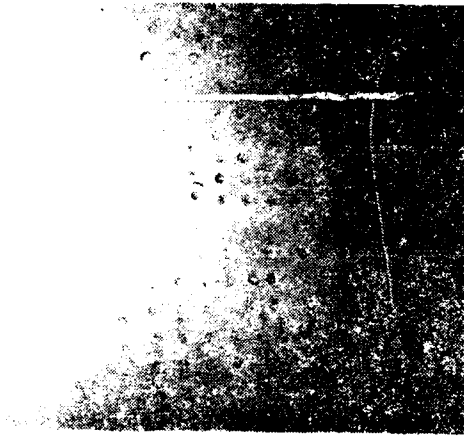


Figure 7

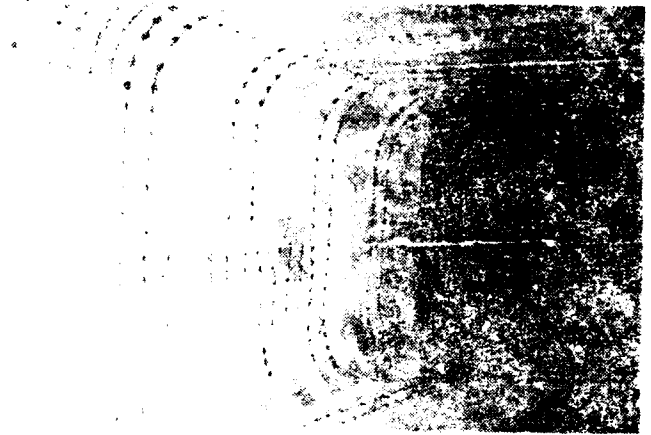


Figure 8



Figure 9

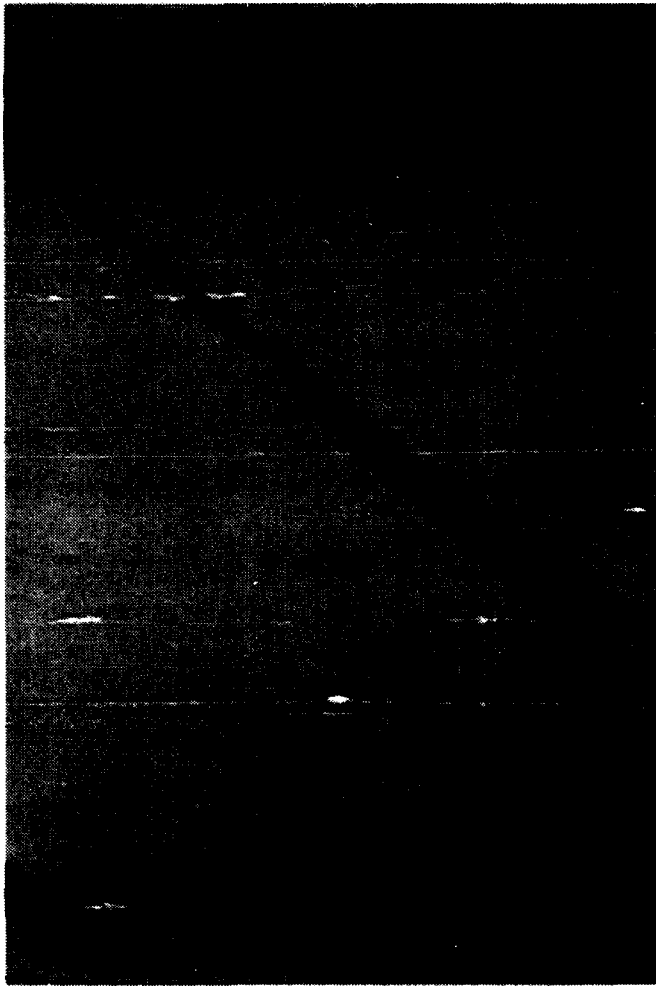


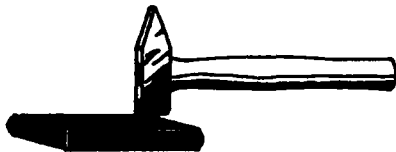
Figure 10

Compressive stress

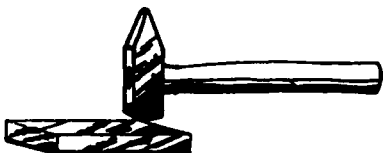
Correlation of the hardness between
blasting media and substrat material



Soft media to hard substrat



Hard media to soft substrat



Hard media to hard substrat

Figure 11

Dry Stripping Strahlversuche auf 2024 T3
 Druckvergleichsdiagramm
 Strahlmittel: Poly Plus
 Strahlmittelfluß: 30%

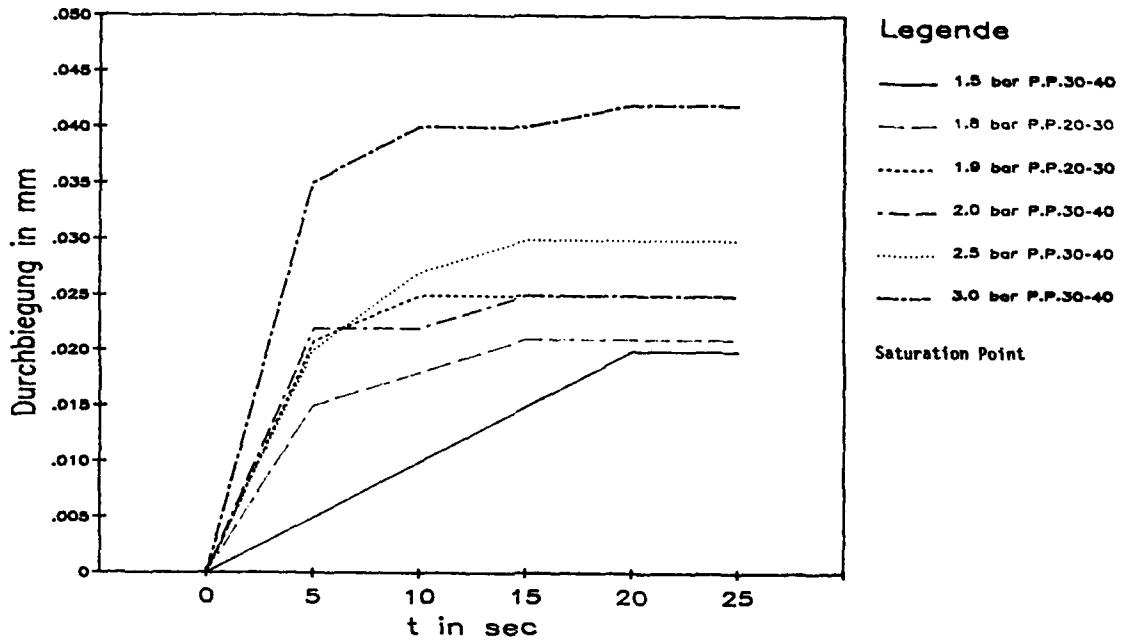


Figure 12

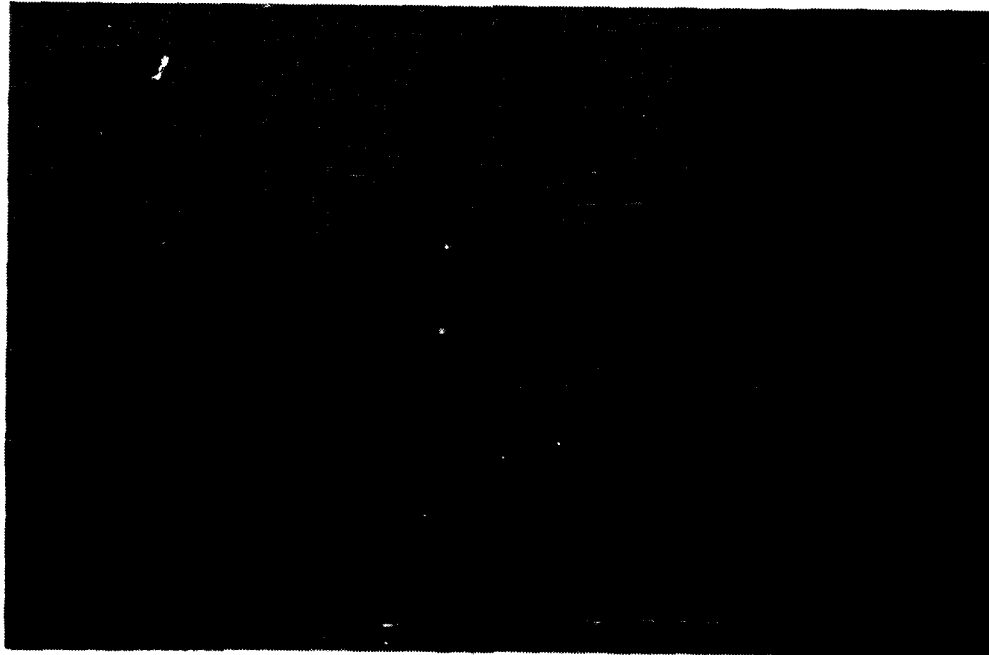


Figure 13

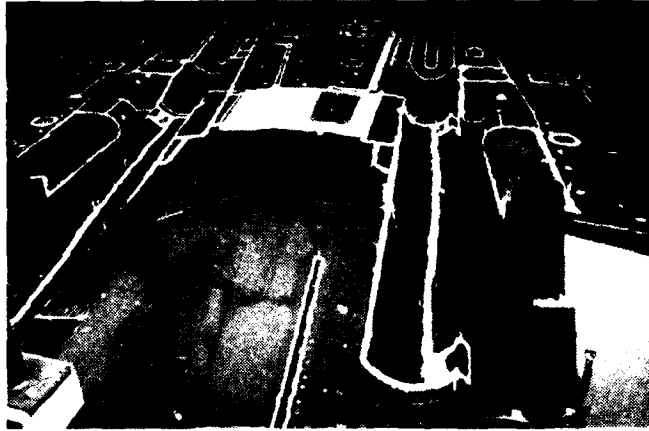


Figure 14

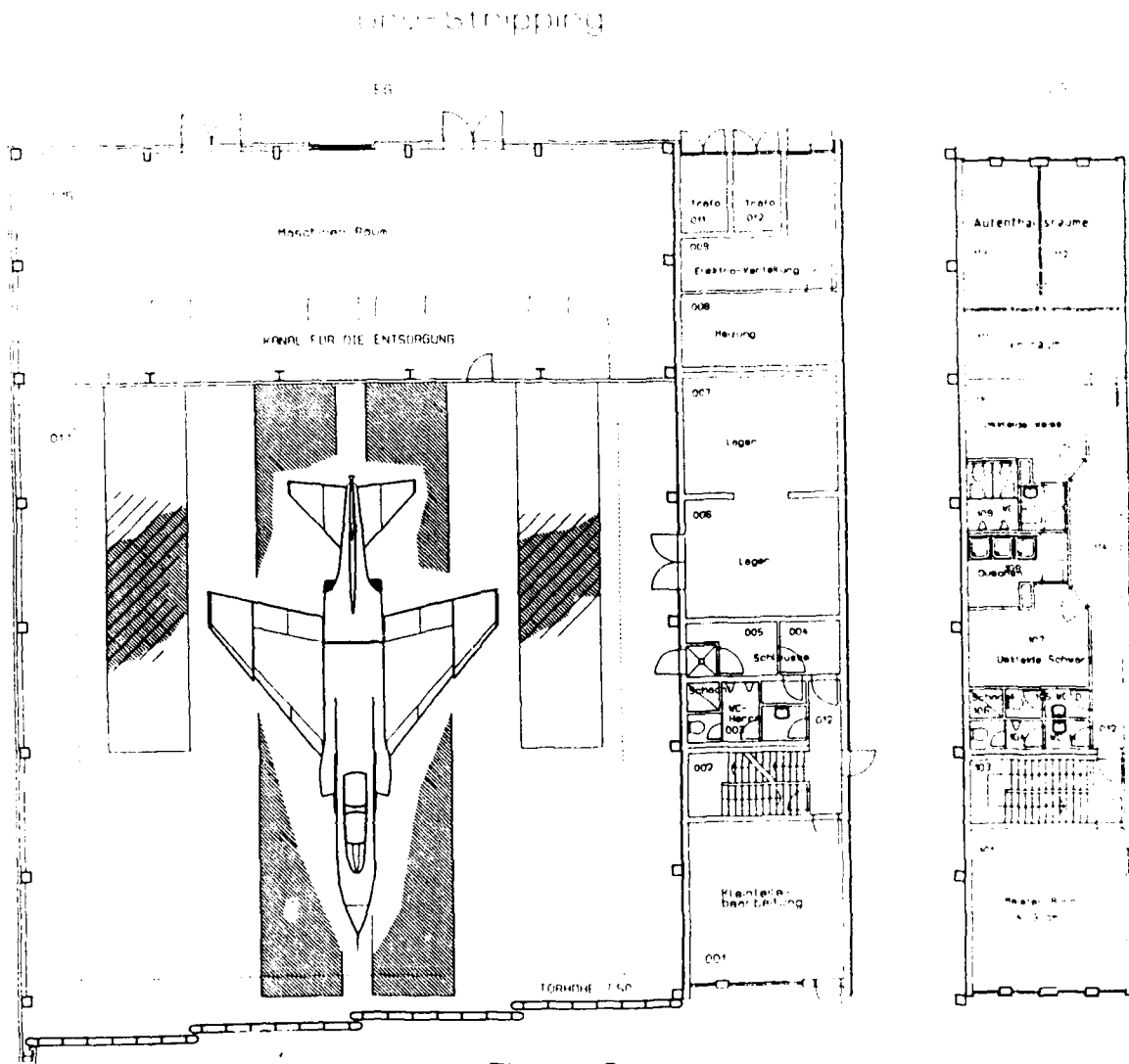


Figure 15

Flugzeug - Entlackung

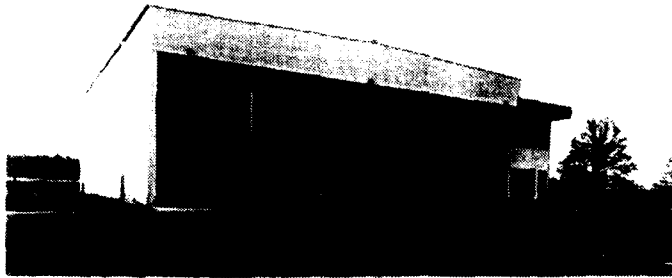


Figure 16

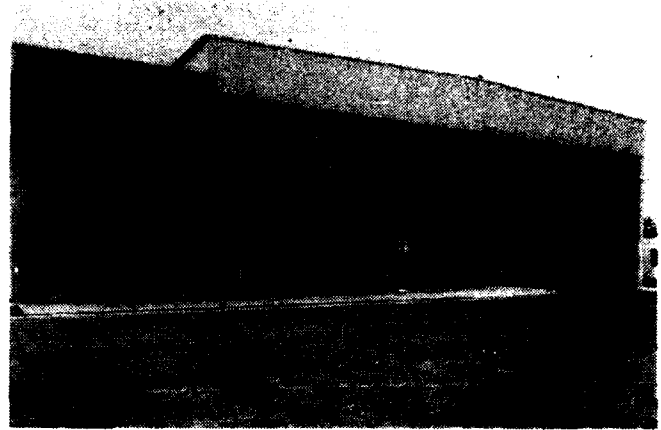
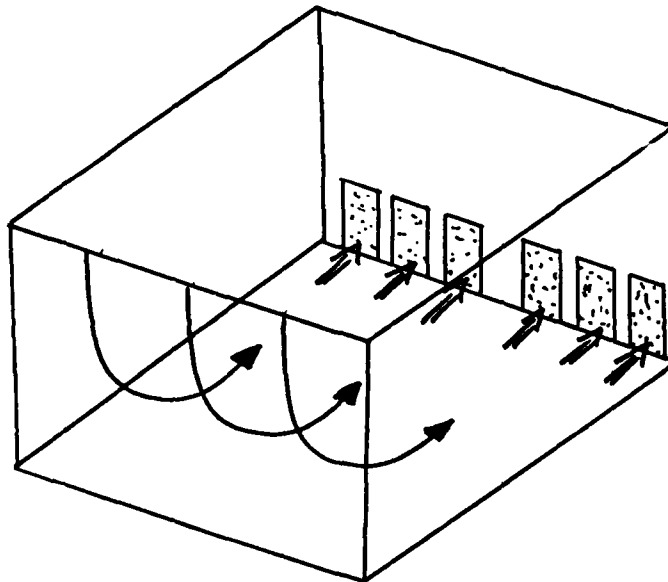


Figure 17

DRY - STRIPPING

AIR FLOW 160 000 m³ h



VOLUME

$$V_H = 25 \times 25 \times 8 = 5000 \text{ m}^3$$

TOTAL AIR FLOW

$$160\ 000 + 40\ 000 = 200\ 000 \text{ m}^3 \text{ h}$$

HANGAR LOCAL EVACUATION

$$V = \frac{V_L}{A} = \frac{200\ 000}{25 \times 8 \times 3600} = 0.28 \text{ ms}$$

AIR EXCHANGE / h

$$\frac{V_{\text{AIR}}}{V_{\text{HANG}}} = \frac{200\ 000}{5\ 000} = \text{times/h}$$

Figure 18

DRY - STRIPPING

LOCAL EVACUATION m³/h

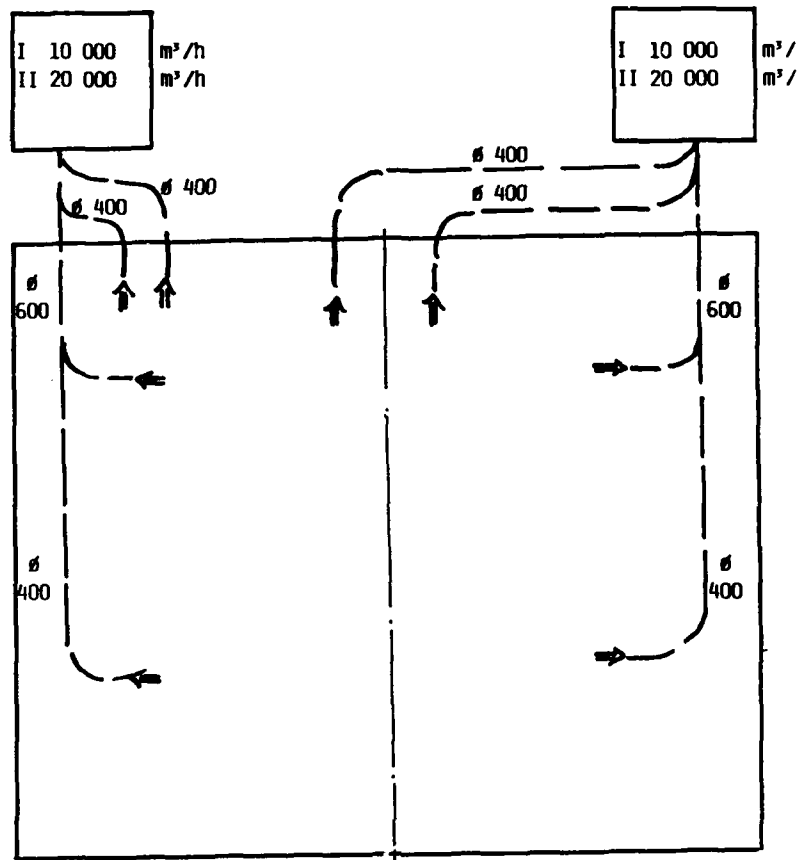
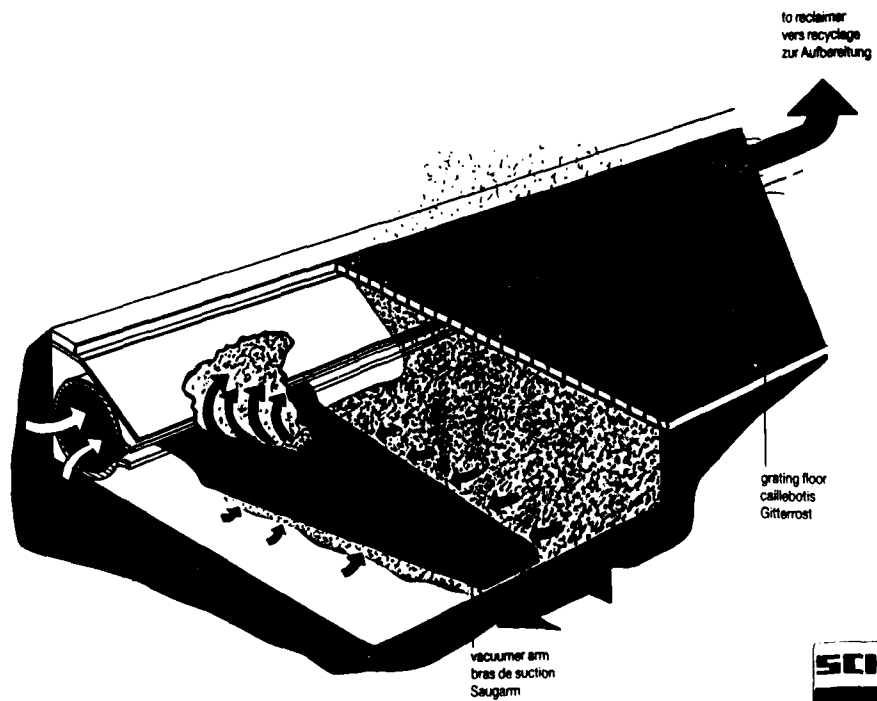


Figure 19



Detail drawing of the media recovery floor type VACUUCT
 Croquis détaillé du système de récupération de média type VACUUCT
 Detailzeichnung des Aufbereitungsystems VACUUCT



Figure 20

DRY - STRIPPING - SYSTEM

LOCAL EVACUATION

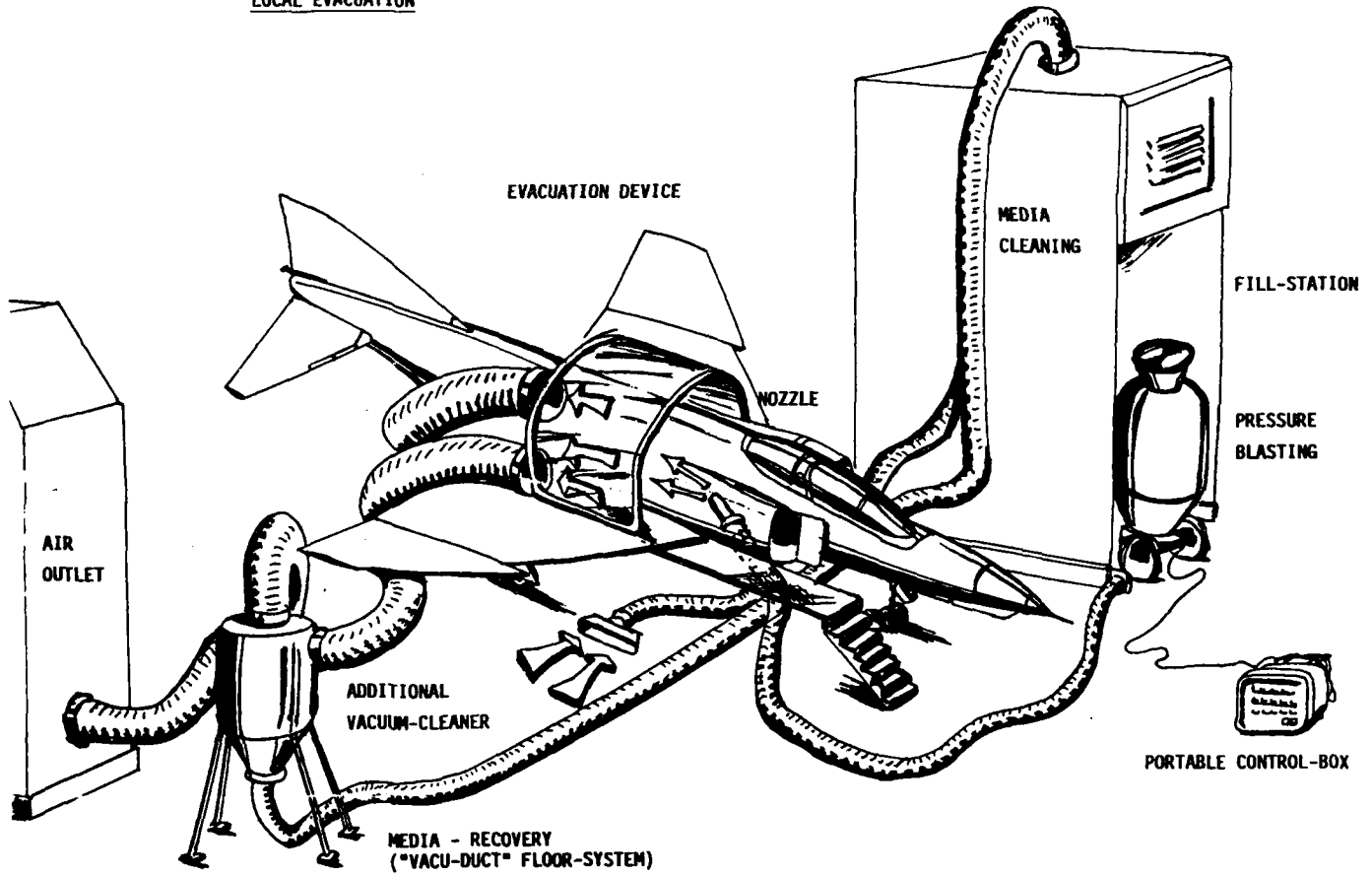


Figure 21

National Association of Corrosion Engineers NACE
12th International Corrosion Congress, September 19-24, 1993
Houston, Texas

**A New Eddy Current Inspection System for Quantitative Corrosion Depth
Measurement on A/C Wing Skins**

E. Grauvogl
Deutsche Aerospace AG (DASA)
8072 Manching Germany

F. Regler
Deutsche Aerospace AG (DASA)
8072 Manching Germany

Dr. H.-M. Thomas
BAM-Berlin
Unter den Eichen 87
1000 Berlin 45 Germany

Abstract

A NDI test system for determination of the depth of attack of open corrosion damage in the form of cavity corrosion and pitting is presented. This system is based on eddy current method, where the signals from a special probe are correlated with a curve, which is derived in many practical tests. The test result is presented in graphical form ("C-Scan") which can then be quantitatively evaluated on a PC monitor.

This test system was used in field for quantitative determination of corrosion at the underside of the wing surface of German TORNADO aircraft. Based on the test results of more than 100 aircraft a rank order for removal of the corrosion was developed.

Key terms: NDI, eddy current, open corrosion

1. Introduction

In non-destructive inspection (NDI) by eddy current methods, the test results obtained depends not only on the general testing conditions resulting from the particular situation, but also to a great extent on the measurement probe used. In the inspection of aircraft components, the achievement of reliable test results is particularly problematical in the area of riveted or bolted connections due to the large number of variables influencing the testing process. As these joints are a favorite starting point for corrosion attack, quantitative description of any damage as early as possible is of great interests. For this application, a computer aided testing system, which permits visual display of the corrosion damage with high image quality on the basis of the measured eddy current signals has been developed. In conjunction with an eddy current probe specifically developed for imaging purposes, this system facilitates quantification of the corrosion depth. The theoretical principles and the special measuring probe were developed at BAM, Berlin. At DASA in Manching, the hardware required for this specific application was developed, the overall system adapted and optimized, and the system used on a large number of aircraft of type TORNADO owned by the German Luftwaffe and German Marineflieger. Test system software, adapted for this specific problem, was compiled by the engineering company EMA Elektronik in Berlin.

2. Description of the testing system

A schematic diagram of the testing configuration can be found in Figure 1. The testing system consists of a standard commercial eddy current tester whose vector component outputs are connected to an analogue/digital converter in a personal computer. The signals are digitized with a resolution of 12 bits. Display and evaluation of the measurements takes place on the PC monitor screen. During the measurement process, the PC controls the two axis slide table used to guide the measurement probe. Acquisition of the measured values is triggered by the separate stepping motor controller, thus facilitating reliable assignment of the measured values to specific locations. The simplicity of the structure makes the testing system universally usable. For the same reason, any component in the system can for example easily be replaced by a different make. Control of the measurement and representation program is extremely clearly structured due to the menu guidance system to SAA standard which has been implemented. Preparation of the slide unit for measurement is effected with the cursor keys and mouse, and is facilitated by the graphical representation of the probe position and measurement voltage. The scanning surface and distance between measuring points are freely selectable within the bounds of the scanning range and computer memory. During the measurement process itself, an image of the measured value is generated in the form of a projected three-dimensional function topography. This means that the results of time consuming measurements can be assessed directly and the measuring process prematurely discontinued if necessary. Single and two channel measurements can be carried out. With two channel measurements, the vector quantity can be represented. On completion of measurement, the data recorded are stored to hard disk. Numerous configurations are possible for the graphical representation. For example, a 3-D diagram can be observed at any angle of rotation or inclination. All the axes are scaleable. Amplitude related colours increase clarity and the facilities for interpretation. With topographical representation, the line to line distance and the starting threshold can be influenced. Imaging by grey scales has proved the most appropriate for the evaluation of measurement data taken on a flat plane. Pseudo-colour representation

can also be used for rapid location of extreme values. The relevant depth indications are derived from the amplitude values by means of a calibration curve.

3. Probe configuration

The test results are decisively influenced by the selection of the eddy current probe used. On this topic, intensive studies were carried out at BAM [1], finally leading to the development of a special test probe optimized for imaging purposes [2,3,4]. For assessment of the suitability of a testing probe, the directional characteristic is determined at a point defect. Conventional absolute probes exhibit a drop in sensitivity at the centre of their detection area, which has adverse effects on the further signal processing. The probe type developed at BAM avoids this disadvantage, as can be seen from the comparison in figure 2. The "blind spot" leads to false results, in particular in the problem of corrosion depth determination. The use of both probe types on a corrosion cavity in the vicinity of a titanium bolted joint is shown in Figure 3. The corrosion depth curve is inaccurately represented by the conventional probe (left). The probe without blind spot (right) produces a truer image with much greater detail. Thus, for example, the corrosion directly at the edge of the bolt head can be better recognized. The differences in imaging characteristics become particularly clear when the results are compared with the photograph of the area tested in Figure 4.

4. Application on aircraft

The application of the testing system on a TORNADO aircraft is shown in Figure 5. The probe manipulator is fastened to the underside of the wing surface. A detailed view is shown in Figure 6. The maximum scanning area is $110 \times 90 \text{ mm}^2$. The minimum track to track distance is 0.02 mm. The maximum possible scanning speed depends first and foremost on the computer used. With a 386 PC, a speed of approx. 20 mm/s can currently be achieved. The schematic structure of the area to be tested is shown in Figure 7. A wing has a length of approx. 3.5 m. There are 174 titanium fasteners in this length. These fasteners are used to join the skin and rear spar together. The nominal sheet thickness in the area of these bolted joints is 4.1 mm. The depth range to be covered by the probe configuration is derived from this figure. On the basis of the probe design developed at BAM, several scanning probes were subsequently developed at DASA. The aim was to achieve as great a depth penetration as possible with simultaneously high lateral resolution capability. The calculated relationship between probe distance and measurement voltage for one of the probes manufactured is illustrated in Figure 8. As a result of the saturation behaviour, accurate results have to remain limited to a depth equivalent to half the sheet thickness. This is justifiable in that greater damage depths would in any case necessitate repair work. The directional characteristic at a point defect is shown in Figure 9. The detection area in this case is approx. $0.8 \times 1.2 \text{ mm}^2$. Imaging results of good quality are achieved here. With a greater detection area, of course, the depth range available for assessment could also be increased, but the poorer lateral resolution would then result in an underassessment of small area defects. As a representative example, the evaluation of a testing area with corrosion removal is shown in Figure 10. The test area represented $25 \times 25 \text{ mm}^2$. The track to track distance for these measurements was set to the standard value of 0.5 mm due to time constraints. As a result, the image appears to have a somewhat coarse grid. The amplitudes of the vector component which the tester supplies are also shown. The geometry of the fastener can be clearly seen. Adjacent to this, at the top left,

there is a corrosion cavity. A calibration curve is required for an indication of the depth (cf. Figure 8). This is determined on a perfect sheet, for example by inserting film strips of known thickness. The thickness of any paint coating must also be taken into account. For example, on recording of the calibration curve on an uncoated test specimen, a film of 0.24 mm thickness was used as a substitute for the wing coating. In this case, shown in Figure 8, the curve can be described by a logarithmic model. The coefficients A and μ thus determined are used by the computer to calculate the depth from the amplitudes. For evaluation, the tester first has to set a reference point on the monitor, representing the zero-point. Among other things, this can be used to improve the zero-point compensation somewhat. The locations in the image then selected with the mouse pointer are supplied with the corresponding depth values by the computer. The mouse pointer is assigned in this operation to a quadratic aperture within which an average is calculated from the measured values. The size of this aperture can be adapted to meet the requirements of reliable measured value determination. Rapid and precise location of the maximum value is facilitated by the use of pseudocolour values (e.g. red). In the case illustrated in Figure 10, the maximum corrosion depth of 0.58 mm was located approx. 2 mm away from the edge of the fastener.

For verification of the test results, the corroded areas on five TORNADO aircraft were machined out. Figure 11 shows a series of fasteners after removal of the corrosion by grinding [5]. The maximum depths of the machined out cavities was then determined by means of a dial gauge. The results of testing were then compiled in the graphic in Figure 12. This reveals the following: the overwhelming number of corrosion points found had a corrosion depth of less than 0.4 mm. The depths found were fundamentally confirmed by the mechanical measurements. The deviations are difficult to interpret in individual cases. It must be pointed out that mechanical measurement is also not without its problems, because the relationship to an uncorroded surface has to be established in each case. It is fundamentally to be expected that eddy current testing tends towards relatively lower depth indications, because grinding was carried out until no further corrosion was visible. As the sheet thickness was reduced by approx. 0.1 mm during every careful grinding operation, the cavity then certainly became somewhat deeper than necessary. If deeper values were obtained by eddy current testing, the reason is probably to be found in probe lift off. This can be caused in particular by a swelling up of corrosion products. Such lift off signals cannot at present adequately be distinguished from the useful signals proper.

5. In field inspection

This test system was used in field for quantitative determination of corrosion at the underside of the wing surface of German TORNADO aircraft. For this inspection, coating was not removed. In performance of the test, the depth values calculated in the analysis program are assigned to the relevant fastener numbers (Figure 13) and entered into measurement charts (Figure 14). Based on the test results of more than 100 aircraft a rank order of the aircraft for removal of the corrosion was developed. Parameters for the rank order of the aircraft were the numbers of corrosion, depth and diameter of the corrosion, and strength calculation. The aircraft with the most severe corrosion are to repaired first. Of course, aircraft based in the near of the Northern Sea were affected more severe than aircraft based in the inner country. In the most cases the corrosion starts at the interface fastener - skin due to contact corrosion between Al-skin and Titanium fastener and this corrosion is than visible as bulged paint.

In some cases where the corrosion product caused a large heightening of some tenth of a millimeter these areas had to be flattened before the EC-inspection. The signal discrimination wasn't enough to decide between the corrosion caused signal part and the lift-off caused signal part.

The evaluation of 10 aircraft which had been treated in the mean time gave a good conformity between the EC measured corrosion depth and the mechanically measured depth of material removal.

A new project will use a multifrequency EC-technique and signal inverse filtering technique for an improved discrimination of the corrosion depth-signal and the "noise" signal.

6. Conclusions

With the test system described, the problem of quantitative determination of the attack depth of open corrosion damage by eddy current processes has been successfully solved in principle and implemented in practice. An expansion to cover related testing situations appears appropriate. Over and above this, the approach also contains a general potential for other testing jobs, such as concealed corrosion. Improvements in the following areas are to be aimed at for the application described above: the depth detection of the probes should be improved. To increase the imaging properties, and in particular their independence of direction, the directional characteristic should be as punctiform as possible, but at least small and circular. Probe modelling procedures could be of assistance in achieving this aim. The testing accuracy can be further improved if the disruptive influences such as lift off effect, edge effect and fastener signal can be successfully reduced. Apart from optimization of the testing parameters, image processing could certainly also make a good contribution to this.

7. Literature

[1] Thomas, H-M., Weigelt, G.: Anwendung von Wirbelstromverfahren zur quantitativen Bestimmung der Tiefenausdehnung von Korrosionsschäden an Aluminiumstrukturen (Application of eddy current processes for the quantitative determination of the depth penetration of corrosion damage on aluminium structures). Concluding report on DECHEMA research project L9. 1/8, May 1991

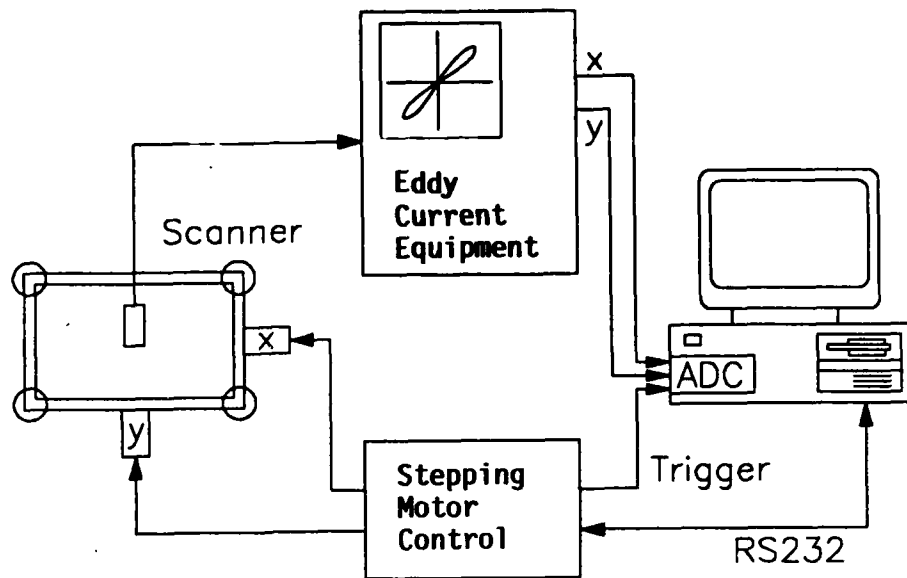
[2] Thomas, H-M., Wittig, G.: Problematik der quantitativen Bestimmung flächenhafter Korrosion mit Wirbelstrom (The problems of quantitative depth determination of surface corrosion with eddy current. DGZfP Annual Congress, 25th - 27th September 1989 in Kiel, Congress Report

[3] Thomas, H-M., Wittig, G.: Methode zur Analyse von offenen Korrosionsschäden mittels Wirbelstromverfahren (Method for analysis of open corrosion damage by means of eddy current processes). DACH Annual Congress, 6th - 8th May 1991, in Lucerne, Congress Report

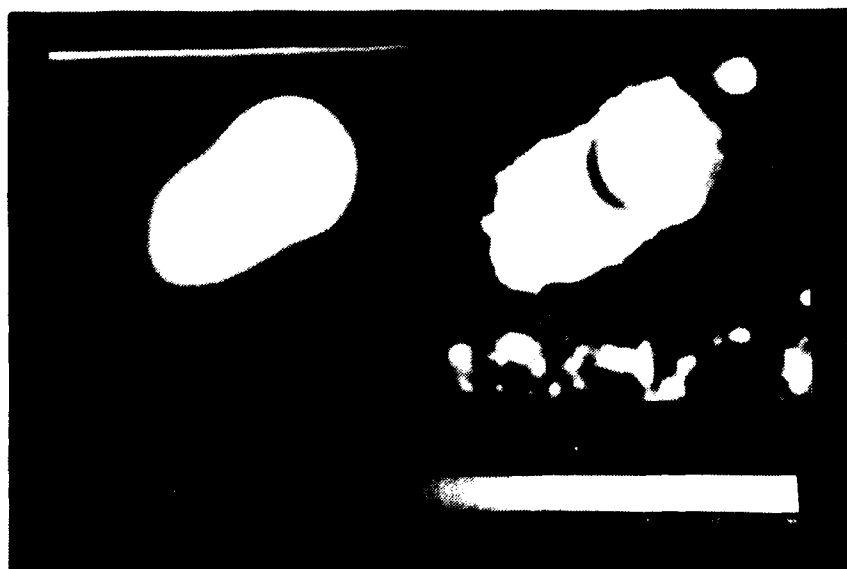
[4] Thomas, H-M.: Bildverarbeitung unterstützt Wirbelstromprüfung, Teil 1: Eine spezielle Tastsonde bewertet Oberflächenkorrosion quantitativ (Image processing assists eddy current testing, part 1: a special scanning probe quantitatively assesses surface corrosion). Materialprüfung magazine volume 5/92

[5] Grauvogl, E.: Ersterfassung Korrosion Tragflächenunterseite TORNADO (Initial detection of corrosion on the underside of Tornado wings). Test report no. 45/08/91 from DASA Manching

Figure 1:→
Block diagram of the test system used for corrosion depth determination.



← Figure 2:
Comparison of the directional characteristics of two eddy current testing probes:
Left: The standard commercial probe exhibits a loss of sensitivity at the centre.
Right: The probe developed at BAM has maximum sensitivity at the centre.



← Figure 3:
Comparison of the testing results for the eddy current scanning probes from figure 2:
Left: The conventional probe provides an inadequate description of the damage.
Right: The probe without blind spot provides a sharp image of the damage.



← Figure 4:
Photograph of the
testet area of figure
3.



Figure 5:
Application of the testing system on the
underside of the wing of a TORNADO
aircraft.

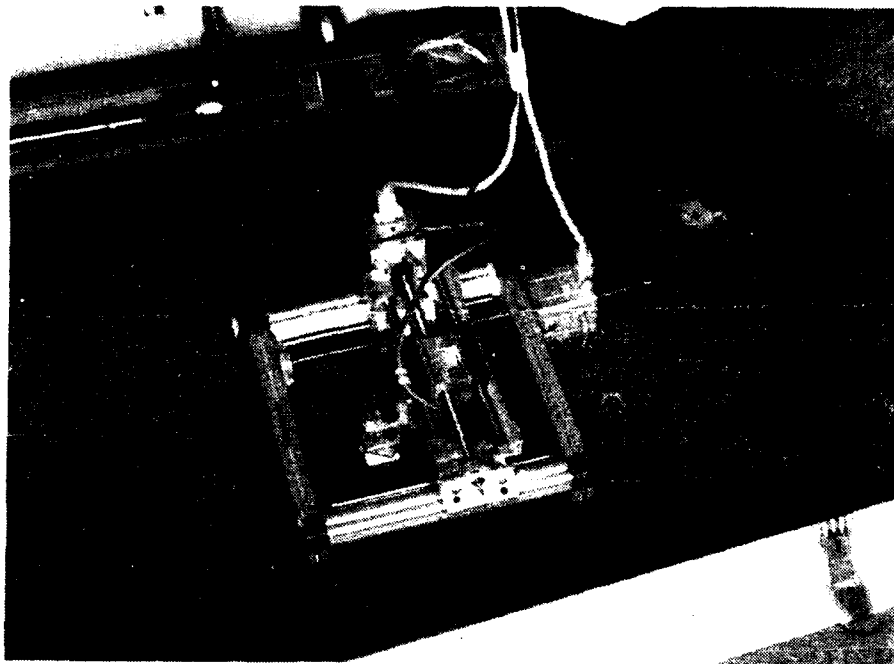


Figure 6: →
Detailed view of the
two axis probe
manipulator.

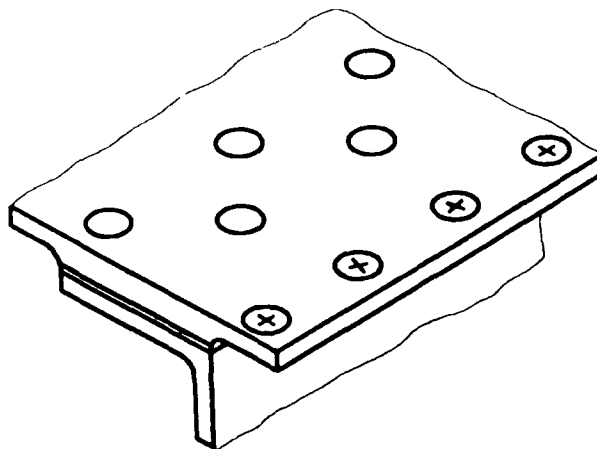
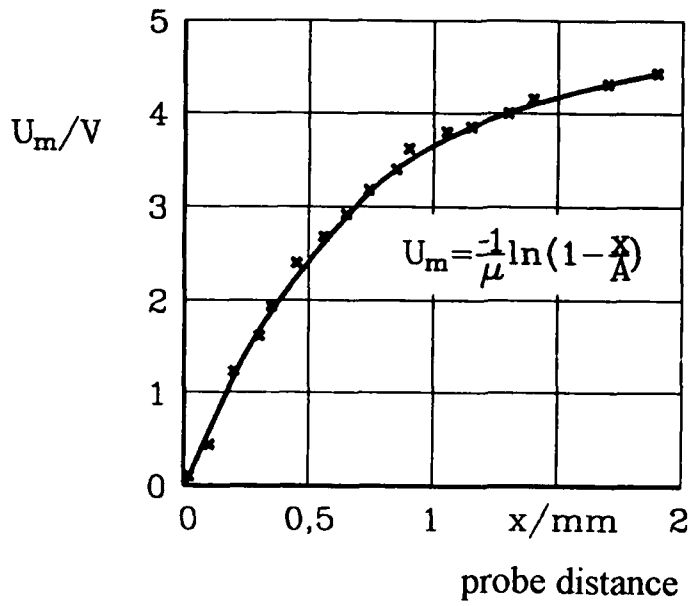
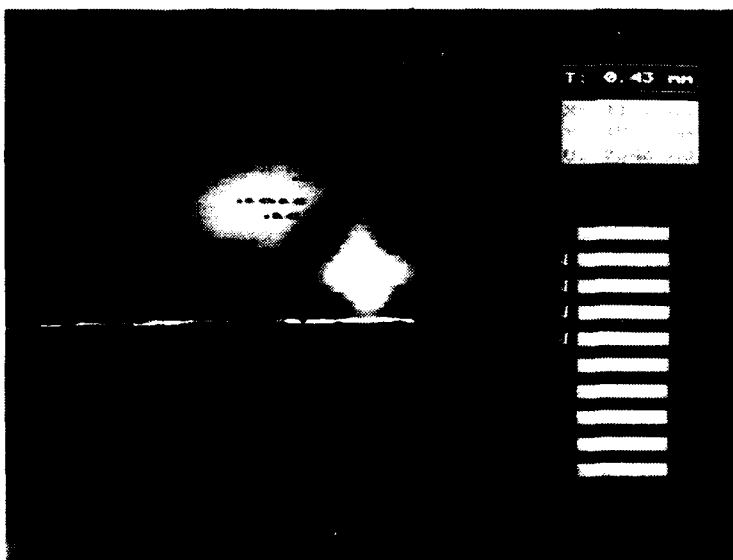
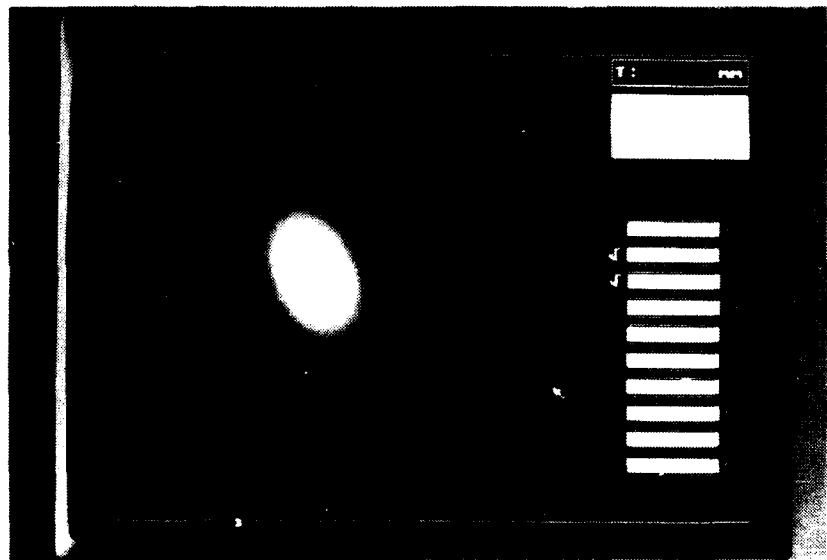


Figure 7: ↓
Schematic structure
of the wing in the
testing area.

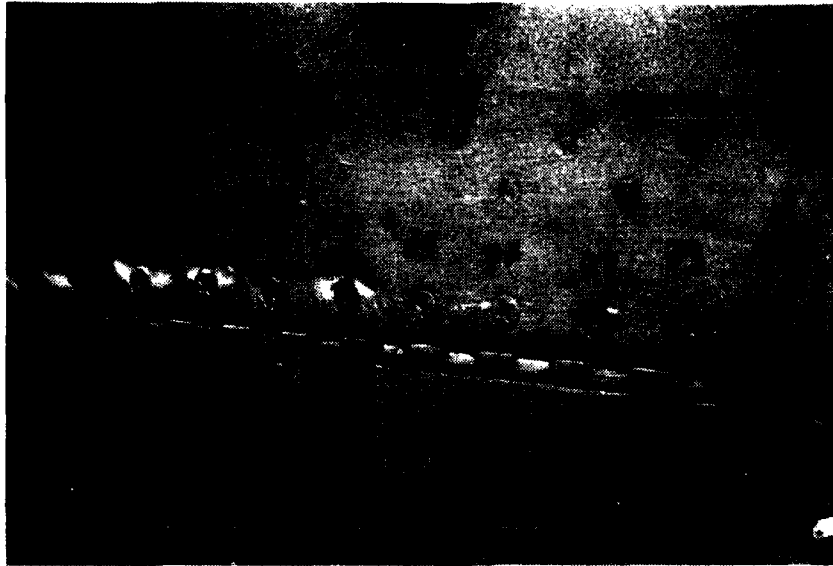


← Figure 8:
 Calibration curve for a scanning probe used for corrosion depth determination. The functional relationship can be approximately described by a logarithmic model.

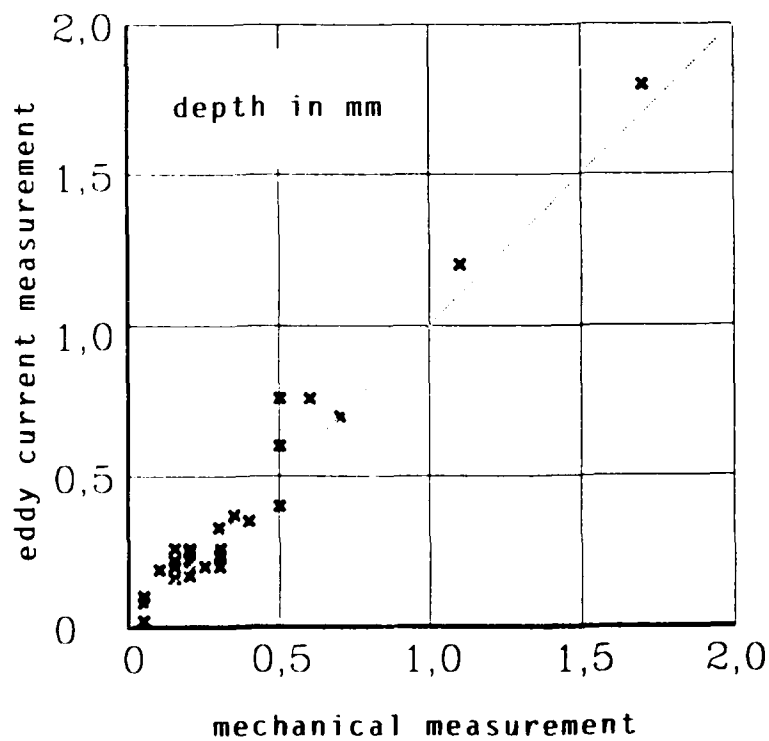
Figure 9: →
 Directional characteristic of the scanning probe used on a point defect.



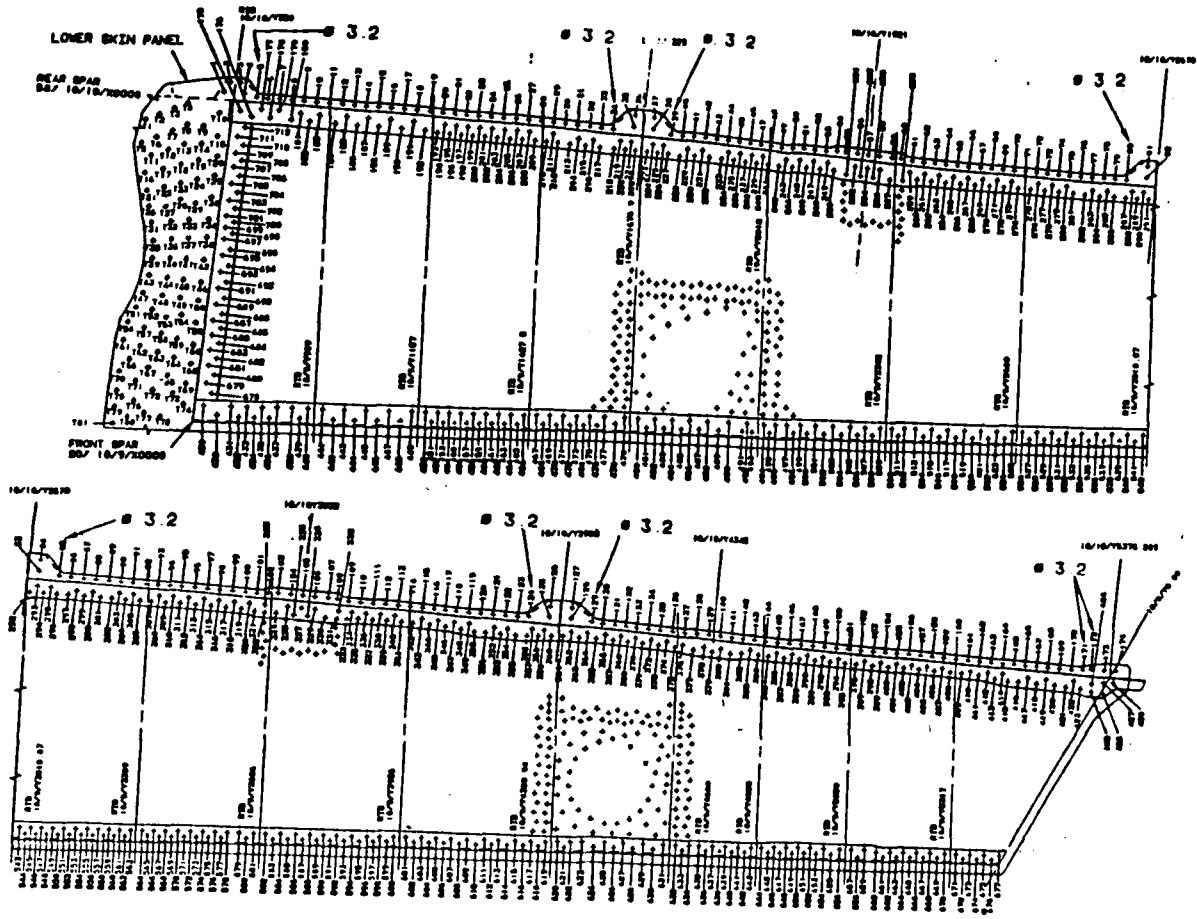
← Figure 10:
 Representative example of depth evaluation for a corrosion cavity in the vicinity of a titanium fastener.




↑ Figure 11:
View of the underside of a wing after removal of the corrosion by grinding.



← Figure 12:
Comparison of the test results from eddy current measurement and a mechanical measurement. The mechanical measurement was carried out by means of a dial gauge after grinding out of the corrosion.



↑ Figure 13:
Sketch of the underside of the TORNADO wing with all fastener numbers.

| KORROSION - DATENBLATT SONDERAKTION: TRAGFLÜGEL | | |  | | |
|----------------------------------------------------|--------------------------|-------------------|-------------------------------------------------------------------------------------|--------------|-----------------|
| POSITION | AUSGEARBEITETE KORROSION | TIEFE FLÄCHE (mm) | ERSTMALIG | WIEDERHOLUNG | NEIN BEHANDLUNG |
| | NEIN BEHANDLUNG | JA | | JA | |
| POSITION | AUSGEARBEITETE KORROSION | TIEFE FLÄCHE (mm) | ERSTMALIG | WIEDERHOLUNG | NEIN BEHANDLUNG |
| | NEIN BEHANDLUNG | JA | | JA | |

| | |
|------------|------------------|
| VERBAND | LOWER SKIN PANEL |
| ERSTELLER: | P-125516-801 LH |
| ABTEILUNG: | P-125516-802 RH |
| DATUM: | |

↑ Figure 14:
Measurement chart for the test results of in field eddy current measurement.

Computer Assisted Aircraft Paint Stripping Technology

Robert M. Carnes
Striptech International, Inc.
6 Park Avenue
Sumter, SC 29150

Abstract

Removing coating from delicate aviation substrates has numerous times been more damaging to aircraft than the in-place corrosion discovered after the stripping process. Corrosion inspections and damage repair are essential for aircraft safety of flight. Chemical paint stripping with methylene chloride has long been the accepted method of paint removal. Due to the more stringent controls placed on methylene chloride by both the United States Environmental Protection Agency (EPA) and the Occupational Safety and Health Administration (OSHA), numerous alternate methods of paint stripping have been under development.

Our ten year investigative effort into alternate coating removal methods led us to build a large aviation facility and use computer controlled and calibrated plastic media dry stripping equipment. The entire facility was systems designed, balanced and computer interfaced. This computer network covers hangar air handling, plastic media size grading and cleanliness, dense particle separation, plastic media dispensing dry strip air pressure, and analysis of heavy metals in the waste stream.

Our dry strip computer parameters are determined by Messerschmitt, Bölkow and Blohm (MBB) for each particular substrate through a consortium agreement. By very accurately controlling the size of very clean media, weight of plastic media dispensed and the dispersing air pressure, the media velocity is kept constant as is the energy available to each substrate and coating.

Only through very exacting computer controls and calibrated equipment have we been able to achieve the totally acceptable damage free results of paint removal from all aviation substrates.

I. Initial Investigation

A ten-year investigative effort into all aviation paint stripping technologies was recently completed. A selection was made of what our company considered the best present day and future stripping process, the best available equipment, and the best associated symbiotic systems application. During the past three years, we have looked at the national need for a large aircraft paint stripping, corrosion control and painting facility; a good facility location and size; and adequate financing for such a large private venture.

II. Previous Outdated Method of Paint Removal

We all realize that the true necessity for aviation paint removal is: corrosion control, inspections, and weight reduction. Other items such as change in aircraft ownership and/or paint scheme may necessitate aircraft stripping, too. What most people fail to realize is that many times the damage done to an aircraft during the paint removal process may be greater than the in-place corrosion damage that the stripping process discovered. (No, the resolution to this induced damage is not to leave the aircraft skins unpainted and polished.) Little to no testing has ever been done to assess the aircraft damage imposed by the accepted method of methylene chloride wet chemical paint stripping. There are numerous bad side effects which can be attributed to this chemical stripping and the associated maintenance events which accompany this process. Increased pressure by EPA and OSHA will soon eliminate methylene chloride chemical paint stripping.

III. Alternate Paint Removal Methods and Considerations

Alternate methods of paint removal have undergone extensive testing and scrutiny. Striptech International, in our search for the best method, process and equipment, had to consider:

- A. Aircraft and process insurability
- B. Present and possible future EPA regulations
- C. Present and possible future OSHA regulations
- D. Present and potential RCRA regulations
- E. Waste
 - 1. quantity
 - 2. transportation
 - 3. disposal methods
 - 4. cost
 - 5. liability
- F. Initial cost of the stripping media and recyclability
- G. Maintained cleanliness of initial use and recycled media
- H. Size grading and control of stripping media
- I. Dust, contamination and dense particle removal

- J. Potential damage to metal skins and verification testing
 - 1. Almen arc height
 - 2. crack growth
 - 3. fatigue life
- K. Partial alclad, cadmium, anodize, IVD removal
- L. Potential damage to composites, structural tapes, honeycomb, bonded metallics, tin-zinc lightening suppression tape
- M. Repeatable and reproducible results
- N. Controllability of the process
- O. Overall economics of the different processes and equipment
- P. Speed and accuracy of paint removal
- Q. Long-term environmental impact

IV. Investigation Conclusions

Stripstech decided on the plastic media dry stripping method. Most people in the aviation world have not embraced plastic media due to: damage imparted to aviation substrates, little repeatability of results, training problems, dense particle contamination, entrained dust, high waste production and lack of precise parameter controls. We found all "negatives" associated with plastic media dry stripping could be solved with technology and superb equipment. All too often, we heard people say with a voice of authority that plastic media damages aircraft. We found damage was caused by poor equipment. Most plastic media systems were a means or method of paint removal and were not a "process." Our investigation found that most all plastic media systems severely lacked the controls necessary for aviation quality work. We found it was essential to have exacting, integrated and calibrated computer controls coupled with: precision media classification and dispensing, air pressure and volume, dust and contamination removal, dense particle separation and ionized static electricity elimination. Only by having these did we actually have a plastic media dry paint stripping process.

All other methods of researched paint removal had numerous problems also. None we investigated had solutions readily or near term available. The combination of the 98 +/-2% accurate calibrated computer controls, 95% media size grading accuracy, and high media volume 99.98% cleaning capacity package made plastic media dry stripping extremely cost effective and able to safely strip all aviation substrates with totally acceptable results. This integrated, calibrated and well-balanced package gave repeatable and reproducible results for each specific aviation substrate and coating system. Dry stripping problems that so many people complained about had now been solved with technological advances. For numerous years, plastic media dry stripping has been referred to as an operator dependent art form. Expert training coupled with an artistic ability, color change recognition, superb eye-hand coordination and an almost uncanny sixth sense was necessary for good results. Our researched plastic media machine process package now makes plastic media dry stripping a machine-dependent science. Computer controls insure the energy delivered to a substrate is maintained at below the maximum energy saturation level that could impart damage.

V. Computer Controls

The computer controls are not magic nor are they complicated. Each and every aviation substrate is tested for the exact non-damaging dry strip parameters by Messerschmitt, Bölkow and Blohm (MBB). This exacting information and all future testing information on new substrates is provided through a consortium agreement. Data such as media type and hardness, loose grain media sieve size and tolerances, independently controlled air pressure, independently controlled media flow rate and angle of impingement are provided. It is a "given" that all media ejected must always be 99.98% clean and free from all dense particles, trash and dust.

Each hose and nozzle PC controller can store 199 different parameters of media flow rate and air pressure. A master list of MBB verified aviation substrates by type and thickness have been provided with a matched computer entry code. When a specific air pressure code and a separate media flow rate code are selected on the PC controller, an exacting weight of clean, dry, static-free, size graded media is ejected from a nozzle, at a precise particle velocity that dry strips that specifically selected substrate. Computer controls allow changes in either air pressure or media flow rate without effecting the other. (This, of course, is not so with a gravity flow controlled media delivery system which when you increase pressure, you also increase the amount of media dispensed). Each hose dispensing system has its own PC controller. A master panel operator monitors all operations, sets the PC controllers and monitors the substrate mapped aircraft.

When training new dry stripping operators, computers can be set to maintain parameters to the most delicate substrate on the aircraft and "no damage" is thus insured. This does slow the paint stripping rate, but a quality, damage-free job is much more important than speed. This gives the operator more "visual time" to assess their developing paint removal skills and the layer by layer removal capability. This also allows time for each trainee to discover the different reactive and visual qualities of each type top coat, primer, sealant and skin filler under actual stripping conditions, but not at the speed of production operations. Computers make training a non-threatening experience for the novice and reduce the anxiety of the aircraft owner, our insurance company, and our facility management team.

Aviation skin damage is of paramount concern for companies looking at alternative methods to methylene chloride paint stripping. There are many ways aviation skin damage can occur using non-computer controlled plastic media dry stripping equipment. For any dry strip system to work properly, the same exacting events must occur in the media cleaning, media grading, dispensing, recovery, and air delivery packages. If this occurs, then predictable results occur each and every time.

VI. Computer controlled, high tech solutions to plastic media dry stripping.

A computer controlled, and calibrated media feed auger delivers the exact weight (98 +/-2% accurate) of specific size and type media (95% accurate) to the very dry, computer controlled air stream. The weight of the plastic media is precisely computer controlled from MBB derived data. At no time does the dosage of media to the blasting air stream rely on gravity or pressure pot selected pressure. Because the auger feeds the media at a smooth

rate, no spurts or surges occur at the nozzle and only a smooth stream of media is delivered to the substrate. This is what prevents substrate damage.

All of our delivery systems use only air which has been stripped of moisture and oil vapors. Monitors are installed to measure air moisture and are located at the master computer control panel. Plastic media storage hoppers and processing centers, where media may stand, have dryer-heaters to eliminate condensation problems. Plastic media thus stays in a loose grain consistency.

High velocity air wash, high efficiency cyclones and vibrating screens insure all paint/primer material, dust and trash are extracted from the recycled plastic media. Only plastic media and any dense particles now remain to be separated.

A dense particle separator system removes all particles greater than the density of plastic (1.5 grams/cc) regardless of the size or quantity of contamination. A 99.98% (minimum) clean factor can be achieved with only one pass through the cleaning system. A very sophisticated computer system analyses cleaned media samples and provides parts per million of all possible dense particle contaminants.

Pre-selected purchased sizes of media as governed by MBB for specific jobs are re-graded by sieve size to a 95% accuracy by vibrating screens. Numerous screens can be used to recycle any specific sizes of media. The combination of media sizing, cleaning and dense particle separation, allow us to purchase cheaper plastic medias and clean it better than the expensive virgin materials. The cleaning capability also allows us to recycle plastic media 18-20 times instead of 1-3 times, as do most operations. At \$1.50 to \$2.30 per purchased pound of media and a disposal cost of \$.23 to \$1.92 per pound, the economics of our computer system are good. All these computer controlled and high tech factors allow the same results to be achieved on a given substrate, over and over again without variance, when the same MBB input factors are used and followed.

Computer controls have made plastic media dry stripping a method which was once "suspect" in its ability to properly strip aviation substrates into our method of choice. Our dry strip system has over 400 input and output lines to electronically and computer monitor and control functions. Our entire dry strip system is also computer linked to our facility air handling system. If any out of tolerance condition occurs within the entire PC controller, recovery, cleaning, dense particle separation, storage or pressure pot systems, then a systems analysis and fault diagnostic board will illuminate showing the problem area and the system will shut down.

The facility air handling system moves over 640,000 cubic feet of air per minute at 100 linear feet per minute and cleans the air to 99.99% at 5 microns. Each filter is reverse pulse cleaned only when needed via sensors and information as to filter conditions are shown. Air handling loads, back pressure and automated louvers are handled by computer. High efficiency motors are monitored by electronic sensors as are the large exhaust fans. Any out-of tolerance conditions will shut down the dry strip and air handling system. The large air compressors are also electronically monitored to keep equal time on each, keep a watch on critical servicing items, record temperatures, alarm any carbon monoxide levels and automatically shut down all systems in case of a critical condition.

All filter dust, paint and primer chips are automatically separated from good plastic media and relegated to a holding area. Our waste is analyzed by the spectrometric photo analysis computer for levels of arsenic, barium, cadmium, chromium, lead, mercury, selenium and silver. The contained parts per million are automatically displayed for reference with the EPA allowable limits.

A master control and fault diagnostic room monitors, displays and controls many hundreds of functions necessary for "top-notch" aviation plastic media stripping. Computer controls and high tech equipment brought aviation dry stripping from the damaging dark days to a new age of gentle paint removal. It is only through computers that Striptech can remove paint from all present day aviation substrates and be ready to handle future substrates.

Air handling is computer controlled by zones, depending on the size of aircraft. The facility actually fits around a large aircraft such as the DC-10 or Airbus 300. Smaller aircraft such as the B-737 are stripped in one side of the hanger. Fighter size aircraft and large helicopters are stripped in the nose dock portion of the hangar. This versatility allows computer controlled air flow to specific regions where stripping is occurring but not in others where masking, demasking or other functions are occurring. This is good economics.

Our under floor plastic media vacuum recovery system operates under a computer controlled system based on the aircraft length (vacuum travel distance and number of systems operating) and the amount of plastic media being dispersed (vacuum travel speed). This is good economics.

VIII. Messerschmitt's Investigations and Results

MBB, who is a certifying and approving laboratory both for the German government and their national aviation agency, has spent millions of dollars conducting the most extensive test ever performed on plastic media dry stripping and equipment. They have concluded that damage-free aviation dry stripping can be performed on all substrates but only with the correct computer controlled and calibrated equipment. MBB, over many years of research, has helped develop a complete dry strip set of equipment and a paint removal facility. They now dry strip three aircraft per week. We have duplicated and updated their facility in our facility in San Antonio, Texas.

The Canadian government had a problem in trying to chemical strip the McDonnell Douglas CF-18 fighter due to large amount of .020" graphite epoxy composite skin areas. Their investigation into alternate methods still left them with problems of skin damage due to both the composites and the .012" 7075 T6 alclad aluminum skin flight controls. They hired MBB to perform definitive tests to find a way to non-chemically strip the CF-18 with acceptable results. MBB's test report led the Canadian government to duplicate the MBB system ... a computer controlled and calibrated plastic media dry strip system.

The following were the overall conclusions derived after four complete paint and strip cycles (all edges included) of numerous composite and metal test samples. American Society of Testing and Measurements' conditions were followed and all substrate coatings, bonding and preparation were in accordance with the manufacturer's (McDonnell Douglas) specifications.

Specimens stripped were .020" graphite epoxy composite and .012" 7075 T6 alclad aluminum.

A. Overall Composite Test Results for Four Strip Cycles

1. Composites - ultrasonic inspection
 - a. no delamination
 - b. no disbond
2. Composites - x-ray inspection
 - a. no delamination
 - b. no disbonds
3. Composites - light microscope inspection
 - a. no damage after the first PMB strip
 - b. no damage after the second PMB strip, slight roughness of top resin
 - c. a decrease in surface quality occurred on the top resin of the top laminate due to slight matrix pullout
 - d. slight fiber damage was visible on the fourth strip cycle
 - e. other test performed showed that if 70% of the primer was left on the composite surfaces, that no rough matrix pullout occurred. By using the primer as a stripping "flag," damage is eliminated.
4. Composite - compression tests
 - a. In the worst case of the 0.020" graphite epoxy bonded panel PMB stripped four times, there was a 4% higher compression strength than a panel that had never been stripped.
 - b. The worst case in a decrease in strength and strain to failure was less than 15% for a 0.020" test panel stripped four times.

B. Overall Metal Test Results for Four PMB Strip Cycles

1. Metal - ultrasonic inspection
 - a. No delamination between core and skin occurred.
2. Metal - x-ray inspections
 - a. No delamination between core and skin occurred.
3. Metal - light microscope inspections
 - a. A slight roughness was observed due to number of strip cycles.

C. Other Tests and Their Results

1. Ion-vapor deposit (IVD) of aluminum on steel
 - a. PMB on 0.040" steel IVD aluminum plating painted and stripped.
 - b. Results: No weight loss occurred showing no aluminum removal and the surface became smoother due to the small tips of the IVD plating being flattened by the PMB action.
2. Cadmium Plated Steel
 - a. PMB on 0.040" steel, cadmium plated, painted and stripped.

- b. Results: No thickness loss could be measured, but a slight weight loss did occur (.000227 of one percent). Depending on 4 or 5 PMB strips and a later repainting, no corrosion can be expected. Aircraft fasteners will have much more cadmium removed using wrenches, screwdrivers, apexes, and sockets than PMB could ever remove when used in the correct aviation grade equipment.
- 3. Paint removal by dry stripping from tin zinc lightening-protected substrates
 - a. PMB removed the paint from tin-zinc bonded to aircraft skins
 - b. Results: Components with lightening protection should not be stripped down to the tin-zinc layer due to created damage to this thin, soft film.
 - c. PMB stripping should only go to the primer layer.
- 4. Paint adhesion after PMB dry stripping
 - a. Numerous types of coatings were applied at different thicknesses and stripped at different parameters on different types of substrates to determine what effect PMB had on paint adhesion.
 - b. Using the same primer and paint application methods, prep, and conditions, no basic differences in paint adhesion for PMB stripped and non-stripped aluminum panels could be determined.

IX. CONCLUSION

The remainder of the equation to support our computer and high tech dry strip facility includes:

- A. A corrosion treatment, repair and control facility. Full and in depth support in this area is also provided by the Dee Howard Company and Fairchild under contract agreement.
- B. A full service down draft paint facility is available as well as a full service aircraft wash pad

Computers and high tech have taken the worry out of removing paint so inspection and corrosion control can be accomplished.

Accelerating Factors in Galvanically Induced Polyimide Degradation

M. L. Rommel
Northrop Corporation
Aircraft Division
1 Northrop Avenue 3853/MF
Hawthorne, CA 90250

A. S. Postyn
Northrop Corporation
Aircraft Division
1 Northrop Avenue 3853/MF
Hawthorne, CA 90250

T. A. Dyer
Northrop Corporation
Aircraft Division
1 Northrop Avenue 3853/MF
Hawthorne, CA 90250

Abstract

Polyimides reinforced with graphite fibers possess superior mechanical properties in the 250°F (120°C) to 550°F (288°C) temperature range compared to their epoxy counterparts. Polyimides such as bismaleimides (BMI) are susceptible to hydrolysis which results in physical degradation of the composite. Hydrolysis can occur when a graphite fiber bismaleimide composite is coupled to a metal, such as aluminum, in a sump-type environment. If the aluminum corrodes, the composite since it is electrically coupled to the metal becomes the cathode. Water reduction in the presence of oxygen occurs at the cathode which leads to the formation of hydroxyl ions which attack the bismaleimide resin. This study has identified the factors required for degradation and the effect of different variables on the reaction rate. Temperature was found to be the greatest reaction accelerator and the elimination of exposed graphite fibers presents the best method of slowing the reaction. It was also found that the galvanic current correlates to the amount of visual degradation observed in the composite as well as the rate of metal corrosion.

Key Terms: polyimides, bismaleimides, galvanic corrosion, composites, graphite

I. Introduction

The increased demand for aircraft operating at higher Mach numbers has stimulated the development of low density materials with higher operating temperatures. Some of the most attractive materials are polyimide based composites reinforced with graphite fibers. These materials offer an attractive combination of low density, increased toughness, and higher operating temperatures than their epoxy counterparts. However, recent work has shown that polyimide based composites such as bismaleimides with graphite reinforcement are susceptible to galvanically induced hydrolysis¹. The mechanism for this process is shown in Figure 1. The anodic reaction consists of the oxidation of a metal which increases its valence state through the production of electrons. The electrons are then consumed by the cathodic reaction which in this case is the reduction of water in the presence of oxygen to produce hydroxyl ions. The graphite reinforcement in the composite acts as the cathode in this galvanic couple. Therefore, the hydroxyl ions accumulate at the composite and attack the imide-carbonyl linkage of the polymer which results in degradation of the polymer.

The purpose of this work was to verify the mechanism of polyimide degradation and further identify the conditions that are required for the reaction to occur. Electrochemical techniques were used to quantitatively evaluate galvanically induced hydrolysis of graphite reinforced bismaleimide composites and determine the variables that influence the rate of degradation. Corrosion potential measurements were conducted in 3.5 weight percent sodium chloride solutions at room temperature to construct a galvanic series. This formed a basis for predicting the corrosion tendencies of various metal/bismaleimide composite combinations. Measurements of the galvanic current were made over 150 days between various metal/composite combinations under different experimental conditions. Visual damage to both the metal and the composite was recorded and evaluated during the galvanic current experiments. This information will provide a baseline to formulate accelerated tests to predict the service life of polyimide composites in airframe applications.

II. Experimental

The cathodic material used in this study consisted of a woven IM7/5250-4 five-harness satin cloth produced by BASF Structural Materials. The anode depending on the test condition was either aluminum 7075-T6, titanium 6Al-4V, or stainless steel 321.

A. Specimen Preparation

All metal specimens were polished to a 600 grit finish, vapor degreased (except titanium), and rinsed in deionized water. The titanium and composite specimens were wiped with isopropyl alcohol and rinsed in deionized water. The surface resin was removed from the top of the composite by sanding to expose graphite fibers and permit electrode contact. The specimens used for the potential and current measurements were all 1 inch (2.54 cm) by 4 inch (10.2 cm) by 0.125 inch (0.32 cm). The procedures used to conduct the experiments are summarized below.

B. Test Cells

The test cells used for the galvanic current experiments are shown in Figure 2. The distance between the anode and cathode was 4.6 cm. The test cells were filled with 400 ml of test solution. All test cells were identical to facilitate the elimination of experimental error.

C. Measurements

1. Corrosion Potential. All measurements were conducted in 3.5 weight percent NaCl solution at room temperature using an ESC multichannel potentiostat with a saturated calomel reference electrode (SCE) and glassy carbon counter electrodes. The corrosion potential was recorded three times a week. The value reported was the average of 250 days of measurements.

2. Current Versus Time Measurements. Current versus time measurements were performed for metal/BMI couples under the conditions described in Table 1. A Princeton Applied Research 273 potentiostat/galvanostat was used in a potentiostatic mode to monitor current. The BMI specimen was connected to the working electrode input of the potentiostat. The metal specimen was connected to the counter and reference electrode inputs. In this configuration, the potentiostat functioned as a zero resistance ammeter. The specimens were placed initially in the test cell and allowed to equilibrate in the test solution for one hour. Galvanic current measurements were conducted for one hour on each cell every seven days. A saturated calomel reference electrode was used for all measurements. After the measurement, the anode and cathode were electrically connected using copper wire. The galvanic current reported is the average of the current recorded during the one hour measurement.

III Results

A. Mechanism Verification

In order to verify that the attack of the polyimide occurred via hydroxyl ions, the original General Dynamics "tin" can test² was used to reproduce the attack of the BMI. This test consisted of placing a graphite/BMI specimen in a tin can with equal amounts of 3.5 weight percent sodium chloride solution and JP5 jet fuel. The can was heated to 140°F (60°C) and observed until attack of the composite was visible. Attack occurred within 24 hours, upon which the specimen was removed from the solution and subjected to Fourier Transform Infrared Spectroscopy (FTIR) on a Spectra Tech IR-Plan microscope. The scan associated with this sample as well as an untreated BMI sample is shown in Figure 3. The scan of the untreated BMI showed an imide-carbonyl peak at 1800 cm⁻¹ while the specimen exposed to the tin can test showed a peak at 1650 cm⁻¹. The peak at 1650 cm⁻¹ corresponds to a carboxylic acid (the by-product of an imide-hydroxyl ion reaction). To further characterize the attack, a sample of BMI exposed to a 10 weight percent solution of sodium hydroxide (pH = 10) was scanned using FTIR. As shown in Figure 3, the resulting scan was virtually identical to the scan of the specimen exposed in the "tin" can experiment.

B. Requirements for Degradation

The requirements for galvanic corrosion of metals have been summarized by Balboian and Pohlman³ as a common electrical path, a common electrolyte, and materials possessing different corrosion potentials. To verify that galvanically induced BMI degradation follows the same general principles, the tests summarized in Table 2 were conducted. The tests to evaluate the need for a conductive fiber, corroding metal, and electrical contact were all conducted at 180°F (82°C) in equal amounts of 3.5 weight percent sodium chloride solution and JP5 jet fuel. These test conditions duplicate the conditions of the original General Dynamics "tin" can test. During the tests, the BMI specimens were periodically inspected for visual damage.

The tests summarized in Table 2, showed that a conductive fiber and electrical contact is needed for degradation of the BMI composite. When S glass/BMI was placed in an iron can, no degradation occurred. The same observation was made for the case when there was no electrical contact between BMI/graphite and the metal can. This satisfies the condition of a common electrical path. The need for electrolyte bridging was evaluated using a concentration cell. The bismaleimide was

electrically connected to aluminum 7075-T6 with both the composite and the metal specimen immersed in separate electrolyte solutions. The metal corroded but no degradation in the IM7/BMI 5250-4 was observed.

C. Galvanic Series

The third requirement for galvanic corrosion is a potential difference between the two materials. To evaluate the potential difference between various metals and bismaleimide IM7/5250-4, a galvanic series was constructed from the corrosion potential data. The galvanic series is usually a good indication of the possible galvanic effects as indicated by the magnitude of the potential difference between the two materials. In general, a potential difference of approximately 250 mV between materials indicates a tendency towards galvanic corrosion³. As shown in Figure 4, the IM7/5250-4 was the most cathodic material with a corrosion potential of 200 mV versus SCE, followed by the Ti-6Al-4V, and stainless steel 321. The most anodic or active material measured was a rapidly solidified magnesium alloy, followed by the aluminum alloys 7075-T6 and 3003. The potential difference between the aluminum alloys and the IM7/BMI 5250-4 was 950 mV versus SCE, while the potential difference between the titanium and IM7/BMI 5250-4 was only 150 mV versus SCE.

In order to further assess the galvanic corrosion tendencies, the effect of coupling IM7/BMI 5250-4 with various metals was examined. The data is summarized in Figure 5. This data allowed an assessment of the effect of coupling on the polarization tendencies of the various metal/bismaleimide combinations. The current produced by a galvanic cell depends on both the resistance of the electrolyte and the degree of polarization of the anode and cathode. However, in cells where the anode and cathode are in close proximity to each other, the resistance of the electrolyte is usually a secondary factor compared to polarization. Of the couples examined, the aluminum/IM7/BMI 5250-4 was the only couple that was cathodically controlled. Specifically, the corrosion potential of the couple was closer to that of the aluminum anode and hence the corrosion rate is controlled primarily by the aluminum. The stainless steel and Ti-6Al-4V coupled to IM7/BMI 5250-4 polarized to some degree at both the anode and the cathode. In this case, the corrosion rate of the couple is synergistically determined by the properties of the two materials in the couple.

D. Galvanic Current

Measurements of the galvanic current between couples of BMI/graphite and various metals were conducted for 150 days and are shown in Figure 7. These measurements were conducted using a zero resistance ammeter technique. The magnitude of the galvanic current provides an indication of the severity of galvanic corrosion in various environments through Faraday's Law⁵. Faraday's law states that the weight of reacting metal is proportional to the product of galvanic current and time. Therefore, by measuring the amount of current between couples of IM7/BMI 5250-4 and 7075-T6, the severity of corrosion and the influence of time on the corrosion tendencies of the various metal/bismaleimide combinations can be assessed. Metal weight loss measurements were used to determine the corrosion rate of the metal and to correlate metal corrosion with the degree of bismaleimide degradation. A summary of the metal weight loss measurements is shown in Figure 6. Polyimide damage was based on visually inspecting the composite specimens and rating the degree of attack using the rating scale shown in Table 3. A plot of the composite visual damage, for the galvanic couples, versus time is shown in Figure 8.

1. Effect of Metal. The galvanic current of the IM7/5250-4 Al 7075-T6 couple was initially 400 μ A and increased to a maximum of 1150 μ A after 150 days. The corrosion rate of the aluminum was 7 mils per year (0.175 mm/year). The composite visual damage was rated an eight, after exposure, according to the scale given in Table 3. The galvanic current between couples of

BMI/5250-4 and Ti-6Al-4V and stainless steel 321 remained constant with time and was 3 μA and 5 μA , respectively. The corrosion rate of the Ti-6Al-4V and SS321 was negligible, less than 0.0003 mm/year (0.01 mils per year). Sectioning of the corresponding bismaleimide specimens showed that no attack of the composite in either specimen.

2. Effect of Temperature. The effect of temperature on the reaction rate was evaluated by comparing test cells at different temperatures. The temperatures investigated were 140°F (60°C), 120°F (49°C), and 77°F (25°C). The metal in each case was Al 7075-T6 coupled to the IM7/BMI 5250-4 and immersed in 3.5 percent NaCl. The test cell at 140°F (60°C) exhibited the highest currents. The 140°F (60°C) test cell had an initial current of 675 μA which increased to a maximum of 5400 μA after 34 days. The test was then discontinued at this point because the composite incurred enough damage to be rated a 10 according to the scale given in Table 3. The corrosion rate of the metal in the 140°F (60°C) test cell was 70 mils per year (1.78 mm/year). The test cell at 120°F (49°C) had intermediate currents compared to the 140°F (60°C) and 77°F (25°C) test cells. The initial current was 850 μA , which is higher than the 140°F (60°C) test cell. However, the maximum current measure was only 2940 μA . The 120°F (49°C) test cell was discontinued after 108 days because the composite had suffered maximum visual damage. The corrosion rate of the metal in this test cell was 21.7 mils per year (0.55 mm/year). The 77°F (25°C) test cell exhibited the lowest currents. The initial current was 400 μA which increased to 1150 μA after 150 days. The composite specimen was rated an 8 after 150 days of exposure. The corrosion rate of the metal was 7 mils per year (0.175 mm/year).

3. Effect of Exposed Edges. The effect of having no exposed graphite fibers was investigated by coupling an Al 7075-T6 specimen to a IM7/BMI 5250-4 with no edges exposed to the electrolyte. In this test cell, the metal was coupled to the surface of the BMI. The average galvanic current was approximately 40 μA and did not increase with respect to exposure time. The corrosion rate of the metal in this test cell was 0.1 mils per year (0.003 mm/year). No visual attack of the composite was observed after 150 days of exposure.

4. Effect of Area. The effect of the anode to cathode area was determined by comparing three different anode to cathode ratios. The highest galvanic current was measured in the couple that had an anode to cathode ratio of approximately 0.5. This corresponds to the specimen with the largest amount of exposed graphite fibers. The corrosion rate of the metal in the test cell with an anode to cathode ratio of 0.5 was 15.6 mils per year (0.40 mm/year). Visual composite damage, for this test, was somewhat less than that observed for the anode/cathode ratios of one and two. Presumably this is because the specimen was larger and the attack was somewhat diluted over the area. The next largest current was the test cell that had an anode to cathode ratio of one. The metal in this test cell showed a corrosion rate of 7 mils per year (0.175 mm/year). The least amount of current measured was in the test cell with an anode to cathode ratio of two. In this case, the smaller cathode area translated to a 46 percent decrease in corrosion rate. The corrosion rate of the metal in this case was 2.2 mils per year (0.06 mm/year).

5. Effect of Electrolyte. Four different concentrations of salt solution, the effect of real seawater, and the addition of jet fuel to the baseline salt solution were investigated. The 5.0 weight percent sodium chloride solution produced the highest galvanic current while the 0.1 weight percent solution produced the least amount of current. The 5.0, 3.5 and 1.0 weight percent solutions all increased in current with increased exposure times while the 0.1 weight percent solution showed a decrease in current initially which eventually leveled off to a constant value. The amount of damage suffered by the metal and composite correlated very well with solution concentration. The higher concentrations resulted in more metallic corrosion as well as composite damage. Real seawater behaved in a manner similar to the 0.1 weight percent sodium chloride solution. The sodium chloride concentration of the seawater was approximately 3.8 weight percent. The reaction rate was lower than that of the 3.5 percent NaCl test cell. The lower galvanic current and consequently lower reaction rates associated with real seawater is probably

due to buffering effects caused by the different types of ions found in natural seawater. The effect of adding jet fuel to the salt water was investigated and found to approximately double the galvanic current. The corrosion rate of the metal was 15.5 mils per year (0.40 mm/year) which is approximately twice that of the same test cell without jet fuel. Attack of the composite in the test cell containing jet fuel was also accelerated compared to the baseline test cell. The jet fuel seemed to promote swelling which would increase the amount of exposed fiber.

6. Effect of Nitrogen Purge. The effect of reducing the oxygen concentration was investigated by purging with nitrogen at a rate of 150 cm³/minute with nitrogen gas. Based on the mechanism shown in Figure 1, reducing the oxygen concentration should slow the cathodic reaction which will result in decreasing the amount of hydroxyl ions produced. The galvanic current measured while purging with nitrogen was approximately 60 μ A as compared to the baseline cell which started at 400 μ A. The current in the nitrogen purged cell remained fairly steady over the two weeks of measurements.

IV. Conclusions

The following conclusions based on the data presented in this paper can be made regarding the mechanism of galvanically-induced polyimide degradation:

- The mechanism of polyimide degradation, when coupled to a corroding metal, was shown to occur via a galvanic reaction. Hydroxyl ions liberated at the cathode then attack the imide-carbonyl linkage which degrades the bismaleimide composite.
- Examination of the polarization behavior of the IM7/BMI 5250-4 and aluminum 7075-T6, stainless steel 321 and titanium 6Al-4V showed that the only couple that exhibited cathodic control was the IM7/BMI and Al 7075-T6 couple.
- The greatest increase in reaction rate was found when the temperature was increased and the amount of exposed graphite fibers were increased.
- The greatest decrease in reaction rate was found when exposed graphite fibers were eliminated.
- The magnitude of the galvanic current correlated with the corrosion rate of the metal and also with the amount of visual degradation observed in the composite.

References

1. J. Boyd, BASF Structural Materials, Private Communication, April 1990.
2. M. Faudree and D. Kinnard, "Polyimide Degradation Meeting", Wright-Patterson AFB, June 1990.
3. R. Balboian, and S. Polman, "Volume 13. Corrosion", Metals Handbook, ASM International, Metals Park, Ohio, September 1987.
4. M. Fontana, "Corrosion Engineering", McGraw-Hill, New York, NY., 1986.
5. H. Uhlig, and R. Revie, "Corrosion and Corrosion Control", John Wiley & Sons, New York, NY., 1985.
6. R. Balboian, "Predicting Galvanic Corrosion Using Electrochemical Techniques", Electrochemical Techniques for Corrosion Engineering (Houston, TX: National Association of Corrosion Engineers, 1986).

Table 1. Current Versus Time Test Cells

| Cell No. | Composite | Metal | Electrolyte (Weight %) | Variable |
|----------|------------------|------------|------------------------|---------------------------|
| 1 | BMI (5250-4)/IM7 | Al 7075-T6 | 3.5% NaCl | Baseline |
| 2 | BMI (5250-4)/IM7 | Al 7075-T6 | 3.5% NaCl and JP5 | Jet Fuel |
| 3 | BMI (5250-4)/IM7 | Ti 6Al-4V | 3.5% NaCl | Metal |
| 4 | BMI (5250-4)/IM7 | 321 SS | 3.5% NaCl | Metal |
| 5 | BMI (5250-4)/IM7 | Al 7075-T6 | 5.0% NaCl | Concentration |
| 6 | BMI (5250-4)/IM7 | Al 7075-T6 | 1.0% NaCl | Concentration |
| 7 | BMI (5250-4)/IM7 | Al 7075-T6 | 0.1% NaCl | Concentration |
| 8 | BMI (5250-4)/IM7 | Al 7075-T6 | 3.5% NaCl | Anode/Cathode Ratio = 0.5 |
| 9 | BMI (5250-4)/IM7 | Al 7075-T6 | 0.5% NaCl | Anode/Cathode Ratio = 2 |
| 10 | BMI (5250-4)/IM7 | Al 7075-T6 | 3.5% NaCl | Temperature: 120°F (49°C) |
| 16 | BMI (5250-4)/IM7 | Al 7075-T6 | Hermosa Seawater | Type of Electrolyte |
| 18 | BMI (5250-4)/IM7 | Al 7075-T6 | 3.5% NaCl | Temperature: 140°F (60°C) |
| 19 | BMI (5250-4)/IM7 | Al 7075-T6 | 3.5% NaCl | No Exposed Edges |

Table 2. General Dynamics "Tin" Can Tests of Bismaleimide 5250-4

| Variable Investigated | Fiber | Environment | Contact With Metal | Degradation |
|-------------------------------------|---------|-------------------------|----------------------------------------------------|-------------|
| Electrical Contact Conducting Fiber | IM7 | Iron Can | Yes | Yes |
| | IM7 | Iron Can | No | No |
| | IM7 | Iron Can | No | No |
| | S Glass | Iron Can | Yes | No |
| Corroding Metal | IM7 | Ti-6Al-4V | Yes | No |
| | IM7 | Al 7075-T6 | Yes | Yes |
| | IM7 | Al 2024 | Yes | Yes |
| Electrolyte Bridging | IM7 | Al 7075-T6 (3.5 % NaCl) | Electrical Contact With No Bridging Of Electrolyte | |

Table 3. Visual Rating System Used to Evaluate IM7/5250-4 Damage

| Rating | Description |
|--------|---------------------------------------------------------|
| 1 | Mild Discoloration |
| 2 | Significant Discoloration |
| 3 | Significant Discoloration With Exposed Fibers |
| 4 | Numerous Exposed Fibers |
| 5 | Delaminated More Than One Ply |
| 6 | Delaminated More Than Two Plies |
| 7 | Severely Delaminated With No Surface Resin Left |
| 8 | More Severe Delamination With No Surface Resin Left |
| 9 | More Severe Delamination With No Resin In Several Plies |
| 10 | Severely Delaminated With No Resin (Maximum damage) |

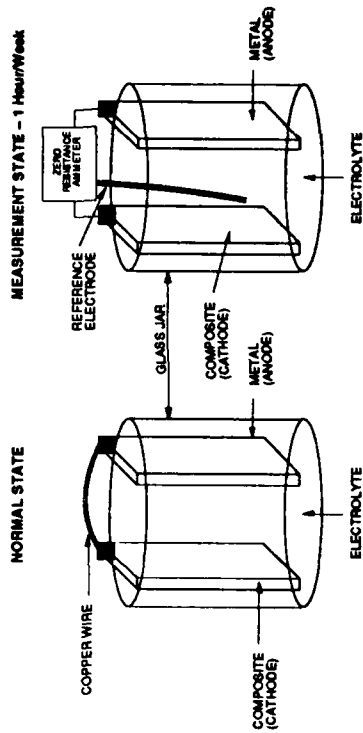


Figure 2. Test Cell for Galvanic Current Measurements.

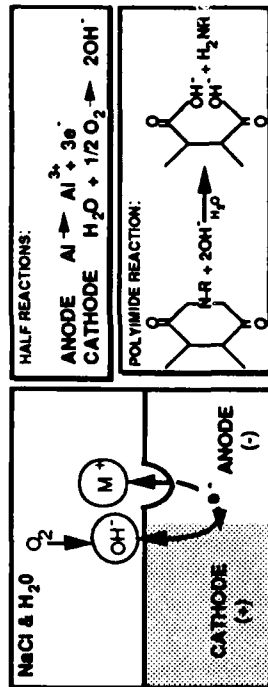


Figure 1. Mechanism of Galvanically Induced Imide Hydrolysis.

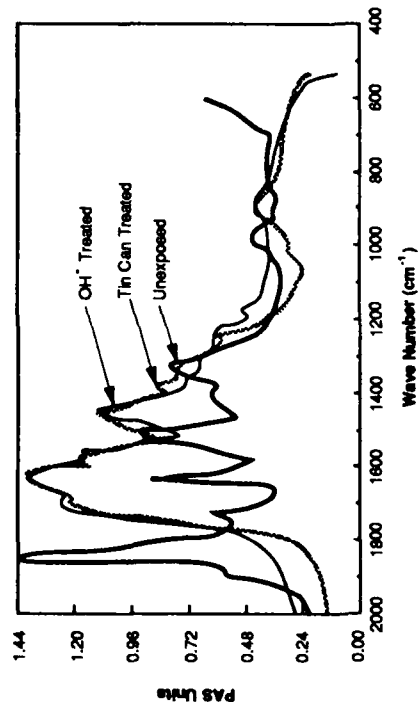


Figure 3. FTIR Spectrograph of Untreated IM7/BMI 5250-4, "Tin Can Treated" IM7/BMI 5250-4, and OH⁻ Treated IM7/BMI 5250-4.

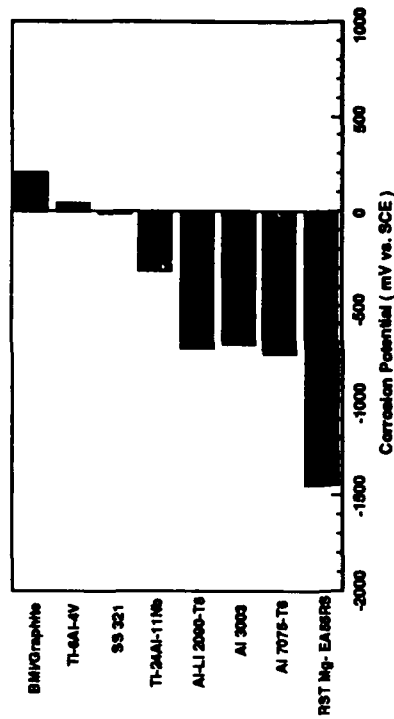


Figure 4. Galvanic Series in 3.5 Weight Percent Sodium Chloride.

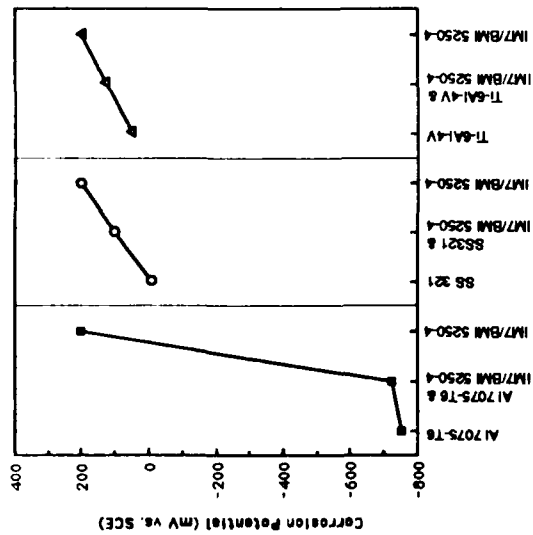


Figure 5. Corrosion Potential of Various Couples in 3.5 Weight Percent Sodium Chloride

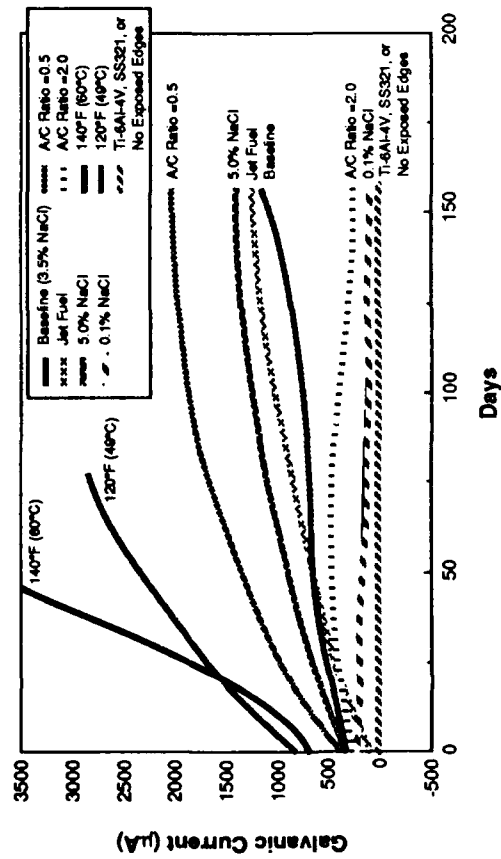


Figure 7. Summary of Galvanic Current or Reaction Rate vs. Time.

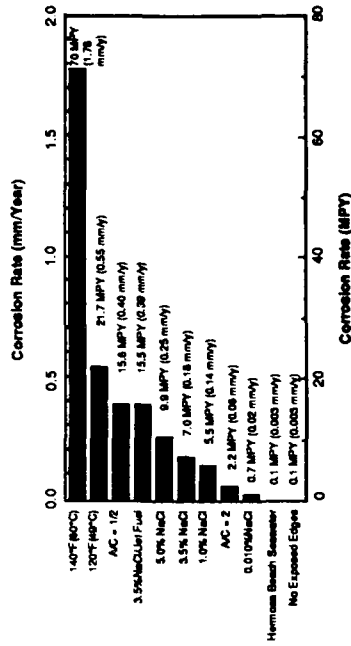


Figure 6. Metal Corrosion Rate in the Various Test Cells.

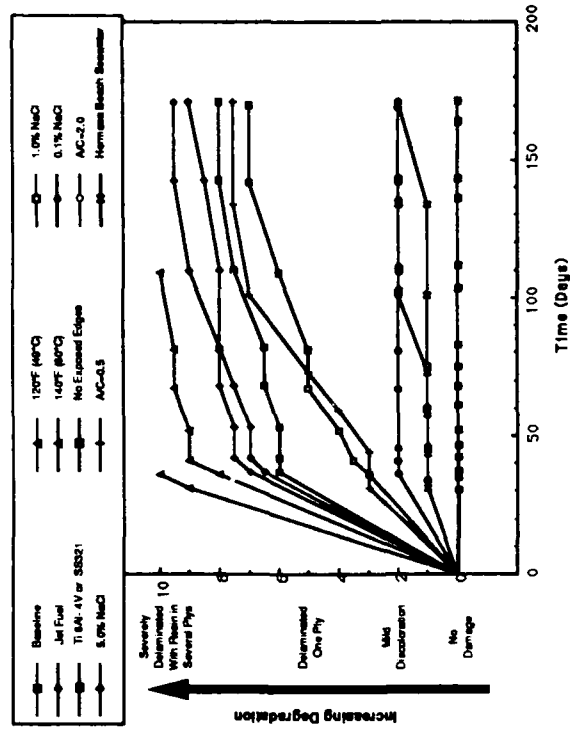


Figure 8. IM7/BMI 5250-4 Damage Versus Time For the Various Test Cells.

Reducing Aircraft Corrosion With Desiccant Dehumidifiers

David McCarthy
Government Applications Department
Munters Cargocaire
79 Monroe St.
Amesbury, MA 01913 USA

Douglas Kosar
Manager of Applications Engineering
Munters Cargocaire
79 Monroe St.
Amesbury, MA 01913 USA

Steven Cameron
Project Engineer, C/KC-135 Program
Oklahoma City Air Logistics Center
Tinker Air Force Base
Oklahoma City, OK 73145-5609 USA

Abstract

Aircraft corrosion represents a multi-billion-dollar annual expense for military and commercial operators. Much of this costly waste can be eliminated or reduced by keeping the aircraft dry when it is on the ground. In the last ten years, many aircraft owners and operators have been successful in attaching desiccant dehumidifiers to aircraft, circulating dry air through corrosion-sensitive components such as engines, radar, avionics and the air frame itself. This paper outlines four of the principal corrosion and excess moisture issues in aircraft, and describes how each problem has been addressed through the use of specially-designed desiccant dehumidifiers.

Principal Issues

Aircraft corrosion costs the United States taxpayer more than \$1 billion dollars every year.¹ This figure includes only the cost of corrosion within the Air Force. When one adds the cost of aircraft corrosion in the Navy, Army and Marine Corps, estimates exceed \$2 billion annually. When the cost of corrosion of the commercial air fleets is added to the military figures, one can see clearly that aircraft corrosion has become a significant waste of our national resources. The problem deserves close attention from the engineering community, since economic realities have forced extension of the useful life of aircraft. Military fleets cannot be replaced at the rates of the past because of reductions in defense budgets, and competitive pressures in the commercial marketplace require that we make use of civilian aircraft for longer periods than the designers may have originally anticipated.²

A traditional response of a well-trained corrosion engineer to a corrosion problem is to seek a material change or design modification to avoid the problem entirely. Failing those remedies, the engineer often seeks a coating or other surface treatment to limit the negative effects of corrosion. While these are certainly valid responses, there is another technology, perhaps less familiar to the corrosion engineer, which has been effectively applied to reduce the cost of atmospheric corrosion in large, exposed machinery. This technology—humidity control—has been effective in reducing costs of several types of corrosion commonly found in aircraft.

Dry air prevents corrosion by eliminating moisture. The atmospheric corrosion reaction requires three elements—the base material, oxygen and an electrolyte, which allows electrons to flow from an area of

high potential to an area of lower potential within the base material. By removing condensed moisture from aircraft, corrosion is slowed or halted because no electrolyte remains to sustain the reaction. Humidity control, like any technology, does not solve all of the complex problems of aircraft corrosion, but it has been applied with cost-effective results in a wide variety of situations. These include:

a. Propulsion System Corrosion

In some engines, operation in a marine environment has a highly corrosive effect. Alluding to this problem, John DeLuccia of the Naval Air Development Center's Aerospace Materials Division recently joked: "An F-14 on a carrier deck is almost biodegradable!"³

In Denmark, the J-35 fighter aircraft routinely operates at low level over salt water, and had experienced significant corrosion of turbine blades. In 1975, the Danish Air Force began a program to connect industrial desiccant dehumidifiers to the engine air intakes whenever the aircraft returned from a mission. The dry air removed condensed water from the engine assembly, which effectively eliminated the electrolyte, slowing corrosion from visually obvious flakes to levels so low they were difficult to measure. The Danish Defense Forces estimate annual savings from this program at \$970,000 in return for a one-time capital cost of \$323,000 and an annual energy cost of \$284,000.

b. Corrosion Effects on Avionics

The cost of computers and other aviation electronics now often exceeds the cost of the aircraft itself. Earl T. Startzman of Boeing's Aviation Software & Electronics Laboratory in Wichita, Kansas expressed this new hardware-software relationship succinctly when he said: "We like to think of the airplane as just another peripheral".⁴

There are two humidity-related problems that have been addressed successfully by the use of desiccant dehumidification equipment; contact corrosion and changes in insulation resistance due to adsorbed moisture. The source of this moisture is humid air, which condenses within the aircraft in two situations. First, when humid air trapped in the airframe is lifted aloft on take-off, moisture condenses as the aircraft skin encounters the much colder temperatures of the atmosphere at altitude. Secondly, as the aircraft descends to the more humid air at ground level, the surfaces chilled at high altitudes once again condense water as humid air re-enters the aircraft on landing.

In high-reliability aircraft electronics, circuit boards are generally protected by conformal coatings, so corrosion on the board itself is quite minimal. The connectors, however, are more sensitive to condensed moisture. Current must flow freely through contact points that are exposed to humid air, and in some cases, exposed to actual water droplets. The potential for corrosion at these points is obvious, and indeed is notorious in aircraft and in military electronics.

A second problem results from changes in resistance of cable insulation due to condensed moisture. For example, a typical resistance value for nylon at 10% relative humidity is 10^{14} OHM. At 90% rh, that value drops to 10^7 OHM. This more-than-million-fold change in resistance can, over the miles of electrical cable in modern aircraft, create problems in performance of computer hardware. If the designer assumes a fixed resistance value, and that value changes by over a million-to-one ratio, the circuit can develop problems.

Avionics reliability was the principal concern of the Swedish Air Force when, in 1981, they applied desiccant dehumidification technology to the problem. In a test of the Draken fighter aircraft, dry air was supplied to the cabin and electronics areas whenever the aircraft was scheduled to be on the ground for more than two hours. The results were impressive. The mean time between failures (MTBF) for radar and cabin electronics increased from 7.2 hours (with no humidity control) to 14.2 hours. This doubling of the MTBF saved money and improved mission readiness—a key concern of defense aircraft program managers.

c. Airframe corrosion fatigue

In his September 1992 article entitled *Industry seeks tonic for aging aircraft*, Alan Brown of Aerospace America begins by saying "Some engineers knew U.S. airliners were aging even before the top of an Aloha Airlines 737 unzipped over Hawaii four years ago. Now everyone knows." That tragic event, which any air traveler has difficulty forgetting, has shown the potential dangers of fatigue corrosion of the air frame in very compelling terms.

Fatigue corrosion is strongly accelerated by condensed moisture, as Mr. Brown describes in his article. Moderate laboratory humidity cuts the fatigue life of many aluminum alloys by 50% or more. Moisture actually condensing into microcracks has an even more harmful effect.⁵ As with electronics, condensation caused by altitude changes leaves moisture inside the air frame, where it accelerates corrosion.

Supplying dry air to the aircraft cabin on the ground can help remove this frame-bound moisture, and several organizations are designing systems to measure the results. For example, the Boeing 707 airframe, used as the EC-135 and KC-135 aircraft by the US Air Force, is now being supplied with dry air in test installations at Hickham Air Force Base in Hawaii and at Mildenhall Air Force Base in England. Additionally, operators of the Lockheed Hercules aircraft recently reported favorable results of similar programs that have been in progress since 1985⁶.

d. Adsorbed moisture

Condensed moisture is expensive to lift. Studies conducted by commercial fleet operators in Europe show that carrying an extra kilogram of weight costs about \$14,285 per year (1993 dollars). The same studies have also shown that large commercial aircraft can adsorb as much as 250 to 400 Kg in condensate into cracks, crevices and especially into cabin insulation.⁷ By circulating dry air to remove the unwanted moisture, it may be possible to save between \$3.5 and 5 million dollars per aircraft per year in fuel costs.

Odors and microbiological infestation are also a direct result of adsorbed moisture. Many of the unsavory odors which disturb humans originate from fungi, and fungal growth is greatly accelerated by high humidity and especially by condensed moisture. For example, Figure 1 shows that the growth rate for *Aspergillus Ruber*, one of the fungi responsible for odors in buildings, is 40 times greater at 90% rh than at 70% rh.⁸ Figure 2 shows another characteristic of humidity, which is that many bacteria, some of which contain viruses, survive longer at high humidity than at low humidity. The figure shows that at 35% rh, all but 5% of the *poliomyelitis* virus are dead within the first five hours of exposure, but at 80% rh, the virus continues to multiply. By keeping materials dry, fungal and bacterial growth can be greatly reduced or eliminated entirely, as has been shown in studies of the fungal infection of buildings.⁹

High humidity is the thread which runs through all four of these issues. If an aircraft can be kept dry, the problems caused by moisture can be reduced or eliminated, which is the reason that dry air technology has been more widely utilized in aircraft applications over the last ten years.

Dry Air Technology

In aircraft applications, desiccant wheel (DEW) dehumidifiers are generally used because of their ability to remove moisture from air regardless of the ambient temperature or moisture level. The more familiar cooling-based dehumidifiers are generally not used, because in aircraft operations, the engineer must plan for cold temperatures as well as high humidities. Cooling-based dehumidifiers cannot dry air efficiently when the ambient is below 15°C (60°F).

As the name implies, DEW dehumidifiers use a desiccant—a material which can easily attract and remove water vapor from air. Most people are familiar with the small packages of desiccant normally

shipped with consumer electronics and cameras, and often contained in bottles of vitamins and other pharmaceutical tablets. The desiccant in dehumidifiers is similar, except that where a package of desiccant eventually becomes saturated, a dehumidifier has a heating cycle to reactivate (dry) the desiccant so the unit can produce dry air continuously.

Figure 3 shows that in dehumidifiers, the desiccant is impregnated into a corrugated ceramic composite material, which is formed into a wheel¹⁰. Air passes easily through the flutes, contacting the desiccant. The wheel rotates slowly (6 to 10 rph) between two air streams. The incoming process air stream—the larger one—gives off its moisture to the desiccant. The process air is dry as it leaves the wheel. The humidity-laden wheel rotates slowly into a second, smaller air stream which has been heated. This smaller exhaust air stream—called the reactivation air—warms the desiccant. The warmed desiccant gives off its moisture, which is then carried away by the reactivation air. The newly-dried desiccant material is rotated back into the process air, where it absorbs moisture once again.

Figure 4 shows how this basic operating principle is expressed in the hardware commonly used in aircraft dehumidification. A desiccant wheel with fans and heaters is mounted on a cart, which is large enough to carry the flexible duct which connects the dehumidifier to the aircraft. A retractable power cable is also mounted on the cart, as power connections may be located some distance away from the aircraft.

Figure 5 shows a desiccant dehumidifier connected to the engine air inlet of a fighter aircraft. The entry point for the dry air varies according to the aircraft configuration and the reason for connecting the dry air. Engine corrosion, clearly, requires only a simple connection through the cover normally placed over the air inlet. Avionics and radar protection requires a connection to the cabin and nose of the aircraft, and preventing airframe corrosion requires air distributed throughout the aircraft. In most cases, these connections are fairly straightforward. In older aircraft without specific dry air connections, the method of attachment varies, and in some cases, multi-point connections have proven useful. From a practical perspective, operators find that the simpler and faster the connection, the more likely it will actually be used by the ground crew.

Experience With Specific Aircraft

Dry air technology has been applied to a wide variety of aircraft, including Air Force One, the Boeing 747 which carries the President of the United States. Other fixed wing aircraft include the P-3 Orion, DC-9, C-130 Hercules, F-16, J-37, Nimrod, Tornado, P-3 Orion, EA-6B Prowler, C/F-16 and the AV-8B Harrier and many more. Favorable results have also been obtained with helicopters including the Cobra, UH-1, B-105 and the Sea King and others. To illustrate some interesting points, we have chosen four different types of aircraft to describe how dehumidification technology is used.

Engine Corrosion - Danish Air Force Fighters (F-16, F-104, J-35 and J-37)

The land-based Danish Air Force has, in common with all naval aircraft, a low-level marine flying environment. This inevitably means that salt-laden sea spray will flow through the engine during many flights. The J-35 aircraft, for example, uses the RM-6C engine, which has difficulty resisting salt spray corrosion, particularly on the rotor and stator blades in the first stages of the compressor.

In the early 70's, the Danish Air Force experimented with several remedies. Flushing the engine with fresh water after each flight helped somewhat with the corrosion on the outer-most blades, but water left inside the engine tended to aggravate corrosion in places that were hard to reach. Corrosion-retardant coatings were also tried, but with limited success. The most effective coatings caused performance problems, because the layers of corrosion inhibitor built up on the compressor blades, altering their aerodynamic profile and reducing their effectiveness. These deposits had to be cleaned

off regularly, which in some cases required engine de-mounting and disassembly, a process not far removed in cost from replacing corroded blades.

In 1975, program managers began to explore a dry air option. The Danish Army had used dry air preservation for many years to eliminate corrosion on stored military hardware, so there was a body of knowledge concerning desiccant dehumidification technology in the military environment, but less experience with aircraft. In warehouse applications, the application a dehumidifier is relatively obvious. The building is sealed, or a lightweight plastic sheet enclosure is built inside a larger building. The permanently-mounted dehumidifier recirculates dry air through the enclosure whenever a humidistat indicates the relative humidity is above 50%.¹¹ In an active-duty aircraft, there are different challenges.

To begin with, there is the question of enclosing the object. To eliminate corrosion, dry air must surround the item in question, and it would hardly be practical to build hangers or lightweight plastic tents to hold all active duty aircraft. The answer, which seems obvious in retrospect, took some time to discover. The engine was the only item at issue, and jet engines are designed for the flow of large amounts of air. Project engineers realized they only needed to seal the intake and outflow, and circulate dry air through the engine.

The standard engine inlet covers were drilled with a hole about 10mm (4") in diameter, and fitted with a short collar to accept the dry air supply hose from the dehumidifier. New covers were made for the leaving side of each engine, and these covers had a similar hole covered by a small flexible rubber patch to act as a simple one-way air valve, allowing air to leave the engine, but not to enter. To keep the installation procedure simple and quick, the project engineers did not bother to return the dry air to the dehumidifier. This dehumidifier configuration is called an "open" system, reflecting the fact that dry air is blown through the engine and out to the weather. A return air or "closed" system would have required extra ductwork, and would have raised the issue of spark-proof (costly) dehumidifiers, since the aircraft were kept fueled and ready for instant operation.

The program was a success from the beginning. Since 1980, dehumidifiers have been connected to all fighters any time they are on the ground for more than two hours. These include the F-16, F-104, J-35 and the J-37 type aircraft. Based on a four-year period, the program managers calculated a consolidated annual labor and material cost savings of \$970,000. The cost of running the dehumidifiers is approximately \$284,000 per year (at an electrical cost of \$0.08 kwh). The initial capital expense of dehumidifiers and flight line power connections was about \$323,000. So a ten-year net savings estimate would be over \$6.5 million. That estimate is conservative, as it does not include the additional cost reduction which comes from lower parts inventory charges, nor has there been any estimate of the dollar value of the operational benefit of having nearly all aircraft mission-ready.

Avionics Corrosion - J-37 aircraft

The Swedish Air Force operates the J-37 fighter aircraft, and began experiments with dry air technology in 1981 after the successful Danish program was brought to their attention. In the Swedish case, there was no major issue of engine corrosion. The engine metallurgy was somewhat different in the J-37, and Swedish aircraft do not have the same percentage of low-level, maritime operations that was typical of the Danish experience. Also, these particular aircraft are kept inside hangers rather than left outdoors, exposed to the weather.

The J-37, however, is like many modern aircraft in that it has a high percentage of aircraft electronics, and the reliability of the aircraft as a whole is strongly dependant on the reliability of that equipment. The Swedish program focused on improving the mean time between failures (MTBF) of the avionics and radar gear. At approximately one major failure for every 7 flying hours, the MTBF was less than desirable.

One of the especially annoying aspects of J-37 maintenance was the "no-fault-found" problem. That is to say, a radar or avionics set would fail on start-up, so it would be replaced, taken to the repair bench and connected to power. When the technician ran through the diagnostic procedure, no fault could be found to explain its failure to work properly in the aircraft. Project engineers suspected that these were humidity-related problems. They speculated that as the equipment warmed up on the test bench, moisture which had been adsorbed into insulation and condensed into connectors, would be driven off by heat, which solved whatever problem prevented start up in the aircraft. As a practical matter, however, each fault delayed launch of an aircraft, and leaving electronics and radar on continuously generated more problems than it solved.

Over a one year period from January to December of 1981, the Swedish Defense Forces conducted a test of failure rates for dehumidified vs. non-dehumidified aircraft. 10 aircraft were equipped with desiccant dehumidifiers, which provided dry air to the air frame through hoses similar to those in the Danish program. 23 aircraft were left without such protection as a test control. After a year, the MTBF of the dehumidified aircraft was about twice that of the "humid" aircraft (7.2 hrs vs. 14.2 hrs) In terms of the radar sets specifically, the MTBF of the 23 humid aircraft was 32.7 hrs compared to 55.7 hrs for the dry aircraft.

Following the test program, all the aircraft were equipped with dehumidifiers. Figure 6 shows how the MTBF continued to improve as the years moved on. During the 12 months of 1985, a follow-up analysis was performed on 52 of the J-37 aircraft that had been dehumidified. In those units, the overall MTBF had lengthened to 20.2 hours—nearly a 300% increase over the "humid" aircraft. Likewise, for the radar sets alone, the MTBF had increased from 32.7 hours for humid aircraft to 101.1 hours for dehumidified aircraft.

One consequence of this success is that the new Saab-built Gripen fighter aircraft has been built with dehumidification in mind. In older aircraft, bulkheads and other structural elements block the flow of dry air through the air frame. In the Gripen, the Swedish Defense Forces decided to design a dry air distribution system into the frame itself, so dehumidified air connected at a single point in the fuselage can be carried directly to each compartment where electronics and other corrosion-sensitive components are located. A similar dry air distribution system is part of the design specification for the new European Fighter Aircraft.

Airframe Corrosion - Boeing 707 aircraft

The Boeing 707 aircraft, in use throughout commercial airlines for over 30 years, has also been widely used by the U.S. Air Force. The EC-135 is used as an electronics platform and the KC-135 is used for airborne refueling operations. Corrosion-related repair costs for these aircraft exceed \$76 million dollars annually, so they have become the subject of a test program which began in December 1991.

The C/KC-135 program office at the Air Logistics Center at Tinker Air Force Base in Oklahoma City, Oklahoma, has placed two aircraft under test at Hickam Air Force Base in Hawaii and two more aircraft at Mildenhall AFB in England. In each location, one aircraft is being supplied with dry air and the other left without such protection. Sensors are located at several points inside the air frame to record temperature and relative humidity. In addition, both passive and active corrosion sensors are placed inside the aircraft so that the internal corrosion rate can be directly compared with fluctuations in relative humidity.

Corrosion at Hickam had been especially severe. In one of the test aircraft, daylight was visible from inside the fuselage at the tail of the aircraft after the vertical stabilizer panels were removed. Corrosion was also extreme in the area around the cannon plug connectors that penetrate the skin. The severity of that corrosion is perhaps due to the electrical current often present at that point. Before the test began, both the test aircraft (dry) and the control aircraft (humid) were inspected and all corrosion damage repaired.

In September, 1992, both aircraft were inspected once again. The dry aircraft showed no visible corrosion in the areas inspected (the wing leading edges, engine struts and forward and aft "hell-holes"). In contrast, the humid aircraft showed exfoliated corrosion damage on the rib structure behind the leading edge flaps on the right wing. There were also spots of exfoliated skin just under the refueling boom pod. Slight pressure from a pen knife produced a hole through the skin at that point. Overall, the damage on the humid aircraft corresponded to a 20% increase in corrosion over the 9-month period, where the corrosion increase on the dry aircraft was limited to less than 1%.

In the less severe humidity of Mildenhall in England, differences between the humid aircraft and the dry aircraft were less obvious as of an inspection performed at the end of February 1993. However, both aircraft had just completed phase inspection, and resulting repair records were not available as of the deadline for completing this paper. A review of the phase inspection repairs may show differences between the humid and dry aircraft for the preceding year. Informally, the maintenance crew chiefs report that the avionics on the dry aircraft seem to be performing more reliably than normal. Standard equipment performance monitoring systems will, at the end of the test period, be able to define this performance improvement quantitatively. Overall, the test results to date show that dry air technology shows promise of limiting airframe corrosion, a widespread problem that has resisted solution through other methods.

Removing Condensed Moisture - Fokker F-28, Boeing 720-B and McDonnell-Douglas DC-9 aircraft
Water vapor which enters an aircraft at ground level can cause problems when it condenses to a liquid in the cooler temperatures at altitude. The problems can be corrosion-related as seen above, and condensed water can cause other problems as well. Specifically, when materials are moistened, the fungal spores present in all environments (typically 3,000 to 5,000 spores per cubic meter in humid weather at ground level¹²) can begin to grow, producing the characteristic musty odors common to some older aircraft. Additionally, condensed water represents a significant amount of weight, which the aircraft operator must pay for with extra fuel consumption. To reduce fuel costs, eliminate odors and limit corrosion, several research projects have focused on drying commercial aircraft interiors between flight operations.

The Fokker F-28 is a short-range passenger jet used extensively through Europe. In 1988, an F-28 aircraft operating from Linjeflyg airport in Sweden was equipped with a datalogger and sensors to record temperature and humidity changes during ground and flight operations. Readings were taken continuously from October 11th through October 31st and again from November 24th through December 14th. The aircraft made several flights every day, operating within Sweden. Sensors were mounted at three points: inside the passenger compartment, between the cabin wall and cabin insulation and inside the insulation batts themselves. (see figure 7) The data showed that because of wide temperature changes from ground to cruising altitude, the relative humidity generally rose above 90% inside the insulation and to over 70% between the cabin and the insulation surfaces. While there was no sensor located at the external skin on the far side of the insulation, one can see by the temperatures inside the insulation that at the colder outer skin of the aircraft, condensation was taking place because the dew point exceeded the surface temperature. This condensation phenomenon prompts the question of how much water is actually produced by the process in a commercial airliner. In other words, how important is this problem?

In 1986, a test was performed on a Boeing 720 aircraft in Denmark. A single aircraft became available for experiments while undergoing extensive maintenance inside a hanger. A desiccant dehumidifier was attached to the ground cooling connection and dry air was circulated through the aircraft while maintenance operations were underway. Of the 15-day test period, the doors of the aircraft were open for maintenance (exposed to the humid air of the hanger) for over 110 hours, or about 30% of the elapsed time. In the 250 hours when the dehumidifier could be fully effective, the dry air removed 250 Kg of water from the aircraft, an average of one kilogram per hour. At 1993 fuel costs and engine efficiencies, removing those 250 kilos saves the aircraft operator more than \$3,500,000 per year. (\$14,285 per kilo per year, as estimated by SAS project engineers in February, 1993)

Commercial airliners, however, do not normally sit in one place for 15 days. They are very active and must be fully utilized to generate profits for their operators. So although there may be a condensation problem which leads to excess fuel costs and corrosion—can the problem be effectively controlled by drying during the short layovers which are typical of commercial flight operations? Some reasons for optimism concerning this issue are found in the results of a test to dry a DC-9 aircraft operated by Scandinavian Airlines (SAS) in Sweden.

In that 8-week test, the aircraft was connected to desiccant dehumidifiers at the end of each day's flight. Connections were made through the ground cooling system, and air was returned to the dehumidifier from the ground cooling outlet. Returning the cabin air allows the dehumidifiers to dry it more deeply than would be possible with an "open" system, which would have used fresh air, which is somewhat more humid. Figure 8 shows the results of that test. The dehumidification system consistently removed between 17 and 35 kilos per drying period.

The project engineers noted that moisture desorbs from different materials at different rates. The moisture contained in the air was removed quite rapidly—it represented about 1.5 kg and cabin air was dried to its minimum moisture content within 20 minutes. Moisture in carpet and upholstery totaled approximately 24 Kg, and to reach a dry state (the point below which no further drying could be measured), the upholstery and carpets required approximately 3 hours. The rest of the moisture removed by the dehumidifiers came from foam in the seat cushions and from insulation in the cabin walls. These results are quite encouraging, and the project engineers feel that even faster drying rates can be achieved by designing a means of passing dry air more directly through the insulation.

Summary

In summary, these and other dehumidification programs suggest that:

1. Drying Engines is simple and inexpensive

As engines are designed for airflow, and come equipped with standard covers, keeping them dry with desiccant dehumidifiers is very simple and need not disrupt the normal maintenance routine. If engine corrosion is a problem, dehumidifiers can provide an economical solution.

2. Using dehumidifiers to dry avionics saves a great deal of money

Disruptions and repairs caused by corroded avionics are very expensive. Keeping them dry with desiccant dehumidifiers does involve some custom fitting of air hoses, but can save the installation cost within the first year.

3. Airframe corrosion merits additional research in different aircraft

Airframe corrosion is very complex, but favorable results have been obtained with desiccant dehumidifiers in several cases. Aircraft operators may wish to examine the technique further as fleets age and become more sensitive to this problem.

4. Removal of condensate may save both fuel and corrosion costs

Research has established that condensation can occur inside an airframe because of surface temperature changes at altitude. Using dehumidifiers is one promising way to remove the condensation and avoid odors, excess fuel costs and corrosion accelerated by the condensate.

Finally, in most corrosion problems, the environment is not a variable. In recent years, however, desiccant dehumidification technology has begun to provide the corrosion engineer with a new tool: the ability to remove the electrolyte from the corrosion reaction and therefore solve complex problems in a simple, cost-effective way.

References

- ¹ G. Cooke, P Vore, C. Gumeinny, G. Cooke Jr., E. Lunsford & H. Kealy. *A study to determine the annual direct cost of corrosion maintenance for weapons systems and equipment in the United States Air Force.* (Final Report, Contract #F09603-89-C-3016, 1979) Prepared for the Warner-Robbins Air Logistics Center, Robins Air Force Base, GA 31098 USA.
- ² Brown, Alan S. *Industry seeks tonic for aging aircraft* (Materials Performance, September, 1992. NACE, Houston, TX USA)
- ³ Ibid
- ⁴ Allen, Frederick, *The airplane as a computer peripheral* (American Heritage of Invention & Technology, Winter 1992, Forbes Inc. New York, NY USA)
- ⁵ Ailor, W.H. (Ed) *Influence of water vapor (on fatigue life of metals)* (pp 971-972 of *Atmospheric Corrosion*, 1982, Wiley-Interscience, NY, NY USA)
- ⁶ Hercules Operator's Conference - HOC'92 (Lockheed Airfield Service Department, October 1992, Marietta, GA USA)
- ⁷ Fristad, Stig, *Report to SAS on drying rates of DC-9 aircraft* (1986, A.B. Carl Munters, Sollentuna, Sweden)
- ⁸ Brundrett, G.W. *Criteria for moisture control* (1990, Butterworth-Heinemann Publishing, London, UK)
- ⁹ Executive Engineers Committee Report, *Mold & mildew in hotels and motels* (1991, American Hotel & Motel Association, Washington, DC USA)
- ¹⁰ Harriman, L.G. III *The Dehumidification Handbook* (2nd Edition) (1990, Munters Cargocaire, Amesbury, MA)
- ¹¹ Harriman, L. G. III *Prevention of metallic corrosion in storage areas* (1985, Proceedings of the 1985 symposium on moisture & humidity, Instrument Society of America, Research Triangle Park, NC USA)
- ¹² *Mold & mildew in hotels & motels*

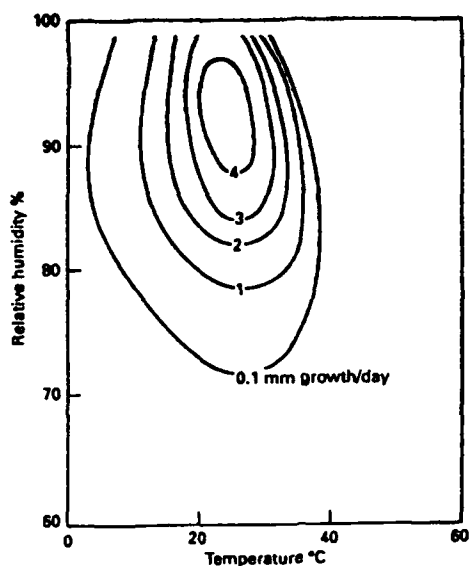


Figure 1
 At high humidities, fungal spores can dissolve the nutrients they need for growth from the surfaces on which they have landed. This graph shows that the growth rate for *Aspergillus Ruber*, a common fungus responsible for musty odors, is 40 times greater at 90% rh than when humidity is kept below 70% rh. (Brundrett, G.W., *Criteria for moisture control*)

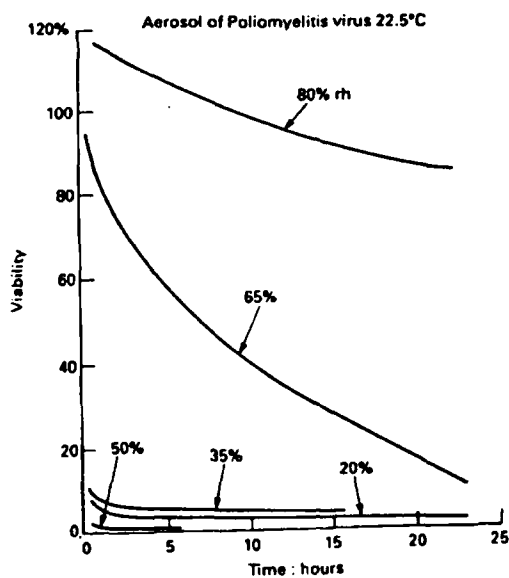


Figure 2
 Many bacteria and viruses also thrive at high humidity but perish when humidity is low. The polio virus, for example can survive far longer in humid environments than in dry air. (Brundrett, G.W., *Criteria for moisture control*)

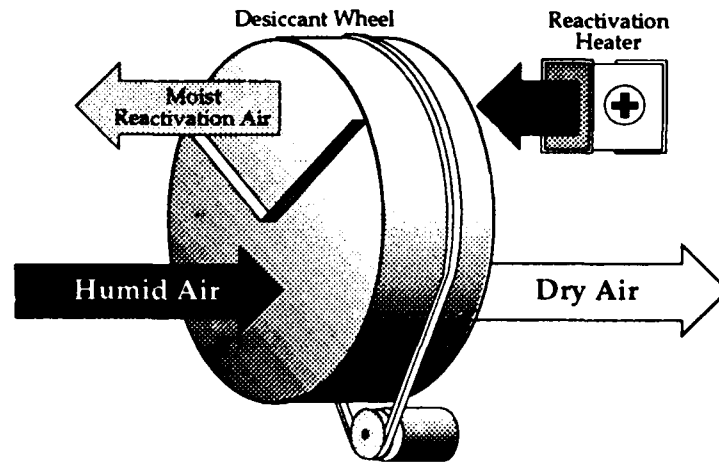


Figure 3
In a desiccant wheel dehumidifier (DEW), a high-capacity desiccant is impregnated into a lightweight corrugated ceramic matrix shaped like a honeycomb wheel. The wheel rotates between air being dried (process air) and air which reactivates the desiccant for re-use (reactivation air) Dry air is produced continuously, and the unit can dehumidify air even at temperatures below freezing.

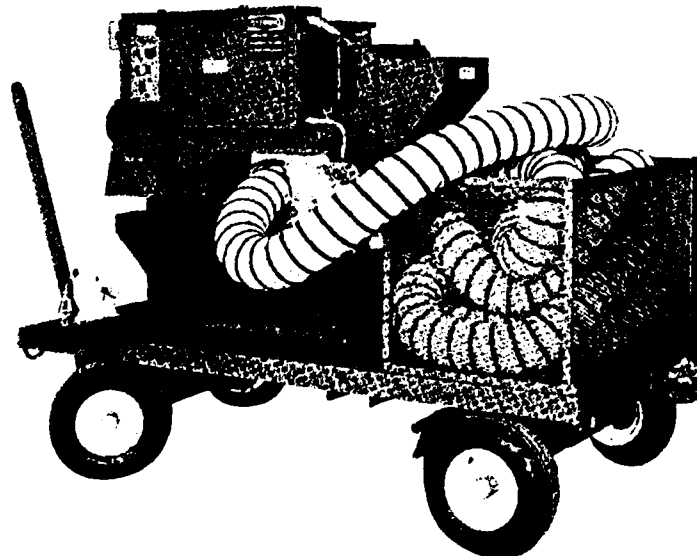


Figure 4
A typical desiccant dehumidifier used for drying aircraft.

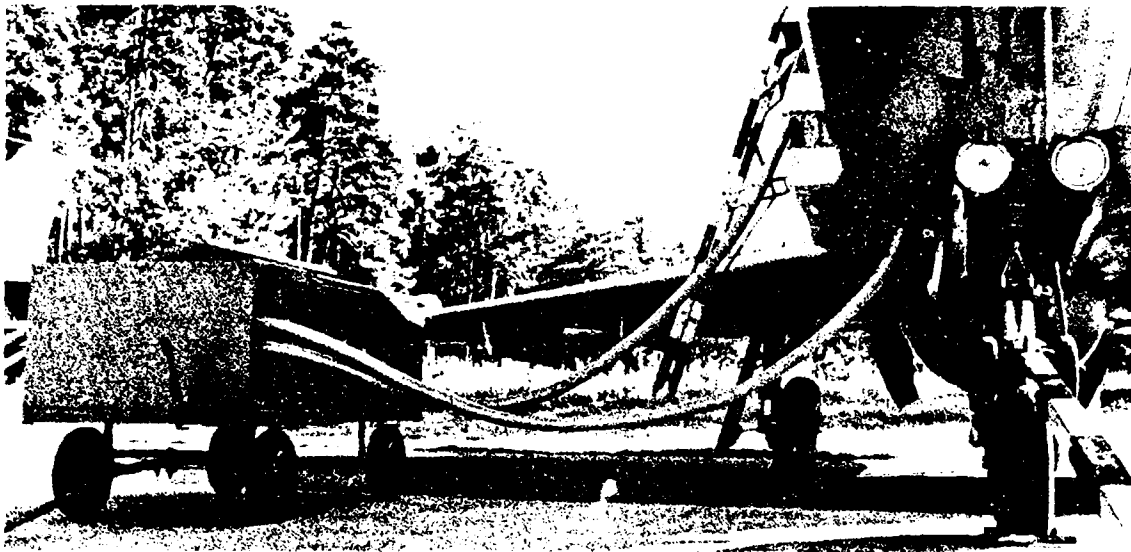


Figure 5
Connections between a desiccant dehumidifier and an aircraft vary according to the purpose of the project. In this case dry air is distributed to both the cockpit electronics and the engine air inlets.

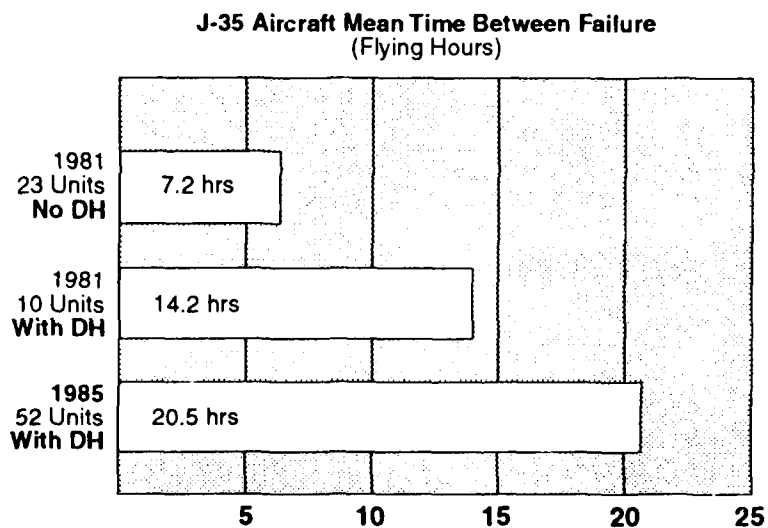


Figure 6
Following the 1981 test, 52 aircraft were equipped with desiccant dehumidifiers and the MTBF continued to improve. The figure shows the 1985 MTBF was 20.5 hours with dehumidification where without such equipment the original MTBF was 7.2 hours.

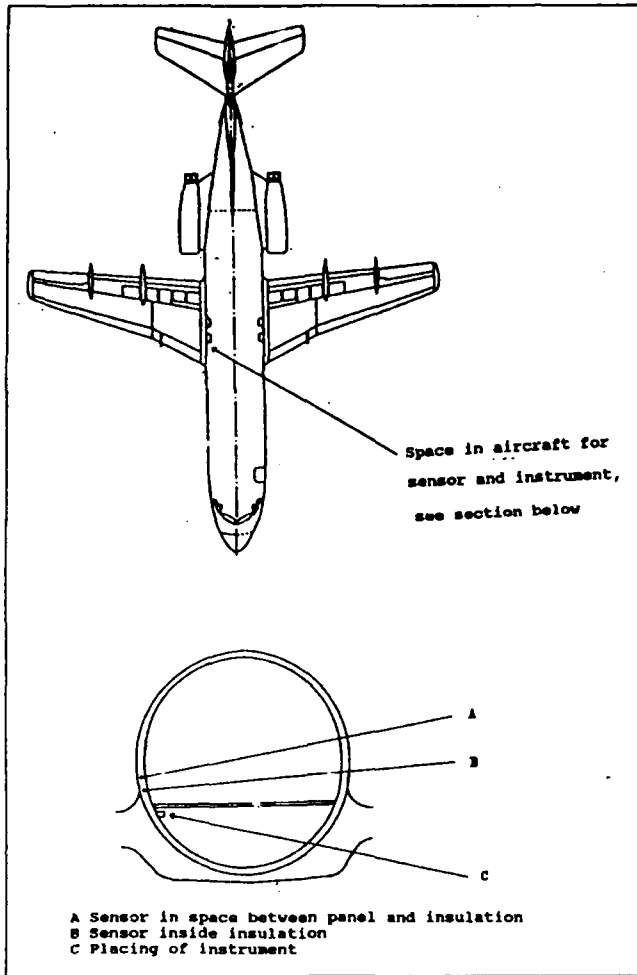


Figure 7
 A Fokker F-28 aircraft was equipped with temperature and humidity sensors to track humidity changes during normal flight operations. The test showed that the relative humidity in the insulation regularly exceeded 90%, which indicates that condensation occurs on the cold side of the insulation, where surface temperatures are frequently below the air dew point.

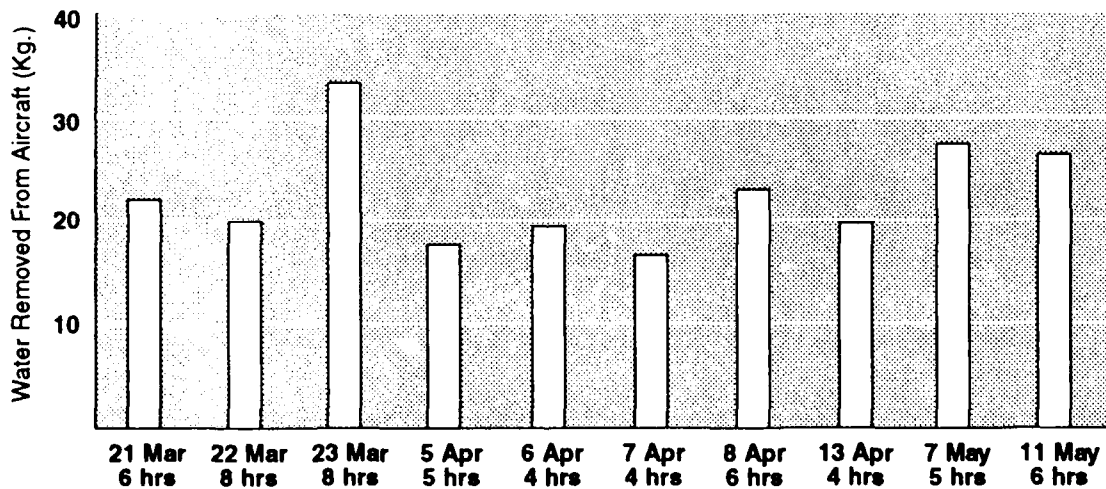


Figure 8
 A test program was conducted on an SAS (Scandinavian Airlines) DC-9 to determine how much water could be removed by dehumidifiers in the short time between normal flight operations. As the graph shows, a great deal of moisture was removed, which indicates that drying operational aircraft is indeed practical even when very little time is available for connecting dehumidifiers.

Corrosion Contribution to Environmental Cracking Failures of Critical Aircraft Parts

John J. DeLuccia, Ph.D.
Senior Materials Engineer
Naval Air Warfare Center/Aircraft Division
Warminster, PA 18974

Abstract

Four separate and distinct failures, attributable to corrosion are presented and analyzed. They are: A fuselage crown failure caused by multisite damage; A steel landing gear lug fitting caused by Hydrogen embrittlement; A high pressure engine disc caused by pitting; and a helicopter transmission gear caused by crevice corrosion. Each of these failures were catastrophic in that they occurred without warning. The contribution of corrosion to the initiation and/or propagation of the failure is noted. Failure avoidance is discussed.

Key terms: corrosion, stress corrosion, corrosion fatigue, environmental embrittlement

Introduction

Aging aircraft fleets are experiencing increased structural failures due to corrosion. The effects of undetected and untreated corrosion can lead to catastrophic consequences, and this is especially true of older aircraft which may have experienced cumulative corrosion and fatigue damage. As described elsewhere, aircraft corrosion events can be viewed from the standpoints of time dependent, time-related, and time-"independent" mechanisms.⁽¹⁾ Time dependent corrosion such as pitting, exfoliation, and crevice corrosion will, if not prevented or controlled, accumulate to unsafe limits. Often times these mechanisms act as the precursors to cracking that ultimately results in catastrophic failure. At least two of the failures described here fall in that category. The time related and time independent corrosion events involve superimposed mechanical effects that can adversely affect aircraft structural integrity. The interaction of the electrochemical event of corrosion with the accumulated or simultaneous action of stress, either sustained or cyclic, can lead to cracking damage. The phenomenon of corrosion fatigue of airframes is not always acknowledged because of its complexity.

Fatigue failures are time related and cycle dependent. Thus, the number of flights (stress cycles) plays a key role in this type of airframe failure. The phenomena of stress corrosion cracking and environmental embrittlement are neither strongly time dependent or cycle related. All that is needed is a specific corrodent or embrittling agent and an enduring tensile stress. Thus even a new aircraft with the proper combination of stress and environment can experience cracking over a very short period of time. Since a finite, albeit short, amount of time must pass before cracking occurs, these phenomena are described as time "independent" with the independent in quotation marks. As an example, when smooth tensile bars of forged 7075-T6 aluminum are stressed, usually at 50% of the yield strength, and then alternately immersed in a 3 1/2% salt (NaCl) solution, stress corrosion cracks form within 24 hours. The cracking of aluminum alloys thus described is classified as stress corrosion cracking. The event occurs by the combined and simultaneous action of corrosion and a static tensile stress.

The other "time independent" event that can lead to failure is environmental embrittlement where a particular embrittling species enters the metal through an electrochemical or physical process. Hydrogen embrittlement of high strength steel is an example.

The four failures presented here will be identified as to their corrosion time dependency as well as to the mechanism of failure.

Fuselage Crown Failure

In 1988, a commercial airliner operating out of Honolulu, Hawaii experienced an explosive decompression and structural failure at 24,000 feet. Approximately 18 feet of the cabin fuselage skin and structure aft of the cabin entrance door and above the passenger floorline separated from the airplane during flight. This spectacular failure is depicted in Figure 1. The National Transportation Safety Board described the probable cause of failure as a result of fuselage lap joint disbonding, ensuing corrosion, and finally fatigue cracking around fasteners leading to multisite damage (MSD).⁽²⁾ The failure path is traced to the fastener patterns of the mid-fuselage cold bond lap joint. A portion of the inner bonded surface of the failed bonded and riveted lap joint is shown in Figure 2. Note the absence of the bonding material and the extensive corrosion of the aluminum skin. Figure 3 is a portion of the fuselage that shows the multisite damage of the upper row of rivets from the subject aircraft.

The mechanism of this failure is simple and straightforward. The lap joints of the fuselage contain three rows of rivets as well as a cold cured epoxy faying surface bond. With time and the marine environment that this particular aircraft endured, the faying surface bond degraded so that ingress of a corrosive electrolyte was facilitated. The electrolyte was provided by the daily condensation of salt laden moist air. The corrosion that resulted was accompanied by low cycle fatigue of the fuselage that endured a cycle of stress upon each cabin pressurization-depressurization (each ascent and descent). This aircraft was exposed to this conjoint action for nineteen years. With the degradation of the bond, the epoxy and scrim cloth acted as a wick for moisture causing subsequent corrosion of the 2024-T3 aluminum skin surface. With cabin pressurization cycles, the phenomenon of multisite damage by corrosion fatigue ensued (Figure 3). This ultimately led to the failure. Thus the time dependent event of general corrosion, (Figure 2), led to the time and cycle related event of corrosion fatigue with its accompanying catastrophic consequence.

Main Landing Gear Lug Failures

In 1980, the U.S. Navy took possession of five new F-18 fighter aircraft. Within months, all five of the aircraft experienced main landing gear lug failures. All failures were discovered while the aircraft were sitting on the tarmac. All of the failures occurred in a stressed lug on the axle beam. The gear is stored under stress during flight. During this period, these aircraft were undergoing tests and the landing gear were being assembled, disassembled and instrumented. During the disassembly the bearings were removed from the lugs and the internal surface of the lugs were chemically treated. It should be pointed out that the landing gear of forged, high strength 300M steel was coated with aluminum by the ion vapor deposit (IVD) process. When the snug fitting bearings were removed from the lugs, much of the thin aluminum coating was removed exposing the underlying high strength steel. Oblivious to this fact, the maintenance technician treated the surface with a chromate conversion coating appropriate for aluminum. The conversion coating, containing an acid etchant, corroded and embrittled the underlying steel. The embrittlement of the steel was caused by the entrance of hydrogen atoms, a concomitant to acidic corrosion, and was sufficient to cause failure of the lug under sustained loading. The characteristic intergranular fracture surface was noted on the failed steel surfaces as is shown in the lower right photograph of Figure 4. Within 24 hours after one of the failures occurred, the diffusible hydrogen content within

the axle beam adjacent to the lug was measured by an electrochemical technique (barnacle electrode). The amount measured was over 4 times higher than untreated steel. The barnacle electrode method for measuring hydrogen is described in reference (3).

Engine Compressor Disk Failure

In the spring of 1991, a commercial, cargo jet airliner aborted a flight on the takeoff roll after unsuccessfully attempting to extinguish a fire in a failed engine. The fire spread to the cabin and destroyed the aircraft along with its cargo of U.S. mail. It was reported that the fire was caused by the rupture of the engine's ninth stage high pressure compressor disk.⁽⁴⁾ Fragments from the engine severed fuel, oil, and hydraulic lines and penetrated the fuselage. Examination of the engine showed the ninth through twelfth stage high pressure compressor disks to be severely corroded and pitted. Figure 5 depicts the corrosion and pitting on the 11th stage compressor disk. The compressor disks are made of high strength, low alloy steel that were initially electroplated with a combination of nickel and cadmium. With time and exposure to corrosive environments, the plating is corroded away thereby exposing the underlying steel. In this particular case, the engine in question is sparingly used. That is, the engine was not used on a regular basis. Because of corrosion problems associated with low use, these engines are now getting more attention. Specifically borescope inspections of the high pressure disks are now being made to detect corrosion as depicted in Figure 5. Figure 6 shows the failure of the ninth compressor disk of the subject aircraft. Note the total circumferential rupture (crack) of the disk. Investigators traced this failure to metal fatigue caused by corrosion. It is precisely the corrosion as shown in Figure 5 that can initiate/facilitate fatigue. The corrosion pits shown in Figure 5 can act as chemical notches that concentrate stresses and hence facilitate crack initiation in the fatigue mode. If the cyclic loading is occurring while the crack is wet, the fatigue propagation is further accelerated by corrosion. This type of failure is a classic example of a time dependent corrosion event, pitting, occurring in the down time of the engine, i.e., moist air contaminated with the chlorides or other pollutants, condensing on the cold surface of the disk daily provides the electrolyte for corrosion. If the engine is under utilized this electrolyte acts on the surface for extended periods giving the corrosion and pitting observed in Figure 5. The situation can then degenerate to a failure mode that is time/cycle related when the part is mechanically loaded, i.e., when the engine is used. It is theorized that the rupture in the subject disk was caused by corrosion in the "down time" followed by corrosion fatigue. The fatigue crack propagated to the point of overload resulting in the complete circumferential rupture of the disk.

Helicopter Transmission Gear Failure

In the fall of 1986 a helicopter providing transportation for North Sea off shore oil workers experienced a forward transmission gear failure that resulted in the loss of the aircraft with the attendant loss of 38 lives. The gear in question is the steel spiral bevel ring gear held in place by 24 steel bolts with an aluminum bronze shim on its upper surface to retard fretting. The location of the gear and a typical corrosion site is shown in Figure 7. The catastrophic failure of this gear was determined to be the result of the combined action of the environment (corrosion); imposed stresses; as well as environmental surface wear (fretting).⁽⁵⁾ The gear in question was recovered from the accident and discovered to have unusual circumferential corrosion grooves under the shim. For corrosion of the gear to occur, the environment must have access to the metal that is corroding. In this particular case the environment consists of an aqueous film containing chlorides at the faying surface of the gear and shim. It is believed that this film

gained access to the subject gear as a result of condensation of the moist, salt laden air surrounding the transmission during the down time, e.g., overnight.

The enlarged depiction of Figure 7 is a sketch of the cross section showing the gear, shim and condensed film of moisture. The operative mechanism for the corrosion grooves is crevice corrosion caused by the geometry of the gear and differences in the partial pressure of oxygen in the condensed film. In Figure 7, this differential aeration causes region A on the gear to have a lesser O_2 concentration than region C. This difference creates a differential aeration electrochemical cell causing region A to act as an anode (that which corrodes) and region C to act as a cathode (that which does not corrode). It should be noted that the presence of the Al bronze shim could also act as a cathode thereby causing greater corrosion at the A region. With time, the anode region, A, corrodes causing a build up of electropositive ferrous ions, Fe^{++} . These ions attract chloride ions and then hydrolyze (combine with water). The products of this hydrolysis reaction are ferrous hydroxide and free hydrochloric acid. Thus even if the pH of the film is neutral at the outset, after a period of time, the pH in the crevice where the hydrochloric acid is collecting is much lower and hence much more aggressive. This type of corrosion attack is considered autocatalytic in nature.⁽⁶⁾

This gear failure is further complicated by the accompanying phenomenon of fretting (wear). In the absence of a specific corrodent, fretting tends to occur at the gear shim interface. Thus the corrosion previously described is accompanied by fretting and fretting wear particles (oxides). The previously described condensed film of salt laden moisture combined with the fretting wear particles form a corrosive slurry that under the conditions of dynamic loading (gear motion) accounts for the observed grooves and trenches that lead to the failure. Thus the corrosion/wear mechanism acted as a precursor to failure. It is believed that cracking (either stress corrosion or corrosion fatigue) was initiated at the base of the previously described trenches in the corrosion grooves. The cracking then proceeded via a corrosion fatigue mode, circumferentially to a point and then went radially to total gear failure. This is another example of a catastrophic failure that was initiated by a time dependent corrosion event; crevice corrosion.

Summary

From the four failures described herein, it is evident that chemical deterioration (corrosion) of susceptible aircraft structures can lead to catastrophic failures of critical parts. Because of the unforgiving nature of aircraft failures, it is not sufficient to treat the inevitable corrosion of aircraft as a low level maintenance problem that can be handled routinely. The fuselage crown failure and the helicopter gear failure show the importance of initial design on subsequent corrosion events. Both configurations allowed for corrosion access. The landing gear failure shows the importance of a thorough knowledge of maintenance chemical actions on high strength materials, e.g., embrittlement of high strength steel exposed to a chemical conversion coating meant for aluminum. The engine disc failure points to frequency of inspection and consideration of corrosion during the down time of an engine. The seemingly benign environmental conditions of parts not in use can cause serious corrosion over a period of time.

Thus it is evident that aircraft corrosion in general, and the more time critical phenomena of corrosion fatigue, stress corrosion, and environmental embrittlement in particular demand new approaches that include factoring in corrosion at the design stage of the aircraft (damage tolerance to include corrosion), the use of new products, alloys and processes, and a vigilance in maintenance and inspection techniques not now in evidence.⁽⁷⁾

Acknowledgments

Mr. Fred Sobeck, the Aging Aircraft Program Manager for the FAA is gratefully acknowledged for helpful discussions and photographs of some of the work presented. Mr. Roy Cunningham of the Boeing Corporation is also gratefully acknowledged for information, advice, and discussions he provided. Finally, Dr. Thomas Fluornoy of the FAA Technical Center is acknowledged for his support of this work.

References

1. DeLuccia, John J., "The Corrosion of Aging Aircraft and its Consequences," 32nd Structures, Dynamics, and Materials Conference of the American Institute of Aeronautics and Astronautics, Conference Proceedings, April 1991, Part 2, p. 1667.
2. Aircraft Accident Report #NTSB/AAR-89/03, National Transportation Safety Board, Washington, DC, June 14, 1989.
3. DeLuccia, J. J., and Berman, D. A., "An Electrochemical Technique to Measure Diffusible Hydrogen in Metals (Barnacle Electrode)," Electromechanical Corrosion Testing, ASTM-STP 727, American Society for Testing and Materials, 1981, pp. 256-273.
4. Aviation Week and Space Technology, June 24, 1991, p. 68.
5. DeLuccia, J. J., "Report on the Failure of a Spiral Ring Bevel Gear from the Forward Transmission of a British Airways Helicopter," Unpublished Report to Boeing Helicopter Co. #229, of Jan. 22, 1988.
6. Fontana, M. G., "Corrosion Engineering," 3rd Ed., McGraw Hill, (1986), pp. 109-151.
7. DeLuccia, J. J., "Aircraft Materials and Processes for Corrosion Prevention and Control." Durability of Metal Aircraft Structures, Proceedings of International Workshop on Structural Integrity of Aging Airplanes, Atlanta Technical Publications, Atlanta, GA, (1992), pp. 311-324.

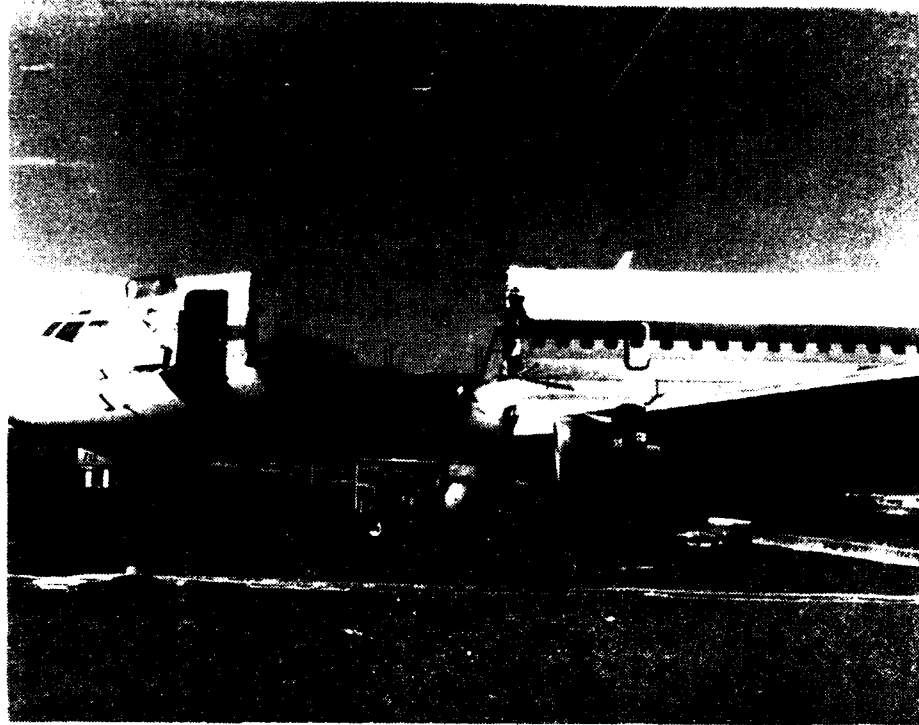


Figure 1. Aircraft showing fuselage crown failure Manifested by missing upper lobe.



Figure 2. Failed inner bonded lap joint surface. Note missing adhesive and corrosion. (magnified 3X)

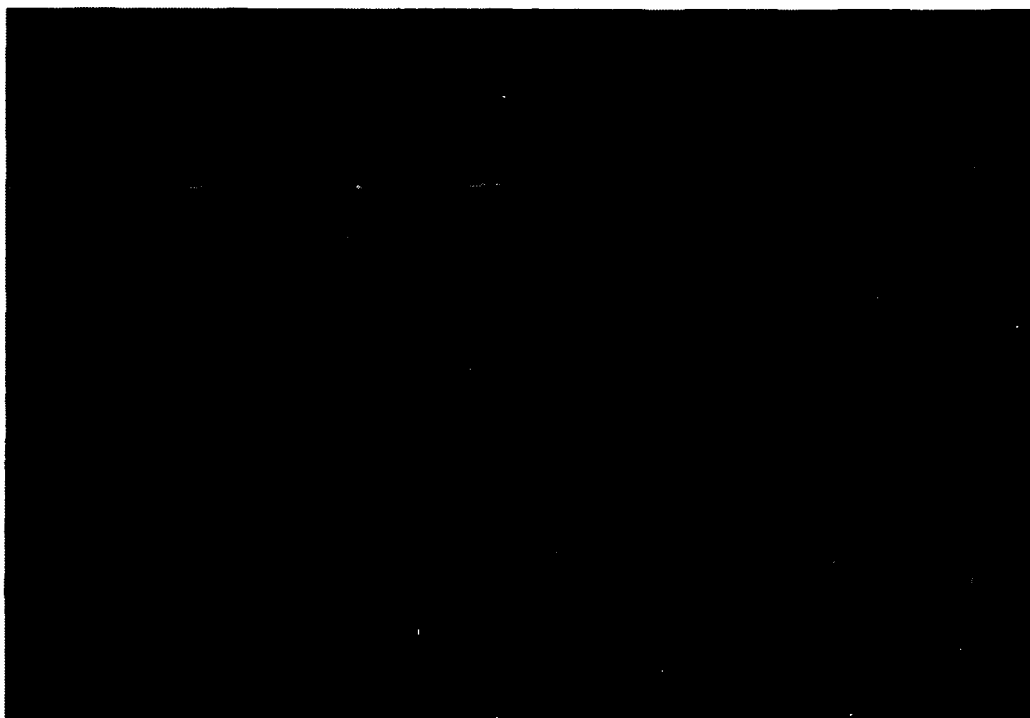


Figure 3. Outer surface of lap joint showing multisite damage around upper row of rivets. (magnified 3X)

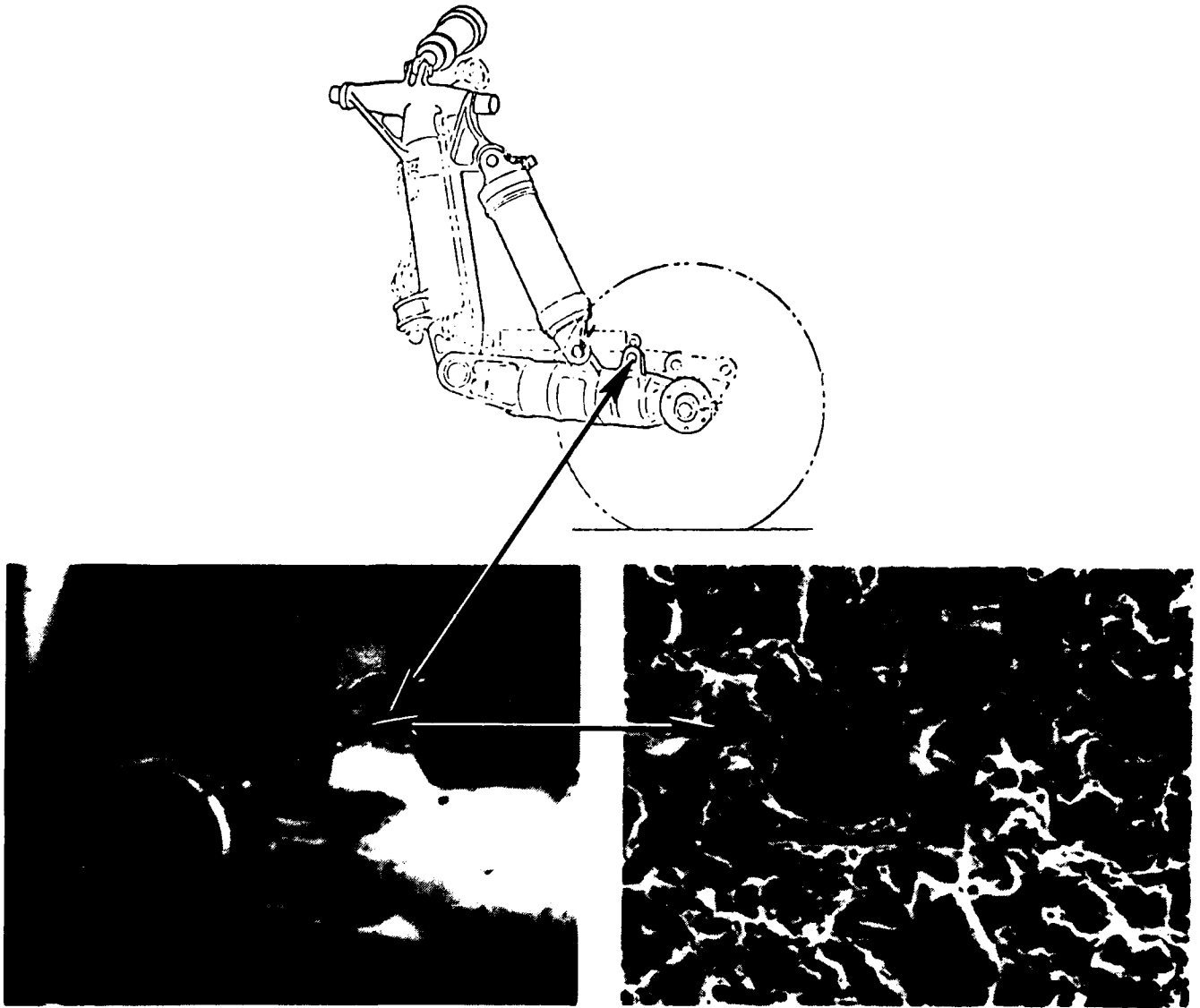


Figure 4. Navy F-18 main landing rear lug failure caused by hydrogen embrittlement. Fracture surface of 300 M steel lug in lower left photograph. (magnified 1000X)

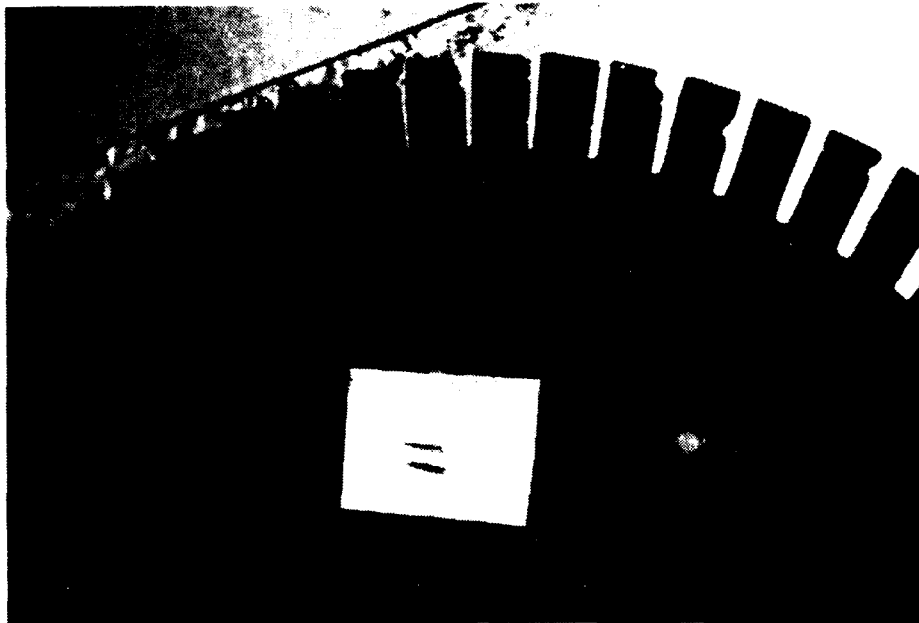


Figure 5. Eleventh stage compressor disk of Ni-Cd plated steel showing Corrosion pitting.

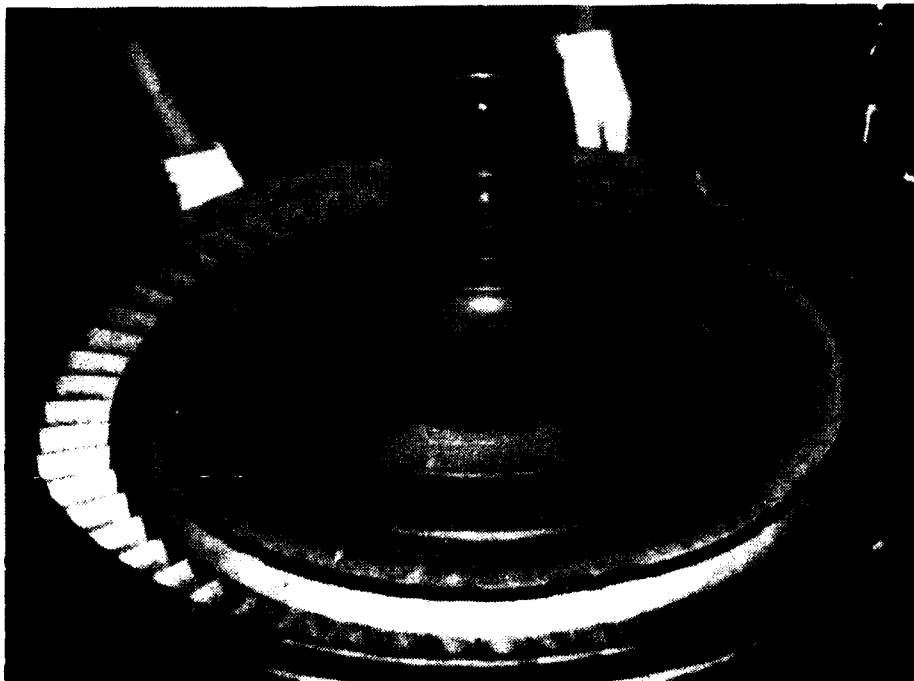


Figure 6. Circumferential rupture (crack) of ninth stage compressor disk.

FORWARD TRANSMISSION GEAR TRAIN

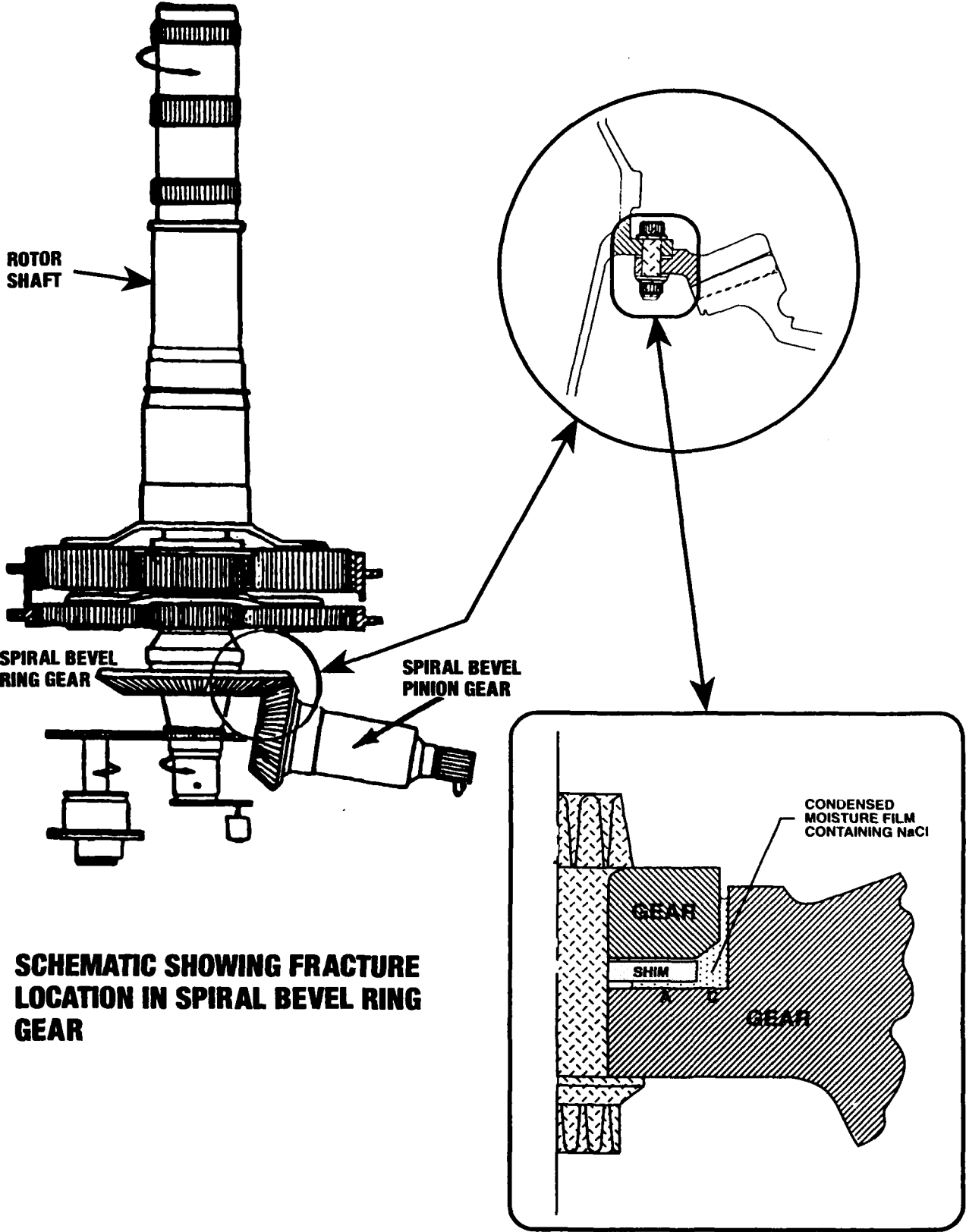


Figure 7. Failure location of steel spiral bevel ring gear form a helicopter transmission.

Use of Volatile Inhibitors (VCI's) for Aircraft Protection

Alex Eydelnant
Cortec Corporation
4119 White Bear Pkwy
St. Paul, MN 55110

Boris Miksic
Cortec Corporation
4119 White Bear Pkwy
St. Paul, MN 55110

Stephen Russell
Commander Corps & Fort Louis
AFZH-DEQ
Fort Louis, WA 98433-5000

ABSTRACT

A variety of tests were performed to evaluate the feasibility of VCI's application for maintenance and protection of Navy aircraft from corrosion damage.

In the test program such procedures, as a Salt Fog Cabinet ASTM B-117 and Humidity Chamber ASTM D-1748 were performed to evaluate the protection properties of inhibitor A to be applied primarily on airframes, armaments and mechanical parts.

Inhibitor A is a complex mixture of amine salts of aromatic sulfonic acids in the carrier, and volatile carboxylic acid salts as a vapor phase inhibitor. Inhibitor A possessed both contact and vapor phase inhibition properties.

Inhibitor B, a polyethylene film extruded with VCI compound was specified in the test program. Inhibitor B is a mixture of amine carboxylates. This inhibitor was evaluated as a barrier material possessing VCI and desiccant properties. Specially designed climatic tests have been performed to assess protection properties of this inhibitor.

Inhibitor C, containing triazoles, amines, carboxylic acids, salts and esters, was tested using the Battelle Flowing Mixed Gas test + ASTM-1748. The Battelle Flowing Mixed Gas Test and ASTM-1748 have been applied on the following metals: steel, aluminum, copper, gold, silver, solder, brass in order to simulate the effect of indoor environments on electronic components and materials. The Battelle test is considered to be a realistic, accelerated environmental test since it takes into account the synergistic effect of low concentrations of relevant pollutants, temperature and humidity. The test condition simulated was a Class III environment.

KEY TERMS: Vapor corrosion inhibitor, Navy aircraft maintenance, protection of avionics equipment.

INTRODUCTION

This paper will address VCI materials developed by Cortec Corporation that have provided advances in corrosion control of naval aircraft.

Prevention of aircraft deterioration is the central theme of any maintenance effort including the Naval Aviation Maintenance Program (NAMP). The possibility of significant corrosion damage is greatest when aircraft are inactive, in transport, in storage, or when poorly protected and maintained. As a general rule, tactical aircraft spends only about 40 % of their time in active flight missions. Therefore their reliability and sustained performance are a direct result of protective and preventive maintenance measures on the flight deck or hanger.

The materials used in the construction of aircraft include aluminum alloys, magnesium alloys, high-strength steels, titanium alloys, composite materials and other non-ferrous metals used in the avionics equipment. Numerous corrosive agents can have an adverse effect on the aircraft structural materials. Water is always present, usually not from exposure to rain, but as a result of condensation; spillages and leaks of hydraulic fluids, lubricants and fuel; highly corrosive chloride and sulfate ions in the air - to name just a few. This list of potential environmental dangers to naval aircraft is not all inclusive. It is influenced and continually altered by advances in technology, geographical location and strategic/tactical threat.

It is not surprising that over the years, examples of all the common types of corrosion have been found on aircraft. These include crevice, pitting and exfoliation corrosion on aluminum alloy components; galvanic corrosion at dissimilar metal contacts and dynamic corrosion processes such as stress corrosion cracking; all types of electronic corrosion; corrosion fatigue and fretting corrosion.

In order to maintain military aircraft as a ready to mission unit, different maintenance schemes can be employed. The protection schemes currently used on military aircraft have been evolved over a period of 30 to 40 years and are designed to protect the aircraft throughout its life. There are six traditional classes of corrosion preventive systems commonly used in the military and commercial aviation. They are: protective coatings (polyurethanes, epoxies); inorganic finishes (chrome, cadmium plating, anodizing); corrosion-inhibitive compounds (water displacing oils); sealants (silicones, polysulfides); corrosion-resistant alloys; desiccants.

A largely overlooked application for aircraft protection is the technology of volatile corrosion inhibitors (VCI). This paper is an attempt to fill this gap and provide the interested audience with prospects of possible use of these compounds for aircraft maintenance and protection.

EXPERIMENTAL PROCEDURE

Materials and Apparatus

The procedures for the general corrosion tests performed on inhibitor A followed the ASTM practices B-117 and D-1748. Low carbon steel Q-panels were utilized according to SAE 1010 as the surface preparation before inhibitor A application. The original finish was used and cleaning with methanol was performed to avoid surface contamination.

A special apparatus (see Fig. 1) was designed for the testing of Inhibitor B (extruded with vapor corrosion inhibitor in polyethylene film). All metal samples were polished, degreased and cleaned with methanol. Steel, copper, brass and aluminum panels of 7x5x0.2 cm each were mounted on the test holder and packed into inhibited polyethylene film bag, and a bag of nontreated polyethylene as a control. The bags were sealed airtight. Inside each bag was approximately 20 grams of water in the form of a saturated sponge. The samples were arranged inside the test assembly so as not to be touched by the bag. The bags were placed in a temperature cycling climate chamber so that water within the bags could condense on the samples and the bag walls. The temperature settings were 45° C (113° F) and 15° C (59° F) respectively for each cycle. Every four hours the temperature was switched from one setting to another. The duration of the test was 42 cycles or 168 hours. Water condensed on the samples was monitored periodically by visual inspection. The surface area of the bag interior was 0.1 m².

As the test procedures for the inhibitor C - a product specially formulated for protection of the aircraft electronic equipment - two methodologies were used:

- * ASTM D-1748 Humidity Cabinet Method
- * Battelle Flowing Mixed Gas Test

The ASTM D-1748 accelerated corrosion test was performed at elevated temperature and humidity. The extent of protection provided by the inhibitor C was determined. The following metals were used in the test: silver, solder, copper, brass and steel. Test panels of 3.75 x 7.5 x 0.16 cm were cleaned with methanol before use. For each metal one panel was untreated, another one was sprayed with the inhibitor C. Panels were allowed to air dry and then placed in an ASTM D-1748 humidity cabinet with relative humidity of 100 % and temperature of 50° C.

The Battelle Flowing Mixed Gas Test was used to determine the effectiveness of the inhibitor C in a polluted environment. The test was developed in Battelle Laboratories to simulate the effect of indoor operating environments on electronic components and materials. The following metals were used in the test: copper, silver, gold and steel. The metal samples were cleaned with methanol before the application of inhibitor C. Environmental conditions inside the chamber were:

| | | | | |
|----------------------------------|---|---------|---|--------|
| a) Temperature | : | 30° C | ± | 2° C |
| b) Relative humidity | : | 75 % | ± | 2 % |
| c) Cl ₂ concentration | : | 20 ppb | ± | 5 ppb |
| d) NO ₂ | : | 200 ppb | ± | 50 ppb |
| e) H ₂ S | : | 100 ppb | ± | 20 ppb |
| f) Exposure time | : | 7 days | | |

After stabilization, the test samples and control coupons were placed in the chamber no closer than 5 cm from each other or the chamber. After placement of the samples in the chamber, it was allowed to re-stabilize and adjust as required to maintain the specified concentrations and conditions.

RESULTS AND DISCUSSION

The anti-corrosion performance of the inhibitors

Inhibitor A performance in ASTM D-1748 and B-117 tests

The performance of inhibitor A is shown in Fig.'s 2, 3 and 4. As it can be seen, the film of inhibitor A with a thickness of 12.5 microns provided protection for 1500 hours and 37.5 micron film provided protection for more than 2500 hours respectively for steel. A similar pattern of performance was observed for aluminum coated with inhibitor A.

In ASTM B-117 salt spray test the duration of protection is 200 hours and 500 hours, respectively, for 12.5 and 37.5 microns film. The control sample failed in 2 hours in humidity cabinet and in 30 minutes in salt fog cabinet. Such a performance of the inhibitor A can be attributed to both contact and vapor inhibition abilities of the compound. The inhibitor A is a complex mixture of amine salts of aromatic sulfonic acids in the carrier, as a contact inhibitor component, and volatile carboxylic acids salts, as a vapor phase inhibitor. The thin polar layer composed of surfactants, like sulfonated salts, is tightly bound to the metal surface by mechanism of chemisorption. Between this thin polar layer and the corrosive environments is the thicker barrier layer which is usually made up of hydrocarbons. The reason combinations of different surface active components are used in the formulation of inhibitor A is that a metal surface has many active sites where corrosion can begin. These active sites have a great range of energy levels. A surface active component of the inhibitor will be strongly chemisorbed or adsorbed at active sites having energy levels complimentary to the energy levels of the polar group. Thus, it would form much tighter and more uniform layer over the metal surface.

The barrier layer has three important characteristics:

- * low permeability by moisture and other corrosives
- * compatibility with the oleophilic ends of the polar layer molecules so that the barrier is held firmly in place
- * good solubility in the carrier so it is possible to apply the polar and barrier layers to the metal surface

Inhibitor A also provides protection in vapor phase for metal surfaces not covered or not sufficiently covered with the product due to presence of the volatile part in the formulation. Inhibitor A releases a vapor of corrosion inhibitor which migrates to recessed areas or areas not sufficiently protected with the contact part of the inhibitor.

It is believed that these ionic vapors form a thin, monomolecular layer on the metal surface providing protection by the mechanism of passivation for steel and aluminum. VCI film barrier reheals and self-replenishes through further evaporation and condensation of the inhibitor on the metal surface. Inhibitor A has a much greater affinity for a metal surface than for water. The sulfonate part of the inhibitor displaces water from the metal and becomes chemisorbed on the surface.

Therefore, inhibitor A has multifunctional properties: corrosion-inhibitive compound, water displacing compound and vapor corrosion inhibitor.

These properties are critically important for protection of airframes, mechanical parts of aircraft and armaments during storage and operation in highly corrosive environments. Inhibitor A is also more economical to apply, because it combines in itself protective parameters of three currently used preventive systems.

Inhibitor B performance

The test results on the inhibitor B are presented in Table 1. As it is shown, the control metal samples in non-treated polyethylene bag were severely corroded. Metal samples protected with VCI extruded polyethylene bag are practically free from any corrosion attack. The mechanism of protection for inhibitor B material is basically the same as it was described above. The carrier for the vapor phase inhibitor is polyethylene film by itself. Inhibitor released by polyethylene matrix migrates through the volume of air to the metal surface and forms a thin protective layer at the surface. It is believed that steel and aluminum are protected by the mechanism of passivation. The works of Miksic and Sparrow (6) revealed that mechanism of protection for copper and copper based alloys, (i.e. brass) is different and based on chemisorption of the inhibitor on the surface and formation of insoluble organometallic complex on the surface. It is important to mention here that inhibitor B is a dual function product, as it also provides action of dehumidification along with inhibition. Therefore, inhibitor B can be used in the form of insert bags, flexible covers and barrier material in order to protect different parts of aircraft during shipment, storage etc.

Inhibitor C performance

The number of days to failure of the metal panel when exposed in the humidity cabinet is summarized in Table 2 and Figure 5, for each metal used in the test. It can be seen that solder, copper and brass have an extremely long period of protection when treated with inhibitor C. Steel and silver have somewhat less, but still sufficient duration of protection.

The results of the Battelle flowing mixed gas test are shown in Table 3. The most dramatic and explicit visual results were observed for copper, silver and gold, three metals that are very common in different types of electronic devices. Copper control sample was dark black after 1 day of testing, control gold coupon was extensively damaged by pitting with a substantial amount of corrosion creep from the pores and silver was covered with thick black deposit of corrosion products. In comparison copper and gold treated with inhibitor C did not show any signs of corrosion and silver sample was only slightly discolored near edges. The proposed mechanism of protection is chemisorption of the inhibitor on these particular metals. In the case of aluminum, steel and solder, it is believed that absorption is purely physical with subsequent passivation of metal surface.

CONCLUSIONS

The purpose of this paper was to investigate the possibility of application of different types of vapor corrosion inhibitors for aircraft protection during maintenance, storage, transportation and active mission periods.

Inhibitors that can be used for protection of aircraft bodies, armaments, avionics were tested on selected metals mostly common in the aircraft construction, and under specific conditions of accelerated testings.

On the basis of test results it can be concluded that multifunctional VCI systems are technologically feasible and are an economical method for providing corrosion protection to military.

References

1. Rosenfeld, I.L. "Atmospheric Corrosion of Metals", NACE, Houston, TX, 1973.
2. NAVAIR 15-01-500. Preservation of Naval Aircraft., Direction of Commander, Naval Air Systems Command, 1991.
3. McLoughlin, V.C. "Corrosion Control Measures for Military Aircraft - Present UK requirements and future developments", AGARD conference proceedings, Vol. AGARD-CP-315, London 1981.
4. Ketcham, S.J. et al. "Recent Developments in Materials and Processes for Aircraft Corrosion Control", AGARD Conference proceedings, Vol. AGARD-CP-315, London 1981.
5. Smithy, C.J.F. "The Protection of Aircraft Against Corrosion", Corrosion Prevention and Control, Vol. 28, NO. 5. pp. 9-11. Beaconsfield Scientific Ltd., 1981.
6. Miksic, B.A., Tarvin, M., Sparrow, G.R. "Surface Analytical Techniques in Evaluation of the Effect of VCI Organic Corrosion Inhibitors on the Surface Chemistry of Metals". NACE - Corrosion, paper No. 607. New Orleans, LA 1989.
7. Abbot, W.H. "Corrosion of Electrical Contacts: Review of Flowing Mixed Gas Test Development", Br. Corros. J., 24, 2, 1989, pp. 153-159.
8. Contec Research, Inc. Report. Interoffice communication.

Table 1.

| Material | Inhibitor B | Non-treated polyethylene |
|------------------|----------------------------|-----------------------------------|
| STEEL | Free from corrosion | Uniform corrosion, pitting |
| COPPER | Slight darkening | Dense black film |
| BRASS | Free from corrosion | Black specks |
| ALUMINIUM | Free from corrosion | Gray-black cast |

Table 2.

| TYPE | DAYS TO FAILURE | | | | |
|--------------------|------------------------|---------------|---------------|---------------|--------------|
| | Ag | Solder | Cu | Brass | Steel |
| Control | 3 | 10 | 4 | 1 | 3 |
| Inhibitor C | 18 | 66 | >80 | >80 | 63 |

Table 3.

| Metal | Control | Inhibitor C |
|---------------|-------------------------|-------------------------------|
| COPPER | Dark deposit | Free from corrosion |
| BRASS | Dark deposit | Discoloration of edges |
| SILVER | Black film | Discoloration of edges |
| GOLD | Pitting | Free from corrosion |
| STEEL | 100 % Brown rust | 3 % Brown rust |

Figure 1. Test Apparatus

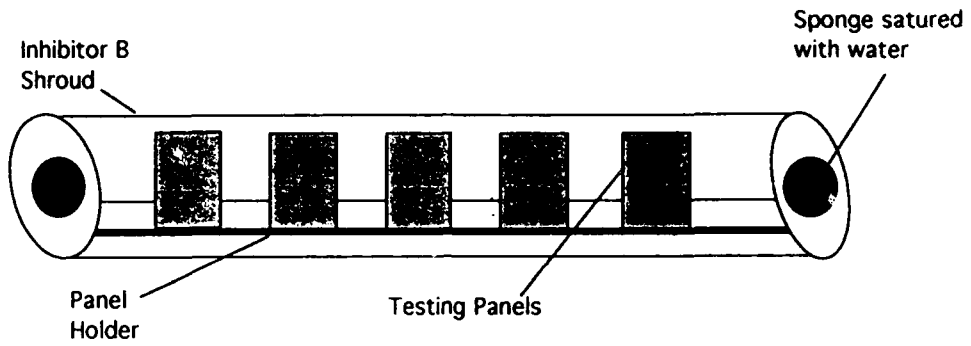


Figure 2. ASTM D-1748

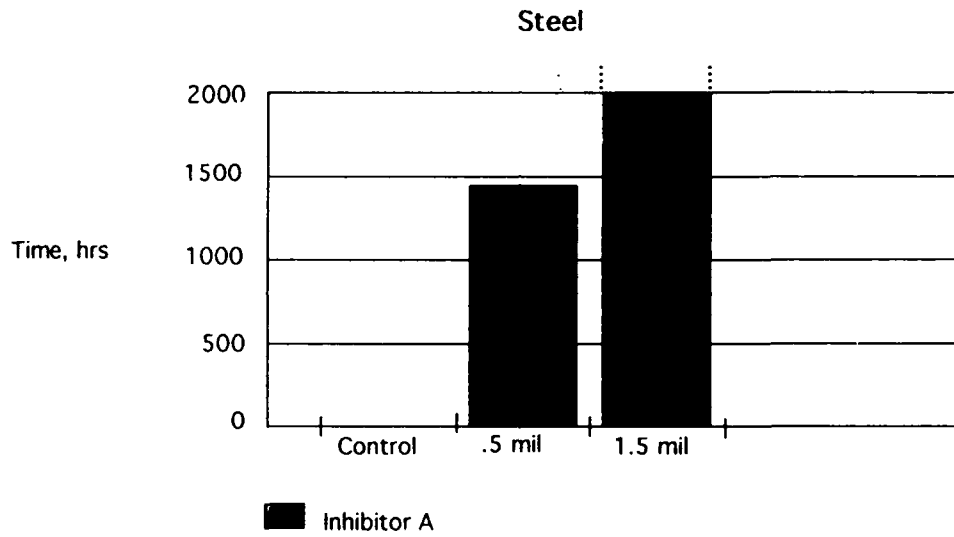


Figure 3. ASTM B-117 Test

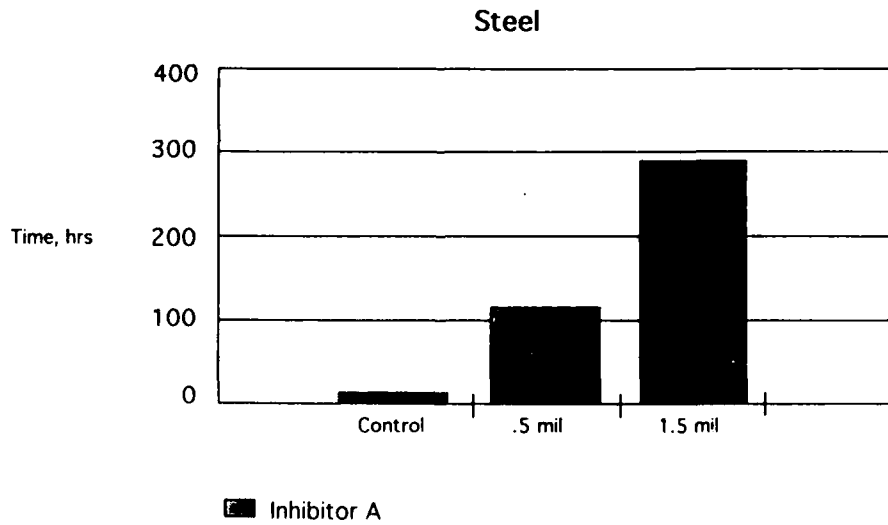


Figure 4. ASTM D-1748

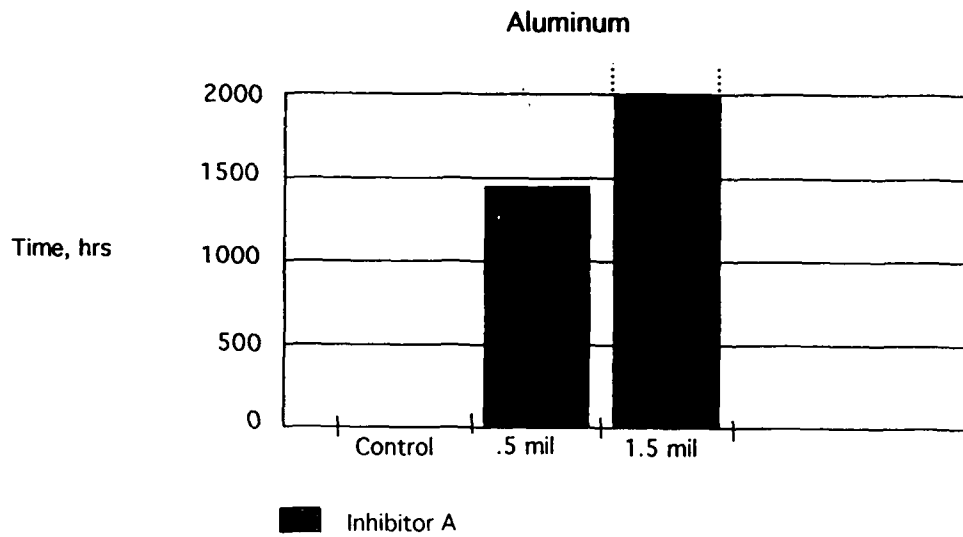
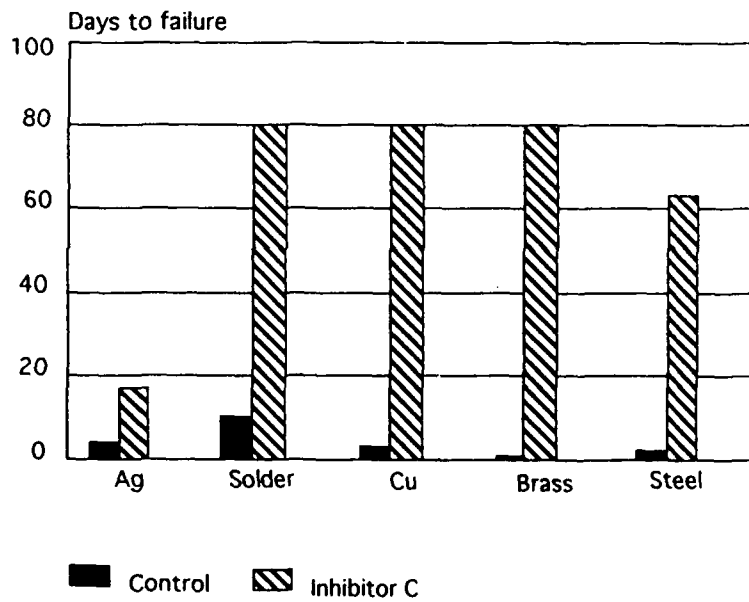


Figure 5. ASTM D-1748 Humidity Cabinet



DESIGNING METALLIC SURFACE COATINGS FOR IMPROVED CORROSION RESISTANCE

Raj Narayan
Department of Metallurgical Engineering,
Indian Institute of Technology,
KANPUR - 208016 , INDIA

ABSTRACT

Metallic surface coatings have often been used to improve corrosion resistance of various engineering components. The paper discusses how a better understanding of the protection mechanism has helped in designing coating systems having improved corrosion resistance.

INTRODUCTION

Corrosion is defined as the deterioration of useful properties of a material as a result of its interaction with the environment. Both direct and indirect losses due to corrosion are huge. A substantial amount of government and industrial funds are being spent all over the world for combating corrosion. A wide variety of techniques have been used for corrosion prevention⁽¹⁾ (Table 1). Use of coatings, particularly metallic coatings, constitute a very important domain of these methods. A thorough understanding of various techniques, their limitations, advantages and the effect of various process parameters on coating properties and the mechanism of protection has enabled corrosion engineers to design and develop metallic coatings with improved corrosion resistance.

SURFACE COATING TECHNIQUES

A wide variety of techniques are available (Table 2) for applying metallic coatings for improving surface sensitive properties like wear, corrosion etc. Advantages, limitations and typical applications of these techniques have been discussed in an earlier publication.⁽²⁾ It is evidently clear that by proper selection of the coating technique and control of process parameters it is possible to control various coating properties like composition, structure, thickness, porosity, bond strength etc. All these properties are extremely important and effect the ability of coatings in preventing or delaying corrosion.

MECHANISM OF CORROSION PREVENTION BY COATINGS

Protection of metals from corrosion by use of metallic

coatings has been practiced for centuries. Coatings primarily protect the underlying metal by physically separating it from the environment. Ideally, coatings should not have any porosity. However, all coatings have pores. Pore area and density depends upon the nature of the coating process and the process variables. At these pores, underlying metal is exposed to the environment. Performance of a coating system depends upon the nature of the coating metal, pore density and nature of the interfacial region between the coating and the substrate.

Metallic coatings could either be cathodic or anodic to the substrate. If the coating is cathodic (noble) to the substrate, corrosion of the substrate at the pores is accelerated due to galvanic cell formed between the coating and the substrate (Fig.1A). On the other hand if the coating is anodic (active) to the substrate, corrosion of the coating metal around the pores is accelerated.(Fig. 1B) If coating-substrate interface is a sharp and well defined region then the problem is further magnified due to lateral spread of the corrosive attack. Such lateral attack can result in coating lift off, exposing more substrate surface to the environment, resulting in its enhanced corrosion.

COATING DESIGN FOR IMPROVED CORROSION RESISTANCE.

A wide variety of coating techniques, and improved knowledge of the effect of various process parameters on coating properties and mechanism of protection by coatings has enabled design and development of coating systems with improved corrosion resistance. Various factors which make this possible are:

a. COATING METAL :

This will be basically determined by the application of the coated component and the nature of the corrosive environment. Coating metal should, naturally have good corrosion resistance in the environment in question. Customer acceptance, bond strength, life, cost and toxicity are some of the other factors. For example, we know that galvanic coatings of zinc and aluminum can effectively protect steel from atmospheric corrosion but one would hardly accept such coatings on household appliances like electric kettle, coffee percolators etc. largely due to their dull appearance.

b. COATING PROCESS

Once the coating metal has been selected, one has to choose the most appropriate coating process for applying that metal. Various factors which affect the choice of the coating process may include

- Component size and quantity
- Maximum permissible deposition temperature
- Coating thickness
- Coating deposition rate
- Throwing power of the process

- Bond strength of the coating
- Coating structure
- Environmental considerations.
- Component size
- Economic considerations

c. COATING STRUCTURE

It is often possible to obtain much improved corrosion resistance by changing coating structure. Amongst other things pore size and distribution in the coating is extremely important. It has been mentioned earlier that all coatings contain pores. The environment comes in contact with substrate at these pores. It is, therefore, obvious that control of pore size and distribution should effect corrosion resistance of metallic coating. At the outset it would appear that reducing the pore area should improve corrosion resistance. However, this may not be true in all cases. When coating is anodic to the substrate, reducing pore size and number will improve corrosion resistance. Improved corrosion resistance would also result when these pores are sealed with some filler. Well known example exhibiting such behavior is the use of anodic coatings of zinc and aluminum on steel and subsequent painting to improve their corrosion resistance.

However, when coatings are cathodic to the substrate reducing pore diameter and density may actually accelerate corrosion, specially when pores are not completely eliminated. This is due to the fact that in such cases anodic area, metal exposed at the pores, is very small as compared to cathodic area which is the coating itself. Reducing the pore area results in a lowering in anode to cathode area ratio. This causes almost same amount of corrosion over a smaller anodic area or in other words increased intensity of attack resulting in deeper pit and consequently accelerated coating failure.

d. COATING SCHEME

Multi layer coatings have been used to improve appearance and corrosion resistance of coated components. In such cases top layer gives the desired decorative finish whereas the second layer gives corrosion resistance. In some cases exposure of the substrate is delayed by another layer below the first layer.

All the above considerations have helped in designing coatings with improved corrosion resistance. While a lot has been written on the effect of first two factors listed above, full potential of the last two factors has not been fully appreciated except in a very few cases. Design and development of nickel chromium coating system for corrosion prevention is perhaps one of the few examples where these considerations have been fully exploited. Some of these developments are discussed below.

NICKEL-CHROMIUM COATING SYSTEM FOR CORROSION PREVENTION OF FERROUS MATERIALS

Steel when exposed to an atmosphere containing moisture is susceptible to corrosion which is commonly called rusting. Apart from being a cause of material damage, rusting is also unsightly. Attempts have, therefore, been made to develop techniques for rust prevention. Coatings are one of the common techniques for doing so.

Soon after their development in 1837, nickel coatings have been used for corrosion prevention of iron & steel components. Although, the earlier nickel coatings provided a reasonably good protection, they had to be polished to produce a bright appearance. Further, they quickly tarnished on exposure to the atmosphere and had to be frequently polished. With the advent of chromium coatings, it became possible to prevent rapid tarnishing of nickel by electrodeposition of a thin coating of chromium on it. Failure of this nickel plus chromium coating took place due to corrosion of nickel layer at pores in the chromium coating.

Concurrent development of bright nickel plating which overcame the need of expensive post plating polishing aggravated the corrosion problem. It was soon realized that this was due to poorer corrosion resistance of bright nickel which was contaminated with organic brighteners and leveling agents present in the plating bath.

Corrosion resistance of nickel plus chromium coating system can be improved by delaying the penetration of the underlying nickel coating. This can be achieved by :

- a. Increasing thickness
- b. Decreasing the intensity of galvanic attack between chromium (cathodic) and nickel (anodic) at the pores in the chromium coating by modifying the chromium coating structure.
- c. Delaying exposure of the substrate on penetration of nickel coating by spreading corrosion pits laterally rather than vertically before it reaches the substrate by modifying the nickel coating.

While the first alternative listed above increases life of the nickel chromium coating system it is rarely used due to increase in the cost of thicker nickel coatings. Next two alternatives are widely used. They are discussed below in some detail.

MODIFICATION OF CHROMIUM COATING

Failure of nickel-chromium coating system occurs due to penetration of the nickel coating due to galvanic action between nickel and chromium at pores in the chromium coating. It is, therefore, obvious that life of this system can be increased by either eliminating these pores in the chromium coating by using a crack/pore free chromium or by increasing the number of these

pores so that the galvanic attack of nickel is spread out over a large anode area resulting in shallower pits. This technique of increasing life of nickel chromium coating system has resulted in development of micro-cracked and micro-porous chromium.

Crack Free Chromium

Crack free chromium over nickel coating gives, in general, better corrosion resistance than conventional chromium coating.⁽³⁾ But if chromium coating gets slightly damaged either in use or due to plastic deformation of the substrate, accelerated corrosion occurs at these few isolated exposed areas due to a most unfavorable anode/cathode area ratio.

Micro Cracked Chromium

A micro-cracked chromium coating is one which contains a continuous and uniform network of fine cracks, usually between 25 to 80 cracks per millimeter. Such a fine network of cracks spreads the anodic attack on the underlying nickel at many more sites. This in turn results in shallow pits in nickel (Fig. 2B) as compared to conventional chromium having much lower crack density. (Fig. 2A). These micro-cracks are so fine that they do not effect the brightness of the chromium coating.

Various techniques have been used⁽⁴⁻⁸⁾ to deposit micro-cracked chromium. Factors affecting crack pattern and crack density include

- concentration of chromium tri-oxide
- concentration and type of catalyst
- nature and concentration of metallic impurities
- bath temperature
- current density
- current wave form
- nature of the underlying metal/coating

Micro-porous Chromium

One major limitation of micro-cracked chromium is the difficulty in controlling crack density and crack pattern due to so many variables involved. This can adversely effect corrosion behavior of these coatings. This problem has been overcome to some extent in micro-porous chromium. In micro-porous chromium, pores (100 to 300 per square millimeter) are induced in the chromium coating as a result of incorporation of small inert particles (approximately 0.02 micron in diameter) in the underlying nickel coating.⁽⁹⁻¹¹⁾ This layer containing inert particles is generally applied over bright nickel or double layer nickel discussed later. The inert particles present in the surface prevent subsequent deposition of chromium at these regions, hence a porous chromium coating is formed.

Corrosion resistance of micro-porous chromium is similar to that of micro-cracked chromium since in both cases corrosion is spread over a larger number of anodic sites resulting in

shallower pits and consequently delayed penetration of underlying nickel coating.

Earlier attempts to produce micro-porous chromium by incorporating inert particles like graphite⁽¹²⁾, alumina⁽¹³⁾ and WC⁽¹⁴⁾ etc. in chromium coating itself have not been successful. However, the work at author's laboratory has shown⁽¹⁵⁻¹⁷⁾ that it is possible to incorporate such particles in chromium coating. Corrosion behavior of these coatings is currently under investigation.

MODIFICATION OF NICKEL COATING

Once corrosion starts at pores in chromium, conventional or modified, coating life of the coated component depends upon penetration of the underlying nickel coating. Life of such a coating system, as mentioned earlier, could be increased if the pits in the nickel coating do not reach the substrate. This has been done by designing double and triple layer nickel and sandwich coatings.

Double Layer Nickel Coating

It was mentioned earlier that bright nickel coating is more electronegative (active) than conventional dull nickel coating. A double layer nickel coating consists of a initial layer of semi-bright sulphur free ($< 0.005\% S$) conventional nickel coating followed by sulphur containing bright nickel coating. Relative coating thickness ratio being 70 - 80 % semi-bright plus 30 - 20 % bright nickel. Chromium overlay could be either conventional bright chromium or modified chromium, micro-cracked or micro-porous, discussed earlier. In such a coating system once a corrosion pit at a pore in the chromium coating, has penetrated bright nickel layer, it meets a noble dull nickel layer. Since bright nickel is anodic to dull nickel, exposed dull nickel area is cathodically protected by galvanic action of bright nickel. As a result, corrosion pit now spreads laterally rather than vertically.⁽³⁾ This delays exposure of the steel substrate and thereby extends the useful life of the component without formation of unsightly brown spots.⁽¹⁸⁻²¹⁾

Triple Layer Nickel

The main drawback of of two layer nickel plus chromium coating system is the formation of large flat bottom pits that form. Although these pits are not so detrimental as brown rust spots but they are unpleasant and are unsightly. This problem has been overcome, to some extent, by designing three layer nickel plus chromium coating system.^(22,23) In this system a layer having very high sulphur content is deposited between semi-bright and bright nickel layers. In such a system, once the corrosion pit penetrates the top nickel layer (bright nickel), it spreads laterally due to sacrificial corrosion of intermediate nickel (high S nickel) layer. To a casual viewer this flat bottom pit is not visible since it is still covered with top nickel and chromium layers.(Fig. 4) Only after fairly

long exposure period this hanging top nickel + chromium layer cannot support itself and collapses. Once this occurs appearance deteriorates rapidly. In any case the component appears in a better condition for a longer time than single or two layer nickel plus chromium coating systems. Because of extra complications in depositing three types of nickel layers these type of coatings are limited to specialized applications only.

Sandwich Coatings

Multilayer coatings, also known as sandwich coatings have been designed in which a layer of a metal other than nickel is deposited between two bright nickel coatings followed by chromium coating. (Fig. 5) Crack free chromium⁽²⁴⁾, copper⁽²⁵⁾, silver⁽²⁶⁾ and gold⁽²⁶⁾ coatings have been used for this purpose. When such a multilayer coating system is exposed to a corrosive environment, the top nickel layer is penetrated but further penetration is delayed at the intermediate chromium or copper layer which is cathodic to top nickel layer. (Fig. 5) For brown rust spots to appear pits have to penetrate second nickel layer. This substantially increases the total life of the component. Apart from complexity of producing such coatings there might be polarity reversal under specific environmental conditions. These limitations have restricted the use of sandwich coatings, like three layer nickel coatings, for specialized applications.

CONCLUSIONS

The exciting possibility of designing surface coatings with almost tailor-made corrosion behavior has been highlighted for decorative nickel chromium coating system. It is hoped that future publications will discuss this aspect for other systems also.

REFERENCES

1. Raj Narayan, An Introduction to Metallic Corrosion and Its Prevention, New Delhi, India : Oxford IBH Publishing Co., 1983
2. J.R. Ross, Raj Narayan & J.P. Celis, Corrosion Reviews, 7(1), 1(1987)
3. E.J. Seys, A.A. Johnson and A.C. Tuomello, Proc. Amer. Electroplaters' Soc., 44, 29(1957)
4. E.J. Seyb, Product Finishing, 23, 64(1959)
5. W.E. Lovell, E.H. Shotwell & J. Boyd, Proc. Am. Electroplaters' Soc., 47, 215(1960)
6. W.H. Safranek & R.W. Hardy, Plating, 47, 1027(1960)
7. T.E. Such & M. Partington, Trans. Inst. Metal Fin., 42, 68(1964)

8. A. Du Rose, K. Wilson & G. Tejada, U.S. Patent 3563864(1971)
9. N.V. Research, Holland, U.K. Patent 1020285(1966),
1039741(1966)
10. P.F. Turner, Prod. Finishing, 19(12), 61(1966)
11. J.M. Oderkerken, Electroplating & Metal Fin., 17(1), 2(1964)
12. W. Kampschulte & Co., U.K. Patent 1098066(1968)
13. S.E. Beacom, D.W. Hardesty & W.R. Dotty, Trans. Inst. Metal
Finishing, 42, 77(1964)
14. J.P. Young, Plating & Surface Fin., 62, 348(1975)
15. Raj Narayan & B.H. Narayana, J. Electrochem. Soc., 128, 1704(1981)
16. Raj Narayan & S. Chattopadhyay, Surface Tech., 16, 227(1982)
17. Raj Narayan & Surjit Singh, Metal Finishing, 81, 45(1983)
18. S.A. Watson, Trans. Inst. Metal Fin., 31, 190(1954)
19. M.M. Beckwith, Plating, 47, 403(1960)
20. S.H. Melbourne O.N. Flint, Trans. Inst. Metal Fin., 39, 85(1962)
21. J.M. West, Trans. Inst. Metal Fin., 39, 117(1962)
22. H. Brown, Electroplating & Metal Fin., 15, 398(1962)
23. Udylite Res. Corp., U.S. Patent 3090733(1963)
24. H. Brown & M. Weinberg, Proc. Am. Electroplaters Soc., 46, 128(1959)
25. P.F. Turner & A.G.B. Miller, Trans. Inst. Metal Fin., 47, 50(1969)
26. M & T Chemicals Inc., U.K. Patent 1188350(1964)

TABLE I CLASSIFICATION OF CORROSION PREVENTION METHODS

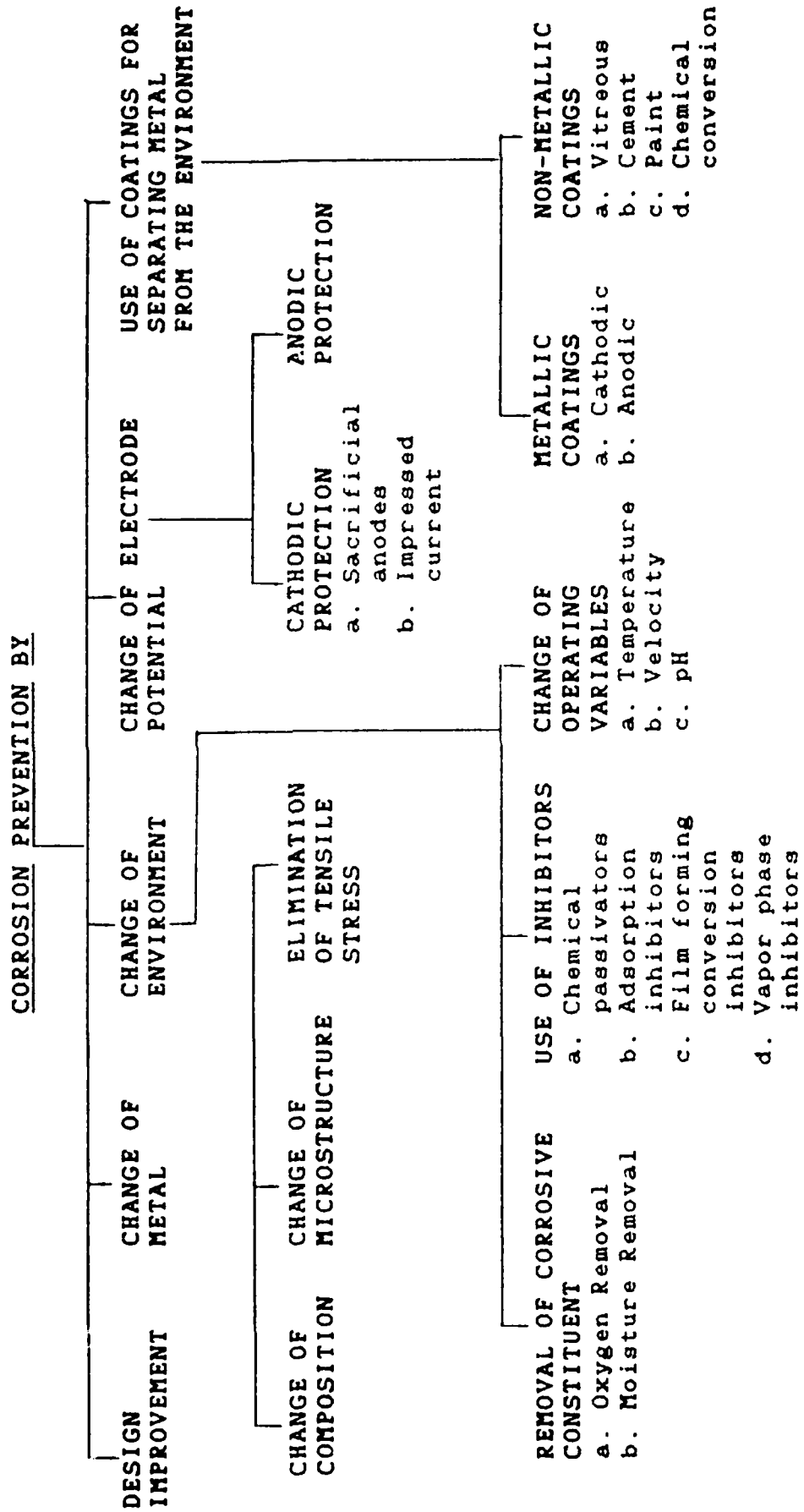
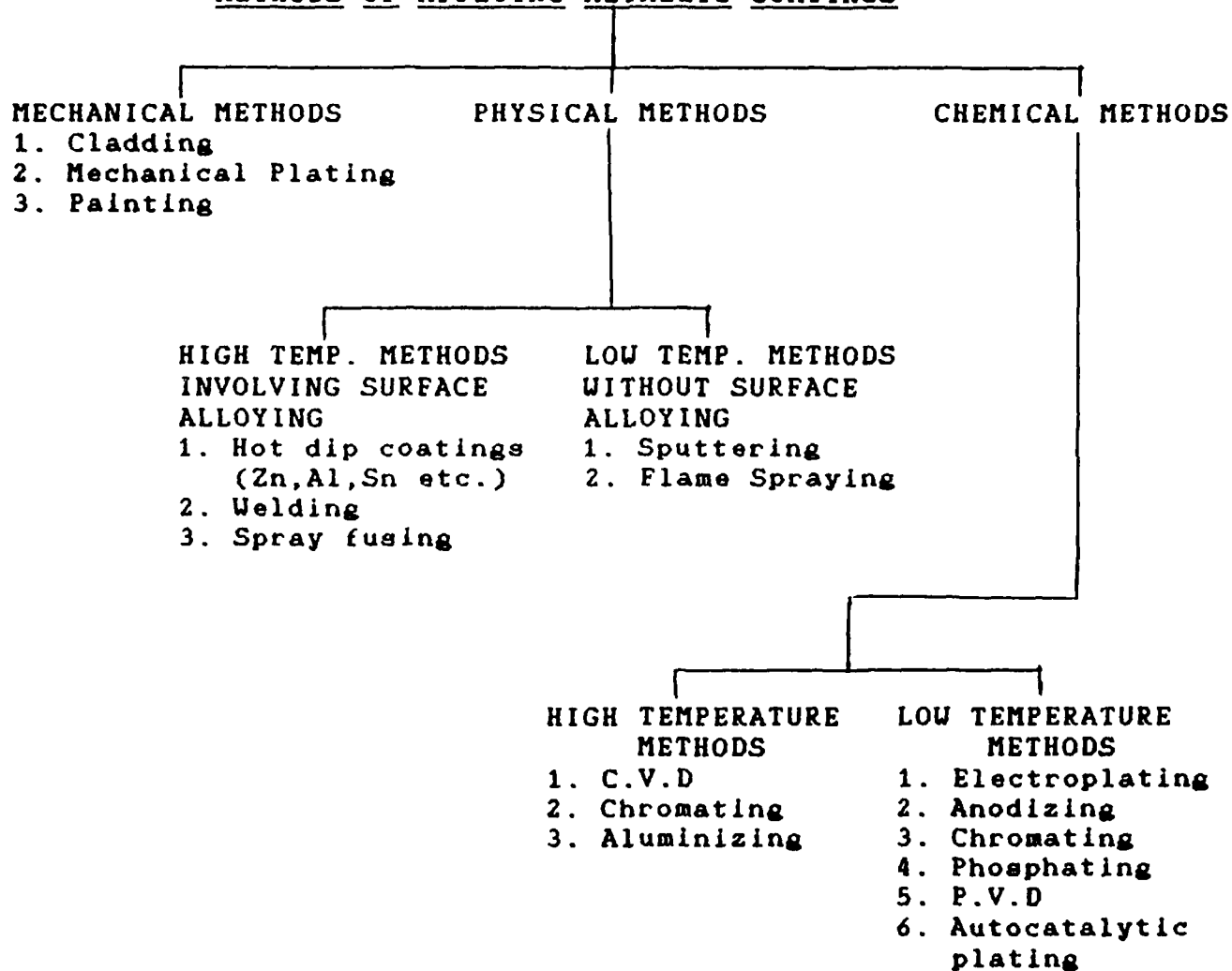


TABLE II APPLICATION OF METALLIC SURFACE COATINGS

METHODS OF APPLYING METALLIC COATINGS



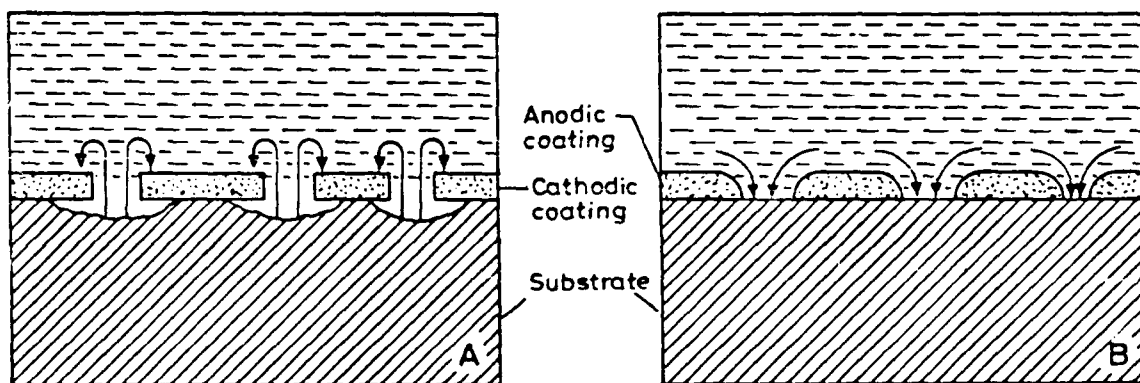


FIG. 1(A) AT PITS IN A CATHODIC COATING, SUBSTRATE CORRODES.

(B) AT PITS IN A ANODIC COATING, THE COATING METAL AROUND THE PORES CORRODES.

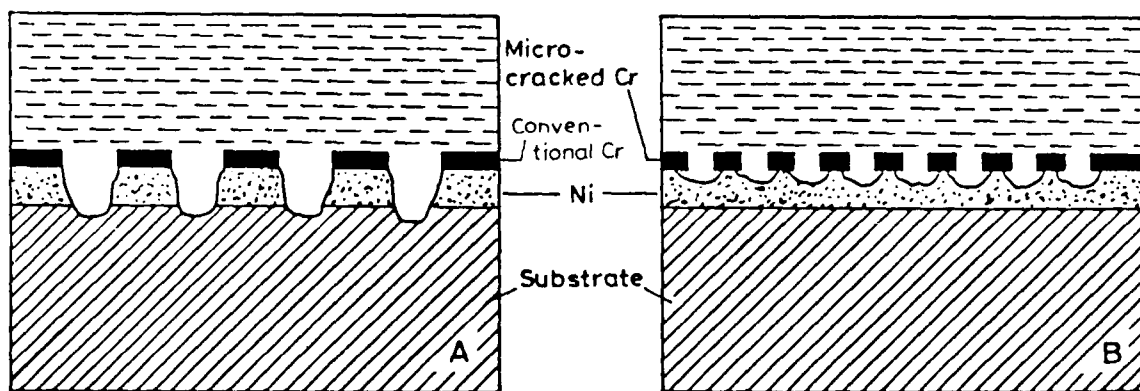


FIG. 2(A) CORROSION PITS IN A NI + CONVENTIONAL CHROMIUM COATING ARE FEW AND DEEP.

(B) CORROSION PITS IN A NI + MICRO_CRACKED CHROMIUM ARE MANY AND SHALLOW.

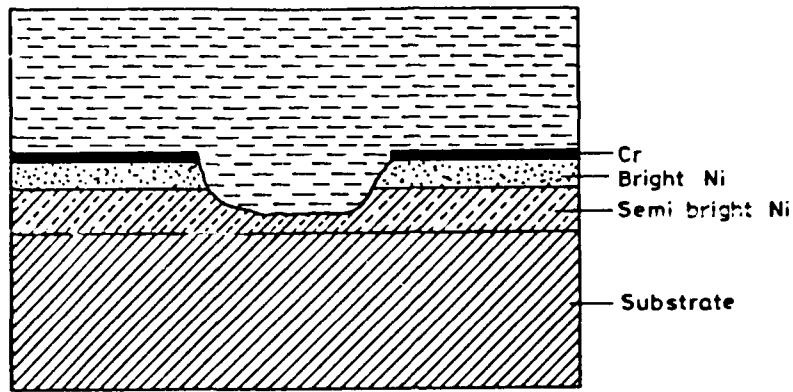


FIG. 3 CROSS-SECTION THROUGH A CORROSION PIT IN A DOUBLE LAYER NICKEL PLUS CHROMIUM COATING ON STEEL SUBSTRATE

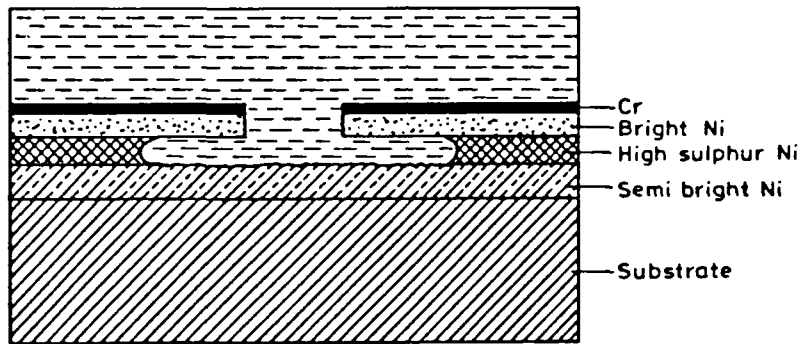


FIG 4 CROSS-SECTION THROUGH A CORROSION PIT IN A THREE LAYER NICKEL PLUS Cr ON STEEL SUBSTRATE

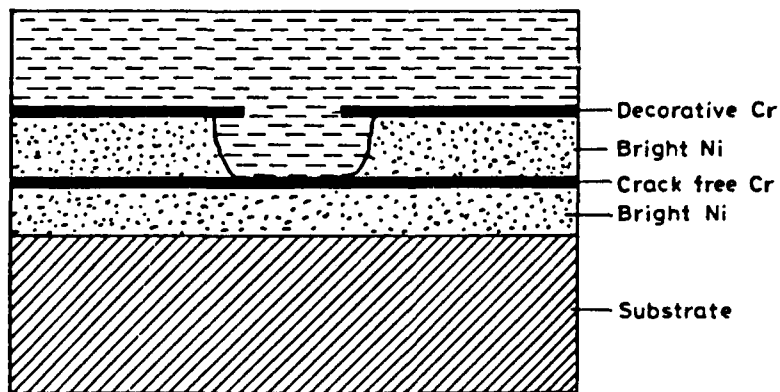


FIG 5 CROSS-SECTION THROUGH A CORROSION PIT IN A MULTI LAYER NICKEL (Ni+Cr+Ni) PLUS CHROMIUM COATING ON STEEL SUBSTRATE

CORROSION BEHAVIOR OF W IMPLANTED ALUMINUM

J.C.S. Fernandes
Department of Chemical Engineering
Instituto Superior Técnico
1096 Lisboa Codex, PORTUGAL

M.G.S. Ferreira
Department of Chemical Engineering
Instituto Superior Técnico
1096 Lisboa Codex, PORTUGAL

Abstract

Ion implantation is a technique that allows the insertion of various elements in the superficial part of materials, forming surface alloys. Moreover there is the possibility of forming solutions beyond the limits of solubility imposed by the thermodynamic relationships, which is of particular interest when the low solubility of the alloys avoids them to reach the desired level of a certain element in order to improve a certain property.

The present investigation looks at the influence of tungsten implanted in aluminum, from the point of view of improved corrosion resistance. Comparative electrochemical results in neutral and alkaline solutions in the presence of chlorides are presented. The results show that for pH's where AlOOH is insoluble the WO_3 stabilizes the oxide film, making the alloy less prone to pitting corrosion.

Key words: Ion implantation, aluminum, tungsten

Introduction

Aluminum alloys are widely used in the transport industry, especially in aeronautics, because of their light weight, high strength and good resistance to uniform corrosion. However, they exhibit very poor resistance against localized attack and, in particular, to pitting in chloride-containing solutions.

It is known that many of the alloying elements used in stainless steels can also improve the corrosion resistance of aluminum. However, improvements in the localized corrosion resistance of aluminum using conventional alloying techniques are difficult to achieve. In fact, to enhance passivation an alloying element should be retained in solid solution without the formation of precipitates that normally act as microgalvanic cells, increasing the localized attack. Thus, the low solubility in aluminum of the transition metals such as Cr, Ta, Mo, W or Zr (below 1% a/o) does not allow them to influence markedly the corrosion behavior of the alloys.

In the past ten years, several authors [1-6] have investigated the metastable Al alloys obtained by nonequilibrium alloying additions of elements such as Mo, Cr, Ta, Zr and Si, using ion implantation or sputter deposition techniques that allow the amount of solute in solid

solution to be increased by several orders of magnitude. From their results it seems that all the above elements lead to an improvement of the pitting resistance of the alloy, being Mo the most promising one. Since molybdenum and tungsten have similar metallurgical and chemical behaviors, a few works devoted to the supersaturated Al-W alloys have appeared recently [7-10].

From the potential vs pH diagrams [11] of aluminum and tungsten (Fig. 1) it can be concluded that aluminum undergoes uniform corrosion in aqueous solutions for pH below 4 or above 8.5, whereas tungsten corrodes for pH above 4. Based on this fact, three different ranges of pH can be established: a zone for pH below 4 where aluminum corrodes and tungsten is passivated, a zone from pH 4 to pH 8.5 where aluminum is passivated and tungsten corrodes and a zone above pH 8.5 where both metals corrode uniformly. In this investigation, we study the effect of W implanted in pure aluminum on the corrosion behavior in neutral and alkaline solutions in the presence of chlorides.

Experimental

Pure aluminum specimens were implanted with W, to fluences of 1×10^{16} W^+/cm^2 and 4×10^{16} W^+/cm^2 at a energy of 40 KeV and in some cases 150 KeV.

Tungsten concentration depth profiles were obtained by Rutherford Backscattering Spectrometry (RBS) with a 2 MeV Van de Graaff accelerator at LNETI (Sacavém, Portugal), as described elsewhere [9,12].

Anodic potentiodynamic polarization plots at a scan rate of $100 \mu V/s$ were carried out in N_2 -deaerated 0.01M Na_2CO_3 + 0.01M NaCl, 0.1M Na_2SO_4 + 0.6M NaCl and 0.6M (3.5% w/w) NaCl solutions. Data acquisition was made through a HP-87 microcomputer.

The open circuit potential vs time was also measured in relation to a saturated calomel electrode, using a high impedance voltmeter and a data acquisition system.

All the potentials are referred to the saturated calomel electrode (SCE).

Results And Discussion

Implantation profile

A typical W depth profile obtained by RBS for the as-implanted samples (4×10^{16} W^+/cm^2 , 40 KeV) is presented in fig. 2, showing a maximum of tungsten concentration (13 at%) for a depth of approximately 35 nm. For the samples obtained with the same dose and an implantation energy of 150 KeV a deeper and more uniform implant distribution is expected [13].

Electrochemical studies in carbonate solutions

Cyclic polarization plots in chloride containing solutions (0.01M Na_2CO_3 +0.01M NaCl) show a breakdown of the film for both the pure aluminum and the W implanted specimens (Fig. 3). However, the breakdown potential (pitting potential) is lower for the W implanted specimens, which can be attributed to an easy pitting nucleation in sites made

available by previous tungsten dissolution.

A potential vs time plot for the implanted specimens is shown in Fig. 4. Initially the potential is -1175 mV, but after a short time it becomes -1700 mV, i.e., the value of the free corrosion potential of pure aluminum.

The analysis of the above results can be done on the basis of the E-pH diagrams [11] of aluminum and tungsten, Fig. 1. Fig. 1A shows that aluminum corrodes in aqueous solutions for $\text{pH} < 4$ and $\text{pH} > 8.5$; thus, in our case ($\text{pH} = 11$) the domain will be of general corrosion. Tungsten, according to Fig. 1B, suffers dissolution for $\text{pH} > 4$, being also in a corrosion domain in the solution used. Therefore, no beneficial effects can be expected from alloying, as passivation is not effective in alkaline solutions.

Electrochemical studies in sulfate solutions

Anodic polarization plots were obtained on pure aluminum and W implanted aluminum in 0.1 M Na_2SO_4 + 0.6 M NaCl, Fig. 5. For the non-implanted aluminum a passive behavior can be observed with residual passive currents of magnitude of 10^{-7} - 10^{-6} A.cm⁻², followed by breakdown, at -740 mV. For the implanted specimens a significant increase of the free corrosion potential was observed, simultaneously with an increase of the pitting potential.

The residual passive currents are of the same magnitude of those found for pure aluminum. The W implantation was carried out at energies of 40 KeV and 150 KeV, the results indicating a better pitting corrosion performance for the latter ones.

Electrochemical studies in sodium chloride solutions

Anodic potentiodynamic polarization plots relative to pure aluminum and W implanted aluminum (40 KeV) in 0.6M NaCl are shown in Fig. 6.

For the non-implanted aluminum a passive behavior can be observed with residual passive currents of magnitude 10^{-7} A.cm⁻², followed by breakdown at --730 mV.

For the implanted samples a significant increase of the free corrosion potential is observed, simultaneously with an increase of the pitting potential to values of --500 mV. The residual passive current densities are of the same magnitude but slightly larger than those found for pure aluminum.

From the above results it can be concluded that there is as beneficial effect of the addition of W in the localized corrosion resistance of aluminum in neutral solutions. However, as it will be discussed later, this effect is not as important as for Al-W supersaturated alloys obtained by cosputter deposition of Al and W onto Si single-crystal wafers [7,8], where pitting potentials as high as 1937 mV vs SCE were reported for Al-10.3at%W alloy.

The superior corrosion performance provided by alloying with transition metals has been attributed by various authors to the presence of the oxidized element in the passive layer [4,6]. According to those authors, binary alloys such as Al-Mo, Al-Cr or Al-Ta show an enhanced passivity because their passive films become enriched in MoO_4^{2-} , CrOOH or Ta_2O_5 , being more resistant to chloride attack as a result of electrostatic repulsion or modification of the oxide structure. For Al-W alloys, where only a very thin film with low concentration of WO_3 is found, the corrosion resistance is explained as resulting from a synergetic interaction between W and Al_2O_3 [8].

Natishan et al. [2,5] proposed another explanation based on the pH_{zch} (pH of zero charge) of the oxides of the alloying metals. According to those authors, the pH of zero charge affects the surface charge and the adsorption characteristics of the film, determining whether the adsorption of Lewis acids or Lewis bases is favored. At pH's lower than the pH_{zch} the surface has a net positive character and attracts anions such as chloride, whereas for pH's higher than the pH_{zch} a net negative charge will attract cations to the surface. The increase in the pitting potential of the various Al alloys should then be attributed to the low pH_{zch} of the oxides of alloying elements.

All the above theories try to explain the enhanced corrosion resistance of Al alloys on the basis of a more protective film. However, as can be seen in figures 5 and 6, the passive current density is almost identical for both pure and W-implanted aluminum. This similarity in the passive current is also found in the polarization curves obtained by Shaw et al. [8] for several supersaturated Al alloys. This fact seems to indicate that the passive films of all the alloys are identical to the passive film on pure aluminum. Thus, the different resistance to pitting corrosion should not be associated with the bulk characteristics of the passive film.

According to Smialowska [14], the diameters of the chloride ion and the water molecule are 0.36 nm [15] and 0.31 nm [16] respectively, whereas the grain boundary thickness in Al_2O_3 is 8.5 nm [17]. Thus, even in the passive region, below the pitting potential, chloride ions and water would reach the bottom of the defects that always exist on the oxide film and react with Al^{3+} from the metal. However, for a pit to be stable it requires the establishment of a critical value of the pH that dissolves the passive film and, as proposed by Galvele [18], this critical pH is related to the product of the minimum local current density within the pit (i) and a characteristic defect dimension (x). Thus, the pitting potential should depend upon the dimensions of defects on the metal surface. In fact, as reported by Smialowska [13], E_p is more positive for sputter-deposited Al film (grain size 40nm) than for conventional Al (grain size 44 μm), being expected that fine grained aluminum should have a smaller defect size than conventional Al. This could be used to explain the difference between the results obtained in this work using ion implantation and those obtained by Shaw et al [7,8] using cosputter deposited Al-W. As the average grain size for the sputter-deposited Al-W alloys is 30nm, whereas ion implantation uses a conventional Al surface, the effect of a reduced grain size could be pointed out as the reason for the best results obtained by those authors. The fact that a very slight increase in the passive current is observed for the implanted aluminum can also be explained as a result of a slight increase of the number of defects in the metal surface due to radiation damage during ion bombardment.

The above theory can also be used to explain the beneficial effect of tungsten additions as a result of the low solubility of WO_3 in acidic conditions. The lower the critical pH the higher the critical $x \cdot i$ value needed to create a stable pit and thus the higher the pitting potential. An element such as W, whose oxide is insoluble at the low pH's existing within pits, will then lead to high pitting potential in neutral solutions such as sodium chloride or sodium sulfate + sodium chloride solutions. In alkaline solutions such as sodium carbonate solutions, where both metals undergo general corrosion, no beneficial effect should be expected.

The fact that higher implantation energies lead to better results from the point of view of corrosion, might be due to a deeper penetration of the aluminum as shown by Ives et al. [13] for the implantation of Mo in stainless steels. The formation of a thicker implanted layer where insoluble WO_3 can be formed, makes more difficult the progression of nucleated pits.

Conclusions

The role of implanted tungsten on the pitting corrosion of aluminum depends on the pH of the solution. In alkaline solutions where AlOOH and WO_3 are not stable the presence of W is deleterious. In neutral solutions the WO_3 stabilizes the oxide film and a low a critical pH is necessary to nucleate pits.

Acknowledgments

The authors thank Prof. J.C. Soares (Centro de Fisica Nuclear) for performing the RBS analysis.

References

1. A. H. Al-Saffar, V. Ashworth, A. K. O. Bairamov, D. J. Chivers, W. A. Grant and R. P. M. Procter, *Corros. Sci.*, **20**, 127 (1980)
2. P. M. Natishan, E. McCafferty and G. K. Hubler, *J. Electrochem. Soc.*, **133**, 1061 (1986)
3. W. C. Moshier, G. D. Davis, J. S. Ahearn and H. F. Hough, *J. Electrochem. Soc.*, **133**, 1063 (1986)
4. W. C. Moshier, G. D. Davis, J. S. Ahearn and H. F. Hough, *J. Electrochem. Soc.*, **134**, 2677 (1987)
5. P. M. Natishan, E. McCafferty and G. K. Hubler, *J. Electrochem. Soc.*, **135**, 321 (1988)
6. G. D. Davis, W. C. Moshier, T. L. Fritz and G. O. Cote, *J. Electrochem. Soc.*, **137**, 422 (1990)
7. B. A. Shaw, T. L. Fritz, G. D. Davis and W. C. Moshier, *J. Electrochem. Soc.*, **137**, 1317 (1990)
8. B. A. Shaw, G. D. Davis, T. L. Fritz, B. J. Rees and W. C. Moshier, *J. Electrochem. Soc.*, **138**, 3288 (1991)
9. R. C. Da Silva, M. F. Da Silva, A. A. Melo, J. C. Soares, E. Leitão and M. Barbosa,

Nuclear Instruments and Methods in Physics Research, **B50**, 423 (1990)

10. J. C. S. Fernandes and M. G. S. Ferreira, *Surface and Coatings Tech.*, **56**, 75 (1992)
11. M. Pourbaix, *Atlas of Electrochemical Equilibria in Aqueous Solutions*, NACE, Houston (1974).
12. M. F. Da Silva, M. R. Da Silva, E. Alves, A. Melo, J. C. Soares, J. Winand and R. Vianden, in *Surface Engineering*, eds. R. Kossowsky and S. C. Singhal (Martinus Nijhoff, 1984) NATO ASI Series E85, p.74
13. M. B. Ives, W. G. Akano, Y. C. Lu, G. Ruijin and S. C. Srivastava, *Corros. Sci.*, **31**, 367 (1990)
14. Z. Szklarska-Smialowska, *Corros. Sci.*, **33**, 1193 (1992)
15. *CRC Handbook of Chemistry and Physics* (ed. R. C. Weast), p. F187, CRC Press, Boca Raton (1989-90)
16. A. F. Wells, *Structural Inorganic Chemistry*, p.537, Clarendon Press, Oxford (1975)
17. C. B. Carter, A. M. Donald and S. L. Saas, *Phil. Mag.*, **A41**, 467 (1980)
18. J. R. Galvele, *J. Electrochem. Soc.*, **123**, 464 (1976)

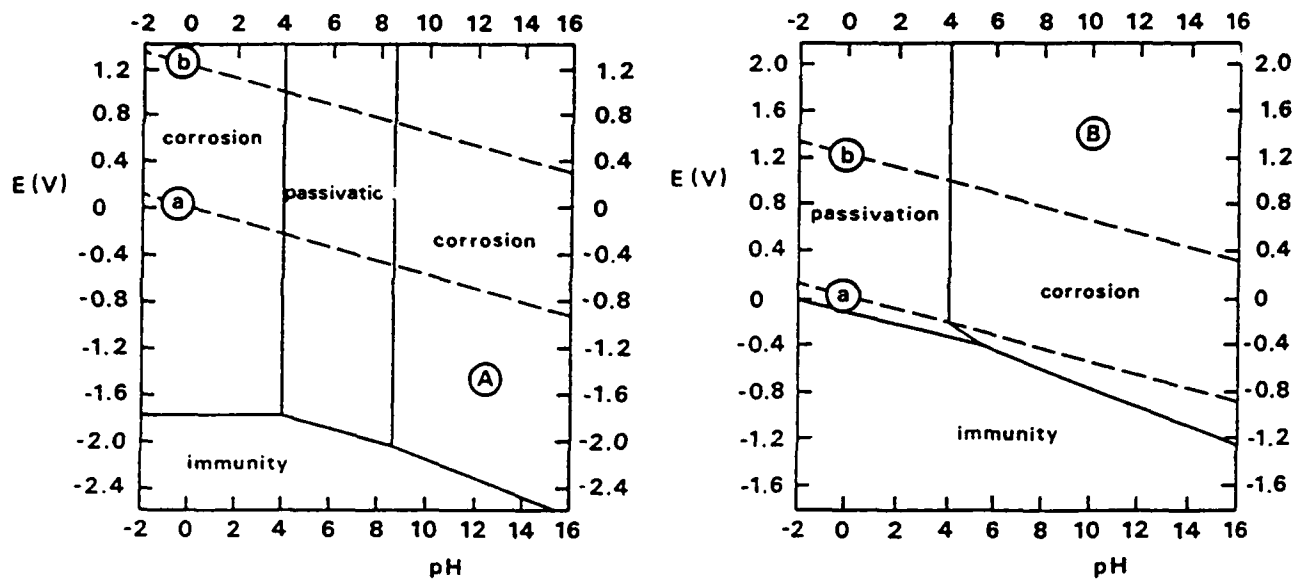


Fig. 1. E-pH diagrams for (A) aluminum and (B) tungsten, in aqueous solutions.

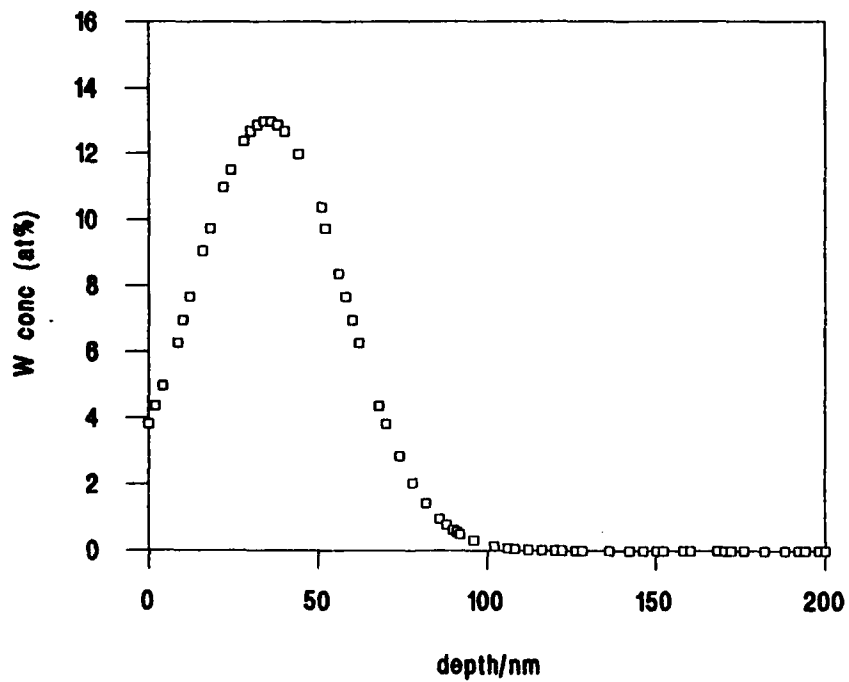


Fig. 2 - Typical W depth profile obtained by RBS for the as-implanted samples ($4 \times 10^{16} \text{ W}^+/\text{cm}^2$, 40 KeV)

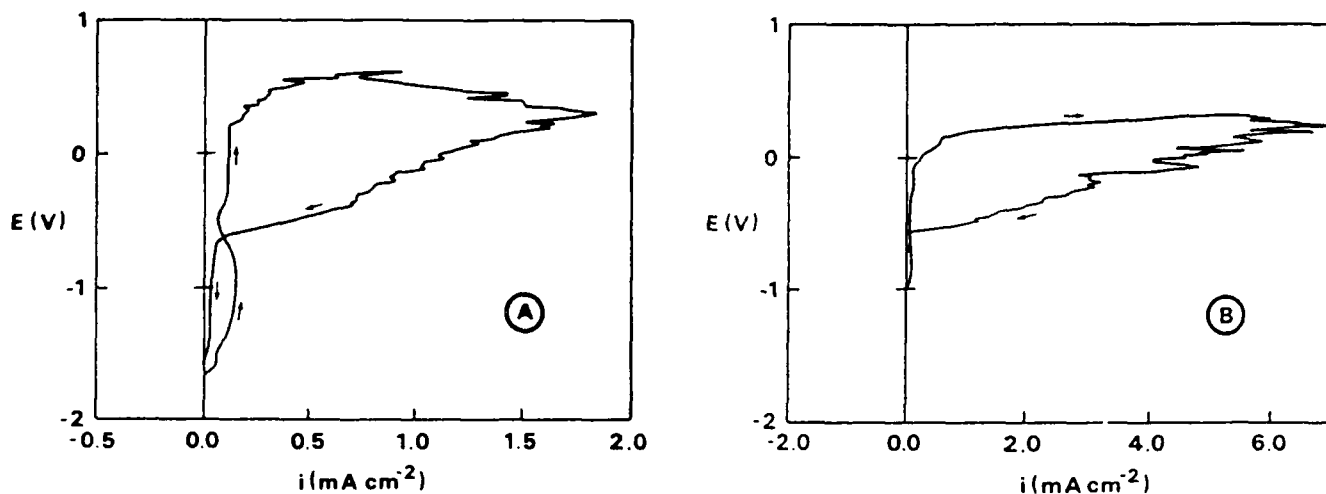


Fig.3. Cyclic anodic polarization plots in 0.01 M Na_2CO_3 + 0.01M NaCl for (A) pure aluminum and (B) W implanted aluminum.

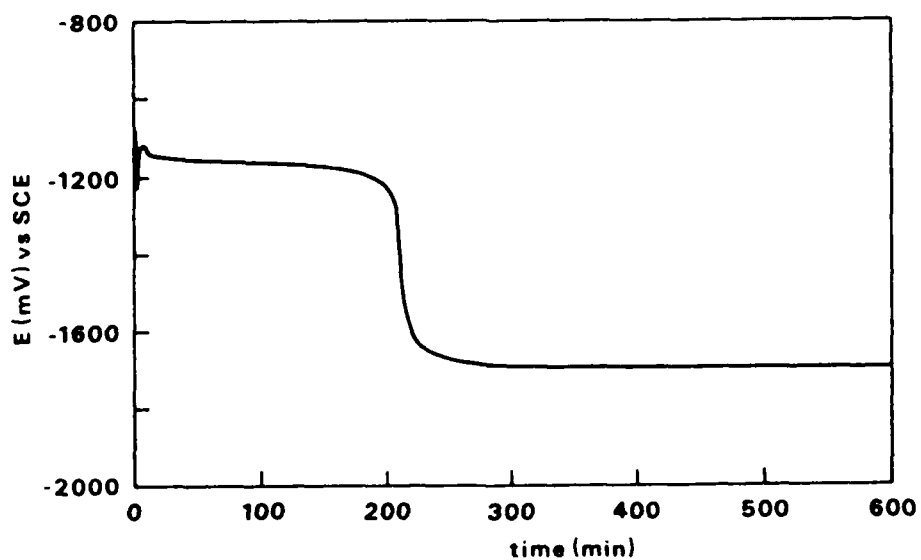


Fig.4. Potential vs time for W implanted aluminum in 0.01 M Na_2CO_3 .

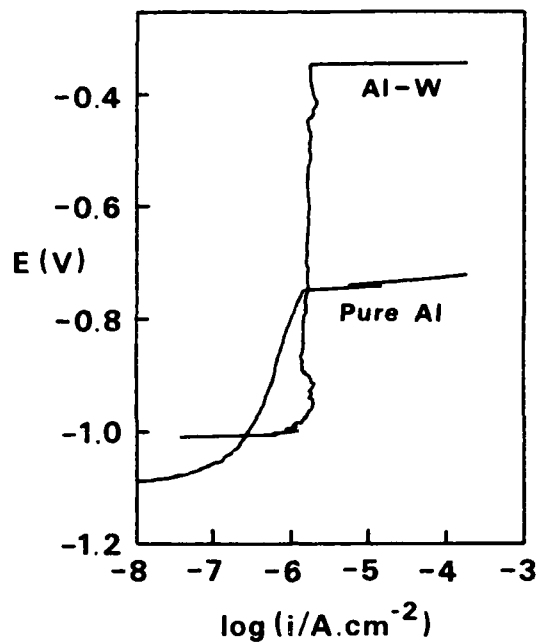


Fig. 5. Polarization plots in 0.1 M Na_2SO_4 + 0.6 M NaCl for pure aluminum and W implanted aluminum (implantation energy: 150 KeV).

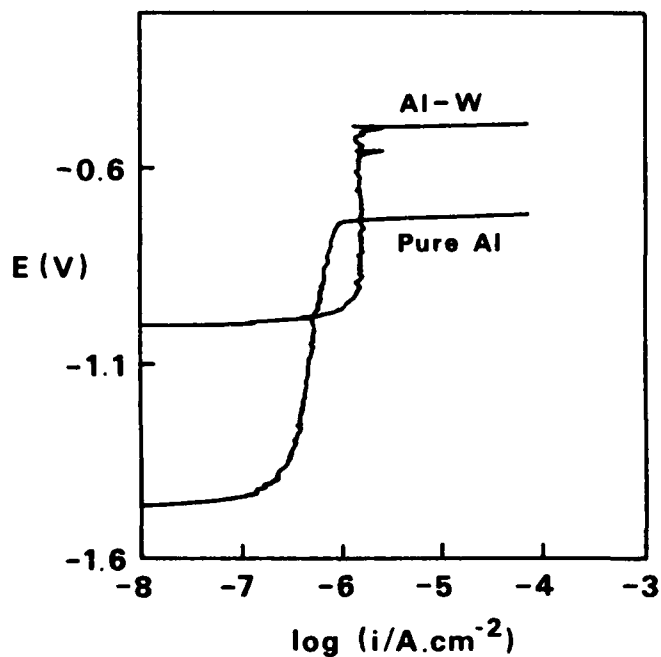


Fig. 6. Anodic polarization plots in 0.6 M NaCl for pure aluminum and W implanted aluminum.

DEVELOPMENT OF CHROMIUM BASED COMPOSITE COATINGS FOR TRIBOLOGICAL APPLICATIONS

Raj Narayan,
Professor,
Department of Metallurgical Engineering,
Indian Institute of Technology,
Kanpur-208016, INDIA

ABSTRACT

Chromium coatings are commonly used for tribological applications due to their high hardness, good corrosion resistance and low coefficient of friction. Applicable range of these coatings has been further extended by incorporating hard or self lubricating particles within the chromium matrix. The paper describes the work done at IIT Kanpur on the effect of various operating variables on electrodeposition of chromium based composite coatings.

INTRODUCTION

Since tribological properties, specially wear, are surface sensitive engineers have employed different techniques to modify surfaces for improving tribological behavior of engineering components. Development of electrodeposited composite coatings has been mainly due to their potential tribological applications. These coatings are produced by suspending bath insoluble particles in the plating electrolyte by agitation during the entire plating operation. A variety of materials including TiO_2 , ZrO_2 , TiC , WC , SiN , $PTFE$, Graphite etc. have been co-deposited with a wide range of matrix metals and alloys e.g. Ag, Au, Co, Cu, Co, Pb, Zn etc.

Electrodeposited chromium coatings have been used for tribological applications due to their high hardness, low coefficient of friction and good corrosion resistance. It was therefore natural to explore the possibility of extending the applicability range of these coatings by incorporating hard and self lubricating particles in them. However, earlier attempts⁽¹⁻⁵⁾ to co-deposit particles such as Al_2O_3 , SiO_2 etc. from a conventional hexavalent chromium bath were unsuccessful. Addison and Kedward⁽⁶⁾ were able to obtain composite coatings from a trivalent chromium plating bath. However, there were

serious limitations due to poor throwing power and inability to obtain thick deposits from these baths. Young⁽⁴⁾ showed that for codeposition to occur presence of thallium ions (Tl^+) was essential in hexavalent chromium plating baths. Contrary to these observations, Skominas et. al.⁽⁷⁾ reported co-deposition of Al_2O_3 , SiO_2 , ZrO_2 from a hexavalent chromium bath without any bath additives. Successful codeposition of SiO_2 ^(4,5), TiO_2 ^(4,5,7), B_4C ^(4,5), B_6C ^(4,5), Cr_3C_2 ⁽⁶⁾, TiB_2 ⁽⁴⁾, ZrB_2 ^(7,9), and diamond in a chromium matrix from a hexavalent bath has been claimed by some investigators. However, in most cases detailed information regarding the effect of various operating variables on codeposition is not readily available. Work was undertaken at our institute to obtain this vital information.

EXPERIMENTAL

Mild steel flat strip specimens (5 x 1 x 0.125 cm) were first ground with 80 grit emery followed by 220 grit. The specimens were then polished with 4/0 paper. All sharp corners and edges were rounded off to avoid burnt deposits at these places. The specimens were then cleaned with acetone and anodically etched in a mixture of CrO_3 and sulfuric acid at 25 A/dm^2 . They were then washed in warm water and immediately placed in the plating bath.

A schematic diagram of the experimental setup is shown in Fig.1. Second phase particles were added to hexavalent chromium plating bath containing 250 g/l chromic acid and 2.5 g/l sulfuric acid operated at 50°C and 50 A/dm^2 , unless otherwise stated. Solution containing suspended particles was blended for adequate time to ensure good wetting and distribution in the plating solution. Amount of particles co-deposited was determined gravimetrically by dissolving the coating in concentrated acid containing few drops of formaldehyde, diluting 4:1 and filtering.

RESULTS

Effect of various operating variables on codeposition of graphite, Al_2O_3 and WC in a chromium matrix has been studied at our institute.

hours. Blending beyond 3 hours did not have any significant effect. (Fig.2A). Room temperature aging of the plating bath up to 4 days (Fig.2B) and variation of current density between 20 to 60 A/dm² at different bath loads (Fig.2C) had practically no effect on the amount of graphite content in the coating.

Amount of codeposited graphite increased with increase in its content in the bath (bath load). (Fig.3) Increasing the bath temperature also increased the amount of graphite in the coating. Optimum co-deposition took place at 50°C. (Fig.4)

Cr-Al₂O₃ COMPOSITE COATINGS⁽¹²⁾

Initial attempts to co-deposit as-received alpha Al₂O₃ with chromium were unsuccessful. Codeposition was possible only when Al₂O₃ powder particles were coated by electroless nickel. However, this coated powder was not stable in chromium plating bath. Further investigations showed that co-deposition was also possible by using dry ground alumina powder. Further work was carried out with alumina powder dry ground for 12 hours in a ball mill. Average particle size of this powder was 1.7 microns.

Aging of the plating bath had practically no effect on the amount of Al₂O₃ in the coating at all bath loads and current densities except at a bath load of 20 g/l operating at a current density of 30 A/dm². Under these conditions aging about 10 days was essential for optimum co-deposition to occur (Fig.5)

Bath temperature also effected the amount of Al₂O₃ in the coating with maximum co-deposition occurring at 40°C (Fig.6). At bath temperatures lower than 40°C the deposits were very rough and heavily cracked. Optimum bath temperature for smooth deposits was 50°C.

Amount of co-deposited alumina increased on increasing its content in the plating bath. (Fig.7) Increasing current density also increased the amount of Al₂O₃ in the coating. (Fig.8) Maximum codeposition occurred at 35 A/dm².

Cr-WC COMPOSITE COATINGS⁽¹³⁾

Increasing the chromic acid concentration in the bath at a H_2SO_4 to chromic acid ratio of 1:100 at $55^\circ C$ and $55 A/dm^2$ increased the amount WC in the coating. Optimum co-deposition took place at about 240 g/l. (Fig.9)

Increasing the blending time at $55 A/dm^2$, $50^\circ C$ and chromic acid concentration of 240 g/l, increased the amount of WC in the coating. The effect leveled off after about 300 minutes of blending. For blending times less than 30 minutes no co-deposition took place. (Fig.10)

Increasing the plating bath temperature up to $55^\circ C$, at all bath loads, increased the amount of codeposition. Increasing bath temperature beyond $55^\circ C$ had practically no effect. (Fig.11)

MECHANISM OF CO-DEPOSITION

Various mechanisms of codeposition have been proposed. Detailed analysis of the above results has shown⁽¹⁰⁻¹³⁾ that two stage adsorption mechanism proposed by Gullielmi⁽¹⁴⁾ is applicable for co-deposition of Graphite, Al_2O_3 and WC in a chromium matrix .

CONCLUSIONS

Possibility of co-deposition of Graphite, Al_2O_3 and WC in a chromium matrix has been clearly established. Effect of various operating parameters like blending time, bath aging, bath load, current density and bath temperature on the amount of codeposition has been studied. By controlling these variables it is possible to control the amount of second phase particles in chromium matrix.

REFERENCES

1. S.E.Beacom, D.W.Hardestay & W.R.Dotty, Trans. Inst. Metal

- Finishing, 42, 77(1964)
2. E.A.Brandes and D.Goldthorpe, Metallurgica, 75, 195(1967)
 3. E.C.Kedward et.al., Trans. Inst. Metal Finishing, 54, 8(1976)
 4. J.P.Young, Res. Directorate, Weapons Lab., Rock Island Arsenal, IL, Report No. NB SIR 74, 615(Nov.1974)
 5. J.P.Young, Plating & Surface Fin., 62, 348(1975)
 6. C.A.Addison and E.C.Kedward, Trans. Inst. Metal Finishing, 55, 46(1977)
 7. L.H.Wagner and R.P.Ericson, NTIS, AD No 74-7767(1972)
 8. E.C.Kedward, et.al., Tribol. Inst., 7, 221(1974)
 9. E.C.Kedward, et.al., U.K.Patent 1220331(1971)
 10. Raj Narayan and B.H.Narayana, J. Electrochem. Soc., 128(8), 1704(1981)
 11. B.H.Narayana, M.Tech.Thesis, Indian Institute of Technology, Kanpur, 1980
 12. Raj Narayan and S.Chattopadhyay, Surface Tech., 16, 227(1982)
 13. D.Prabhakaran, Electrodeposition of Cr-WC Composite Coatings, M.Tech. Thesis, Indian Institute of Technology, Kanpur, 1992
 14. N.Guglielmi, J. Electrochem. Soc., 119, 1009(1972)

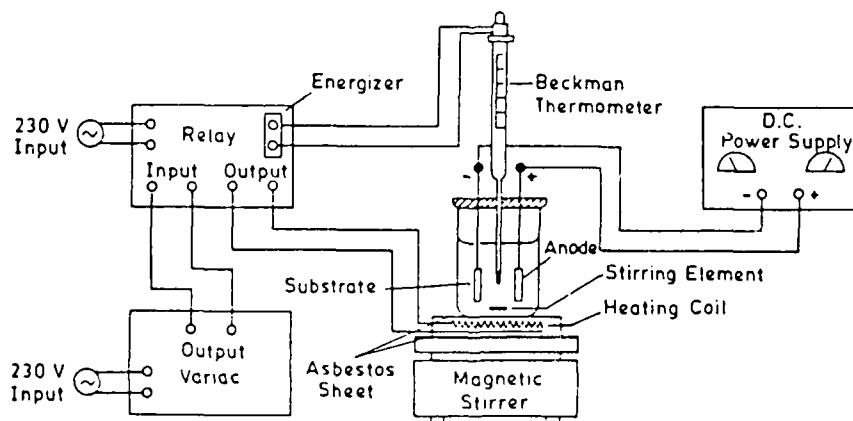


FIG. 1 EXPERIMENTAL SET-UP FOR DEPOSITING COMPOSITE COATINGS.

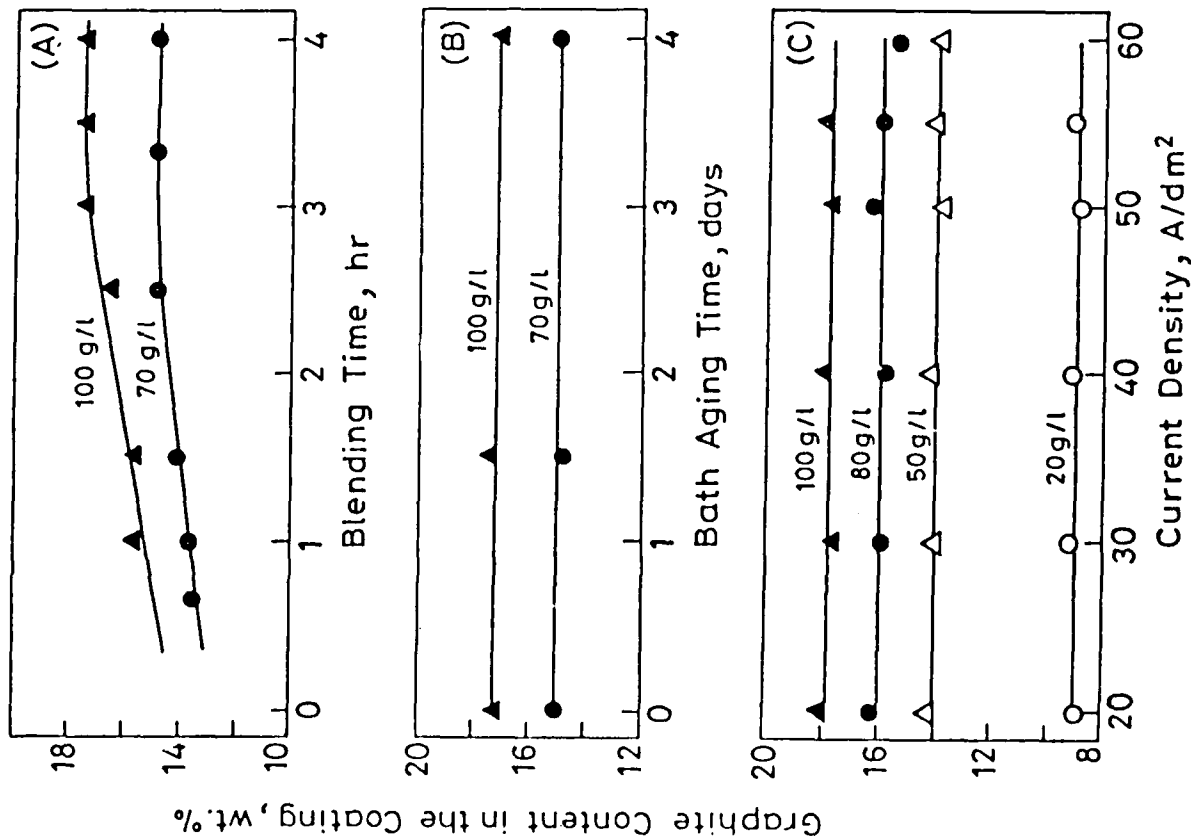


Fig. 2 Effect of blending time, bath aging time and current density on the amount of graphite codeposited with chromium⁽¹¹⁾

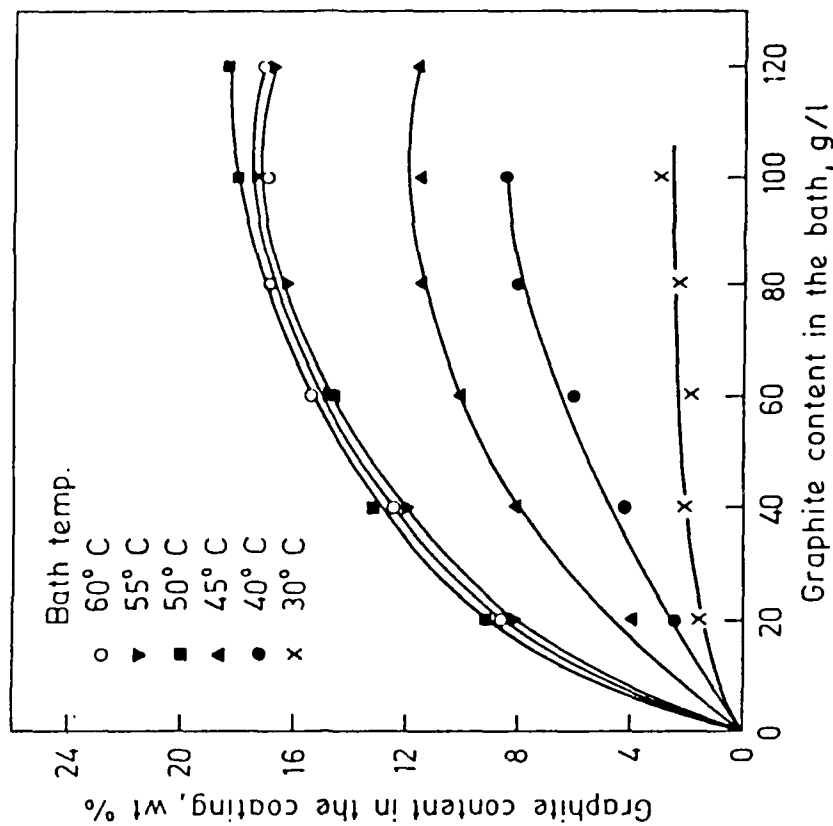


Fig. 3 Effect of graphite content in the plating bath on its content in the coating at 50 A/dm² and different temperatures⁽¹⁰⁾

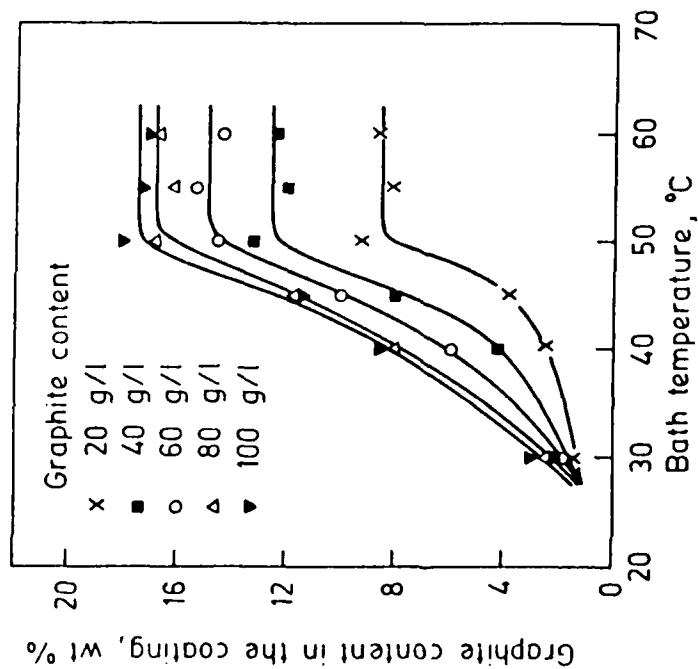


Fig.4 Effect of plating bath temperature on the graphite content in chromium coating at 50 A/dm² and different graphite contents in the bath.(10)

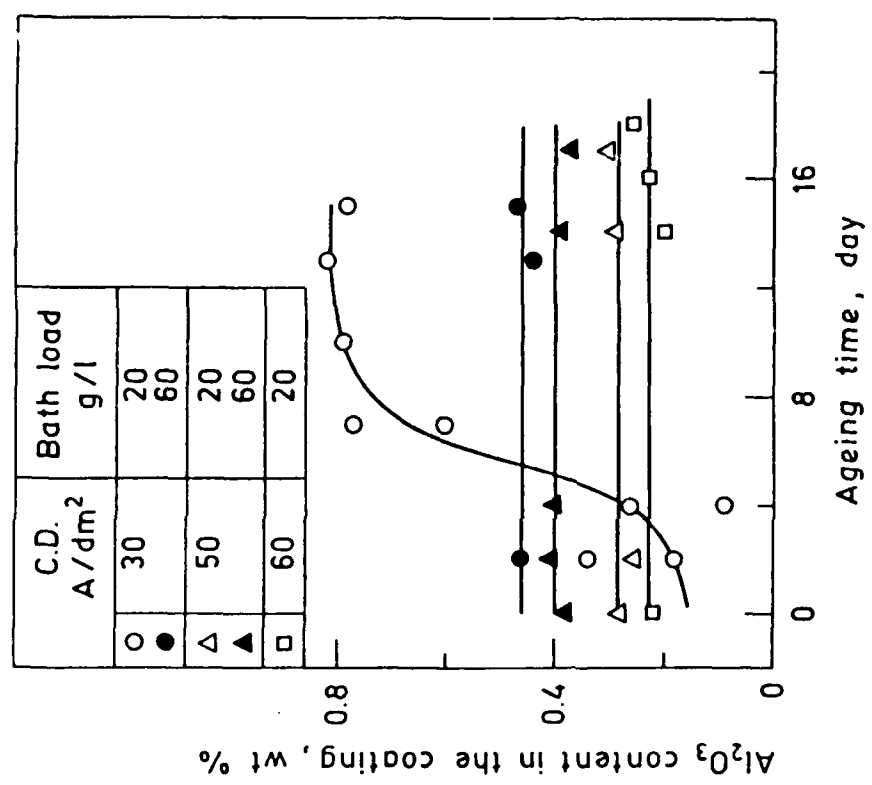


Fig.5 Effect of ageing time of the plating bath on the amount of alumina codeposited with chromium at different current densities and different bath load of Al₂O₃ at 50°C.(12)

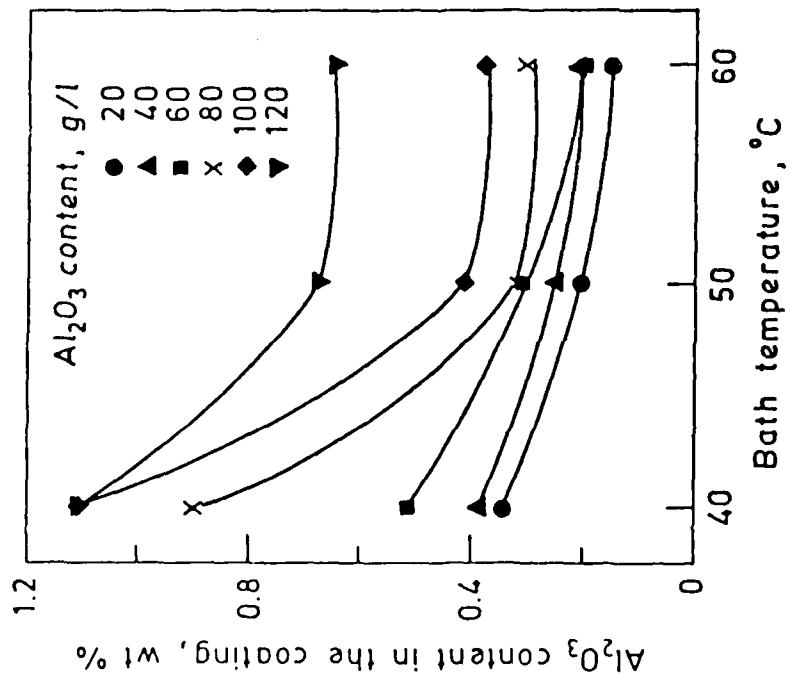


Fig.6 Effect of plating bath temperature on the alumina content in the coating at 30 A/dm² and different alumina content in the bath (12)

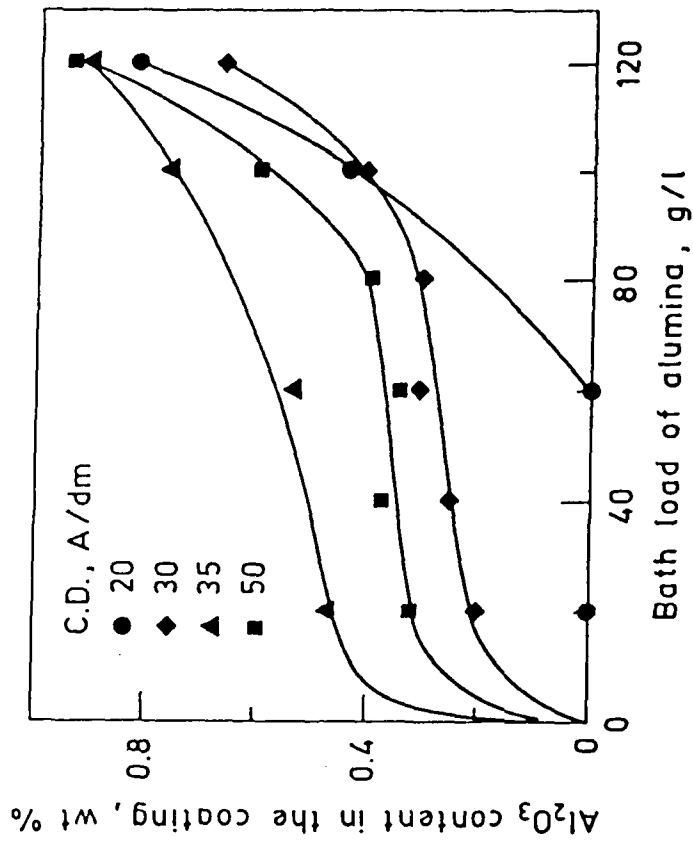


Fig. 7 Effect of bath load of Al₂O₃ on its content in the coating at 50°C. (12)

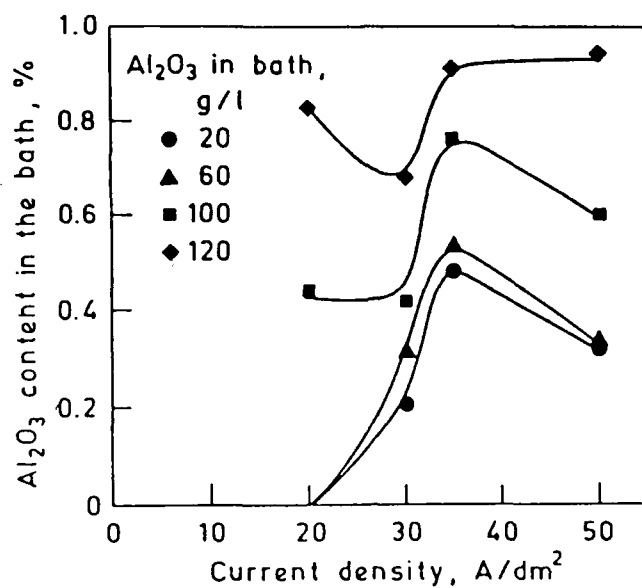


Fig.8 Effect of current density on the Al₂O₃ content in Cr-Al₂O₃ composite coating at different bath loads.⁽¹²⁾

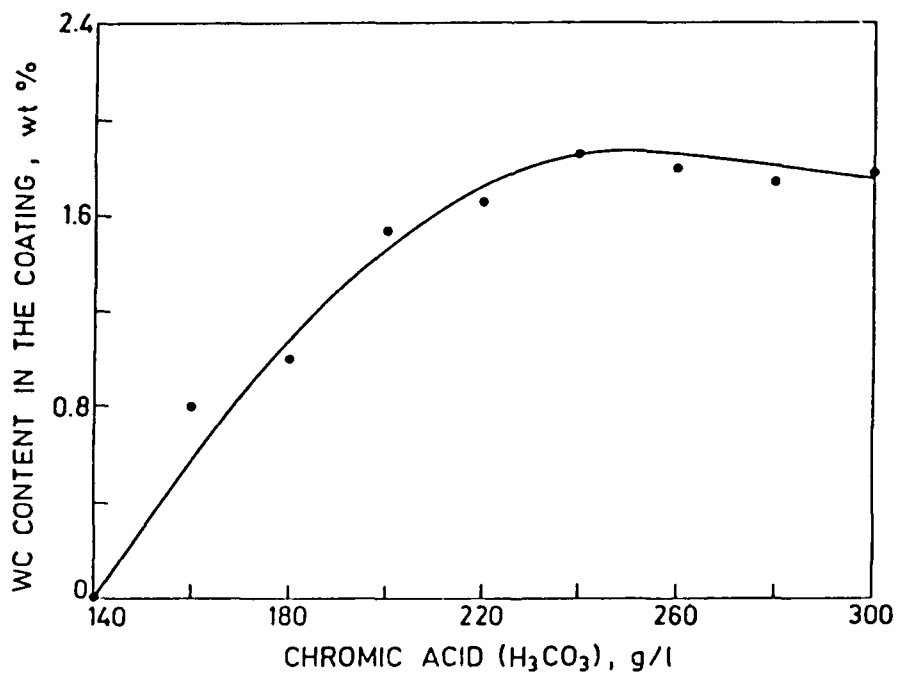


FIG. 9 EFFECT OF CHROMIC ACID CONCENTRATION ON THE AMOUNT OF WC IN THE COATING AT 55°C AND 55A/dm² WITH A BATH LOAD OF 90 g/l.⁽¹³⁾

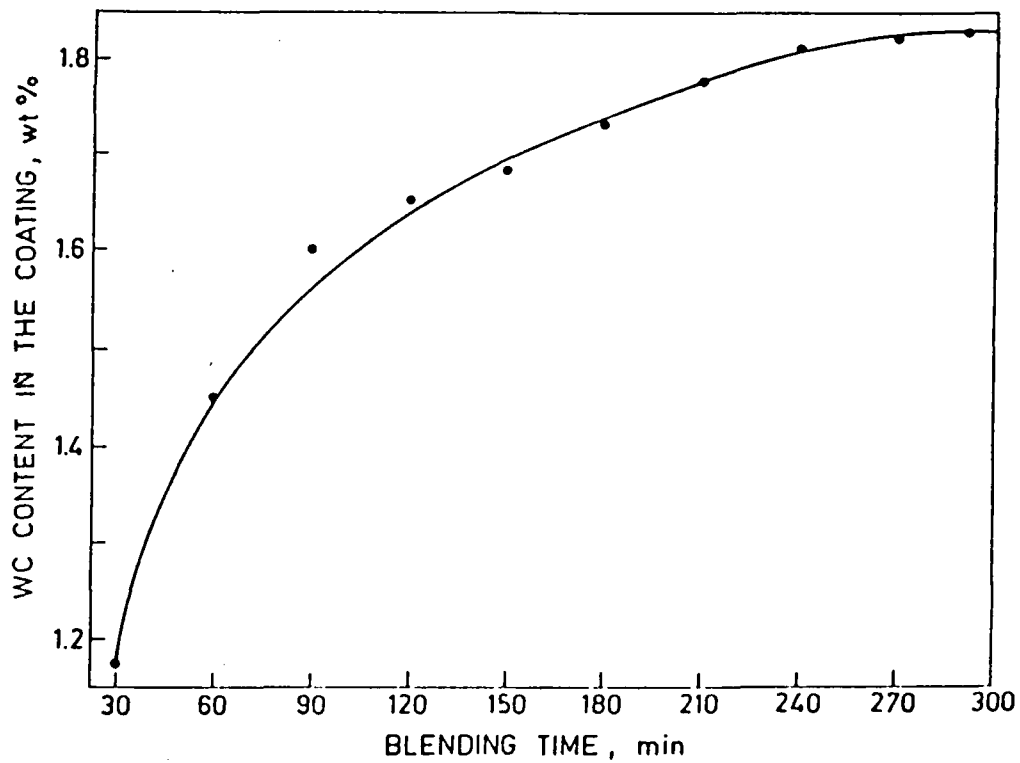


FIG. 10 EFFECT OF BLENDING TIME ON THE AMOUNT OF WC CODEPOSITED WITH Cr AT $55A/dm^2$, $55^\circ C$ AND IN THE BATH 90 g/l OF WC.⁽¹³⁾

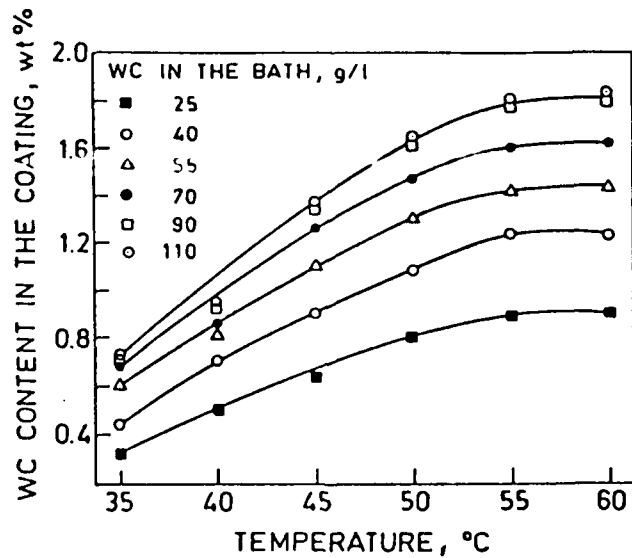


FIG. 11 EFFECT OF PLATING BATH TEMPERATURE ON THE WC CONTENT IN CHROMIUM COATING AT $55A/dm^2$ AND DIFFERENT WC CONTENT IN THE BATH.⁽¹³⁾

Evaluation of Chromate Free Corrosion Inhibited Primers for Airbus Aircrafts

C.W. Matz
Deutsche Aerospace Airbus GmbH
Huenefeldstr. 1 - 5
D-2800 Bremen 1, Germany

Abstract

The economical repair life of transport aircrafts is limited by the increasing maintenance expenditures, which are today mostly due to repair corrosive defects of aging structures. Therefore replacing the well proven chromate leaching corrosion inhibiting primers by chromate free materials needs thorough investigations in order to minimize the technical and economical risks.

Based on available service experience and taking into account the present state of surface protection technology the valid specifications for corrosion inhibiting primers were reviewed and a new profile of requirements developed. This draft specification includes, besides changes in well known standard tests, a new specimen for testing crevice corrosion by an alternating immersion exposure.

Additionally basic studies were performed on the electrochemical influence of chromates in corrosive environments. These tests were performed with various in the aerospace industry applied aluminium alloys. Generally cladding turns out to be clear disadvantage in the crevice situation of joints.

The overall results of the investigation showed the equivalence of chromate free materials with their predecessors in nearly all properties with some important restrictions:

Sufficient filiform corrosion resistance is achieved only in combination with an anodizing pretreatment. Crevice corrosion resistance does not reach the performance level of the high chromate leaching EP primers, but equals to the performance of the older chromate containing PU primer generation.

Key terms: Chromate free primer, corrosion, corrosion inhibition

Introduction

The economical repair life of transport aircrafts is limited by the increasing maintenance expenditures, which are today mostly due to repair corrosive defects of aging structures. Since decades the aircraft industry relies upon the unique corrosion inhibiting properties of chromates. The protection of aluminium alloys inclusive the safeguarded integrity of load carrying primary structures built out of Al, is not only demonstrated in laboratory tests, but also well proven by in service experience. The need to replace soluble chromates (mainly Zn- and Sr-chromates are used) derives from the fact that these materials possess also cancerogenic potential. Thus a conflict between technical and economic advantages versus health, safety and environmental demands is obvious.

Concept for Evaluation of Replacements

By analyzing the currently valid specifications for corrosion inhibiting primers, one can easily detect that these are not fully applicable for chromate free materials due to several reasons:

- Often tests are included, which can only be performed with conventional materials (e.g. chromate leaching rate).
- Due to historic reasons tests are defined which are no longer valid for current production (e.g. surface treatment).
- The layer thickness is designed to conventional materials.

On the other hand not all really needed properties are asked for. An example is the wetting ability, which is most important for touch up processes of riveted structures.

Faced with this situation it was decided to create a completely new specification for chromate free corrosion inhibiting primers (CFCIP).

Following principles were applied:

- The materials and processes included in the requirements should be used in current production and reflect the most critical configuration for the general structure.
- The exposure conditions should correlate to circumstances in reality.
- The test design should take care of proven in service experience and simulate well known damage scenarios.
- The tests should create unambiguous results, i.e. natural scatter should be a minimum and reproducibility should be proven.

Main Features of a Draft Specification for CFCIP

Most of the test are to be performed with the Al alloy 2024. If convenient, we used partly chemically milled sheets (Fig. 1) with clad and bare surfaces, which are typical for today interior structures. Generally both areas are tested simultaneously. With exception for flexibility tests (T0) the heat treatment condition is T3.

Three different surface pretreatment processes were applied. Two of them, the chemical conversion coating (CCC)¹ and the chromic acid anodizing (CAA)² are well known and applied in original equipment manufacturer (OEM) production. The third one is the nitric acid pickle treatment (NAP), which contains a degreasing step, followed by an alkaline etch and the final nitric acid brightening. This process was selected to simulate in reproducible manner surfaces gained by low pretreatment technology like solvent degreasing or mechanical processes, which are often used in repair situations.

Concerning the exposure conditions following important changes were introduced:

- A flexibility test at -55°C
- Immersion in a mixture of water, hydraulic fluid and toilet fluid (simulation of bilge area fluids)

Also reworked were the temperature and time parameters, e.g. the exposure condition applied for toilet fluid is 1500 h at 35°C.

Special care was taken for the corrosion tests. In service experience generally shows following weak points:

- Corrosion starting from local accidental damage (by scratches or impacts)
- Corrosion starting from edges with insufficient protection (coverage of coatings, probability of damage)
- Crevice corrosion

The scenarios of accidental damage and insufficient edge protection are covered satisfactorily by the well known test procedures of salt spray test³, filiform corrosion test⁴ and alternate immersion test⁵, because the specimens are exposed with artificially produced scratches. For crevice corrosion testing purposes a new specimen design was created (Fig. 2). This specimen is normally exposed in corrosive fluid⁽¹⁾ by an alternate immersion procedure.

For the tests, approved paint manufacturers were asked to supply their latest technology chromate free corrosion inhibiting primers together with compatible top coats, suited for interior structural application.

Significant Test Results

With exception of the corrosion inhibiting properties the CFCIP's are at least equivalent to their chromated counterparts. This includes adhesion properties, where e.g. no problem is indicated also on NAP surfaces. A positive surprise are extremely good values reached in the ISO 1518 scratch test, (Fig. 3).

Also improved with comparison to the chromated materials is the behaviour in chemicals resistance. As an example the resistance against hydraulic phosphoric ester fluid is shown (Fig. 4).

The main difference in corrosion performance can be seen in the filiform corrosion test and the crevice corrosion test. Extremely important for the CFCIP's seems to be the surface pretreatment. If anodizing is used the overall performance of the surface protection system meets the specified requirements (Fig. 5). In combination with e.g. chromic sulfuric acid etched (CSA)⁶ aluminium the performance can hardly be accepted (Fig. 6).

The crevice corrosion test indicates also performance differences, which showed clearly that clad Al is a disadvantage in a crevice configuration (Fig. 7).

This was the reason to look more in depth in this situation by electrochemical methods.

Electrochemical Tests

For simulating crevice corrosion a simple electrochemical test configuration with two separate half cells connected with each other by an KNO_3 -solution filled conductance bridge was chosen (Fig. 8). In the basic worst case set-up the cathodic half cell, simulating the exposed edge of a crevice, used bare 2024 sheet material as electrode and neutral 0.1 N NaCl-solution as an electrolyte. This half cell was aerated. The anodic half cell, simulating the non-aerated situation within the crevice,

⁽¹⁾ e.g. 30 g/l NaCl; 1,25 g/l Boric acid; 0,19 g/l NaH_2PO_4 + Na_2CO_3 solution (100 g/l) to make pH 8

used clad 2024 sheets (with covered edges) as electrode and acidic 0.1 N AlCl₃-solution (pH 3,5-4,0) as electrolyte. The corrosion current density measured was about 22,000 nA/cm² (Table 1, experiment 1). Stopping the aeration or changing the anodic material to bare 2024 creates a significant drops of that value (experiments 2 to 4). Compared to experiment 1 the effectivity of chromate was tested at the edge and in the crevice by addition of 0.01 N Na₂Cr₂O₇ · 2H₂O to the electrolyte (Table 1, experiment 5 to 7).

The cathodic inhibiting effect of solved chromate is convincingly demonstrated.

These effects are qualitatively confirmed with other Al alloys. Currently a procedure for testing unknown inhibitors in paint primers is under investigation.

Conclusions

The evaluation of CFCIP's showed advantages and disadvantages in comparison to chromated materials. In connection with anodizing pretreatment processes for aluminium the replacement can be performed. The corrosion tests indicated also that in repair situations this exchange of materials should not yet be carried out.

This complex situation creates some scepticism on customer side. We therefore invite airlines to participate in an in service evaluation program with specimens flown in corrosion prone areas of aircrafts.

References:

1. AECMA prEN 2437 "Chromate conservation coating for aluminium and aluminium alloys"
2. AECMA EN 2101 "Chromic acid anodising of aluminium and aluminium wrought"
3. ISO 7293 "Paints and varnishes - Determination of resistance to neutral salt spray"
4. AECMA EN 3665 "Paints and varnishes - Filiform corrosion resistant test"
5. AECMA EN 3212 "Paints and varnishes - Corrosion resistance test by alternate immersion in a sodium chloride buffer solution"
6. AECMA EN 2334 "Acid chromate pickling of aluminium alloy"

Table 1: Current density measurements

| Experiment No. | Cathode | | | Anode | | Current density [nA/cm ²] |
|----------------|-----------|-------------------------|----------|-----------|--------------------------------------|---------------------------------------|
| | Material | Electrolyte | Aeration | Material | Electrolyte | |
| 1 | 2024 bare | NaCl | + | 2024 clad | AlCl ₃ | 22,000 |
| 2 | 2024 bare | NaCl | - | 2024 clad | AlCl ₃ | 7,000 |
| 3 | 2024 bare | NaCl | + | 2024 bare | AlCl ₃ | 1,900 |
| 4 | 2024 bare | NaCl | - | 2024 bare | AlCl ₃ | 700 |
| 5 | 2024 bare | NaCl + Cr ^{VI} | + | 2024 clad | AlCl ₃ | 20 |
| 6 | 2024 bare | NaCl | + | 2024 clad | AlCl ₃ + Cr ^{VI} | 16,000 |
| 7 | 2024 bare | NaCl + Cr ^{VI} | + | 2024 clad | AlCl ₃ + Cr ^{VI} | 10 |

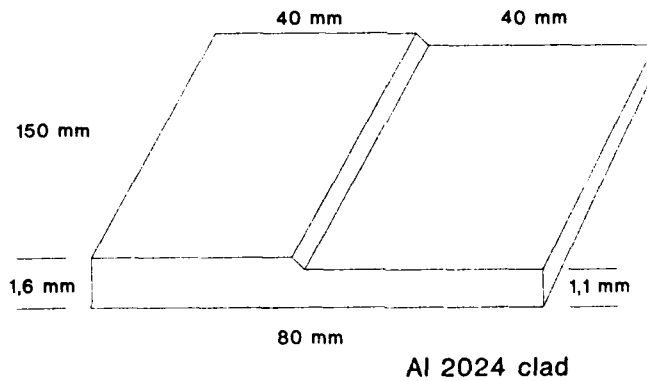


Figure 1: Specimen design for paint testing
(partly chemically milled Al coupon)

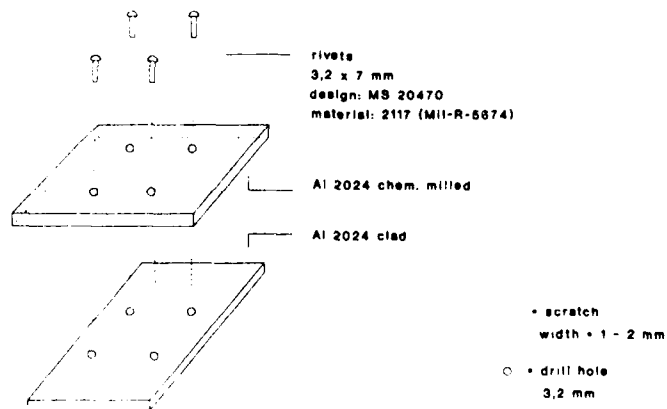


Figure 2: Test Specimen for Crevice Corrosion Test

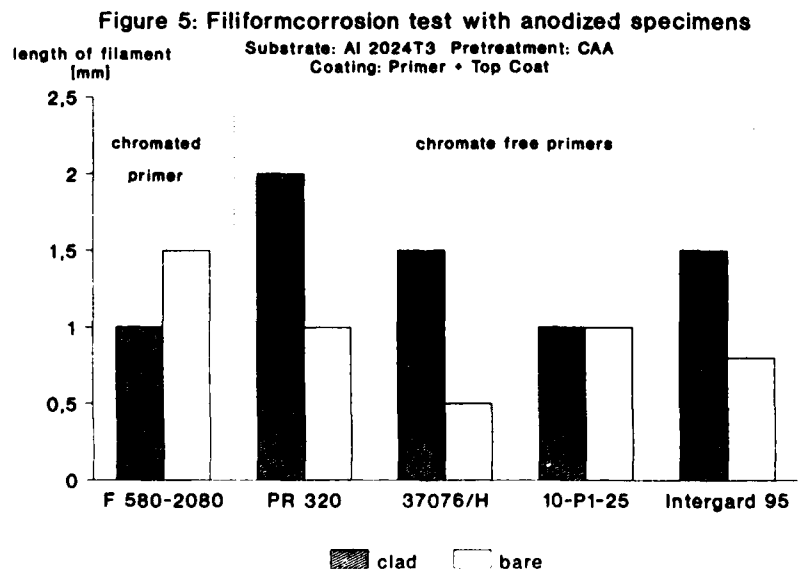
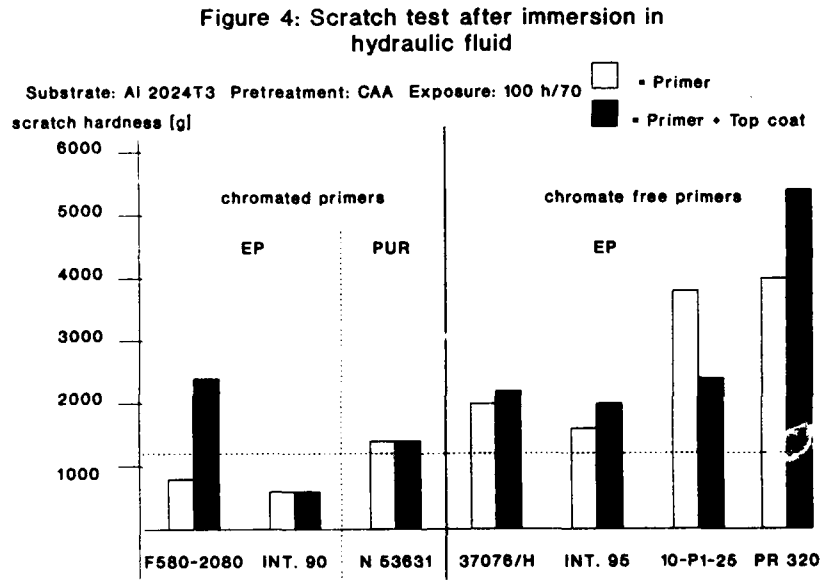
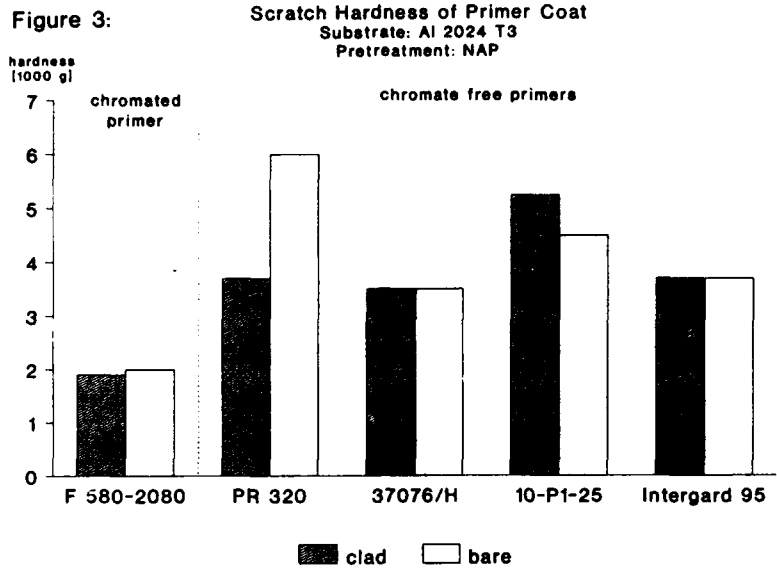


Figure 6: Filiform corrosion test with etched specimens

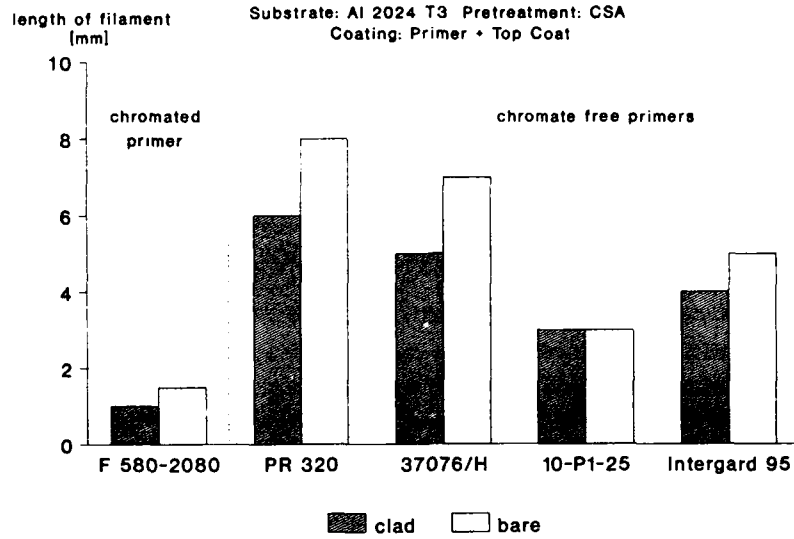


Figure 7: Crevice Corrosion test

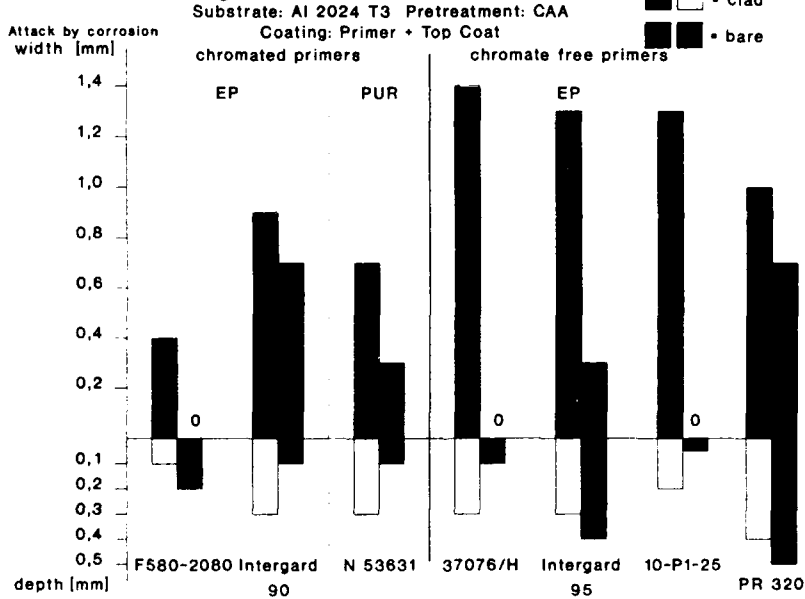
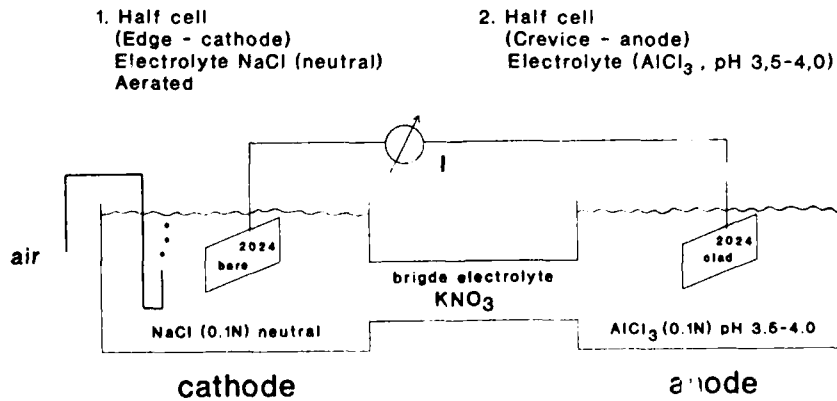


Figure 8: Set-up for Current Density Measurements



Development of a Non-Cyanide Cadmium Pulse Plating Process

James J. Steppan
Martin Marietta Electronics, Information, and Missiles Group
P.O. Box 5837 MP 88
Orlando, Florida 32855-5837

Dana M. Rocca
Martin Marietta Electronics, Information, and Missiles Group
P.O. Box 5837 MP 88
Orlando, Florida 32855-5837

John B. Carraway
Martin Marietta Electronics, Information, and Missiles Group
P.O. Box 5837 MP 88
Orlando, Florida 32855-5837

Vinod S. Agarwala
Naval Air Warfare Center
Code 6062
Warminster, Pennsylvania 18974-0591

Abstract

Cadmium is the coating of choice for high strength steel fasteners in many Navy applications, even though it is electrodeposited primarily from hazardous cyanide baths. A government initiative has been established to replace cyanide baths used in the plating industry. The objective of this study was to develop a pulse plating process capable of producing cadmium deposits which rival those from cyanide baths using a sulfate bath formulation with no complexing agents and near neutral in pH.

The bath formulation for this investigation contained 0.234M cadmium sulfate, 0.282M sodium sulfate, 0.400M boric acid, and was maintained at a pH of 5.5 and an operating temperature of 30°C. Direct current (dc) deposits from this formulation produced large grain deposits with only partial substrate coverage. Taguchi experimental designs were used to evaluate the effects of pulse plating (PP) variables (cathodic current density (CCD), symmetry (SYM), anodic current density (ACD), pulse recurrence frequency (PRF), surfactant concentration, and hydrodynamic conditions) upon cadmium deposit characteristics. The results provided criteria for selection of plating conditions which were effective in reducing the grain size, improving the deposit coverage, and significantly decreasing plating times.

Introduction

Cadmium is utilized in military systems as an electrodeposited coating for structural metals because of attributes such as corrosion protection, lubricity, solderability, electrical contact resistance, and appearance. Cadmium coatings are widely used to minimize galvanic corrosion between high strength steel fasteners and aluminum in the aerospace industry. An additional benefit of cadmium coatings is their lubricity, or low coefficient of friction, which reduces fastener tightening torque and

Key terms: cadmium, non-cyanide, pulse plating, deposition

allows repetitive dismantling ¹. Cadmium is readily solderable with non-acid (electronic) fluxes ². The contact resistance of cadmium is lower than zinc, and cadmium forms tightly adherent corrosion products, while zinc has the disadvantage of forming voluminous corrosion products ^{1,2}. This attribute of cadmium electrodeposits allows for proper functioning of moving parts, threaded assemblies, valves, and delicate mechanisms during corrosive exposure without tight clearances being filled with corrosion debris ¹.

Cadmium coatings are applied by vacuum deposition, mechanical plating, and electroplating. More cadmium is used for electroplating than for any other industrial use ². Cadmium is almost exclusively plated from cyanide baths which are easy to control and produce fine-grained, uniform deposits over complex shapes. With the recent trend toward reduction of hazardous chemical waste generation, a number of non-cyanide plating processes have been developed, but these have been shown to be inferior to cyanide baths. Thus, the development of a high-speed, non-cyanide cadmium pulse plating process which utilizes a plating formulation without complexing agents or toxic organic additives is of paramount importance, especially for military applications.

The objective of this investigation is to improve non-cyanide cadmium plating technology by developing non-cyanide bath formulations without complexing agents or toxic organic additives and by utilizing pulse plating to obtain cadmium deposits which rival those from cyanide baths. This paper describes our efforts to determine the effects of pulse plating variables upon cadmium deposition and to define those plating conditions leading to cadmium deposits with the finest grain size and most complete substrate coverage with a minimal number of experiments.

Figure 1 shows an overview of the approach to this investigation. The first step was to review the results of others who have performed non-cyanide cadmium plating investigations. Sulfate, acetate, and bromide were selected from the many bath formulations revealed by the literature survey as candidate supporting electrolytes. Bath screening studies were performed to characterize the physical, chemical, and electrochemical properties of candidate plating bath formulations prior to initiating the pulse plating experiments. Cyclic voltammetry (CV) was performed at a platinum rotating disk electrode (RDE) to examine the effects of agitation, pH, temperature, cadmium concentration, supporting electrolyte, and surfactant concentrations upon cadmium electrodeposition. The results of these experiments led to the selection of a sulfate bath formulation for the dc and pulse plating experiments. Taguchi experimental design techniques were used to evaluate the effects of six pulse plating variables (CCD, SYM, ACD, PRF, surfactant concentration, and hydrodynamic conditions) upon cadmium deposition. Energy dispersive X-ray fluorescence (EDXRF) techniques were implemented for characterizing the cadmium concentration in solution and the thickness of cadmium electrodeposits. The results of pulse plating optimization were used to produce 24 samples which were prepared to demonstrate that the process is reproducible and to be used in subsequent corrosion resistance and hydrogen embrittlement evaluations. Prior to producing the demonstration samples, it was necessary to develop and implement a process for reproducibly cleaning high strength steel (4340) substrates before electroplating in order to produce samples with uniform coverage and good adhesion.

Experimental

Experimental Setup and Electrodes

A diagram of the experimental setup for the dc and pulse plating studies is shown in Figure 2. A cadmium counter electrode, positioned as shown in Figure 2, was used when plating disks. Three cylindrical cadmium anodes were used when plating cylindrical substrates. The reference electrode

was mercury/mercury sulfate (MMS). High strength steel (4340) disks (2.54 cm diameter x 0.229 or 0.318 cm thick) and cylinders (1.194 cm diameter x 0.803 cm long) were used as the substrate material for a rotating cylinder electrode (RCE) and a RDE (Pine Instrument Company). The resistance between the high strength steel disk or cylinder and contact brushes when installed in the precision rotator was verified to be less than 1 ohm prior to each run.

The galvanostat used for the low current (less than 1A) experiments was an EG&G Princeton Applied Research (PAR) Model 273 galvanostat. The galvanostat used for the high current experiments (1A to 20A) was a Kepco 20-20M Bipolar Operational Power Supply/Amplifier. A calibrated current shunt was connected in series with the cathode and the potential drop across the shunt was used to determine the plating current.

Steel Pretreatment for Initial Studies

The 4340 steel substrates were machined, ground, heat treated in accordance with MIL-H-6875 (Linberg Heat Treat Company, Orlando, Florida). The hardness (Hauser 292DR Hardness Tester) of the disks was determined to be 47.6 +/- 0.3 Rockwell C after heat treatment. The disks and cylinders were again heat treated at 185 °C for 30 minutes before cleaning and plating⁴. After heat treatments, the disks and cylinders were polished with 600 grit silicon carbide paper on an automatic polisher (Leco AP-600) and a lathe, respectively, and vapor degreased. Each disk or cylinder electrode was polished immediately before each run using 0.05 micron alumina on microcloth.

Test Solutions

All of the test solutions were prepared using water from a commercially available water purification system (Millipore Milli-Q). Purge and trap gas chromatography-mass spectroscopy was used to verify that no organics were present in the water. The cadmium sulfate was at least 98% pure (Aldrich Chemical Company). The sodium sulfate and boric acid were both certified American Chemical Society grades. None of the salts were dried prior to separation of the test solutions.

Two bath formulations, Solution I (0.234M cadmium sulfate, 0.282M sodium sulfate, 0.40M boric acid) and Solution II (Solution I plus 0.0345M nonylphenol ethoxylate), were used for the dc and pulse plating experiments. Both solutions were maintained at a pH of approximately 5.5 and an operating temperature of 30 +/- 0.5 °C. The solutions were not deaerated prior to performing dc and pulse plating experiments.

Bath Characterization

The concentrations of the constituents of the plating baths used in the dc and pulse plating formulations were routinely monitored. EDXRF (Tracor Spectrace 5000) and ultra-violet spectroscopy (Bausch and Lomb Spectronic 2000) were performed for cadmium and surfactant concentration determination. Boric acid concentration was periodically determined by titration⁵. The pH of the plating solutions was determined using a pH meter (Corning) which was standardized daily using standard buffers with pH values of 7.00 and 4.00. The temperature of the test solutions was maintained at 30.0 +/- 0.5°C.

Deposit Characterization

The appearance and coverage of cadmium deposits were rated on a scale from 0 to 10 after examining the deposits with an optical microscope (40 to 120 times magnification) and a scanning electron microscope (50 to 2500 times magnification). Typical deposit morphology photographs were taken in the center of the disks. In addition, EDXRF was used to characterize the thickness and

coverage of the cadmium deposits. Independent metallurgical cross-section thickness measurements were performed in conjunction with EDXRF to develop a quantitative nondestructive technique for measuring the thickness of cadmium deposits.

Results

Bath Formulation

The bath formulation for this investigation contains 0.234M cadmium sulfate, 0.282M sodium sulfate, and is maintained at a pH of 5.5 and an operating temperature of 30 +/- 0.5 °C. In addition, boric acid was added to all bath formulations at a concentration of 0.40M. Boric acid is reported to increase the nucleation density during deposition of nickel ^{6,7}, cobalt-zinc alloys ⁸, nickel-zinc alloys ⁹, iron-nickel ¹⁰, and cadmium ¹¹. Nonylphenol ethoxylates were chosen as a class of surfactants to be added to the plating bath formulations to decrease surface tension, and increase the overpotential necessary for cadmium electrodeposition. This type of surfactant was used by Tomassi et.al ¹² in acid sulfate cadmium plating formulations.

dc Plating

Figure 3 and Figure 4 show the morphologies of cadmium deposits produced under dc plating conditions at a steel disk rotating at 97 rpm (Reynold's number, $Re = 1500$) in Solutions I and II, respectively. Increasing the current density from 10 to 20 mA/cm² improved the coverage due to the larger overpotential. The presence of 30 g/L nonylphenol ethoxylate decreased the grain size and increased the substrate coverage of the cadmium deposit, but caused the deposit to become dull and powdery. Similar results were obtained for dc deposits when the hydrodynamic conditions were turbulent ($Re = 40,000$).

Initial Taguchi Experimental Design

The Taguchi method of experimental design ^{13,14} was selected as a means of screening a large number of variables with a minimum number of experiments. The pulse plating and hydrodynamic conditions at the cathode have a significant effect upon the rate of cadmium electrodeposition and the deposit quality. A good fundamental understanding of the effects of pulse plating and hydrodynamic conditions upon the electrodeposition process facilitates the selection of the variables and ranges for optimization.

Pulse Plating Conditions. Pulse plating offers the possibility of achieving enhanced instantaneous mass transport and provides additional process parameters which can be varied independently to influence deposit properties ¹⁵. There are four independent variables (ACD, CCD, and anodic (t_a) and cathodic (t_c) pulse times) which can be varied during pulse plating, but only one (current density) for dc plating. These independent parameters enable one to vary mass transport, electrocrystallization and/or adsorption and desorption conditions during both the anodic and cathodic pulse periods ¹⁶.

Hydrodynamic Conditions. High electrolyte flow velocities enable the use of high current pulses during pulse plating. Well-defined hydrodynamic conditions ensure reproducible plating conditions and are important for scale-up considerations. Most non-cyanide cadmium investigations were performed at stationary electrodes in either quiescent or stirred solutions. A few investigators ^{17,18,19} have performed non-cyanide cadmium electrodeposition studies under well-defined hydrodynamic conditions.

Table I outlines the pulse plating variables and ranges selected for optimization in the initial experimental design. The levels of variables shown in Table I were selected after examining the results of the cyclic voltammetric bath screening studies, the operating conditions used in other pulse plating investigations^{16,17,19,20}, and practical issues such as size and speed limitations of commercially available power supplies and rectifiers. The $L_8 (2^7)$ design matrix shown in Table II was selected for preliminary experiments designed to determine the effects of pulse plating conditions upon deposit appearance and coverage. Column 3 (variable C) is reserved for interaction effects between CCD (variable A) and SYM (variable B). Interaction effects between variables A and B were observed by other investigators^{17,20} and one would expect this interaction to be significant as the product of A times (1-B) is the cathodic charge per pulse cycle. The low and high levels for Re (variable G) correspond to laminar and fully developed turbulent flow, respectively. All of the runs in Table II were performed under conditions of constant total (net) charge of 125 coulombs which corresponds to a theoretical thickness of 16.6 microns (0.652 mils) assuming 100 % efficiency and the density of the cadmium deposit is 8.642 g/cm³. The last column in Table II shows the run times in minutes.

Results from Initial Taguchi Experimental Design. The pulse plating experiments performed as part of the $L_8 (2^7)$ Taguchi design were effective in obtaining a significant amount of information with a minimal number of experiments. The results of the experiments are summarized in Table III. Table IV is a response table calculated from the results shown in Table III. The response results show that the effects of PRF and ACD upon deposit quality are negligible (difference less than 1.0). The remaining variables significantly influence the deposit quality. There is a strong (A x B) interaction effect between CCD and SYM. In fact, this interaction effect is stronger than the other main effects. The Taguchi responses shown in Table IV predict that the optimal deposit will be obtained under the conditions of $A_1B_1D_1E_2F_1G_2$. The confirmatory experiment showed that deposits (Figure 5) produced under these conditions had the best average deposit rating ($(8.0 + 9.8)/2 = 8.9$) and showed an improvement over dc plating (Figure 3) in an additive-free formulation. Although the confirmatory experiment gave results which provided the best average deposit rating, there were still voids in the deposit and the plating time was 21.6 minutes.

Prior to initiating another Taguchi experimental design, the previous results and program objectives were reviewed. The goals were to decrease the grain size, enhance the coverage of the deposit, and decrease the plating time as well. The grain size decreases with increasing CCD, but higher CCD values cause excessive deposition in the high current density areas.

Final Taguchi Experimental Design

In order to accomplish the above-mentioned goals, a Taguchi experimental plan was designed to optimize CCD, ACD, and SYM. Table V shows the ranges of the variables to be optimized. There was no surfactant in the bath formulation due to the negative influence observed from the initial $L_8 (2^7)$ Taguchi experimental results. The rotation rate was fixed at $Re = 40,000$ in order to ensure a high flux of cadmium ions to the rotating electrode when plating at high CCD values. The PRF was fixed at 500 Hz as it was observed during the initial Taguchi experiments that the anodic and cathodic disk potentials (vs MMS) never reached a steady state value at a PRF of 5000 Hz. The final Taguchi $L_9 (3^4)$ design matrix is shown in Table II.

Results from Final Taguchi Design. The results from the final pulse plating experiments are summarized in Table VII. Table VIII is a response table calculated from the results shown in

Table VII. The Taguchi responses shown in Table VII predict that the optimal deposit will be obtained under the conditions of $A_3B_1C_3$. The confirmatory experiment showed that deposits (Figure 6) produced under these conditions had the best average deposit rating ($(9.5 + 8.0)/2 = 8.8$) and showed a significant reduction in grain size compared to Figure 5 and a significant reduction in plating time (0.56 minutes). Although the confirmatory experiment gave results which provided the best average deposit rating, there were still some excess cadmium grains on the surface indicating the need for additional refinement. The excess cadmium grains on the surface may be attributed to insufficient cadmium being etched from the surface during the anodic portion of the pulse cycle. Figure 7 and Figure 8 show the actual current and potential (vs MMS) waveforms for the final confirmatory experiment. The desired anodic and cathodic current values were not reached and maintained as the maximum power output capacity of the bipolar power supply (20 Volts, 400 Watts) was exceeded. Although the waveform shown in Figure 7 is not desirable from a technology transfer standpoint, it was reproducible for our cell geometry. Efforts were taken to minimize the solution resistance (iR drop) by moving the anodes as close as possible and increasing the anode surface area. Future efforts will require a larger capacity power supply or a decrease in the resistance between anodes and cathode.

All of the substrates used in the initial and final Taguchi pulse plating optimization studies were cleaned as outlined previously, but did not reproducibly pass adhesion tests²². It was felt that some of the bare spots observed in the pulse plated deposits may have been caused by inclusions and/or dirty spots on the steel substrates.

Steel Cleaning Methods for Process Demonstration

It was necessary to develop a chemical/electrochemical cleaning procedure to ensure good adhesion of cadmium electrodeposits to the 4340 steel substrate. Table IX outlines the cleaning procedure used for the high strength steel disks and cylinders. This procedure is similar to that used by others^{4,21} and produces cadmium electrodeposits which pass an adhesion tape test²².

Process Demonstration

The production of demonstration samples requires the integration of the results from the pulse plating optimization, steel cleaning, and bath and deposit characterization tasks. Twenty four (24) samples; three (3) sets of four high strength steel test rings and four high strength steel disks, each coated with a different cadmium plating thickness (12 rings and 12 disks) were fabricated for future corrosion tests, salt spray resistance, and hydrogen embrittlement tests. Table X summarizes the plating thicknesses for each sample as determined by X-ray fluorescence. Figure 9 and Figure 10 show typical morphologies of the cadmium deposits on cylinders and disks, respectively. The disks and cylinders were cleaned as shown in Table IX, pulse plated using the current waveform shown in Figure 7 in Solution I under turbulent ($Re = 40,000$) hydrodynamic conditions.

Discussion

The results from this investigation are consistent with the results of other investigations of pulsed electrodeposition of cadmium from non-cyanide baths^{16,17,18,19,23,24,25,26,27,28}. Non-cyanide plating formulations for dc plating require organic additives to increase the overpotential for cadmium electrodeposition and obtain good cadmium deposits. Pulse plating enables one to increase the overpotential for cadmium electrodeposition and obtain good cadmium deposits from additive-free bath formulations. Abd El-Halim and co-workers^{23,24} report that superimposed ac modifies the growth morphology and produces brighter cadmium deposits than those produced by dc from both

chloride and acetate baths. Puippe and Ibl¹⁷ report that pulse plating improves the covering power and decreases the grain size of the cadmium deposits from acid sulfate baths. This improvement is attributed to an enhancement of nucleation by the high pulsed CCD and the resulting high overpotential, which allows metal to grow on sites that are inhibited under conditions for dc plating. Varma and co-workers^{18,19} found that the use of high CCD pulses was instrumental in nucleating fine-grained, near hydrogen-free cadmium electrodeposits from fluoborate solutions. The nucleation of a fine-grained cadmium deposit minimized the codeposition of hydrogen since hydrogen enters steel through the pores of the coating and the hydrogen overpotential of steel is much lower than that of cadmium²⁹. In addition, any codeposited hydrogen can be desorbed or oxidized during the anodic pulse period.

The non-cyanide cadmium pulse plating process developed under this effort shows promise as an additive-free environmentally-friendly alternative to cyanide cadmium plating bath formulations. However, additional refinement and development are necessary to implement such a process for commercial and military applications. The greatest process concerns are with the hydrodynamic and bipolar power supply requirements when plating large amounts of small parts or large surface area parts. The hydrodynamic requirements for small parts can be met with plating barrels while the effluent from filtration pumps can be directed across large parts.

The other concern is that future environmental legislature may eliminate the use of cadmium. If cadmium is absolutely necessary for naval aircraft applications, then it is necessary to develop and implement methods to minimize and recycle cadmium waste. For example, it is possible to reclaim cadmium from spent plating solutions and rinse waters by electroplating the cadmium on mesh electrodes in a fluidized bed electrochemical cell.

Another approach is to consider environmentally safer alternatives to cadmium plating^{30,31,32}. Zinc alloys show promise as safer alternatives to cadmium, however a significant amount of development will be necessary to define and develop suitable plating processes and to verify corrosion performance.

Acknowledgements

This research was supported by the Naval Air Warfare Center under Contract N62269-91-C-026.

References

1. ASTM B766-86, "Standard Specification for Electrodeposited Coatings of Cadmium."
2. W.H. Safranek, "Cadmium," The Properties of Electrodeposited Metals and Alloys, 35-44, American Electroplaters and Surface Finishers Society, Orlando, FL, (1986).
3. H. Morrow, "Cadmium Plating," 58th Metal Finishing Guidebook-Directory, 179-182, Metals and Plastics Publications, Inc., Hackensack, NJ, (1990).
4. ASTM B-242-54, "Standard Practice for Preparation of High-Carbon Steel for Electroplating," (1985).
5. D.G. Foulke, and F.E. Crane, Jr., Electroplaters' Process Control Handbook, Reinhold Publishing Corporation, New York, p. 203, (1963).
6. J.P. Hoare, "On The Role of Boric Acid in the Watts Bath," J. Electrochem. Soc., 133 (12), 2491-2492, (1986).
7. J.P. Hoare, "Boric Acid as a Catalyst in Nickel Plating Solutions," J. Electrochem. Soc., 134, (12), 3102-3103, (1987).
8. C. Karwas, and T. Hepel, "Morphology and Composition of Electrodeposited Cobalt-Zinc Alloys and the Influence of Boric Acid," J. Electrochem. Soc., 136(6), 1672-1678, (1989).

9. C. Karwas, and T. Hepel, "Influence of Boric Acid on Electrodeposition and Stripping of Ni-Zn Alloys," J. Electrochem. Soc., **135**(4), 839-844, (1988).
10. J. Horkins, "Effect of Plating Parameters on Electrodeposition of NiFe," J. Electrochem. Soc., **128**(1), 45-49, (1981).
11. R.E. Dueber, and D.H. Fritts, "The Effect of Boric Acid Additions on Cadmium Electrode Migration in Potassium Hydroxide Electrolytes," J. Electrochem. Soc., **133**(7), 1292-1296, (1986).
12. P. Tomassi, J.A. Weber, and T. Zak, "Optimization of the Composition of the Sulphate Bath for Cadmium Plating," Surface Technology, **7**, 493-503, (1978).
13. Taguchi Methods: Introduction to Quality Engineering 5-Day Workshop Course Manual, American Supplier Institute, Inc., Dearborn Michigan, (1989).
14. G. Taguchi, and S. Konishi, Taguchi Methods: Orthogonal Arrays and Linear Graphs, American Supplier Institute, Dearborn, Michigan, (1987).
15. M. Datta, and D. Landolt, "Experimental Investigation of Mass Transport in Pulse Plating," Surface and Plating Technology, **25**, 97-110, (1987).
16. N. Ibl, J.Cl. Puipe, and H. Angerer, "Electrocrystallization in Pulse Electrolysis," Surface Technology, **6**, 287-300, (1978).
17. J.Cl. Puipe, and N. Ibl, "The Morphology of Pulse-Plated Deposits," Plating and Surface Finishing, 68-72, June, (1980).
18. R. Varma, H. Shimotake, T.L. Hoeller, and V.S. Agarwala, "Electrodeposition of Cadmium from Aqueous Fluoborate Electrolytes," Materials Performance, 39-44, May, (1988).
19. R. Varma, T. Hoeller, L. Ross, V.S. Agarwala, "Reduced Hydrogen Cadmium Plating," J. Electrochem. Soc., **138**, 162-165, (1991).
20. P. Leisner, D. Ulrich, and P. Moller, "The Application of The Taguchi Statistical Method in Pulse Plating. Example: Hard Chromium Plating," AESF Pulse Plating Symposium, January, 1991, Orlando, Florida.
21. E.C. Groshart, "Preparation of Basis Metals for Plating," Metal Finishing Guidebook and Directory, 154-157, (1992).
22. ASTM D3359-83, "Standard Methods for Measuring Adhesion by Tape Test," (1983).
23. A.M. Abd El-Halim, A.O. Baghlaf, and M.I. Sobahi, "Influence of A Superimposed A.C. on Cadmium Electroplating from An Acidic Chloride Bath," Surface Technology, **22**, 143-154, (1984).
24. A.M. Abd El-Halim et al, "Electroplating of Bright Cadmium from An Optimized Acetate Bath under The Influence of Superimposed Alternating Current," J. Applied Electrochem., **17**, 49-56, (1987).
25. V.S. Kublanovskii et al, "Selection of Optimal Parameters of A Pulsating Current from Electrodeposition of Cadmium (II) from A Trilonate Electrolyte," Soviet Progress in Chemistry, **52**, 32-36, (1986).
26. W. Paatsch, "Pulsed Electrodeposition of Zinc and Cadmium," Theory and Practice of Pulse Plating, 93-100, American Electroplaters and Surface Finishers Society, Orlando, Fl, (1986).
27. Y.A. Popkov, V.V. Grinina, and Y.M. Polukarov, "Current Yields in Copper and Cadmium Electrodeposition with Periodic Currents," Soviet Electrochem., **24**, 1146-1149, (1989).
28. J.Cl. Puipe, and N.Ibl, "Influence of Charge and Discharge of Electric Double Layer in Pulse Plating," J. Applied Electrochem., **10**, 775-784, (1980).
29. V.P. Maksimchuk, "Development of Cadmium Plating Baths with Low Hydrogenating Tendency," Soviet Electrochem., **23**, 609-611, (1987).
30. R. Griffin, and P.F. Kasper, "Environmentally Safer Alternatives to Cadmium Plating," Metal Finishing, 51-52, April, (1990).
31. G.F. Hsu, "Zinc-Nickel Alloy Plating: An Alternative to Cadmium," Plating and Surface Finishing, 52-55, April, (1984).
32. C.H. Ko, C.C. Chang, L.C. Chen, and T.S. Lee, "A Comparison of Cadmium Electroplate and Some Alternatives," Plating and Surface Finishing, 46-49, October, (1991).

Table I. PULSE PLATING VARIABLES

| VARIABLE NO. | DESCRIPTION | LOW VALUE (1) | HIGH VALUE (2) |
|--------------|-------------------------------------------------|---------------|----------------|
| A | Cathodic Current (i_c (mA/cm ²)) | 2 | 2000 |
| B | (SYM (%)) | 5 | 95 |
| C | A x B Interaction | | |
| D | Anodic Current (i_a (mA/cm ²)) | 0.0 | -50 |
| E | Pulse Recurrence Frequency (PRF (Hz)) | 50 | 5,000 |
| F | Surfactant Concentration (SUR (g/L)) | 0 | 30 |
| G | Reynold's Number (Re) | 1,500 | 20,000 |

Table II. INITIAL PULSE PLATING L₈ (2⁷) TAGUCHI EXPERIMENTAL DESIGN

| EXPERIMENT No. | VARIABLES | | | | | | | RUN TIME (MIN) |
|----------------|------------|--------------|---|------------|---------------|----------------|---------|----------------|
| | A i_c | B SYM (%) | C | D i_a | E PRF (Hz) | F SUR (g/L) | G Re | |
| 1 | 1 | 1 | 1 | 1 | 1 | 1 | 1 | 21.6 |
| 2 | 1 | 1 | 1 | 2 | 2 | 2 | 2 | 24.9 |
| 3 | 1 | 2 | 2 | 1 | 1 | 2 | 2 | 411.2 |
| 4 | 1 | 2 | 2 | 2 | 2 | 1 | 1 | NA |
| 5 | 2 | 1 | 2 | 1 | 2 | 1 | 2 | 0.2 |
| 6 | 2 | 1 | 2 | 2 | 1 | 2 | 1 | 0.2 |
| 7 | 2 | 2 | 1 | 1 | 2 | 2 | 1 | 4.2 |
| 8 | 2 | 2 | 1 | 2 | 1 | 1 | 2 | 8.0 |

Table III. INITIAL PULSE PLATING L_8 (2^7) TAGUCHI EXPERIMENTAL RESULTS

| EXP. No. | VARIABLES | | | | | | | RESULTS | | |
|----------|------------|-----------------|---|------------|------------------|-------------------|---------|------------|----------|----------|
| | A i_c | B SYM (%) | C | D i_s | E PRF (Hz) | F SUR (g/L) | G Re | COVER RATE | APP RATE | AVG RATE |
| 1 | 1 | 1 | 1 | 1 | 1 | 1 | 1 | 8 | 7 | 7.5 |
| 2 | 1 | 1 | 1 | 2 | 2 | 2 | 2 | 10 | 4 | 7.0 |
| 3 | 1 | 2 | 2 | 1 | 1 | 2 | 2 | 0 | 0 | 0.0 |
| 4 | 1 | 2 | 2 | 2 | 2 | 1 | 1 | 0 | 0 | 0.0 |
| 5 | 2 | 1 | 2 | 1 | 2 | 1 | 2 | 10 | 7 | 8.5 |
| 6 | 2 | 1 | 2 | 2 | 1 | 2 | 1 | 2 | 2 | 2.0 |
| 7 | 2 | 2 | 1 | 1 | 2 | 2 | 1 | 4 | 3 | 3.5 |
| 8 | 2 | 2 | 1 | 2 | 1 | 1 | 2 | 10 | 6 | 8.0 |

EXP DEPOSIT DESCRIPTION
No.

- 1 Bright, silvery, grainy deposit with dendrites on the edges
- 2 Dull gray deposit with blade-like features and nodules covering surface, excellent coverage
- 3 No deposit
- 4 No deposit
- 5 Bright, silvery, fine grained deposit, excellent coverage, areas of excess deposit buildup, no dendrites
- 6 Dull, streaked, powdery, nonuniform deposit with bare spots
- 7 Dull, streaked, powdery deposit
- 8 Dull gray deposit with blade-like features all over surface, excellent coverage

COVER RATE = Arbitrary rating of deposit coverage of the substrate on a scale of 1 to 10.

APP RATE = Arbitrary rating of deposits appearance on a scale from 1 to 10.

AVG RATE = Average of the coverage and appearance ratings.

NA = Not Applicable

Table IV. INITIAL PULSE PLATING L_8 (2^7) TAGUCHI RESPONSE TABLES

| VARIABLES | | | | | | | |
|---------------------------------|------------|-----------------|------|------------|------------------|-------------------|---------|
| LEVEL No. | A i_c | B SYM (%) | C | D i_a | E PRF (Hz) | F SUR (g/L) | G Re |
| 1 | 3.63* | 6.25 | 6.50 | 4.88 | 4.38 | 6.00 | 3.28 |
| 2 | 5.50 | 2.88 | 2.63 | 4.25 | 4.75 | 3.13 | 5.88 |
| Difference Between Levels | -1.87 | 3.37 | 3.87 | 0.63 | -0.37 | 2.87 | 2.50 |

* Using average coverage ratings from experiments with A_1 level in Table III,
 $(7.5 + 7.0 + 0.0 + 0.0)/4 = 3.63$

A x B (C) INTERACTION RESPONSE

| | A_1 | A_2 |
|-------|-------|-------|
| B_1 | 7.25+ | 5.25 |
| B_2 | 0.0 | 5.75 |

+ Using average coverage ratings from experiments with A_1 and B_1 levels in Table III,
 $(7.5 + 7.0)/2 = 7.25$

Table V. PULSE PLATING VARIABLES FOR FINAL TAGUCHI DESIGN

| VARIABLE NO. | DESCRIPTION | LOW VALUE (1) | MID VALUE (2) | HIGH VALUE (3) |
|--------------|-------------------------------------------------|---------------|---------------|----------------|
| A | Cathodic Current (i_c (mA/cm ²)) | 500 | 1000 | 2000 |
| B | Symmetry (SYM (%)) | 30 | 45 | 60 |
| C | Anodic Current (i_a (mA/cm ²)) | -250 | -550 | -1000 |
| FIXED | Pulse Recurrence Frequency (PRF (Hz)) | | 500 | |
| FIXED | Surfactant Concentration (SUR (g/L)) | | 0 | |
| FIXED | Reynold's Number (Re) | | 40,000 | |

Table VI. FINAL PULSE PLATING L₈ (2³) TAGUCHI EXPERIMENTAL DESIGN

| EXPERIMENT No. | VARIABLES | | | |
|----------------|-----------|-----------|---------|----------------|
| | A i_c | B SYM (%) | D i_a | RUN TIME (MIN) |
| 9 | 1 | 1 | 1 | 13.8 |
| 10 | 1 | 2 | 2 | 25.1 |
| 11 | 1 | 3 | 3 | 13.8 |
| 12 | 2 | 1 | 3 | 1.3 |
| 13 | 2 | 2 | 1 | 1.6 |
| 14 | 2 | 3 | 2 | NA |
| 15 | 3 | 1 | 2 | 0.5 |
| 16 | 3 | 2 | 3 | 1.1 |
| 17 | 3 | 3 | 1 | 1.5 |

Table VII. FINAL PULSE PLATING L_9 (3^4) TAGUCHI EXPERIMENTAL RESULTS

| EXP. No. | VARIABLES | | | RESULTS | | | |
|----------|-----------|-----------|---------|----------------|------------|----------|-----|
| | A i_c | B SYM (%) | C i_a | RUN TIME (MIN) | COVER RATE | APP RATE | AVG |
| 9 | 1 | 1 | 1 | 13.8 | 7.0 | 10.0 | 8.5 |
| 10 | 1 | 2 | 2 | 25.1 | 4.0 | 4.0 | 4.0 |
| 11 | 1 | 3 | 3 | 13.8 | 9.0 | 8.0 | 8.5 |
| 12 | 2 | 1 | 3 | 1.3 | 9.5 | 6.0 | 7.8 |
| 13 | 2 | 2 | 1 | 1.6 | 9.5 | 6.0 | 7.8 |
| 14 | 2 | 3 | 2 | NA | 0.0 | 0.0 | 0.0 |
| 15 | 3 | 1 | 2 | 0.5 | 10.0 | 5.0 | 7.5 |
| 16 | 3 | 2 | 3 | 1.1 | 9.8 | 7.0 | 8.4 |
| 17 | 3 | 3 | 1 | 1.5 | 9.0 | 7.5 | 8.3 |

EXP NO. DEPOSIT DESCRIPTION

- 9 Bright, silvery, grainy deposit, no dendrites on the edges
- 10 Poor coverage and appearance
- 11 Areas with excess Cd deposits, uniform deposit underneath, no dendrites
- 12 Dark gray deposit with excess Cd powder balls
- 13 Dark gray deposit with excess Cd powder balls & blades
- 14 NA
- 15 Dark gray deposit with excess Cd powder balls
- 16 Grainy deposit with excess Cd blades
- 17 Bright, silvery deposit with excess Cd

COVER RATE = Arbitrary rating of deposit coverage of the substrate on a scale of 1 to 10.
 APP RATE = Arbitrary rating of deposits appearance on a scale from 1 to 10.
 AVG RATE = Average of the coverage and appearance ratings.
 NA = Not Applicable

Table VIII. FINAL PULSE PLATING L₉ (3⁴) TAGUCHI RESPONSE TABLES

| VARIABLES | | | |
|--------------|---------------------|-----------------|---------------------|
| LEVEL No. | A i _c | B SYM (%) | C i _a |
| 1 | 7.00 | 7.92 | 5.63 |
| 2 | 5.17 | 6.72 | 6.67 |
| 3 | 8.05 | 5.58 | 5.47 |

Table IX. CLEANING PROCEDURE FOR HIGH STRENGTH STEEL 4340 PRIOR TO CADMIUM ELECTROPLATING

| STEP | DESCRIPTION | TIME (MINUTES) |
|------|----------------------------------------------------------------------------------------------------------------------------|----------------|
| 1 | 50% (v/v) HCl, Room temperature (RT) | 5 |
| 2 | Deionized water rinse | 2 |
| 3 | Deionized water rinse | 2 |
| 4 | Alkaline Clean in Ferroprep 390 (Allied Kelite) 80 °C, 90 mA/cm ² , reverse polarity every 30 seconds | 5 |
| 5 | Hct (60 °C) deionized water rinse | 2 |
| 6 | RT deionized water rinse | 2 |
| 7 | RT deionized water rinse | 2 |
| 8 | RT 25% (v/v) HCl | 2 |
| 9 | RT deionized water rinse | 1 |
| 10 | RT deionized water rinse | 1 |
| 11 | Anodic Clean (160 mA/cm ²) 150 ml/L H ₂ SO ₄ /125 g/L Na ₂ SO ₄ | 1 |
| 12 | Running deionized water rinse | 0.5 |
| 13 | Transfer disk or cylinder to arbor | |
| 14 | RT 25% (v/v)HCl | 0.5 |
| 15 | RT deionized water rinse | 0.25 |
| 16 | RT deionized water rinse | 0.25 |

Table X. SUMMARY OF CADMIUM PLATED DELIVERABLES

| Part Type | Part Number | Thickness (Microns) | Morphology Shown in |
|-----------|-------------|---------------------|---------------------|
| Ring | 51 | 4.1 | Figure 9 |
| Ring | 61 | 4.2 | |
| Ring | 65 | 4.8 | |
| Ring | 72 | 3.5 | |
| Ring | 56 | 6.1 | Figure 10 |
| Ring | 67 | 6.2 | |
| Ring | 68 | 5.5 | |
| Ring | 71 | 5.5 | |
| Ring | 54 | 7.6 | Figure 10 |
| Ring | 59 | 7.4 | |
| Ring | 64 | 6.5 | |
| Ring | 73 | 6.7 | |
| Disk | 82 | 5.2 | Figure 10 |
| Disk | 84 | 3.0 | |
| Disk | 90 | 4.2 | |
| Disk | 95 | 3.2 | |
| Disk | 83 | 4.9 | Figure 10 |
| Disk | 103 | 7.1 | |
| Disk | 104 | 6.4 | |
| Disk | 114 | 6.7 | |
| Disk | 101 | 7.5 | Figure 10 |
| Disk | 102 | 7.2 | |
| Disk | 108 | 8.5 | |
| Disk | 109 | 8.9 | |

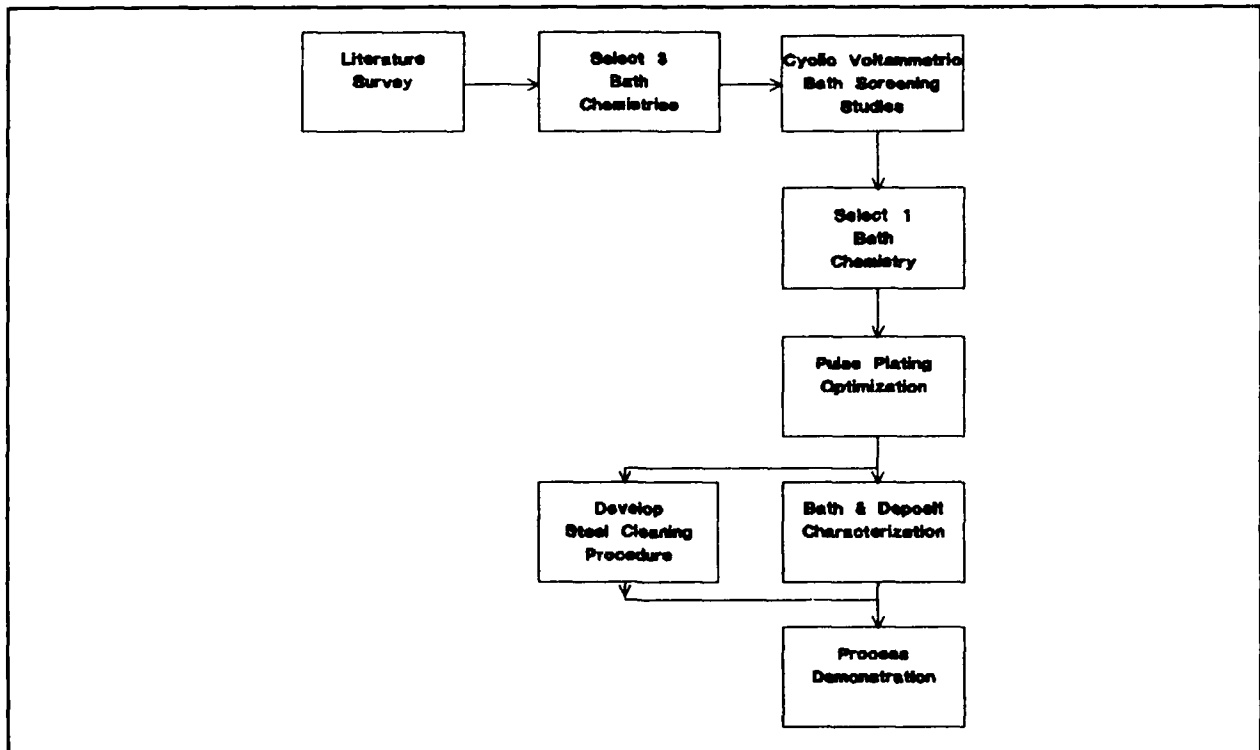


Figure 1. Flow Chart of Non-Cyanide Cadmium Pulse Plating Process Development Approach

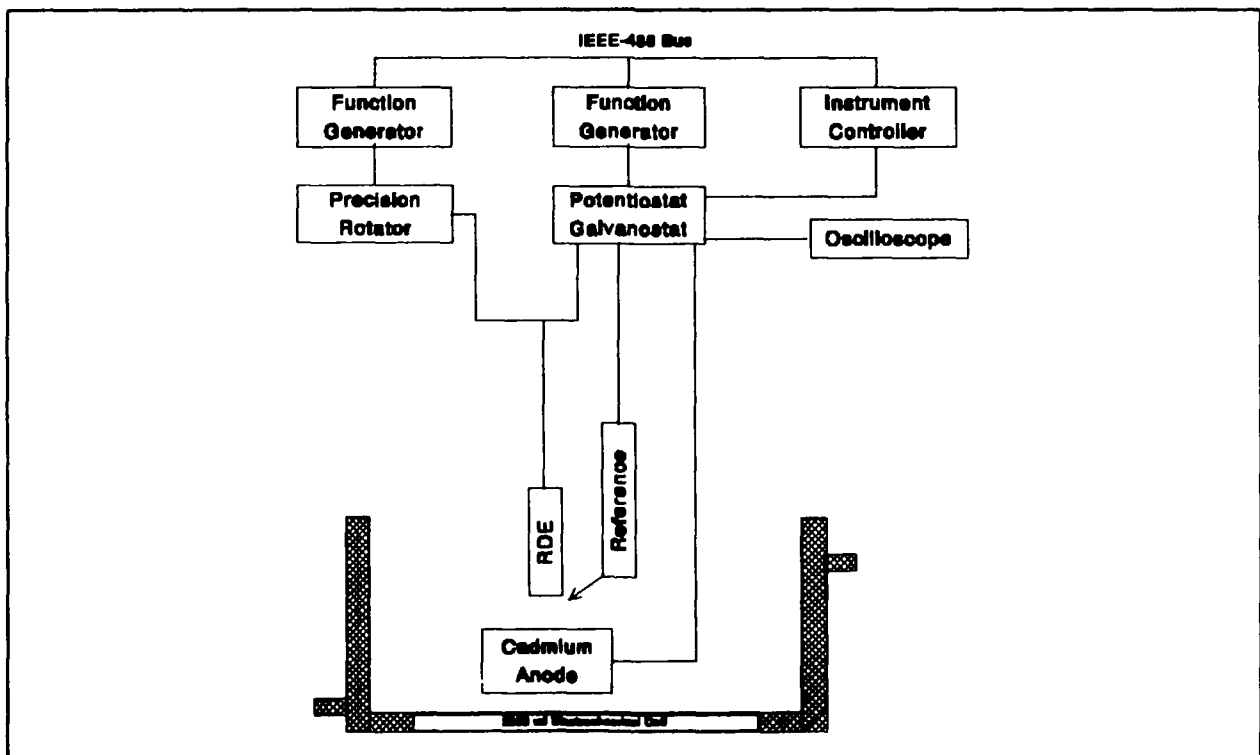
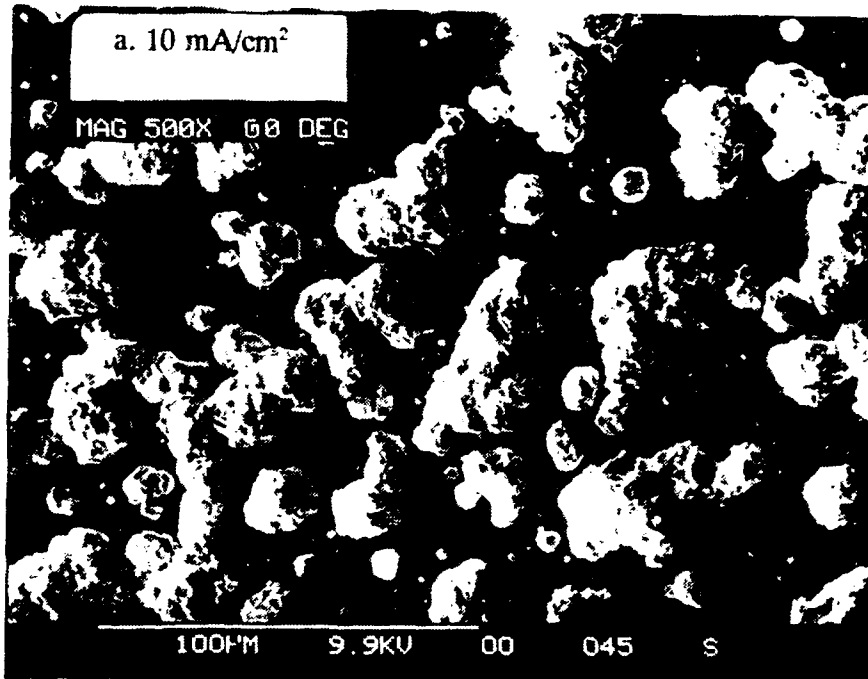
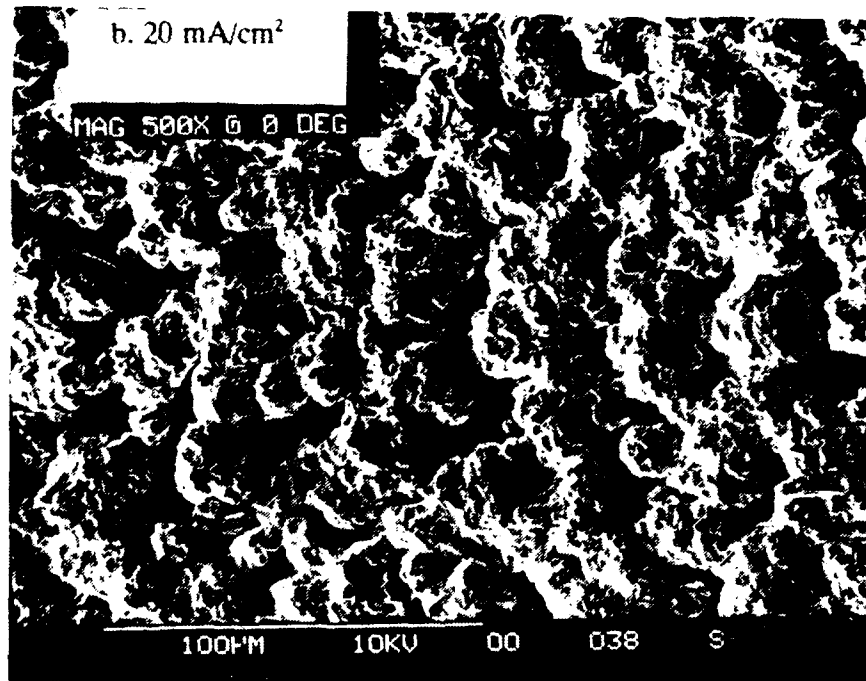


Figure 2. Experimental Setup for dc and Pulse Plating

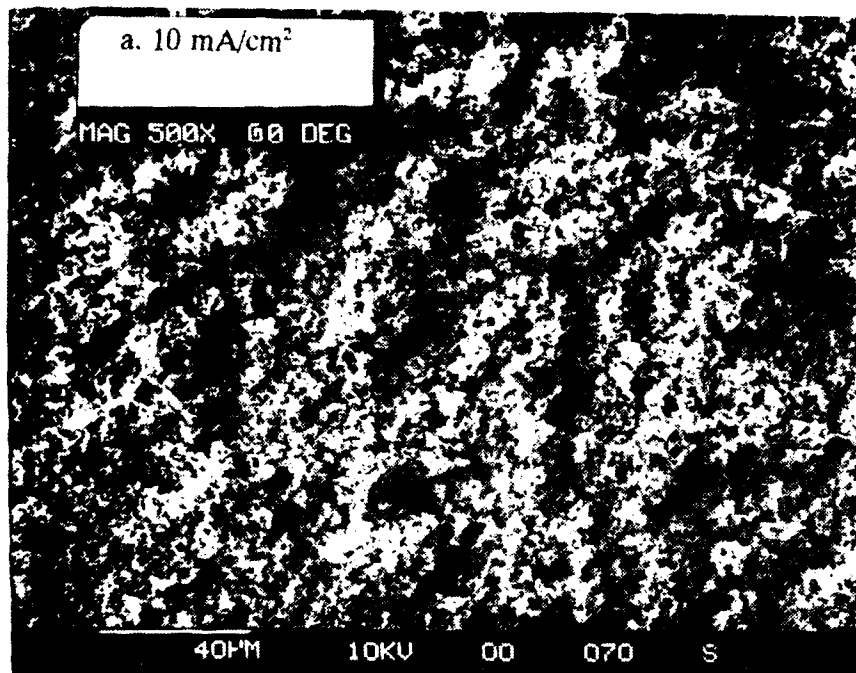


a) 10 mA/cm²

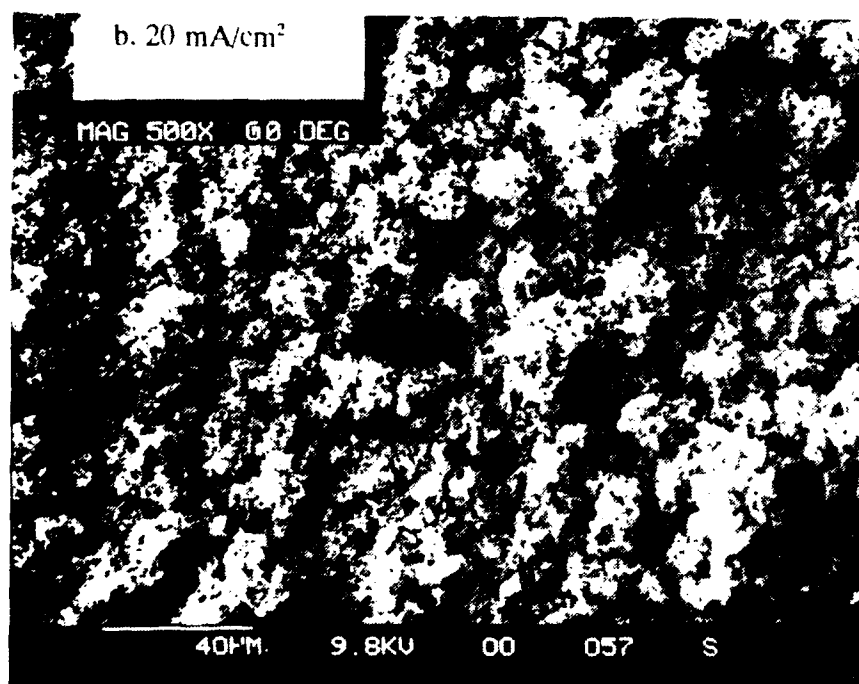


b) 20 mA/cm²

Figure 3. DC Plating Results at A High Strength Steel RDE (97 rpm) in Solution I

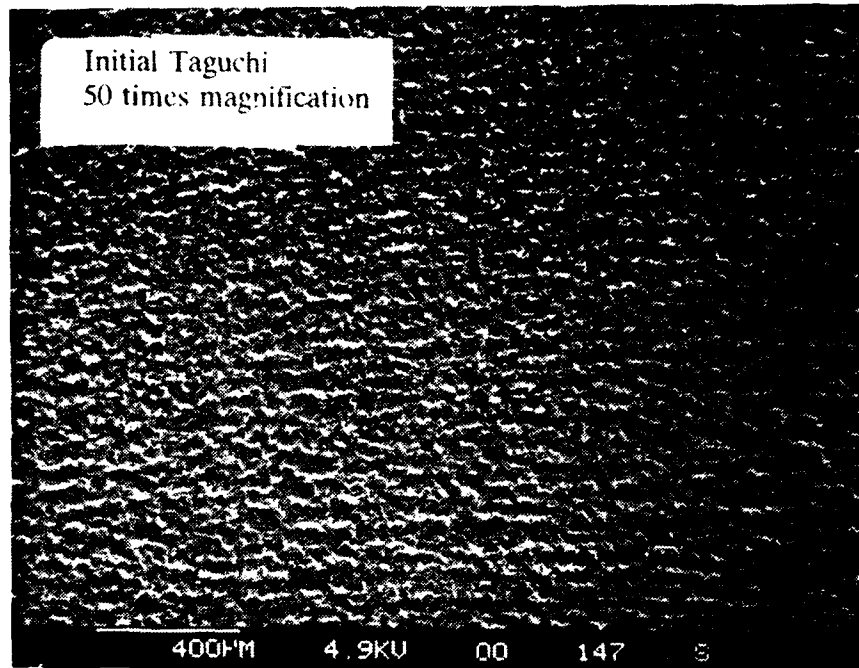


a) 10 mA/cm²

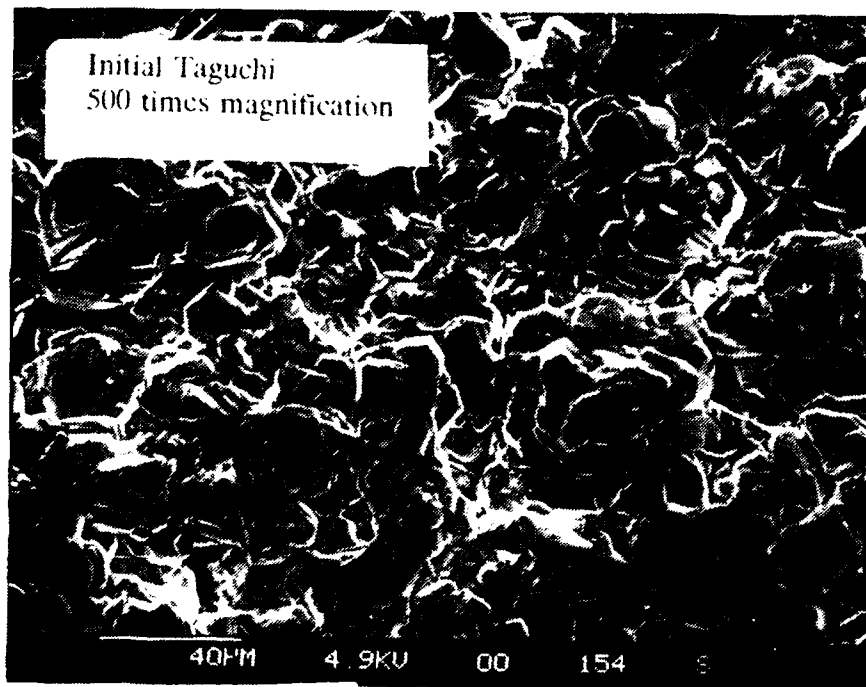


b) 20 mA/cm²

Figure 4. DC Plating Results at A High Strength Steel RDE (97 rpm) in Solution II

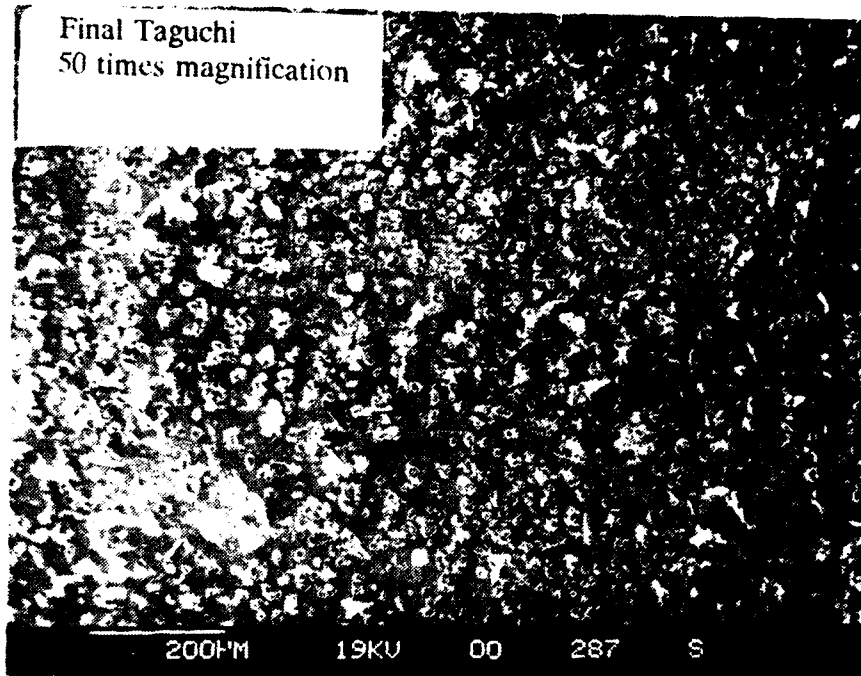


a) 50 times magnification

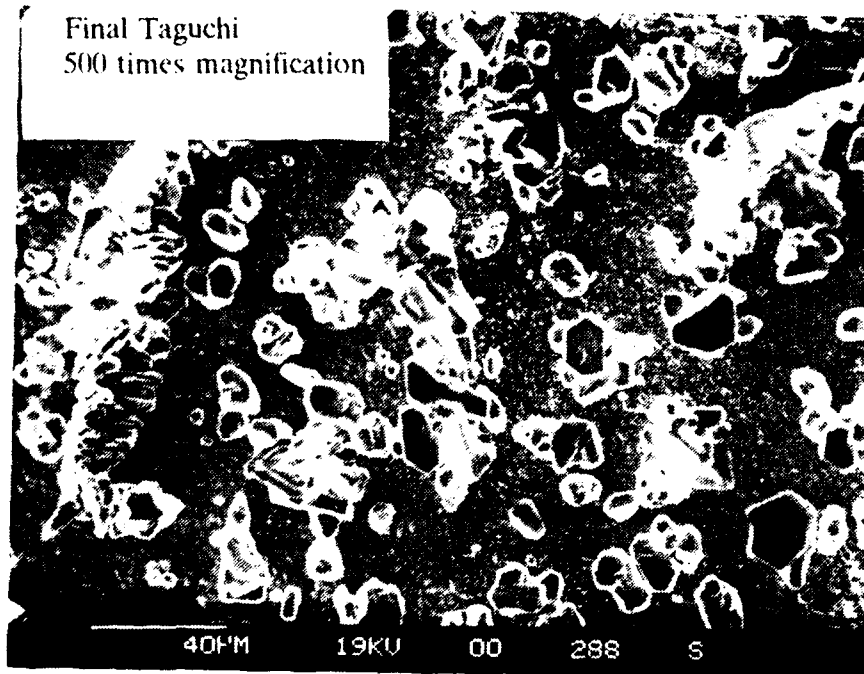


b) 500 times magnification

Figure 5. Pulse Plating Results from Initial Taguchi Confirmatory Run



a) 50 times magnification



b) 500 times magnification

Figure 6. Pulse Plating Results from Final Taguchi Confirmatory Run

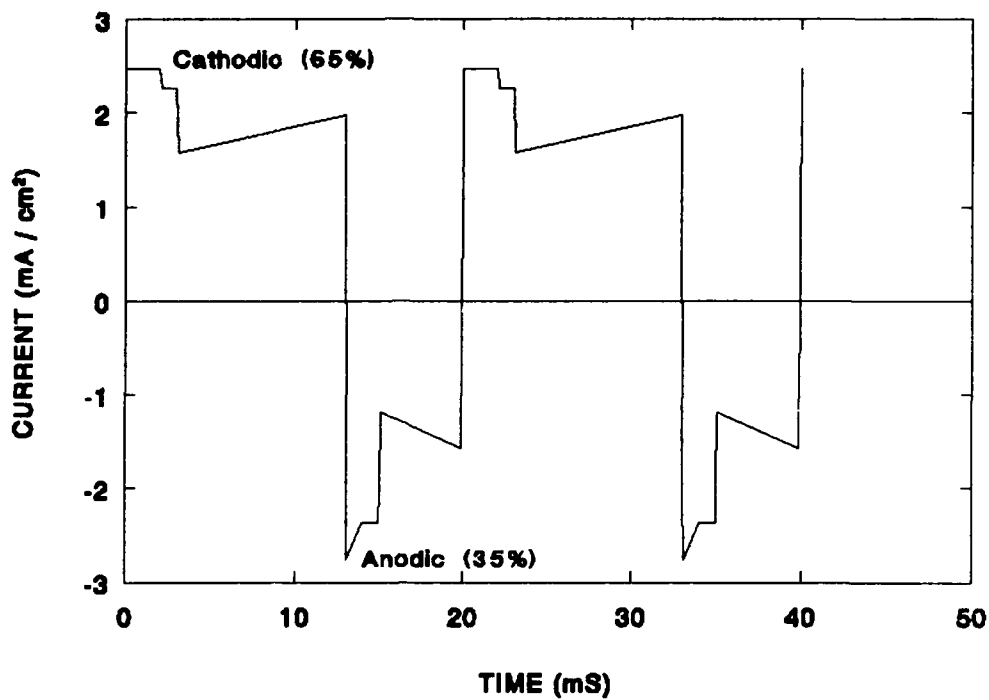


Figure 7. Current Waveform for Final Taguchi Confirmatory Run

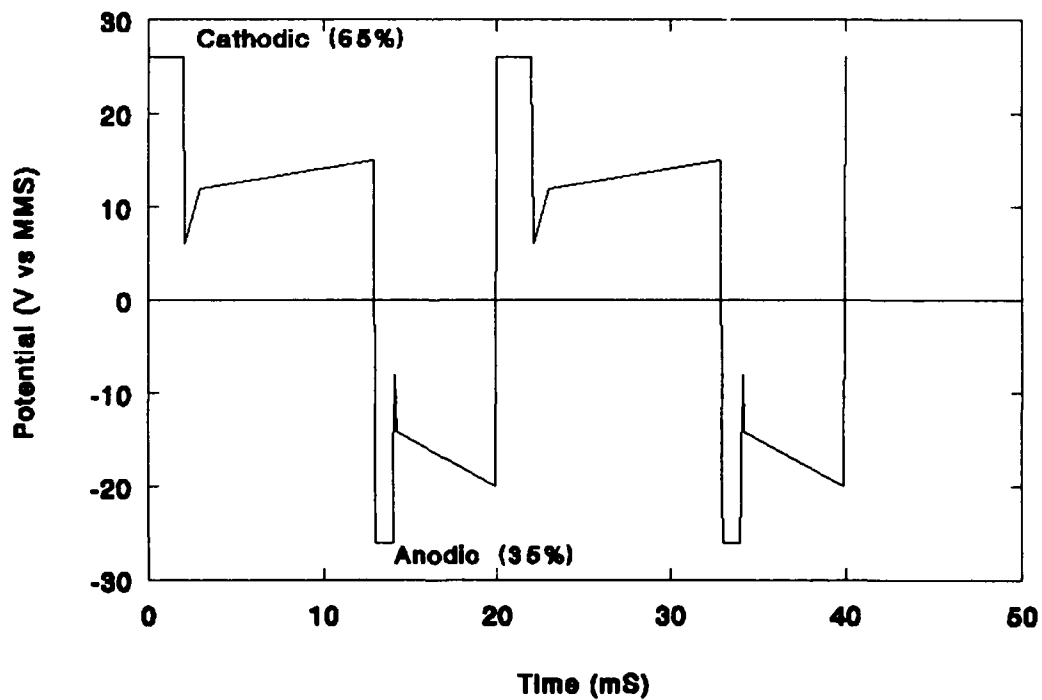
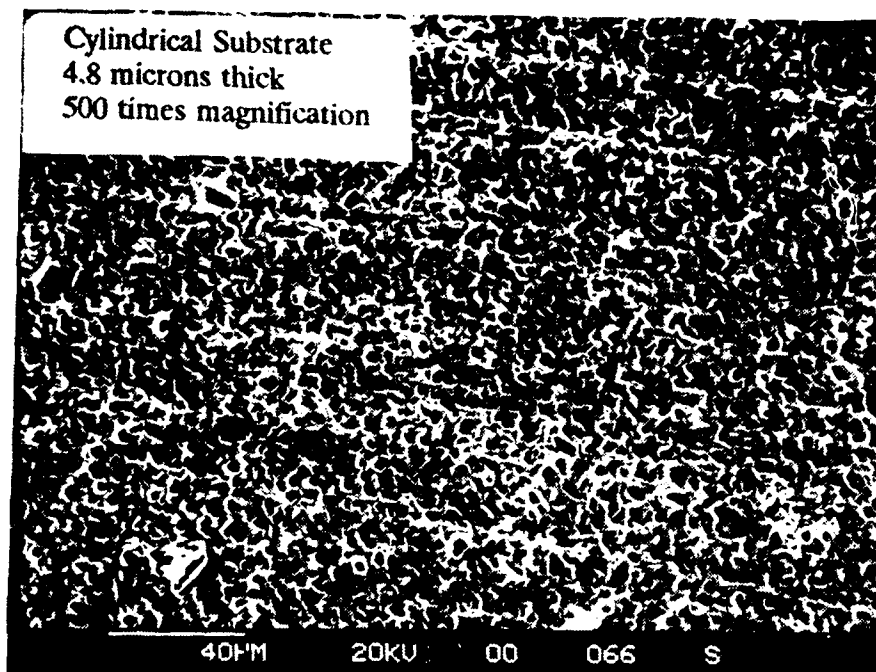
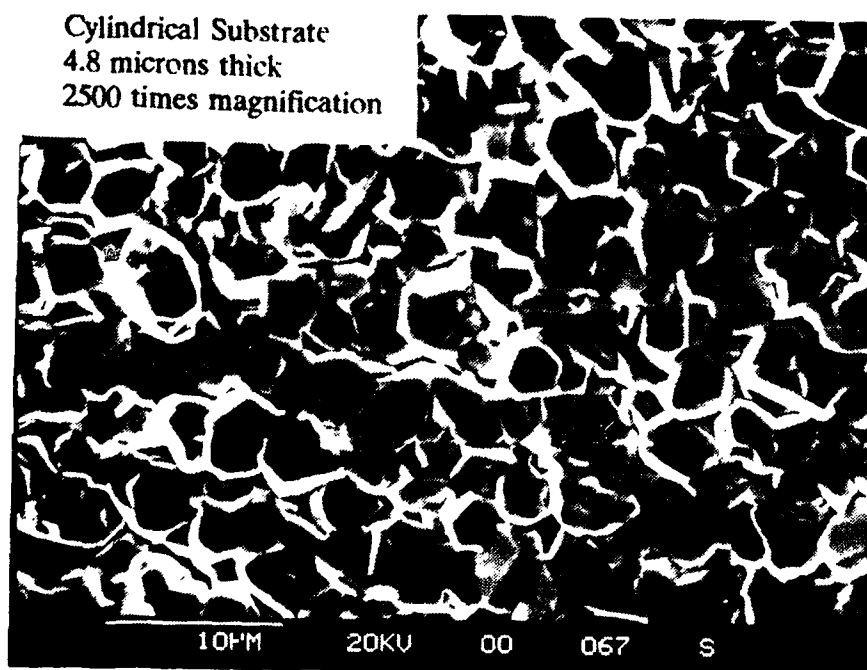


Figure 8. Potential Waveform for Final Taguchi Confirmatory Run

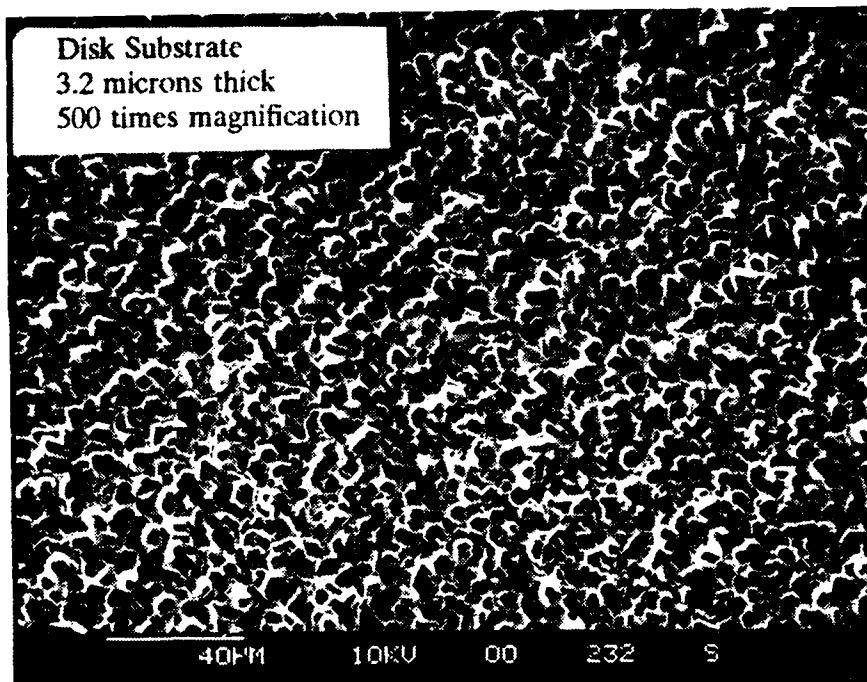


a) 500 times magnification

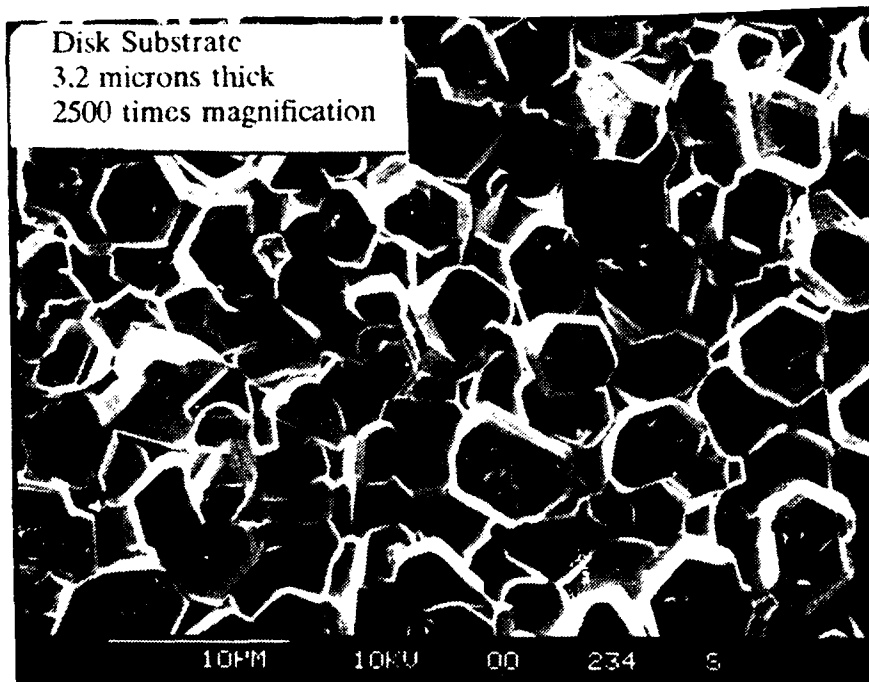


b) 2500 times magnification

Figure 9. Typical Cadmium Electrodeposit Morphology on A High Strength Steel Cylinder



a) 500 times magnification



b) 2500 times magnification

Figure 10. Typical Cadmium Electrodeposit Morphology on A High Strength Steel Disk

Effect of Surface Impurities on the Corrosion
Behavior of Type 434 Stainless Steel

Robert Baboian
Texas Instruments Incorporated
34 Forest Street, MS 10-13
Attleboro, MA 02703

Abstract

Stainless steels are widely used for exterior trim on automobiles. These material are subjected to an extremely aggressive environment and therefore, the stainless steel must be corrosion resistant. Bulk metallurgy and surface characteristics are important factors affecting the resistance to corrosion. This paper addresses reduced resistance to cosmetic localized corrosion observed with stainless steel surfaces which have been subjected to processing including the application of a protective plastic film (polyfilm). Cyclic immersion corrosion tests, Auger analysis and gas chromatography coupled with Fourier Transform Infrared Analysis (FTIR) have been used to determine the mechanism of reduced corrosion resistance and methods to restore the resistance to this type of degradation.

INTRODUCTION

Corrosion problems associated with exterior automotive trim include: 1) effects of the trim system on the auto-body and, 2) corrosion of the trim itself. The problems are caused by the severe corrosivity of the automotive environment as well as the inherent crevice geometry, attachment requirements in the trim/auto-body system, and the susceptibility of paint damage in this area.¹

The inherent corrosion resistance of the material, the quality of the surface and the design configuration are three important factors which affect the durability of trim systems. The increasing severity of the corrosive automobile environment has required changes in the selection, processing, and design of trim materials. Systems which were satisfactory in the 1950's became unsatisfactory during the 1960's. Those that were satisfactory during the 1960's and 1970's have now become susceptible. Trim systems must therefore be designed for corrosion resistance in an environment which now consists of harmful salts both from road salting and marine atmospheres, and atmospheric pollutants in the form of acid deposition.^{2,3,4}

Stainless Steel Exterior Trim

Stainless steel trim materials have been used for many years to provide a number of important functions on automobiles. Properties such as formability, strength, appearance, and corrosion resistance are considered important in choosing a trim material. Therefore, stainless steel materials such as bimetal (stainless steel clad aluminum) have been used widely in these applications.

Factors affecting the corrosion behavior of stainless steel in automotive trim include bulk composition, surface characteristics and trim design.⁵ Quality is affected by the first two of these factors. The bulk composition plays an important role in providing corrosion resistance. Type 430 stainless steel with 17% chromium was used widely up to the early 1960's, however, with the increased corrosivity of the automotive environment, this alloy was no longer corrosion resistant. Type 434 stainless steel with 17% chromium and 1% molybdenum was therefore developed. In recent years, even higher alloys have been developed for stainless steel trim applications.

Bulk impurities can be very important in the performance of the stainless steel. Carbon and nitrogen can precipitate as chromium carbides and nitrides in grain boundaries leading to reduced corrosion resistance. The chemistry of inclusions is another important factor. For example, calcium sulfide in inclusions is known to be a pit initiator in stainless steels and therefore make these alloys susceptible to localized corrosion.

The surface of the stainless steel is directly exposed to the environment in exterior trim applications and therefore its characteristics are extremely important. Chromium depletion at the surface can occur during the bright annealing process resulting in reduced corrosion resistance. Rolled in impurities during stainless steel production can also be a problem.

One of the most important factors today is the introduction of surface impurities during the trim manufacturing process. Processes used today include the application of chemicals, heat, adhesives, rubber and plastic strips, plastic protector film, roll forming lubricants, etc. The corrosion resistance of stainless steel can be affected by all of these. Therefore, even the most corrosion resistant stainless steel can become susceptible to corrosion in the aggressive automotive environment. This is demonstrated by the results reported in this paper on the effect of polyfilm protector on the corrosion resistance of stainless steel.

In recent years, some automotive trim manufacturers have applied a PVC polyfilm protector to the stainless steel surface before processing (such as rollforming) in order to prevent damage to the bright surface. An adhesive, applied to one side of the polyfilm, facilitates bonding to the stainless steel surface. The polyfilm protector is subsequently removed prior to service on the automobile. This study was conducted in order to determine what effect the application of the PVC polyfilm protector could have on the corrosion behavior of stainless steel trim.

Experimental

The cyclic immersion test was used (according to Table 1) to assess the corrosion behavior.⁶ Bimetal material which consisted of Type 434 stainless steel clad to 5052 aluminum alloy was used in the study. In all of the corrosion tests, the aluminum side of the bimetal was masked so that the stainless steel would not be cathodically protected by sacrificial corrosion of the aluminum. Two types of PVC polyfilm protector currently used in trim production was used in this study: clear PVC polyfilm and blue PVC polyfilm protectors. These contained acrylate adhesives to facilitate adhesion to the stainless steel surface. Prior to testing, the stainless steel surface was cleaned with a mag oxide or a lightalconox detergent. The mag oxide clean is an aggressive treatment to remove surface chemicals. The lightalconox clean is intended to remove only airborne deposits and not surface chemicals introduced during trim fabrication. The materials used in this study consisted of bimetal production material in the as-shipped condition, as-received by a roll former, roll formed and stamped bimetal trim parts with blue or clear polyfilm protector. All corrosion tests were performed with five specimens each and ratings are reported in Table 1 as the average for the five specimens.

Results

Initial cyclic immersion tests on current production bimetal both mag oxide andalconox cleaned, resulted in all 0 ratings for all specimens. (see Table 2) This is in agreement with the ongoing quality test program to insure excellent resistance to localized corrosion of bimetal stainless steel.

Cyclic immersion tests were conducted with as received (by rollformer) bimetal before polyfilm was applied and after polyfilm was applied and removed - both blue and clear. The results show a definite susceptibility of the stainless steel to localized corrosion where blue or clear plastic had been applied and removed. The as-received bimetal stainless steel was corrosion resistant (see ratings in Table 2).

In order to determine if corrosion resistance could be restored to bimetal stainless steel which had blue or clear polyfilm applied, the polyfilm was removed and the surface was mag oxide cleaned prior to testing. Comparison specimens were prepared by alconox clean only. The results showed that cleaning these materials with mag oxide restored the corrosion resistance and therefore removed corrosion initiating substances from the surface. The comparison parts which were only cleaned with alconox performed poorly.

At this point, it appeared that the application of protective blue and clear polyfilm was introducing a substance to the bimetal stainless steel surface which was causing reduced resistance to localized corrosion. We therefore removed a portion of blue protective polyfilm from a production part and applied it to the stainless steel surface of bimetal current production material with a known excellent corrosion resistant behavior. Results of cyclic immersion tests on this material with the polyfilm removed showed very poor rating (Table 2) and therefore, the current production bimetal had lost its corrosion resistance. The mag oxide cleaned material performed as expected restoring the excellent corrosion resistance. This test demonstrated that the observed reduction in corrosion resistance was not caused by the rollforming process but was actually caused by the polyfilm.

One important result showed that there was a time dependence of removal of the plastic polyfilm on corrosion performance. When the cyclic immersion test was conducted immediately after removal of the blue plastic, the bimetal stainless steel performed well. However, if the test was conducted 24 hours after removal of the plastic, it performed poorly (Table 2).

All of the above results indicate that the application of the protective polyfilm on bimetal stainless steel reduces the resistance to localized corrosion of that stainless steel. The time dependence indicates that there is a reaction with the residue on the surface after the plastic is removed, or/and absorption properties of the residue are such that corrosive agents are attracted to the surface. The conclusion is that the residue reduces the corrosion resistance of the stainless steel.

Residual Deposits

Auger spectral analysis was used to analyze the surface for elements that were present on production bimetal (as shipped) stainless steel and bimetal stainless steel after the plastic film (clear and blue) was applied and removed. Argon ion sputtering allowed an Auger profile to be obtained from the outermost surface to the bulk metal.

The Auger spectra for the surface of current production bimetal stainless steel (Figure 1) shows substantial peaks for iron, oxygen, and carbon with barely detectable amounts of sulfur and chlorine. The carbon is likely due to normal absorption of organic vapors from the atmosphere. The iron oxide is the typical species found on the topmost surface of type 434 stainless steel. The argon ion sputter profile for this surface in Figure 2 shows that the carbon layer sputters away in a very short time. The profile also shows a chrome-rich oxidized layer just under the topmost surface. Further sputtering penetrates the chrome-rich layer to show the bulk composition of the alloy.

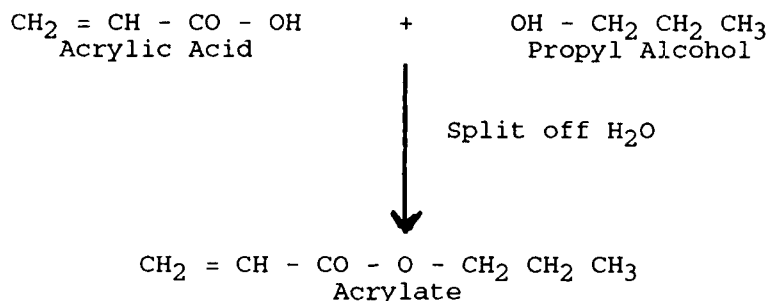
The Auger spectra for the stainless steel surface with the blue polyfilm applied and then removed (Figure 3) shows iron, oxygen, and carbon along

with sulfur. Typical sputter profiles (Figure 4) show areas of carbon rich deposits are significant indicating the residue remains after the polyfilm is removed. When this surface was exposed to atmosphere for 60 hours, the Auger spectra showed that significant quantities of chloride had been absorbed on the surface (Figure 5). This would explain the time dependence of polyfilm removal on corrosion test results.

Analysis of the organic deposit was conducted using FOURIER TRANSFORM INFRARED (FTIR) SPECTROSCOPY. Infrared Spectroscopy is a well established technique for polymer characterization. Gas Chromatography (GC) is used to separate the components by volatilizing the sample in a carrier gas stream and then conducting FTIR on the effluent.

FTIR spectra of adhesives removed from the clear and blue plastic films respectively compare to known spectra for acrylate adhesives. The FTIR for the residual deposit on the bimetal stainless steel was also identified as an acrylate adhesive.

Acrylates are esters which are formed by the reaction of acrylic acid with an alcohol as follows:



When this reaction is complete, residual acrylic acid can frequently be found in the acrylate due to unreacted excess. In fact, the adhesive associated with the blue film was found to contain acrylic acid using FTIR and gas chromatography.

Acrylic acid, a colorless liquid, miscible with water, alcohols, and ethers, is hygroscopic and known to be corrosive. On the surface of stainless steel, it could then attract moisture and subsequently absorb other contaminants. This chemistry could therefore react with the passive film on stainless steel and therefore destroy the protective film in these locations. Such a surface would be susceptible to localized corrosion such as pitting and crevice corrosion in the aggressive automotive environment.

Removal of Residual Deposits

Identification of the residual deposits due to the application of polyfilm protector to the stainless steel surface is important in order to determine what solvents could be used to clean the surface. However, solvents such as MEK, Toluene, Xylene, and alcohols were not successful in restoring corrosion resistance to the stainless steel. Those solvents were used at room temperature and at elevated temperatures without success. (Table 3). Although an alconox clean at room temperature did not restore corrosion resistance to the bimetal stainless steel surface after polyfilm removal, some improvement was observed. It was therefore tried with a hot solution with success. Full corrosion resistance was restored to the stainless steel surface using a 20 to 25 percent aqueous alconox detergent solution at 70°C with moderate agitation and a DI water rinse.

This procedure has been used on materials with polyfilm removed and which when tested by cyclic immersion, fails due to localized corrosion. Using this procedure, these materials pass the cyclic immersion test and therefore resistance to localized corrosion is restored. (See Table 3) It is felt that the hot alconox treatment removed residual deposits such as acrylates, neutralizes acrylic acid, and restores the passive film in areas where the protective film has been damaged due to surface reactions.

Polyfilm Development

The development of polyfilm protector which does not reduce the corrosion resistance of the stainless steel surface has been focused on the chemistry of the adhesive material. The presence of residual acrylic acid is an important factor and therefore elimination of an excess in the adhesive manufacture is beneficial. Results of cyclic corrosion tests show that acrylate adhesives without residual acrylic acid provide substantially improved performance over conventional acrylate adhesives. Rubber base adhesives completely eliminate the effect of reduced corrosion resistance. However, these adhesives do not have optimum properties required for this application.

Summary

Results of corrosion tests show that the corrosion resistance of stainless steel is reduced considerably when PVC polyfilm protector is applied and then removed after trim processing. The results show that the reduced resistance is due to a residual deposit which remains on the stainless steel surface after the polyfilm is removed. Auger analysis and gas chromatography coupled with Fourier transform infrared spectroscopy has shown that the residual deposits are acrylate adhesives containing residual acrylic acid used to bond the polyfilm to the stainless steel surface. These chemicals can react with the stainless steel passive film to yield reduced corrosion resistance. Since the acrylate/acrylic acid chemistry is hygroscopic, aggressive agents can then be absorbed on the stainless steel surface at the exact areas where the passive film has reacted. Removal of the residual adhesive deposits has been achieved through a hot aqueous alconox detergent treatment and therefore restoring corrosion resistance to the stainless steel surface. Development of acrylate adhesives without residual acrylic acid has also provided a polyfilm which does not reduce the stainless steel corrosion resistance after it is applied.

Acknowledgments

The authors wish to acknowledge that the corrosion tests were conducted by William Gorman and that Auger analysis was conducted by Al Hopkins and FTIR analysis was conducted by Marvin Cowens.

1. Baboian, R., Causes and Effects of Corrosion Relating to Exterior Trim on Automobiles, SAE Technical Paper No. 831835, 1983.
2. Baboian, R., Editor, Automotive Corrosion and Protection, NACE, Houston, TX, 1992.
3. Baboian, R., Editor, Automotive Corrosion by Deicing Salts, NACE, Houston, TX, 1981.
4. Baboian, R., Editor, Materials Degradation Caused by Acid Rain, American Chemical Society, Washington, DC, 1986.
5. Baboian, R., Localized Corrosion of Stainless Steel Exterior Automotive Trim, NACE CORROSION/90, Paper No. 91, April, 1990.
6. General Motors Corporation Test Specification PETM 1025.

TABLE 1
Cyclic Immersion Test

| | |
|-------------------------|--------------------------------------------------------------------------------------------------------------------------------------------------------------------------------------|
| Specimen Size | 50 x 50 mm |
| Test Solution (Aqueous) | 4.5% NaCl, 4.5% CaCl ₂ .2H ₂ O, NA ₂ SO ₄ , 0.022% Na ₂ SO ₃ , Na ₂ S ₂ O ₃ |
| Test Conditions | PN = 9.3, 300ml, Solution Temp = 42°C Air Temp = 40°C |
| Immersion Time | 1-2 Seconds |
| Dry Time | 98-102 Seconds |
| Test Duration | 100 Cycles |

TABLE 2
Cyclic Immersion Corrosion Tests on Bimetal Stainless Steel (100 cycles)
Showing the Effect of Polyfilm Polyfilm Application

| <u>MATERIAL</u> | <u>RATING</u> |
|--------------------------------------------------------------------------|---------------|
| Current Production (as shipped) | |
| Alconox clean | 0 |
| MgO clean | 0 |
| As Received (rollformer) (alconox clean) | |
| No polyfilm | 0 |
| Blue polyfilm (removed) | 3.5 |
| As Received (rollformer) (alconox clean) | |
| No polyfilm | 0.75 |
| Clear polyfilm (removed) | 2.25 |
| Roll formed with Blue Polyfilm (removed) | |
| Alconox clean | 2.5 |
| MgO clean | 0 |
| Stamped with clear polyfilm (removed) | |
| Alconox clean | 4.5 |
| MgO clean | 0 |
| Blue Polyfilm applied to current production bimetal stainless surface | |
| Blue polyfilm (removed) | 4 |
| MgO clean | 0 |
| Roll Formed with Blue Polyfilm (alconox clean) | |
| Tested immediately after polyfilm removal | 0.75 |
| Tested 24 hours after polyfilm removal | 3 |

TABLE 3

Cyclic Immersion on Bimetal Stainless Steel After Treatments to Remove Deposits (Trim Parts with Polyfilm Removed)

| Treatment | Rating After 100 Cycles |
|---------------|-------------------------|
| None | 2.5 |
| Xylene (RT) | 2.5 |
| Xylene (HOT) | 2.5 |
| Toluene (RT) | 2.0 |
| Toluene (HOT) | 1.5 |
| MEK (RT) | 1.5 |
| MEK (HOT) | 1.5 |
| Alconox (RT) | 2.5 |
| Alconox (HOT) | 0 |

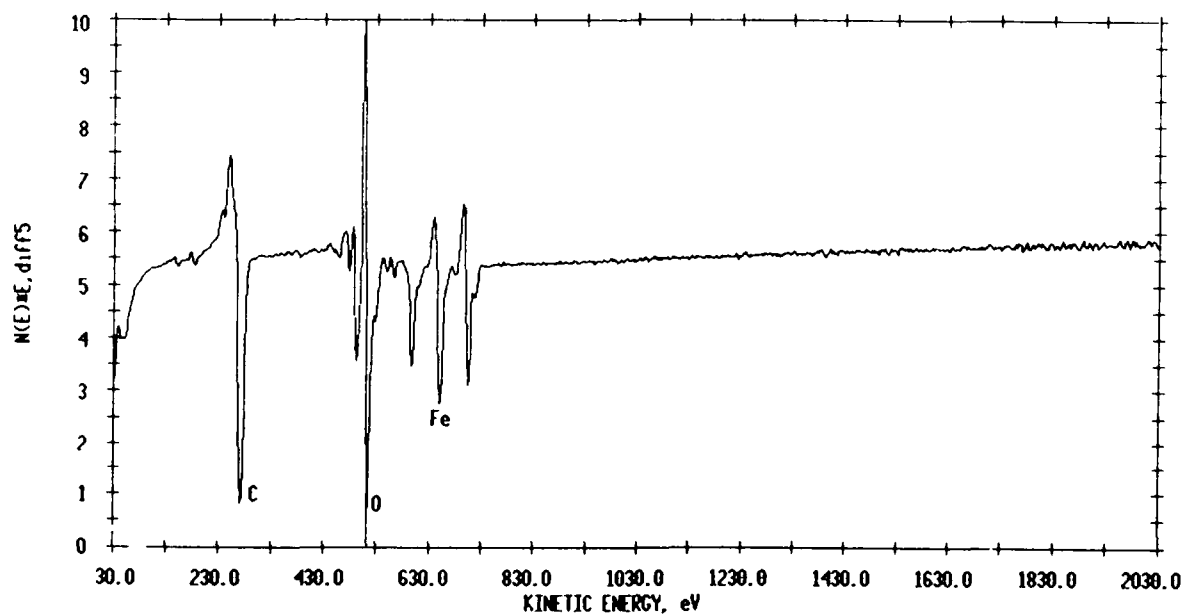


Figure 1 - Auger spectra of the surface of current production bimetal stainless steel surface.

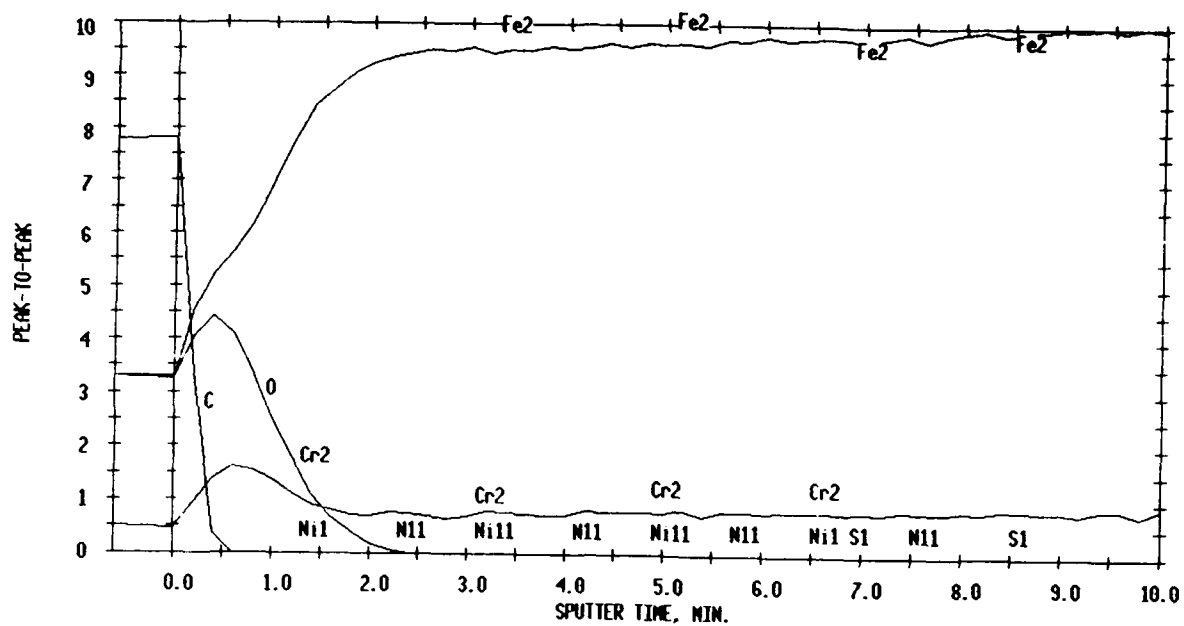


Figure 2 - Argon ion sputter profile for the surface of current production bimetal stainless steel.

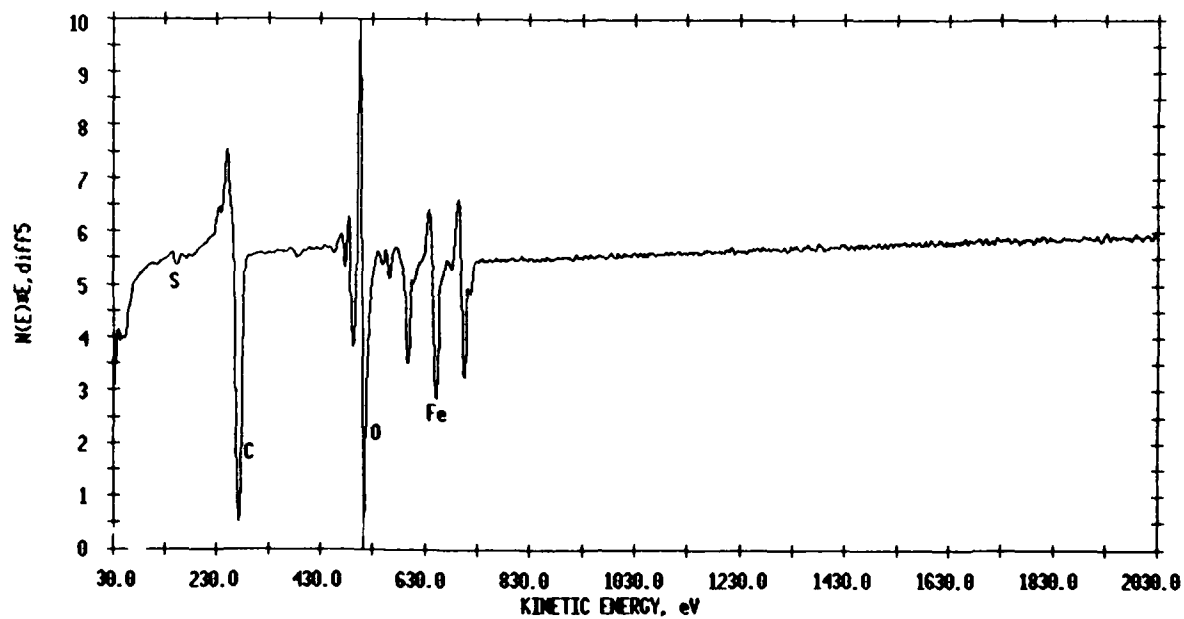


Figure 3 - Auger spectra for the surface of bimetal stainless after polyfilm protector was applied and then removed.

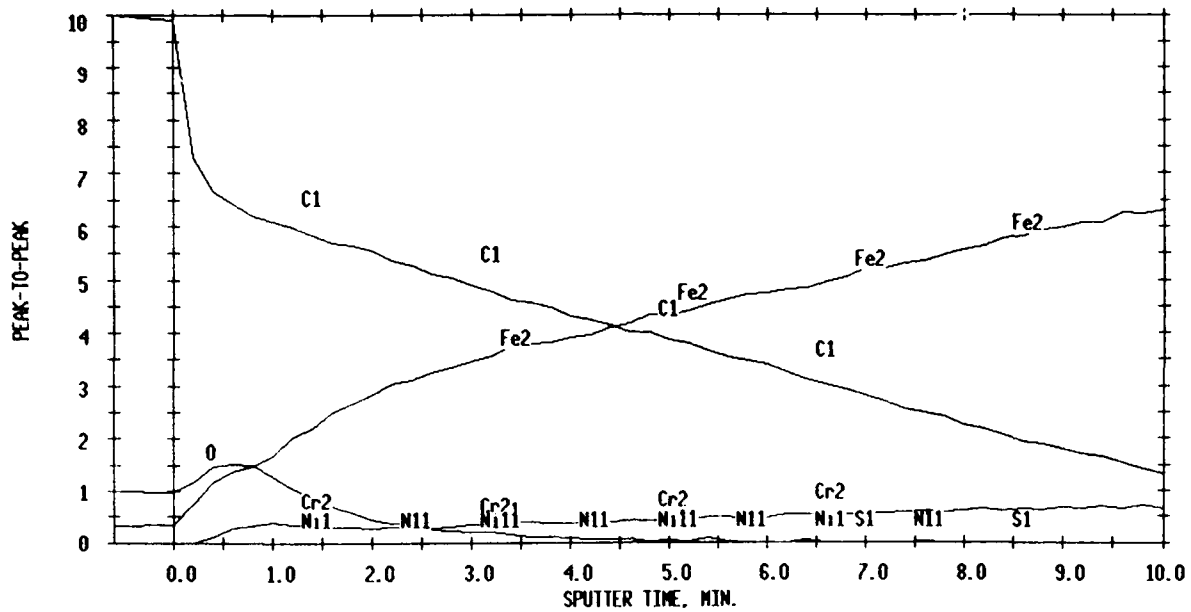


Figure 4 - Argon ion sputter profile for the surface of bimetal stainless steel after polyfilm protector was applied and then removed.

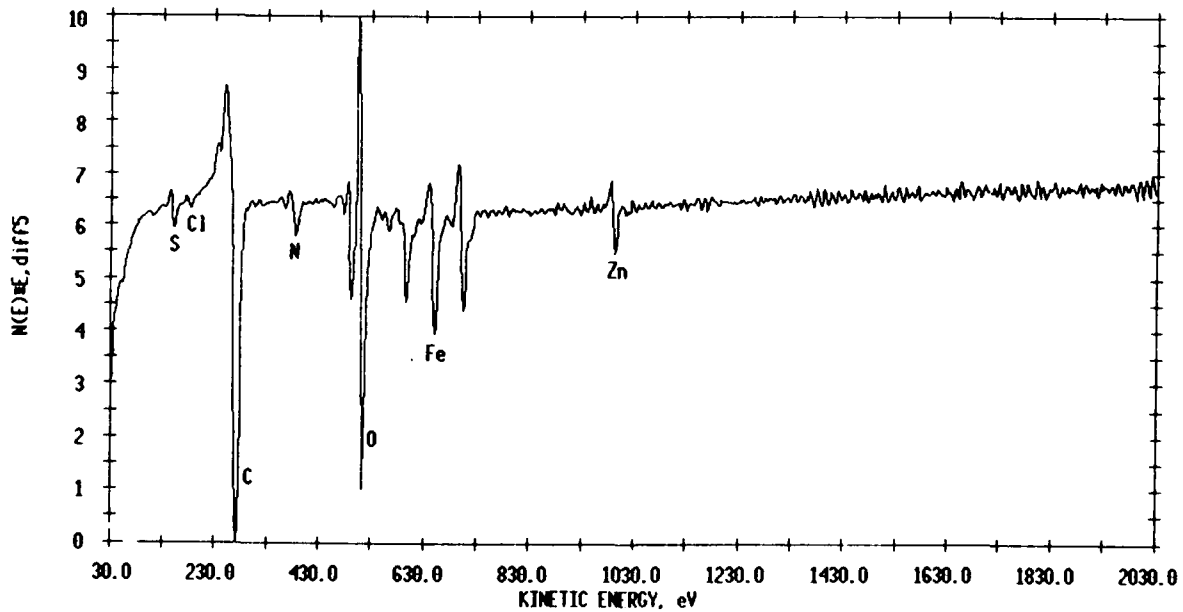


Figure 5 - Auger spectra for the surface of bimetal stainless steel exposed to atmosphere for 60 hours after polyfilm protector was applied and then removed.

Optimization of Corrosion and Wear Properties of Steel Component Surfaces by Controlled Gas Nitriding

Marek BIESTEK
Institute of Precision Mechanics
3, Duchnicka Street,
01-769 Warsaw, Poland

André CZELUSNIAK
NITREX METAL, Inc.
3480 Poirier Blvd.
St. Laurent, Québec
Canada H4R 2J5

Jerzy IWANOW
Institute of Precision Mechanics
3, Duchnicka Street,
01-796 Warsaw, Poland

Michel KORWIN
NITREX METAL, Inc.
3480 Poirier Blvd.
St. Laurent, Québec,
Canada H4R 2J5

Witold LILIENTAL
NITREX METAL, Inc.
3480 Poirier Blvd.
St. Laurent, Québec,
Canada H4R 2J5

Jan TACIKOWSKI
Institute of Precision Mechanics
3, Duchnicka Street,
01-796 Warsaw, Poland

Abstract

NITREG, a modern, controlled gas nitriding process, has been successfully applied to simultaneously enhance corrosion and wear resistance of various grades of steel.

Emphasis is placed on unalloyed and low alloyed structural steels, used for automotive components, including those of hydraulic systems, e.g. dump-truck lifting mechanisms, exposed to especially great corrosion hazards, while requiring enhanced wear resistance. In this case, an oxy-nitro-carburizing treatment (ONC) improves the corrosion resistance of as-nitrided surfaces. The application of surface impregnating agents, containing corrosion inhibitors, brings about a further enhancement of their corrosion resistance. This effect has shown itself to be the most substantial.

Corrosion resistance was evaluated by the salt spray test, administered per ASTM B-117. Additionally, some electrochemical investigations were carried out on 1006 steel to complement the salt spray tests. Material samples were evaluated metallographically in order to correlate corrosion behavior to thickness and microstructure of the nitrided layer. Optimum conditions of layer formation were formulated.

Wear resistance of nitrided and ONC-treated layers, optimized for corrosion resistance, remained satisfactory.

Key terms: gas nitriding, white layer, porosity, corrosion resistance, wear resistance

I. Introduction

Increased pollution of the atmosphere in all industrialized countries, as well as some widely practised procedures, such as de-icing of snow-bound roads with salt, expose automotive and other machine parts, especially those used outdoors, to greater corrosion hazards than in the past.

At the same time, advancing technology places increasing demands on part surface properties. Among these are high corrosion resistance, high wear resistance and controlled roughness, often required simultaneously, as in the case of components of hydraulic systems. Meeting all the above by way of nitriding is a complex problem because of many and varied factors influencing the overall result. Of paramount importance is the thickness and morphology of the nitrided layer, dependent on process conditions, i.e. temperature, time and nitriding potential. This last factor is considered the basic parameter of the nitriding process, determining the nitriding capability of the atmosphere. It is expressed by the ratio of partial pressures of ammonia to hydrogen and its optimum value is selected experimentally.

II. Historical Development

Traditionally, many parts requiring both high corrosion and wear resistance have been hard chrome plated. Although a source of numerous problems besides being ecologically polluting, hard chrome plating has, for many years, been regarded as the best, or even the only method.

Nitriding, a diffusion process for steels, known since the beginning of this century, has been used in the past for one or the other application, i.e. to enhance corrosion or wear resistance but not both. In the latter case, process temperatures have been traditionally high, even above 600°C, which limited the scope of application of nitrided parts to such where core strength was not a major requirement. Besides, thickness of the so-called white (compound) layer obtained in such processes is very big, reaching 75 μm which renders it useless for wear applications. In the case of stainless steels, nitriding has been known to actually impair the corrosion resistance of the surface.

In recent years, nitriding has, however, proven itself to be a substantial improvement over hard chrome plating and, in many instances, has replaced the hitherto practiced technology. To this day, most of the nitriding carried out on automotive components is accomplished in various proprietary modifications of the salt bath process. A further development was the finding that a complex oxide layer deposited over a nitrided layer increases corrosion resistance without significant loss to wear resistance of the as-nitrided surface.

Nitriding in a salt bath, however, means carrying out of the process in a medium with a fixed nitriding capability. In such a process, time and temperature are the only factors determining the final result. The additional, microprocessor controlled variables available in the gas process, e.g. atmosphere composition and flow rate, give it much more flexibility needed to arrive at a nitrided layer with predetermined properties, tailored to any particular application.

Nitriding of stainless steels with a high Cr content requires separate mention. These steels are clad by an extremely thin but compact protective oxide film, impermeable to nitrogen. That film must, therefore, be destroyed before nitriding can take place. This is referred to as surface activation. The aggressive medium of salt bath readily activates stainless steels, which cannot be said of commonly used gas media.

Gas nitriding of automotive parts, constitutes a much needed replacement of the salt bath process. It is ecologically non-polluting and does not pose the known hazards and problems of waste disposal. The advent of ONC

- an oxy-nitro-carburizing treatment, has further enhanced this controlled technology. ONC gives nitrided parts an attractive, black appearance and a corrosion resistance superior to that of parts nitrided in salt bath processes. Substantial corrosion protection of steel components can be obtained by the application of corrosion-inhibitor bearing surface impregnation agents.

III. Aim of Investigation

With the above considerations in mind, our team, composed of metallurgists and corrosion engineers set out to investigate controlled gas nitriding conditions in order to obtain an optimum white layer, enhancing both corrosion and wear resistance on selected grades of steel, meeting the stringent requirements and industrial standards of modern technology.

IV. Materials Used

A. Steels for Automotive Parts.

For tests concerning automotive components, the following steels were selected:

- a-1006 unalloyed carbon steel
- b-1010 unalloyed steel
- c-MM2 microalloyed steel
- d-1045 unalloyed steel

B. Steels for other applications

For tests concerning specialized applications, e.g. aero components, 17-4 PH precipitation hardening steel was selected.

V. Experimental Procedure

A. Sample preparation.

Steel samples used in the tests were polished to an initial roughness of 2-4 μ l prior to nitriding. Actual parts were nitrided with surface roughness as manufactured.

B. Nitriding Processes.

Nitriding processes were carried out at temperatures ranging from 520°C to 580°C in atmospheres composed of 100% NH₃, as well as various combinations of NH₃ and N₂ which resulted in different nitriding potentials. Processing times varied from 0.5 h to 7 h. The ONC process, where performed, was applied for 30 to 40 mins at 520°C.

C. Post-Process Evaluations.

1. Roughness evaluation. After each process, samples were roughness tested.
2. Hardness Measurements. Surface hardness measurements were taken, using 500 pf, 1 kpf and 5 kpf loads. These were only to demonstrate that the surface does exhibit enhanced wear resistance but were not used as a parameter against which corrosion tests were evaluated.
3. Metallography. Metallographical observations were carried out on mounted, polished and etched cross-sections, with the aid of a metallographical microscope, using magnifications from 200X to 1,000X.
4. Corrosion Testing. Corrosion tests were carried out in a salt spray cabinet, per ASTM B-117 on samples which were nitrided only or nitrided and ONC-treated. The medium used was an aqueous solution of NaCl. Some samples and parts were additionally treated by impregnation with various corrosion inhibitors. Daily inspections

determined the progress of corrosion with time. One criterion used for evaluation was time to the appearance of the first corrosion spot. In some cases, the severity of corrosion attack on the tested surface after a fixed time in the fog chamber was compared to evaluate the effect on corrosion resistance of the various modifications of the nitriding and ONC processes.

Electrochemical studies were carried out on nitrided and oxynitrided 1006 steel. This portion of investigations, accomplished in Poland, employed a Russian made PI-50-1 potentiostat with automatic polarization curve recording. Current density was measured with an accuracy of ca. 0.1 mA/cm².

5. Wear Testing. Wear tests quoted in this report were carried out by the cone and three cylinder (Bekker) method. In this method, three nitrided (oxynitrided) cylinders are worn against a rotating cone, made of the equivalent of 4140 steel, hardened and tempered to 30 HRC. The cone was spun at 576 r.p.m. and constant lubrication was used. Every 10 mins, the test was interrupted to measure the wear scar and the load force was accordingly adjusted to maintain a constant unit pressure. These tests were carried out only to demonstrate that nitriding does indeed enhance wear resistance by increasing the surface hardness of the nitrided steel. In these investigations, wear test results were not used systematically as a factor to correlate with corrosion behavior of layers.

VI. Results

A. Roughness Tests

Typical roughness values (R_a expressed in μ l) obtained on three grades of steel nitrided at 530°C and 570°C are shown in Fig. 1. As can be seen, low initial roughness is conducive to lower final roughness after nitriding. These results indicate that roughness increase is a factor that must be taken into account when designing a nitriding process. This is especially true of some applications, e.g. hydraulics system components, for which the final R_a value may not exceed 25 μ l.

B. Hardness and Wear Tests.

Ranges of surface hardness values obtained on steels nitrided in this study are shown in Table 1. As is clearly seen, both carbon content and alloying additions raise surface hardness, thereby enhancing wear resistance. It should be pointed out that relatively low surface hardness readings on low carbon steels are resultant of combined white layer and substrate hardness. The true hardness of white layers even on unalloyed steel is min. 700 HV.

The results of 2 groups of wear tests, all carried out on nitrided or nitrided + ONC-treated 1045 grade steel are put together in Fig. 2. The plots contain delineations to show the extent of the particular phase components of the white layer. It is seen that the most wear resistant component, yielding stable wear characteristics is the ϵ phase with a chemical formula of $Fe_2N_{(1-x)}$. Nitrided only steels exhibit a slightly better wear resistance than those which were additionally ONC-treated but even the latter are considered to have very good tribological characteristics, compared to non-nitrided steel surfaces. The same set of plots illustrates how the formula of the impregnating agent, besides enhancing corrosion resistance, may affect wear characteristics, by acting as a lubricant.

C. Corrosion Tests

1. Initial Selection of Nitrided Layers. This study was carried out on 1010 and MM-2 steels. Several samples of both of the above grades were nitrided only or nitrided and ONC-treated in different processes and placed in the salt spray chamber for a total time of 300 hours. Fig. 3a shows the appearance of 1010 samples and Fig. 3b the appearance of MM-2 samples as taken out of the chamber after the completion of the test. They were classified into two categories, depending on the severity of corrosion attack. "Good" exhibited no corrosion or only minimum effects, not exceeding 10%, concentrated near edges. The remaining samples, all classified "bad", exhibited substantial corrosion. All samples were subsequently sectioned and evaluated metallographically to determine the thickness of the compound ("white") layer and its phase composition. Classification, corresponding process information, as well as results of metallographic evaluation for the 1010 grade are put together in Table 2. Analogous results for the MM-2 microalloyed grade are put together in Table 3.

Results from the two tables demonstrate that layers belonging to any one classification share some common characteristics. These are: total white layer thickness, its uniformity and the thickness of the porous zone. The layer on low carbon and low alloy steels comprises the compound layer, termed "white" because it does not etch easily and a deeper lying diffusion zone, where nitrogen is in solution with dispersed precipitates of nitrides. On these steels, this last zone is significant only from the point of view of fatigue strength and plays no part in wear or corrosion resistance. The outer white layer is composed of a mixture of ϵ ($\text{Fe}_2\text{N}_{1-x}$) and γ' (Fe_4N) nitrides. The outermost, porous zone has a predominance of ϵ . The deeper lying compact, truly white zone has a predominance of the γ' nitride. On steels with very low carbon content, a thin sublayer of pure γ' can be observed at the interface with the diffusion zone. On ONC-treated steels, a thin gray zone of complex oxides is visible above the porous sublayer. Fig. 4a shows a typical "good" layer, while Fig. 4b a typical "bad" layer on 1010 steel. "Good" layers are generally characterized by greater total thickness, good uniformity and a substantial participation of the ϵ phase. The deeper situated non-porous, compact $\epsilon + \gamma'$ phase does not appear to have such good anti-corrosion properties. Corresponding microstructures of layers on MM-2 steel are shown in Figs. 5a and 5b. In this case too, the outermost porous zone appears to be of vital importance to good corrosion behavior and it should constitute at least 40% of the total white layer thickness. Its role is that of a self-lubricating reservoir for impregnating agents containing corrosion-inhibitors. Layers with ONC-treatment generally exhibit better anti-corrosion properties but ONC has little effect on corrosion behavior if the underlying white layer is otherwise poor. Since roughness rises with layer thickness, poor layers with small thicknesses usually exhibit low roughness. In other investigations, not reported in the present paper, it was found that the phenomenon of surface roughness is related to conditions of nucleation and growth of the layer¹. From literature it is apparent that increasing carbon content in steel favors the nucleation of the ϵ nitride first², hence the formation of the porous zone. This porous zone is believed to enhance roughness. Since it is advantageous to corrosion protection, a compromise must be sought between the latter and roughness exceeding specified limits. However, no direct correlation has been found between roughness per se and corrosion behavior: the same results have been reached in a related study³.

2. Optimization of White Layer Thickness. The second round of experiments consisted of correlating white layer thickness with corrosion behavior, measured as the time in the salt spray chamber required to produce first corrosion spot. This investigation covered steel grades 1010 and MM-2, both used in the automotive industry for hydraulics.

After the completion of the test, steel samples were sectioned for metallurgical evaluation. Typical trends obtained for the two steel grades are shown graphically by Figs. 6 and 7. For any given white layer thickness (very thin, poor layers excluded), the application of ONC significantly enhances corrosion resistance. For the two investigated grades, corrosion resistance clearly rises with increasing white layer thickness. The thickness and microstructure of the white layer depend on temperature and time and on the nitriding potential which in our process is automatically controlled.

3. Effect of Impregnating Medium. Fig. 8 shows the effect on corrosion resistance of the nitrided steel surface of liquid impregnating agents, containing corrosion inhibitors. The two agents used in this study were code-named KO-1 (oil-base) and NL-4 (wax-base). Both were applied by immersion. It is seen that impregnation significantly extends times in salt spray to the appearance of the first corrosion spot which can be regarded as protection times. The example shown here is for MM-2 steels. Same trends and similar results were obtained for other grades.

4. Polarization Test. Fig. 9 shows anodic polarization curves obtained on electrodes made of 1006 steel, after: a) oxidation, b) controlled nitriding and c) controlled nitriding + oxy-nitro-carburizing(ONC). All three versions were tested with and without impregnation by the KO-1 agent. The electrolyte used was 1.0 M solution of NaCl. Potentials shown in the plot relate to the Normal Hydrogen Electrode. The results obtained indicate a substantially positive effect of impregnation on the anti-corrosion properties of nitrided and nitrided + ONC-treated steel surfaces. This effect on only oxidized surface is insignificant. Also, the positive effect of the ONC treatment is noted. The existing correlation between the results of salt-spray and polarization tests bodes well for the development of a simple and fast method of evaluation of the quality of various nitrided and nitrided + ONC-treated surface layers on steels, as well as of the effectivity of various impregnating agents.

5 Testing of Nitrided Stainless Steel. In this application, the requirement was to nitride a component of aircraft undercarriage braking system, manufactured from 17-4 PH precipitation-hardening stainless steel without excessively compromising corrosion resistance. A batch of the components was nitrided in a specially developed proprietary mode of the controlled process for stainless steels, involving surface activation. As a result, uniform diffusion layer of 0.004" thickness, with a hardness of over 1000 HV was obtained. A piece that was not nitrided was placed in the salt-spray chamber along with one that was nitrided and impregnated with the NL-4 agent. After 130 hours, the test was discontinued when it was observed that the nitrided piece is actually behaving better than the one which was not nitrided.

VII. Conclusions

The results of this study allow the following conclusions to be drawn:

1. Controlled gas nitriding is capable of producing layers which are resistant to both corrosion and wear.
2. Corrosion resistance of the white layer depends on its thickness, uniformity and microstructure, above all, on the participation of the outer, porous zone with a predominance of the ϵ phase.
3. For low alloy steels, best results in corrosion protection were obtained on layers of 20 to 25 μm thickness with the porous zone constituting at least 40% of the total layer thickness. The participation of the porous zone can be controlled.
4. ONC - treatment consisting of generating a thin complex oxy-nitro-carbide layer over the white layer enhances corrosion resistance while loss in wear resistance is insignificant.

5. Surface impregnation with agents containing corrosion inhibitors serves to further substantially enhance corrosion protection of nitrided steels.
6. Although surface roughness has no direct effect on corrosion behavior, it is associated with the porous ϵ zone. A project is currently underway to optimize the white layer for both roughness and corrosion behavior.
7. Metallurgical analysis of the investigated layers allowed the determination of what type of layers are optimum, in terms of total thickness and morphology, to which carefully preselected process parameters correspond. These include: temperature, time and the nitriding potential which determines nitriding capability.
8. A combination of activation, controlled nitriding and subsequent impregnation resulted in a uniform, hard nitrided layer on stainless steel without compromising corrosion resistance.

References:

1. Application of the NITREG-ONC Process to Hydraulic Systems Components. - Interim Report on study performed for the National Research Council of Canada. (Unpublished) . October 15, 1992.
2. M.A.J. Sommers, E.J. Mittermeier. Verbindungsschichtbildung während des Basnitrierens und des Gas- und Salzbadcarbonitrierens. HÄRTEREI-TECHNISCHE MITTEILUNGEN 47 (1992) 1 pp. 5-12
3. J. Iwanow, J. Tacikowski, M. Biestek, M. Korwin. Increasing of Corrosion Resistance of Gas Phase Nitrided Low Carbon Steels by Inhibitors. Paper to be presented at the 10th European Corrosion Congress, Barcelona, Spain. September, 1993.

Table 1.

| Steel Grade | HV0.5 | HV1 | HV5 | Corresponding white layer (μm) |
|-------------|-----------|-----------|-----------|---------------------------------------------|
| 1006 | 360 - 400 | 340 - 384 | ----- | 20 - 30 |
| 1010 | 356 - 409 | 378 - 413 | 317 - 332 | 9 - 27 |
| 1045 | 453 - 481 | 395 - 413 | 310 - 323 | 12 - 28 |
| MM-2 | 727 - 765 | 686 - 713 | 603 - 628 | 10 - 24 |

Table 2.

| Results of Initial Corrosion and Metallurgical Evaluation of Nitrided 1010 Steel After 340 Hours in Salt Spray Chamber per ASTM B-117 | | | | | | |
|---------------------------------------------------------------------------------------------------------------------------------------|-----------------------|------------------------|---------------------------|--------------------------------------------|-------------------------------|----------------------------------------------------------------------------------------------------------------------------------------------------------------------------------------------------------|
| Classification | Sample No per Fig. 3a | Type of Process | White Layer μm | ϵ (porous sublayer) μm | Roughness R_a μl | Remarks |
| Good | 1 | Contr. Nitriding | 21.5 | 9.5 | 12.5 | White layer continuous and uniform in thickness White Layer continuous and uniform in thickness White layer continuous and uniform in thickness White layer continuous and uniform in thickness |
| | 4 | Contr. Nitriding + ONC | 21 | 9 | 11 | |
| | 7 | Contr. Nitriding + ONC | 22 | 8.5 | 27 | |
| | 10 | Contr. Nitriding + ONC | 27.5 | 12 | 21.5 | |
| Bad | 3 | Contr. Nitriding + ONC | 13 | 2-3 | 11 | White layer fairly uniform |
| | 11 | Contr. Nitriding | 11 | 2-3 | 10.5 | White layer fairly uniform |
| | 2 | Contr. Nitriding + ONC | 6-14 | 1-2 | 7 | White layer very non-uniform in thickness |
| | 5 | Contr. Nitriding + ONC | 10-14 | none | 8.5 | White layer fairly uniform |
| | 6 | Contr. Nitriding + ONC | 6-10 | none | 12 | White layer uniformity poor |
| | 8 | Contr. Nitriding + ONC | 5-6 | none | 20 | White layer fairly uniform |
| | 9 | Contr. Nitriding | 11 | almost none | 11 | White layer fairly uniform |

Table 3

| Results of Initial Corrosion and Metallurgical Evaluation of Nitrided MM-2 Steel After 340 Hours in Salt Spray Chamber per ASTM B-117 | | | | | | |
|---------------------------------------------------------------------------------------------------------------------------------------|-----------------------|------------------------|---------------------------|--------------------------------------------------|-------------------------------|----------------------------------------------------------------------------------------------------|
| Classification | Sample No per Fig. 3b | Type of Process | White Layer μm | ϵ (porous sublayer) μm | Roughness R_a μl | Remarks |
| Good | 5 | Contr. Nitriding + ONC | 22.5 | 12-15 | 24 | White layer continuous and uniform in thickness White Layer continuous and uniform in thickness |
| | 6 | Contr. Nitriding + ONC | 18 | 7-9 | 54 | |
| Bad | 2 | Contr. Nitriding | 21.5 | 12-15 | 46 | White layer continuous and uniform in thickness White layer fairly uniform |
| | 1 | Contr. Nitriding | 12-16 | mostly none, sporadically, up to 6 μm | 15 | |
| | 3 | Contr. Nitriding + ONC | 6-9 | none | 12.5 | White layer fairly uniform |
| | 4 | Contr. Nitriding | 7-8 | 1-3 | 10 | White layer fairly uniform |

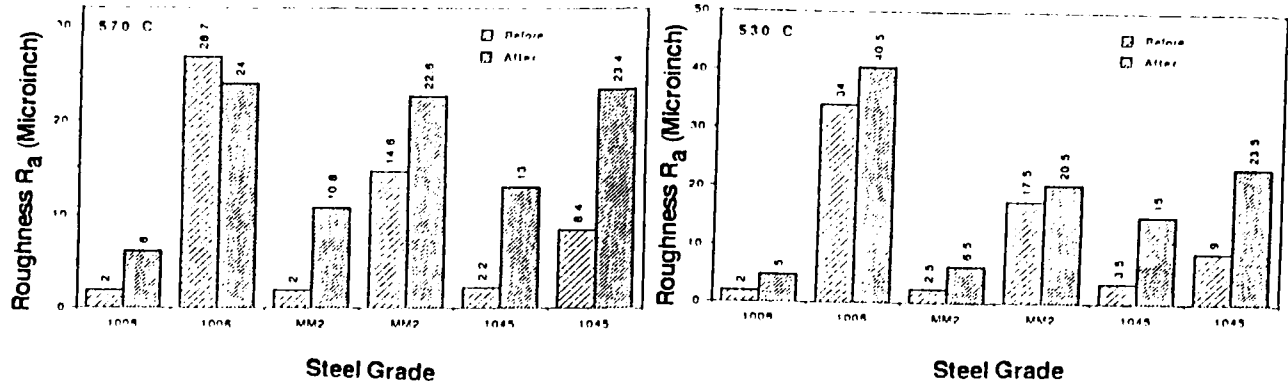


Fig. 1. Typical Ra values on three steel grades before and after nitriding at 570°C (left) and 530°C (right). Other process parameters varied.

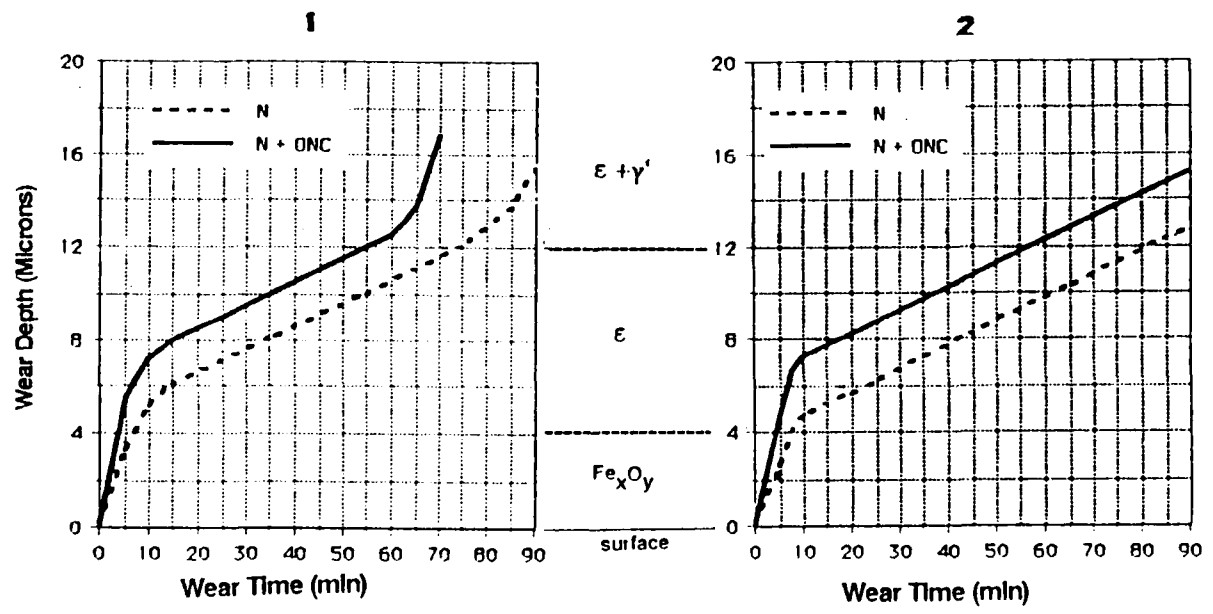


Fig. 2. Linear wear of samples made of nitrided and nitrided + ONC-treated 1045 steel, with the application of two different types of impregnating agents. Symbols between plots show extent of constituent phases of white layer.

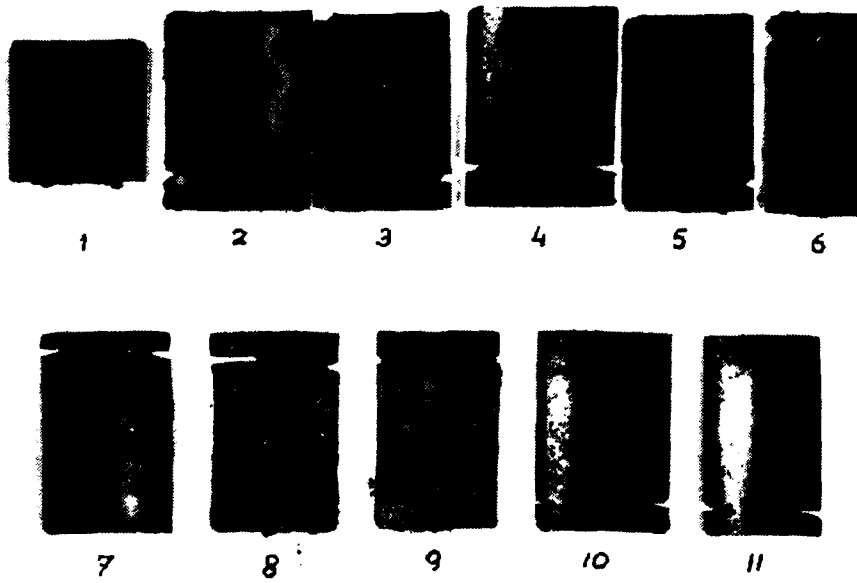


Fig. 3 a. Appearance of 1010 steel samples after 300 hours in salt spray.

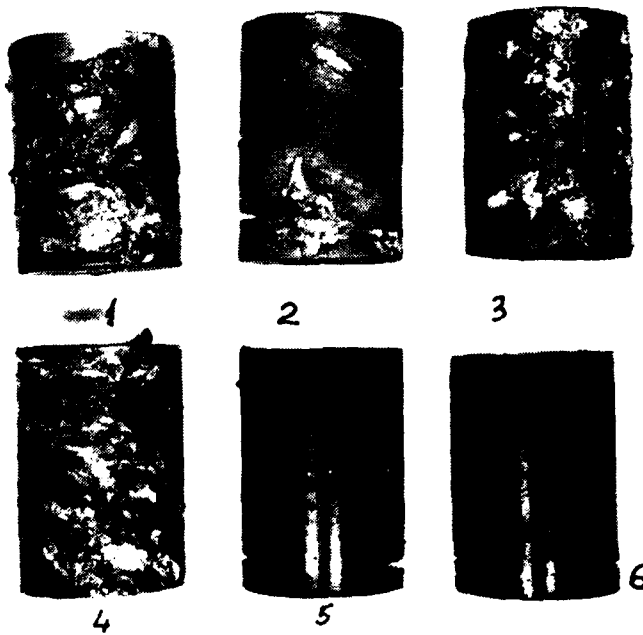
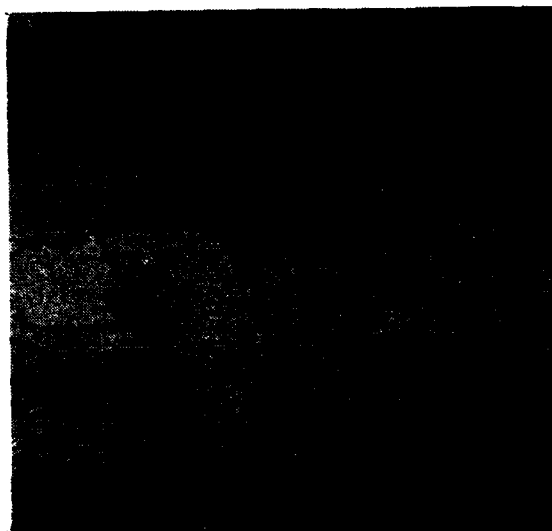
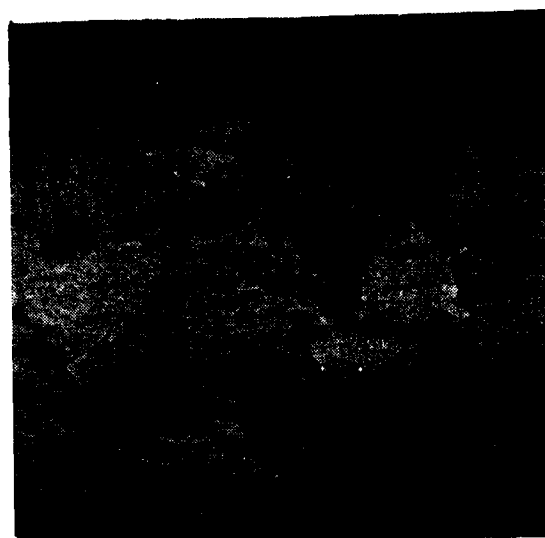


Fig. 3 b. Appearance of MM-2 steel samples after 300 hours in salt spray.

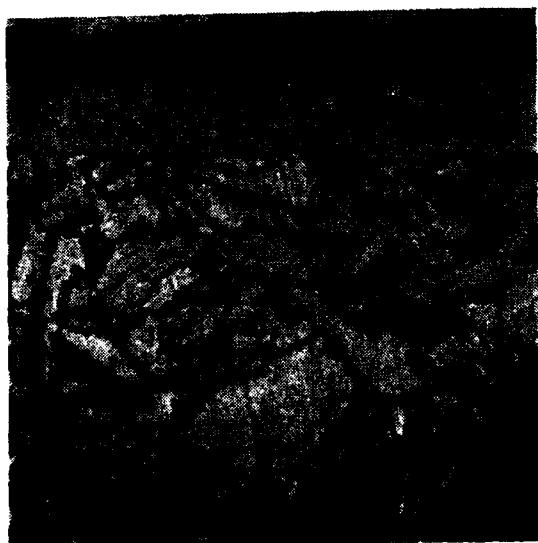


a

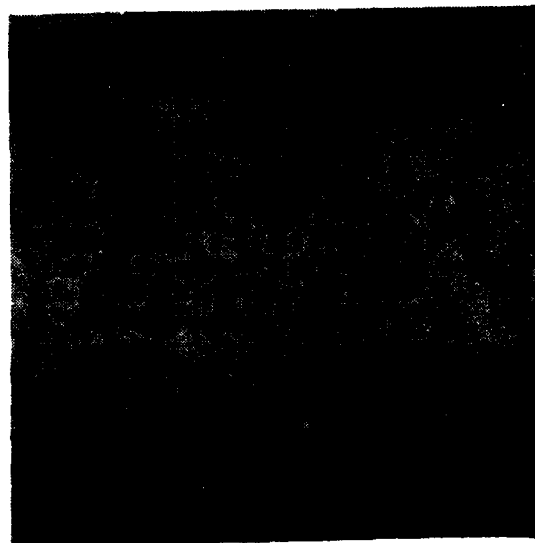


b

Fig. 4. Typical "good" (a) and "bad" (b) white layers on 1010 steel.
Etched with 2% Nital. 1000 X.



a



b

Fig. 5. Typical "good" (a) and "bad" (b) white layers on MM-2 steel.
Etched with 2% Nital 1000 X.

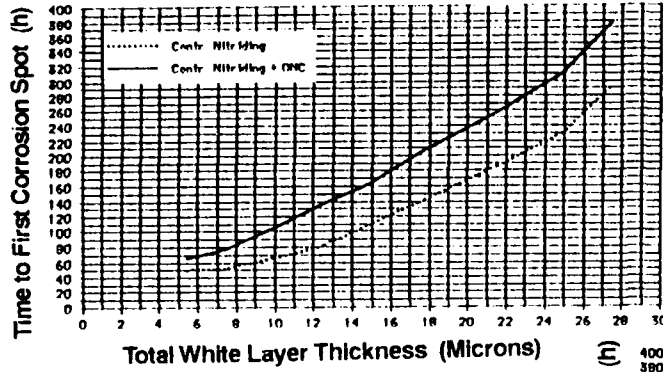


Fig. 6. Typical trend in the correlation between white layer thickness and corrosion protection for 1010 steel.

Fig. 7. Typical trend in the correlation between white layer thickness and corrosion protection of MM-2 steel.

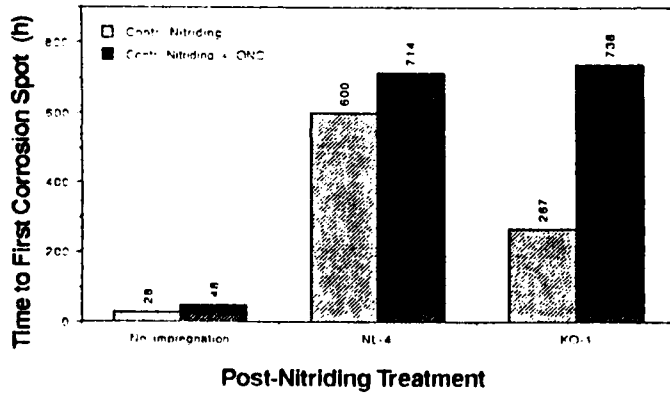
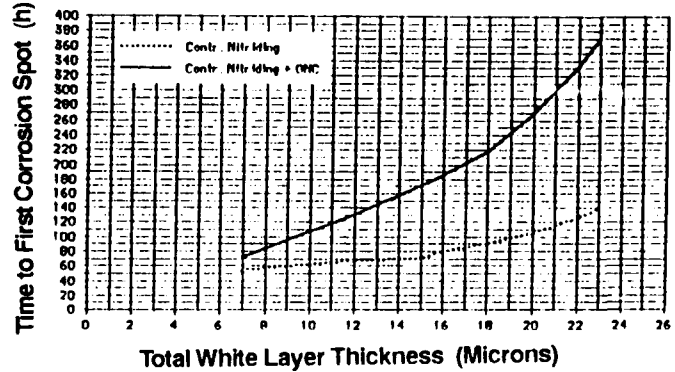


Fig. 8. Enhancement of Corrosion Protection of MM-2 Microalloyed Steel by the Application of Post - Process Impregnation.

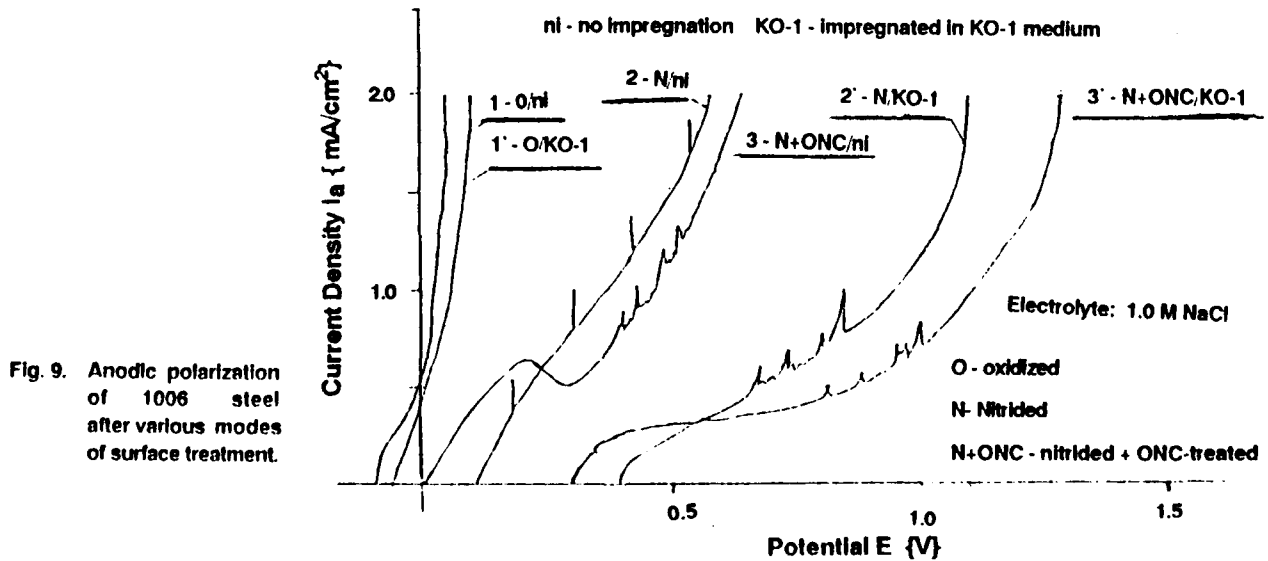


Fig. 9. Anodic polarization of 1006 steel after various modes of surface treatment.

In Situ Analysis of Corrosion in the Crevice of Automotive Body by AC Impedance Measurements.

SAKAE FUJITA
MATERIALS AND PROCESSING RESEARCH CENTER
NKK CORPORATION
1 Kokan-cho, Fukuyama, Hiroshima Pre, 721, Japan

KATSUMI MASAMURA
MATERIALS AND PROCESSING RESEARCH CENTER
NKK CORPORATION
1 Minami-Watarida, Kawasaki, Kanagawa Pre, 210, Japan

Abstract

A new AC impedance technique was developed to investigate the basic corrosion mechanism of steel in the crevice of lapped portion of automotive body, using a model consisting of two identical steel panels facing each other with a small gap. It was shown that impedance at high frequencies above 10kHz gave information about the degree of wetness in the crevice. Impedance at low frequencies less than about 0.01Hz was used to evaluate the variation of the corrosion rate in the crevice. The wetness and the corrosion rate in the crevice of the lapped panels were measured continuously in the wet and dry corrosion test. The relationship between the degree of wetness and corrosion rate was discussed.

Key terms: AC impedance, Automobile, In situ measurement, Crevice, Wetness, Dry, Atmosphere, Accelerated corrosion test

Introduction

Corrosion protection of steel in the crevice at lapped portion of automotive bodies is very important because the throwing power of the conversion coating and the electrodeposition paint is not sufficient to coat such areas, where corrosion species such as chlorides tend to accumulate. However, corrosion mechanism in the crevice of lapped portion has not yet been established because of limited information on the relevant environment and on the variation of the corrosion rate by the change of the environment. The degree of wetness is an important factor that affects corrosion of metals in wet and dry corrosion cycles. Various types of time-of-wetness meter have been proposed for flat panels¹⁻²⁾, but not for crevice areas.

AC impedance spectroscopy has been widely used for analysis and evaluation of corrosion behavior of bare and painted metal. AC impedance measurement using two frequencies³⁻⁴⁾ was first designed by S.Haruyama and T.Tsuru for corrosion monitoring. This system has been applied to field corrosion monitoring of certain structures.

In the present study, a new AC impedance technique was developed, using a model consisting of two identical steel panels facing each other with a small gap, to measure the degree of wetness and the corrosion rate. Solution resistance measured by the AC impedance technique was compared with the mass gain of the solution in the crevice and it was demonstrated that the degree of wetness could be calculated from the measured solution resistance in the crevice. The AC impedance technique was also used to determine the change of the corrosion rate with time in the crevice. In situ measurements of the time dependence of the wetness and corrosion rate in the crevice of the lapped panels were carried out in the laboratory wet and dry corrosion test. Based on the results, the basic corrosion mechanism of steel in the crevice of lapped portion was discussed.

Experimental Method

Specimen

Figure 1 shows the schematic of lapped panels used for measuring the mass gain and impedance in the crevice. The lapped panels were made of two steel sheets coated with the conventional conversion coating and electrodeposited paint (24-30 μ m thick) for automobile body except for the center portion (10mm x 20mm). Spacers (66-70 μ m thick) were placed between the two panels. The uncoated surfaces were facing each other inside the lapped panels. The edges of the lapped panels except for the solution inlet were covered with a small amount of epoxy resin. The clearance between the unpainted inside surfaces was not measured, but estimated to be a little more than 1.14 mm considering the thickness of the electrodeposition coating and the spacers.

Accelerated corrosion tests

The wet and dry cycle was repeated daily in the following manner; (i) immersed vertically in 5wt% NaCl solution for 1 hr at room temperature, (ii) placed horizontally in air maintained at 20-23°C and 18-22%RH for 14 hrs, (iii) left horizontally for 9 hrs in vacuum chamber at room temperature to eliminate all the water remaining in the crevice. The mass loss through the last procedure showed the amount of water in the crevice. A cycle of 1 hour immersion and 23 hours drying was also used.

The mass gain of the lapped panels was measured in the laboratory wet and dry test to a precision of 0.1mg in order to determine the inward and outward migration of the solution with respect to the crevice during the wet and dry cycle. The solution outside the lapped panels was removed by wiping with filter paper immediately after the panels were taken out from the 5wt% NaCl solution. The mass gain of a flat panel covered totally with the conversion coating after one hour immersion in 5wt% NaCl solution was also measured to correct the error of the mass gain caused by water absorption in the electrodeposition coating.

AC impedance measurements

The instruments used for AC impedance measurements consisted of Solartron 1250 frequency response analyzer (FRA) and electrochemical interface 1285. The effective applied AC signal amplitude was 5 mV. The AC frequency was scanned down logarithmically from 60kHz to 0.01Hz.

Results and discussion

The mass gain in the crevice

The saturated mass gain of the lapped panels in 5wt% NaCl solution was 0.045g (about one hour immersion). On the other hand, the corresponding mass gain of fully coated panel was 0.003g/sheet. The mass gain of the lapped panels included an error of $0.003 \times 2 = 0.006$ g. However, all the water absorbed in the coating of the panel sheet disappeared in approximately 1 hr from the start of indoor exposure. The mass gain of the coating by absorption of water was negligible after one hour from the start of indoor exposure.

Figure 2 shows the variation of the mass gain of the lapped panels in the laboratory wet and dry test at room temperature. Obviously, the solution quickly entered the crevice. The mass gain during immersion, however, became smaller as the number of corrosion cycles increased. On the other hand, the mass loss during the dry period decreased with increase of the number of cycles.

Impedance in the crevice

Figure 3 shows the Bode diagram for the lapped panels in 23 hrs from the start of indoor exposure. Solution resistance was measured at 10kHz-60kHz and corrosion resistance

at lower frequencies. It was found that the solution resistance and corrosion resistance in the crevice of the lapped panels could be measured simultaneously by using the two electrode AC impedance technique.

It was assumed that both of the unpainted surfaces in the crevice of the lapped panels were wetted with incoming solution because the gap was narrow as shown in Figure 4. The effective surface area, S , where the unpainted surfaces are in contact with the inside solution is as follows.

$$S = d \cdot \rho / R_s, \quad (1)$$

where R_s is the solution resistance, d is the clearance in the crevice of the lapped panels and ρ is the specific resistance of the solution in the crevice. The value of ρ became constant in few cycles as the solution was saturated with NaCl (approximately 25wt%). Based on Equation(1), S is proportional to $1/R_s$.

Figure 5 shows the time dependence of the reciprocal of the solution resistance in the crevice of the lapped panels in the laboratory wet and dry corrosion test. Besides the first quick mass gain, the variation with time of $1/R_s$ in Figure 5 and the mass gain in Figure 4 are in parallel.

Figure 6 shows a relationship between the mass gain and $1/R_s$ in 5 cycles of the laboratory wet and dry corrosion test. Up to the saturation amount of the crevice solution, a good correlation exist between the mass gain and $1/R_s$ as indicated by the data in Figure 6. The first mass gain was due to water absorption in electrodeposition coating and epoxy resin. It can be concluded that the solution in excess of about 0.033g(saturation amount of crevice solution) is that which permeated other than the unpainted surface.

Corrosion monitoring in wet and dry corrosion tests

Impedance at lower frequencies was assumed to provide the relative corrosion rate in the crevice. Figure 7 shows the time dependence of the reciprocal of corrosion resistance and the degree of wetness of the lapped panels. Corrosion resistance was determined at a frequency 0.01Hz. The degree of wetness was evaluated as follows,

$$\text{Wetness} = R_s(\text{sat}) / R_s, \quad (2)$$

where $R_s(\text{sat})$ is the solution resistance of the lapped panels at the mass gain of 0.033g. The highest corrosion rate was observed immediately after immersion in 5wt% NaCl solution. It rapidly decreased with decrease of the degree of wetness, reaching a minimum at 20% wetness, and increased again when the degree of wetness decreased further.

It was speculated that the initial high corrosion rate was caused by the oxidizing action of the corrosion products and the final increase of the corrosion rate was due to oxygen that diffused into the crevice at the low wetness stage. When significant amount of solution exists in the crevice, supply of oxygen to the crevice solution was extremely limited because of the narrow crevice clearance. Thus, the state of intermediate wetting accelerates corrosion in the crevice.

Conclusion

From the results obtained, the following conclusions can be drawn.

1. The AC impedance technique is useful for simultaneous measurements of the degree of wetness and the corrosion rate in the crevice at the lapped portion. The degree of wetness is given by impedance at high frequencies above 10kHz and the corrosion rate by impedance at low frequencies less than 0.01Hz.

2. The state of intermediate wetting provides relatively easy entry of oxygen and hence accelerates corrosion in the crevice of lapped portion.

Acknowledgment

The authors wish to express their thanks to Dr. Iwao Matsushima of Materials and Processing Research Center, NKK Corporation for his helpful suggestions to this study.

Reference

1. Standard Practice for Measurement of Time-of-Wetness on Surfaces Exposed to Wetting Conditions as in Atmospheric Corrosion Testing, ASTM G84-89, Annual Book of Standards, 03.02, (Philadelphia, PA:ASTM, 1989) p347.
2. Fred H. Haynie and David C. Stiles, *Materials Performance*, No6, 48(1992)
3. S. Haruyama and T. Tsuru, "Electrochemical Corrosion Testing", ASTM STP 727, Florian Mansfeld and Ugo Bertocci, Eds., American Society for Testing and Materials, (1981). p.167.
4. T. Tsuru and S. Haruyama, *Boshoku Gijutsu*, 27, 573 (1978)

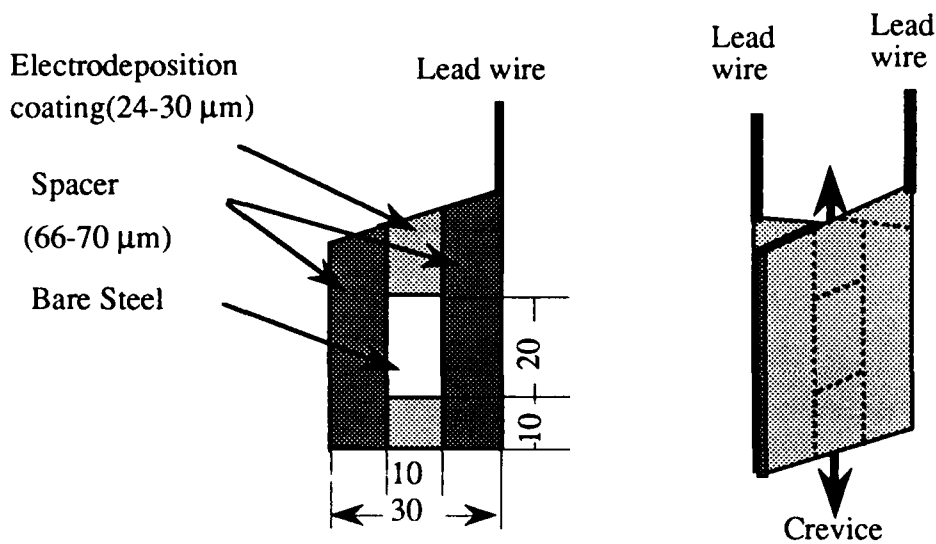


Figure 1 The schematic of the lapped panels used for measuring the mass gain and impedance in the crevice.

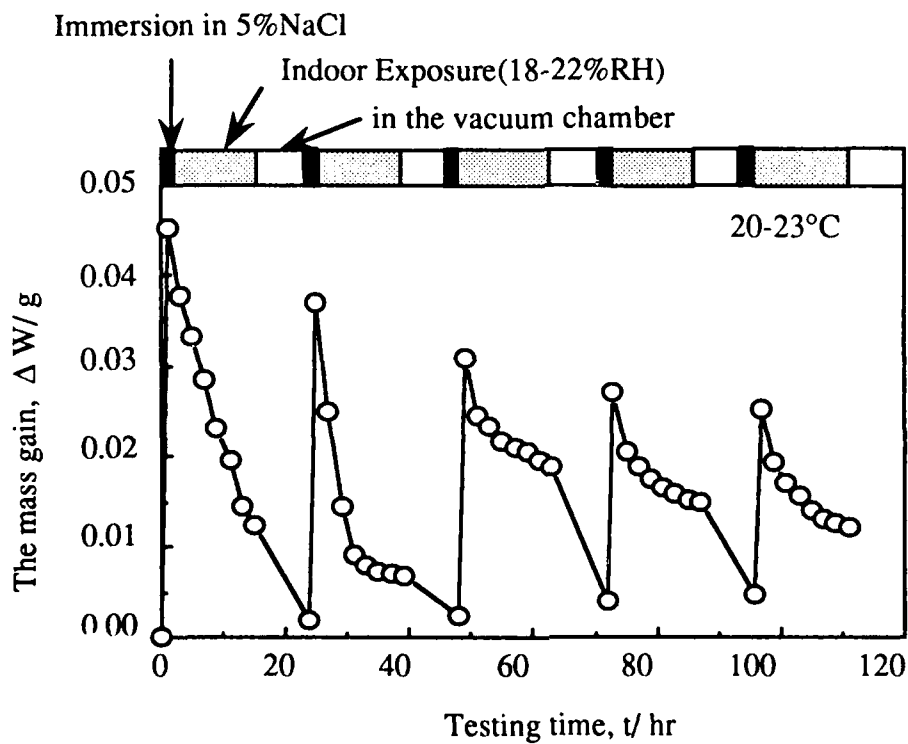


Figure 2 The variation of the mass gain of the lapped panels in the laboratory wet and dry corrosion test at room temperature.

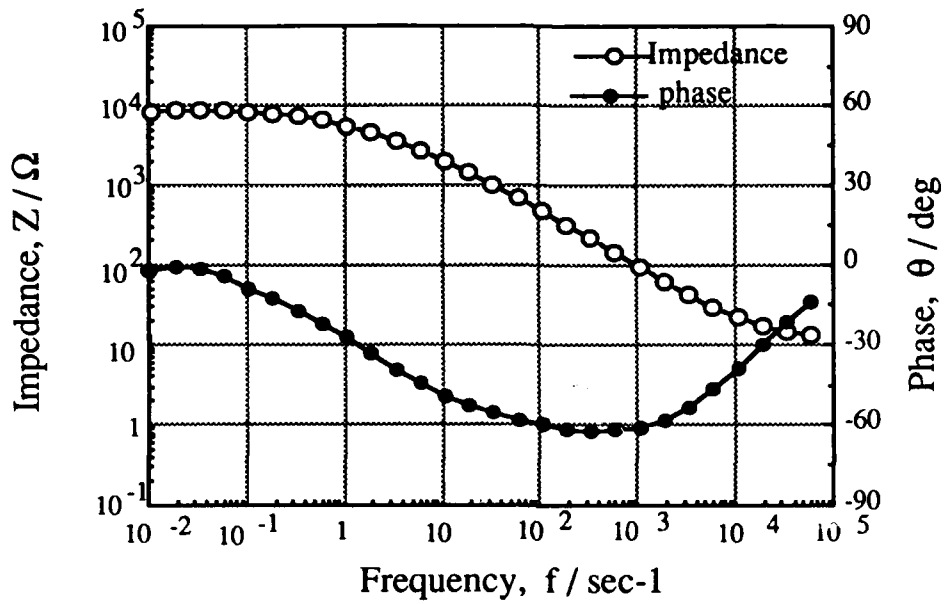


Figure 3 Bode diagram for the lapped panels at 23 hrs from the start of indoor exposure.

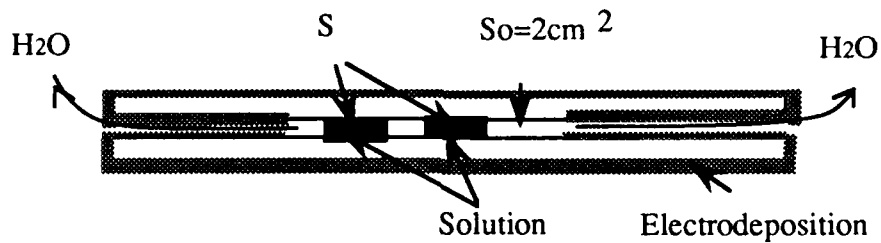


Figure 4 The schematic of the inside solution

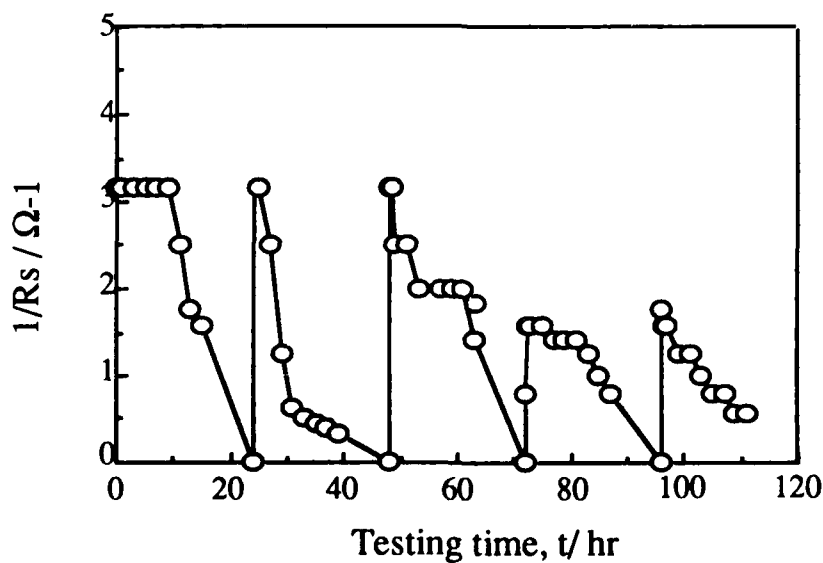


Figure 5 The time dependence of reciprocal of the solution resistance in the crevice of the lapped panels.

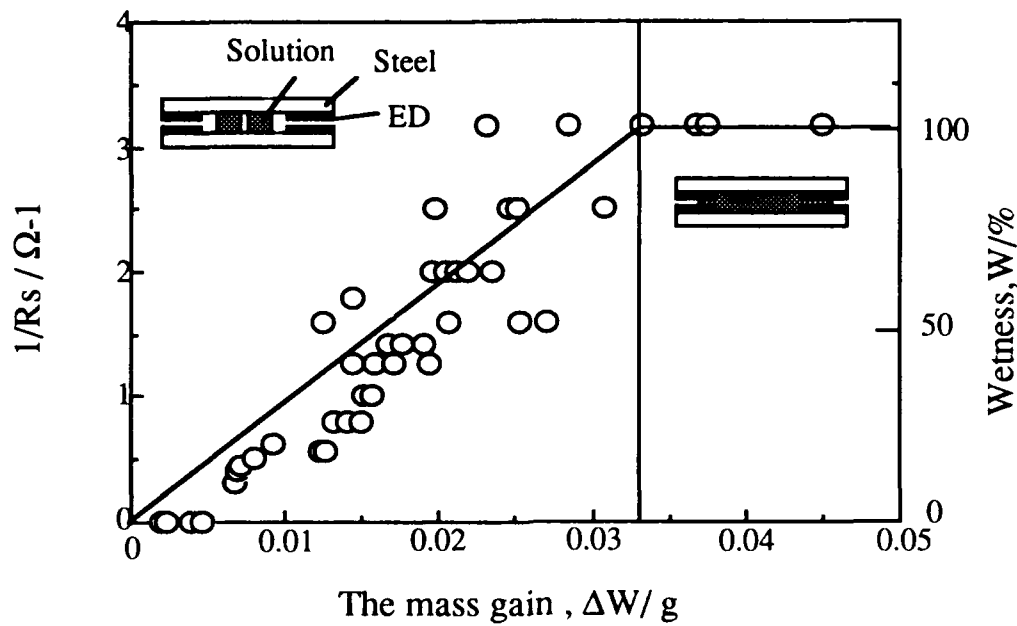


Figure 6 The relationship between the mass gain and reciprocal of the solution resistance in 5 cycles of the laboratory wet and dry corrosion test.

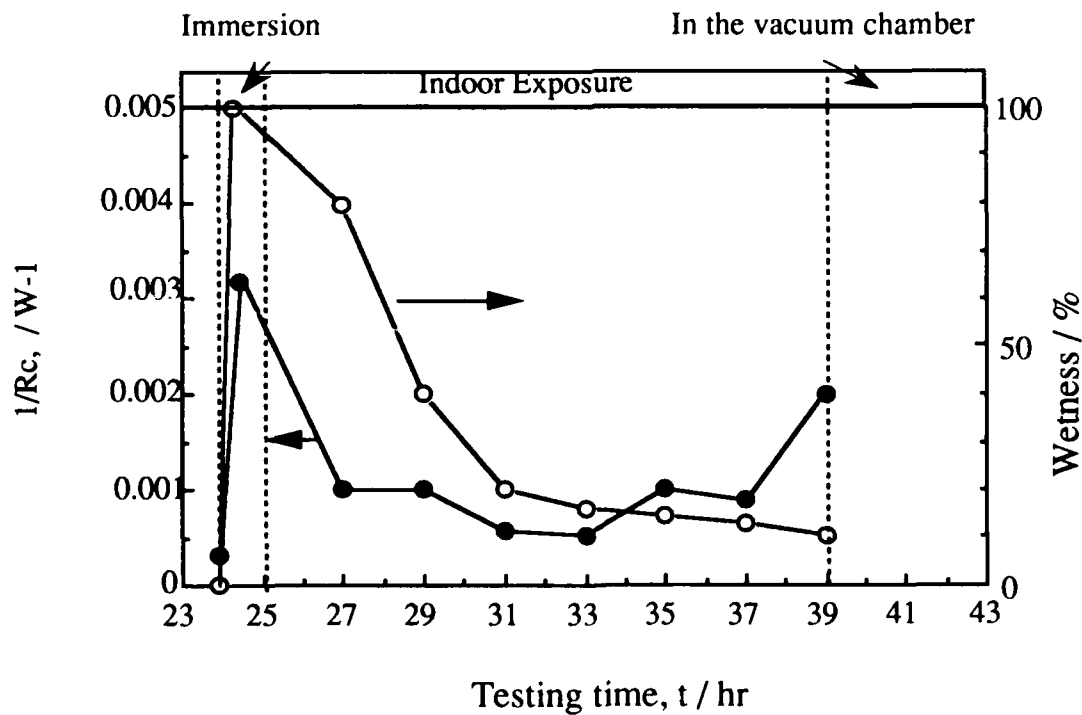


Figure 7 The time dependence of reciprocal of corrosion resistance and the degree of the wetness of the lapped panels.

Designing a Reinforced Concrete against Corrosion in Chloride Containing Environments : Choosing the Cement by Applying a Diffusion Model and Using Electrochemical Methods

Ezzedine Triki

Ecole Nationale d'Ingénieurs de Tunis. Laboratoire de corrosion
B.P. 37 Le Belvédère
Tunis (Tunisia)

Leila Dhouibi-Hachani

Ecole Nationale d'Ingénieurs de Tunis. Laboratoire de corrosion
B.P. 37 Le Belvédère
Tunis (Tunisia)

André Raharinaivo

Laboratoire Central des Ponts et Chaussées
58 Boulevard Lefebvre
75732 Paris CEDEX 15 (France)

Abstract

The object of this investigation is to select the cement to be used in reinforced concretes which are able to resist to chloride diffusion and therefore to the rebar corrosion. For all the tested concretes, the cement contents were equal to 250 kg/m^3 and the water-cement ratio was equal to 0.6, but the cement type varied.

The experimentation was focussed first on the determination of the diffusion coefficient of chloride into concrete, then on plotting stationary polarization curves and measuring the electrochemical impedances of the embedded rebars.

The diffusion study has shown out that the cement type is a major parameter influencing the chloride diffusion into concrete. The polarization curves of embedded rebars have the same shape, whatever the cement type. They include a passivation plateau and a current peak at about $-600 \text{ mV}_{\text{SCE}}$. The length of the passivation plateau and the height of the peak are related with the cement type, therefore with the chloride diffusion.

Finally, the electrochemical impedance of a rebar embedded in concrete was modelled with an equivalent circuit which takes into account the real products formed on steel. In this model, a dispersion constant α has been introduced and the experimental results have shown that this constant is related with the cement type.

The results of this investigation were applied to a real case.

Key terms : concrete, reinforcement, electrochemical tests, chloride diffusion

Introduction

The corrosion of rebars in concrete is due to chloride ions and similar agents which are coming from the environment and can depassivate the metal surface. It means that corrosion occurs when the chloride content close to rebars is high enough, i.e. after a delay which is related to the chloride migration into concrete.

So, for designing a concrete which prevents the rebar corrosion, it is needed to choose the cement type, the cement content and the water-cement ratio, as well. In this paper, only the effect of the cement was investigated.

The cement to use in real structures, had to be selected out of the cements which were available in the concerned area. The chosen cement had to have the following properties :

- it gives the lowest diffusion coefficient of chloride ions.
- rebars embedded in it are passivated.

The environments tested in this investigation were aqueous solutions, which were similar to ground waters encountered in Tunisia.

Experimental

Concrete design

The cements used in this investigation were tunisian. It dealt with :

- ordinary Portland cement "CPA", from Enfida plant.
- composed Portland cement "CPC 1", from Karouba plant.
- Portland cement with a high resistance against sulphates "CPA HRS 45", from Karouba plant.

Table I gives the compositions of these cements. The two cements from Karouba plant were "sulphate resistant", because these requirements are met concerning the following contents : $[\text{CaO Al}_2\text{O}_3] < 5\%$. $\{2[3\text{CaO Al}_2\text{O}_3] + [4\text{CaO Al}_2\text{O}_3 \text{Fe}_2\text{O}_3]\} < 20\%$ and $[\text{SO}_3^{--}] < 2.3\%$.

The concrete design corresponded to that of real, industrial, low cost products, for which the cement type was to be determined (table II). The water-cement ratio was equal to 0.6. The concrete was mixed manually and compacted by vibrating, before pouring into moulds. Concrete specimens were cured in a climatic chamber, with a relative humidity a little higher than 50 %, during 48 hours. At this age, they were taken out of the moulds. Then they were immersed and stored in tap water, at 20°C, during 28 days.

Specimens for electrochemical tests

The reinforced concrete specimens were parallelepipeds, 4x4x16 cm. A plain carbon steel wire, 6.5 mm diameter and 120 mm long, was placed in the longitudinal axis of the specimen. Table III gives the steel composition. The wires were polished with abrasive papers, rinsed with distilled water and dried with warm air, before being embedded in concrete.

The polarization (potentiodynamic) curves were plotted with reinforced concrete specimens which had been cured during 28 days, then immersed in salt solution during one hour.

For the electrochemical impedance spectroscopy, the specimens were first cured during 28 days, then they were continuously immersed in the aggressive salt solution, during 72 weeks. At this time, the electrochemical impedance was measured on specimens which were immersed in the salt solution.

Aggressive solution

The reinforced concrete specimens were immersed in a solution containing 90 g/l sodium chloride (pH = 6.5). This content corresponded to that of a real water in a tunisian site. Some reference tests were made with immersing concrete specimens in distilled water.

Methods for studying chloride diffusion

The chloride diffusion in concrete was studied with the following procedure, which uses a "diffusion cell". A concrete plate was placed in a cell, with salt solution on one side of the plate and a lime solution (saturated with calcium hydroxide, pH = 12.4), on the other side. This technique has been used without any supplementary applied potential which could enhance the diffusion process (Figure 1). Only the chloride content gradient has made the ions flow from the aggressive solution to the lime solution, through concrete. The chloride content in the lime solution was measured in function of time. The curve giving chloride content in this solution, versus time, yields an apparent diffusion coefficient.

The concrete specimens were small plates 160 x 160 x 20 mm³ in dimensions. They were 28 day old, when the diffusion test started. The specimen faces contacting solutions, had been in contact with the mould during concrete hardening. The volume of every solution (salt solution and lime solution) surrounding the concrete specimen was $V = 1\ 250\ \text{cm}^3$.

The chloride diffusion tests lasted at least 250 days.

Procedures of the electrochemical test

Polarization curves Potentiodynamic curves were plotted for the steel wires embedded in concrete. The reference electrode was a saturated calomel electrode (SCE) placed on the concrete surface. The counter-electrode was a stainless steel ([Cr] : 18%, [Ni] : 10%) sheet, placed on the concrete surface.

The potential sweep started one hour after the reinforced concrete specimen had been immersed in aggressive solution. A one-way potential sweep was made, starting from $E = -1200 \text{ mV}_{\text{SCE}}$, up to $+650 \text{ mV}_{\text{SCE}}$, at the rate of 50 mV/min .

Electrochemical impedance spectroscopy (EIS) The aggressive medium was placed in a plastic vessel where a specimen was immersed. For measuring the electrochemical impedance, the experimental arrangement was the same as that for plotting potentiodynamic curve.

The frequency of the applied potential ranged between 50 kHz and 10 mHz . The (peak to peak) amplitude of the potential ΔE was about 8 mV .

The measurements were made after the ageing tests, at rest (zero current) potential. The impedance results were plotted as a Nyquist diagram, having, for a given applied frequency, the real part R as abscissa and the imaginary part $-j G$ as ordinate.

An example of the electrical circuit equivalent to the concrete-steel system was proposed in ¹ : this model has been improved.

Results and Discussion

Results concerning chloride diffusion

The curves giving chloride content C versus $\text{Ln } t$ (logarithm of time) are of the same shape. Figure 2 gives an example of such a curve. It appears that chloride diffusion obey two laws, with a change at a time which was determined in the following way ². A theoretical law was assumed for the chloride diffusion during the first stage. A software, using the "least square" method, was used for fitting the experimental curve with the theoretical curve. It appears that a sudden decrease of the correlation coefficient occurs at a given time (the end of the first stage) : it means that an other diffusion law is then to be used. More precisely, the diffusion processes were assumed as being as follows. During the first stage, the chloride content profile in the concrete plate is not stable and changes with time. Then, during the second stage, it is stable.

For the first stage, the chloride content C at a depth e (thickness of the concrete plate) and at time t , is deduced from FICK's law, knowing the diffusion coefficient D_1 :

$$\ln C\sqrt{t} = \ln A - \frac{e^2}{4 D_1 t}$$

where A is the plate area.

Table IV gives the results concerning the first diffusion coefficient D_1 , which ranges between 546 and 1160. $10^{-9} \text{ cm}^2\text{s}^{-1}$.

The transition times, between the two stages, were : 50 days for CPC1, 60 days for CPA and 120 days for CPA HRS cement.

For the second diffusion stage, the chloride content profile in the concrete plate is stable and the chloride content C_2 in calcium hydroxide solution, at time t is deduced by the FICK's law :

$$C_2 = C_1 \frac{D_2 A}{V e} (t - t_0)$$

where C_1 is the chloride content in salt solution, e the plate thickness, V the solution volume and t_0 a constant.

Table IV gives the values of second diffusion coefficient D_2 , which are ranging between 34 and 230. $10^{-9} \text{ cm}^2\text{s}^{-1}$.

The comparison of the two diffusion coefficients D_1 and D_2 , shows that :

- D_1 is higher than D_2 , for a given concrete design,
- the rankings of concretes designs by using either D_1 or D_2 are the same,
- the highest diffusion coefficients correspond to cement CPC 1 and the lowest values correspond to CPA HRS 45, but cement CPA is similar to CPA HRS 45.

So, according to the results of the chloride diffusion study, the composed Portland cement (CPC 1) is not to be recommended.

Results concerning potentiodynamic curves

The potentiodynamic curves were plotted with using reinforced concrete specimens. Figures 3 and 4, correspond to a sound (reference) concrete, 40 day old, and concretes immersed in salt solution for one hour, respectively.

It appears that

- the potentiodynamic curves have the same shape, whatever the cement type,
- an oxidation peak is visible near $E = -600 \text{ mV}_{\text{SCE}}$, followed by a passivation plateau,
- the peak heights are higher for chloride contaminated concretes than for sound concretes,

- the length of the passivation plateau depends on the cement type. As a rule, ordinary Portland cement (CPA) gives the longest passivation plateau and the lowest current density in this potential range.

During the test, the salt solution pH was stable (equal to 6.5), so that it has no influence on the results concerning the obtained potentiodynamic curves.

It means that, after this method, out of the three cements tested, the ordinary Portland cement (CPA) is the most protective. The composed Portland cement (CPC 1) is not to be recommended.

Results concerning electrochemical impedance

The electrochemical impedance Nyquist diagrams were plotted for steel in the various concrete samples.

Steel in sound concrete Figure 5 gives the Nyquist diagram for steel in a sound concrete, about 40 days old. It shows only one loop, which is a circular arc, having its center below the "real" axis. It corresponds to passivated steel 1,3,4,5,6,7,8, as supplementary visual examinations have confirmed (whitish products are formed on steel surface). It is to be noticed that for a steel rod which was directly immersed in a saturated $\text{Ca}(\text{OH})_2$ solution, during 1 hour or 24 hours, a similar Nyquist plot (with a single loop) was obtained (Figure 6).

Steel in concrete contaminated by salt solution Whatever the cement type, the Nyquist diagram of steel in concrete contaminated by salt solution includes two loops. Some authors have already obtained such results 1, 4,9. The centers of these circular loops are not on the real axis, but a little lower. The loop which corresponds to high frequencies, is far smaller than the low frequency loop (Figure 7). The high frequency loop may be attributed, according to 1, to the lime layer on the rebar. More generally, this high frequency impedance loop corresponds to products formed in the cement paste closed to the steel surface. The low frequency loop corresponds to the direct interface between steel and concrete.

For interpreting the impedance results, a model was established (Figure 8). It includes the concrete resistance, the impedance corresponding to the products formed in cement pores near steel, and the impedance of the steel-concrete interface. It is to be noticed that when no product is formed in the cement paste (in calcium hydroxide solution, for example), the corresponding part of the impedance vanishes.

The interface resistance R_2 is similar to a polarization resistance, but when the embedded steel is highly corroded the area between oxidized metal and concrete may not be assumed as being a pure metal-electrolyte interface. So, it appears (table VI) that the R_2 values does not depend only on the cement type.

The dispersion parts of the impedance correspond to the hardened cement porosity which results in a inhomogeneity of the products distribution. The parameters α_1 and

α_2 describe this dispersion and they are defined in the following way. For a given loop (high frequency or low frequency loop), the dispersion part of the impedance Z_d obeys

$$\frac{1}{Z_{d_i}(\omega)} = \frac{1}{R_{d_i}} + j C_i \omega$$

where ω is the pulsation (frequency), R_d and C a capacitance. Then, parameters α_i (with $i = 1$ or 2) and are defined by

$$R_{d_i} = \omega C_i \operatorname{tg} \frac{\pi \alpha_i}{2}$$

Table VI give the results concerning α_1 and α_2 . It appears that :

- parameters α_1 and α_2 are higher for concrete contaminated by chlorides than for sound concrete of the same design,
- parameter α_2 has the highest values in the case of cement CPC 1,
- supplementary visual examinations have confirmed that when α_2 value is low (case of cement CPA HRS 45), the film formed on steel surface is homogeneous.

So, the electrochemical impedance spectroscopy, which is applied along with the new interpretation model, has shown that cement CPC 1 is not to be recommended.

Conclusion

The results obtained have shown that

- the three procedures for choosing cement give consistent and complementary results,
- Portland cements CPA and CPA HRS 45 have similar properties concerning chloride diffusion and rebar protection, as well.
- composed cement CPC 1 is not to be recommended because as far as chloride diffusion and rebar protection are concerned.

These results had been used for designing concrete in real structures in Tunisia.

References

- 1 F. WENGER Métaux, Corrosion. Industrie No 742, p. 317 (1987)
- 2 L. HACHANI , E. TRIKI , A. RAHARINAIVO, M. T. CHAIEB , Materials and Structures, 24, No 141, p. 172 (1991)
- 3 A. G. JOHN . P. C. SEARSON.J. L. DAWSON, British Corrosion Journal 16, No 2, p. 102
- 4 J. L. DAWSON, D. J. JOHN, Journal of Electroanalytical Chemistry , No 110. p 37 (1981)
- 5 C. ANDRADE, V. CASTELO , British Corrosion Journal , 19, p. 99 (1984)
- 6 F. WENGER, L. LEMOINE,J. GALLAND, 9th International Congress on Metallic Corrosion, Toronto (Canada) (June 1984)
- 7 C. ANDRADE, V. CASTELO, C. ALONSO, J.A. GONZALEZ, in ASTM STP 906 , V. Chaker Ed. .(American Society for Testing Materials), p. 43 (1966)
- 8 T. DE MIRANDA, F. WENGER , 3rd American Congress of Corrosion and Protection, Rio de Janeiro. Brasil , p. 3 (June 1989)
- 9 L. HACHANI, J. CARPIO, C. FIAUD, A. RAHARINAIVO, E. TRIKI, Cement and Concrete Research 22, p. 56 (1992)

Tables

Table I : Compositions of the cements tested (in weight percent)

| Cement | SiO ₂ | Al ₂ O ₃ | Fe ₂ O ₃ | CaO | MgO | SO ₃ | CaO (free) | Loss on ignition | Insoluble |
|------------|------------------|--------------------------------|--------------------------------|-------|------|-----------------|------------|------------------|-----------|
| CPA | 21.73 | 5.39 | 3.36 | 61.99 | 1.19 | 2.04 | 0.49 | 1.9 | 0.70 |
| CPA HRS 45 | 21.75 | 3.85 | 4.68 | 64.14 | 1.44 | 1.74 | 0.30 | 1.0 | 0.32 |
| CPC 1 | 18.50 | 3.80 | 3.80 | 62.30 | 1.50 | 1.20 | 0.35 | 4.5 | 1.60 |

Table II :

a) Design of concrete for electrochemical tests

| Component | Content (kg/m ³) |
|------------------------------|------------------------------|
| Cement | 250 |
| Sand (dia.<5 mm) | 650 |
| Fine gravel (5 < dia. < 8mm) | 635 |
| Gravel (8 < dia. < 12 mm) | 850 |
| Water | 150 |

b) Design of concrete for studying chloride diffusion

| Component | Content (kg/m ³) |
|-------------------------------|------------------------------|
| Cement | 250 |
| Sand (dia.<3 mm) | 650 |
| Fine gravel (3 < dia. < 5 mm) | 635 |
| Water-cement ratio | 0.6 |

Table III : Chemical composition of steel wire

| Element | C | Mn | Si | S | P |
|--------------------|------|-------|------|-------|-------|
| Weight percent (%) | 0.22 | 0.089 | 0.24 | 0.016 | 0.046 |

Table V

Diffusion coefficients D₁ and D₂ of chloride through concrete (in 10⁻⁹ cm². s⁻¹)

| Cement | CPA | CPA HRS | CPC 1 |
|----------------|-----|---------|-------|
| D ₁ | 680 | 546 | 1180 |
| D ₂ | 130 | 34 | 230 |

Table VI :

Values of interface resistance R₂ (kΩ. cm²), dispersion parameters α₁ and α₂ after EIS measurements

| Concrete Parameter | Sound | | In distilled water | | | In chloride solution | | |
|--------------------|----------------|----------------|--------------------|----------------|----------------|----------------------|----------------|----------------|
| | α ₂ | R ₂ | α ₁ | α ₂ | R ₂ | α ₁ | α ₂ | R ₂ |
| CPA | 0.10 | 400 | 0.19 | 0.10 | 875 | 0.56 | 0.41 | 2 |
| CPA HRS | 0.001 | 500 | 0.13 | 0.06 | 140 | 0.50 | 0.44 | 214 |
| CPC1 | 0.11 | 294 | 0.20 | 0.18 | 1120 | 0.45 | 0.60 | 41 |

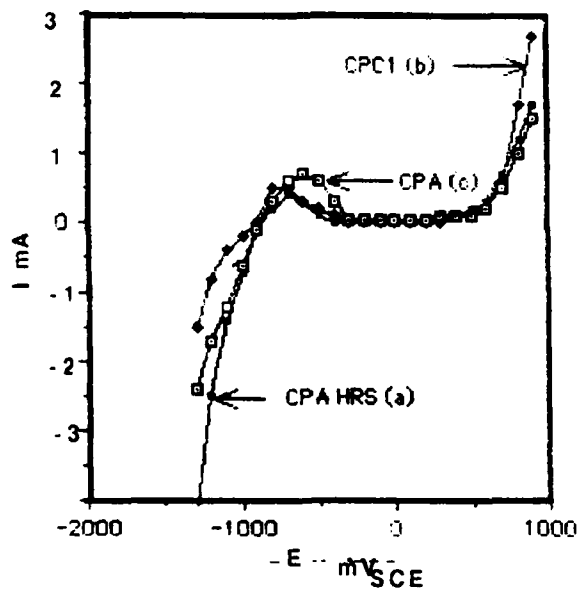


Figure 3 : Potentiodynamic curves of steel in sound concretes (steel area : 24.5 cm^2)
 These reference concretes were cured during 28 days in tap water and for 12 days in atmosphere.

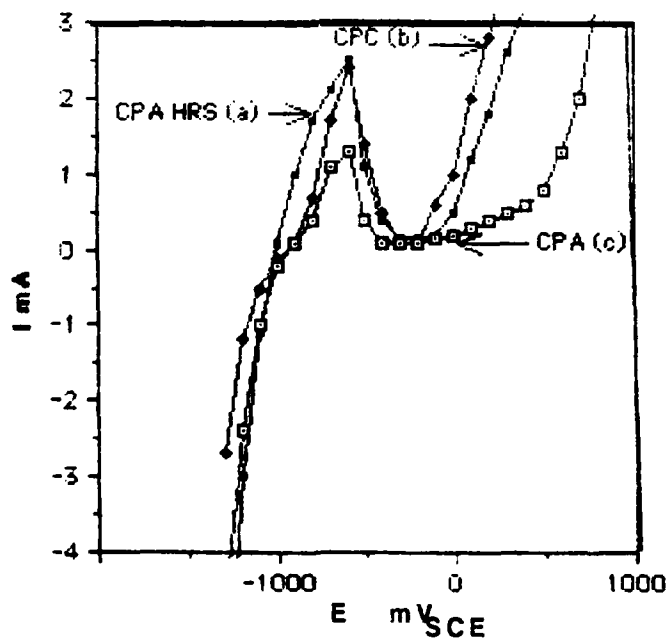


Figure 4 : Potentiodynamic curves of steel in concretes contaminated with chloride
 (steel area : 24.5 cm^2). These reinforced concrete specimens were cured during 28 days, then
 immersed in chloride solution ($\text{pH} = 6.5$) during one hour, before plotting the potentiodynamic curve.

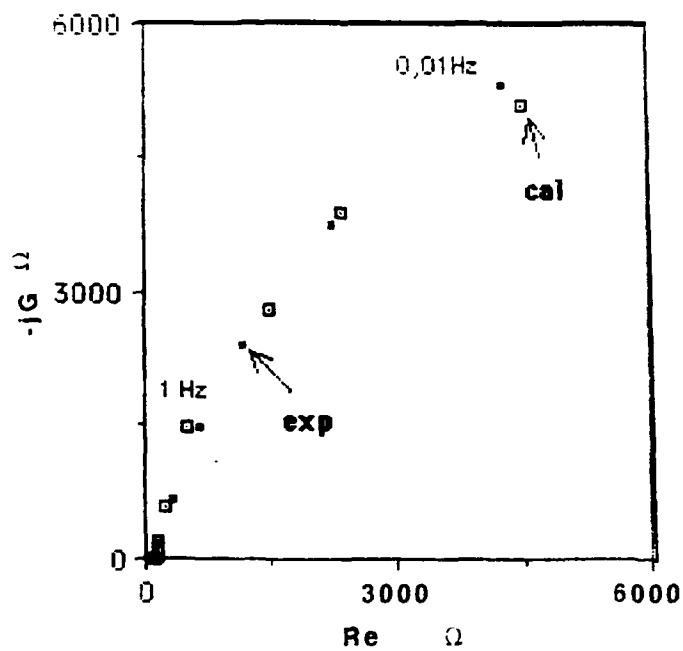


Figure 5 : Nyquist plot of the impedance of steel in sound (reference) CPC 1 concrete , 40 day old. (steel area : 24.5 cm²).

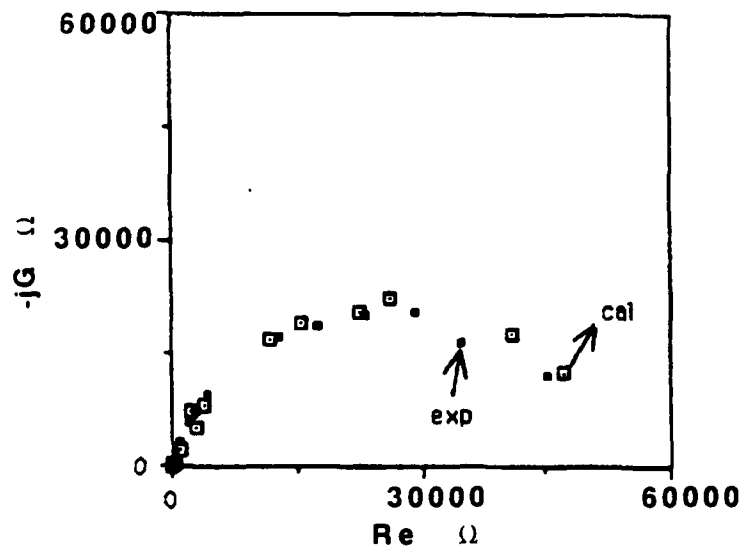


Figure 6 : Nyquist plot of the impedance of steel placed in calcium hydroxide saturated solution (steel area : 24.5 cm²).

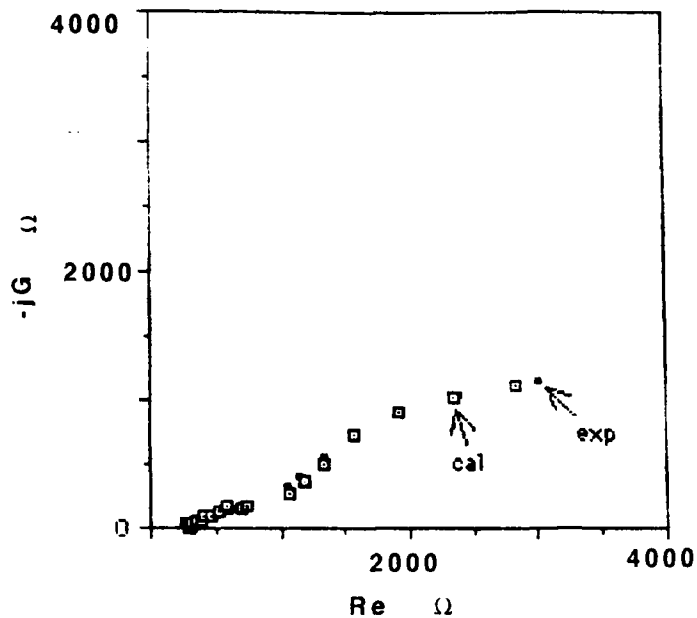


Figure 7 : Nyquist plot of the impedance of steel in CPA HRS concrete, contaminated with chloride (steel area : 24.5 cm^2). These reinforced concrete specimens were cured during 28 days, then immersed in chloride solution for 72 weeks, before measuring the steel electrochemical impedance.

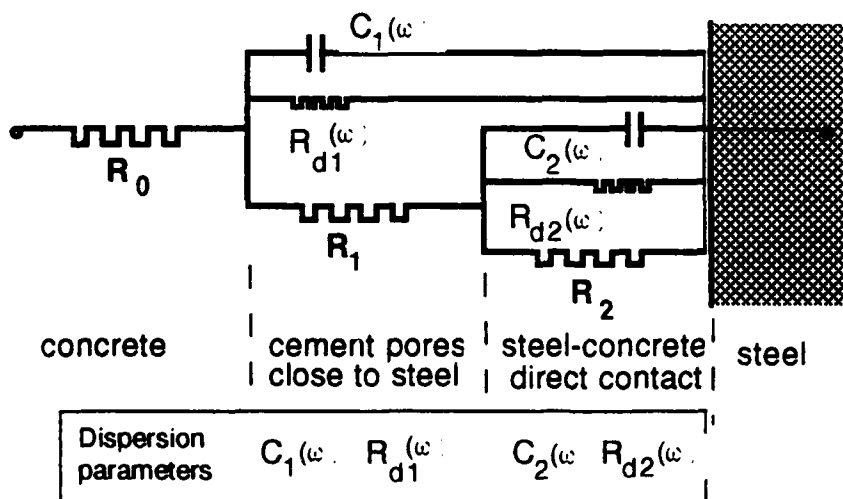


Figure 8 : Equivalent circuit for the electrochemical impedance of steel in concrete

Figures

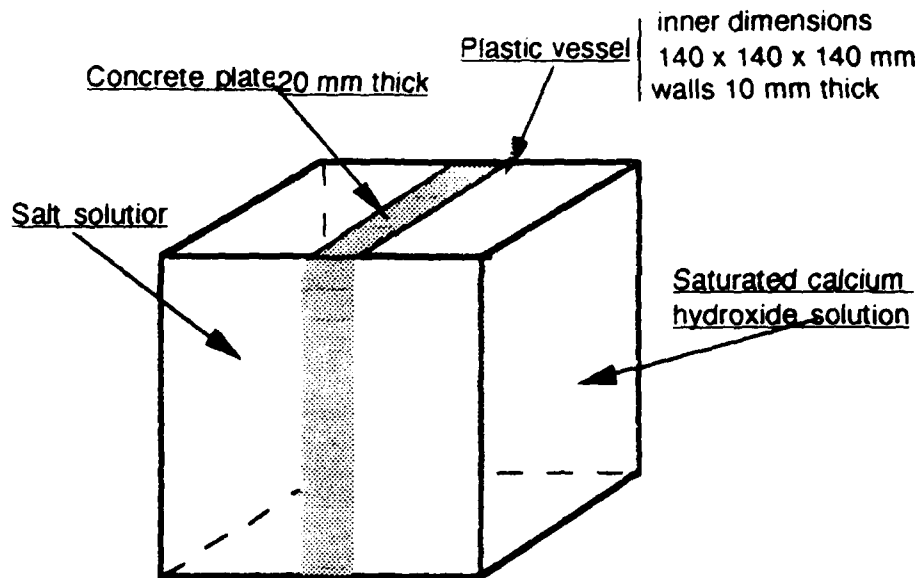


Figure 1 : Experimental arrangement for studying chloride diffusion. The pH of the sodium chloride solution is equal to 6.5.

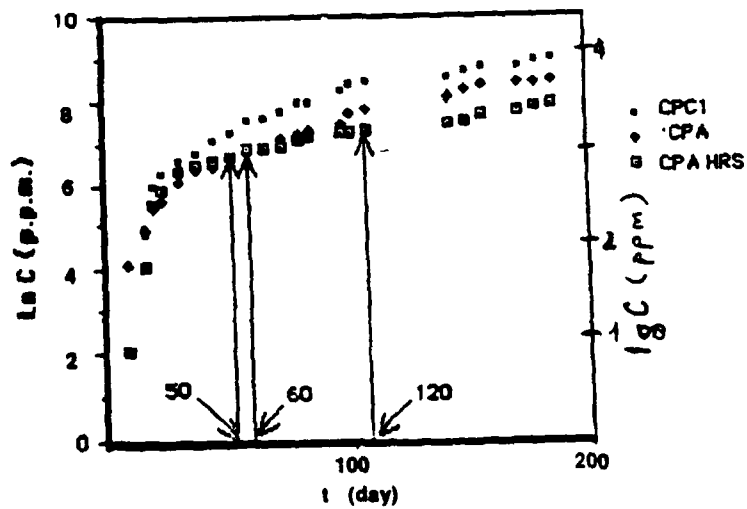


Figure 2 : Typical curve giving chloride content in lime solution, versus time

A Current-Based Criterion for Cathodic Protection of Reinforced Concrete Structures

Jack Bennett
ELTECH Research Corporation
625 East Street
Fairport Harbor, Ohio 44024

Abstract

Several criteria have been proposed to measure the effectiveness of cathodic protection of reinforced concrete structures. Most of these techniques have been adapted from their use in the underground and submerged cathodic protection industry, and have not been vigorously verified in concrete. Many of these criteria are difficult to interpret and apply. In this paper, a new current-based criterion is suggested which is simple to use and technically accurate throughout the life of the system.

Laboratory data are presented which establish the actual corrosion rate of cathodically protected steel as a function of salt concentration, pH and polarization. The amount of polarization needed to achieve an acceptable rate of corrosion is especially sensitive to salt concentration and pH. At pH 13.37, polarizations ranging from zero to 170 millivolts were needed at chloride concentrations ranging from 1 to 30 pounds chloride per cubic yard (0.16 to 4.80% by weight of cement). One unit of pH was found to change the rate of corrosion by over an order of magnitude. These data illustrate the complexity of trying to apply criteria based on steel potential.

Corrosion rate data are also presented as a function of macrocell current flowing to or from the test specimens. Macrocell current was found to represent a relatively small portion of the corrosion occurring on the test specimens. The application of cathodic protection current was found to effectively eliminate both macrocell and microcell corrosion, however. Based on these data, a cathodic protection criterion is proposed based on current flow to or from probes constructed from corroding steel within the structure. This proposed criterion is simple, easy to apply, technically accurate throughout the life of the system, and does not rely on the long-term stability of embedded reference electrodes. Limited field experience is also provided.

Key words: concrete, corrosion, criteria, cathode, cathodic protection, polarization

Introduction

Cathodic protection (CP) is rapidly becoming accepted as a repair option for reinforced concrete structures undergoing corrosion due to the presence of chlorides. Experience over the past 15 years has shown cathodic protection to be both technically effective and economically viable.

Despite this success, however, there still exist confusion and disagreement over the methods used to measure the effectiveness of CP systems. A variety of CP criteria have been proposed, including those using electrode operating potential, potential shift, potential decay, current-potential relationship (E-log I) and a statistical treatment of static potentials. Many of these criteria are complex and difficult to apply.

A field survey conducted in 1989 by Battelle¹ determined the cathodic protection criteria being used on 466 CP installations in North America. The survey showed that the most number of structures were being controlled using the 100 mV depolarization technique (223 structures). Second in popularity was the E-log I criterion (146 structures). Both of these criteria are listed in NACE Standard Recommended Practice². The E-log I criterion, typically used as a start-up procedure, is often difficult to interpret and apply, and is normally performed by consultants or service firms specializing in cathodic protection. The most popular criterion, 100 mV depolarization, was developed in the underground CP industry and was first applied to reinforced concrete structures in the early 1980s. This criterion is simpler than E-log I, but the proper amount of depolarization needed, as well as the procedure for measurement, is still debated. Its use in concrete was reported by Bennett and Mitchell who conducted an empirical investigation of the criterion and recommended that it be raised from 100 mV to 150 mV³. In a technical review of polarization shift criteria, Funahashi and Bushman suggested that polarizations of 155 to 240 mV are needed, depending on the chloride content of the concrete⁴. This finding was reinforced by a subsequent study by Funahashi and Young in 1992⁵. Other authors have suggested that 100 mV of polarization is too high, and results in excessive polarization of steel reinforcement⁶.

Uncertainties in the test procedure further complicate the 100 mV depolarization criterion. The amount of polarization measured depends significantly on the time period used for the test. NACE Standard Recommended Practice suggests that a four hour time period be used for the test². A recent survey of cathodic protection on North American bridges shows that as little as 25% of the total depolarization may be recorded in four hours, however⁷. Determination of the IR-free potential, which is the starting point for the depolarization test, is also dependent on procedure. If the IR-free potential is taken too soon, the initial starting potential will be too high since capacitance decay and charge balancing effects are slow in concrete³. If, conversely, the IR-free potential is taken too long after current-off, then the full depolarization will not be included in the measurement. Most authors suggest that the IR-free reading be taken between 0.01 and 1.0 second after current off^{3,8}.

Contributing to the uncertainty regarding criteria is the lack of corrosion rate data in concrete. Such data could provide a sound experimental basis for CP criteria. With this realization, work began on Strategic Highway Research Program (SHRP) Contract SHRP-91-C-102D in April of 1991. It was the objective of Task 5 of this contract to determine the actual rates of corrosion of reinforcing steel in concrete as a function of chloride concentration, pH, temperature, and cathodic protection current and to use this data to justify cathodic protection criteria. Oxygen was generally accessible to the steel for this study, and the availability of oxygen was not studied as a variable.

Experimental Procedure

A corrosion cell approximating concrete construction with a double mat of reinforcing steel was built from Schedule 40 PVC (see Figure 1). The cell was comprised of two chambers separated by a cation exchange membrane. The anode chamber was filled with Ottawa sand (ASTM C 778-91, "Standard Specification for Standard Sand") and saturated with simulated pore water solution containing chloride ion. The cathode chamber contained Ottawa sand saturated with pore water solution containing no chloride. The cation exchange membrane prevented chloride ion from migrating out of the anode compartment and contaminating the catholyte. Two flat steel coupons were placed in the cell, one on each side of the ion exchange membrane. During operation the two coupons were shorted

together to induce macrocell corrosion. A 10 ohm resistor was placed in the circuit to allow for the monitoring of corrosion currents. Catalyzed titanium anodes were placed on each side of the anode coupon for impressed current tests. The steel sample coupons were manufactured from SAE 1020 steel which contained 0.2% carbon.

The corrosion rate experiments were conducted at various levels of Cl⁻ ion concentrations, ranging from 1 to 30# Cl⁻/yd³ (approximating 0.16 to 4.8% by weight of cement). This was achieved by adding simulated concrete pore water to the sand. Standard pore water solution with chloride contamination was prepared with the following composition:

0.20% Ca(OH)₂
3.20% KCl
1.00% KOH
2.45% NaOH

When Ottawa sand is wetted with solution of this composition, and then drained to create an unflooded condition, the resultant Cl⁻ ion concentration was 10.2#/yd³ (approximating 1.63% by weight of cement). The percentage of KCl in the pore water was adjusted to yield various other concentrations of chloride ion. The use of wet sand in this way permitted access for the oxygen needed to sustain corrosion reactions. Experiments were also conducted at different pH levels by adjusting the amount of NaOH and KOH that were added to the pore water solution. This cell and test procedure are described in detail in another recent publication⁹.

The corrosion rate experiments were conducted on both freely corroding and polarized coupons. A set of five coupons were tested for every set of conditions. Due to the sensitivity required to determine weight losses, extra care was taken during handling to minimize contact with the surface of the coupons. Each experiment lasted 20 days during which corrosion currents were measured three times per week. Depolarization data was periodically collected on the polarized coupon tests using a Saturated Calomel Electrode. Determination of net current flow, either anodic or cathodic, was accomplished by the application of Kirchoff's laws according to the schematic in Figure 2. Typical observations included average weight loss, average depolarization and average current flow, either anodic or cathodic.

Weight loss determinations were conducted by rinsing the test coupons in tap water to remove residual sand. Corrosion products were removed from the surface using ASTM G 1-90, "Standard Practice for Preparing, Cleaning, and Evaluating Corrosion Test Specimens". Several procedures were tested until one was found that did not significantly attack the substrate. The procedure chosen involved dipping the coupons for ten minutes in a room temperature solution containing 20g of Antimony trioxide and 50g of Stannous chloride dissolved in concentrated hydrochloric acid (sp. gr. 1.19) to 1000 ml. After all five coupons were cleaned, a blank untested coupon was cleaned using the same procedure and any weight loss imparted by the etching solution was included in the final weight loss determinations.

Two concrete specimens were used to study corrosion current flow in reinforced concrete. One of these specimens was a 4 ft² (0.37 m²) slab constructed according to Ohio bridge deck specifications. It contained a double mat of reinforcing steel, with the upper mat in chloride contaminated concrete and the lower mat in non-chloride contaminated concrete. This arrangement facilitated development of macrocell corrosion. The second specimen was approximately 0.28 ft² (0.026 m²) containing two #4 reinforcing bars, one in an upper, chloride containing environment, and another in a lower non-chloride environment. Catalyzed titanium mesh anodes were installed on each specimen and covered with a one inch concrete overlay. The upper and lower mats were electrically shorted through a 10 ohm resistor. The resistor served as the path for macrocell currents while also serving as a means for measuring the currents.

Results and Discussion

Corrosion rate experiments conducted as described above in sand wetted with pore water solution closely simulate conditions in an unsaturated concrete environment. Oxygen is generally available for the corrosion process, unlike experiments conducted in aqueous solution where oxygen availability is limited. Diffusion constants are likely to be much higher in wetted sand than in concrete, however. For this reason, corrosion rates developed in this study are expected to be similar to those which occur when cathodic protection is first applied. After a significant amount

of current is passed, concentration gradients can be expected to develop in concrete as a result of electrochemical reaction and ionic migration. Chloride ions will be depleted at the surface of the steel, while hydroxide ions will accumulate, tending to decrease corrosion rate with time. Under such conditions the corrosion rate relationships developed in this study are still expected to be relevant, but the exact chloride and hydroxide concentrations at the surface of the steel may be unknown.

Corrosion rate experiments conducted in sand cells have significant advantages over experiments conducted in concrete. Test coupons can be easily removed from the sand and weighed to establish weight loss data. Weight loss of samples embedded in concrete is much more difficult to establish. Some authors have suggested the use of corrosion probes in concrete.¹⁰ Corrosion in concrete is characterized by a large amount of pitting corrosion. This pitting corrosion, especially present in freely corroding specimens, tend to confound corrosion rate experiments using a corrosion probe, which assumes a uniform corrosion.

Corrosion Rate Experiments

Figure 3 shows the relationship between corrosion rate and chloride concentration at about 20° C and a pH of 13.37. Each point is an average of five cells operated under identical conditions. The graph shows a steadily increasing corrosion rate as chloride concentration was increased from 1 to 30 #/yd³ (approximating 0.16 to 4.8% Cl⁻ by weight of cement).

Figure 4 shows the strong relationship between pore water pH and corrosion rate in the sand cells at 10 #Cl⁻/yd³ (approximating 1.6% by weight of cement) and a cathodic protection current of 0.68 mA/ft² (7.32 mA/m²). An increase of one pH unit reduced the corrosion rate 1½ orders of magnitude under these conditions. This is considered to be especially significant for cathodic protection since cathodic reactions will increase pH at the surface of the steel with time.

Figure 5 shows the effect of cathodic protection current on corrosion rate at concentrations of 10 and 30 #Cl⁻/yd³ (approximating 1.60 and 4.80% by weight of cement). These data confirm cathodic protection to be highly effective in a concrete-like environment.

The objective of any cathodic protection criterion is to allow the user to reduce the rate of corrosion to an acceptable level. It is therefore necessary to define an "acceptable" rate of corrosion. Studies conducted by Kenneth C. Clear indicated that cracking of concrete may result from as little as 2 mil (0.05 mm) of corrosion¹¹. Another recent study by Clemena et al indicated that a metal loss of 3 to 6% was the threshold of corrosion necessary to initiate delamination in reinforced concrete decks¹². Calculating for #5 bar (16 mm dia.), this metal loss equates to a corrosion loss of 4.7 to 9.5 mil (0.12 to 0.24 mm). For the purposes of this study, we will assume the more conservative figure of 2 mils (0.05 mm) of corrosion is required to initiate cracking. Assuming that a minimum of 20 years is needed without delamination, an acceptable corrosion rate of 0.10 mil/yr (0.0025 mm/yr) can be calculated.

One objective of this study was to determine the amount of polarization necessary to maintain an acceptable corrosion rate of 0.10 mil/yr. (0.0025 mm/yr.). This relationship has, unfortunately, been determined to be very complex. Figure 6 shows the relationship between polarization (measured as depolarization) and corrosion rate at chloride concentrations ranging from 1 to 30 #/yd³ (approximating 0.16 to 4.8% by weight of cement). Each data point is an average of data from five cells. Although general relationships can be seen (i.e. increasing chloride concentration increases corrosion rate, and increasing polarization sharply decreases corrosion rate), much more data would be needed to establish the relationships quantitatively. These relationships are complicated further by changes in pH. It therefore appears that a procedure attempting to define the exact amount of polarization necessary for each case would be too complicated for practical use. Another approach is to define and apply the amount of polarization necessary for the worst case, in which case all the steel should receive adequate protection. This approach commonly results in overprotection, however, which is undesirable.

Nulling of Corrosion Current

Figure 7 shows an interesting and relatively simple relationship between corrosion current (flowing to or from the anode) and corrosion rate. The entire range of chloride concentrations, from 1 to 30 #Cl/yd³ (approximating 0.16 to 4.8% by weight of cement), are plotted on this same line. This graph implies that if corrosion current could be measured and controlled, it could be used as an accurate and relatively simple criterion. In other words, making the anode net cathodic effectively stops corrosion. This is a well accepted principle of cathodic protection¹³, but this is the first confirmation of its effectiveness in concrete. It is clear from this graph that most of the corrosion occurring in these tests can be attributed to localized pitting corrosion. Measured weight losses far exceed that predicted by Faraday's Law. But it is also clear that cathodic protection current is capable of eliminating both macrocell and pitting corrosion.

The concept described above, that of measuring corrosion current and applying cathodic protection to null or reverse that current, is applied when using a "rebar probe"¹⁴. Rebar probes are typically constructed by casting a 5 inch (12.7 mm) long piece of #5 rebar (16 mm dia.) in salty mortar, usually 15 #Cl/yd³ (2.4% by weight of cement). This probe is then installed in an excavation in the structure where reinforcing bars have been exposed on all sides, and the excavation is patched with chloride-free concrete. When the probe is connected to the system negative, through a 10 ohm resistor for monitoring purposes, a strong macrocorrosion cell is created. Cathodic protection current is then applied to null or reverse the measured corrosion current, making the probe a net cathode. The rebar probe is usually constructed to be the most anodic site for the structure. It may then be assumed that if the probe is sufficiently protected, the rest of the structure will be protected as well.

Although rebar probes are considered useful, especially for start-up, they are not generally regarded as a cathodic protection criterion, and are not mentioned as such in NACE Recommended Practice². One common criticism of rebar probes is that they indicate a decreasing CP current with time as chloride migrates away from the probe. This is precisely what should happen, however, and it is appropriate that a criterion reflect this process. It is the view of this author that rebar probes have been under utilized in past practice, and deserve further consideration.

Based on the above data and observations, a Corrosion Null Probe (CNP) concept was developed. The CNP is similar to the rebar probe described above, except that it is constructed from reinforcing steel and concrete native to the structure. Corrosion rate monitored in this way will be site specific, and cathodic protection requirement will be completely relevant for the structure at the time of the test.

To verify this concept, the sand cells described above were set up to null macrocell corrosion currents established at several different salt concentrations. The results of these tests are shown on Figure 8 and Table 1. For these tests, cathodic protection current was gradually increased using auxiliary anodes placed near the corroding steel coupon. The null point was recorded when the corrosion current was exactly balanced by cathodic protection current. The range of the data again shows the scatter caused by localized pitting corrosion. Table 1 lists the average cathodic protection current requirements along with the average polarization of the steel at the null point. It is interesting to note that even though the cathodic protection current requirement increases about two orders of magnitude from 1 to 20 #Cl/yd³ (approximating 0.16 to 3.2% by weight of cement), 100 to 150 mV of polarization is adequate protection over most of this range. These data tend to confirm the 100 mV depolarization criterion as a technique, although, as has been suggested by other authors, the criterion should be increased to 150 mV total polarization for worst-case protection. The amount which should be measured in a 4 hour time period is still in question.

The Corrosion Null Probe technique was then tested on two concrete test yard specimens. Results of these tests are shown on Figures 9 and 10. The specimen in Figure 9 was a 4 ft² (0.37 m²) concrete slab which had top mat reinforcement in a state of mild corrosion. In this case, a cathodic protection current of 0.05 mA/ft² (0.54 mA/m²) of concrete was required to null out corrosion current. A second test was then performed on a 0.28 ft² (0.026 m²) test yard slab which was badly delaminated. The slab was in an outdoor test yard, wet and corroding at the time of testing. For this slab, a cathodic protection current of 3.0 mA/ft² (32.3 mA/m²) of concrete was required to null corrosion current, as shown on Figure 10. Following this test, the slab was brought indoors and allowed to dry out for a period of about one month. The nulling test was again performed, and a cathodic protection current of 0.94 mA/ft² (10.1 mA/m²) was then required. The slab was then maintained indoors with weekly ponding and a constant

current of 0.94 mA/ft² (10.1 mA/m²). After 84 days-on-line, the nulling test was again performed and a cathodic protection current of 0.21 mA/ft² (2.26 mA/m²) was determined. This drop of required current from 3.0, to 0.94 to 0.21 mA/ft² (32.3 to 10.1 to 2.26 mA/m²), a result of concrete drying and of cathodic protection current, is considered reasonable. This illustrates how the CNP test responds correctly to changes in environment and conditions.

Field Testing

Figure 11 shows the construction of the Corrosion Null Probe. To create the CNP, a short piece of strongly corroding reinforcing bar is isolated by dry saw-cutting. A wire is attached to one end of the bar for monitoring purposes. The cut ends of the bar and the wire contact are then sealed with non-conducting epoxy. The remainder of the excavation is filled with cementitious grout. The lead wire from the CNP is attached to the cathodic protection system negative through a 10 ohm resistor for monitoring purposes.

In order to verify this concept, Corrosion Null Probes were installed in Wawecus Hill Road Bridge in Norwich, Connecticut. An ELGARD™ cathodic protection system was installed on 12,100 ft (1125 m²) of the deck of this bridge in November of 1992. The cathodic protection system was separated into 4 separately controlled zones, and it was decided to install 2 CNPs in each zone (total 8). Prior to installation, delaminated concrete was extensively removed. The deck was not patched since it was intended to place the concrete in a single pour. It was therefore necessary to locate and construct the probes in the existing concrete before any patching was completed. This is probably not ideal since the potential survey is likely to change somewhat after patching.

After verifying the electrical continuity of steel in the deck, a potential survey was conducted using ASTM C 876-91 "Standard Test Method for Half-Cell Potentials of Uncoated Reinforcing Steel in Concrete". The procedure was conducted using a saturated calomel (SCE) half-cell and Fluke 27 high impedance voltmeter. The survey was first conducted on 4 ft (1.2 m) center to approximately locate the most anodic sites. After this was complete, the most anodic (negative) areas were re-surveyed on 1 ft (0.3 m) center to more closely locate the most anodic reinforcing bars. The exact positions of the bars selected for the probes were determined using a CT-4950 Micro Covermeter, made by ELE International, Inc. The static potentials of the selected bars, before cutting, are given on Table 2.

The reinforcing bars selected for CNPs were then isolated by dry-cutting using a diamond saw. The cutting process is shown on Figure 12. A monitoring wire was attached to one end of the CNP by drilling and tapping one end of the bar. The connection and the cut ends of the bar were coated with non-conducting epoxy. The installed CNP is shown on Figure 13 prior to mesh installation and overlay. The slots which were cut to isolate the CNP were filled by the overlay.

Unfortunately, the wires to the CNPs were left disconnected for 43 days during the construction process. This interrupted the macrocell corrosion and caused the corrosion currents to decrease. When the cathodic protection system was energized, corrosion currents on the probes was still very low, and the required cathodic protection current averaged only 0.05 mA/ft² (0.54 mA/m²). This was not considered valid for start-up and the system was energized at 1.5 mA/ft² (16.1 mA/m²).

After the cathodic protection system on Wawecus Road Bridge had been operating for 34 days, the probes were again tested. During this period of operation the probes were connected to the system negative and had equilibrated to their operating conditions. The required cathodic protection current indicated by each probe is shown on Table 2. The required cathodic protection currents, ranging from 0.23 to 0.75 mA/ft² (2.5 to 8.1 mA/m²) are not unreasonable since the CP system had been operating for 34 days, and since this test was conducted on January 20 when temperatures were very cold. Two of the eight probes were apparently not functioning properly, indicating a negative cathodic protection current requirement. At this time there is no obvious explanation for this behavior.

ELGARD™ is a trademark of ELGARD Corp.

This approach appears to offer a technically accurate and simple to apply criterion for cathodic protection in reinforced concrete. It is site specific, and will reflect diminishing cathodic protection current requirement with time. Installation is simple, and the test is quick and easy to perform. Significantly, it does not rely on the long-term stability of embedded reference electrodes. The CNP technique does require that reinforcing steel be cut and isolated, however, and in certain cases this may be objectionable. One such case would be where prestressing steel is involved. Another concern is the need to select the most anodic area for the construction of the CNP. This must be done very carefully. If the CNP is installed in the wrong location, the cathodic protection current may be grossly misjudged.

On the strength of these tests and results to date, additional field tests of the Corrosion Null Probe are recommended. As of this writing, monitoring of the probes in Connecticut is continuing and other field tests are being initiated.

Conclusions

1. Cells filled with sand wetted with simulated pore water solution provide a useful simulated environment for corrosion studies of steel in concrete.
2. Cathodic protection current can effectively stop corrosion of steel in a concrete environment.
3. The rate of corrosion of steel in concrete is strongly dependent on chloride concentration and pH.
4. The amount of polarization needed to stop corrosion is variable, depending on chloride ion concentration, pH and temperature.
5. The 100 mV polarization criterion is reasonably appropriate as a worst case criterion, but as such the requirement should be increased to 150mV total polarization. The 4-hour time period typically used for depolarization measurement may be inadequate in some cases, which could lead to overprotection.
6. The Corrosion Null Probe (CNP) is proposed as a simple and effective criterion for cathodic protection of steel in concrete.
7. Additional field testing and experience are needed to verify the CNP technique.

Acknowledgements

This research was funded by the Strategic Highway Research Program (National Research Council). The publication of this article does not necessarily indicate approval or endorsement by the National Academy of Sciences, the United States Government, or the American Association of State Highway Transportation Officials (or its member states), of the findings, opinions, conclusions or recommendations either inferred or specifically expressed herein.

The author would also like to express his thanks to Eric Lohrey of the Connecticut DOT and Walt Eager of the Oregon DOT for their willingness to install the first Corrosion Null Probes on field highway structures.

References

1. M.K. Han, et al, "Cathodic Protection of Concrete Bridge Components," Strategic Highway Research Program, Progress Report for Contract SHRP-87-C-102B, April 14, 1989.
2. Standard Recommended Practice, NACE Standard RP0290-90, Item No. 53072, April, 1990.
3. J.E. Bennett and T.A. Mitchell, "Depolarization of Cathodically Protected Reinforcing Steel in Concrete," Paper No. 373, NACE Corrosion/89, New Orleans, April 1989.
4. M. Funishashi, J.B. Bushman, "Technical Review of 100 mV Polarization Shift Criterion for Reinforcing Steel in Concrete," Corrosion, Vol. 47, No. 5, National Association of Corrosion Engineers, Houston, Texas, 1989.

5. M. Funihashi and W.T. Young, "Investigation of 100 mV Polarization Shift Criterion for Reinforcing Steel in Concrete," Paper No. 193, NACE Corrosion/92, Nashville, 1992.
6. R.C.G. Laird, "Performance Evaluation Testing of Conductive Coating Cathodic Protection Systems on Thin Parking Garage Slabs," Paper No. 553, NACE Corrosion/91, Cincinnati, 1991.
7. J.P. Broomfield, "Field Survey of Cathodic Protection on North American Bridges," Materials Performance, Vol. 31, No. 9, National Association of Corrosion Engineers, Houston, Texas, September, 1992.
8. Cathodic Protection of Reinforced Concrete, Technical Report No. 36, Concrete Society, Corrosion Engineering Association, London, 1989.
9. J.E. Bennett, J.J. Bartholomew, T.R. Turk, "Cathodic Protection Criteria Related Studies Under SHRP Contract," Paper No. 323, NACE Corrosion/93, New Orleans, 1993.
10. J.A. Keldsen, "Measuring Steel-in-Concrete Corrosion with an Electrical Resistance Probe," Paper No. 123, NACE Corrosion/80, Houston, 1980.
11. K.C. Clear, "Measuring Rate of Corrosion of Steel in Field Concrete," June, 1988. (Available from Kenneth C. Clear, Inc. Rt. 1, Box 347, Boston, VA 22713).
12. G.G. Clemena, D.R. Jackson, G.C. Crawford, "Inclusion of Rebar Corrosion Rate Measurements in Condition Surveys of Concrete Bridge Decks," Transportation Research Record 1347, p. 37-45, 1992.
13. L.S. Ed Van Delinder, "Corrosion Basics, An Introduction," National Association of Corrosion Engineers, p. 184, Houston, Texas, 1984.
14. N.D. Burke and J.B. Bushman, "Corrosion and Cathodic Protection of Steel Reinforced Concrete Bridge Decks," FHWA Report No. FHWA-IP-88-007, p. 45, 56, 58, CORRPRO Companies, Inc., 1988.

Table 1. Average CP Requirement and Polarization vs. Salt Concentration

| Salt Concentration # Cl/yd. ³ (% by wt. cement) | Avg. CP Requirement mA/ft. ² steel (mA/M ²) | Avg. Polarization mV |
|---------------------------------------------------------------|-----------------------------------------------------------------------|-------------------------|
| 1 (0.16) | 0.05 (0.5) | 9 |
| 3 (0.48) | 0.34 (3.7) | 53 |
| 5 (0.80) | 1.64 (17.6) | 114 |
| 8 (1.28) | 2.14 (23.0) | 102 |
| 10 (1.60) | 5.98 (64.3) | 140 |
| 20 (3.20) | 10.90 (117.3) | 155 |

Table 2. Static Potential and Cathodic Protection Current Requirement for Corrosion Null Probes, Wawecus Hill Rd., Norwich, Connecticut, January 20, 1993.

| Zone | Probe No. | Static Potential mV vs SCE | Cathodic Protection Current mA/ft. ² Concrete (mA/M ²) |
|------|-----------|-------------------------------|----------------------------------------------------------------------------------|
| 1 | 1-1 | -436 | 0.23 (2.5) |
| 1 | 1-2 | -430 | * * |
| 2 | 2-1 | -385 | 0.36 (3.9) |
| 2 | 2-2 | -485 | 0.32 (3.4) |
| 3 | 3-1 | -424 | 0.45 (4.8) |
| 3 | 3-2 | -482 | 0.75 (8.1) |
| 4 | 4-1 | -400 | * * |
| 4 | 4-2 | -345 | 0.31 (3.3) |

* negative CP current indicated

CORROSION MACROCELL DESIGN

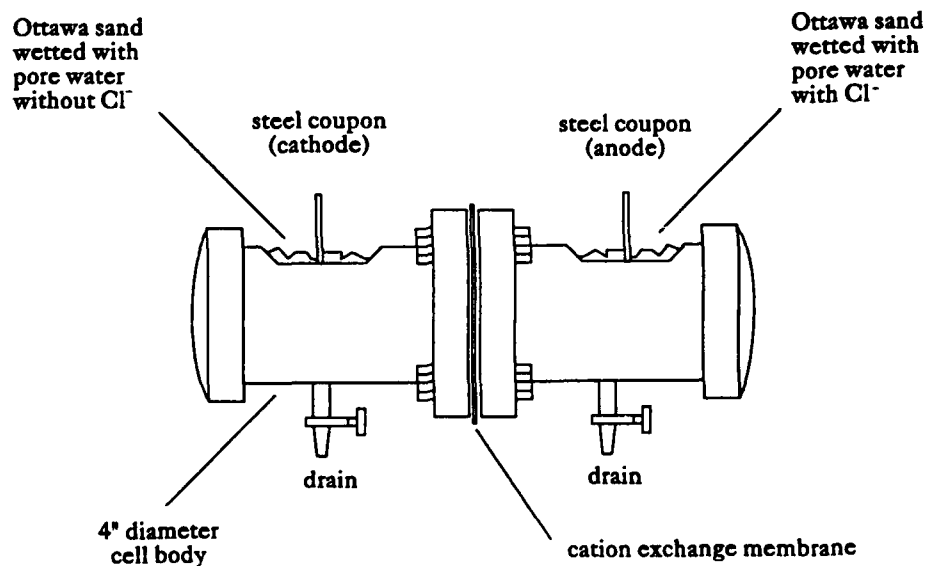


Figure 1. Corrosion Macrocell design

ELECTRICAL SCHEMATIC FOR THE SAND/PORE WATER CELLS

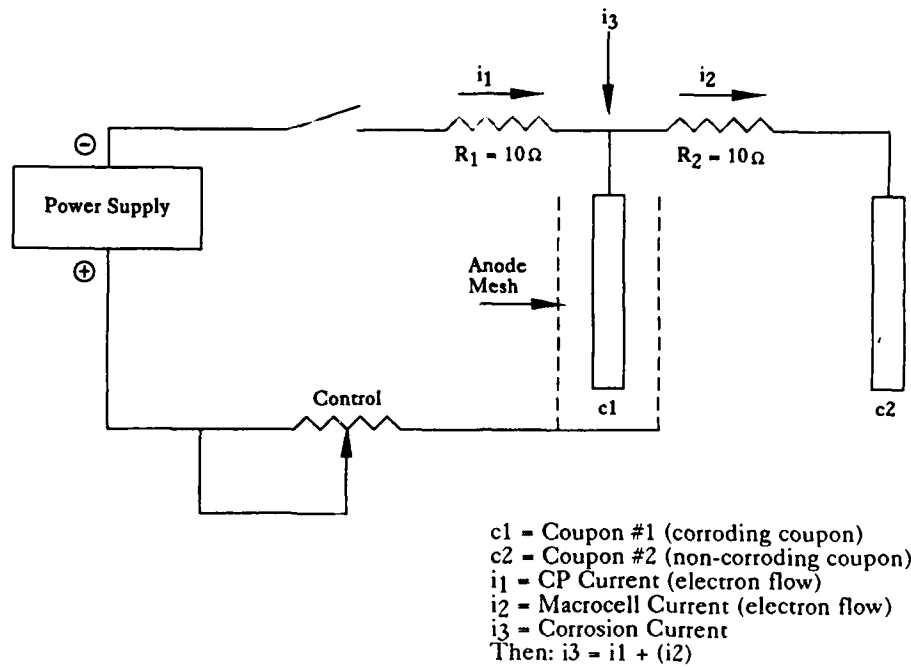


Figure 2. Electrical Schematic for the Sand Cells

SALT CONCENTRATION vs. CORROSION RATE

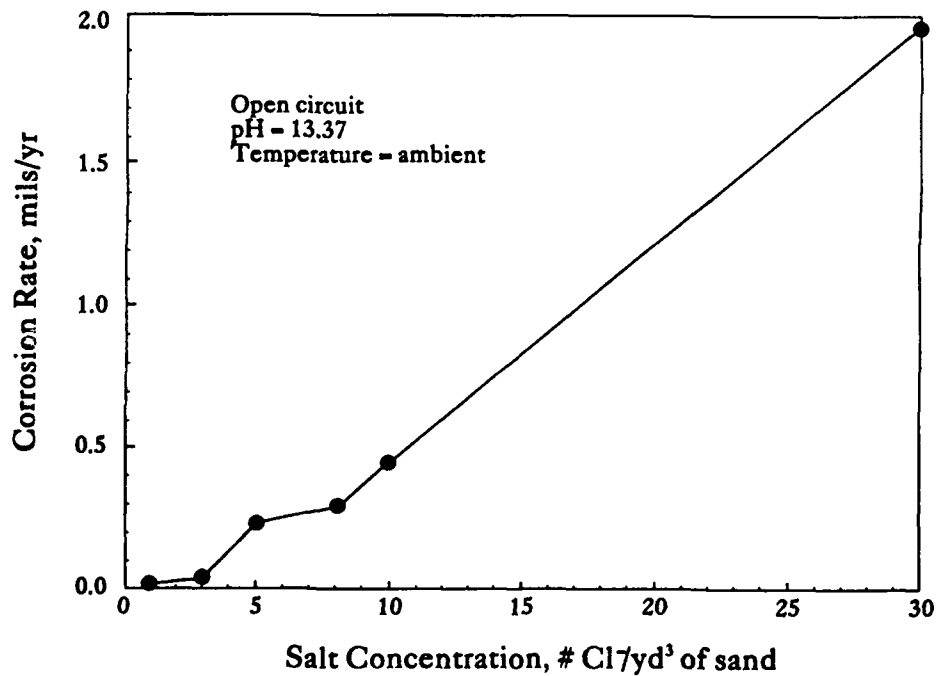


Figure 3. Corrosion Rate vs Salt Concentration

pH vs. CORROSION RATE Under Applied CP Current

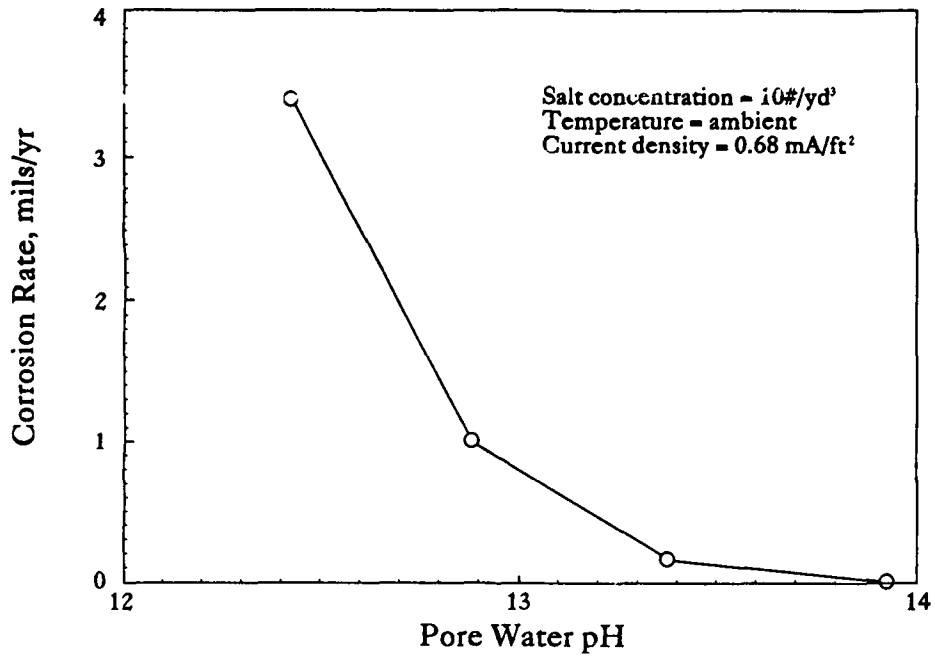


Figure 4. Corrosion Rate vs pH Under Applied CP Current

CATHODIC PROTECTION CURRENT DENSITY vs. CORROSION RATE

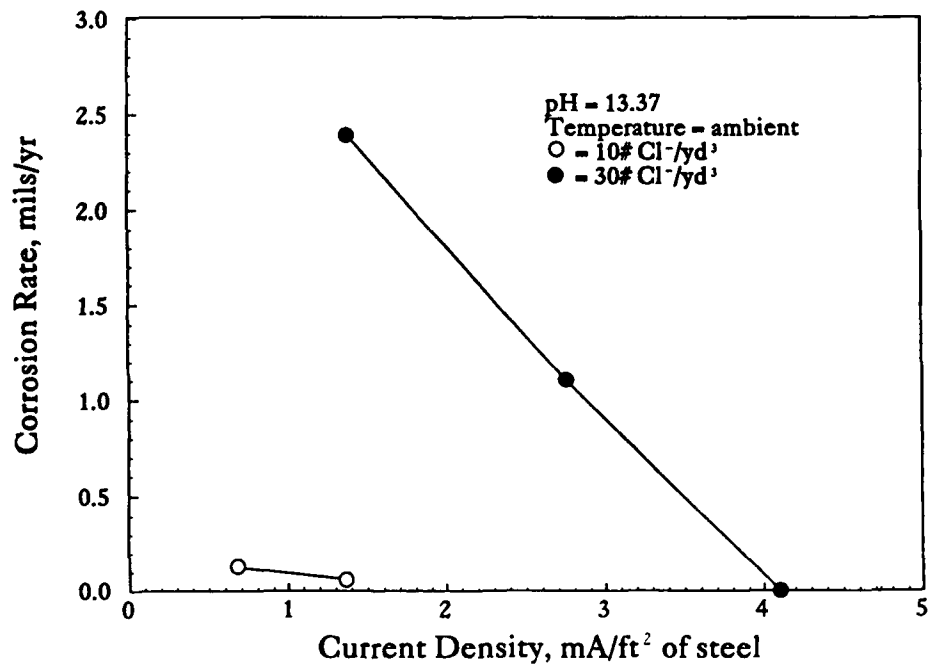


Figure 5. Corrosion Rate vs Cathodic Protection Current

AVG. DEPOLARIZATION vs. CORROSION RATE

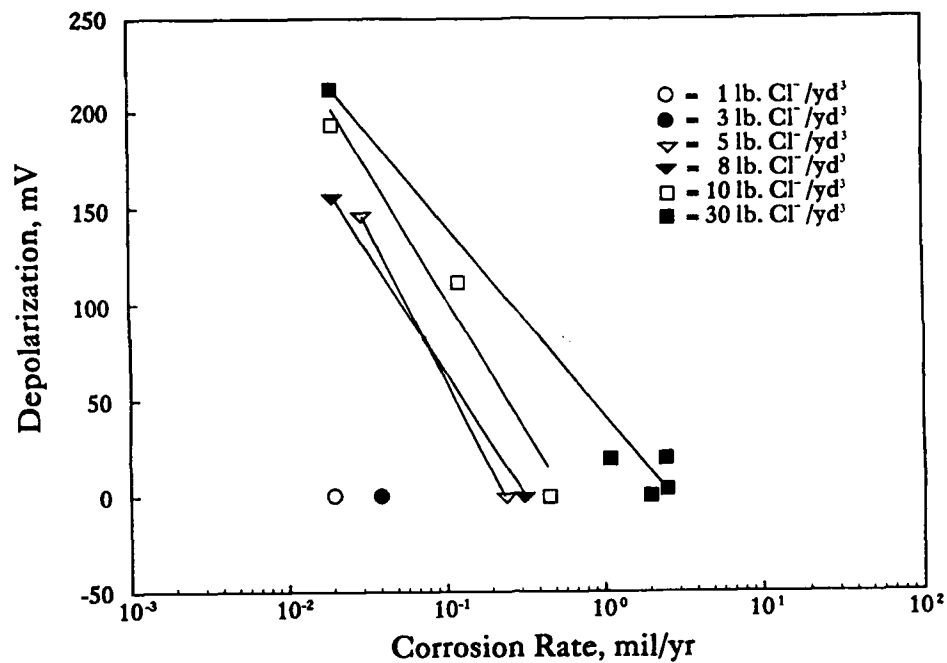


Figure 6. Corrosion Rate vs Average Depolarization

CORROSION CURRENT vs. CORROSION RATE

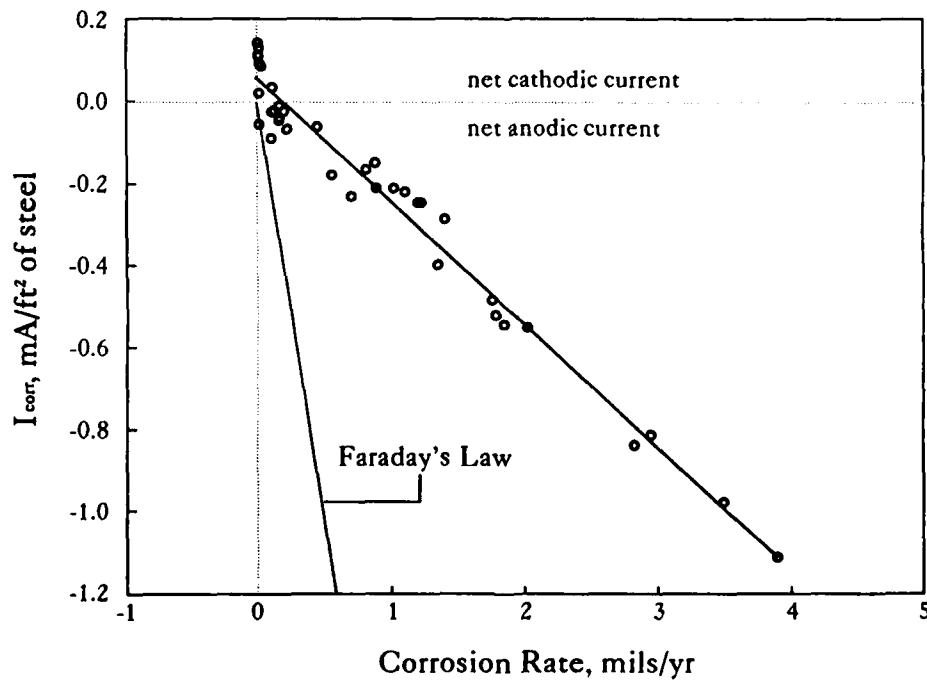


Figure 7. Corrosion Rate vs Macrocell Corrosion Current

CATHODIC NULLING CURRENT vs. SALT CONCENTRATION

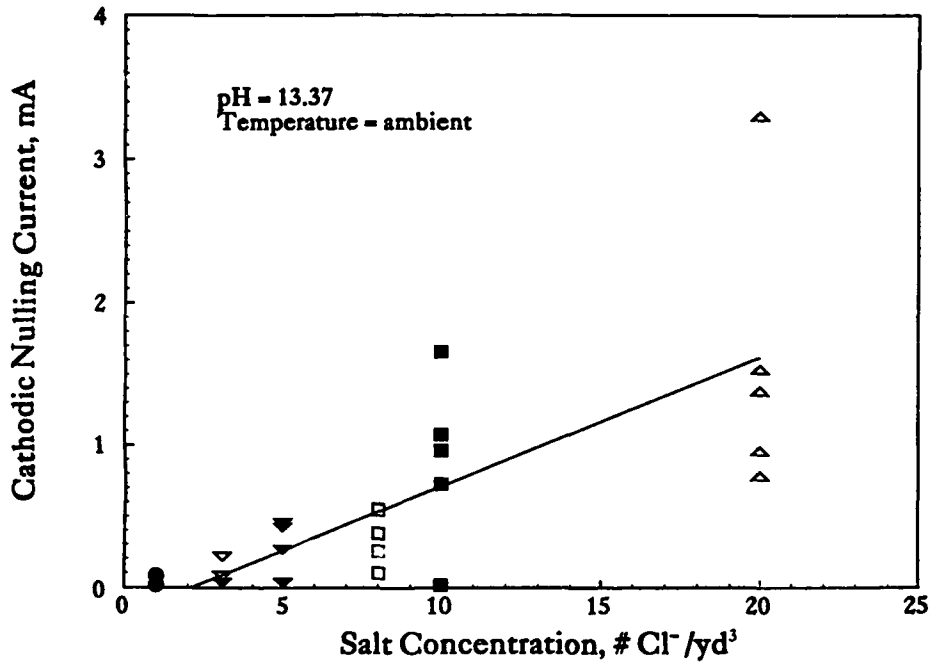


Figure 8. Cathodic Nulling Current vs Salt Concentration

CATHODIC PROTECTION CURRENT REQUIREMENT Mildly Corroding Concrete Specimen

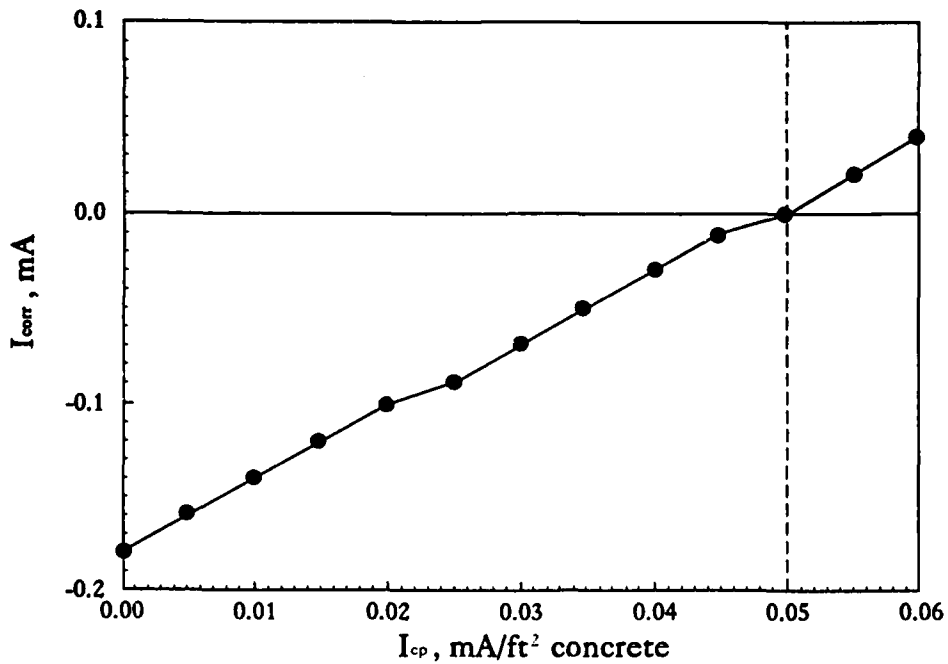
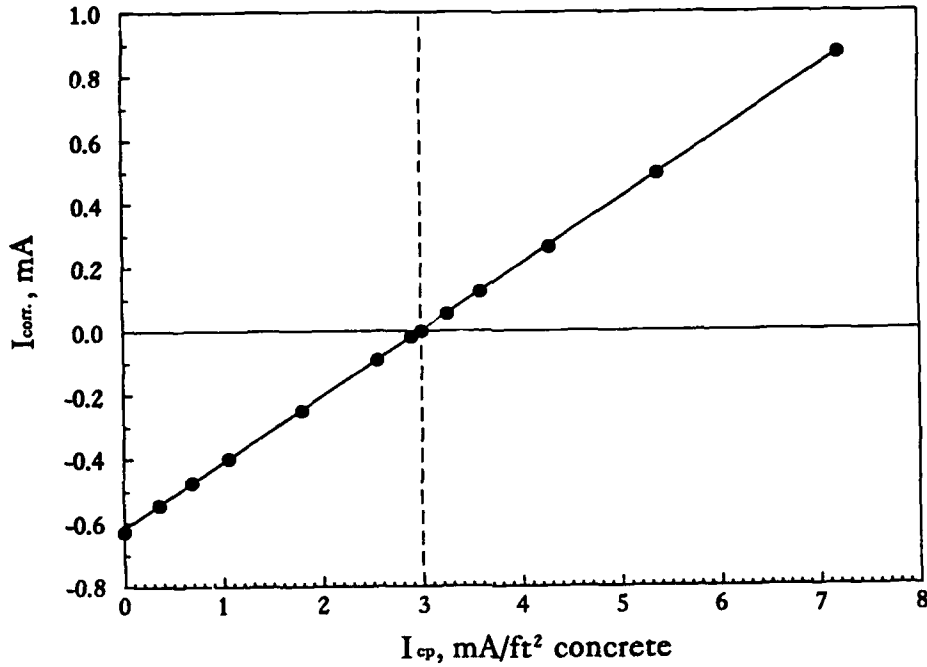


Figure 9. Cathodic Protection Current Requirement for Mildly Corroding Concrete Specimen

CATHODIC PROTECTION CURRENT REQUIREMENT Badly Corroding Concrete Specimen



**Figure 10. Cathodic Protection Current Requirement
for Badly Corroding Concrete Specimen**

CORROSION NULL PROBE INSTALLATION NOT TO SCALE

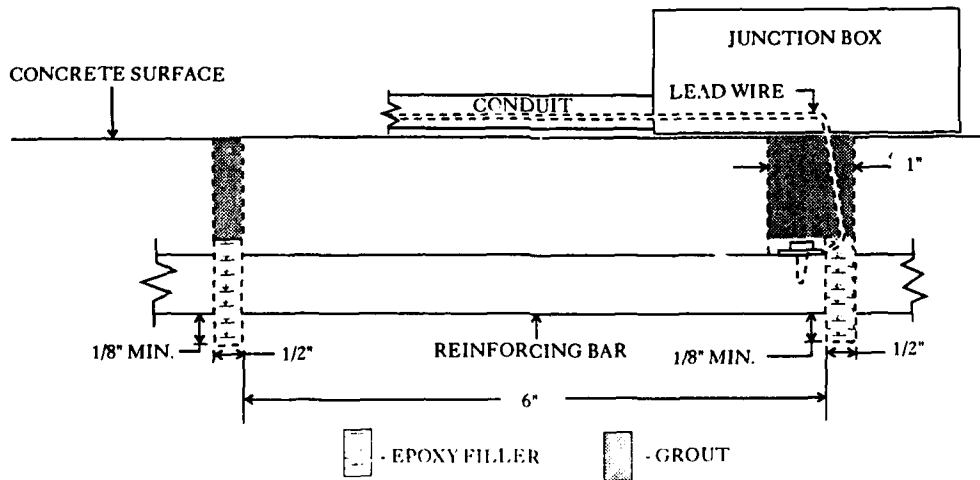


Figure 11. Construction of the Corrosion Null Probe



Figure 12. Cutting Reinforcing Bar for the Corrosion Null Probe

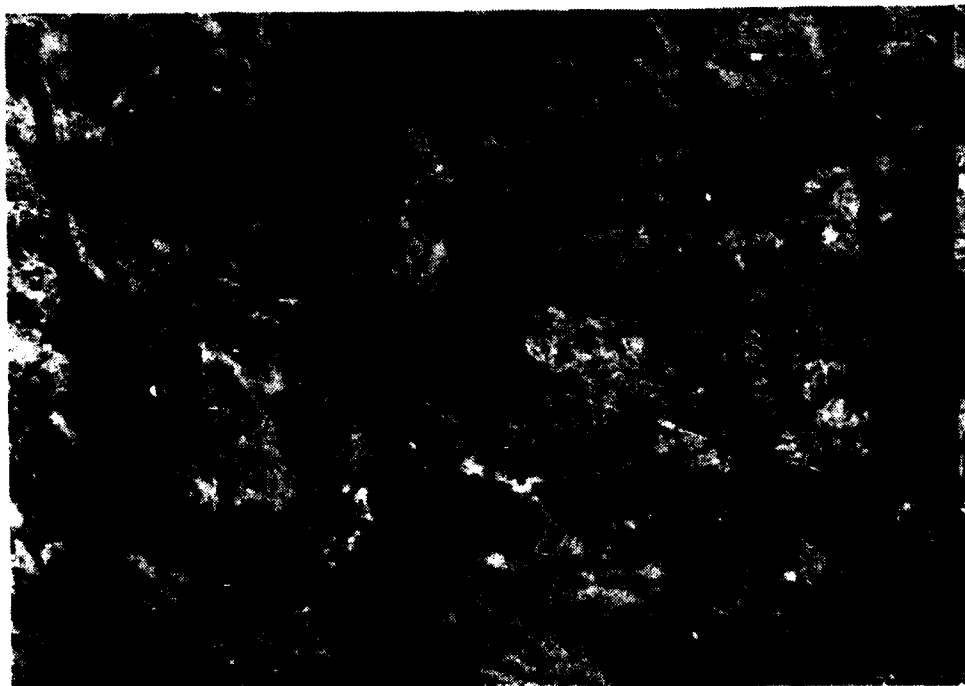


Figure 13. Installed Corrosion Null Probe Prior to Mesh Installation and Overlay

Carbonation of Flyash-Containing Concrete. Electrochemical Studies

M.F.Montemor
Departamento de Engenharia Química, Instituto Superior Técnico
1096 Lisboa codex, Portugal

A.M.P.Simões
Departamento de Engenharia Química, Instituto Superior Técnico
1096 Lisboa codex, Portugal

M.G.S.Ferreira
Departamento de Engenharia Química, Instituto Superior Técnico
1096 Lisboa codex, Portugal

M.M.Salta
Laboratório Nacional de Engenharia Civil
1769 Lisboa codex, Portugal

Abstract

Addition of flyash to concrete has been finding increasing applications in recent years. Although a number of studies have been made in order to evaluate the mechanical properties of concrete with flyash addition, only few tests have been reported concerning the influence of flyash on the electrochemical behavior and corrosion of concrete reinforcement. One of the processes which leads to reinforcement corrosion is carbonation of the calcium hydroxide in the concrete pores, which leads to a pH drop, with consequent depassivation of the metal surface.

Electrochemical impedance spectroscopy - EIS - has proved to be a useful technique for the study of corrosion problems, both for mechanistic interpretation and for monitorization. However, most of the applications in the literature deal with localized corrosion under chloride influence.

This study deals with the corrosion of steel due to concrete carbonation and also with the influence of concrete composition and curing time on that process. Electrochemical Impedance Spectroscopy and Open Circuit Potential measurements were used, as well as pH tests for determination of carbonation depths. The results have shown that the addition of flyash leads to higher carbonation rates.

Both the techniques of potential monitoring and EIS showed sensitivity to the phenomena occurring on the surface, the combination of the two being particularly useful in the interpretation.

Key terms : Concrete, flyash, impedance, potential, carbonation.

Introduction

The alkaline nature of concrete provides reinforcing steel with good corrosion protection. The high pH (> 12.5) in concrete results in passivation of reinforcing steel¹. However, corrosion can occur if the concrete is not of adequate quality, the structure was not properly designed for its service, or due to an aggressive environment, namely the presence of chlorides and / or carbon dioxide^{1, 2}.

The importance of carbonation, which is a slow process under natural conditions, has grown in recent years due to the increase in structures age and associated risk of corrosion.

Carbonation occurs when CO_2 from the environment reacts with $\text{Ca}(\text{OH})_2$, lowering the pH to about 8 - 8.5.

Carbonation rate is a function of concrete moisture content; it is very slow in dry concrete and in water saturated concrete, maximum carbonation rates being usually found at 50 - 60 % of relative humidity^{3,4}. Carbonation rate is dependent upon other factors, namely: the type and content of cement, composition and porosity of concrete, thickness of concrete cover⁵.

In order to have a good quality concrete, the addition of flyash to the cement has become a common practice in recent years. Flyash is a finely divided residue, resulting from the combustion of coal in power plants. It possesses pozzolanic properties and reacts with $\text{Ca}(\text{OH})_2$ to form compounds with cementitious properties.

In this work, the corrosion process induced by carbon dioxide is studied on reinforced concrete blocks having different flyash contents under conditions of natural and accelerated carbonation. The corrosion behavior is studied by electrochemical impedance spectroscopy (EIS) and open circuit potential (OCP) measurements. Carbonation depths were determined by the phenolphthalein test.

Experimental procedure

A - Concrete blocks:

The concrete mix proportions were:

Portland cement + flyash = 350 kg

Water = 200 l

Sand = 1400 kg

Aggregates = 360 kg

The w/c ratio was 0,57 and samples had 0%, 30%, 50% of flyash in partial substitution of Portland cement.

Two kind of blocks were prepared:

—For electrochemical experiments - Two commercial steel bars ($\phi = 1$ cm) were embedded in each concrete block, under a cover thickness of 1cm. The dimensions of the blocks were 10x10x16 cm. When not mentioned, steel bars were polished with SiC grit up to 600.

—For carbonation depth measurement - Small concrete prisms were prepared. The bottom and top of each prism were isolated with an epoxy paint in order to control the carbonation direction.

All samples were cured in a saturated humidity chamber before starting the experiments.

B - Exposure:

Accelerated carbonation conditions:

Samples having different curing time (7 and 28 days) were exposed in a 5% CO_2 atmosphere at about 65% of relative humidity. Carbonation tests, using the phenolphthalein method and electrochemical measurements were made.

Natural carbonation conditions:

Samples having different curing time (7, 28 and 90 days) were exposed in an urban atmosphere (% $\text{CO}_2 \sim 0.03$). Only tests of carbonation depth (using the phenolphthalein method) were made.

C - Electrochemical Techniques:

Open circuit potential (OCP):

The open circuit potential of each steel bar was measured versus a saturated calomel electrode whose tip was involved in a sponge previously immersed in distilled water. The electrode was slightly pressed against the prism surface. The measurements being taken with a high impedance (10 M Ω) voltmeter.

Electrochemical impedance spectroscopy (EIS) :

The measurements were made between the two steel bars of each concrete block, across a concrete thickness of 6cm. The range of frequencies analyzed was generally between 100 kHz and 5 mHz. A 1255 Solartron FRA and a 1286 Solartron electrochemical interface were used.

Results

A - Carbonation Rates

Fig. 1 shows the results of carbonation depth as a function of time, for the accelerated tests (5% CO₂). To a first approximation, the evolution can be considered as linear, with a slope depending both on the curing time and on the composition of the concrete (% of flyash amount). As expected, higher carbonation rates were observed for the blocks with the lower curing time.

On the other hand, higher carbonation rates were observed for the blocks with higher flyash amounts, this result being observed both for 7 and for 28 days of cure. Approximate carbonation rates for the accelerated tests can be found in Table I.

Table I - Carbonation rates (mm/year)

| Flyash amount (%) | 7 days of cure | 28 days of cure |
|-------------------|----------------|-----------------|
| 0 | 170 | 49 |
| 30 | 452 | 76 |
| 50 | 576 | 169 |

For the blocks under natural exposure (Fig. 2), observed carbonation rates were significantly lower in all cases. The dependence on the concrete composition was identical to the accelerated tests, i.e., carbonation becomes a slower process in the absence of flyash. The process, however, seems to be independent of the curing time, even for a very long cure (90 days).

B - Potential Measurements (vs. SCE)

The potential of the embedded steel bars (Fig. 3) shows an evolution which is characterized by values around [-100, 0] mV at the end of the cure, followed by a potential drop after a period of time. The potential values observed after curing are typical of a passive state, whereas the drop to lower values can be interpreted as being due to activation of the metal. These "active potentials" are independent of the curing time, being rather a function of concrete composition, i.e., of the flyash amount. Thus, typical potential ranges for activity are: [-500, -600] mV for the 50% blocks; [-400, -500] mV for the 30% blocks, and ~ -300 mV for blocks with no flyash. The time for activation significantly decreases with the amount of flyash, this tendency being true also for 28 days of cure.

After a period of time at the active potentials, most of the steel bars showed a slow raise of the

OCP, towards the same potential range as observed at the beginning of the tests.

To determine the effect of surface preparation, a few concrete blocks were prepared using rusted steel bars. OCP measurements made on rusted and pre-polish steel bars showed that the time for potential decay, and therefore for metal activation, were quite similar, as illustrated in fig.4.

C - E.I.S. measurements

Fig.5 shows the impedance spectra for a block with 50% of flyash, at the following exposure times and potentials (vs SCE): 1 day (-256 mV), 3 days (-556 mV), 10 days (-566 mV) and 20 days (-537 mV). For one block without flyash addition - fig.6 - a spectrum obtained after 39 days (-60 mV) shows a passive behavior, whereas the other spectra - after 126, 134 and 150 days - refer to OCP values in the range [-310, -328] mV. The OCP evolution of these blocks is plotted in Fig.3.

At the beginning of the exposure, i.e., before the arrival of the carbonation front to the electrode surface, the impedance spectra - figs. 5a) and 6a) - are typical of a capacitor, therefore revealing a passive state.

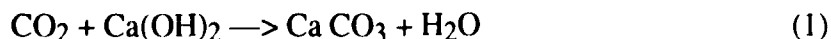
After a period of time, which corresponds approximately to the time for potential decay, two time constants develop in the Nyquist plot: one at high frequencies, with a very small capacitance (1-50 nF/cm²) and a resistance which increases with the time of exposure, and which is also a function of the amount of flyash; and one other at lower frequencies, with values of resistance and capacitance which are significantly different for blocks with different compositions. Thus, for the 50% blocks, the low frequency process leads to a semicircle which is very well resolved in a first state, but becomes gradually more depressed in time, Fig.5c)d). The resistance is approximately constant (35-40 kΩ.cm²) and the capacitance increases from approximately 10 to 80 μF/cm². This low frequency process was attributed to the slow corrosion of the reinforcement, the raise in the measured capacitance suggesting an increase in the attacked area.

For the blocks made with plain cement - Fig. 6 - the low frequency region of the spectra is characterized by a very high resistance (3-5 MΩ.cm²) and an apparent capacitance which starts at values attributable to an electrochemical double layer (15-20 μF/cm²), later rising to much higher values (200-500 μF/cm²), suggesting a diffusion controlled process. Comparable results were obtained by other workers⁶ for carbonation in ordinary Portland cement.

Visual inspection of the steel bars when the concrete samples were broken revealed generalized corrosion, the surface being covered by corrosion products.

Discussion

In agreement with other workers⁷ we have found that concrete with high flyash contents carbonates faster. This conclusion is based on both the electrochemical measurements (OCP and EIS) and the phenolphthalein tests. It is well known that the carbonation of concrete follows according to the reaction:



The presence of calcium hydroxide is a result of the hydration reaction of CaO (a main component of cement). In the presence of flyash, the amount of CaO added to the concrete is lower, and thus less Ca(OH)₂ will be available for reacting with CO₂. This can explain why carbonation, proceeds faster in flyash-containing concrete. In addition to this effect, the presence of flyash retards the setting time of concrete⁸. For this reason, porosity can be expected to be

higher in a first stage, thus allowing carbon dioxide penetration. This negative influence of flyash on the protective properties of concrete was observed both for the accelerated tests and for the natural exposure tests.

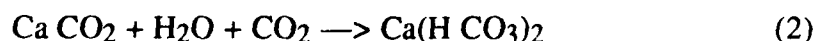
An increase in the curing time, on the contrary, has resulted in a retardation of the carbonation rate. This effect is a consequence of a higher degree of hydration at the start of carbon dioxide exposure, which corresponds both to a lower porosity and to a higher amount of $\text{Ca}(\text{OH})_2$. For the natural exposure tests, however, no significant effect of the curing time on the rate of carbonation was observed. This can be explained by the comparatively low CO_2 concentration, which permits the evolution of the hydration processes during exposure.

Three different tests were used in this work for the evaluation of concrete carbonation and consequent reinforcement corrosion : pH test, OCP measurements and EIS.

The phenolphthalein pH test, although inexpensive and easy to use, is not a precise test and only gives information on whether the acidity of the concrete is above or below a pH value around 9. Such low acidity, however, does not necessarily mean that the reinforcement has become active. This explains the large differences in time for complete carbonation determined by the phenolphthalein test and the potential measurements (figs. 1 and 3).

Potential measurements normally give information on the surface state of the metal, and have revealed useful for previous studies using immersed blocks^{9,10}. For low moisture contents, however, the measurements may be affected by an ohmic drop^{11,12}. Potential measurements made on blocks dried in air and after wetting with distilled water showed only a small decay in the potential, indicating that, for the working conditions, the ohmic drop did not significantly affect the results.

As mentioned above, the active corrosion potentials were dependent on the composition of the concrete, this observation being related with the alkaline content. According to the literature⁷ the carbonation of $\text{Ca}(\text{OH})_2$, reaction (1) — leads to a pH decrease to a value around 8. However, in the presence of water and of a CO_2 excess, another reaction may proceed, leading to bicarbonate formation, which lowers the pH to a value around 6 :



Therefore, in the presence of a large excess of CO_2 , the pH is expected to become lower leading to higher corrosion rates and more negative corrosion potentials. This explains why samples with 50% of flyash showed corrosion potentials in the range [-500, -600] mV whereas concrete without flyash showed less negative potential values (~ - 300 mV).

The fact that potential evolution is identical for polished and non-polished rebars suggests that the fundamental factors are the concrete composition and namely its pH, and not the steel pre-treatment.

After complete carbonation, the potential of samples having 0 e 30% of flyash increased towards more noble values. An explanation for this behaviour is probably due to the fact that when carbonation is complete, the high resistivity of concrete hinders carbon dioxide diffusion and bicarbonates precipitate as Ca CO_3 . In other works, reaction (2) is reversed, and this tends to raise the pH to more alkaline values.

The EIS results clearly confirmed the potential measurements, which is another indication of the unimportant effect of the ohmic drop on the OCP measurements, for the cover thickness used.

At the beginning of the exposure, when the potentials are in the passive range, the spectra are mainly capacitive, irrespective of the concrete composition. After the potential drop, the spectra changed to reveal a process which can be described by two time constants, whose resistances vary both with time and with the flyash amount. The high frequency time constant,

characterized by very low capacitance values and a time increasing resistance, suggests the presence of a film of corrosion products which becomes thicker as corrosion proceeds, and which was detected by visual inspection at the end of the tests. A small semicircle at the high frequencies had been observed in previous studies on immersed blocks under pitting corrosion, and was attributed to the concrete properties^{8,9}. In this work, however, the high frequency process has higher time constants and appears only after corrosion initiation, suggesting a different origin.

The charge transfer process, which was also observed for all the compositions, was significantly influenced by the amount of flyash. Thus, for the 50% block which, as mentioned above, had lower corrosion potentials and lower pH values, corrosion proceeded more easily and for that reason the Nyquist plot shows a well defined semicircle, in opposition with the spectra of the 0% block, which reveals a very large and incomplete semicircle, revealing a slow corrosion process; for longer exposure times, a Warburg develops at the low frequencies, revealing diffusion controlled attack. This difference in behavior is probably related not just with the concrete composition, but rather with the lower porosity of the 0% block, since corrosion started in this case only after long exposure times, therefore giving way to a decrease in concrete porosity.

Conclusions

The addition of flyash to concrete in partial substitution of Portland cement has shown, for the concentrations used in this study, an undesirable effect concerning reinforcement corrosion under concrete carbonation.

This effect, which was observed in both natural and accelerated tests, and for all the curing times, was evidenced by an acceleration in the carbonation rate determined by the phenolphthalein test, and by the smaller values of the charge transfer resistance from the electrochemical impedance spectra.

For the accelerated tests, an increase in the curing time has led to lower carbonation rates, for all the concrete compositions tested, although this effect was not observed in atmospheric exposure.

The large gap observed between the time for carbonation front arrival to the steel surface and the time for corrosion potential drop reveal that the results from the phenolphthalein test cannot be extrapolated for estimating the time for corrosion initiation.

The interpretation of the steel corrosion behavior by OCP measurements was confirmed by EIS, this technique being particularly useful in the monitoring of the system.

References

- 1 - S.K. Somuah, J.K. Boah, P. Leblanc, *ACI Mat. J.*, Jan./Feb., (1991): p.49.
- 2 - Corrosion of metals in concrete, *ACI Mat. J.*, Jan./Feb., (1985): p.3.
- 3 - G.K. Glass, C.L. Page, N.R. Short, *Corr. Sc.* 32, (1991): p. 1283.
- 4 - J.A. Gonzalez, C. Algaba, C. Andrade, *Br. Corr. J.* 15, 3 (1980): p. 135.
- 5 - K. Tuutti, *Corrosion of Steel in Concrete*, (Swedish Cement and Concrete Research Institute 5-100 44, Stockholm, 1982).

- 6 - D.G.John, A.T.Coote, K.W.J.Treadaway, J.L.Dawson, in " Corrosion of Reinforcement in Concrete Construction ", (Ed. A.P. Crane, London, 1983), p.263.
- 7 - J.A. Gonzalez, C. Alonso, C. Andrade, in "Corrosion of reinforcement in Concrete Construction", (Ed. A., P. Crane, London, 1983), p.159.
- 8 - ACI Report, ACI Mat. J., Sept./Out., (1987): p. 381.
- 9 - M.F. Montemor, A.M.P. Simões, M.M. Salta, M.G.S. Ferreira, "Advances in Corrosion and Protection", Paper nº 393, (Manchester, U.K. 1992), to be published in Corrosion Science.
- 10 - M.F. Montemor, A.M.P. Simões, M.M. Salta, M.G.S. Ferreira, to be presented in "10th European Corrosion Congress", paper nº 243, (Barcelona, Spain, 1993).
- 11 - R.D. Brown, M.P. Geoghegan and A.F. Baker, in "Corrosion of Reinforcement in Concrete Construction", (Ed. A.P. Crane, London, 1983), p.193.
- 12 - A. Sehgal; D. Li, Y.T. Kho, K. Ossea-Asare, H.W. Pickering, Corrosion,48, 10 (1992): p.706.

Performance of Concrete with Microsilica in Chemical Environments

N. S. Berke, PhD
W. R. Grace & Co., Conn.
Construction Products Division
62 Whittemore Avenue
Cambridge, MA 02140

T. Durning, P.E.
W. R. Grace & Co., Conn.
Construction Products Division
62 Whittemore Avenue
Cambridge, MA 02140

M. C. Hicks
W. R. Grace & Co., Conn.
Construction Products Division
62 Whittemore Avenue
Cambridge, MA 02140

Abstract

Concrete sewer pipe is a cost effective means of providing sewage transport. The recently mandated elimination of toxic chemicals in effluents has resulted in an increase in bacterial activity and the formation of localized high concentrations of sulfuric acid in the sewers. This has led to relatively rapid degradation of the concrete and ultimately to failure of the sewers. In this paper, we determine the effect of microsilica (silica fume) on the resistance of concrete pipe to acid attack. In addition to sulfuric acid, the resistance of laboratory specimens to formic and acetic acid as well as various acid salts was examined. It was found that in general, microsilica can result in substantial improvements in the life expectancy of concrete in chemical environments, and that the performance of concrete specimens containing microsilica in slurry form was superior to specimens made with densified microsilica. In the presence of magnesium sulfate and aluminum sulfate, however, the improvement in durability is negligible and not sufficient to make practical extensions in life expectancy.

Keywords: Chemical resistance, microsilica, sewer, sulfuric acid, acetic acid, formic acid, magnesium sulfate, aluminum sulfate, ferric chloride, ammonium nitrate, zinc sulfate, aluminum chloride, anaerobic bacteria, aerobic bacteria.

Introduction

Portland Cement concrete is an extremely versatile and cost effective structural material. Unfortunately, many natural and industrial environments exist where the highly durable nature of concrete is compromised. Perhaps the most common example of this is the deterioration of reinforced concrete in our roads and bridges due to chloride induced corrosion of the embedded reinforcing steel.

When concrete deteriorates due to chloride induced corrosion of reinforcing steel, the concrete itself is not corroding or being chemically altered in any significant manner. Instead, it is rupturing in response to the high internal stresses which the expansive corrosion products produce.^{1,2} However, many environments do exist where the portland cement paste and/or the aggregate may be chemically attacked, resulting in deterioration.

Previously published papers have reported on the use of microsilica to increase concrete's durability in exposure to several aggressive chemical environments.²⁻⁵ This paper reports the results of a test program designed to expand the realm of aggressive environments where the impact of microsilica is documented. In addition, brief accounts of several field applications of microsilica in aggressive environments are presented.

Background

There are essentially two basic modes whereby a chemical agent will attack and degrade concrete. In one, the product of the chemical reaction is soluble and is leached away into the attacking solution. This leads to loss of material, higher porosity, and loss of strength. In the other deterioration mode, the reaction product is insoluble and expansive. The formation of expansive reaction products builds high internal stresses, leading to heaving, cracking and spalling of the concrete.

When Portland cement hydrates, the resulting paste matrix is a combination of calcium silicate hydrate gel (CSH), and crystals of calcium hydroxide ($\text{Ca}(\text{OH})_2$). Since this Portland cement paste matrix is an alkaline material (the pH of the pore water is typically 12 to 13),^{6,7} it is particularly susceptible to attack by acidic solutions. In general, all acids will react with the calcium hydroxide component of the paste. In addition, very low pH solutions and certain specific compounds (regardless of pH) will react with and degrade the CSH paste. The actual rate of deterioration will be extremely dependent upon the permeability of the concrete to the attacking solution, as well as the solubility or expansive nature of the reaction products. As a result, merely knowing the pH of a solution without knowing its chemical composition is not sufficient to predict its aggressiveness toward concrete.

The Sewer Environment

One of the purposes of this work is to attempt to characterize the performance of microsilica in increasing the concrete durability in a sanitary sewer environment. Although not as visible as our deteriorating roads and bridges, the problem of deteriorating concrete in the sewer and wastewater treatment systems is almost of the same magnitude.⁸

The mechanism of deterioration of concrete exposed to a sanitary sewer environment is primarily that of sulfuric acid attack. The sulfuric acid which attacks the concrete is not present in the sewage stream, but it is produced on surfaces above the sewage stream by sulfide oxidizing bacteria. These bacteria oxidize hydrogen sulfide gas, produced by sulfur reducing bacteria in the sewage stream, to produce sulfurous and sulfuric acids.

Sulfur is generally present in wastewaters in the form of sulfate ion. Anaerobic bacteria (disulfovibrio) that are present in sewers can, under certain conditions, reduce the sulfate to sulfide. The required conditions include the absence of oxygen and the presence of organic nutrients, conditions that usually exist in the slime layer that builds up on the concrete surface below the water line. The microbially generated hydrogen sulfide and volatile organic sulfides enter the atmosphere above the water line and are deposited on the concrete surface as shown in Figure 1 (Obtained from Ref. 8). Here, aerobic bacteria (thiobacillus) oxidize the sulfides to sulfuric acid which then proceeds to attack the concrete. Note that the attack takes place in the non-wetted portion of the pipe so the sulfuric acid that is produced is not diluted by the sewage stream.

It is interesting to note that some studies have concluded that recently enacted regulations limiting the dumping of hazardous materials into municipal sewers have exacerbated the situation by creating a more hospitable environment for the sulfur reducing bacteria which produce the hydrogen sulfide gas.⁹

Published empirical relationships for predicting the rate of buildup of sulfide in a sewer indicate that the sulfide concentration in a sewer increases with the biological oxygen demand (a measure of the concentration of biodegradable organics) of the sewage and the wetted perimeter of the pipe, and decreases with the velocity of the flow.¹⁰ Note that the size of the slime layer in which the sulfate reduction occurs increases with the wetted perimeter, but decreases with increasing velocity of the sewage due to mechanical attrition.

Sulfide concentrations in flowing sewage of up to 4 mg/L have been reported.¹⁰ The rate at which hydrogen sulfide enters the atmosphere above the sewage depends on the fraction of the total sulfide that is present as hydrogen sulfide; this fraction increases significantly with decreasing pH. It is believed that sulfide concentrations of 0.4 mg/L are sufficient to lead to significant corrosion of reinforced concrete structures.¹¹ Sulfuric acid concentrations may be as high as 5,000 mg/L (equivalent to a pH of 1).^{9,11}

Acid attack in the sewer environment. Once the sulfuric acid is formed, it must be transported to the vulnerable concrete components before it can do harm. Subsequently, the reaction products must be transported out of the concrete matrix. It is the rate of these transport processes that ultimately determines the rate of degradation of the concrete. Transport of aggressive chemical solutions into the concrete matrix is dictated primarily by the concrete permeability.

A standard design practice to account for the acid attack in sewer pipe is to provide some thickness of sacrificial concrete. The thickness of this sacrificial layer is calculated based on predicting the amount of hydrogen sulfide to be produced over the design life of the sewer. The assumption is then made that this will be converted to sulfuric acid, and then that some high percentage of the sulfuric acid produced will be neutralized by reacting with the alkaline concrete. This has been an accepted practice for several decades, but it ignores the contribution of concrete permeability, and it ignores the expansive sulfate reaction which accompanies the sulfuric acid attack.

The amount of acid required to neutralize a certain mass of concrete can be calculated, once the alkalinity of the concrete is known. However, with sulfuric acid, the reaction product formed in this neutralization process with calcium hydroxide is calcium sulfate. This calcium sulfate will then react with the aluminate phase of cement to form ettringite, an expansive product which will cause further deterioration of the concrete. So, attack by sulfuric acid will result in damaging ettringite reaction in addition to loss of material through acid neutralization. The more porous the concrete, the further into the matrix this expansive ettringite will be produced, and the more disruptive its action.

With sulfuric acid attack in a sewer environment, the concrete attacked is above the sewer stream. As the permeability of the concrete is decreased, less of the aggressive material will permeate into the concrete,

and more of it will drip back down into the sewer stream. Unfortunately, the methods of testing utilized in this testing program do nothing to simulate this behavior. The method used to expose concrete samples to the various attacking media in this study was to immerse them (and in some cases to cycle between immersion and drying). Immersion tests are simple to carry out, they provide comparability with other published tests, and they are accurate for modeling conditions similar to immersion; but it is quite possible they fail to capture the full benefit of lowered permeability in exposure conditions similar to that of sewer pipe. The testing carried out here did not simulate the effects of concrete mix proportions or matrix characteristics on the ability of the bacteria ecosystem to grow and thrive.

Other Aggressive Chemical Environments

In addition to studying the applicability of microsilica for the sewer environment, testing was performed to characterize the advantages of using microsilica to increase durability in many other chemical environments. Many inorganic salts can lead to the rapid degradation of concrete. Generally, the more acidic the salt solution, the more rapid the attack, but this is not universally true. With some exceptions, basic salts are not usually a problem, but once again, this is not universally true.

Microsilica

Microsilica is an extremely fine high silica material that acts both physically and chemically to alter the pore structure of concrete. Adding microsilica to concrete in the range of 5 to 30 percent by weight of cement will result in drastically reduced permeabilities, and reduced amounts of calcium hydroxide. It has been reported in several papers that an addition of 30% microsilica (by weight of cement) will virtually eliminate any calcium hydroxide. The decrease in permeability afforded by 7 to 15 percent microsilica has been reported to be by as much as a factor from 10 to 100.^{5,14}

The importance of reducing permeability has previously been discussed. Reducing calcium hydroxide is also important since this is the component that is most easily attacked by virtually all aggressive media. Further, it has been reported that the calcium silicate hydrate resulting from the reaction of the microsilica with calcium hydroxide has a lower calcium-to-silica ratio and a high degree of polymerization. This enables concretes containing microsilica to accommodate foreign ions without associated degradation action. In combination with the reduction in permeability, it is expected, and has been found in practice, that microsilica is able to reduce the rate of attack of a range of chemical media.

Experimental Investigation

In these tests, pipe sections and pipe cores supplied by several manufacturers, as well as cylinders produced in our laboratory were exposed to sulfuric acid solutions of different strengths. The pipe samples were received with and without pozzolan additives. The cylinders were made from a range of mix designs to determine the effect of microsilica on the resistance of concrete to a range of salt solutions.

The concrete samples were exposed to the test solutions in two ways. In one method, the samples were immersed continuously in the test solution, whereas in the other the samples were subjected to wet-dry cycles of one week submerged followed by one week dry. The loss of mass of the sample was used as a measure of the amount of degradation and was calculated from:

$$\text{Mass loss, \%} = \frac{\text{Initial mass (ssd)} - \text{Current mass (ssd)}}{\text{Initial mass (ssd)}} \times 100$$

The initial mass is obtained by immersing the concrete samples in water for at least 24 hours, removing them, and then weighing them after lightly wiping off the excess moisture. The mass obtained in this way

is known as "surface saturated dry" (ssd). The exposed samples were periodically removed from the test solution, wire brushed to remove loose material, lightly blotted to remove excess surface moisture, and then weighed. After weighing, the samples were either returned to a fresh test solution (continuously exposed) or left to dry for one week and then returned to a fresh solution (cyclic exposure). In the case of continuously exposed samples which were weighed at intervals of greater than one week, the pH of the test solution was adjusted weekly.

The exposure and weighing continued until the sample "failed," that is, the mass loss reached 25%.

The cyclic exposure method is selected as a means of accelerating the degradation. It is thought that the dry period serves to increase the concentration of the attacking medium in the concrete pores. The wire brushing technique is used mainly to ensure all the loose material is removed before weighing. The brushing also removes any gypsum layer that may form on the surface of the concrete, and which in practice might serve to reduce the rate of attack by providing a barrier between the concrete and the attacking solution. Both test procedures therefore provide an accelerated rate of attack that is suitable for comparison purposes, but which is different from degradation rates that might be found in the field.

Tests In sulfuric acid

Pipe Sections. The pipe sections were obtained from pipes manufactured for sewage conveyance by a west coast supplier. Pipes made from three different mix designs were obtained. These included controls with 320 kg/m^3 (542 lb/yd^3) cement content, a mix with 123 kg/m^3 (208 lb/yd^3) fly ash plus 74 kg/m^3 (125 lb/yd^3) microsilica, and a third mix with 296 kg/m^3 (500 lb/yd^3) cement content, 99 kg/m^3 (167 lb/yd^3) fly ash plus 49 kg/m^3 (83 lb/yd^3) microsilica. The water to cement ratio was not provided, but was probably below 0.3 which is typical of the very dry mixes used for pipe manufacture. Four samples of each mix design were exposed to a 1% (by mass) sulfuric acid solution (pH=1.2) at 22°C (72°F). Both continuous and cyclic exposure methods were used for these samples.

Pipe Cores. Two sets of pipe cores were obtained. One set included three different mix designs. The control had a CF of 244 kg/m^3 (412 lb/yd^3) and 90 kg/m^3 (152 lb/yd^3) fly ash with a Water/Cementitious ratio of 0.35. The other two mixes had 20 % microsilica (49 kg/m^3 - 82 lb/yd^3). Two types of microsilica, namely a "densified" powder and a slurry, were used. Two to three samples of each mix design were also exposed continuously to a 1% (by mass) sulfuric acid solution (pH=1.2) at 22°C (72°F). These samples were also exposed to a 5% sulfuric acid solution (pH=0.6) at 22°C (72°F).

The second set of pipe cores were from packerhead pipe. Samples from seven different mixes were provided, each having a cementitious content of 361 kg/m^3 (609 lb/yd^3). Details of the mix proportions are given in Table 1. As before, Water/Cementitious ratios were low (around 0.3) as is customary with pipe mixtures. Four samples of each mix design were tested in sulfuric acid solutions with pH=1, 2 and 3 at 38°C (100°F).

Other Aggressive media testing

Cylinders produced in our laboratory 76 mm in diameter and 152 mm long (3" by 6") were used for these tests. The samples were demolded after 24 hours and moist cured at 100% RH and 22°C (72°F) for 28 days before exposure to the various aggressive chemicals.

In these tests, we tried to obtain information on the effectiveness of microsilica in protecting concrete against attack by a number of salts and acids. The solutions and their pHs were as follows:

| | |
|-------------------------|----------|
| • 20% aluminum chloride | pH = 1.0 |
| • 10% aluminum sulfate | pH = 3.2 |
| • 10% ferric chloride | pH = 1.0 |
| • 20% ammonium nitrate | pH = 5.9 |
| • 10% magnesium sulfate | pH = 5.9 |
| • 15% zinc sulfate | pH = 4.9 |
| • 5% acetic acid | pH = 2.5 |
| • 5% formic acid | pH = 1.9 |

The cyclic exposure method was selected for these tests. The mix proportions and physical properties of the concrete used are given in Table 2. The microsilica used was a water-based slurry⁽¹⁾. The concrete mixtures were prepared at 22 °C (72 °F). Again, the samples were cast in 76 mm diameter by 152 mm long (3" by 6") cylinders which were demolded at 24 hours and moist cured at 22 °C (72 °F) for 28 days. Three samples of each mix were tested.

Results and Discussion

Sulfuric Acid

The rate at which the pipe sections and pipe cores lost weight in the low pH sulfuric acid solutions (pH = 1 to 1.2) are shown in Figures 2 to 5. In all cases, the rate of degradation was rapid with little variation amongst the different mix designs. By contrast, the rate of degradation at the higher pHs (pH = 2) was much slower as can be seen in Figure 6, which shows that after one year exposure, all the samples are still gaining mass.

As shown in Figure 4, addition of microsilica to the mix does extend the life over that achieved with fly ash alone. Furthermore, it appears that there is a significant advantage to using microsilica in the slurry form as opposed to the densified product. This might be due to incomplete breakup and dispersion of the densified product in this very dry mix. Note that increasing the concentration of the sulfuric acid to 5% (pH=0.6) had no effect on the relative performance of the concrete specimens (Figure 7).

Effect of microsilica in various acid and salt environments

The concrete deterioration in the presence of the two organic acids tested, namely 5% acetic acid and 5% formic acid are shown in Figures 8 and 9. The effect of microsilica on the rate of degradation in the presence of various salt solutions is shown in Figures 10 to 15.

The data for the organic acids tested had been presented in a previous paper.² These tests have now been completed and the data for the 5% formic acid solution show that there is a 2, 3 and 4 fold improvement over the concrete without microsilica, by the addition of 10%, 20% and 30% microsilica respectively (Figure 9). The acetic acid solution was a more detrimental solution than the formic acid solution for concrete with no microsilica and for the 7.5% and 15% microsilica. However, a marked improvement was achieved by the addition of 30% microsilica, as can be seen in Figure 8. An eleven fold improvement was observed over the controls for a mass loss of only 20%.

(1) Force 10,000, a 50% water based slurry, trademark of W. R. Grace & Co. - Conn.

The two chloride solutions (Figures 10 and 11) were as acidic as some of the sulfuric acid solutions tested, yet the microsilica had a marked beneficial effect on the resistance to degradation. The aluminum chloride was by far the more aggressive, and the control specimens failed after (38 cycles) cyclic exposure. The greater aggressiveness of the aluminum chloride relative to the ferric chloride is attributed to the effect of the aluminum ion. After 38 cycles, the specimens containing 10 percent microsilica had lost only 8 percent of their mass, and the rate of mass loss was still relatively low. In the case of ferric chloride, the control specimens had lost 8 percent of their mass after (48 cycles) exposure. By contrast, specimens containing 20 percent microsilica had lost only 2 percent of their mass.

It is clear that although the pH is a measure of the strength of the acid, it is not necessarily the most important indicator of aggressiveness. This is illustrated further in Figure 12 which shows the mass loss in the presence of ammonium nitrate. Although this solution had a pH of 5.9, the rate of degradation is about the same as that of ferric chloride at pH = 1 (Figure 11). It is also seen that microsilica is effective in reducing the attack by the ammonium ion. After 80 cycles, the mass loss in specimens with 25 percent microsilica was less than half that of the controls.

Variable results were obtained in the case of the three sulfate salts tested (Figures 13 to 15). In the case of aluminum sulfate (pH = 3.2, Figure 13), the attack was relatively rapid and the microsilica had little effect. Both the aluminum and the sulfate ions probably contribute to the aggressiveness of this salt. Zinc sulfate (pH = 4.9, Figure 14), is not very aggressive, and the microsilica is able to significantly reduce the little attack that does occur.

Some researchers,^{15,16} have noticed that magnesium sulfate was particularly aggressive to concrete with microsilica. However, here, the attack of concrete up to 20% microsilica was found to be insignificant. At 30% microsilica there was an increase in attack, but the overall attack was still low.

Field Experience

City of Houston Sewer System

Microsilica has now been used for several years in the certain portions of the sewer system of the City of Houston. To date it has been used mainly in shotcrete for repair of leaking manholes and lift stations. It has also been used in manufacture of new precast manhole and lift stations, and one contract has now been let with microsilica specified to be used in the sewer pipe as well as the manholes and lift stations. This is not to imply that the City of Houston has embraced microsilica as the solution to their hydrogen sulfide induced corrosion problems. They are evaluating it and using it on an experimental basis in portions of the sewer where conditions are known not to be extremely aggressive.

Recently, an evaluation was done of a concrete lift station containing microsilica located near Houston Intercontinental Airport that had been in place for over three years. Detailed petrographic examination of cores taken near the high water level showed absolutely no sign of acid attack on the surface of the concrete. Unfortunately there is no directly comparable reference structure for comparison purposes.

Food Processing Applications

Perhaps one of the most cost effective uses of microsilica is in floor slabs in food processing plants. Floor slabs in many types of food processing plants experience deterioration due to exposure to moderately aggressive organic acids, coupled with abrasion and the effects of aggressive cleaning procedures. Numerous plants across North America have used microsilica to increase durability in this environment with positive results.

In the September 1987 edition of Plant Services magazine, the performance of a microsilica concrete floor in a Durkee Famous Foods plant in Wolcott, NY is detailed. This plant produces French fried onions, and the acidic onion juice that repeatedly falls on the floor had produced an exposed aggregate finish. The deteriorated original concrete floor was repaired using an overlay course of microsilica concrete in 1985. The article attests to how well the microsilica concrete stood up to the environment after 2 years in service. In 1991 this same floor was inspected and reportedly did not show any signs of wear or deterioration.

Another example the beneficial effect of microsilica in a food processing application is the Cuddy Foods chicken parts processing plant in London, Ontario. Constant exposure to the fatty acids, exacerbated by the daily cleanings using high pressure steam, was causing the floors to deteriorate so fast that they required resurfacing almost every year. In 1987 Cuddy used microsilica concrete in a 200,000 sq ft expansion. Last year the floor with microsilica was reported to be showing the first signs of deterioration and wear in particularly aggressive areas.

The durability enhancements provided by microsilica in food processing plants such as those recorded above is not too be expected in all applications. In an extreme example of this, microsilica was used in a battery recycling plant where the concrete was exposed to spills and splashing of 25% sulfuric acid. This was clearly an inappropriate application, and the concrete deteriorated rapidly.

The laboratory test data available at the time this battery recycling project was constructed clearly indicated that this was not a suitable application for microsilica. However, many industrial environments exist where no guidance is available to assess the suitability of microsilica. This is the primary reason for performing the testing reported in this paper, to expand the realm of chemical environments where the performance of microsilica is documented. Even with these results, numerous environments exist where microsilica has not been tested. In these situations, it is essential that microsilica concrete be tested in the environment to determine its performance before its use is contemplated.

Conclusions

Based upon the work presented here, the following conclusions can be reached concerning the resistance of concrete to chemical attack:

1. In general, additions of microsilica to concretes improved the resistance to attack by aggressive chemicals.
2. In the extremely dry mixes, as those used in concrete pipe fabrication, the slurry form of microsilica was more effective than the densified form.
3. Microsilica has been successfully used to improve resistance to chemical attack in the field.
4. Pretesting is needed to determine if concrete mixtures are resistant to specific chemicals, since pH and ions present are not necessarily accurate indication of performance.

References

1. N. S. Berke, D. W. Pfeiffer, T. G. Weil, "Protection Against Chloride-Induced Corrosion", *Concrete International*, 10 12, (1988): p. 45.
2. T. A. Durning, M. C. Hicks, "Using Microsilica to Increase Concrete's Resistance to Aggressive Chemicals", *Concrete International*, 13 3, (March 1991): p. 42.
3. P. K. Mehta, "Studies on Chemical Resistance of low Water/cement Ratios Concrete", *Cement and Concrete Research*, 15 6 (1985): p. 969.
4. E. J. Sellevold, "Condensed Silica Fume in Concrete: A world Review." International Workshop on Condensed Silica Fume in Concrete, Montreal, May, 1987.
5. N. S. Berke, "Resistance of Microsilica Concrete to Steel Corrosion, Erosion and Chemical Attack", SP-114, American Concrete Institute, Detroit, (1989): p. 861.
6. H. G. Wheat, Z. Eliezer, "Some Electrochemical Aspects of Corrosion of Steel in Concrete", *Corrosion*, 41 11 (1985): p. 640.
7. C. J. Newton, J. M. Sykes, "Effect of Mix Specification on Corrosion of Steel in Mortars immersed in Chloride Solutions", *Br. Corrosion Journal*, 26 1 (1991): p.31.
8. U. S. Environmental Protection Agency, Office of Water (WH-59F), "Hydrogen Sulfide Corrosion in Wastewater Collection and Treatment Systems", Washington, D.C. 20460, May 1991.
9. F. Mansfeld, H. Shih, A. Postyn, et. al. "Corrosion Monitoring and Control in Concrete Sewer Pipes", CORROSION/90, paper no.113 (Houston, TX: National Association of Corrosion Engineers, 1990).
10. K. K. Kienow, "Concrete Interceptor Sewer Corrosion: Protection - A State of the Art Review", Third International Conference on the Internal and External Protection of Pipes, BHRA Fluid Engineering, Cranfield, Bedford, England, September 1979.
11. J. L. Villalobos, "Corrosion of Reinforcing Steel by Hydrogen Sulfide Induced Corrosion in Wastewater Facilities", CORROSION/90, paper no. 321 (Houston, TX: National Association of Corrosion Engineers, 1990).
12. E. Bock, "Examination of the Resistance of Cement Mortar Linings of Ductile Cast Iron Pipes to Biogenous Sulfuric Acid Corrosion." Department of Microbiology, Hamburg University, Germany, (1992).
13. H. Grube, W. Rechenberg, "Durability of Concrete Structures in Acidic Water." *Cement and Concrete Research*, 19 (1989): p. 783.
14. H. Cheng-Yi, R. F. Feldman, "Hydration Reactions in Portland Cement-Silica Fume Blends", *Cement and Concrete Research*, 15 4 (1985): p. 585.
15. M. S. Eglinton, *Concrete and its Chemical Behaviour*, Thomas Telford Ltd, London 1987.
16. M. D. Cohen, A. Bentur, "Durability of Portland Cement-Silica Fume Pastes in Magnesium Sulfate and Sodium Sulfate Solutions", *ACI Materials Journal*, May-June 1988: p.148.

Table 1 -- Properties of the plastic and hardened concrete used in the manufacture of the Packerhead pipe

| | CF kg/m ³ | Aggregates | | Total Water kg/m ³ | Set Retarder* mL/m ³ | Silica Fume % | Fly Ash Type C kg/m ³ | 7 day p MPa |
|-------|-------------------------|-----------------------------|---------------------------|-------------------------------------|---------------------------------------|---------------------|----------------------------------------|-------------------|
| | | Coarse kg/m ³ | Fine kg/m ³ | | | | | |
| Mix 1 | 361 | 969 | 1007 | 107 | - | - | - | 41 |
| Mix 2 | 361 | 969 | 1007 | 107 | 696 | - | - | 41 |
| Mix 3 | 361 | 969 | 1007 | - | 696 | 10 | - | 71 |
| Mix 4 | 290 | 969 | 1007 | - | 696 | 12.5 | 71 | 75 |
| Mix 5 | 363 | 969 | 1007 | - | - | 20 | - | 72 |
| Mix 6 | 290 | 969 | 1007 | - | 696 | 20 | 71 | 49 |
| Mix 7 | 290 | 969 | 1007 | - | - | 18 | 71 | 36 |

* Daratarad HC, a Trade Mark of W. R. Grace & Co., Conn

1 kg/m³=1.69 lb/yd³ 1 mL/m³=0.026 oz/yd³ 1 MPa= 145 psi

Table 2 - Properties of the plastic and hardened concrete

| Chemical Tested | CF kg/m ³ | Coarse Aggregate kg/m ³ Type | Fine Agg. kg/m ³ | Silica Fume % | W/C | Air % | Slump mm | 28 day Comp Str. MPa |
|-----------------------------------------------|-------------------------|-----------------------------------------------|--------------------------------|------------------|------|----------|-------------|-------------------------|
| 10% Aluminum sulfate and 20% Ammonium nitrate | 385 | 1033 River Gravel | 730 | 0 | 0.36 | 5.4 | 158 | 42 |
| | 385 | 1048 River Gravel | 684 | 12.5 | 0.36 | 3.7 | 191 | 60 |
| | 385 | 1048 River Gravel | 626 | 25 | 0.36 | 3.7 | 191 | 67 |
| 20% Aluminum chloride | 442 | 1016 River Gravel | 781 | 0 | 0.40 | 2.5 | 184 | 54 |
| | 444 | 1020 River Gravel | 734 | 10 | 0.40 | 2.4 | 210 | 76 |
| 10% Ferric chloride | 457 | 1066 River Gravel | 757 | 0 | 0.31 | 1.0 | 210 | 45 |
| | 345 | 1094 River Gravel | 821 | 10 | 0.42 | 1.3 | 203 | 72 |
| | 350 | 933 River Gravel | 948 | 20 | 0.42 | 1.4 | 210 | 85 |
| 10% Magnesium sulfate | 386 | 1025 River Gravel | 898 | 0 | 0.33 | 2.2 | 203 | 47 |
| | 387 | 1026 River Gravel | 855 | 10 | 0.33 | 2.5 | 182 | 74 |
| | 388 | 1030 River Gravel | 814 | 20 | 0.33 | 2.0 | 133 | 83 |
| | 385 | 1020 River Gravel | 763 | 30 | 0.33 | 2.3 | 89 | 64 |
| 15% Zinc sulfate | 283 | 777 River Gravel | 861 | 0 | 0.42 | 4.4 | 182 | 35 |
| | 459 | 1263 River Gravel | 568 | 7.5 | 0.31 | 1.7 | 222 | 55 |
| | 463 | 1101 River Gravel | 689 | 16 | 0.31 | 2.6 | 191 | 81 |
| 5% Acetic acid | 412 | 1031 River Gravel | 713 | 0 | 0.36 | 4.2 | 165 | 43 |
| | 411 | 1030 River Gravel | 676 | 7.5 | 0.36 | 5.5 | 121 | 48 |
| | 411 | 1030 River Gravel | 640 | 15 | 0.36 | 6.9 | 171 | 59 |
| | 420 | 1100 River Gravel | 606 | 30 | 0.36 | 4.0 | 191 | 74 |
| 5% Formic acid | 349 | 1048 River Gravel | 957 | 0 | 0.28 | 3.2 | 13 | 49 |
| | 348 | 1045 River Gravel | 915 | 10 | 0.28 | 3.6 | 38 | 68 |
| | 351 | 1055 River Gravel | 893 | 20 | 0.28 | 3.2 | 76 | 79 |
| | 353 | 1057 River Gravel | 845 | 30 | 0.28 | 2.8 | 38 | 79 |

1 kg/m³ = 1.69 lb/yd³ 1 mL/m³ = 0.026 oz/yd³ 1 mm = 0.04 inches 1 MPa = 145 psi

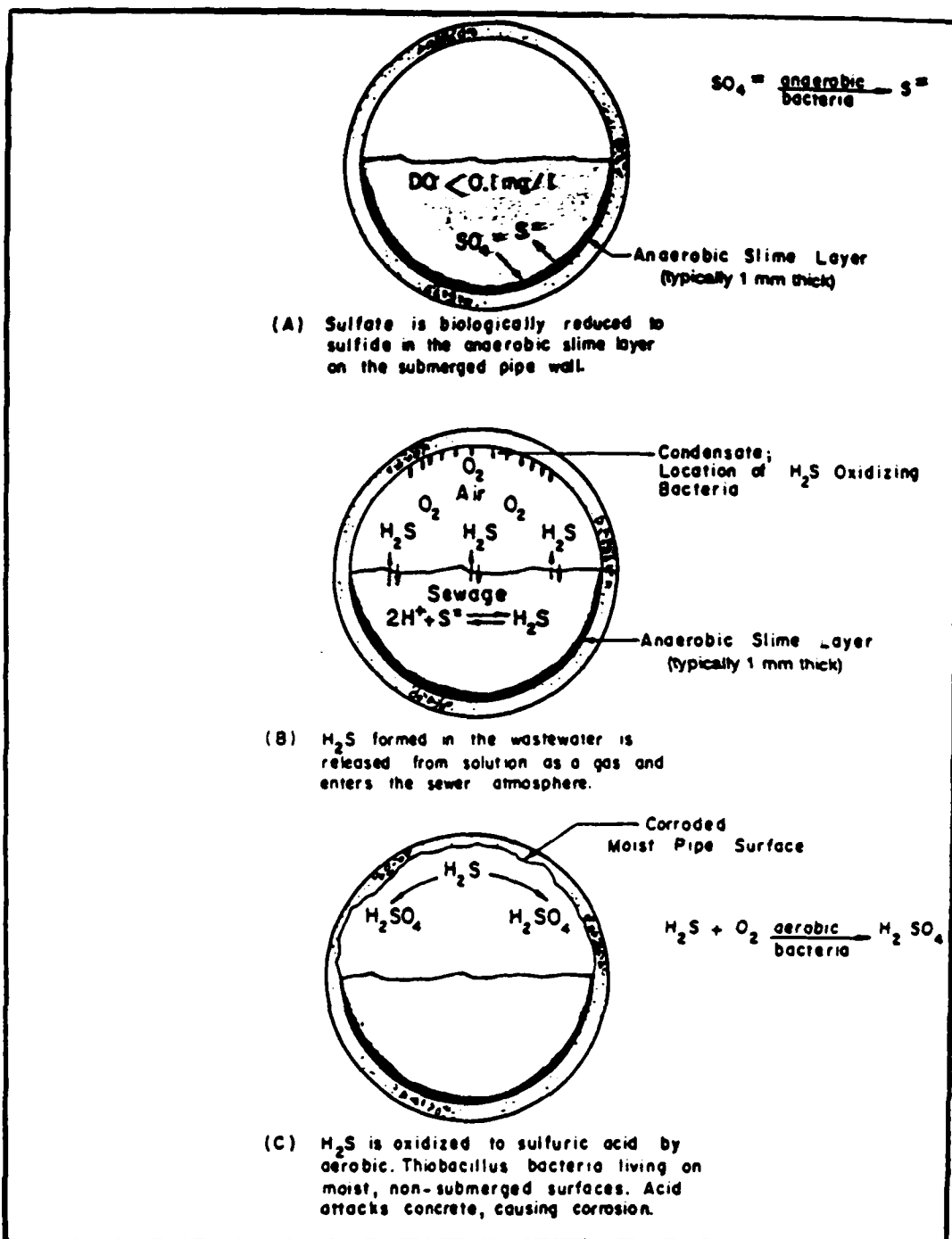


Figure 1
 Mechanism of Sulfide Generation and Corrosion in Sewers
 (From Reference 8)

Effect of Microsilica on Sulfuric Acid Resistance

Continuous Soaking in 1% Sulfuric Acid

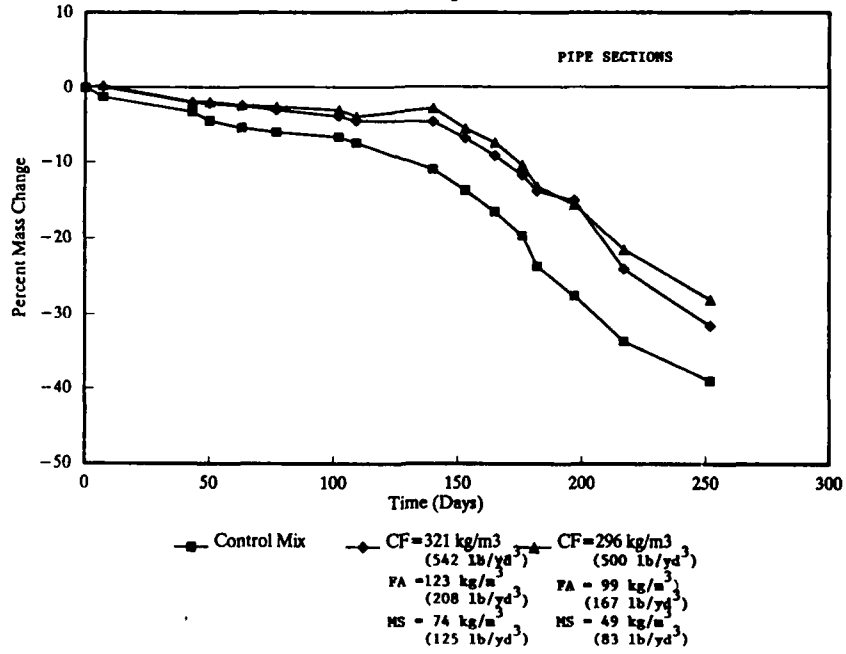


Figure 2

Effect of Microsilica on Sulfuric Acid Resistance

Wet/Dry Cycling in 1% Sulfuric Acid

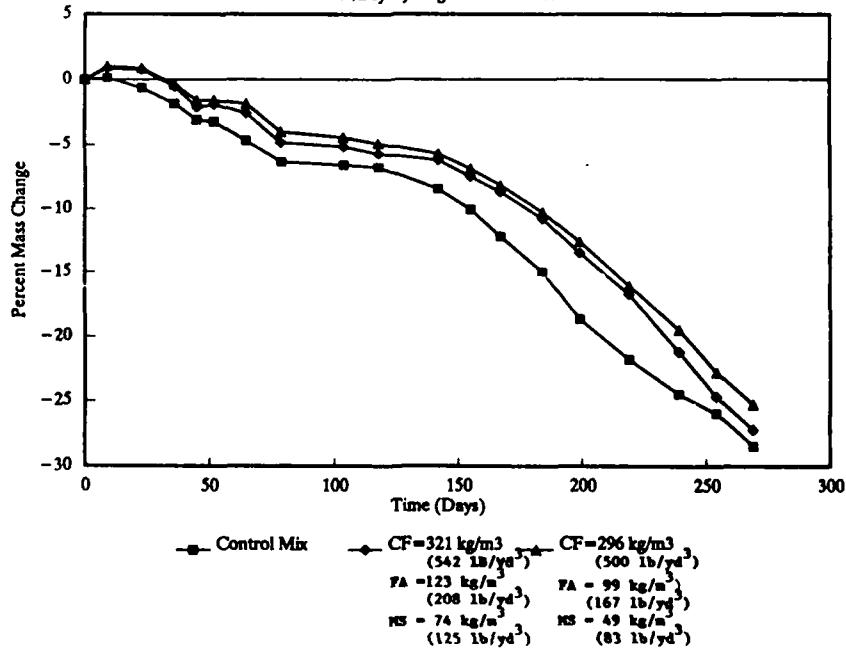


Figure 3

Effect of Microsilica on Sulfuric Acid Resistance

Continuous Soaking in 1% Sulfuric Acid

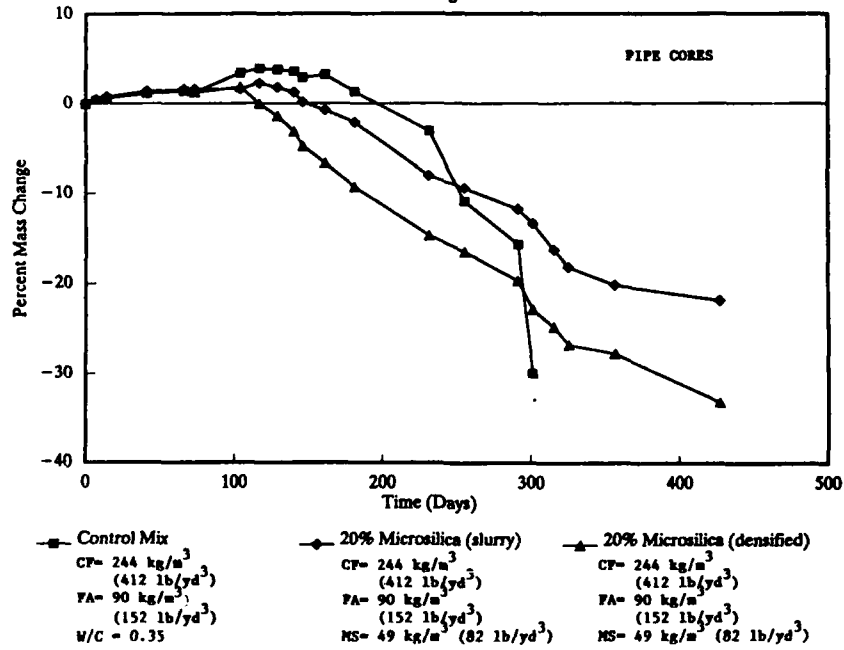


Figure 4

Mass loss of concrete pipe cores

38 C, sulfuric acid pH=1

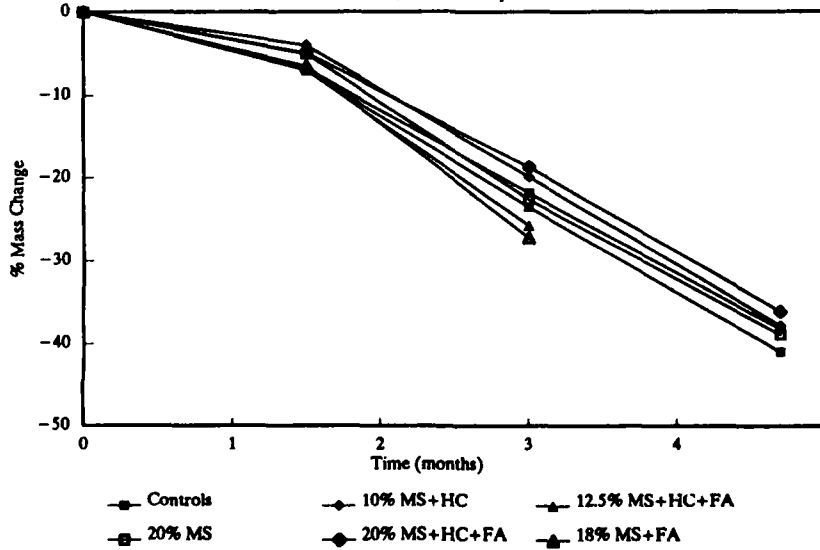


Figure 5

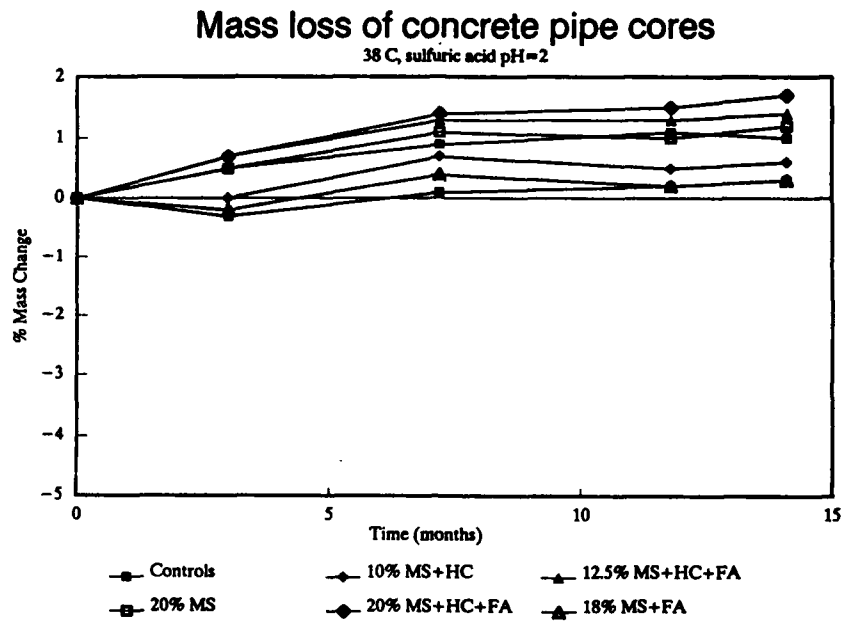


Figure 6

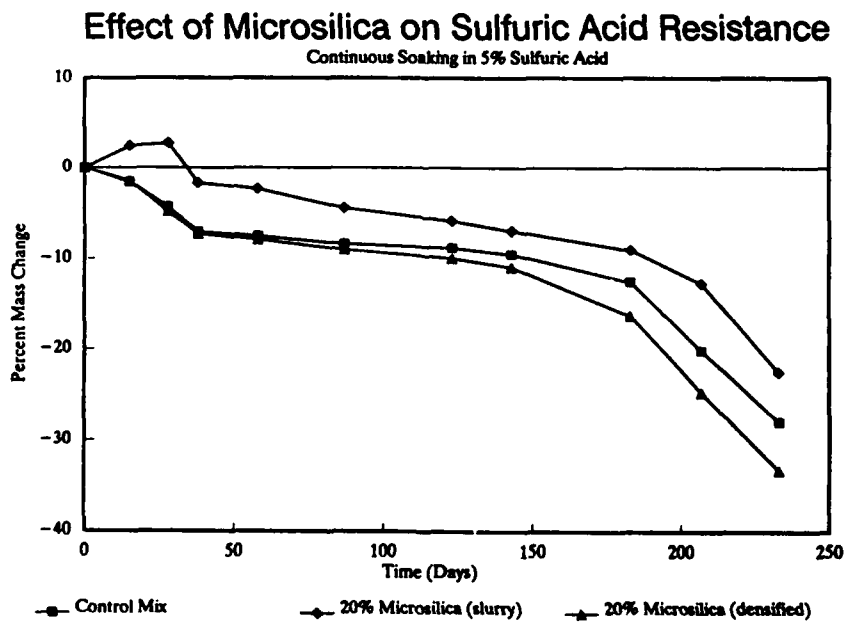


Figure 7

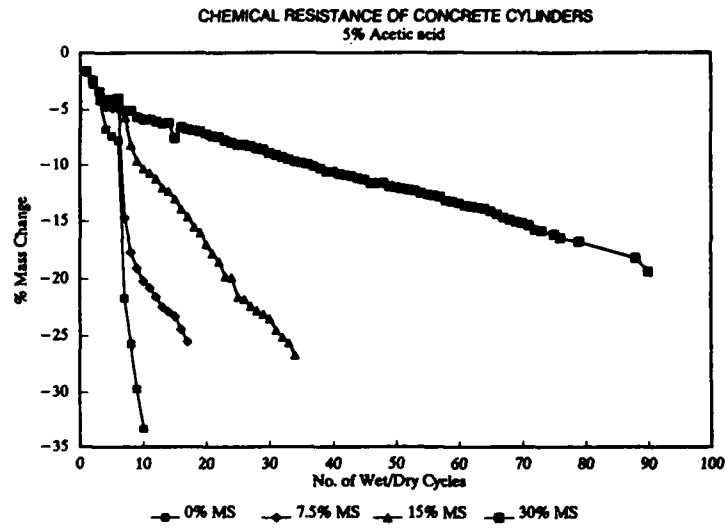


Figure 8

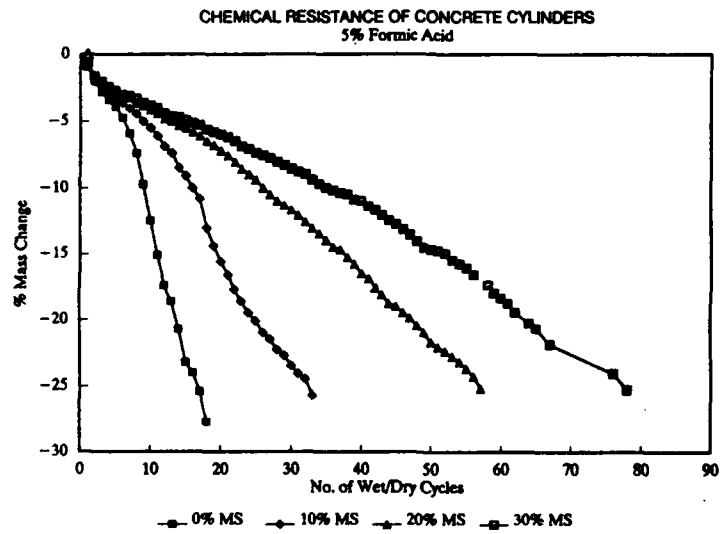


Figure 9

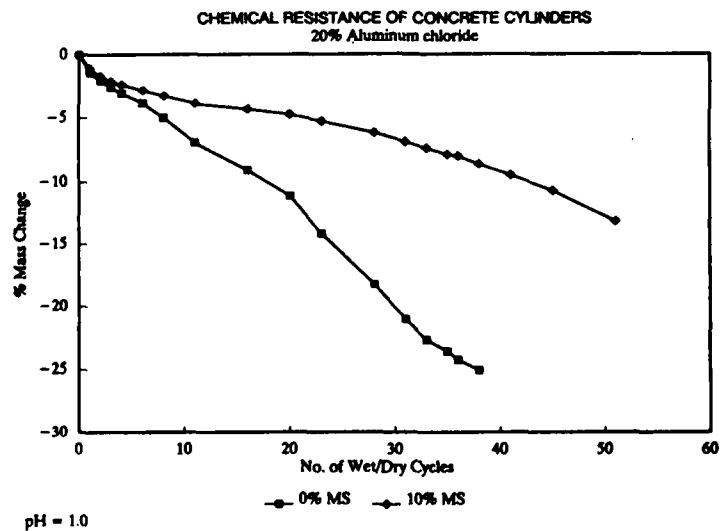


Figure 10

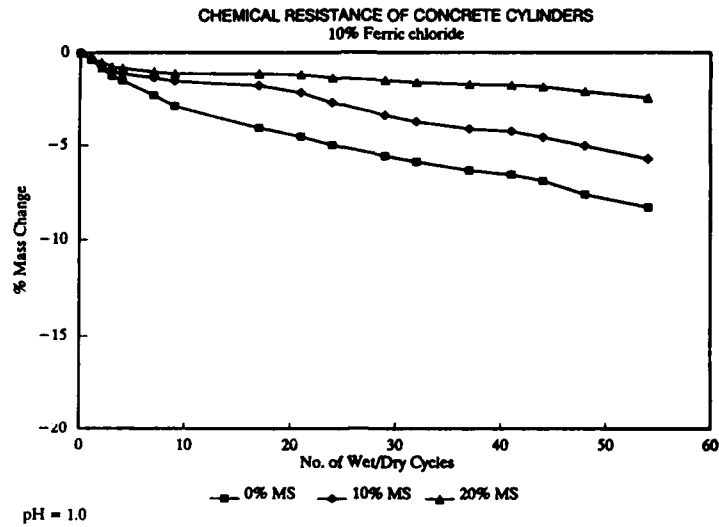


Figure 11

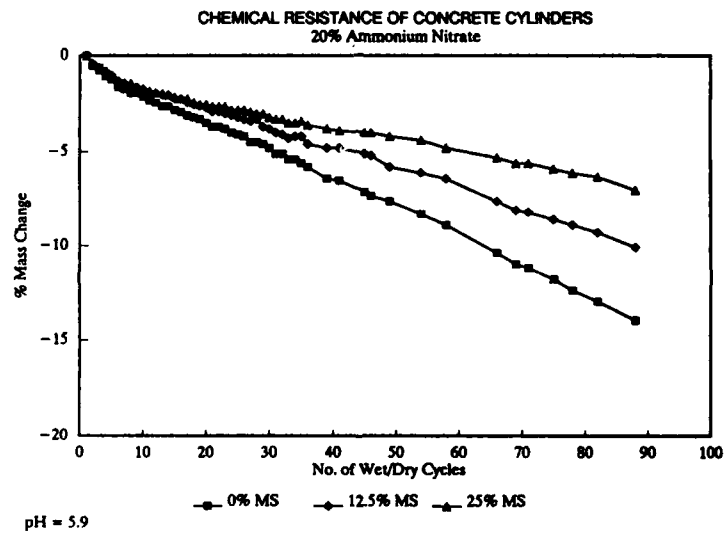


Figure 12

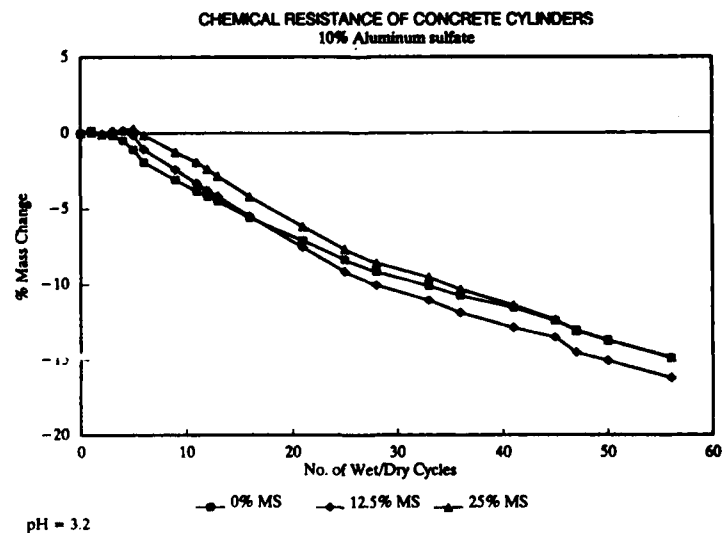


Figure 13

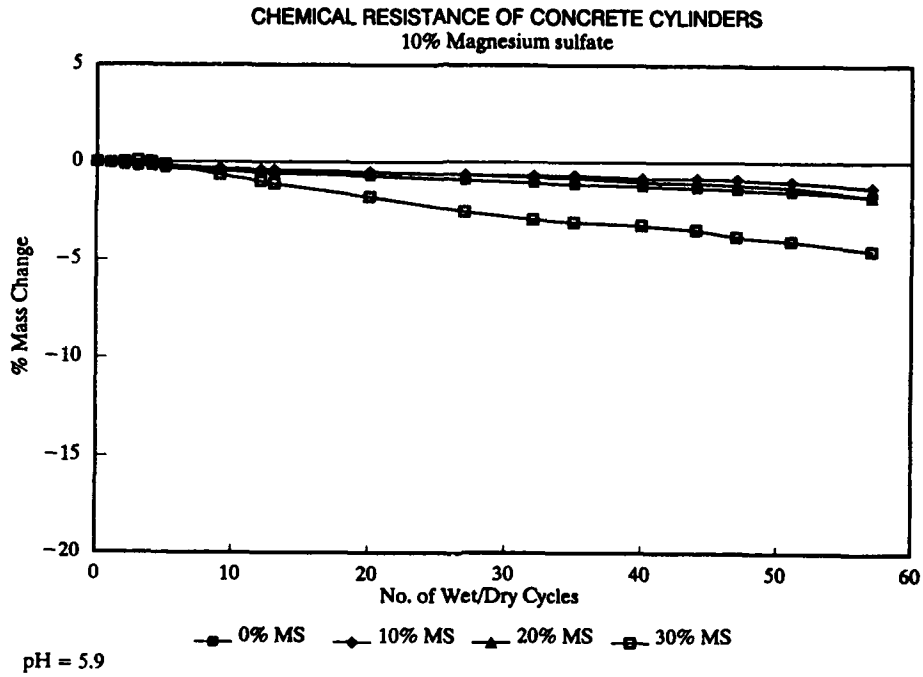


Figure 14

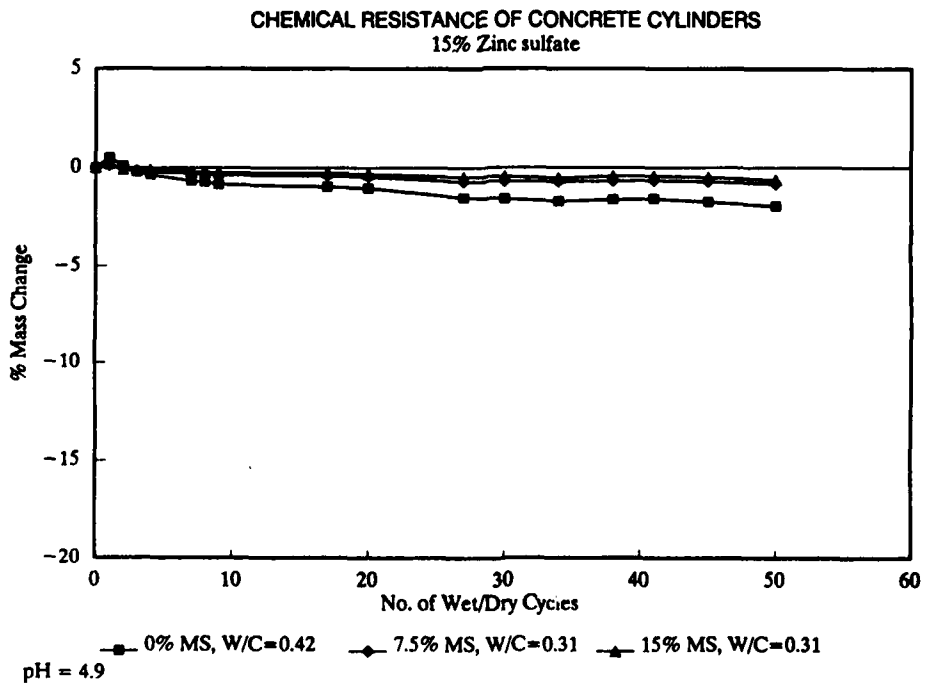


Figure 15

Inspection and Monitoring of Reinforced Concrete Structures - Electrochemical Methods to Detect Corrosion

B. Elsener, H. Wojtas and H. Böhni

Institute of Materials Chemistry and Corrosion
Swiss Federal Institute of Technology,
ETH Hönggerberg, CH-8093 Zurich (Switzerland)

Abstract

Maintenance and planning of the restoration work on reinforced concrete structures need a rapid, non-destructive inspection technique that detects corrosion at an early stage. In this paper the field experience with electrochemical techniques are reported. The results of potential surveys on bridge decks and walls realized with a new computer controlled eight-wheel measurement system clearly show that a fixed potential value (as proposed in ASTM C 876-87) for the identification and location of active corrosion of steel in concrete does not exist. A statistical elaboration of the potential data allows to identify the potential value for corroding and passive rebars for each structure individually.

A rapid new technique using galvanostatic pulse measurements was tested successfully on site. It gives clear, unambiguous results on the corrosion state of the rebars when half-cell potentials are uncertain. In addition, the ohmic resistance and the apparent polarization resistance are determined from the evaluation of the transients. From these values the concrete resistivity and the actual corrosion rate of the rebars may be estimated.

Keywords: non-destructive, monitoring, potential mapping, pulse technique

Introduction

Corrosion of the rebars is the main cause of damage and early failure of reinforced concrete structures [1]. The increasing use of deicing salts has resulted in severe damage to the bridges of the Swiss highway system, chloride concentrations in the concrete up to 4 % by weight of cement are found resulting in pitting attack of the rebars. Maintenance and planning of the restoration of these structures as well as quality control needs a *rapid, non-destructive inspection technique* that detects corrosion of the rebars at an early stage and defines adequately which areas of bridges require repair. The traditional method of inspection of reinforced concrete structures is too limited for two reasons:

- o relying on a visual inspection in combination with physical techniques to detect disbondment and cracking, damage is detected too late and only when it reaches a significant level of deterioration.
- o The results of laboratory tests on core samples (chloride penetration, porosity, carbonation) are always limited in their number and thus not representative of the whole structure.

The main problem, the corrosion - especially the dangerous pitting attack - of the reinforcing steel, can not be detected rapidly and at an early stage in this way. Due to the *electrochemical nature* of corrosion of steel in concrete electrochemical methods are well suited for the inspection and monitoring of concrete structures. The location of corroding zones is a comparably simple task, on site corrosion rate measurements are of great practical interest and of fundamental research concern. In this paper, the theoretical basis and field experience with electrochemical methods (potential mapping and galvanostatic pulse measurements) are reported and discussed.

Electrochemical Fundamentals

Steel embedded in good quality concrete is protected by a very thin oxide film (the passive film) that forms spontaneously in the high alkaline pore water. The loss of alkalinity due to carbonation of the concrete or the penetration of chloride ions (arising either from marine or deicing salts) to the steel can destroy this protective passive film [2 - 5]. In the presence of oxygen and humidity in the concrete corrosion of the reinforcement starts, alternating wetting and drying of the concrete are the more dangerous conditions. Chlorides are transported with the water and changing humidity gradients result in a transport zone at the concrete surface (Figure 1). Rebars located behind this transport zone will not corrode rapidly. A characteristic feature for the corrosion of steel in concrete is the development of macrocells (Figure 2). The coexistence of passive and corroding areas on the same rebar form a short circuited galvanic element with the corroding area as anode and the passive surface as cathode. The cell voltage ΔU in this macroelement equals the potential difference between corroding and passive steel and may reach up to 0.5 Volt. The resulting current flow I (which is directly proportional to the mass loss of the steel)

$$I = \Delta U / (R_E + R_A + R_C) \quad (1)$$

where

I = current flow, A

ΔU = cell voltage in the macroelement, Volt

R_E = electrical resistance of the concrete, Ohm

R_A = anodic reaction resistance, Ohm,

R_C = cathodic reaction resistance, Ohm

is determined by the electrical resistance of the concrete and the anodic and cathodic reaction resistance [5, 6].

The electric field can be measured at the concrete surface, resulting in equipotential lines (*potential field*) that allow the location of corroding zones at the most negative values. This is the basis of potential mapping, the principal electrochemical technique applied to the routine inspection of reinforced concrete structures [7 - 12]. Its use and interpretation are described in the ASTM Standard Test Method for Half Cell Potentials of Reinforcing Steel in Concrete C876-87.

When surface potentials are taken they are measured essentially remote from the reinforcement due to the concrete cover. The measured potentials are affected by the ohmic potential drop in the concrete and are in fact mixed potentials. Several factors as concrete resistivity (humidity) [8, 13], high resistive surface layers [8, 9, 14], oxygen access [15], concrete cover depth and chloride content have a significant effect on the potentials measured at the concrete surface as already discussed [6, 10 - 12]. Thus the results of potential mapping need careful interpretation. It becomes obvious that absolute potential values for assessing the corrosion hazard in a structure are not applicable. In addition, a rapid new monitoring technique that can overcome the difficulties in interpreting potential measurements is needed.

Potential mapping - location of corroding zones

Procedure

The procedure for measuring half-cell potentials is comparatively straightforward: a good electrical connection is made to the reinforcement, an external reference electrode (copper / copper sulfate, CSE) placed on the concrete surface and potential readings are taken on a regular grid on the surface. To facilitate the potential survey of large bridge decks, walls, or parking decks, the IBWK (Institute of Materials Chemistry and Corrosion, Swiss Federal Institute of Technology) developed a novel eight-wheel electrode measuring system (for details see [6, 10 - 12, 17]) that allows a survey of 200 square meters per hour with grid dimensions of 15 cm using computer-assisted data acquisition and processing. The optimum way of representing the data has been found to be a colour map of the potential field, where every individual point can be identified.

Results and Interpretation

The interpretation of the potential readings according to the ASTM C876-87 standard is based on a fixed potential value of -350 mV. More negative potentials were found to indicate corrosion with 95% probability [16]. Practical experience has shown, however, that for different conditions (that is concrete cover, humidity, chloride content) different potential values indicate corrosion [8 - 12, 17]. As is shown in figure 3, the most positive potential values where corrosion of the rebars was detected can range from as high as -200 mV down to -570 mV CSE. Examples of our recent work on potential mapping were presented in more detail already [10 - 12].

Probability distribution of potentials

One of the main advantages of using a computerized data acquisition in the potential mapping technique is that the very large number of potential readings taken on a bridge deck or a wall can be treated statistically. It has been found that the standard deviation of the half cell potentials remains fairly constant at $\sigma = 55 - 60$ mV for passive and $\sigma = 100 - 110$ mV for active regions [18]. In the cumulative probability distribution plots (figure 4) for most structures a mixed slope of $\sigma = 115 - 125$ mV appears [11, 17, 18] corresponding to the geometric sum of the passive and active zone. The potential difference observed between the distribution of passive and corroding rebars in the example of the San Bernardino tunnel clearly shows that these two zones have very different concrete humidity. Indeed, near the expansion joints the concrete was very wet and the resistivity in these areas was much lower [6, 11, 19].

Measurements in the project phase

Our experience from the restoration of bridge decks shows that potential surveys should be taken already in the project phase of a restoration to get a precise idea of the degree of damage of the structure. Only based on the results of the potential measurements core sampling for chloride analysis or resistivity measurements can be performed at the most representative points. Usually at this stage potential readings can be taken only from the underside of the bridge deck or through holes in the asphalt cover, thus a much larger grid of measuring points has to be used. The cumulative probability distribution of the potentials measured on a bridge deck of 400 m² shows ([figure 5](#)) that the information on the degree of damage and the location of large corroding zones is still maintained at large grid size.

Field experience on a large number of bridge decks investigated with the potential mapping technique has shown a clear correlation between the measured potential value and the chloride content in the concrete [18, 19]: the most negative potentials coincide with the areas of high chloride content. This is especially important in choosing the adequate points for core sampling in the project phase of a restoration and it allows - with a non-destructive technique - an insight in the chloride distribution on a structure.

Summarizing our experience with potential surveys, the interpretation of the potential field, that is the location of corrosion, can not be based on an absolute value as proposed by ASTM C 876-87. The examples presented (among numerous others [8 - 12, 17]) show that the structure of the potential field and the local potential gradient are better ways to identify the type of corrosion (general corrosion, pitting attack) and to locate corroding rebars. The statistical evaluation of potential data and recent experience [19] have shown that measurements from the underside of a bridge deck with a grid spacing of about 100 cm are sufficiently accurate to assess the degree of damage in the project phase and to locate large corroding zones. In addition, only based on the results of the half cell potential data core sampling for chloride analysis or resistivity measurements can be performed at the most representative points

Galvanostatic Pulse Measurements

The potential mapping technique has provided a very useful, non-destructive means of delineating areas of corrosion in the project phase as well as during restoration work. It is an early warning system that can assess the magnitude of the problem of corrosion and can be used to control the effectiveness of a restoration. The technique, however, suffers from two main disadvantages. Firstly, there is no direct assessment of the corrosion rate, although the corrosion rate may be estimated from the potential gradient and the concrete resistivity [11, 20]. Secondly, the measured potentials can not always be interpreted in a straight forward manner: negative potentials may occur due to polarization effects or due to lack of oxygen in very wet, dense or polymer-modified concrete and may thus lead to misinterpretations. The galvanostatic pulse method is a rapid, non-destructive technique to overcome these difficulties and to obtain unambiguous information on the corrosion state of the rebars with a single measurement. In addition, the resistivity of the concrete is determined and according to eq. (1) the corrosion risk on different points of the structure can be estimated.

Theory

When an instantaneous current step I_{app} is applied to a simple corrosion system, the potential, V_t , at a given time t can be expressed as [21]:

$$V_t = I_{app} [R_p [1 - \exp(-t / (R_p C_{dl}))] + R_\Omega] \quad (2)$$

| | | |
|------------|--------------------------|--------------|
| R_p | polarization resistance | [Ω] |
| C_{dl} | double layer capacitance | [μF] |
| R_Ω | ohmic resistance | [Ω] |

This equation may be rewritten in a form suitable for curve fitting, from which all the parameters can be determined:

$$V_t = K_0 - K_1 \exp(-t / K_2) \quad (3)$$

| | |
|-------|------------------------------------|
| K_0 | $(I_{app} R_p + I_{app} R_\Omega)$ |
| K_1 | $I_{app} R_p$ |
| K_2 | $(R_p C_{dl})$ |

Procedure

A short-time anodic current pulse (typically eight seconds) is imposed galvanostatically on to the reinforcement from a small counter electrode ($d = 14$ cm) [11] on the concrete surface and the resulting change in potential is monitored. The potentials are measured with a Cu/CuSO₄ reference electrode (in the center of the CE) and a high input impedance differential voltmeter. The output of the voltmeter is connected to the A/D converter of the computer. The pulse response is registered with 10 msec / point, each curve consisting of 1000 points. In the experiments performed, current pulses from 0.05 mA to 0.3 mA were used. To avoid any electrical connection between the rebars and the ground of the mains a special battery powered precision current source was used as a galvanostat. A typical example of a pulse response and the fit according eq. (3) is shown in figure 7.

Lollipop samples

The pulse measurement technique (GPM) with the evaluation according to eq. (3) has been tested on a series of lollipop samples with different chloride content at various exposure conditions in the laboratory. A good agreement with the results of impedance spectroscopy (EIS) for the values of R_Ω and R_p (figure 6) has been found. Systems which involve more than one time constant show deviations from the fit according eq. (3). This has been noted especially at very short time of the pulse in agreement with the occurrence of a high frequency loop in impedance spectra [11, 22]. These problems are currently in elaboration.

Application on site

Potential-time transients (fig. 7) were measured on a reinforced concrete wall heavily contaminated with chlorides from deicing salts at the bottom (up to 1 m above the street level). The curves measured at the bottom (corroding area) quickly reach the steady-state potential. Due to the steep polarization curve in the case of localized corrosion, the rebars can be polarized only a few millivolts with the applied current pulse of 0.1 mA. A continuous increase in potential instead showed that passive rebars can be polarized easily for several tenth of millivolts but with a

higher time constant (eq. 3). The results obtained on the reinforced concrete wall at different heights are summarized in table 1.

In contrast to a small laboratory specimen, on large slabs or on site the inhomogeneous current distribution arising from the small counter electrode has to be taken into consideration [18, 23 - 25]. The measured area varies over a wide range due to the variation in resistivity of the concrete and the true polarization resistance (active or passive state of the rebars) [24]. Calculations using an electrical network to model a single rebar in concrete (figure 8) confirmed this fact: for active corroding bars 95% of the current is confined to ± 10 cm from the border of the counter electrode, on passive rebars 95% of the current are dispersed within ± 50 cm (figure 9). The effect of concrete resistivity is notable for passive rebars.

Thus, the current pulse and its response cannot be related *a priori* to any specific electrode area and only effective polarization resistances $R_{p\text{ eff}}$ are determined. The data $R_{p\text{ eff}}$ from table 1 have to be multiplied with the area measured, a rough estimation using figure 9 results in a specific polarization resistance of 2000 $k\Omega\text{cm}^2$ for passive rebars (height 3 m). Another model to overcome these difficulties (spatial distribution of the electrical signals in the structure) is based on transmission lines [23 - 25]. Any approach to estimate the true polarization resistance on a structure has to take into account the rebar density at the different points of measurement and the concrete cover thickness. These values might vary considerably on a structure. To allow a fully quantitative evaluation of the pulse measurements (and of all other electrochemical techniques on site) much work has still to be done.

A more direct approach to evaluate differences in the corrosion rate at least qualitatively can be based on equation (1): for macrocells the corrosion rate is approximately proportional to the concrete conductivity. For the data in table 1 the corrosion rate at the bottom of the wall would be 30 times higher than at the height of 3 m. Due to the simple way of determining the ohmic resistance from galvanostatic pulse measurements this might be a rapid, non-destructive and easy way to obtain on-site informations on the corrosion risk at different points of a structure [26].

Conclusions

The results of field applications of non-destructive electrochemical techniques to assess the corrosion of rebars in concrete show:

1. Potential surveys with a new eight-wheel electrode measuring system are very well suited to locate corroding rebars. However, an absolute potential value for the identification of corrosion as proposed in ASTM C876-87 does not exist. It is shown that the structure of the potential field and the local potential gradient are better ways to identify the type of corrosion (pitting or general corrosion) and to locate corroding rebars.
2. Already in the project phase of a restoration work potential surveys should be performed. The statistical evaluation of half cell potential data from a number of bridge decks and practical experience has shown that measurements from the underside or through holes in the asphalt cover with a grid spacing of 1 m

are sufficiently accurate to assess the degree of damage and to locate large corroding zones.

3. Galvanostatic pulse measurements have been applied in the laboratory and on site. In the laboratory a good agreement with the results of other electrochemical techniques has been found. This rapid and non-destructive technique gives clear information on the state of the rebars in concrete when potential measurements are uncertain. In addition, it provides informations on the concrete resistivity simultaneously and allows to estimate the corrosion risk at different points of a structure.
4. To calculate the true polarization resistance the non-uniform current distribution between the rebars and the small counter electrode on the concrete surface has to be taken into account.

Acknowledgements

This work was financially supported by the Swiss Federal Highway administration within the research program "Brückenunterhaltsforschung".

References

- 1 D. Jungwirth, E. Beyer and P. Gruber: Dauerhafte Betonbauwerke, Beton-Verlag GmbH Düsseldorf (1986) p. 150
- 2 ACI - Committee 222, Corrosion of Metals in Concrete. ACIR-85 American Concrete Institute, Detroit MI 1985
- 3 Page C.L and Treadaway K.W.J., Nature **297** (1982)109
- 4 Corrosion of Steel in Concrete, RILEM Technical Committee 60 -CSC, State of the Art Report (1986)
- 5 Arup H., The mechanism of protection of steel by concrete. In Corrosion of Reinforcement in Concrete Construction, ed. A.P. Crane. Society of Chemical Industry, London, 1983, pp. 151-157
- 6 Elsener B. and Böhni H., Schweiz. Ingenieur und Architekt, **105** (1987) 528
- 7 Stratfull R.F., Corrosion NACE **13** (1957) 173t
- 8 Berkeley K.G. and Pahnmanaban S., Practical Potential Monitoring in Concrete. Proc. Conf. UK Corrosion 1987, pp. 115 - 131
- 9 Baker A.F., Potential Mapping Techniques. Seminar on Corrosion in Concrete - Monitoring, Survey and Control by Cathodic Protection. London Press Centre May 13. 1986, paper No. 3.
- 10 Elsener B., Müller S., Suter M. and Böhni H., Potential Mapping of Steel in Concrete. Proc. Conf. UK Corrosion 1988 Brighton UK. Vol. III pp. 169 - 182
- 11 Elsener B. and Böhni H., "Potential Mapping and Corrosion of Steel in Concrete", Corrosion Rates of Steel in Concrete, ASTM STP 1065, N.S. Berke, V. Chaker and D. Whiting, eds. American Society for Testing and Materials, Philadelphia, 1990 p. 143 - 156
- 12 Elsener B., Müller S., Suter M. and Böhni H., Potential Survey of Reinforced Concrete Structures - Theory and Practice. Proc Conf. Measurement and Testing in Civil Engineering, Lyon (France), 13.-16.9.1988, Vcl. I pp. 227 - 236

- 13 John D.G., Eden D.A., Dawson J.L. and Langford P.E., Proc. Conf. Corrosion/87, San Francisco CA, 9.-13.3.1987, paper 136
- 14 Browne R.D., Geoghan M.P. and Baker A.F., in Corrosion of Reinforcement in Concrete Construction, ed. A.P. Crane. Society of Chemical Industry, London, 1983, pp. 193 - 222
- 15 Popovics S., Simeonov Y., Bozhinov G. and Barovsky N., in Corrosion of Reinforcement in Concrete Construction, ed. A.P. Crane. Society of Chemical Industry, London, 1983, pp. 19 - 38
- 16 Van Daveer J.R., J. American Concrete Institute, **12** (1975) 697
- 17 B. Elsener, S. Müller, M. Suter and H. Böhni: in Corrosion of Reinforcement in Concrete, C.L. Page, K.W. Treadaway, P.B. Bamforth eds. Elsevier Applied Science London, 1990, p. 348 - 357
- 18 B. Elsener and H. Böhni: Materials Science Forum 111/112 (1992) 635
- 19 Hunkeler F., Schweiz. Ingenieur und Architekt **109** (1991) 272 - 278
- 20 Naish C.C, Harker A. and Carney R.F., in Corrosion of Reinforcement in Concrete, C.L. Page, K.W. Treadaway, P.B. Bamforth eds. Elsevier Applied Science London, 1990, p. 314 - 332
- 21 Newton C.J. and Sykes J.M., Corrosion Science **28** (1988) 1051
- 22 Lemoine L., Wenger F. and Galland J., Corrosion Rates of Steel in Concrete, ASTM STP 1065, N.S. Berke, V. Chaker and D. Whiting, eds. American Society for Testing and Materials, Philadelphia, 1990 p. 118 - 133
- 23 Feliu S., Gonzales J.A., Andrade M.C. and Feliu V., CORROSION 87, NACE 1987 paper Nr. 145
- 24 Feliu S., Gonzales J.A., Andrade M.C. and Feliu V., Corr. Science **29** (1989) 105 - 113
- 25 Feliu S., Gonzales J.A., Andrade M.C. and Feliu V., Materials and Structures **22** (1989) 199 - 205
- 26 B. Elsener, in "Erhaltung von Brücken", SIA Dokumentation D099, Schweizerischer Ingenieur und Architektenverein, Zürich (1993)

Table 1:

Results of the galvanostatic pulse measurements on a reinforced concrete wall exposed to splash water with deicing salt. Heavily chloride contaminated up to 1 m height.

| Height | E_{corr} [mV CSE] | K_0 eq.(3) | R_{Ω} [Ω] | $R_{p\ eff}$ [Ω] | t_{const} [sec] |
|--------|--------------------------|--------------|------------------------------|------------------------------|----------------------|
| 0.2 m | - 510 | - 483 | 220 | 60 | 2.25 |
| 0.5 m | - 482 | - 462 | 160 | 38 | 2.47 |
| 1.0 m | - 360 | - 200 | 1380 | 235 | 3.36 |
| 3.0 m | - 138 | + 442 | 5350 | 430 | 4.25 |

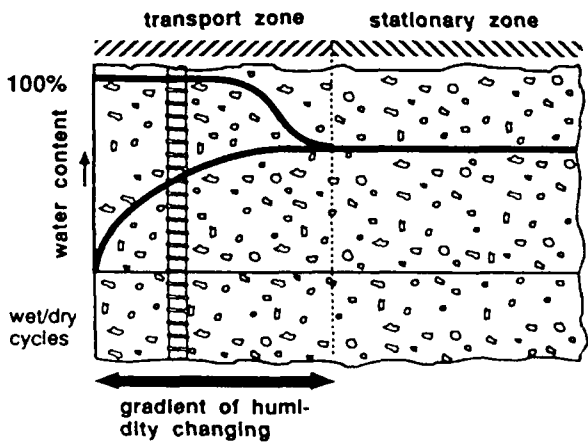


Figure 1. Schematic view of the transport zone on the concrete cover for alternating wet/dry cycles.

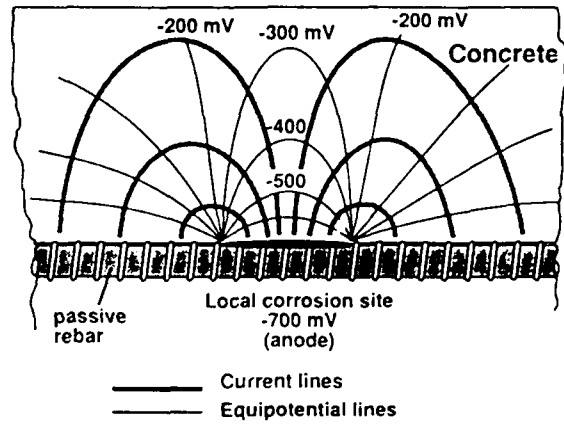


Figure 2. Schematic view of the electric field and current flow of an active/passive macroelement on steel in concrete.

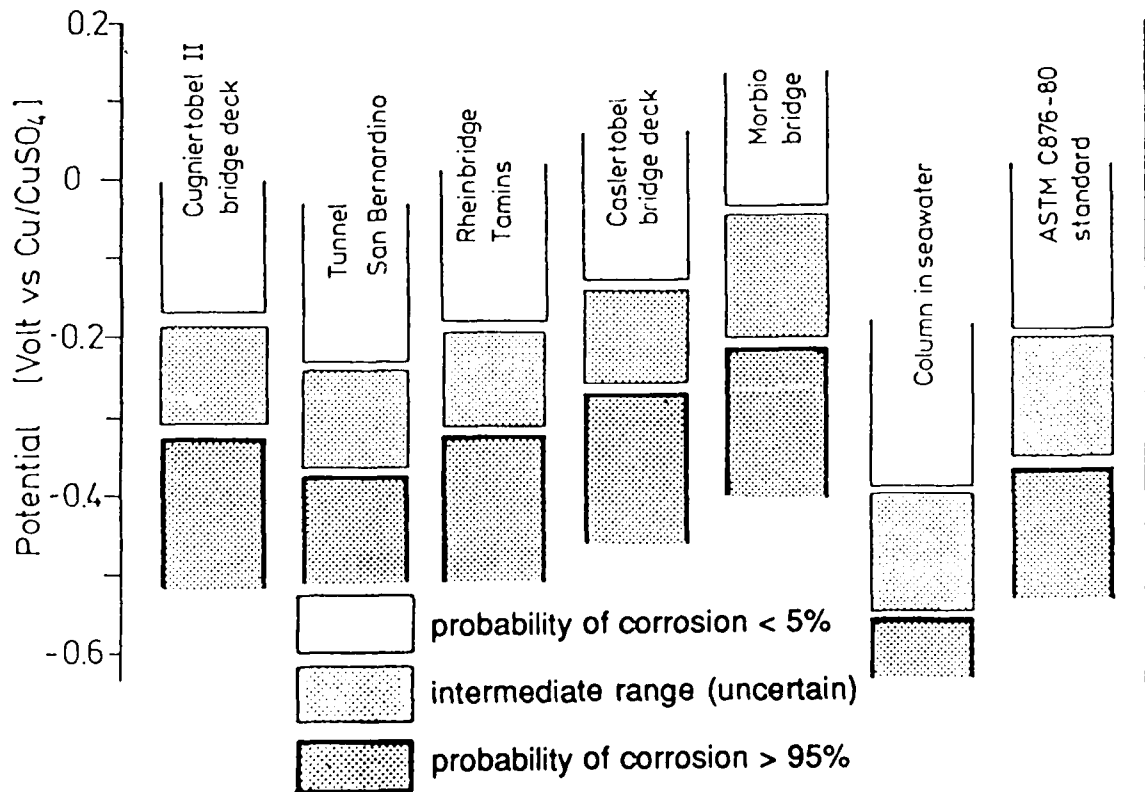


Figure 3. Experimentally determined potential range indicating active corrosion on different bridge decks compared to the ASTM C 876-80 standard.

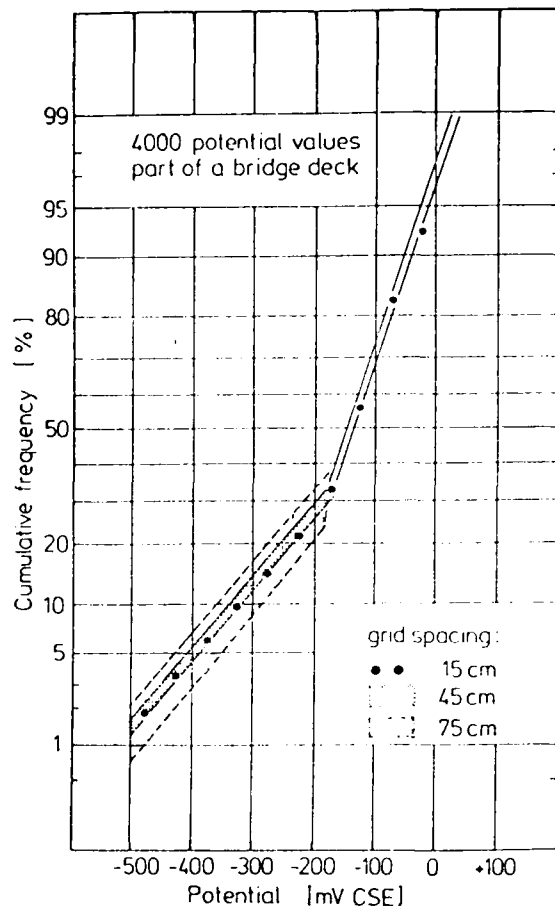
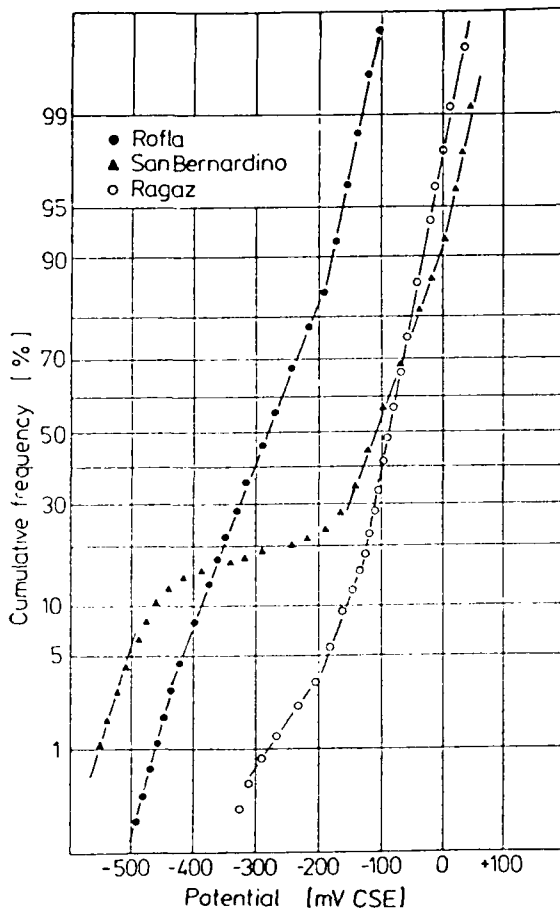


Figure 4. Cumulative frequency distribution of potential values measured on different bridge decks. Note the huge effect of humidity change (corroding zones = wet, passive zones = dry) in the example San Bernardino.

Figure 5. Cumulative frequency distribution of potential values measured on a bridge deck with a grid of 15 cm. Computer simulation for grid spacing of 45 and 75 centimeter performed on the same data set.

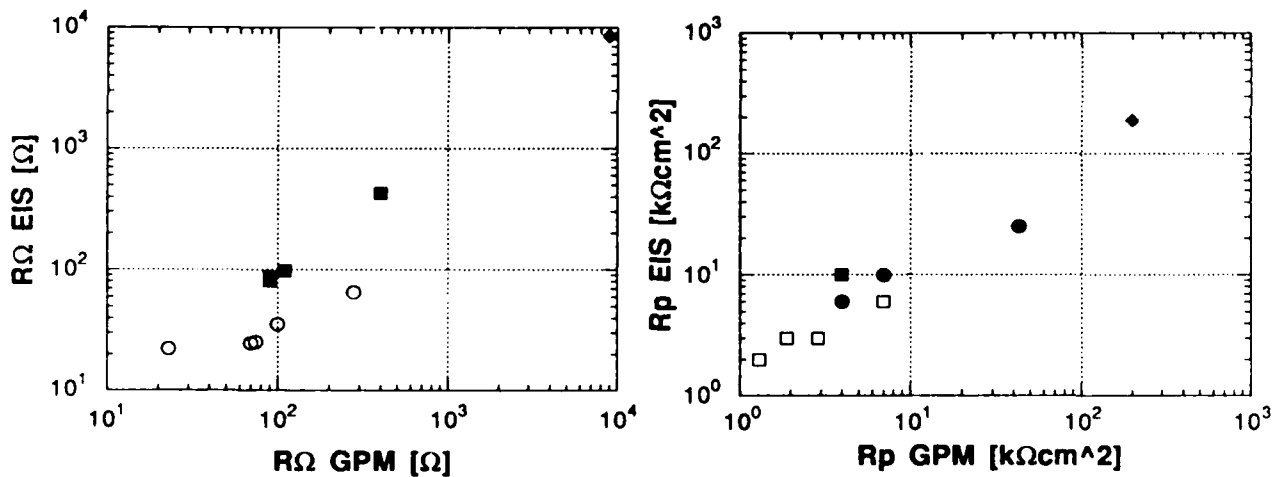


Figure 6: Comparison of polarization resistance R_p and ohmic resistance R_Ω from impedance (EIS) and galvanostatic pulse measurements (GPM) for two sets of lollipops (2% and 1.4% Cl-/cement) in different environmental conditions

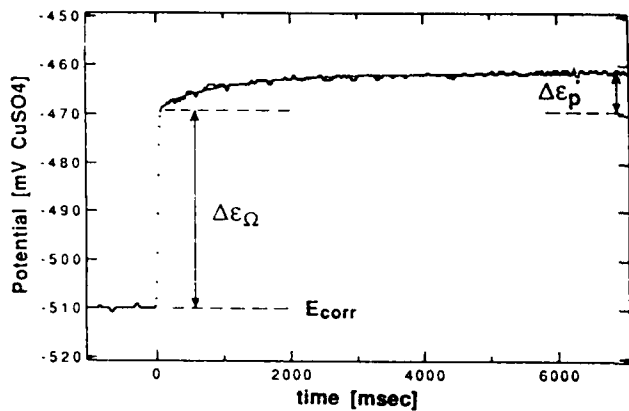


Figure 7. Galvanostatic pulse transient measured at 0.2 m height on a heavily chloride contaminated wall, current $I_{app} = 0.1$ mA.

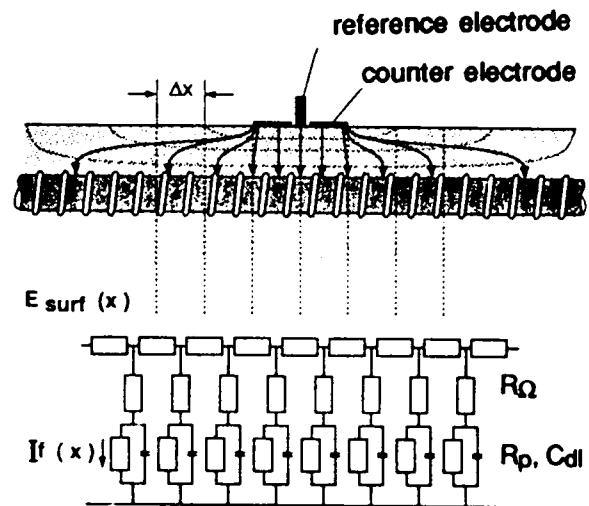


Figure 8: Current distribution from a small counter electrode and equivalent electrical network (schematic)

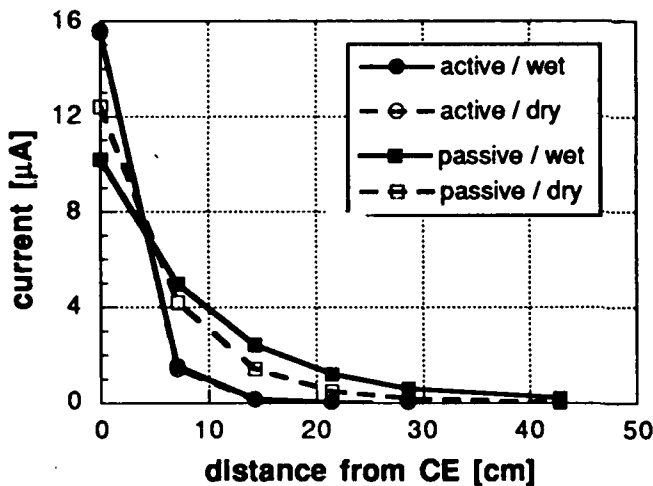


Figure 9: Current distribution from a small counter electrode (calculated with the electrical network) for active and passive rebars.

Evaluation of Concrete Corrosion Inhibitors

N. S. Berke, PhD
W.R. Grace & Co., Conn.
Construction Products Division
62 Whittemore Avenue
Cambridge, MA 02140

M. C. Hicks
W.R. Grace & Co., Conn.
Construction Products Division
62 Whittemore Avenue
Cambridge, MA 02140

P. G. Tourney, P.E.
W.R. Grace & Co., Conn.
Construction Products Division
62 Whittemore Avenue
Cambridge, MA 02140

Abstract

Corrosion of steel in concrete is one of the major causes of the loss of durability in marine and deicing salt environments. Numerous protection systems are commercially available including corrosion inhibiting admixtures. The proper evaluation of corrosion inhibiting admixtures requires determining their effectiveness in the presence of chloride at the steel concrete interface, and on their effect on concrete properties. This paper shows that proper testing in good quality concrete can differentiate between a corrosion inhibitor and water repellent or permeability reducer, and by comparison to other studies shows how erroneous conclusions can be reached by not testing in good quality concretes.

Keywords: corrosion inhibitors, calcium nitrite, concrete, dampproofing admixtures, butyl ester emulsion, oleic acid, dimethylethanolamine, cyclic polarization, polarization resistance, water repellent

Introduction

Corrosion of steel reinforced concrete is a major problem in marine environments and in those environments where deicing salts are used. Though not a major problem in the United States and Canada, carbonation also leads to corrosion of embedded steel. Several protection techniques have been applied and suggested for combating the corrosion problem. These include epoxy-coated reinforcing steel, corrosion inhibiting admixtures, permeability reduction in the concrete by using low water-to-cementitious ratios and pozzolans such as microsilica, protective membranes, sealers, cathodic protection, and replacing the steel with stainless steel or composite materials. In this paper the corrosion inhibitor approach is examined.

The evaluation of a corrosion protection system for steel in concrete is not trivial. Extensive screening and long-term testing is needed to demonstrate that the system is viable for the 40 to 100 year design life of new structures. Though this type of testing has been performed by metal producers before introducing new alloys or coatings, it has not always been the case in the concrete industry. This is illustrated by the current activity of modifying the specifications for epoxy-coated reinforcing steel to address problems that occurred in the Florida Keys and elsewhere.¹⁻³ Inhibitor admixtures need to be evaluated in two areas. One is their effect on concrete properties and the other is their corrosion performance.

Corrosion inhibitors protect steel in the presence of chloride ions. A good definition is that of Rozenfeld which states that a corrosion inhibitor varies the rate of a corrosion process by influencing the kinetics of the electrochemical reactions responsible for this process.⁴ Inhibitors thus must retard either the anodic, cathodic, or both reactions simultaneously. Numerous other protection systems such as epoxy-coated rebar, silica fume, and slag might reduce corrosion, but as they do not affect the kinetics of the corrosion reactions when chloride is next to the steel, they are not corrosion inhibitors.

Corrosion inhibitors added to the concrete in the mixing cycle are chemical admixtures, as such they must not be harmful to the properties of the concrete. Though there is no ASTM specification for corrosion inhibiting admixtures, ASTM C 494 does give guidelines for the effects of admixtures on plastic and hardened properties of concrete. A corrosion inhibiting admixture should not cause excessive retardation or acceleration (unless this can be offset by other approved admixtures), it should not reduce flexural or compressive strengths below 90% of a similar concrete without the inhibitor. Freezing and thawing resistance must also be maintained if the concrete is to be used in regions subjected to temperatures below freezing.

Initial screening tests such as cyclic polarization to determine the effect of the inhibitor in a concrete type solution in the presence of chloride, and ASTM G 109 to determine the effects in concrete of lesser quality are useful. However, testing must also be conducted to demonstrate long-term performance in concrete similar to that specified in the field. The corrosion inhibiting behavior of admixtures needs to be determined in good quality concrete meeting the code requirements of ACI 318 or similar codes. Successful completion of the long-term laboratory program should lead to field applications, starting with small structures.

The long-term evaluation of calcium nitrite as a corrosion inhibiting admixture is complete and shows that it is effective.⁵⁻⁹ Recently a butyl ester of oleic acid emulsion type admixture has been introduced as an ester and amine organic corrosion inhibitor.¹⁰ A comparison of the two products in screening tests is given here, as is a comparison to a dimethylethanol amine (DMEA) product that was recently introduced. The results show that the butyl ester product does not provide significant corrosion inhibition, in contrast to published test data conducted in extremely poor quality concrete,¹⁰ and that the DMEA is ineffective.

These differences are discussed and point to the necessity of longer-term evaluation of new products. An analysis of the concrete properties is also given indicating that there is a marked decrease in mechanical properties when the butyl ester emulsion type product is added.

Preliminary results of long-term experiments with better quality concretes are also presented. The concrete data show a significant decrease in the mechanical properties when the butyl ester emulsion type product is added and virtually no improvement in permeability in field quality concretes. Comparisons to longer-term experiments that were conducted previously with calcium nitrite are also given.

Experimental

Cyclic Polarization

Cyclic polarization is a relatively quick test that gives an indication of the corrosion inhibiting (or lack thereof) properties of metals exposed to a chloride environment. This test provides a useful method of gaining information on the pitting tendency of a metal in a particular environment. This is achieved by shifting the applied potential from the cathodic zone toward the anodic region at a rate slow enough to allow for the formation of a protective film, followed by a scan in the reverse direction. This latter scan should be at a rate fast enough to minimize the amount of time that the specimen is subjected to high current. The method used here is a modified version of ASTM G 61 (Test Method for Conducting Cyclic Potentiodynamic Polarization Measurements for Localized Corrosion, Susceptibility of Iron-, Nickel-, or Cobalt-Based Alloys).¹¹ Because the applied potential brings the sample potential into regions far removed from the corrosion potential (500 mV or more), this technique can be destructive. Under actual field conditions, such high values are not encountered unless large, stray voltages are present.

Because it is destructive, the method cannot be applied to concrete structures in the field, nor is it a monitoring technique. Its use is restricted to the examination of test specimens in the laboratory.

Solutions commonly used are saturated calcium hydroxide at a pH of approximately 12.4 which is very similar to concrete.

These tests were carried out by immersing the rebar specimens machined into 9.5 mm diameter by 13 mm (0.4" by 0.5") long cylinders to fit an EG & G Princeton Applied Research cylindrical specimen holder. The cylinders were degreased with methanol prior to testing. Solutions used were 0.25 M sodium chloride saturated with calcium hydroxide. Additions of calcium nitrite in dosages equivalent to 10 and 15 V/m^3 (2 and 3 gal/yd^3), butyl ester emulsion in dosages equivalent to 5, 10 and 15 V/m^3 (1, 2, and 3 gal/yd^3), and dimethylethanolamine (DMEA) in a dosage equivalent to 0.6 kg/m^3 (1 lb/yd^3), were used.

The potential of the specimens was held at -1 V vs. SCE for 15 minutes prior to starting the cyclic polarization test. A scan rate of 5 mV/s was used in all cases. The potential was scanned from -800 mV vs. SCE in the direction of positive potentials to a maximum current of 255 $\mu\text{A/cm}^2$, at which point the potential was reversed and scanned in the direction of more negative potentials until -700 mV vs. SCE was reached.

The test determines a breakdown potential, E_b , which is indicative of the start of pitting during the scan. The higher the breakdown potential E_b the more effective the inhibitor is, at the given chloride level. The more important value is the pitting potential E_p , at which pitting stops. Severe corrosion cannot occur at potentials more negative than this value. Typically if E_b values are greater than 0 mV then E_p values above -280 mV vs. SCE (-350 CSE) indicate protection.

Macrocell Corrosion

A useful screening test in concrete is the new ASTM G 109 Standard Test Method for Determining the Effects of Chemical Admixtures on the Corrosion of Embedded Steel Reinforcement in Concrete Exposed to Chloride Environments.¹² This method is conducted on a well cured concrete at 0.5 w/c ratio to produce a discontinuous pore structure with a higher permeability than that specified in field concretes. Good performance in this method would be one of several criteria needed to demonstrate effectiveness of a corrosion inhibitor for steel in concrete.

Concrete specimens were made with the mix proportions listed in Tables 1 and 2. Table 1 specimens were made in accordance to ASTM G109,¹² and a modified version of the procedure was used for the other macrocell specimens. Beams 279 mmx114 mmx152 mm (11"x4.5"x6") were made which contained one top bar and two bottom reinforcing bars (#4, 13 mm (0.5") diameter) made of black steel. The bottom bars were 25 mm (1") from the bottom as described in Reference 12. The reinforcing bars were taped with electroplater's tape to expose 203 mm (8") of rebar. After a curing period at 100% RH and 22 °C (72 °F), a plastic dam 152 mmx76 mm (6"x3") was caulked to the top. The four sides of the specimen and the top surface outside the dam were coated with a concrete epoxy. Ground clamps were used to attach a 100 ohm resistor between the top and one of the bottom bars. The two bottom bars were also electrically connected. The samples were cyclically ponded with a 3% solution of sodium chloride on a two-week wet two-week dry cycle. The voltage drop across the 100 ohm resistor was measured every four weeks.

Polarization resistance

Polarization resistance is used to directly measure the total corrosion rate of steel in concrete. It is based upon a variation of ASTM G 59 Standard Practice for Conducting Potentiodynamic Polarization Resistance Measurements.¹³ The method is nondestructive due to the small perturbations applied for only short times, allowing for the long-term monitoring of reinforced concrete specimens.

Specimens used were 76 mm diameter 152 mm long (3"x6") cylinders with embedded #3 steel reinforcing bars (9.5 mm-3/8"). The protruding length of the bar as well as a short length of embedded bar was covered with electroplater's tape, leaving 26 cm² of exposed bar embedded in the concrete. After 28 days curing at 100% RH at 22 °C (72 °F), the specimens were ponded to half their height in 3% sodium chloride. The solution was changed every two months. This type of ponding models concrete exposed to a marine environment in the splash/tidal zone.

The polarization resistance was measured using a PAR model 351 system consisting of a computer-controlled potentiostat and associated software. The applied potential was increased at a rate of 0.1 mV/s from 20 mV below the equilibrium potential to a final potential of 20 mV above the equilibrium potential. To eliminate errors due to the large concrete resistance, the current-interrupt feature of the system was enabled when obtaining the data.

Results and Discussion

Cyclic Polarization Screening Tests

Cyclic polarization is a useful test to demonstrate that a corrosion inhibitor is actually working when chlorides are present at the reinforcing bar level. It clearly eliminates the effects of dampproofing admixtures and concrete permeability reducers, which might appear to have enhanced properties in some concrete tests. Cyclic polarization E_b and E_p values at a chloride level equivalent to 3 kg/m³ (5 lb/yd³) of chloride ion are given in Table 3 and characteristic curves are shown in Figures 1-4. The data indicate that only calcium

nitrite provides resistance to pitting corrosion. The DMEA at recommended levels improved E_p , but actually resulted in a reduced E_p value compared to the control, indicating that it might be detrimental in alkaline environments. The butyl ester emulsion at 5 l/m^3 (1 gal/yd^3) was essentially the same as the control, however, an increased dosage actually worsened its performance indicating that this product is not a corrosion inhibitor. As found in numerous other studies increasing the calcium nitrite content was increasingly beneficial.¹⁴⁻¹⁶

There is some indication that cathodic currents 100 mV active to E_p are slightly reduced for all the additives tested. However, considering extremely large cathode to anode ratios present for steel in concrete, a minor improvement in cathodic inhibition is not enough to stop pitting corrosion. This fact is also mentioned by Rozenfeld as to why cathodic inhibitors, and in particular organic corrosion inhibitors are usually only effective under acidic conditions where hydrogen reduction is the cathodic reaction.⁴ Thus, by increasing the threshold for pit initiation, calcium nitrite is the only admixture that shows corrosion inhibiting properties in this test.

Concrete Testing

Mechanical Properties. The evaluation of a corrosion inhibiting admixture, or for that matter any admixture, must include a study of the effects of that admixture on concrete properties. The effects of calcium nitrite, butyl ester emulsion, and DMEA on concretes produced at a 0.5 w/c ratio for ASTM G109 testing are shown in Table 1. The data show that DMEA does not adversely affect compressive strength, whereas, there was a 5.3% decrease with the butyl ester emulsion. However, this decrease occurred even though there was a 24% decrease in the plastic air content, which should have resulted in an increase in strength. Using the standard 5.5% strength decrease per 1% air increase,¹⁷ the compressive strength for the butyl ester emulsion, at the same air content as the control, would have been 33 MPa (4785 psi) for a 13% decrease in compressive strength. This 13% reduction in strength would not pass the ASTM C 494 requirements. The calcium nitrite specimens showed a significant improvement in compressive strength of over 39%.

Of interest is the extremely high value of air entrainment admixture needed to achieve even a reduced level of air entrainment for the butyl ester emulsion treated concrete. Figure 5 graphically illustrates the substantially increased air entraining dosages needed. In areas subjected to freezing and thawing this could be of major concern.

There was a slight decrease in concrete slump with the calcium nitrite mixture. However, in actual field usage superplasticizers and high range water reducers are used to adjust slump.

In addition to tests in concrete produced according to G109, additional tests were made at w/c = 0.4. This is more representative of a typical field application. Mechanical properties for these concretes are given in Table 2. In this case there was a 13% decrease in compressive strength for the butyl ester emulsion product at 28 days. Again, this 13% reduction in strength would not pass the ASTM C 494 requirements. The calcium nitrite concrete specimens in contrast showed better than a 10% improvement. Once again it was more difficult to entrain air with the butyl ester emulsion.

The concrete data clearly show that butyl ester emulsion negatively affects the compressive strength of concrete, and makes it more difficult to entrain air. Thus, the margin of safety in meeting compressive strength requirements is significantly reduced. Extra cementitious material and increased air entraining agent additions will most likely be needed with this product's use.

Corrosion Testing in Concrete. Figure 6 shows the results of G109 macrocell corrosion testing on the concretes described in Table 1. Note that only the 15 Vm^3 (3 gal/yd^3) 30% calcium nitrite treated concrete was showing no signs of corrosion activity at the completion of the test. The DMEA treated concrete appears to be equivalent to the control and there is only a moderate improvement with the butyl ester emulsion product.

When broken open for visual comparison it was seen that the corrosion on the bars paralleled the corrosion currents for all products tested. Figure 7 shows the measured corrosion areas. It is clear that DMEA is not behaving like a corrosion inhibitor and might even be detrimental. This was not totally unexpected based upon the poor performance in the cyclic polarization tests.

The slightly improved performance with the butyl ester emulsion might be due to the fact that it is reducing the ingress of chloride to a small degree. The chloride analyses given in Table 4 do show a decrease in chloride ingress for the butyl ester emulsion and to a lesser extent for the calcium nitrite treated concrete. However, since corrosion is occurring for the butyl ester emulsion product at a reduced chloride level relative to the control, it can hardly be considered to be a corrosion inhibitor, and is more in the dampproofing admixtures category.^{18,19}

Tests are also being conducted at 0.4 w/c. Preliminary chloride results after one year of ponding show that there is no decrease in chloride ingress over that of control specimens for the butyl ester emulsion. This is in accord with work by T. C. Powers et. al. that showed that dampproofing admixtures have little benefit in good quality concrete.²⁰

Corrosion testing in concrete with 4.7 kg/m^3 (8 lb/yd^3) of admixed sodium chloride at 0.4 w/c is in progress. Figure 8 shows the corrosion currents determined by polarization resistance over 18 months of testing for controls, 5 Vm^3 (1 gal/yd^3) butyl ester emulsion, and 15 Vm^3 (3 gal/yd^3) of calcium nitrite corrosion inhibitor. Corrosion rates above 15 $\mu\text{S/cm}^2$ are indicative of some corrosion activity and above 25 $\mu\text{S/cm}^2$ significant corrosion is occurring.^{21, 22} Thus the butyl ester emulsion is showing signs of corrosion and activity slightly higher than that in the controls, whereas the specimens with calcium nitrite are passive. This is more clearly shown in the integrated currents shown in Figure 9. Once again these results could have been predicted from the cyclic polarization data.

Further Discussion

As noted earlier there is substantial evidence pointing to the effectiveness of calcium nitrite as a concrete corrosion inhibitor. Much of this evidence was obtained from long-term testing in high quality concretes. It was demonstrated that the improvements in corrosion protection were due to protection of the steel in the presence of chloride and not by a decrease in chloride permeability.

In contrast, the published data showing improvements in corrosion performance with butyl ester emulsion have been on concretes with low cement factors, higher w/c values, low cover, and poor curing.^{10,23,24} These papers highlight the chloride permeability reductions and claim corrosion inhibition. As seen in this work the claims for chloride permeability reduction in poor concrete are valid, however, for quality concrete there is little or no improvement. The overwhelming evidence is that the butyl ester emulsion is not an effective corrosion inhibitor for steel in concrete. This is not really surprising since organic inhibitors are mostly used in acid environments.⁴

Furthermore, the studies presented here indicate that long-term tests in better quality concretes are needed, because some products can look better in poor quality concrete than in good quality concrete. For example an updated graph of a long-term lollipop test first described in 1985²⁵ is shown in Figure 10. These data showed that it took approximately 3 years for severe corrosion activity to initiate on control

specimens produced at 0.34 w/c. The specimens with calcium nitrite corrosion inhibitor are still not corroding, after over 8 years of testing, at chloride levels exceeding 10 kg/m^3 (17 lb/yd^3).²⁶ If these tests were ended after 1 year it would have appeared that a high range water reducer was more effective than calcium nitrite, which was not the case.^{21, 26} Therefore, corrosion inhibitors have to be evaluated in long-term tests in concretes representative of those used in the field.

Conclusions

Based upon this work the following conclusions can be made:

1. Cyclic polarization tests give an accurate assessment of the corrosion inhibiting properties of a chemical when chloride is present at the steel.
2. Calcium nitrite is an effective corrosion inhibitor for steel in concrete in chloride environments and protects when chloride is present at the steel.
3. Butyl ester emulsion reduces chloride ingress at 0.5 w/c. However, in concrete at 0.4 w/c it had little effect on chloride ingress.
4. Butyl ester emulsion does not prevent the corrosion of reinforcing steel in the presence of chloride, and therefore is not considered to be a corrosion inhibitor in concrete. It is a fatty acid and falls under the category of dampproofing admixtures.
5. Butyl ester emulsion adversely affects compressive strength and the ability to air entrain concrete.
6. DMEA does not appear to be an effective corrosion inhibitor in alkaline or concrete environments when chloride is present at the steel reinforcement.
7. Long-term corrosion tests in good quality concrete are needed for all newly introduced products to prove performance benefits.

Acknowledgements

The authors wish to thank P. Toner, A. Dressler, J. Lee and M. Dallaire for their assistance in producing specimens and conducting several of the experiments, and the management at Grace Construction Products.

References

1. A. Zayed, A. Sagues, R. Powers, "Corrosion of Epoxy-Coated Reinforcing Steel in Concrete" CORROSION/89, paper no. 379 (Houston, TX: National Association of Corrosion Engineers, 1989).
2. TRB Session 153, Transportation Research Board Meeting, June 10-14, 1993, Washington, D.C.
3. TRB Session 182, Transportation Research Board Meeting, June 10-14, 1993, Washington, D.C.
4. I. L. Rozenfeld, Corrosion Inhibitors, McGraw-Hill, Inc., New York, N.Y. (1981): p. 3.
5. N. S. Berke, A. M. Rosenberg, "A Technical Review of Calcium Nitrite Corrosion Inhibitor in Concrete", Transportation Research Record 1211, Transportation Research Board, National Research Council, Washington, D.C. 1989.
6. N. S. Berke, B. El-Jazairi, "The Use of Calcium Nitrite as a Corrosion Inhibiting Admixture to Steel Reinforcement in Concrete", Corrosion of Reinforcement in Concrete, C.L. Page, K.W.J. Treadaway and P.B. Bamforth Eds., Elsevier Applied Science, p. 571, London (1990).
7. N. S. Berke, T. G. Weil, "Worldwide Review of Corrosion Inhibitors in Concrete", Advances in Concrete Technology, Canada Center for Mineral and Energy Technology (CANMET), V. M. Malhotra Editor, (1992): p. 899.
8. N. S. Berke, "Corrosion Inhibitors in Concrete", Concrete International, 13 7 (July 1991): p.24.
9. N. S. Berke, "A Review of Corrosion Inhibitors in Concrete", Materials Performance, Vol No. (1989): p. 41.
10. C. K. Nmai, S. A. Farrington, G. S. Bobrowski, "Organic-Based Corrosion-Inhibiting Admixture for Reinforced Concrete", Concrete International, 14 4, (April 1992), p. 45.
11. ASTM G 61-86 "Standard Test Method for Conducting Cyclic Potentiodynamic Polarization Measurements for Localized Corrosion Susceptibility of Iron-, Nickel-, or Cobalt-Based Alloys", Annual Book of ASTM Standards, Vol. 03.02 (1992), American Society for Testing and Materials, Philadelphia.
12. ASTM G 109-92 "Standard Test Method for Determining the Effects of Chemical Admixtures on the Corrosion of Embedded Steel Reinforcement in Concrete Exposed to Chloride Environments", Annual Book of ASTM Standards, Vol. 03.02 (1992), American Society for Testing and Materials, Philadelphia.
13. ASTM G 59-91 "Standard Practice for Conducting Cyclic Potentiodynamic Polarization Resistance Measurements", Annual Book of ASTM Standards, Vol. 03.02 (1992), American Society for Testing and Materials, Philadelphia.
14. N. S. Berke, M. C. Hicks, "Electrochemical Methods of Determining the Corrosivity of Steel in Concrete", ASTM STP 1000, R. Baboian and S. W. Dean Eds., American Society for Testing of Materials, Philadelphia, PA, (1989): p. 425.
15. N. S. Berke, "The Use of Anodic Polarization to Determine the Effectiveness of Calcium Nitrite as an Anodic Inhibitor", Corrosion Effect of Stray Currents and the Techniques for Evaluating Corrosion of Rebars in Concrete, ASTM STP 906, V. Chaker Ed., American Society for Testing and Materials, Philadelphia, (1986): p. 78.

16. B. B. Hope, A. K. C. Ip, "Corrosion Inhibitors for Use in Concrete", *ACI Materials Journal*, (November-December 1989): p. 602.
17. S. Mindess, J. F. Young, *Concrete*, Prentice Hall, Inc., Englewood Cliffs, N.J. 07632, (1981): p. 260.
18. M. R. Rixom, N. P. Mailvaganam, *Chemical Admixtures for Concrete*, Second Edition, E & F.N. Spon Publishers, New York, NY, (1986): p. 140.
19. V. S. Ramachandran, *Concrete Admixtures Handbook*, Ed., Noyes Publications, Park Ridge, New Jersey, NJ. USA, (1984): p. 518.
20. T. C. Powers, L. E. Copeland, H. M. Mann, "Capillary Continuity or Discontinuity in Cement Pastes", *Journal of the P.C.A. Research and Development Laboratories*, 1 2, (May 1959): p.38.
21. N. S. Berke, "The Effects of Calcium Nitrite and Mix Design on the Corrosion Resistance of Steel in Concrete - Part 2, Long-Term Results", *CORROSION/87*, paper no. 132, (Houston, TX: National Association of Corrosion Engineers, 1987).
22. J. A. Gonzalez, S. Feliu, C. Andrade, I. Rodrigues, "On-Site Detection of Corrosion in Reinforced Concrete Structures", *Materials and Structures*, 24 (1991): p. 346.
23. G. S. Bobrowski, C. K. Nmai, S. A. Farrington, "Inhibiting Corrosion of Steel: a New Chemical Approach", Master Builders publication (Cleveland, OH).
24. C. K. Nmai, "Effect of Chemical and Mineral Admixtures on the Corrosion of Steel in Concrete" *CORROSION/92*, paper no. 201, (Houston, TX: National Association of Corrosion Engineers, 1992).
25. N. S. Berke, "The Effects of Calcium Nitrite and Mix Design on the Corrosion Resistance of Steel in Concrete - Part 1", *CORROSION/85*, paper no. 273, (Houston, TX: National Association of Corrosion Engineers, 1985).
26. N. S. Berke, K. M. Sundberg, "The Effects of Admixtures and Concrete Mix Designs on Long-Term Concrete Durability in Chloride Environments", *CORROSION/89*, paper no. 386, (Houston, TX: National Association of Corrosion Engineers, 1989).

Table 1

Properties of the fresh and hardened concrete

CF = 356 kg/m³
 Type I cement
 948 kg/m³ 13 mm Trap Rock
 848 kg/m³ fine aggregate
 W/C = 0.50

| | Mix #1 Control | Mix #2 5 L/m ³ butyl ester emulsion | Mix #3 15 L/m ³ 30% sol calcium nitrite | Mix #4 0.6 kg/m ³ DMEA* |
|----------------------------------------|-------------------|---------------------------------------------------------|-------------------------------------------------------------|------------------------------------------|
| Vinsol Resin** (mL/m ³) | 174 | 4831 | 232 | 174 |
| Air (%) | 5.8 | 4.4 | 5.8 | 6.6 |
| Slump (mm) | 76 | 89 | 51 | 89 |
| Compressive Strength (MPa) | | | | |
| 1 day | 11 | 13 | 13 | 12 |
| 7 days | 27 | 27 | 40 | 32 |
| 28 days | 38 | 36 | 53 | 38 |

* Dimethylethanolamine
 ** Air-entraining admixture

1 kg/m³=1.69 lb/yd³ 1 mL/m³=0.026 oz/yd³ 1 mm=0.04 inches 1 MPa=145 psi

Table 2

Properties of the fresh and hardened concrete

CF = 362 kg/m³
 Type I cement
 1037 kg/m³ gravel
 741 kg/m³ fine aggregate
 W/C = 0.40

| | Mix #1 Control | Mix #2 15 L/m ³ 30% sol calcium nitrite | Mix #3 5 L/m ³ butyl ester emulsion |
|----------------------------------------|-------------------|-------------------------------------------------------------|---------------------------------------------------------|
| Set-retarder* (mL/m ³) | 708 | 946 | 708 |
| Vinsol Resin** (mL/m ³) | 58 | 58 | 944 |
| Air (%) | 6.6 | 6.4 | 5.8 |
| Slump (mm) | 159 | 171 | 203 |
| Compressive Strength (MPa) | | | |
| 1 day | 26 | 27 | 25 |
| 7 days | 35 | 46 | 36 |
| 28 days | 46 | 51 | 40 |

* Lignosulfonate/glucose polymer retarder
 ** Air-entraining admixture

1 kg/m³=1.69 lb/yd³ 1 mL/m³=0.026 oz/yd³ 1 mm=0.04 inches 1 MPa=145 psi

Table 3
Cyclic Polarization Data

| | E_b (mV vs. SCE) | E_p (mV vs. SCE) |
|----------------------------------|--------------------|--------------------|
| 0.25 M NaCl | +63 | -463 |
| 10 L/m³ | +370 | -136 |
| 15 L/m³ | +386 | -126 |
| 30% calcium nitrite | | |
| 0.6 kg/m³ DMEA | +241 | -543 |
| Butyl ester emulsion | | |
| 5 L/m³ | +58 | -398 |
| 10 L/m³ | +39 | -541 |
| 15 L/m³ | +72 | -484 |

1 kg/m³ = 1.69 lb/yd³ 1 L/m³ = 0.2 gal/yd³

Table 4
Chloride Concentration after 13 months ponding
(Kg/m³)
ASTM G109

W/C=0.5

| Depth (mm) | Control | Butyl ester emulsion 5 L/m ³ | Calcium Nitrite 30% solution 15 L/m ³ | DMEA 0.6 kg/m ³ |
|------------|---------|--------------------------------------------|--------------------------------------------------------|-------------------------------|
| 9.5 | 6.2 | 6.8 | 5.7 | 12.8 |
| 29 | 4.3 | 1.4 | 2.4 | 9.0 |
| 48 | 0.65 | 0.36 | 0.36 | 2.7 |
| 67 | 0.41 | 0.18 | 0.23 | 0.3 |

1 kg/m³ = 1.69 lb/yd³ 1 L/m³ = 0.2 gal/yd³ 1 mm = 0.04 inches

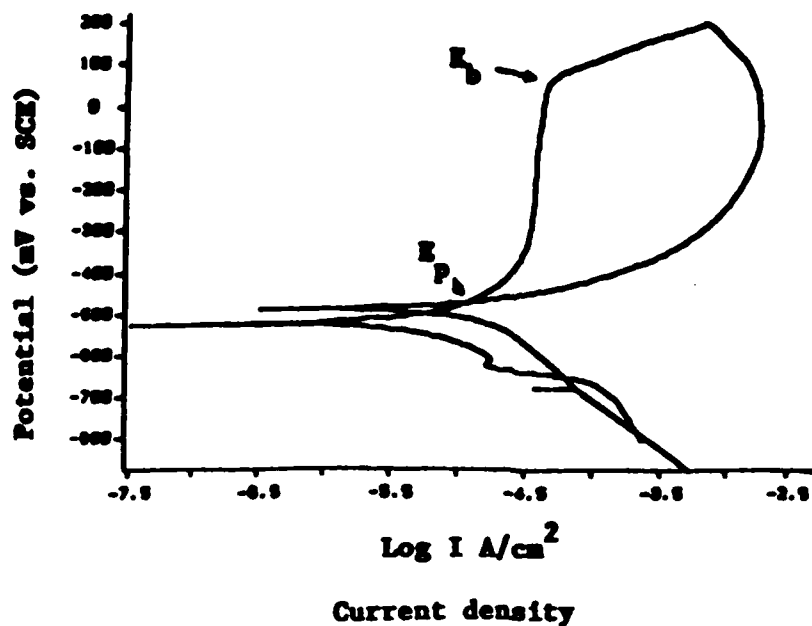


Figure 1
 Cyclic Polarization Curve for 0.25M NaCl
 Sat. Ca(OH)₂

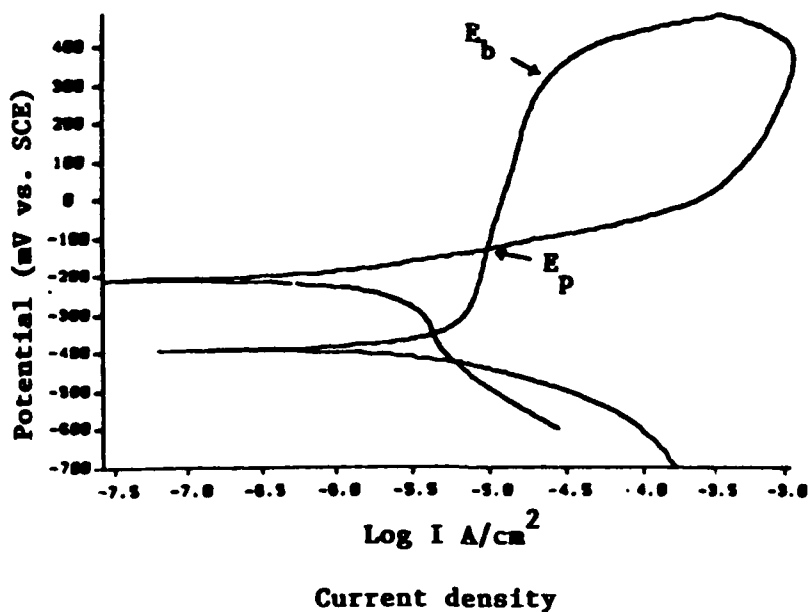


Figure 2
 Cyclic Polarization Curve for 15 L/m³ (3 gal/yd³) Calcium nitrite
 0.25M NaCl, Sat. Ca(OH)₂

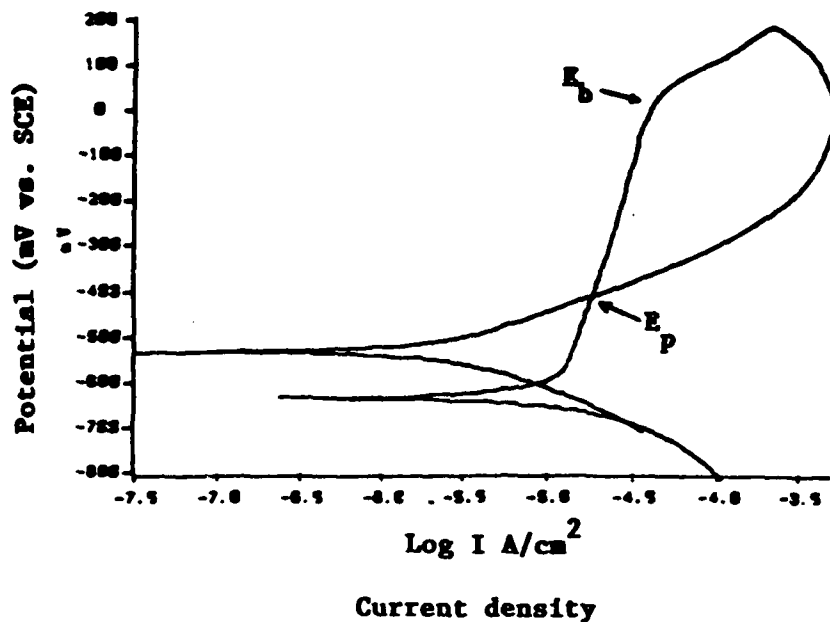


Figure 3

Cyclic Polarization Curve for 5 L/m³ (1 gal/yd³) Butyl ester emulsion
0.25M NaCl, Sat. Ca(OH)₂

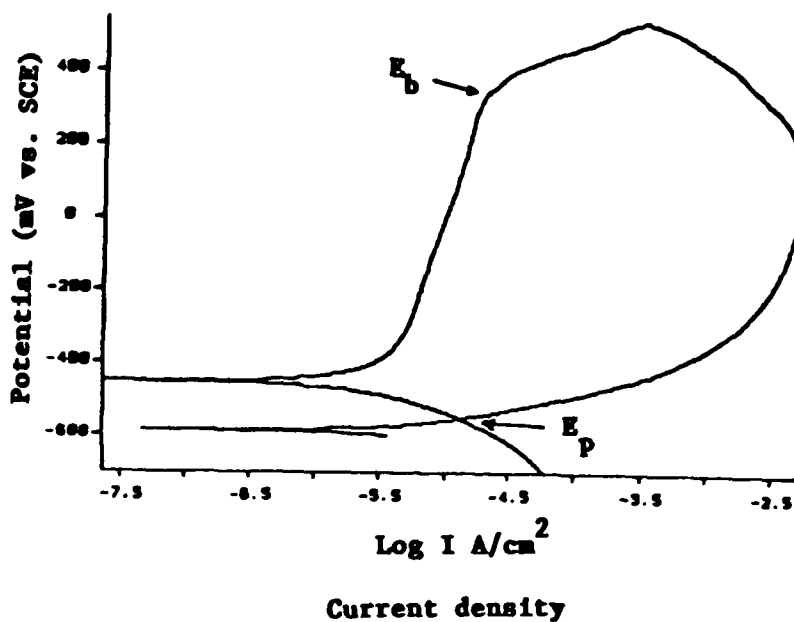


Figure 4

Cyclic Polarization Curve for 0.6 kg/m³ (1 lb/yd³) DMEA
0.25M NaCl, Sat Ca(OH)₂

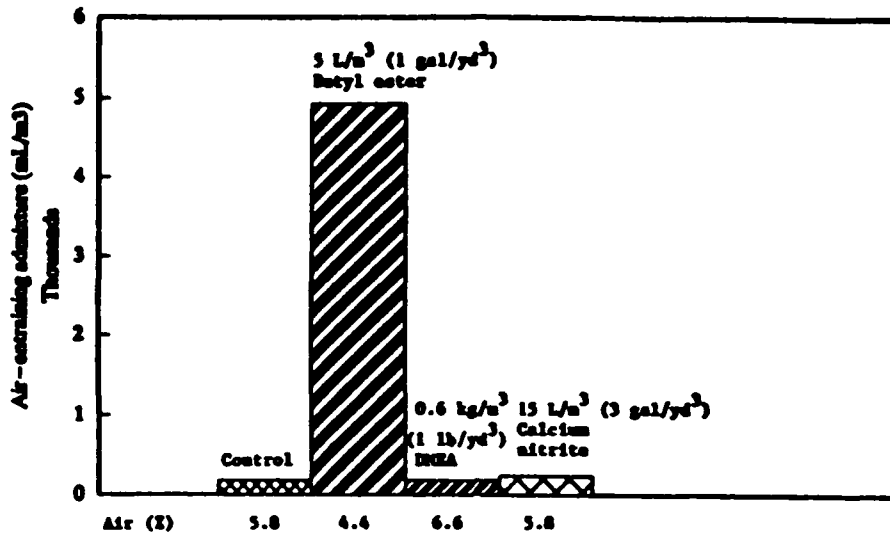


Figure 5

Amount of Air-entraining Admixture Required ASTM G 109

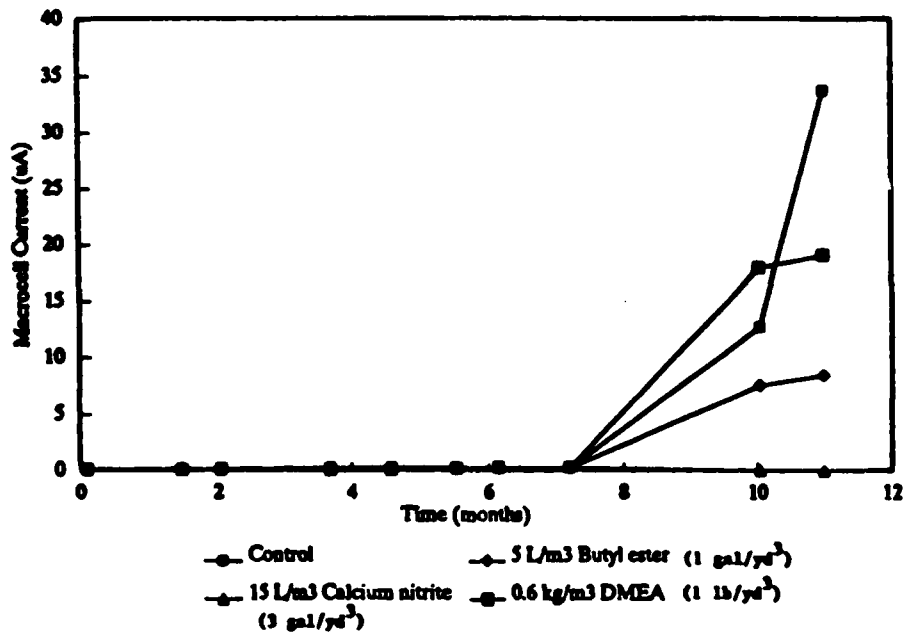


Figure 6

Macrocell Current of Minibeams ASTM G 109

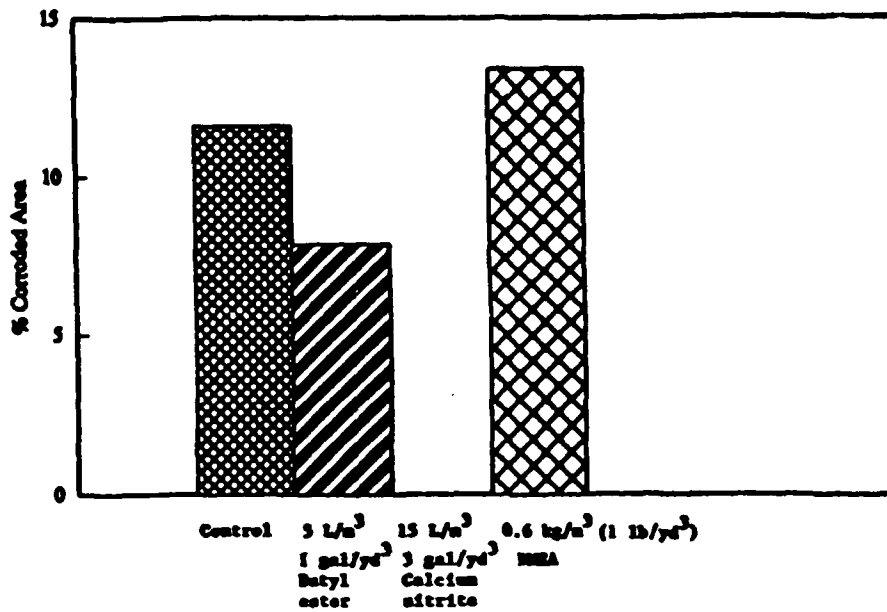


Figure 7

Percent Corroded Area after 13 Months Ponding
ASTM G 109

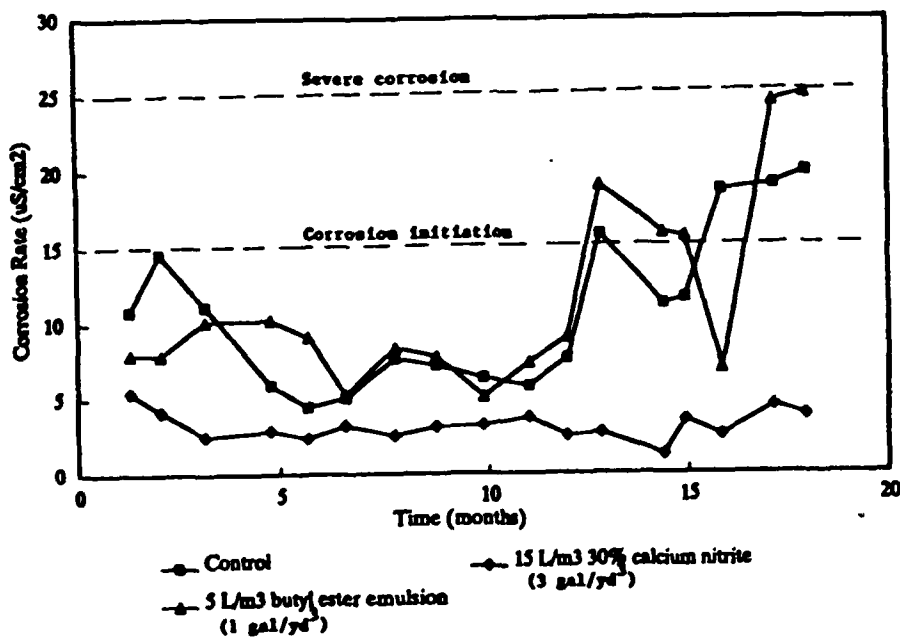


Figure 8

Corrosion Rate of Lollipops
4.7 kg/m³ admixed chloride
(1 lb/yd³)

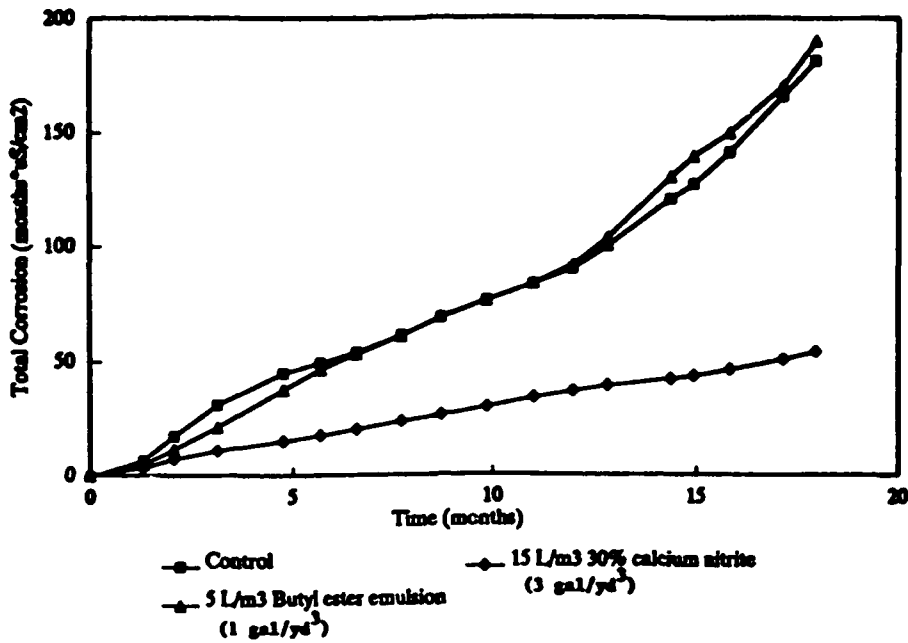


Figure 9

Total Corrosion of Lollipops

4.7 kg/m³ admixed chloride
(8 lb/yd³)

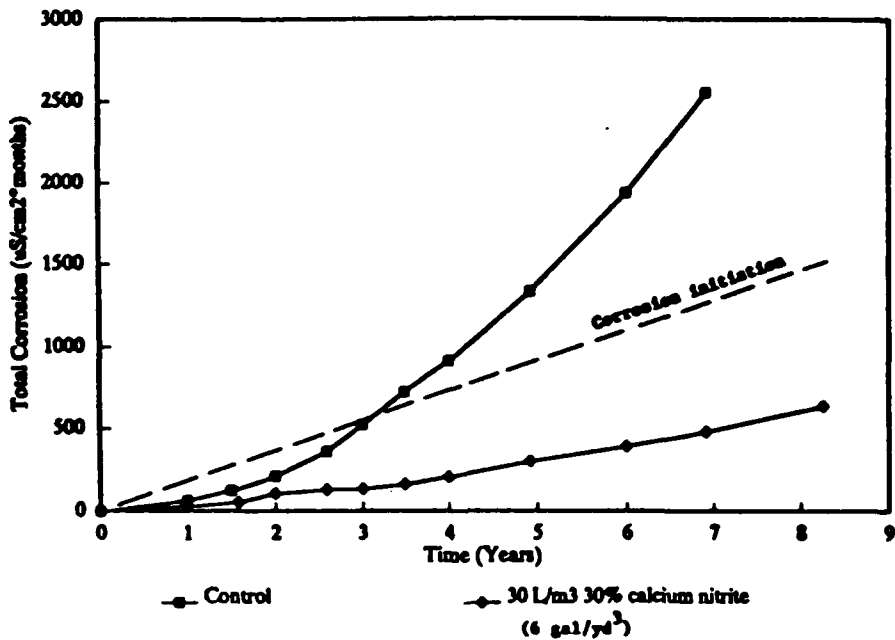


Figure 10

Total Corrosion of Lollipops

W/C=0.34 CF=397 kg/m³(670 lb/yd³)

Cathodic Protection of New Steel Reinforced Concrete Structures

Aladar Tvarusko
ELTECH International Corporation
Geneva Branch
18, chemin des Aulx
1228 Plan-les-Ouates/Geneva
Switzerland

Abstract

Installation of cathodic protection, CP, into new, chloride-free steel reinforced concrete structures should be considered as preventive maintenance in a hostile environment where intermittent or continuous chloride ingress into concrete will occur during the lifetime of the structure, e.g. in marine environment, through application of de-icing salts, in the presence of brackish groundwater close to surface. The decision on the incorporation of cathodic protection into new structures should be taken during the early stages of cooperative design by construction and CP engineers. The installation of strong, but flexible, activated titanium anodes of long lifetime directly onto rebars before concrete pouring is advantageous from both technical and economic viewpoint. Of the more than 500,000 m² total surface area protected by activated titanium anodes, 113,000 m² is on new/quasi new structures, predominantly on viaduct decks and curbs in Italy. Several activated titanium anode mesh and ribbon installation techniques are described for a variety of steel reinforced concrete structures.

Key Terms: Cathodic protection, new steel reinforced concrete structures, activated titanium anode mesh/ribbon, anode installation techniques, preventive maintenance..

Introduction

Reinforced concrete structures are designed for a lifetime of up to around 100 years and are known to have lasted for 50 to 80 years. Steel reinforcement, rebar, embedded in concrete, a complex composite material, is normally passivated in its alkaline environment. However, in the presence of chlorides, the natural passivity of steel is destroyed and the rebar corrodes leading to concrete deterioration in considerably shorter time, sometimes as short as 5 years.

The corrosion products have greater volume than the steel rebar leading to large tensile stresses on the concrete (pressures up to 32 MPa were measured)¹ and inevitable concrete cracking and spalling. The corrosion risk depends, among others, on content and distribution of chlorides, quality, state, and cover of concrete, environmental factors: wetness, water content and their distribution, temperature. The main culprit, chloride's source may be a) the (un)intentional incorporation, as additive, or via brackish water or salt-laden aggregate, and/or b) an ingress from the environment: marine (sea water and/or spray), soil (groundwater), or seasonal (de-icing salt).

There are several rehabilitation techniques for old reinforced concrete structures of which only the cathodic protection of rebars was found to stop corrosion regardless of the chloride and water (wetness) content of concrete.

Application of cathodic protection to new chloride-free steel reinforced concrete structures is to be considered as a preventive maintenance in a hostile environment where intermittent or continuous chloride ingress into concrete will occur during the lifetime of such structures². Some examples are: de-icing salt a) spraying onto concrete bridge decks or roadbeds of tunnels b) splashing onto bridge columns, walls, c) leakage through cracks in blacktop/membrane or through deteriorated joints into deck/roadbed or onto substructure; marine environment a) submerged area, b) tidal/splash zone, c) salt-laden atmosphere (mist, sand) on/around concrete structures such as bridges, offshore platforms, piers, terminals, wharves, sea water cooling, buildings; in/above saline groundwater: underground concrete structures/installations, substructures, basement and lowest floors of buildings, industrial installations, etc.

The decision to incorporate cathodic protection into steel reinforced concrete structures should be taken very early, preferably during the design stage of the structure. The designers of the structure and cathodic protection system should work closely toward a "construction friendly" and cost-effective solution best suited for the structure under the given conditions and environment.

The anode could be installed onto the concrete surface, such as conductive paint, zinc, but such systems a) probably require special formation/preparation of the new concrete surface, b) usually are not suited for wet concrete and in the presence of water on the concrete surface, c) need occasional maintenance, repair of damaged anode/protective surface layer, and d) have the anode reaction zone at the concrete/anode interface just below the outer/protective surface layer.

It is preferred to install a dimensionally stable, strong but flexible anode with long lifetime directly on to the reinforcing steel or into the rebar cage before concrete pouring. Thus, there is no need for surface preparation and no joint in the concrete (single or briefly interrupted concrete pouring). The activated titanium anodes are the most suited for new concrete structures. Their installation onto the reinforcing steel and/or into rebar cage a) is simple, b) hardly interferes with the construction techniques used (concrete pouring, vibrating) and c) is cost effective.

There are three principal requirements for the cathodic protection of steel reinforced concrete structures (new or old) to function properly: 1) the steel reinforcement must be electrically continuous (usually no problem in new structures), 2) a contact between rebar and other steel elements and activated titanium anode must be absent before, during, and after concrete pouring or overlaying, 3) the electrical resistivity of concrete must be below 50,000 ohm.cm. at around 20°C (usually it is well below).

For the design of the cathodic protection, CP system, it is imperative to have the related drawings of the concrete structure, especially dimensions, details, positions of rebars and other embedded steel parts. The choice of anode depends, among others, on the nature of concrete structure, steel density, required protective current density, construction and concreting techniques used, concrete quality, especially cover, environment.

The activated titanium anodes are available as a) expanded mesh of various diamond and strand dimensions and b) ribbon of appropriate thickness and width.

This paper describes the application of proprietary activated titanium anodes, ELGARD™⁽¹⁾, to a variety of new and quasi-new concrete structures.

Anode Mesh Installation

The choice of the activated titanium anode mesh installation and concrete pouring technique will be affected by the nature of the concrete structure/element, among others: orientation (horizontal, vertical, sloping), dimension (length, width, depth), rebar size, quantity and distribution (presence, size of cage[s]) as well as concreting conditions, such as, concrete quality, pumping or dumping, distribution over the surface, compacting (vibrators), access.

Activated titanium anode mesh can be installed directly onto the rebars using concrete spacers or suitable plastic fasteners³, such as horizontal rebar clips, tie-clips or push-on fasteners. In order to prevent a contact (electric short) between the rebars and anode mesh (during the pouring, vibrating, and curing of concrete), a plastic spacer mesh is placed directly onto rebars after the installation of plastic fasteners, as shown in Figure 1, and the activated titanium anode mesh is subsequently fastened to them. It is obvious that such an arrangement will prevent the compaction of poured concrete by vibrators below the installed plastic spacer/anode mesh on horizontal structure elements such as decks of bridges, wharves, parking garages. There is really no hindrance on vertical elements, e.g., columns, walls, coping, as shown in Figure 2, but the vibrating must be done with care. The presence of mesh or mesh strips must always be on the mind of the crew doing the vibrating.

In the simplest installation technique for especially large horizontal surfaces, such as decks, the concrete is pumped in up to a height of minimum 13 mm, practically around 25 mm, above the rebars and levelled to the selected height. The activated titanium anode mesh can be prefabricated into a "carpet" of desired dimensions with spotwelded conductor bars and suitable attached cables. Such rolled up activated titanium anode mesh "carpets" are best suited for smaller areas (ca. 3 x 10 m). The concrete is poured onto the unrolled anode mesh to the required height and its surface is finished to the desired quality.

On larger horizontal areas (e.g. 5 x 30 m), the concrete is poured as described above. As soon as one can walk on the fresh concrete (1-3 hr), or without any delay, the concrete surface is roughened, e.g., by rake, the activated titanium anode mesh is rapidly rolled onto the wet concrete, and a current conductor bar is spotwelded to the anode mesh^{3,4}. On a soft concrete surface, planks are placed onto the unrolled activated titanium anode mesh, as shown in Figure 3; this prevents the feet sinking into the concrete and pushing the anode mesh against the rebars creating an electric short. In both cases, the concrete is immediately pumped onto the activated titanium anode mesh up to the required height which is followed by the usual finishing operation. The installation of activated titanium anode mesh is rapid, and ca. 14 m²/man-hour of mesh installation rate was obtained on a bridge deck. Obviously, the bulk and "overlay" concrete composition is the same, and there is no solid/wet interface between the two concrete pours. It is to be noted that such an installation has been in operation for 5 years⁵.

⁽¹⁾ ELGARD™ is a trademark of ELGARD Corporation

Similar technique, practically a single concrete pouring, was used for the prefabrication of new bridge deck units (1.9 x 10 m) to be installed subsequently onto new steel beams. The prefabricated welded rebar deck unit was placed into a special frame resting on an appropriate steel platform. Concrete was poured up to the predetermined height, vibrated, levelled and its surface roughened, as in all similar techniques. After the installation of the prefabricated activated titanium anode mesh "carpet", concrete was immediately poured onto, and spread out up to the final height and surface finished, as shown in Figure 4. The anode mesh installation rate is around 16 m²/man-hour. The activated titanium anode mesh and titanium current conductor bar, extending from the prefabricated bridge deck units, are interconnected after the placement of deck units onto the steel substructure and concreting of the gaps.

It is to be mentioned that all rebar connections, placement of reference electrodes, sensors, cables, obviously must be done before the concrete pouring.

The majority, (95%), of the new/quasi-new steel reinforced concrete structures with cathodic protection using activated titanium anode mesh/ribbon (113,000 m²) are bridge decks, mainly post-tensioned, and curbs on the Italian Autostrada, Torino-Frejus, and Aquila-Gran Sasso⁶. The decision to incorporate cathodic protection was made after the design, start of prefabrication and installation of box girders. Thus, the activated titanium anode mesh/ribbon had to be incorporated during various stages of the construction of the viaducts. Some of them were already standing with or without concreted New Jersey-type curbs. A large number of box girders were prefabricated and stored for installation onto pillars being constructed. Other box girders were prefabricated and appropriate activated titanium anode mesh and overlay were installed in a separate building erected next to the box girder production hall.

In spite of this large variation of conditions, the installation technique remained practically constant for the deck: a) roughening of the concrete surface for good adhesion of the overlay, b) attachment of the activated titanium anode mesh to the roughened concrete surface with plastic fasteners, and c) spraying of a 10-15 mm thick acrylic polymer modified cementitious overlay onto appropriately prepared concrete surface. Numerous roughening techniques were used: from mechanical grinding through grit blasting to water jet. The same installation technique was used for concreted curbs. However, anode ribbon was installed into a large number of curb rebar cages with subsequent single concrete pouring (see later).

Figure 5 shows the overlay spraying onto the installed activated titanium anode mesh attached to the roughened concrete deck surface of a prefabricated box girder. Figure 6 shows the activated titanium anode mesh installed onto the curb and walkway as well as the cementitious overlay on both parts with the required surface finish. The titanium current conductor bar from the curb goes over the walkway to the bridge deck and finally through it at an appropriate location. It is attached to a cable inside the box girder where all cables, trunking and instrumentation are located.

The prefabricated box girders are installed onto columns. Their curb and walkway rebar cages are exposed and the concreting takes place in-situ. Thus, the activated titanium anode, preferably ribbon could be installed onto the rebars before the placement of the formwork and concrete pouring (see later). It is obvious that this method of activated titanium anode installation will be more economical and technically superior, i.e., absence of two concrete layers of probably different compositions and their interface.

Anode Ribbon Installation

Due to its nature, the activated titanium anode ribbon can be advantageously used for the cathodic protection of new, narrow and long concrete structures, such as beams, walls, columns, barriers, swimming pools. The anode ribbons, well attached to the rebars through plastic fasteners hardly interfere with the vibrating of concrete and rarely touch the rebar(s) causing a short-circuit. It is already a well-accepted practice to contact each ribbon with a separate short cable; thus an eventual short-circuit can be easily identified and rectified by disconnecting the appropriate cable if it cannot be eliminated otherwise. Figure 7 shows the individual cable connections and anode ribbons installed into the rebar cage of a swimming pool wall and overflow. It also shows this concrete structure after the removal of the formwork.

The activated titanium anode ribbon is well-suited for the CP of curbs formed in-situ on viaducts and bridge decks. The anode ribbon is easily installed with plastic fasteners onto rebars in segmented cages, as shown in Figure 8. The connecting cables from the anode ribbons are collected into a junction box already embedded in the concrete base. The installed activated titanium anode ribbons do not interfere with the placement of railing attachment base on the top of the rebar cage. The formwork is easily placed over the rebar cage and hardly anything hinders the concrete pouring and vibrating. In the background of this photo the finished curbs are visible on the parallel viaduct.

It may be advantageous to install activated titanium anode mesh strips² in certain steel reinforced concrete structures located in areas with brackish groundwater, such as multistorey buildings with numerous beams, columns, walls, stairways, especially in their basements and lower floors.

References

1. A. Tvarusko, J.E. Bennett, "Practical Aspects of Cathodic Protection of Steel Reinforcement in Concrete with a Proprietary Activated Titanium Mesh Anode", in Proceedings of 2nd International Conference 'Deterioration and Repair of Reinforced Concrete in the Arabian Gulf', Vol.1, p. 139 (Manama, Bahrain: Bahrain Society of Engineers, 1987).
2. A. Tvarusko, "Cathodic Protection of Various Concrete Structures Worldwide", CORROSION/93, paper No. 335 (Houston, Texas: National Association of Corrosion Engineers, 1993).
3. A. Tvarusko, "Cathodic Protection of Rebars in Old and New Concrete Structures", 'Evaluation and Rehabilitation of Concrete Structures and Innovations in Design', Proceedings ACI International Conference, Hong Kong, 1991, SP-128, p.359 (Detroit, MI, American Concrete Institute, 1991).
4. M. Romagnolo, S. Ferrari, M. Grandi, Autostrade XXX No. 4 (1988); p.77.
5. B. Bazzoni, L. Lazzari, M. Grandi, "Cathodic Protection on Highway Bridge Deck: Five Year Experience", UK Corrosion '92, Vol.3, (Leighton Buzzard, Bedfordshire, Great Britain: The Institute of Corrosion, 1992).
6. M. Grandi, L. Lazzari, "Cathodic Protection Experiences on Highway Bridge Decks", in Proceedings of 11th International Corrosion Congress, 'Innovation and Technology Transfer for Corrosion Control', Vol 2, p. 2.481, (Milano, Italy, Associazione Italiana di Metallurgia, 1990).



FIGURE 1
Plastic spacer mesh and push-on fasteners on rebar ready for placement of activated titanium anode mesh.

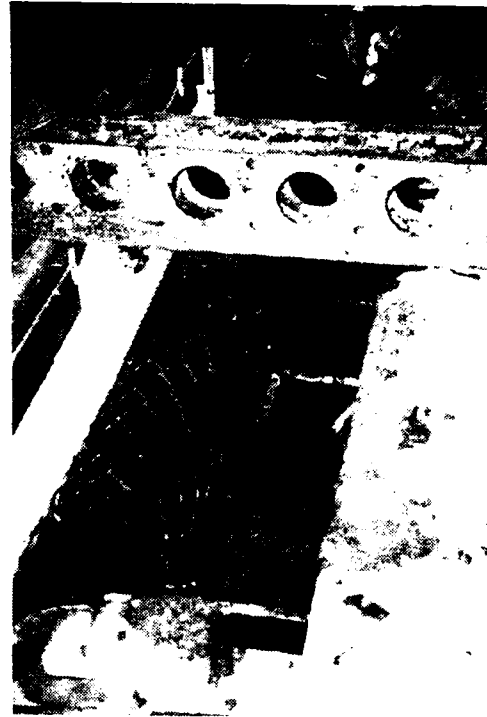


FIGURE 2
Use of vibrators on both sides of a vertical plastic spacer/activated titanium anode mesh during concrete pouring.

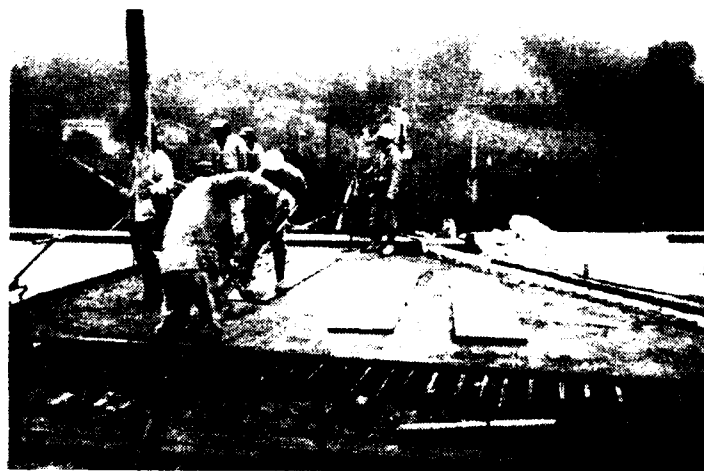


FIGURE 3
Concrete is spread out over unrolled activated anode mesh during an interrupted "single" concrete pouring.



FIGURE 4
Spreading and surface finishing of concrete over installed activated titanium mesh during the prefabrication of a bridge deck unit.

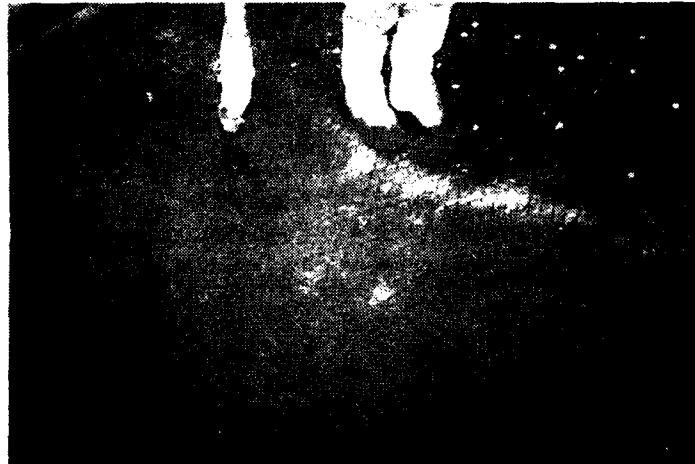


FIGURE 5
Spraying of a thin acrylic polymer modified cementitious overlay onto an activated titanium anode mesh installed on the deck of a box girder.



FIGURE 6
Installed activated titanium anode mesh on a curb and walkway partially covered by a cementitious overlay.

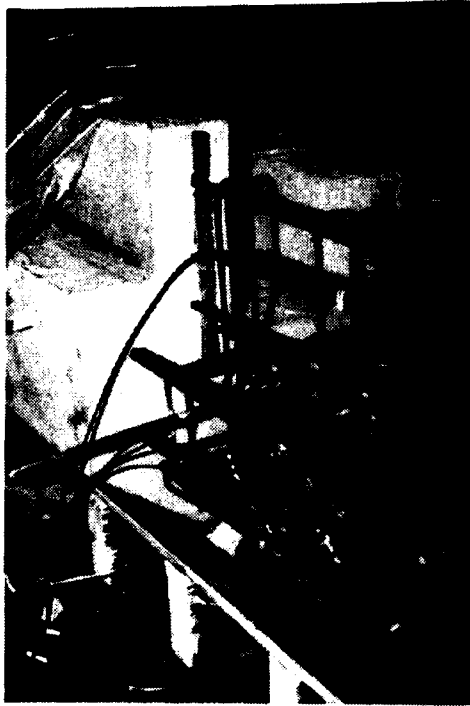


FIGURE 7

Activated titanium anode ribbons in the rebar cage of, and view of, a swimming pool wall and overflow.

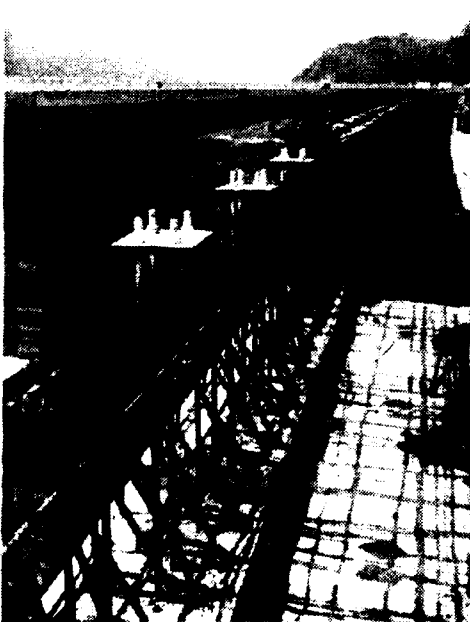


FIGURE 8

Viaduct curb with installed activated anode ribbon and formwork.

MEASUREMENT OF CORROSION RATE OF REINFORCING STEEL AND ELECTRICAL RESISTIVITY OF CONCRETE USING GALVANOSTATIC STEADY STATE POLARISATION TECHNIQUE

V. Lakshminarayanan
Raman Research Institute
Bangalore 560080, India

P.S.Ramesh
Department of Civil Engineering,
Bangalore University,
Bangalore 560056, India

S.R.Rajagopalan
Materials Science Division
National Aeronautical Laboratory
Bangalore 560017, India

Abstract

Measurement of corrosion rate of reinforcing steels in concrete using steady state techniques is beset with the problems of large ohmic drop arising out of the concrete resistance. In this work, a simple and elegant technique for correcting this ohmic drop component from the measured polarisation data has been proposed and tested. Using the corrected values from the galvanostatic steady state technique, the corrosion rates have been evaluated for High tensile steel (HTS), mild steel (MS) and High yield strength deformed steel (HYSD) reinforced in different grades of concrete mixes. Measurements were conducted on specimens cured for one day as well as 28 days. The results indicate that the corrosion rates of different steel specimens are largest in a mix of cement, sand and aggregate ratio of 1:2:4 followed by 1:3:0 and 1:1:2 mixes. The effect of adding chloride ions in the concrete mix has been studied and the results show that for 28 days cured specimens, the corrosion rates of different steels do not significantly increase in the presence of admixed chloride ions. In contrast, under similar conditions, there is a large increase in corrosion rate in the case of one day cured specimens. Measurements were also carried out with several inhibitors such as sodium nitrite, sodium chromate and sodium lauryl sulphate added to the concrete mix. It is also shown that the measured electrical resistivity can be correlated with permeability and pore size distribution of concrete. Since it is the permeability which controls the extent of ionic intrusion which in turn causes corrosion of reinforcing steel, a knowledge of resistivity is quite useful in evaluating the corrosion resistance of reinforced steel.

Key terms: Corrosion rate, galvanostatic charging, concrete, inhibitors
Chloride intrusion, resistivity

I. INTRODUCTION

The p^H of hydrated cement is about 13 at common W/C ratios. At this alkaline range, a passive film is formed on the steel surface which protects it from degradation. This film breaks down under certain conditions like carbonation and attack by chloride ions which penetrate the concrete leading to active corrosion. It is therefore of interest to study the effect of different mix proportions and additives on the corrosion rate of reinforced steel in different environments. In this paper, the results of such a study are presented and discussed. In addition, the resistivity values of concrete are measured using a novel method known as galvanostatic charging technique.¹ This technique is simple and elegant while also minimising the electrode polarisation during measurement.

II. EXPERIMENTAL

A. Instrumentation

The corrosion rates and polarisation resistance values are measured using steady state galvanostatic polarisation technique. Fig 1(a) shows the schematic experimental set-up. A home made potentiostat is used in the galvanostat mode. The specimen (Fig 2) which forms the working electrode is kept with the entire concrete portion immersed in the electrolyte. This is surrounded with a stainless steel sheet acting as a counter electrode and positioned concentrically about 20 mm from the specimen. A saturated Calomel electrode is used as a reference electrode in all the cases along with a suitable salt bridge .

For polarisation resistance measurement, the polarisation range is confined within 20mV from the rest potential on either direction. For the measurement of corrosion rate, the Tafel extrapolation of the anodic curve is carried out with the straight line portion located at a potential $> 60\text{mV}$ from the rest potential. All the potential values are corrected for IR drop which is calculated from the measured uncompensated resistance using the galvanostatic charging technique described below.

In this technique, a small duration current pulse of amplitude I is imposed on the steel-concrete-solution interphase using a galvanostat and the potential response with respect to the sat. calomel electrode was displayed on an oscilloscope. The initial step is equal to the ohmic drop IR_u , from which R_u can be obtained. The current pulse and potential response are schematically shown in Fig. 1(b).

B. Systems studied

- (i) Types of Steel used : (a) High tensile steel (HTS)
(b) Mild steel (MS)
(c) High yield strength deformed steel (HYSD)

- (ii) Types of mix proportion : (a) 1:2:4 (M15): w/c = 0.5
 (b) 1:1:2 (M25): w/c = 0.4
 (c) 1:3 (Mortar) with water based on cement consistency 28%
- (iii) Types of electrolytes : (a) SAT Ca(OH)₂ + 0.1M NaOH
 (b) 0.1 M H₂SO₄ +1M Na₂(SO₄)
 (c) 3% NaCl
- (iv) Curing periods : 1 day ,3 days ,28 days
- (v) Additives used : (a) Calcium chloride (b) Sodium Nitrate
 : (c) Sodium Stannate (d) Stannous Nitrite
 : (e) Sodium lauryl Sulphate

C. Preparation of specimen

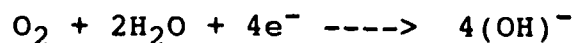
The steel rods used for embedment in concrete was first cleaned thoroughly to remove all rust and oxide film using rough emery and then dipped in 1:1 hydrochloric acid, cleaned, dried and finally degreased in acetone.

A typical specimen used for corrosion measurements is shown in Fig. (2). A particular length (usually 30 mm) was exposed and the remaining portion was made non-conductive using PVC adhesive tape tightly wrapped with several layers on the steel to ensure no seepage of electrolyte into the unexposed portion. An epoxy and PVC tape seal was also used on either end (about 35mm) of the concrete.

The concrete, with the reinforced steel packed in the mold is kept immersed in distilled water for curing after 24 hours of preparation of the sample. The curing is continued for 28 days and then the samples are taken out and kept immersed in the respective electrolyte for 24 hours before performing the measurements. As for the one day cured specimens the samples are kept immersed in water for 24 hours and in the respective electrolyte for 1 hour. Three specimens are prepared under each condition and the results presented are the average of these three values. For the measurement of resistivity change with time of curing, cylindrical specimens were used with full length of the rod exposed to concrete. For a study of resistivity variation with thickness, a tetragonal block of concrete with a square base and constant height (50 mm) was used (i.e., $l = b = h$).

III. RESULTS AND DISCUSSIONS

It is well known that the cathodic reaction occurring during the corrosion of steel in concrete is,



In other words, the system needs supply of oxygen for corrosion to take place under active conditions, while for the formation and continuation of protective passive layer presence of oxygen is necessary. In any steady state polarisation method, applied to steel in concrete, a limitation arises due to slow rate of oxygen diffusion. This leads to inaccuracies in corrosion rate measured by polarisation technique.

For small polarisations, the concentration polarisation is small and the measured polarisation resistance R_p can be considered to be quite accurate. The measured corrosion rate, however, may not be quite correct but yet provides valuable information in comparative evaluation under different environmental conditions.

(A) Study under different electrolytes

The three electrolytes used for measurement represent different environmental conditions to which reinforced steel is subjected to. Sat. $\text{Ca}(\text{OH})_2 + \text{NaOH}$ represents the real world situation of pH 13, 0.1 M Sulphuric acid represents the conditions prevailing due to so-called 'acid rains' in industrial atmosphere and 3% NaCl simulates the marine environment.

From Table 1 it can be seen that for 28 days cured specimen, the corrosion rates of all the steels follow the same trend in different electrolytes, viz., i_{corr} in $\text{Ca}(\text{OH})_2 < \text{in } \text{H}_2\text{SO}_4 < \text{in NaCl}$. Corrosion rate of all the three steels are more or less same in calcium hydroxide. The lowest corrosion rates observed in $\text{Ca}(\text{OH})_2$ is due to the absence of any aggressive ions like chloride and sulphate which tend to disrupt the natural positive film. However, in H_2SO_4 the corrosion rate is higher. This is because of the lowering of p^{H} by H_2SO_4 and consequent active dissolution of the metal. The highest i_{corr} in NaCl confirms the generally observed pattern where diffusion chloride of ions break down the passive layer of the steel surface. R_p values also show the same trend.

(B) Study in different concrete mixes

Table 2 presents the results obtained for three different concrete mix proportions. In all the cases NaCl has been used as the electrolyte as it provides the most aggressive environment among the three electrolytes.

It can be seen that the lowest corrosion rate is obtained in M25 followed by mortar and M15. It is obvious that M25 with the highest cement-sand ratio has the lowest porosity. This is because, at a larger cement to sand ratio, the pores are filled with the more hydrated cement gel which decreases the porosity. Therefore diffusion of Cl^- ions through the pores is limited whereas in M15 due to more voids, the corrosion rate is the highest. Mortar with more impermeable cover than that of M15 has a corrosion rate intermediate between that of M15 and M25.

The corrosion rates of different steels do not show much variation in different concrete mixes. Even though HTS shows higher corrosion rate in M15 compared with mortar and M25, the same is not reflected in other mixes. These results indicate that the nature of steel and its composition are not very important factors which lead to corrosion over a long period of time.

(C) One day cured specimens

The results of study in two different electrolytes are shown in Table 3. It can be seen that corrosion rate is generally higher in NaCl electrolyte as expected. For different steels however, the corrosion rate was least in HTS and highest in HYSD and intermediate value in MS, a trend, which was not observed in the case of 28 days cured specimens. The presence of chromium offering protection in HTS may be a factor in reducing the corrosion rate in HTS steel. This may not be a significant factor in 28 day cured specimens.

(D) Effect of chloride ions

CaCl_2 is being used in concrete as an accelerator for early development of strength and earlier setting time. CaCl_2 acts as a catalyst in the hydration of C_3S and C_2S .

The results of corrosion rate and R_p values for 28 day cured specimen in NaCl electrolyte for different mix proportions with 3.5% CaCl_2 by weight are tabulated in Table 4.

Even though an increase in corrosion rate has been observed in a few cases in M25 mixes for all the steels, it is not quite significant to be attributed to the effect of admixed chloride. In fact, there is a decrease in corrosion rate in the case of HTS steel. A repeat experiment showed the same trend. This shows, for 28 day cured specimens, the admixed Cl^- ions are not quite effective in breaking the passive layer.

The effect of admixed chloride ion on one day cured specimens has been studied in $\text{Ca}(\text{OH})_2 + \text{NaOH}$. As can be seen from the Table 5, the corrosion rates for one day cured specimens with admixed chloride have increased by 4 to 6 times in almost all cases compared to specimens with no admixed Cl^- ions. R_p values also showed similar trend.

When CaCl_2 is added as an admixture, calcium oxychloride hydrate is formed, which accelerates the hydration of cement. Moreover, tricalcium aluminate (C_3A) forms calcium chloroaluminate hydrates.² It is evident that majority of CaCl_2 is present as a complex. Hence Cl^- ions in these complexes cannot be extracted by water. Hence the meagre amount of Cl^- ions cannot induce breakdown of passivity. It is evident that in one day cured specimens not all CaCl_2 gets complexed as in the case of 28 day cured specimens. It is these free Cl^- ions which cause greater corrosion in one day cured specimens. It is evident therefore, that Cl^- ions that diffuse from outside that are more

aggressive than admixed chloride in causing corrosion of reinforced steel. This observation is also substantiated by other works.³

(E) Effect of Corrosion Inhibitors

Corrosion inhibitors are added in concrete mix to protect the steel from corrosion. In this work, sodium chromate and sodium nitrite⁴ and sodium lauryl sulphate have been used as corrosion inhibitors. The amounts of added inhibitors are mentioned in Tables 6-9.

The results of corrosion rate measurements for steel in the presence of sodium chromate for 28 day cured specimens in sodium chloride electrolyte is shown in table 6. The results show that, even though the inhibition is evident only in the case of HTS, there is no significant inhibition in other steels. This shows that in the presence of chloride ions which disrupt the protective film of chromium oxide (Cr_2O_3), there is no inhibition of steel corrosion by chromate addition.

However, it has been found that sodium nitrite is an effective inhibitor of steel corrosion in NaCl electrolyte as can be seen from Table 8. The same trend is observed with sodium lauryl sulphate which incidentally is also used as a porefiller.⁵

Some workers⁴ have suggested using one day cured specimens for inhibitor studies. From the results presented in Tables 7 and 9 it can be seen that the corrosion rates in Sat $\text{Ca}(\text{OH})_2 + \text{NaOH}$ is not significantly decreased even with the addition of inhibitors which were found effective in 28 day cured specimens. The results suggest that measurements conducted with one day cured specimens cannot be used to assess the inhibitor efficiency of the additives.

(F) Resistivity Measurements

The measurement of electrical resistivity of concrete is quite important in evaluating the strength and durability of concrete in addition to the corrosion properties of reinforcing steel. This is because electrical resistivity is indicative of permeability⁶ and pore distribution in concrete. The variation in the resistivity of cement with time is also related to hydration of cement paste and is indicative of the rate at which the chemical reactions occur within the paste.

It has been shown by us¹ that the galvanostatic charging technique provides a simple and elegant method of measuring the electrical resistivity of concrete. The details of the method and instrumentation had been described elsewhere. Fig. (3) shows a typical resistivity curve plotted against the number of days of curing. It can be seen that the resistivity increases steeply at the beginning and asymptotically approaches an upper limit after 25 days of curing. This variation follows a hyperbolic fit of the form

$$y = x/(ax + c)$$

where the constants a and c are found to be characteristic of any particular mix proportion. Since the resistivity of concrete is an indicator of permeability and pore distribution, it is also a measure of compressive strength of concrete. The compressive strength values reported in literature⁵ when plotted against the number of days of curing is found to follow a similar hyperbolic expression.

We have carried out the resistivity measurements on tetragonal concrete blocks with square base ($l = b \neq h$) but with a constant height of 50 mm. Two mild steel plates were embedded at either end of the concrete specimen. The distance of separation (l) is varied for each specimen and the resistivity values are shown in Table 10. The results show that at constant height and at different cover thicknesses the resistance actually shows a slight decrease with increasing cover thickness. The resistivity of course shows a similar trend.

It must be emphasised that for a highly inhomogeneous medium like concrete, with different conduction paths, no simple mathematical expression can be used to calculate resistivity from the measured resistance. This is because the local field intensification or field distortion introduced by different materials of different conductivity must be taken into account which makes any mathematical development quite complex. However, the calculated resistivity values assuming a simple homogeneous, isotropic medium can still be used to gain an understanding of the various phenomena contributing to the porosity, durability and strength of concrete.

IV. SUMMARY AND CONCLUSIONS

Corrosion rates of different steels used for reinforcement in concrete such as HTS, MS, HYSD had been measured in different electrolytes and concrete mixes using steady state galvanostatic polarisation technique after correcting for the ohmic drop. The effect chloride ions on the corrosion rates had been investigated. It was found that the chloride ion intrusion from the electrolyte increased the corrosion rate of steel while the admixed chloride did not significantly affect the rate. A new method of measuring the electrical resistivity of concrete was proposed and tested. It was found that the electrical resistivity of concrete increases in a hyperbolic manner with number of days of curing. This conforms to the pattern observed in the case of compressive strength variation with time .

References

- 1 V.Lakshminarayanan, P.S.Ramesh and S.R.Rajagopalan, Mag. Conc. Res., 44 (1992): 47.
- 2 V.Ramachandran, 'Calcium Chloride in Concrete', (London: Allied Science Publishers, 1976), p.59.
- 3 J. Corbo and H.Farazam, ACI Materials Journal, Sept. (1989):498.
- 4 A.M.Rosenberg, J.M.Gaidis, T.G.Kossivas and R.W.Previte, ASTM STP, 629 (1977): 89.
- 5 A.M.Neville, 'Properties of Concrete', ELBS Longman (1981).
- 6 N.R.Buenfeld and J.B.Newmann, Mag. Concr. Res., 36 (1984):67

Table 1 : Corrosion rate($\mu\text{A cm}^{-2}$) and polarisation resistance(ohm cm^2) of different steels in M15 mix in different electrolytes (28 days curing)

| Electrolyte | HTS | | MS | | HYSD | |
|----------------------------------------------------------------------|-------------------|-------|-------------------|-------|-------------------|-------|
| | i_{corr} | R_p | i_{corr} | R_p | i_{corr} | R_p |
| NaOH+sat.Ca(OH) ₂ | 0.34 | 59.73 | 0.26 | 56.89 | 0.32 | 68.90 |
| 0.1M H ₂ SO ₄ +Na ₂ SO ₄ | 4.38 | 3.10 | 2.73 | 6.33 | 0.35 | 49.40 |
| 3% NaCl | 7.17 | 1.90 | 4.00 | 9.23 | 3.40 | 8.34 |

Table 2 : Corrosion rate ($\mu\text{A/cm}^2$) of different steels in different concrete mixes in NaCl Electrolyte(28 day cured specimens)

| Mix (cement:sand:aggregate) | HTS | MS | HYSD |
|-----------------------------|------|------|------|
| 1:2:4 (M15 Mix) | 7.17 | 4.00 | 3.40 |
| 1:3 (Mortar Mix) | 0.45 | 0.44 | 0.60 |
| 1:1:2 (M25 Mix) | 0.23 | 0.29 | 0.27 |

Table 3 : Corrosion rate ($\mu\text{A/cm}^2$) of different steels in different electrolytes (1 day cured specimens)

| Electrolyte | M15 | | | MORTAR | | |
|-------------------------------|------|------|------|--------|------|------|
| | HTS | MS | HYSD | HTS | MS | HYSD |
| 3% NaCl | 1.34 | 2.91 | 8.05 | 2.22 | 5.16 | 4.37 |
| NaOH +SAT.Ca(OH) ₂ | 1.63 | 1.59 | 3.04 | 0.98 | 1.01 | 4.00 |

Table 4 : Corrosion rate ($\mu\text{A/cm}^2$) of different steels in different concrete mixes in NaCl electrolyte (28 day cured specimens) with 3.5% CaCl₂ by weight of cement added

| Mix | M15 | | | MORTAR | | | M25 | | |
|-------------------------|------|------|------|--------|------|------|------|------|------|
| | HTS | MS | HYSD | HTS | MS | HYSD | HTS | MS | HYSD |
| with Cl ⁻ | 3.95 | 4.53 | 4.77 | 0.35 | 2.08 | 3.22 | 0.43 | 0.33 | 0.63 |
| without Cl ⁻ | 7.17 | 4.00 | 3.40 | 0.45 | 0.44 | 0.60 | 0.23 | 0.29 | 0.27 |

Table 5 : Corrosion rate ($\mu\text{A}/\text{cm}^2$) of different steels in different concrete mixes in $\text{NaOH} + \text{Ca}(\text{OH})_2$ electrolyte (1 day cured specimens) with 3.5% CaCl_2 added.

| Mix | M15 | | | MORTAR | | | M25 | |
|-----------------------|------|------|------|--------|------|------|------|--|
| | HTS | MS | HYSD | HTS | MS | HYSD | HTS | |
| with Cl^- | 4.42 | 4.00 | 6.21 | 4.95 | 6.78 | 6.69 | 1.19 | |
| without Cl^- | 1.63 | 1.59 | 3.04 | 0.98 | 1.01 | 4.00 | 0.27 | |

Table 6 : Corrosion rate ($\mu\text{A}/\text{cm}^2$) of different steels in different concrete mixes in NaCl electrolyte with inhibitor (28 day cured specimens)

| Mix | M15 | | | MORTAR | | | M25 | | |
|-----------------------------------|------|------|------|--------|------|------|------|------|------|
| | HTS | MS | HYSD | HTS | MS | HYSD | HTS | MS | HYSD |
| with 2% Na_2CrO_4 | 3.72 | 0.91 | 3.39 | 0.10 | 0.77 | 0.86 | 0.15 | 0.45 | 0.12 |
| without Na_2CrO_4 | 7.17 | 4.00 | 3.40 | 0.45 | 0.44 | 0.60 | 0.23 | 0.29 | 0.28 |

Table 7 : Corrosion rate ($\mu\text{A}/\text{cm}^2$) of different steels in different concrete mixes in $\text{NaOH} + \text{SAT}.\text{Ca}(\text{OH})_2$ electrolyte (1 day cured specimens).

| | M15 | | | MORTAR | | | M25 | |
|-----------------------------------|------|------|------|--------|------|------|------|--|
| | HTS | MS | HYSD | HTS | MS | HYSD | HTS | |
| with 2% Na_2CrO_4 | 2.12 | 3.15 | 6.75 | 0.43 | 1.42 | 3.40 | 0.30 | |
| without Na_2CrO_4 | 1.63 | 1.59 | 3.04 | 0.98 | 1.01 | 4.00 | 0.27 | |

Table 8 : Corrosion rate ($\mu\text{A}/\text{cm}^2$) and Polarisation resistance (K ohm cm^2) of HTS with and without inhibitors (28 days curing)

| Mix type | Electrolyte | I_{corr} | R_p |
|-----------------------------------|-------------|--------------------------|------------|
| Without chemicals | Mortar(1:3) | NaCl | 0.45 43.3 |
| With 2% NaNO_3 | " | " | 0.18 93.9 |
| With 4% NaNO_3 | " | " | 0.10 111.4 |
| With 2% Na_2CrO_4 | " | " | 0.10 169.2 |
| Without Chemical | M25(1:1:2) | $\text{Ca}(\text{OH})_2$ | 0.40 113.2 |
| With lauryl Sulphate 2% | " | " | 0.30 74.4 |

Table 9 : Corrosion rate ($\mu\text{A}/\text{cm}^2$) and Polarisation resistance (K ohm cm^2) of HTS steels in M25 concrete mix in $\text{NaOH}+\text{SAT}.\text{Ca}(\text{OH})_2$ Electrolyte with and without additives (1 day cured specimens) (average values). The indicated % are with respect to weight of cement.

| | I_{corr} | R_p |
|--------------------------------|-------------------|-------|
| Without chemicals | 0.269 | 46.58 |
| With 3.5% Calcium chloride | 1.197 | 9.90 |
| with 2% Sodium Chromate | 0.303 | 61.90 |
| With 2% Stannous Nitrite | 0.507 | 52.10 |
| With 2% Sodium Stannate | 0.268 | 59.80 |
| With 2% Sodium Nitrite | 0.242 | 29.10 |
| With 2% Sodium lauryl Sulphate | 0.320 | 60.34 |

Table 10 : Resistance and resistivity values for cubic concrete specimens of different cover thicknesses and constant height

Mix proportion(1:1:2):w/c =0.4 :Number of days of curing =3
Height of the specimens = 50 mm

| Length (l) (mm) | Resistance (ohm) | Resistivity (ohm m) |
|--------------------|---------------------|------------------------|
| 47 | 470 | 23.5 |
| 54 | 462 | 23.1 |
| 67 | 441 | 22.0 |
| 77 | 434 | 21.7 |

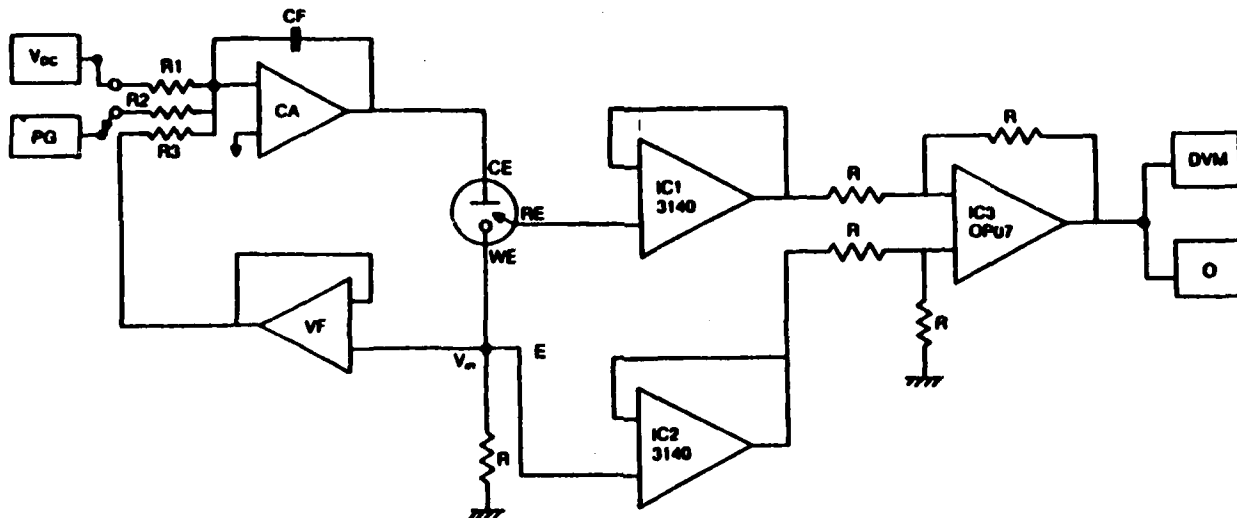


FIG 1 (a): Schematic experimental set-up used in the study.

| | |
|-------------------------|-------------------------------------------------------|
| V dc: DC voltage source | R1,R2,R3,R4 : Resistances |
| PG : Pulse generator | IC1,IC2,IC3,IC4 : Op.amps |
| CA : Control amplifier | DVM : Digital multimeter |
| VF : Voltage follower | CE ,RE, WE : Counter,reference and working electrodes |
| C :capacitor | |

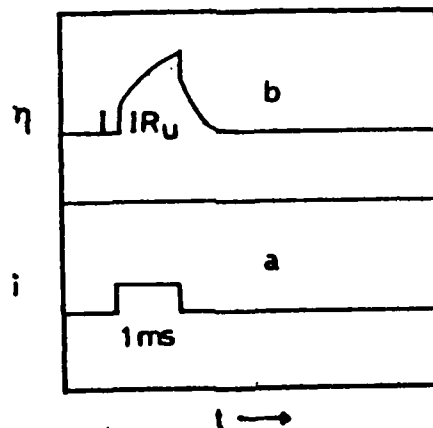


FIG 1 (b): Schematic diagram of the input current pulse (a) and the potential response(b)
 IR_u = potential drop due to resistance of concrete
 u

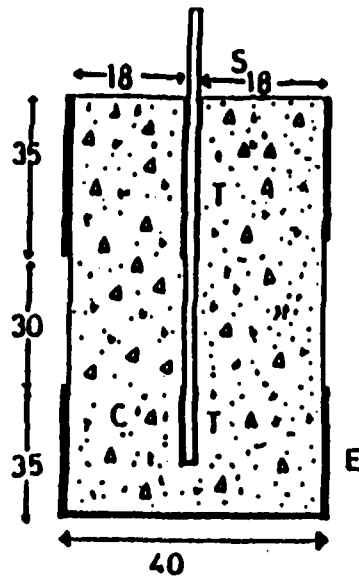


FIG 2: A typical reinforced concrete specimen used for corrosion studies.
 S :Steel E:Epoxy resin cover T = PVC tape

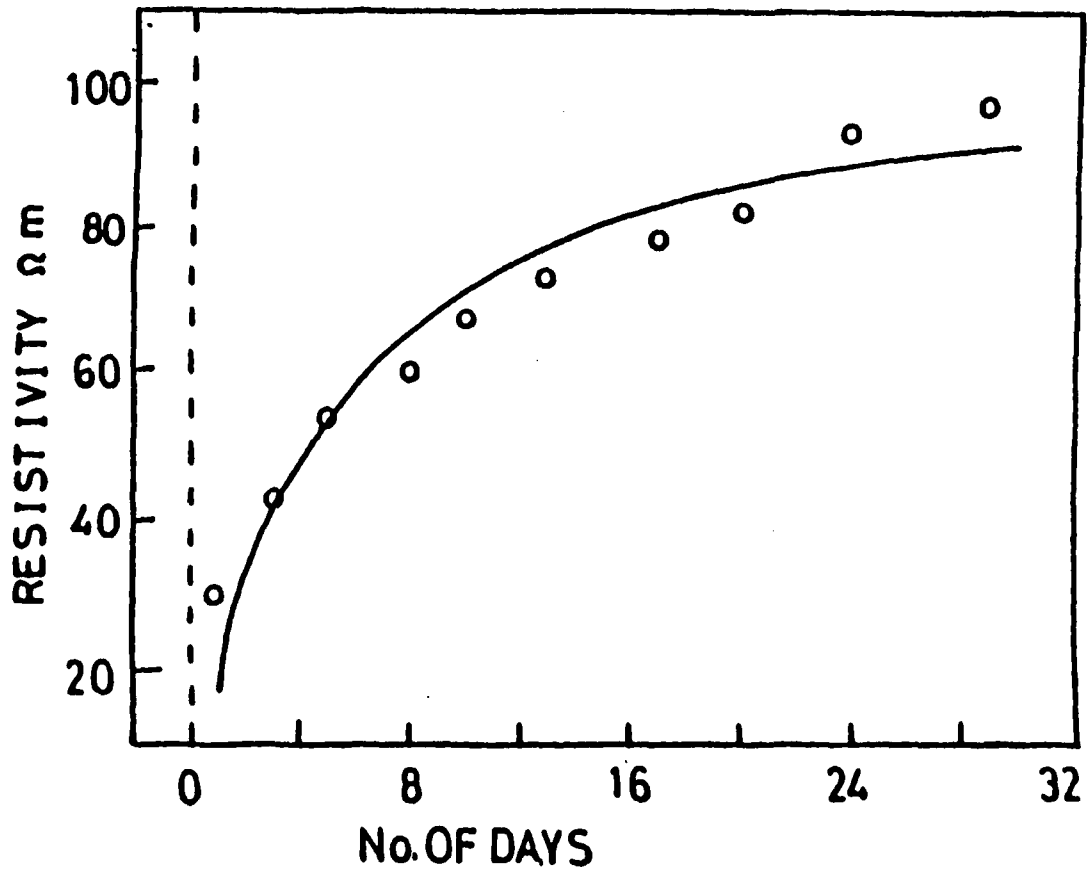


FIG 3: A typical resistivity Vs number of days of curing plot.

Corrosion and Prevention of Ferrocement Roofing Slabs in Electrical Furnace Processing Workshop

Huan Bin Sun
Zhejiang University of Technology
Hangzhou 310014 China

Ming Chou
China Agribusiness Development
Trust & Investment Corporation
Zhejiang Branch

You Yong Yang
Zhejiang Institute of Industrial
Design & Research

Abstract

Ferrocement is a kind of thin-wall reinforced concrete. The main characteristic of ferrocement is that it is lighter than ordinary reinforced concrete. It is economical and durable for industrial buildings, especially high industrial buildings in earthquake areas. Some uses of ferrocement are successful, while some were not because of corrosion. For the purpose of comparison two examples are presented. There is a workshop built in 1959. The slabs were in an environment with fairly high temperature, and corrosive gases. After more than thirty years, the ferrocement suffered varying degrees of damage at different parts. At the top region of the electric furnace, several seriously corroded ferrocement blocks in the slabs fell down onto the ground. Fumes from the electric furnace were sampled and analysed. Carbon dioxide is the main corrosive component. The other workshop is in Shaanxi Province, China. It is also an electric furnace processing workshop, with a 5 tons electric furnace built in 1971. The top surface of the ferrocement roofing slabs were painted with a type of emulsified bituminous materials and the bottom surfaces were painted with polyurethane paints combined with coal tar and other additives. It was discovered that the ferrocement still appears to be performing satisfactorily. This indicates that paints protect ferrocement from carbonation and corrosion.

Key terms : ferrocement, roofing slab, electric furnace, fabric reinforcement, carbonation, emulsified bituminous material, polyurethane paints

I . Introduction

Ferrocement is a kind of thin-wall reinforced concrete using weld-wire fabric and well-graded fine aggregate and gravels¹. The main characteristic of ferrocement is that it is lighter than ordinary reinforced concrete. Thus, the dead loads of the structures are largely decreased. In addition , it is convenient for ferrocement constructions to be transferred and erected. Moreover it is economical and durable for industrial buildings, especially high industrial buildings in earthquake areas, to use ferrocement as roof materials.

Ferrocement is more durable than various metal materials and is more economical than ordinary reinforced concrete^{2, 3} when ferrocement is produced on a large scale in factories using mass-production techniques. Usually use of ferrocement can save 1/3 construction cost, and ferrocement structures are able to last more than 40 years³. However, some ferrocement elements have deteriorated earlier. It is necessary to pay attention to some particular instances, such as corrosive and high temperature environments, where ferrocement is used.

Some uses of ferrocement are successful, while some are not because of corrosion. For the purpose of comparison two examples are presented.

II . The appearance of deterioration

Precast ferrocement roofing slabs (Fig. 1) were used in an electric furnace processing workshop of a metallurgical machine-building factory, Zhejiang Province, China. There was a length of clerestory roof with shelter enhancing ventilation and smoke ejection on the top of a 3 tons electric furnace which produced molten steel day and night. The workshop was built in 1959. The slabs were in an environment with fairly high temperature, and corrosive gases; in addition, water vapour and water formed by condensation and rain water permeated the ferrocement. After more than thirty years, the ferrocement suffered varying degrees of damage at different parts. In the vicinity of the electric furnace , the bottom surface turned black , and its inside became dull yellow. The bottom surface layer of the slabs became somewhat loose. At the top region of the electric furnace, there were serious cracks and fabric reinforcement corrosion in the slabs nearby the clerestory roof. The steel frames of the clerestory roof were seriously corroded and several seriously corroded ferrocement blocks in the slabs fell down onto the ground.

III . Prevention of corrosion

The other workshop is in Shaanxi Province , China. It also is an electric furnace processing workshop , with a 5 tons electric furnace built in 1971. Top surface of the ferrocement roofing slabs were painted with a type of emulsified bituminous materials and the bottom surfaces were painted with polyurethane paints combined with coal tar and other additives. (Fig.2) The operational situation of the electric furnace and the surrounding environment conditions were similar to those described above. In order to improve the ventilation condition , the clerestory roof was expanded and some slabs were removed recently. It was discovered that the ferrocement still appears to be performing satisfactorily. Tests with phenolphthalein indicator solution did not show any sign of carbonation. This indicates that paints protect ferrocement from carbonation and corrosion.

IV . The mechanism of corrosion

Fumes spurted from the electric furnace were sampled and analysed . The chemical constituent by volume are as follows,

Tab.1 Chemical constituent of the fumes

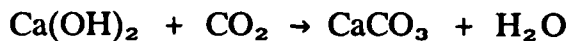
| phase | Chemical constituents(by volume %) | | | |
|-----------|------------------------------------|-----------------|----------------|----------------|
| | CO | CO ₂ | O ₂ | N ₂ |
| melt | 34 | 7.5 | 0.2 | 58 |
| Oxidation | 41 | 8.3 | 0.4 | 50 |
| Reduction | 38 | 1.7 | 0.3 | 60 |

A. Carbonation of the ferrocement

The exposure of porous ferrocement roofing slabs to CO₂ which penetrates the surface of ferrocement through the capillary pores in the presence of moisture or vapour condensation results in carbonation, which is a major cause of corrosion . The other constituents, CO, O₂,N₂, have been shown to cause no damage.

B. Carbonation shrinkage

All compounds of Ca in portland cement paste can be carbonated. Calcium hydroxide, a major constituent of hydrated portland cement, reacts with CO_2 , thus:



dissolution of calcium hydroxide crystals increases compressibility of hydrated Portland cement, and is a significant factor in the carbonation shrinkage of hydrated Portland cement paste. As a result of carbonation shrinkage, the total porosity and volume concentration of large pores are reduced, and fine cracks are caused in the area restrained.

C. Serious cracking of ferrocement

A network of fine cracks occurs on the bottom surfaces of ferrocement roofing slabs. Meanwhile CO_2 penetrates the surface of the cracked slabs, permeates through the cracks and consequentially, promotes carbonation. The vicious circle repeats itself. The more the carbonation takes place, the more the ferrocement roofing slabs crack, and vice versa.

D. Erosion and corrosion

Carbonic acid is capable of dissolving lime from ferrocement, since:



Calcium bicarbonate is very soluble, even small quantities attack ferrocement. Meanwhile CO_2 dissolved in water is known to cause corrosion of carbon steel because of the increased quantity of hydrogen ions, that is,



AS a result of deep carbonation, the alkalinity of the ferrocement is lowered; that is, carbonation of concrete decreases the P^{H} to a value of less than 11.5 and the passivation can no longer be preserved. The passivation layer is formed on the surface of the steel fabric. It is a very thin but dense layer. When it is attacked by the surrounding ferrocement environment, electrical potential develops along the fabric, so that electro-chemical corrosion of the steel fabric is then possible.

V . Preventing corrosion -- paintings

Emulsified bituminous materials containing units derived from butylene and propylene and also bitumen-compatible fillers, surface adhesion promoters and plasticising agents show good resistance to gases and water.

Polyurethane combined with a sufficient amount of coal tar and other chemical additives exhibits excellent properties . It is a sprayable, one-component painting comprising mixtures of polyurethane elastomers, specified isocyanates, polyurethane-compatible coal tars of specified viscosity containing about more than 85% by weight. The constituent make up of coal tar varies with the source; however, it contains mainly hydrocarbons and oxygenated materials. The main characteristic of coal tar is its permeability. Tar penetrates into the capillaries of ferrocement and fills the bottom surface layer forming a thin membrane. The painting possesses high impermeability to gases, vapour and water formed by condensation , and exhibits outstanding adhesion to ferrocement and resistance to aging . The addition of coal tar increases the plasticity , activity and gas resistance of the polyurethane while decreasing the cost, and the addition of polyurethane to tar improves high-temperature softenings.

Conclusion

1. The characteristic of ferrocement element is that it is lighter than ordinary reinforced concrete. It is economical and durable for industrial buildings, especially high industrial buildings in earthquake areas, to use ferrocement as roof materials.
2. ferrocement roofing slabs painted with a type of emulsified bituminous material on the top surfaces and polyurethane combined with coal tar and other chemical additives on the bottom surfaces exhibit excellent behavior under erosive and corrosive environments.

References

1. ACI Committee 549, Guide for The Design, Construction, and Repair of Ferrocement, ACI Sturctural Journal, vol.85, No.3, pp.327 (1988).
2. M.E.Iorns, Laminated Concrete, Concrete International, vol.11, No.10, pp.76 (1989).
3. H.B.Sun, Durable Reinforced Concrete Ribbed Thin Slabs, Procceding of International Conference ' Concrete 2000 ', to be published (1993).

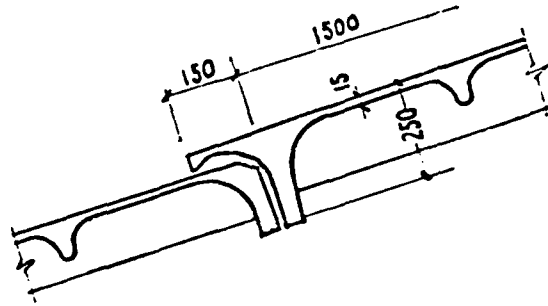
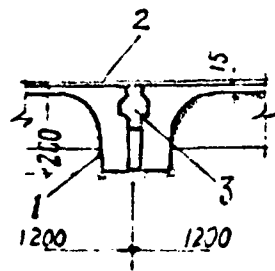


Fig.1 Ferrocement roofing slabs



1. Polyurethane combined painting
2. Emulsified bituminous materials
3. Factice

Fig.2 Ferrocement roofing slabs protected from corrosion

MANAGEMENT OF CORROSION CONTROL OF REINFORCED CONCRETE IN THE CHANNEL TUNNEL

Antoine Pourbaix (Cebelcor, Brussels) and Stephen Cargo (Eurotunnel)

1. THE STRUCTURE

The Channel Tunnel system consists of three separate tunnels - two running tunnels (7.6 m internal diameter) and a central service tunnel (4.8 m internal diameter) - together with terminals at Folkestone in England and Coquelles near Calais in France. The scheme, although based on rail transportation, links both the rail and road networks of the United Kingdom to those of continental Europe. It will carry through trains of both passengers and freight and special shuttle trains which will take drive-on road vehicles. The shuttle trains will take 35 minutes to complete the journey from platform to platform at an average speed of 120 km/hr, but only 26 minutes will be in the 50 km of tunnel. In the early years of operation, passenger shuttles will run approximately every 15 minutes during peak periods and generally every 20 minutes during the day. The minimum service, which will be provided at night, will be one passenger shuttle per hour. For lorries there will be at least one shuttle per hour rising to three per hour at peak periods.

Ideas and proposals for a Channel Tunnel have been contemplated by engineers for nearly 200 years, and go back to Napoleon's time. The present scheme was the outcome of a competition organised by the British and French governments in 1985. The successful scheme used more tried and tested techniques than those put forward by the other competing schemes. The decision to carry road transport on rail wagons was made for very sound safety, technical and driver psychology reasons. This virtually decided the tunnel configuration and diameter. The 7.6 m diameter tunnels could be more easily constructed at speed than the 13 or 14 m diameter tunnel needed for a two-lane road tunnel. The total tunnel length is 50 km, 38 km of which run beneath the sea. The cover from tunnel to seabed is between 25 and 45 metres.

From Folkestone, past Dover and under the Channel for a total distance of about 45 km the tunnels are bored through chalk marl, generally considered to be one of the most consistent and safe tunnelling mediums. As they approach the Folkestone terminal, the tunnels pass through gault clay and other strata, and for the first 5 km from the Coquelles terminal they pass through more faulted zones and sands and gravels. Some idea of the durability and relative impermeability of the chalk marl can be gauged from the fact that the tunnel constructed by Colonel Beaumont's boring machine in the 1880s under Shakespeare Cliff was never lined yet remains there to this day.

The vertical and horizontal alignment of the tunnels was therefore chosen so that the maximum possible length would be in the chalk marl, taking into account the acceptable gradients (not exceeding 1.1%) and the power consumption criteria applicable to a high-speed railway system, as well as drainage and pumping requirements.

Even the risk of earthquakes is not being overlooked in the design of the tunnel. Wide-ranging studies have been made to identify the possible earthquake risks, based on historical records and other on-going investigations.

The tunnels are bored by tunnel boring machines (TBMs) to permit the installation of reinforced concrete linings, or alternatively of bolted cast iron linings (Spheroidal Graphite Iron) where ground conditions would not permit concrete linings to be built to the satisfactory standard.

On the UK side, to sustain high rates of progress, Open Face TBMs were used with expanded concrete linings directly against the excavated ground. Pads on the back of the linings allowed the formation of a 20mm annulus which was filled with cement grout and fly ash. This enabled the lining, which is not in itself watertight, to largely prevent water ingress. Where openings were required, a cast iron concrete hybrid lining was used. Due to the more difficult nature of the ground, on the French side Earth Pressure Balance TBMs were used in conjunction with bolted precast concrete segments, which were sealed with a neoprene gasket.

Main tunnels The scheme comprises two running tunnels, each carrying a single rail track, and a separate service tunnel lying midway between the running tunnels, and connected to them by cross-passages. Two separate running tunnels, rather than a single large-diameter tunnel carrying twin tracks, were chosen to minimise construction risks and to provide greater safety of operation and maintenance.

Service Tunnel The service tunnel has the primary function of providing access to and from the running tunnels throughout their length in both normal and emergency conditions, and it allows the tunnels to be evacuated, following any emergency halting of trains, within 90 minutes. The service tunnel carries its own guided transportation system. In addition, it accommodates water and pumping mains and a drainage channel, and acts as the fresh air supply duct to the tunnel complex in normal operation. It is designed to be kept at a t.

positive pressure in relation to the running tunnels in all conditions to prevent smoke ingress. The service tunnel was designed to act during construction as a pilot tunnel, allowing ground conditions to be investigated more thoroughly in advance of the running tunnel drives. It was also used for ground injection to improve running tunnel driving conditions where this was required near the UK coast.

Cross-passages and equipment rooms The cross-passages connecting the running and service tunnels are at 375 m centres, such that three passages will be directly adjacent to a halted shuttle train. The cross-passages incorporate fire-proof evacuation doors which may be opened and closed in all operational conditions.

Equipment rooms, accommodating transformers, switchgear and signalling equipment, are located between the service and running tunnels, are accessed from the service tunnel.

Pressure relief ducts Differential air pressures and aerodynamic resistance build up rapidly on a train travelling at speed in a very long tunnel. The shuttle stock in particular gives a high blockage ratio (ratio of train to tunnel cross-section); without pressure relief the power required to drive a train at operational speed would greatly increase. The pressure relief system adopted comprises 2 m diameter ducts at 250 m centres connecting the two running tunnels, crossing above the service tunnel. The ducts are fitted with fully closable dampers to prevent the passage of smoke from one tunnel to the other in case of fire.

Pumping stations Three under sea pumping stations serve the whole of the underground works.

Crossovers For operational and maintenance requirements, four double crossovers are incorporated between the two terminals, two in the under sea section, to allow trains to cross from one running track to the other. The crossovers are equipped with fire doors to close the full length of the opening between the running tracks in normal operation.

2. THE CONCRETE

Design Parameters The combination of a 120 year design life with the need for a rapid, accurate and safe lining erection led to a stringent concrete specification, sophisticated detailing and onerous casting accuracy.

With no British, French or other international codes available relating specifically to design of tunnel linings, the design criteria were based on site investigation of linings remaining in previous works abandoned in the 1970s and on full scale load tests on the sophisticated convex knuckle-joint design of the proposed segments.

Durability was the key to meeting the 120-year design life. This required a very high resistance to permeation and diffusion of saline water into the concrete, and this was met by using dense, high strength 60 N/mm² concrete.

Design Differences Fundamental differences between the F and UK designs can be observed. On the UK side, the joints between segments include curved faces and no particular water tightness is sought. Water ingress is considered as normal and a system of closed drainage channels was provided to collect water at the bottom of the tunnel. On the French side, all the segment contact faces are provided with neoprene seals able to withstand the water pressure. An eventual water inflow would be treated as on the UK side, but this would be regarded as exceptional. The result is that, during normal service, the lining on the French side will be subjected to full hydrostatic pressure, whereas, on the UK side, the water ingress can lead to a reduction of the water pressure behind the lining. Segments on either side also differ in their length, measured longitudinally, and in their thickness: on the UK side, the thickness varies as a function of the depth, while, on the French side, it remains the same for a given tunnel diameter. Finally, the reinforcements are also different: on the French side, the TBM ram forces are acting directly on the edge of the last installed segments, whereas on the UK side, the TBM gains its support from radial gripper pads acting on the excavated ground. These differences are at first surprising since they occur within the same structure. They result at the same time from difference in French and UK technical philosophy and practice, in codes, in equipment, and in the fact that the TBMs are of different origins. Despite these divergences, the levels of design safety on both the UK and French sides are very close to each other, and in any case it is very difficult, if not impossible, to assert that one concept is better than the other.

The materials On the UK side, the use of 30% PFA as a cement replacement was for the following reasons.

- to enhance the long-term strength development,
- to produce a more economical mix;
- to produce a more dense concrete
- to reduce the heat of hydration
- to lower the water demand

On the French side, the contractor tried with little success to make use of a mix incorporating silica fume. Apparently, the characteristics of the fume available were irregular. Moreover, the use of silica fume (SF) has drawbacks: mixes incorporating SF are very sensitive to small variations of water ratio, which makes their production more critical. SF mixes also require a longer curing period than normal concrete.

On the French side, crushed limestone from a local quarry was used as an aggregate in conjunction with river sands. In the UK, a low alkaline granite from the west coast of Scotland was used. The problem of Alkaline Silica Reaction (ASR) was resolved by using crushed granite fines from the same quarry, as opposed to the local natural sands, which are high in silica. Because this then increased the water demand significantly, thus reducing the strength of the concrete, amongst other things, the need was identified to use a super plasticiser with a water/cement ratio of 0.35.

The composition of the French and UK concrete is given in Table 1, below. It is worth while

mentioning that the precast lining for the Channel Tunnel on the UK side won the Building and Civil Engineering category of the 1992 Concrete Society Award for outstanding structures.

| France | | UK | |
|------------------------|---------|------------------|-----------------------|
| Ciment CPA55PM | 400 kg | cement | 310 kg/m ³ |
| sable roulé Oise | 325 kg | pfa | 130 kg/m ³ |
| sable concassé LS | 340 kg | 20 mm 32% | 580 kg/m ³ |
| granulat concassé 3/8 | 250 kg | 10 mm 25% | 454 kg/m ³ |
| granulat concassé 5/12 | 1060 kg | fines 43% | 780 kg/m ³ |
| adjuvant sika HR401 | 7 kg | superplasticiser | 5,8 l/m ³ |
| ou chryso durciplast | 5,5 kg | target w/c ratio | 0.35 |
| eau libre | 140 kg | | |

Table 1. Final composition of the concrete for the linings

The erection tolerance required a casting accuracy of ± 0.1 mm. This was checked using technology developed for jet turbine blades. The success of the quality systems is demonstrated by the reject rate of 0.6% over a three-year with only 0.03% rejection for dimensional defects.

Delivery of linings for the UK side to Shakespeare Site, Dover, 100 km from the casting yard, involved 1250 train movements. This major exercise in logistics avoided the environmental problems associated with road haulage and helped to minimise the impact of this immense project on the people of Kent.

On the French side, the casting yard was located on site.

Cover The structural design dictates that the cover cannot be more than 35 mm without the cover spalling at high compressive loads. Whereas a larger cover gives a greater degree of protection against time-related processes such as chloride ion diffusion, the quality of the concrete is such that 35 mm cover should prove adequate to provide the required durability.

Coated rebar It was recognised that the only practical reinforcement material/coating system that was considered viable was epoxy coated rebar. However, whilst epoxy coated rebar would probably provide for a far more durable system, the cost benefit could not be easily quantified.

In view of the anticipated exposure conditions, the predicted performance of the selected mixes, and the intention to use cast iron segments in "severely aggressive" areas, the decision not to use epoxy coated reinforcing bar was supported by the consideration that data on the performance and availability of epoxy coated bar was limited at the time of setting up the original test programme.

3. THE CORROSION PROBLEMS

The environment The environment in the Tunnel has been described as "warm, humid, saline, turbulent and dusty".

Specifically, during operation the interior will have air temperatures in the range of 30 - 35°C, with high circulation rates, hence ample oxygen. It will be generally humid, due to the seepage of water and condensation from the cooling piping, with local areas seeing intermittent drying due to the high circulation of air during train passage. Train operation will occasionally cause "misting", or condensation zones.

The exterior faces of the liners will have salt water, with about 17,000 ppm chloride concentration; essentially the same as the sea.

Trains will operate on high voltage alternating current (25,000 volts) drawing a very high amperage over the 120 year life.

The risks The long-term performance of reinforced concrete structures in general, and precast reinforced concrete segments within the Channel Tunnel project in particular, will be determined by either corrosion of the reinforcement steel or the degradation of the concrete itself.

Corrosion of reinforcement steel can be initiated by one or more of the following mechanisms:

- i. Loss of pH due to carbonation of the concrete
- ii. Chloride attack
- iii. Cracking of concrete, mechanical damage
- iv. Stray current effects

i. With the use of dense concrete of low permeability and a minimum cover of 35 mm, the risk of carbonation in the undamaged linings is greatly reduced. The greatest risk is where the inner face is subject to alternate wetting and drying.

ii. Chloride permeation and diffusion from the outside, including wick action, is certainly a possibility. The impermeability of the concrete, the presence of an annulus of grout, the continuous saturation and consequent lack of oxygen, and the probable formation of secondary gels such as brucite, leading to even lower permeability, are all beneficial in reducing the ingress of chloride.

Perhaps the greatest risk will be at the edges, where the rebars are exposed simultaneously to chloride ingress from outside and oxygen penetration from inside.

iii. Repaired defects, especially spalls, may show early corrosion due to the different levels of chloride and different oxygen permeability characteristics.

iv. Most of the references in the literature indicate that AC induced corrosion is only a small fraction of the corrosion caused by an equivalent DC current. Figures given are between 5% and 0.1% for steel in soils (1-4). We consider that this approach can be misleading; in passive systems such as steel in concrete, AC induced currents produce shifts of electrode potentials and this may eventually cause breakdown of passivity (5). A 3-month test made on the linings of the Channel Tunnel indicated that there was no direct relation between

corrosion and the AC induced current density. The test showed that the conservation or the destruction of the state of passivity was easily detected by potential measurements.

Relevant past experience a) High quality concrete has been successfully used in the marine environment for many decades, with numerous instances of highly durable performance, and little, if any, corrosion of the reinforcing steel.

Examples are:

1. Some twenty North Sea offshore platforms. Note especially that their utility shafts have a comparable external water head and comparable internal environment
2. Floating concrete barges and ships, built during the First and Second World Wars, many of which are still serving as breakwaters.
3. Floating concrete bridges, such as the Hood Canal Bridge in Washington, USA, with essentially no corrosion of the reinforcing steel below their waterline.
4. Quays in Kuwait, built in 1959 - 60, showing no corrosion.
5. Harbour structures and bridges in many locations around the world.

b) On the other hand, there has been a significant number of notorious cases of early severe and destructive corrosion.

Examples are:

1. Dubai Immersed Tunnel
Seepage of water through joints has led to severe corrosion of reinforcing steel, with much cracking and spalling, necessitating major repairs.
2. Hong Kong Mass Rail Transport Tunnels
These tunnels, built with precast concrete segments, with a design life of 120 years, are showing significant corrosion after 4 to 10 years. Most corrosion is apparently occurring on the inside face, in areas of defects and repairs and where cover is deficient.
3. (Jubail) Seawater Cooling Canals and Siphons, Saudi Arabia (Middle East)
These are showing severe corrosion within 3 years, where concrete has been subject to wetting and drying. The corrosion process has been fully arrested by the installation of a sacrificial anode cathodic protection system.
4. Iron Ore Terminal at bin Qasim, near Karachi, Pakistan
This installation has exhibited severe corrosion after 5 to 8 years.
5. The original San Mateo-Hayward Bridge, near San Francisco, California (now replaced).
the bridge showed severe corrosion, commencing even prior to completion.
Repairs merely shifted the corrosion to adjacent areas.

c) Special attention was paid to the existing (1974) service tunnel at Dover. Cores show 0.2 to 0.8% chloride, by weight of cement, which is at or above the commonly accepted threshold of 0.4%. Localised corrosion is reported from those areas which are subjected to ponding of salt water and where cover was deficient.

Prediction of Lifetime "There is a reasonable probability that the reinforcing bars will be depassivated and exposed to corrosion at mid-life, i.e. after 50 to 60 years."

This conclusion was arrived at by the Technical Review Committee in their report on the

Durability of the Concrete Tunnel Liners.

Their recommendation was that Cathodic Protection Systems should be designed now to ensure that these are practicable for application at a later date. These designs should be updated periodically to take advantage of new technology. They also recommend that a rational and effective maintenance management system is put in place and a data base established at an early date, to track each lining segment throughout its life.

This is why CEBELCOR was asked to conduct a feasibility study on cathodic protection and to make recommendations for corrosion monitoring.

4. PROTECTION METHODS; FEASIBILITY STUDY OF CATHODIC PROTECTION

A study on the risk of corrosion was conducted to identify parts of the Tunnel that could be more exposed to corrosion and to identify possible corrosion scenarios.

Corrosion scenarios One possibility is that chloride will diffuse or permeate from the surrounding wet ground and reach the outer rebar mat. If the inner rebar mat is passive, corrosion of the outer rebar will be accelerated by the coupling of the two mats.

A second possibility is that the oxygen initially present in the concrete will be consumed, leading to low potentials of the outer rebar mats (-0.8 to -1.0 V_{sce})(6-7). This situation was extensively studied in connection with the long term storage of nuclear wastes, and there is a consensus that it does not lead to a risk of corrosion (6,8-10). In this case, the coupling with the passive inner mat has little consequence.

The inner mat will be exposed to carbonation, possibly accelerated locally by wet and dry cycles. Normally chloride is kept out of the tunnel by closed drainage channels inside the concrete wall.

The galvanic couple between the inner and outer mats will tend to decrease the corrosion rate of the inner rebar if the potential of the outer rebar is low. Such a situation will exist both when there is cathodic protection of the outer rebar or when oxygen in the concrete on the extrados is depleted.

Cathodic protection is the only way to combat corrosion of the outer rebars of the concrete linings. If a corrosion threat on the inner rebars is identified early enough, coating the concrete is a possible remedy; otherwise, cathodic protection is necessary.

External anodes are best suited for the protection of outer rebars surfaces, and conversely internal surface anodes are more effective to protect the inner rebar mat. It is considered that only 10 % or a little more of the total current reaches the remote mat.

Isolated cases of cathodic protection in concrete date back 30 or 40 years; the number of applications increased much in the last 10 to 15 years, particularly on bridge decks exposed

to winter desalting and on bridge piles in marine splash zones.

Although current density is important as a design parameter, it is not the correct criterium for protection. The primary criterium is a value of the electrode potential. An overview of the literature and the selection for the project for the Channel Tunnel is presented below.

Potential criteria NACE issued in april 1990 a recommended practice RP0290-90 applicable to structures exposed to the atmosphere and to cathodic protection systems with distributed mesh anodes. These recommendations are based on purely empirical evaluation of successful CP systems. The proposed criteria are:

- the instant off-potential should be at least 100 mV lower than the final potential ("final" means a stable potential after some unspecified time, typically 4 hours), or: the instant off-potential measured immediately after application of the CP current should be at least 100 mV higher than the off-potential after a period of time of cathodic protection (typically 4 hours),

- the most electronegative potential must be lowered by at least the standard deviation of the potential values measured before applying CP (potential under polarization is measured by instant off-value),

- E-log i curve analysis: the IR drop free potential is measured when the CP current is incrementally increased. The current required is the one which starts a linear portion of the E-log i curve (after a curved portion).

This latter criterium is often not practical. The NACE recommendation does not reject the simultaneous use of other criteria.

Other criteria concrete were reviewed and discussed at an AFREM-CEFRACOR seminar (11):

- the potentials -0.71 et -0.79 V_{sce} proposed by Vrable (see discussion in (12)) are considered conservative (too low). The same opinion applies to a decrease of 300 mV from the zero current potential.

- Isecke (13) suggests -0.55 to - 0.65 V_{sce} (or -0.7 with time).

- D.A.Hausmann (14) introduced an interesting proposal: prevention of corrosion initiation at -0.44 V_{sce} and arrest of corrosion at -0.65 V_{sce} .

- Taché and Lemoine (15) take over the same approach, with different criteria for uncorroded structures (-0.425 V_{sce}) and for corroded structures (-0.635 V_{sce}).

The scatter of the figures mentioned is an indication of a specific property of steel in concrete which is properly identified only in a small number of papers:

in high alkalinity concrete contaminated with chloride, initiation of pitting corrosion can be prevented by keeping the potential below a critical "pitting potential". If corrosion due to chloride has just started, it is possible to restore passivation by maintaining the potential below another critical potential called "protection potential against localized corrosion", which is slightly lower.

If corrosion has started because of a loss of passivation due to a pH decrease, it is necessary to protect steel by lowering the potential initially below the immunity potential, which is lower than the protection potential against localized corrosion. In the longer term, when a higher pH is restored by the cathodic polarization, the "protection potential against localized corrosion" criterium is again applicable.

Our recommendation is to apply cathodic protection before corrosion starts and to use the "protection potential against localized corrosion" as the criterium for cathodic protection. This is a good combination of safety and economy. The value of this protection potential is in the range of - 0.40 to -0.45 V_{sce}. This potential must naturally be controlled without error due to ohmic drop.

Required current density Data from literature on current density required for cathodic protection of steel in concrete are highly scattered. Examples of extreme values are 0,06 mA/m² (concrete in soil saturated with water) to 42 mA/m² (in sea water) (16) or even 268 mA/m² (17).

More data are reviewed below:

- R.O.Müller (18) : 1 mA/m² in the absence of Cl⁻, and 20 mA/m² with 2% Cl⁻ per weight of cement was enough to bring protection, in ordinary concrete.
- F.Hunkeler (19) found adequate protection on non corroded rebars with 0,5 to 10 mA per m² of concrete surface (for bridges with two mats of rebars), and the current required decreased significantly with time. For corroded steel, initial protection was achieved with 5 to 20 mA/m², and the current required also decreased with time.

Taché and Lemoine (15) presented a series of figures of current densities for buried reinforced concrete pipes (0,4 to 1 mA/m² in a good quality concrete, and 1 to 2 mA/m² in a poor concrete), for bridge decks (1 to 32 mA/m²), for foundations (0.65 to 17 mA/m²), for concrete in sea water (1,2 to 42 mA/m²) and in water saturated soils (0.06 to 12 mA/m²). Taché and Lemoine carried out some tests and used a few hundreds of μ A/m² to reach -0.9 V_{sce} and 1 mA/m² for -1 V_{sce} (15). Other figures mentioned at this conference (15) include 0.1 to 15 mA/m².

At the conference UK Corrosion 90, a general opinion was expressed that the current densities cited are often too large. According to H.Arup, 1 to 4 or even 0.1 to 4 mA/m² is enough, after the reduction of the oxygen initially present in the concrete.

C.M.Preece, F.O.Gronvold, T.Frolund (20) produced polarization curves in OPC concrete, and in concrete containing fly ash or micro silica, immersed in saturated deaerated Ca(OH)₂. All backscan curves show current densities between 0,01 and 0,2 mA/m² for potentials between -400 and -800 mV_{sce}.

The Norwegian Petroleum Directorate (21, page 145) recommends of 0,2 to 4 mA/m² of rebar surface. Most of the offshore designers use 1 to 2 mA/m² of concrete surface. The same publication (page 148) mentions that Den Norske Veritas (DnV) recommended in

1977 0.5 to 1 mA per m² of outer layer of rebar.

It is generally considered that the surface of steel in a structure with two rebar layers is approximately equal to the surface of one face of the concrete. This is true for the prefabricated concrete linings of the Channel Tunnel.

It appears that maintaining passivity can be achieved at lower current density than if passivity must be restored from an actively corroding situation. This is a strong argument for a careful corrosion monitoring programme and for the application of cathodic protection before corrosion starts.

Considering the low permeability concrete used in the Channel Tunnel, and assuming that cathodic protection will be applied before corrosion starts, a current density of 1 mA per m² was recommended as a design value. The estimate current for the three tunnels, including the protection of cast iron linings is 2136 A.

Selection of the cathodic protection system Different systems were considered:

- sacrificial anodes outside the tunnel
- impressed current with groundbeds installed on shore,
- impressed current with distributed groundbeds drilled from the tunnel,
- surface anodes on the inner surface of the tunnel.

Functional and engineering aspects, access during operation of the tunnel, interferences with other structures, electrical safety inside the tunnel, maintenance and costs were analyzed.

Sacrificial anodes:

The sacrificial anodes would be drilled through the concrete linings and forced into the ground. The optimum combinations of the number, size of anodes and lifetime were estimated at 35000 14 kg zinc anodes with a backfill, to be replaced every 8 years, or 50000 6 kg magnesium anodes, with a lifetime of 13 years. Zinc anodes must be distributed on the three tunnels; magnesium anodes can be installed only on the service tunnel.

The advantage is the possibility of protecting limited sections of the tunnel, if required, and the absence of safety and earthing problems in long return conductors. The system with magnesium anodes is cheaper; both are however expensive in the long term.

Impressed current with deep anode groundbeds:

A system with remote anode groundbeds positioned on shore as shown on figure 1 was considered. The cost of the electrical cable to the rectifier at Cap Gris-Nez appeared prohibitive; the system lacks of flexibility, if protection is needed only on specific lengths of the tunnel.

Another impressed current system with anode groundbeds drilled in the ground from the service tunnel looks more attractive presently: 16 one hundred metre deep groundbeds in the subsea section would each protect sections of 2.5 km long (figure 1). With this system, the protection current can be adjusted rather easily, if needed. This system is comparatively less

expensive.

Surface distributed anodes:

Mesh anodes are embedded in a conductive cementitious overlay. Zinc flake sprayed on the surface can also be used as an impressed current anode. In both cases, surface preparation is necessary. Installation raise immense problems in fully equipped and operating tunnels.

This system would not protect the segments below the trackbed, nor the external surface of cast iron linings.

The total cost (material, installation, instrumentation, surface preparation, application of overlay) is estimated at 250 GBP/m², or more than 10 % of the cost of the whole project, and this is considered excessive. The system may be interesting only for very local application, if the need is demonstrated. The joints, or edges between segments is one example of a possible local application of this technique.

In all cases, all the rebar cages must be electrically connected. This is already done under the trackbed, and provisions were taken from the beginning to make it possible in due time. This will be a major item in the cost.

5. CORROSION MONITORING

Corrosion monitoring will indicate when additional protection methods must be implemented. We have seen before that it is important to apply cathodic protection before corrosion really starts.

Corrosion monitoring will indicate which corrosion scenario comes true: chloride ingress from outside, or carbonation from inside, etc. This will govern the selection of the additional protection method. Corrosion monitoring will also indicate if additional protection is needed everywhere or on specific sections.

An investigation was conducted to design a corrosion monitoring programme for the concrete linings of the Channel Tunnel, and a report on guidelines was prepared:

Monitoring the progression of carbonation and chloride ingress from inside is done easily by small core sampling. The surveillance of chloride ingress from outside is done by electrochemical monitoring on probes cast with a reduced concrete cover near the outer skin of the linings. Figure 2 shows a typical arrangement of instrumented linings with such a probe (B-probe). The probe has a known exposed surface; it is accessible from inside the tunnel; a recessed hole allow potential measurements with limited interference due to local currents; polarization measurements can be done, using the rebar cage as a counter electrode.

The instrumented linings also contain a resistivity probe with a reduced concrete cover; four A-probes are designed to monitor corrosion near the edges and corrosion due to AC induced current.

There are 140 instrumented linings distributed on the three tunnels.

The corrosion monitoring programme actually covers more than the instrumented linings; on the whole 1200 linings are controlled, distributed in different groups: wet grounds sections, linings damaged during installation and random zones. If there are condensing zones, these will also be controlled.

The size of the samples (300 in each group) indicates with a degree of confidence higher than 90% that the proportion of bad linings in that group is between 7% and 13%, when the proportion of bad linings in the sample is 10%. The degree of confidence increases when the proportion of bad linings observed increases: if 25% of bad linings are observed, there is a 95% confidence that the number of bad linings in that group is between 20 and 30%.

The monitoring procedures selected are: core drilling and analysis, potential mapping and polarization resistance measurements with a guard-ring cell on the rebar cages, potential and polarization measurements on probes with a reduced concrete cover and on probes near the edges of the linings, AC induced current measurements and corrosion measurements on probes exposed to AC induced current, concrete resistivity and rebound number (measured with a sclerometer). At this time, electrochemical impedance, electrochemical noise, ultrasonic pulse echo, pulsed radar system and infrared thermography were not considered further, although we are convinced that electrochemical impedance will soon become a valuable tool for the operation conditions in the Channel Tunnel.

The detailed monitoring procedures were established, the instrumentation was selected, or developed when specific needs appeared for the Tunnel. The monitoring techniques were tested and demonstrated on mock-up linings brought to the laboratory. Extensive tests were conducted to understand the exact meaning of slow potential drifts observed during potential mapping on dry carbonated concrete (22,23). Polarization resistance is measured under potentiostatic control because this allows shorter stabilization time (24). A portable potentiostat was developed for that application, using a switch-off method to control the applied potential without error due to ohmic drop (23).

Two teams of Eurotunnel technicians were trained for the monitoring operations; the first monitoring campaign is now completed and the data at time zero has been collected. AC induced measurements must still be done under normal traffic conditions. It is planned to conduct such monitoring campaigns once a year during 5 years, then to consider longer intervals and a revised statistical control.

6. INTERPRETATION AND MANAGEMENT

The data collected is interpreted on the base of the general knowledge of electrochemistry in concrete, of recommendations such as ASTM C876 and of critical values determined at the time zero and from measurements on reference mock-up linings. Polarization measurements, coupling currents, potential contours in the depth of the linings, alkalinity measurements and core analysis are used as cross-check methods.

All the data is stored in a single data base. Software has been progressively developed for an automatic interpretation and to provide an early warning alarm, automatically. The software analyses trends in the course of time, verifies the critical values and revises the experimental plan for the statistical control.

Examples of results obtained so far are illustrated in figure 3.

7. CONCLUSIONS

Corrosion monitoring is an essential part of the maintenance programme in the Channel Tunnel. One of the aims is to identify zones at risk and to concentrate future monitoring there, leading to increased confidence with less cost/time impact.

Eurotunnel is working towards a unique system of electronic data capture and analysis, for an early warning system. This corrosion monitoring system is integrated into the daily maintenance management system; the data logger will be used not only to capture the corrosion monitoring data, but for the general and detailed inspection on the conditions of the linings as well.

Due to the time restraints during operations in the Tunnel and cost implication, it was important to collect as much data as possible in a short period of time. We think we have gained the expertise in that respect. A rough estimate of the time for the collection of the data is 0.66 man.year and we expect to decrease this in the future. If we take into account the management of the data and the expertise of Cebelcor to analyse it, the total cost is estimated at 25,000 GBP or 42,000 US\$/year.

Eurotunnel considers that this monitoring programme developed by Cebelcor is a good balance between reliability and cost efficiency. With this programme, Eurotunnel will have a clear picture of the increasing risks of corrosion and therefore be in a confident position to make a well informed judgement on the need for additional protection, and particularly on:

- which protection system
- where to apply it
- and when.

REFERENCES

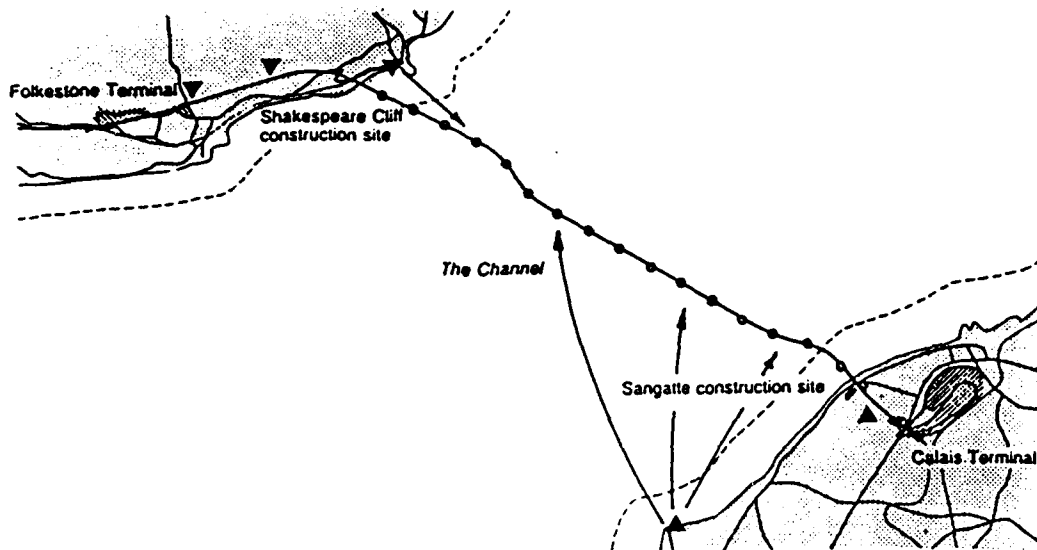
- (1) J.Dabkowski, A.Taflove. Mutual Design Consideration for Overhead AC Transmission Lines and Gas Transmission Lines. Vol 1: Engineering Analysis. EPRI EL-904. American Gas Ass. and EPRI, September 1978.
- (2) A.W.Peabody, C.C.Siegfried. Corrosion Control Problems and Personnel Hazards Control Problems Caused by HVDC and HVAC Transmission Systems on Non-Associated Underground Facilities. CIGRE 1974, Session 36-03.
- (3) B.Jacquet, W.B.Moore. Influence des courants de terre sur les canalisations et câbles enterrés. CIGRE 1988. Session 36-06ref 3 de RT308
- (4) L.V.Collings. Alternating Current can Corrode Pipe. Corrosion 76, Houston, March 22-26 1976, Abstract in The Oil and Gas Journal, April 5, 1976
- (5) A.Pourbaix, R.Muyllé. AC induced corrosion of metals. Rapports Techniques Cebelcor, 161, RT.308, december 1991.
- (6) C.M.Preece. Corrosion of steel in concrete. SKBF-KBS 82-19, Stockholm
- (7) "The hollow leg problem". Steel in concrete, n°1, oct 1978 Korrosionscentralen, Denmark
- (8) C.M.Hansson. The corrosion of steel in anaerobic concrete and the associated hydrogen evolution. SKB, SFR 87- 02, Stockholm
- (9) R.Grauer. The corrosion behaviour of carbon steel in Portland cement. Cédra 88-02E, Baden.
- (10) C.C.Naish, P.H.Balkwill, T.M.O'Brien, G.P.Marsh. Anaerobic corrosion of carbon steel in concrete. Harwell AERE-G50232, February 1989.
- (11) "La protection cathodique et la durabilité des ouvrages en béton armé", Séminaire AFREM-CEFRACOR, St.Rémy-lez-Chevreuse, 15 mai 1990
- (12) B.S.Wyatt and D.J.Irvine. A review of cathodic protection of reinforced concrete. Materials Performance, dec 1987, 19-21
- (13) B.Isecke (BAM, Berlin) Discussion at the 9th European Congress on Corrosion, Utrecht, 2-6 October 1989
- (14) D.Hausman. Criteria for cathodic protection of steel in concrete structures, Mat. Protection, oct 69, 23-25.
- (15) G.Taché, L.Lemoine. Protection cathodique des armatures du béton: principes et généralités. Séminaire AFREM-CEFRACOR "Durabilité et protection des armatures du béton", Paris 15.6.88.
- (16) H.Arup, Korrosion Centralen report 79/02e, 1979.
- (17) L.L.Shreir. Corrosion, Newnes ed. 2d edition, p11.65
- (18) R.O.Müller. Field and laboratory experience with cathodic protection of rebars in concrete. 9th E.C.Corrosion, Utrecht, oct 89)
- (19) F.Hunkeler. Kathodischer schutz von stahlbetonbauwerken (Ceacor, Naples 1989)
- (20) C.M.Preece, F.O.Gronvold, T.Frolund. The influence of cement type on the electrochemical behaviour of steel in concrete. in A.P.Crane, Ellis Horwood, 393-405)
- (21) Design and operational guidance on cathodic protection of offshore structures, subsea installations and pipelines. The Marine Technology Directorate, MTD Ltd publication

90/102, London 1990

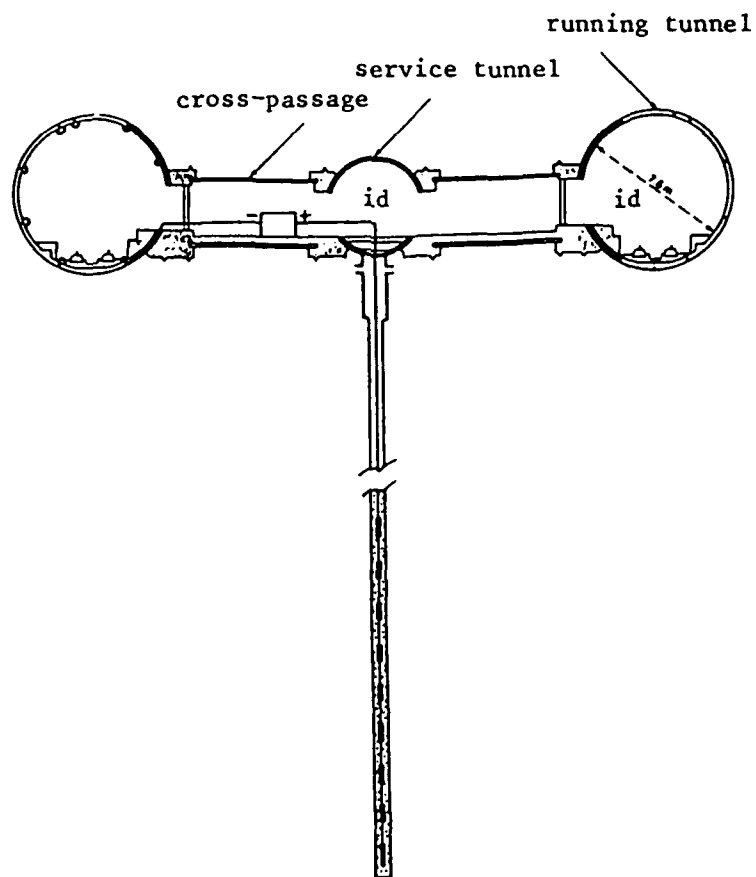
(22) A.Pourbaix. Contrôle de l'état de armatures par mesure de potentiels d'électrode. Journées d'Etude Protection cathodique des armatures du béton armé, ENPC, Paris 26-27.5.92

(23) J.Kissel. Contrôle de la corrosion des armatures du béton par des mesures électrochimiques. Rapports Techniques Cebelcor, 162, RT.310, décembre 1992.

(24) J.A.Gonzalez, A.Molina, M.L.Escudera, C.Andrade. Errors in the electrochemical evaluation of very small corrosion rates. 1. Polarization resistance method applied to corrosion of steel in concrete. Corrosion Science, 25, n°10, 917-930, 1985.



- a) ▲ anode groundbeds on shore
- anode groundbeds drilled through the tunnel



- b) anode groundbeds drilled through the service tunnel

Figure 1 : Projects for impressed current cathodic protection systems

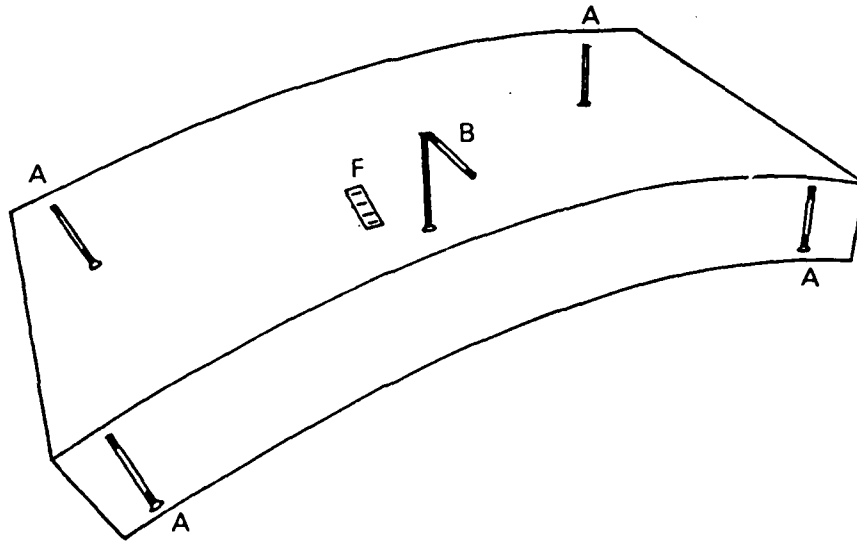


Figure 2: Schematic presentation of an instrumented concrete lining
 Probes with reduced concrete cover:
 A: for AC induced current and edges
 B: for chloride ingress on the extrados
 F: resistivity of concrete

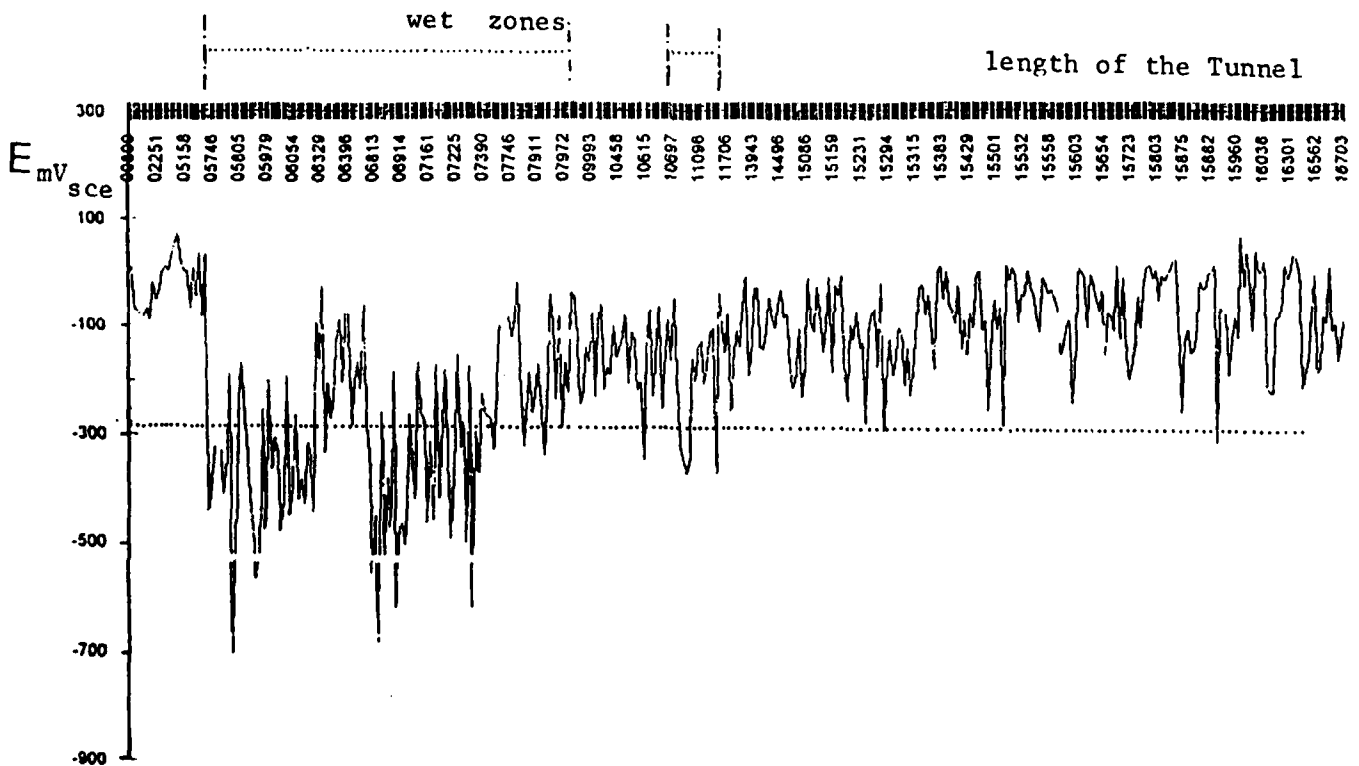


Figure 3: Example of corrosion monitoring data:
 lowest potential along the length of a
 section of the tunnel

RELIABILITY AND CORROSION TESTING OF ELECTRONIC COMPONENTS AND ASSEMBLIES

J. D. Sinclair
AT&T Bell Laboratories
Murray Hill, NJ 07974

R. P. Frankenthal
AT&T Bell Laboratories
Murray Hill, NJ 07974

D. J. Siconolfi
AT&T Bell Laboratories
Murray Hill, NJ 07974

ABSTRACT

Discovering and preventing corrosion and failures requires the use of accelerated-life tests that uncover real-world failure mechanisms. Accelerated-life testing of electronic materials and assemblies has usually been carried out without considering the potential effects of ambient particles in corrosion and other degradation processes. Yet data collected in recent years shows that the mass concentration of corrosive airborne particles is comparable to the total of all acid pollutant gases in most urban environments. The question arises, do the traditional corrosive gas tests realistically represent the degradation, on a macroscopic or molecular scale, that takes place in real-world ambients.

In this paper it is shown that natural and anthropogenically derived sub-micron particles need to be considered in corrosion processes because: (1) many are sufficiently hygroscopic and corrosive to react directly with non-noble metals and passive oxides or to allow harmful electrical leakage currents to flow between metallizations; (2) others will inhibit oxygen and moisture access to the region of the surface under the particle, leading to variations in the electrochemical potential across the surface; (3) others adsorb corrosive gases and moisture leading to corrosion. Following discussion of the importance of particle contamination in corrosion of electronics, this paper describes a prototype submicron particle exposure chamber for accelerated-life testing of electronic devices and assemblies.

Key terms: particle induced corrosion, accelerated life testing, dust chamber, particle deposition.

Introduction

Airborne particle contamination is present in all of the environments inhabited by humans. Most airborne particles are too small to be visible to the unaided eye. Research on atmospheric corrosion and the degradation of electronic materials and assemblies has usually been carried out without considering the potential effects of corrosive submicron particles, in spite of the keen awareness of the undesirable consequences of microbial and inanimate particle contamination by

at least a few manufacturing industries, e.g. pharmaceutical and semiconductor. In two papers in the early 1980s, Wood et al. (1) found that coarse particles of ammonium chloride or nitrate, and some ambient particles, frequently had a marked effect on the corrosion of iron, zinc, and aluminum in the presence of SO_2 . Limited access of moisture/oxygen to surfaces beneath particles or other foreign matter is well known to cause some corrosion processes (2). This differential aeration causes variations in electrochemical potential that drive the corrosion reactions.

The mass concentration of airborne particles in indoor electronic equipment environments has been measured in several different climates (3-5) and found to be in the same range as the concentration of corrosive, acid forming inorganic gases (6). For example, the total mass concentrations of submicron ($0.1\text{-}1.0\mu\text{m}$) and coarse ($>1.0\mu\text{m}$) airborne particles found within telecommunication equipment centers or factories in Wichita, KS (4), Newark, NJ (4), Neenah, WI (4), and North Andover, MA (5), were 5, 9, 2, and $15\mu\text{g}/\text{m}^3$, respectively. In comparison, the concentration of SO_2 was typically found to be $<10\mu\text{g}/\text{m}^3$, and that of NO_x $<35\mu\text{g}/\text{m}^3$ for electronic equipment in several different environments in the United States (6).

The consequences of unintended particle deposition during all types of corrosion experiments are also frequently overlooked in the interpretation of experimental results. Studies over the last 15 years have shown that all surfaces become rapidly contaminated with submicron corrosive particles in ordinary indoor environments.

The question arises, do the traditional corrosive gas accelerated-life-tests realistically represent the degradation, on a macroscopic or molecular scale, that takes place in real-world ambients. In this work it is concluded that natural and anthropogenically derived submicron particles need to be considered because: (1) all surfaces exposed to ambient environments are contaminated with corrosive particles that can cause localized defects and lead to weak-link failures; (2) many are sufficiently hygroscopic and corrosive to react directly with non-noble metals and passive oxides; (3) others will inhibit oxygen and moisture access to the surface; (4) other inert particles can adsorb corrosive gases and moisture from the ambient leading to corrosion.

Following discussion of the importance of particle contamination in corrosion of electronics, a prototype, submicron particle exposure chamber is described for discovering particle related failure processes in electronic devices and assemblies. The same accelerated-life testing chamber can also be used to evaluate the effectiveness of design, materials, or environmental changes in preventing corrosion and failures.

Traditional Corrosive Gas Testing

Corrosive gas testing for electronic equipment used in normal urban environments in the United States evolved in large part through an industry supported program at Battelle Laboratories in the early 1980s (7). The so-called Class II test uses Cl_2 ($31.7\mu\text{g}/\text{m}^3$), H_2S ($15.2\mu\text{g}/\text{m}^3$), and NO_2 ($410\mu\text{g}/\text{m}^3$) as the test gases. The Battelle experiments showed that realistic corrosion products are produced on a variety of connector metallizations with the Class II test. Notably absent are SO_2 in the gas mixture and sulfate in the corrosion product. The author and colleagues have shown (8) that the accumulation of sulfate on zinc and aluminum surfaces in telecommunications

facilities correlates strongly with the local concentration of airborne sulfate, but not with SO₂ concentration, indicating that sulfate accumulation is due to particulate deposition. The European testing community frequently includes SO₂ in the gas mixture, though it seems unlikely to the authors that SO₂ contributes to corrosion in these exposure tests at relative humidity levels below Vernon's critical relative humidity (9). Of course, if hygroscopic particles are present, the humidity at which a moisture film forms may be reduced. However, in a purely corrosive gas test no hygroscopic particles will be present.

Experience With Particle-Related Degradation Processes

Experience with circuit board failures in recent years has demonstrated the impact that particles can have on reliability. The increasing power density in electronic devices demands that forced-air cooling be provided to equipment cabinets. As air velocity across surfaces increases, particle deposition velocity also increases. For example, the deposition velocity of a typical ammonium acid sulfate particle (0.5 μ m diameter) in an office building (typical flow rate of 4-8 ft/min) is about 0.0002 ft/min. In a forced-air cooled cabinet (typical flow rate 30 ft/min) the deposition velocity is about 0.02 ft/min (3-5). Particle accumulation rates (airborne concentration multiplied by the appropriate deposition velocity) are approximately 100 times higher in the forced-air cooled cabinet. This greatly enhanced deposition leads to rapid particle accumulation on circuit boards, devices, and the leads which connect devices to circuit boards.

The submicron particles found in these deposits in urban environments are predominantly derived from fossil fuel combustion. They tend to be hygroscopic above 50-65% relative humidity. In the presence of hygroscopic contamination and elevated relative humidity, an absorbed film of water will form. If the water film extends over a defect in the circuit board covercoat and the defect sits above a conductor pathway operating at a different voltage from that on a nearby lead, current will flow between the lead and the conductor. In an extreme case, with a voltage differential of a few hundred volts, an arc may occur. Component damage will result. Failures of this type underscore the need for both detailed understanding of particle-related degradation processes and new accelerated-life tests that include corrosive, hygroscopic particles.

Particle Sources In The Environment

Particles are usually categorized in three size groups that relate to their predominant sources. Coarse particles (1 - ~20 μ m) are largely derived from mineralogical or biological sources and commonly are formed by mechanical processes. Wind-induced erosion is the most important outdoor generation process. The number density of coarse particles is much lower than that of particles in other size ranges (see Table I), but their mass concentration per unit volume of air is usually about half of the total mass concentration of all airborne particles (4,5,10-12). Fine particles, i.e. <1 μ m diameter, may be sub-divided into two categories. Particles with diameters in the 0.1-1.0 μ m size range are largely anthropologically derived. Their mass distribution peaks at about 0.5 μ m. Their number density is much higher than that of the coarse particles, but their total outdoor mass is usually comparable (4,5,10-12). These particles are designated mature particles here since they originate as much smaller particles that grow predominantly by agglomeration. Once a particle reaches the size range 0.1-1.0 μ m, its diffusivity is too slow to

further agglomerate with other similarly sized particles.

Ultra-fine particles (0.01-0.1 μ m) are mainly attributable to fossil fuel combustion in populated areas, except when volcanic activity is high. They are more plentiful than mature and coarse particles (10,12). Most of the materials in these particles originates from SO₂, NO, NO₂, and volatile organic substances resulting from energy consumption, solvent evaporation, and other sources. Under the influence of sunlight, oxygen, and atmospheric moisture, they are converted to droplets containing sulfuric acid, nitric acid, and a host of organic substances. Ambient ammonia subsequently neutralizes the acid droplets. Because these particles grow rapidly and their composition is continually evolving, they are referred to as adolescent particles in Table I.

Effects Of Moisture On Particle-Contaminated Surfaces

An important characteristic of particles is their critical relative humidity (CRH). The CRHs at room temperature of some relevant compounds are: H₂SO₄ - <5%; NH₄HSO₄ - approximately 40%; (NH₄)₂SO₄ - 80%; NH₄NO₃ - 61% (13-16). In contrast, the effective CRH for many clean metal surfaces, as originally described by Vernon (9), is 70-80%. Particles derived from fossil fuel combustion lower the humidity at which an appreciable film of water exists on metal or insulating surfaces and increase the conductivity of the water film. Comizzoli and others (17) have shown that surface conductance on insulators is exponentially related to relative humidity. Comizzoli has developed a phenomenological model that explains the dependence of surface conductance on temperature and humidity.

Deposition Rate of Particles on Surfaces

Particle deposition rates can be calculated if their size-dependent airborne concentrations are known and a size-dependent deposition velocity appropriate for the air-flow conditions is known or can be estimated. Data on deposition velocities are not entirely consistent and are very sparse for some conditions. The author and colleagues have used the values indicated in Table II for making predictions on deposition rates. These are suggested as guidelines for estimation purposes. Experimentally determined deposition velocities appropriate to the air-flow conditions are needed to insure quantitative results. Deposition velocity is strongly dependent on air-flow velocity and particle size, as shown in Table II (3-5, 18-20). The deposition velocities for the coarse particles are dominated by gravitation and thus increase with size. Deposition velocities for the smallest particles are dominated by their diffusivity and thus increase with decreasing size. The mature particles are affected by both factors.

Outdoors, where wind speeds are typically 500 - 2000ft/min, the average expected deposition rates (deposition rate equals airborne concentration times deposition velocity) of particles to surfaces are $2 \times 10^6 - 2 \times 10^9$, $2 \times 10^3 - 2 \times 10^6$, and 20 - 2000 particles/ft² sec for adolescent, mature, and coarse particles, respectively.

For indoor environments, the airborne concentrations vary considerably, depending on the air-handling-system characteristics (air exchange rate, efficiency of primary and secondary air filters) and indoor sources. For ordinary office buildings where electronic equipment may be

housed (4,5,10,21,23), at typical air flow velocities of 4 - 8ft/min, the deposition rates are calculated to be $3 - 2 \times 10^5$, 200 - 2000, and 0.2 - 20 particles/ft² sec, for adolescent, mature, and coarse particles, respectively. These rates contrast with those for a Class 10 semiconductor manufacturing cleanroom where deposition rates are 0.02 - 15, 0.0003 - 0.03, and 0.001 - 0.02 particles/ft² sec, respectively, for adolescent, mature, and coarse particles. The relevance of these cleanroom data to the study of corrosion of electronics is two fold. (1) The low deposition rates that cause yield degrading defects in semiconductor manufacture are greatly exceeded by field deposition rates. A defect on a semiconductor surface will also be a defect, even if not readily visible to the unaided eye, on a metal surface exposed to atmospheric environments. If a fundamental understanding of corrosion processes in field environments is the objective, these defects ought to be considered. (2) The technology exists to carry out research in environments that are very nearly free of uncontrolled particles. For corrosive gas studies, particle-related complications in the interpretation of gas/surface interactions are avoidable. For studies of particle induced corrosion, unintended particles can be avoided.

Particles Deposition and Reliability

If the service life of an electronic equipment unit is taken to be 10 years, the typical particle loading in the U.S. for mature particles is predicted to be $10^{11} - 10^{12}/\text{ft}^2$ and that for adolescent particles is $10^{10} - 10^{13}/\text{ft}^2$. When these particles, which are rich in ammonium acid sulfate and nitrate, combine with adsorbed moisture, the resulting electrolyte solution is expected to be corrosive to many electronic devices. Clearly, the effects of particles need to be considered in testing of electronic devices and equipment.

New Technologies For Particle Contamination And Control

The reluctance of scientists to consider the effects of submicron particles in atmospheric corrosion and accelerated-life testing of electronics is partly due to the daunting complexity of degradation processes involving particles. The insufficiency of analytical tools to analyze such particles, to count their surface density, and to characterize their effects during experiments, and the lack of methods to carry out accelerated-life tests involving corrosive particles, have also inhibited progress. Decreasing feature size in silicon integrated circuit technology over the last ten years has been paralleled by essential improvements in particle characterization and control. Cleanroom technology is readily available in small, affordable laboratory-scale enclosures. The same tools that have been developed to characterize particles on surfaces and carry out controlled particle deposition on silicon wafers and other substrates are also valuable for atmospheric corrosion research and for reliability studies of electronic devices and equipment (24).

Submicron Particle Exposure Chamber

Numerous chambers exist for life testing of electronic components and devices in the presence of gaseous contaminants. Only a few have been described for testing with dust particles (25-29). All of these were designed to test with coarse particles. Typically, the air flow is either turbulent or undefined. No chambers have been built for life testing using fine ionic particles under conditions of parallel air flow with velocities adequate to accelerate particle deposition (≥ 30 m/min). We have now developed an exposure chamber with the following specifications: 0.01-1 μm particles - $\geq 1 \times 10^{10} \text{m}^{-3}$; flow velocity - up to 35 m/min; parallel air flow; uniform dust concentration.

A schematic drawing of the exposure chamber is shown in Figure 1. Air flows upward through the test area of the chamber. Particles are introduced at a point in the air stream above an ULPA filter that removes contaminant particles with 99.9995% efficiency at 0.12 μm . Injected particles are removed after they have made one pass through the chamber. The chamber, with a 60x60 cm cross section and a height of 110 cm, is sufficiently large to hold a rack that supports up to 48 circuit boards. The ULPA filter, which is situated immediately below the chamber, and a screen just above the filter ensure that the air flow in the chamber is parallel to the vertical walls of the chamber. The air velocity can be controlled at speeds up to 35 m/min.

Submicron (0.01 - 1 μm) ionic particles, such as ammonium sulfate, are generated (24) from an aqueous solution of the salt by compressed, filtered air in an atomizer. The aerosol droplets are dried by a stream of pre-heated air. Residual moisture is removed from the particles by passing them through a diffusion dryer. Charges on the particles are neutralized with a Kr-85 source, which brings them to Boltzmann equilibrium (30). The average size of the particles varies as the cube root of the solution concentration.

The particles are introduced into the exposure chamber through a sixteen nozzle distribution system that was designed to give a uniform concentration of particles throughout the chamber. This was achieved by having all air and particles travel the identical distance and encounter the same type of resistances to flow. The distribution system is made from type 316 stainless steel, the interior of which has been electropolished to minimize particle deposition and shedding.

Steady-state conditions in the dust chamber are achieved by recirculating the air, while constantly introducing new particles immediately downstream from the ULPA filter.

Tests of the exposure chamber included measurements of air velocities and particle concentrations throughout the chamber. The air-velocity distribution, measured at 49 points over the cross section of the chamber at a height corresponding to the middle of the rack that holds the circuit boards is shown in Figure 2. The small variation from point to point is attributed to the interference in the parallel airflow caused by the particle input distribution system.

The concentration and size distribution of $(\text{NH}_4)_2\text{SO}_4$ particles generated from a 0.01 M solution of the salt is shown in Figure 3. The distribution was measured at the same positions as the air velocity with an electrical aerosol analyzer that provides automatic size analysis in increments from 0.01 to 1 μm in diameter. The total concentration is 1.3×10^{10} particles/ m^3 . The mass concentration calculated from this distribution is $18\mu\text{g}/\text{m}^3$. This is slightly more than the typical indoor concentration in air. Acceleration of the deposition rate to the devices or circuit boards being tested is accomplished predominantly by the air flow velocity. The particle-concentration distribution for 0.024 μm -sized particles is shown in Figure 4. The average concentration and standard deviation for this size fraction are 4.13×10^9 and 6.71×10^8 particles/ m^3 , respectively. Similar plots were obtained for the other size fractions shown in Figure 5. To determine whether a constant concentration can be maintained for an extended time, the concentration was measured every two minutes for five hours. The results (Figure 5) show that the average concentration remains steady. The average concentration is 1.27×10^{10} particles/ m^3 with a 95% confidence limit of $\pm 3.17 \times 10^8$ particles/ m^3 .

Research Opportunities In Particle Effects

Failures in electronic devices and equipment usually occur at localized defects. Investigations that evaluate average corrosion effects over large areas may fail to uncover the weak links that lead to failure. Particles cause localized defects and highly non-uniform corrosion. Corrosive gas and solution experiments usually lead to more uniform corrosion and potentially unrealistic failures.

Experiments on particle effects are best carried out in environments that are nearly free of particles. These experiments can be accomplished in small modular cleanrooms that are available at affordable cost. The development of the submicron particle exposure chamber described in this paper and a thermophoretically driven particle deposition apparatus described in a companion paper in this Proceedings (32) provide researchers with the experimental tools needed to carry out well-controlled particle depositions on metal test coupons, electrical test structures, and devices.

Acknowledgement

Many people at AT&T Bell Laboratories have contributed over several decades to the knowledge base that led to this paper. Those currently active in this work include L. Clark, R. B. Comizzoli, G. R. Crane, T. E. Graedel, T. Hastie, R. E. Lobnig, P. W. Morrison, K. Nguyen, G. A. Peins, L. A. Psota-Kelty, J. Rauchut, and A. Swanson. C. J. Weschler at Bellcore has also been an important contributor.

References

1. J. R. Walton, J. B. Johnson, and G. C. Wood, *Br. Corros. J.*, **17**, 59(1982); **17**,65(1982).
2. U. R. Evans, "The Corrosion and Oxidation of Metals: Scientific Principles and Practical Applications," Edward Arnold (Publishers) Ltd., 1961, London, p. 446.
3. J. D. Sinclair, *J. Electrochem. Soc.*, **135**, 89C (1988).
4. J. D. Sinclair, L. A. Psota-Kelty, C. J. Weschler, and H. C. Shield, *Atmos. Environ.*, **24A**, 627 (1990).
5. J. D. Sinclair, L. A. Psota-Kelty, G. A. Peins, and A. O. Ibidunni, *Atmos. Environ.*, **26A**, 871 (1992).
6. R. B. Comizzoli, R. P. Frankenthal, P. C. Milner, and J. D. Sinclair, *Science*, **234**, 340 (1986).
7. W. H. Abbott, *IEEE Transactions On Components, Hybrids, And Manufacturing Technology*, **11**, 22 (1988).
8. J. D. Sinclair and L. A. Psota-Kelty in "Proceedings of the International Congress on Metallic Corrosion," Vol. 2, p. 296, National Research Council of Canada, Ottawa, Ont., Canada (1984).
9. W. H. J. Vernon, *Trans. Faraday Soc.*, **31**, 1668 (1935).
10. R. P. Donovan, D. R. Locke, C. M. Osburn, and A. L. Caviness, *J. Electrochem. Soc.*, **132**, 2731 (1985).
11. K. T. Whitby, R. B. Husar, and B. Y. H. Liu, in "Aerosols and Atmospheric Chemistry," G. M. Hidy, Editor, pp. 237-264, Academic Press Inc., New York (1972).
12. B. Y. H. Liu, J. W. Lee, D. H. Pui, K. H. Ahn, and S. L. Gilbert, *J. Environ. Sciences, September/October*, **22** (1987).
13. R. C. Weast and M. J. Astle, "CRC Handbook of Chemistry and Physics", 59th Edition, CRC Press, 1978, Palm Beach Florida, p. E46.
14. I. N. Tang, *J. Aerosol Sci*, **7**, 361(1976).
15. R. J. Charlson, D. S. Covert, T. V. Larson, and A. P. Waggoner, *Atmos. Environ.*, **12**, 39(1978).
16. A. S. Wexler, J. H. Seinfeld, *Atmos. Environ.*, **25A**, 2731(1991).
17. R. B. Comizzoli, "Materials Developments in Microelectronic Packaging: Performance and Reliability," Proceedings of the Fourth Electronic Materials and Processing Congress, ASM International, Ohio, 1991, p. 311.
18. H. Sievering, *Atmos. Environ.*, **16**, 301 (1982).
19. B. Y. H. Liu, B. Fardi, and K. H. Ahn, *Proceedings - Institute of Environmental Sciences*, San Jose, pp. 19-23, May (1987).

20. J. J. Wu, R. J. Miller, D. W. Cooper, J. F. Flynn, D. J. Delson, and R. F. Teagle, *J. Environ. Sciences, January/February*, 27 (1989).
21. J. D. Sinclair and L. A. Psota-Kelty, unpublished work.
22. M. K. Owen, D. S. Ensor, L. S. Hovis, and W. G. Tucker, and L. E. Sparks, *Aerosol Sci. and Techn.*, 13, 486 (1990).
23. L. A. Clark, T. Hastie, L. A. Psota-Kelty, J. D. Sinclair, and J. W. Rauchut, *Aerosol Sci. and Techn.*, 16, (1992).
24. R. P. Frankenthal, R. Lobnig, D. J. Siconolfi, and J. D. Sinclair, *J. Vac. Sci. Technol.*, in press.
25. R. V. Steenstrup, V. M. Fiacco, and L. K. Schultz, *Proc. 28th IEEE Holm Conf. Electrical Contacts*, 1982, p. 59.
26. EIA Standard RS-364-50, "Test Procedure #50 Sand Dust Test Procedure for Electrical Connectors," Electrical Industries Association, Washington, DC, 1983.
27. Department of Defense, MIL-STD-810D, paragraph 510.2, July 19, 1983.
28. L. White, *Proc. 33rd IEEE Holm Conf. Electrical Contacts*, 1982, p. 87.
29. D. G. DeNure and E. S. Sproles, Jr., *IEEE Trans. Compon., Hybr., Manuf. Technol.*, 14, 802 (1991).
30. B. Y. H. Liu and D. Y. H. Pui, *J. Colloid Interface Sci.*, 49, 305 (1974)
31. R. P. Frankenthal, R. Lobnig, D. J. Siconolfi, and J. D. Sinclair, This Proceedings.

TABLE I. TYPICAL AIRBORNE PARTICLE CONCENTRATIONS (PARTICLES/ft³)

| | <u>Adolescent Pollutants</u> <u>0.01-0.1μm</u> | <u>Mature Pollutants</u> <u>0.1-1.0μm</u> | <u>Minerals, Biologicals</u> <u>1-15μm</u> |
|-----------------------|------------------------------------------------------------------|-------------------------------------------------------------|--------------------------------------------------------------|
| Outdoor | 10 ⁸ - 10 ¹⁰ (11,12)† | 10 ⁵ - 10 ⁸ (4,5,11,12) | 10 ³ - 10 ⁵ (4,5,11,12) |
| Office Building | 10 ⁴ - 10 ⁷ * | 10 ⁶ - 10 ⁷ (4,5,10,21,22) | 10 - 10 ³ (4,5,10,21,22) |
| Class 10 Cleanroom | 10-500(12,23) | 1-10(12,23) | 0.05-1(12,23) |

† The numbers in parenthesis are references

* Estimated - insufficient experimental data

TABLE II. DEPOSITION VELOCITIES FOR AIRBORNE PARTICLES (ft/sec)

| | <u>Adolescent Pollutants</u> <u>0.01-0.1μm</u> | <u>Mature Pollutants</u> <u>0.1-1.0μm</u> | <u>Minerals, Biologicals</u> <u>1-15μm</u> |
|---------------------------------------|------------------------------------------------------------------|-------------------------------------------------------------|--------------------------------------------------------------|
| Outdoor (500-2000 ft/min) | 0.02-0.2* | 0.02(18)† | 0.02 |
| Office Building (4-8 ft/min) | 0.0003-0.02* | 0.0002(3-5) | 0.02 |
| Class 10 Cleanroom (100 ft/min) | 0.002-0.03(19,20) | 0.0003-0.003(19,20) | 0.02 |

† The numbers in parenthesis are references

* Estimated - insufficient experimental data

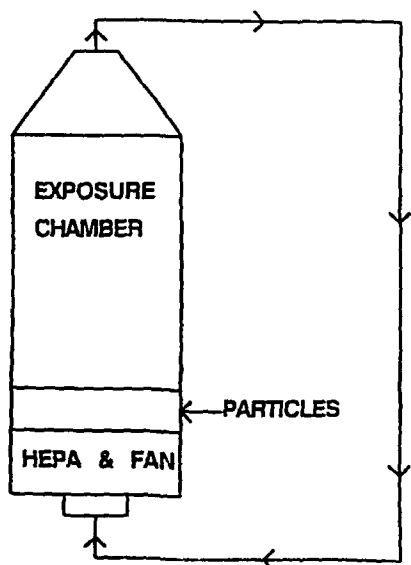


Figure 1. Schematic drawing of the exposure chamber for life testing with submicron ionic dust particles. Particles are introduced into the air stream just above the ULPA filter and are removed from the system by the filter after one cycle. A screen (not shown) just above the ULPA filter ensures parallel air flow.

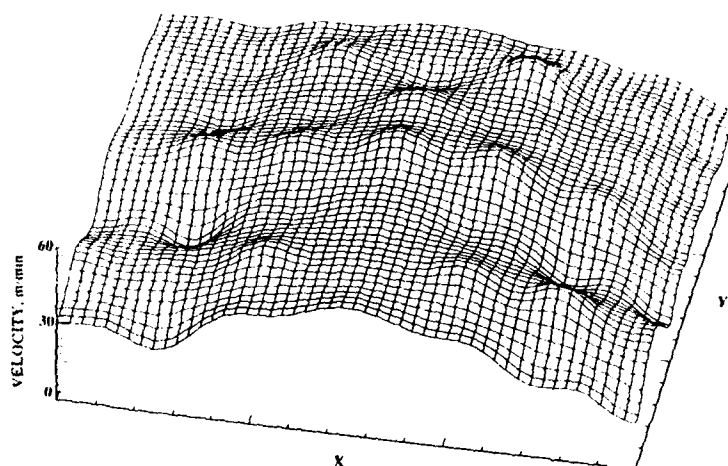


Figure 2. Air velocity distribution profile across the dust exposure chamber at the height of the middle of the test rack.

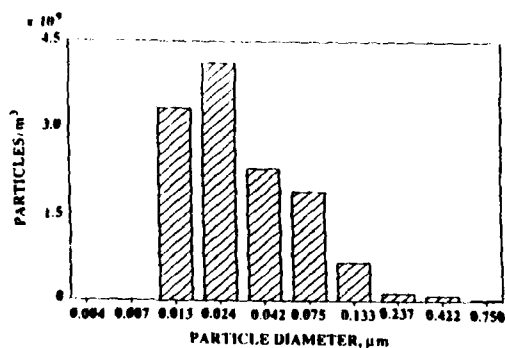


Figure 3. Concentration and size distribution of particles measured across the dust exposure chamber at the height of the middle of the test rack.

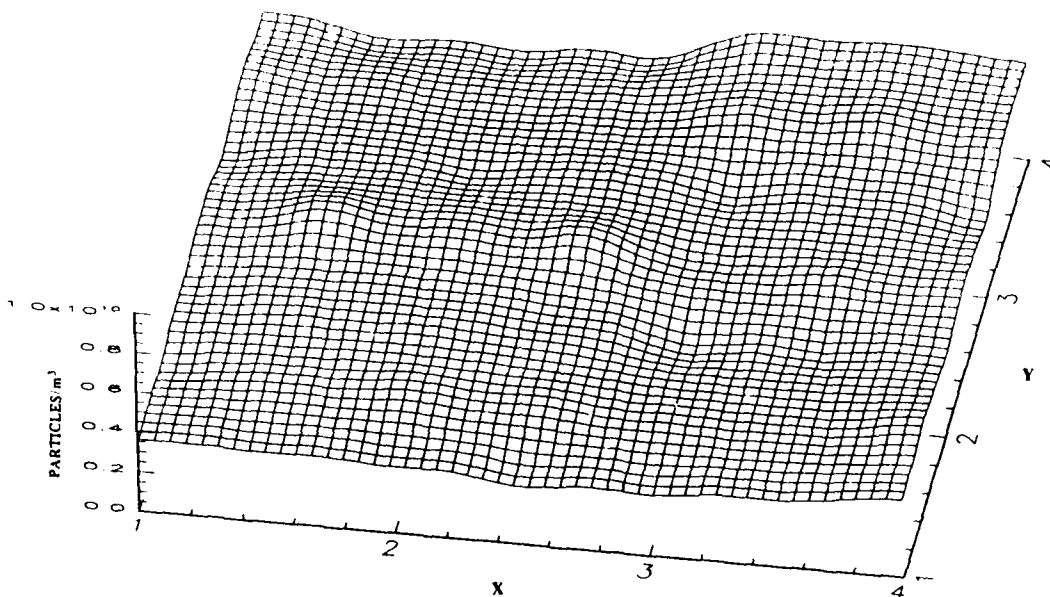


Figure 4. Particle-concentration distribution profile for 0.024 μm -sized particles across the dust exposure chamber at the height of the middle of the test rack.

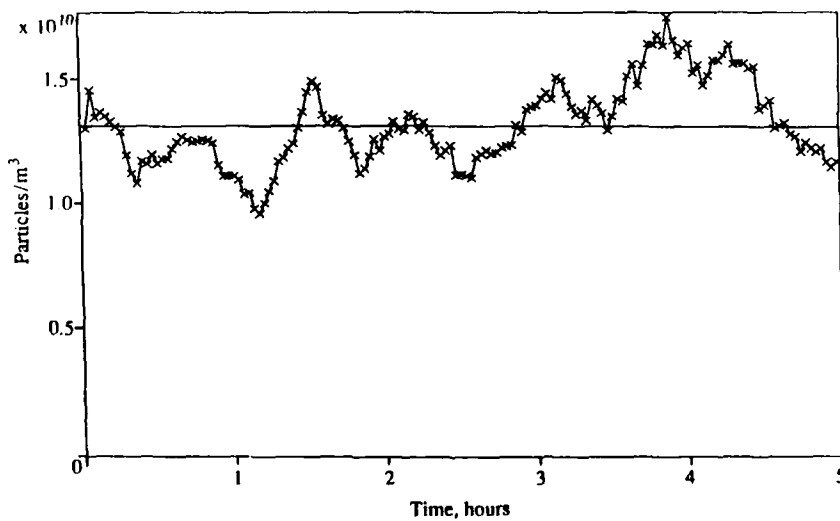


Figure 5. Concentration of particles over an extended time period. Horizontal line is average of all 150 measurements.

In Situ Investigation of the Initial Stages of the Electrochemical Deposition of Metals by Contact Electric Resistance Method

V. A. Marichev

Russian Academy of Science, Institute of Physical Chemistry, currently visiting at the Technical Research Centre of Finland
Metals Laboratory, P. O. Box 26
SF-02151 Espoo, Finland

Abstract

The new in situ Contact Electric Resistance (CER) method was applied for investigation of the very initial stages of electrodeposition in twelve different metal-electrolyte systems. The experiments were carried out at room temperature using precracked specimens in galvanostatic mode for Cu/Cu²⁺ deposition and in potentiostatic mode for the other systems. All the tests were started at positive potentials, where deposition of the investigated cation is impossible, and the potential was lowered stepwise through the potential range of interest. First, the contact electric resistance of each substrate metal was measured as a function of the potential in the supporting electrolyte. Second, the cation was added and the test was repeated starting again from a potential at which deposition is impossible. The potential at which the contact electric resistance during this second run started to differ from the resistance measured in the supporting electrolyte was taken as the potential of electrodeposition of the corresponding metal. The measured underpotential values for electrodeposition of Cu/Cd²⁺, Cu/Sn²⁺, Cu/Zn²⁺ and Ag/Pb²⁺ (0.27 V, 0.16 V, 0.3 V and 0.17 V respectively) are in good agreement with published data. The sensitivity of the CER method for Cu/Cu²⁺ electrochemical deposition in acid electrolytes is about 0.03 monolayers.

Key terms: contact electric resistance, electrodeposition, underpotential deposition

Introduction

The study of the very initial stages of the electrochemical deposition of metals, including underpotential electrodeposition, is important and interesting both from scientific and industrial applications point of view. The main methods of in situ investigation to cover this problem are cyclic voltammetry (VAM)^{1,2} and recently scanning tunneling microscopy (STM)^{3,4}. Both of them have their own advantages and some limitations which make it difficult to use these methods for any "deposited metal/solution/substrate metal" electrochemical system. First of all, it is necessary to avoid interference from parallel electrochemical reactions for both VAM and STM and difficulties of STM observations of atomic-level crystalline lattice for most of metals in contact with electrolyte solutions.

In this paper, we report in situ investigation of submonolayer electrodeposition for twelve different metal-electrolyte systems using new Contact Electric Resistance (CER) method which is sensitive to anions and water adsorption and to oxidation of metals. The sensitivity of the CER method is 10⁻⁹ Ω and it can be used for all conducting materials in any electrolyte at ambient and high temperatures and pressures in a region of potentials including the potentials of intensive evolution of hydrogen or oxygen. CER-method was firstly developed for ambient conditions^{5,6} and later applied for high temperature-high pressure water (300 °C, 150 bar) investigations⁷.

Experimental Procedure

The CER method consists of accurate measurement of the electric resistance (ER) between two periodically contacted metallic specimens. In the present work these two specimens were the walls of a fatigue crack in a single edge notched plate sample cyclically loaded below the corrosion fatigue crack growth threshold.

The samples of the investigated substrate metals were 200 x 25 x 2 mm (Fig. 1a) with a 60° cut and with an air fatigue crack of 3 - 3.5 mm length. The sample and contacts for measuring ER of the central part of the sample with a crack (points A) were plated with a chemically stable varnish (except the 1 cm² surface area near the fatigue crack - nondashed part of the sample in Fig. 1a), placed into an electrochemical cell and fixed in electrically insulated grips of a testing machine Instron 1195. During cyclic loading of the sample this machine provides an accuracy of 0,1 % in reproductibility of maximum and minimum loads of the cycle, which results in the reproducibility of the relative displacement of the cyclically contacting crack walls at the level of 10⁻⁹ m.

A direct current of 10 A was passed through the sample generating a voltage signal depending on the ER of the sample. The ER of the sample during cyclic loading was measured using a double (Thompson) bridge, and was continuously recorded by an X-t-recorder. Since the methods of sample preparation and the details of CER measurement have been described elsewhere^{5,6}, we note only that the precision class of the direct current stabilizer and the double bridge provided the measurement of ER with an accuracy up to 0.02 % and the sensitivity of 10⁻⁹ Ω.

The schematic explanation of the variation of the ER of the sample at cyclic loading is given in Fig. 1b, where points A indicate the points of current supply and connections of the double bridge. If there is no crack in a sample and its ER is equal to R₁, then after growing the fatigue crack at the maximum tension load of the cycle (when the crack is fully open, i.e., its walls do not touch each other) the sample resistance grows by a factor of R₂ due to decrease of its cross-section area. At the minimum load of the cycle (zero or compression) the crack walls will touch each other which is equivalent to shunting the resistance R₂ by the contact resistance R equal to the ER sum of the successive chain: metal-film-electrolyte between the crack walls-film-metal. Thus, at the cyclic loading of a sample with a crack its ER cyclically varies from R₁ + R₂ at the maximum load and the full opening of the crack to R₁ + R₂R/(R₂ + R) at the minimum load. The variation of ER of a sample during each cycle (ΔR) is determined by the equation (1) and the contact ER at the minimum load of the cycle (R) by equation (2):

$$\Delta R = \frac{R_2^2}{(R_2 + R)} \quad (1)$$

$$R = \frac{R_2(R_2 - \Delta R)}{\Delta R} \quad (2)$$

Resistance R₂ is a constant which depends upon the specimen size, fatigue crack length and specific electric resistance of the investigated substrate metal. For any particular specimen the ΔR value depends upon R (eq. 1), i.e. upon the electrolyte composition and the electro-

chemical potential. ΔR values corresponding to different potentials are continuously measured and recorded, and then used to account R from equation (2).

In this work the potential dependence of R was investigated at room temperature in several electrolytes (see Table 1), prepared from distilled water and chemically pure reagents. Deairation of the electrolytes with pure argon gas was used only during experiments with Cu/Cu²⁺-electrodeposition. The specimens of Ag, Cu and Ni (substrate metals) were of 99.99 % purity grade. The electrode potentials were measured using Ag/AgCl-reference electrode, then recounted and reported in this paper vs. SHE.

Experimental Results and Discussion

Some experimental data and conclusions from the previous works^{5,6} devoted to CER-method are important for this investigation and have to be shortly listed as following:

1. The contact electric resistance (R) is independent of the ionic electrolyte conductivity, but is defined by electronic conductivity between the crack walls.
2. R is assumed to be zero at the most complete reduction of the films on the crack walls during cathodic polarization. Any increase in the R obtained by polarization to more positive potentials is due to an increase of the electric resistance of the films on the contacting crack walls.
3. The changes of the cyclic loading frequency (0.04 - 0.4 Hz) and direct current value through the specimens (0.03 - 30 A) have no noticeable effect on the R-potential behavior, but the changes of minimum and/or maximum loads or stress ratio of the cycling loading do have an effect on this behavior. For this reason, all the runs in the present work were carried out by constant values of direct current (10 A), frequency (0.2 Hz) and stress ratio (0.25) of cyclic loading.

The usual procedure to obtain the R dependence upon the potential during adsorption and/or oxidation of metals consists of the initial reduction of the crack walls by cathodic polarization up to high enough negative potentials. After reducing all films on the contact surfaces the R-potential dependence was studied by increasing the potential stepwise by 0.025 - 0.1V after an exposure of 2 - 5 min at each potential value. Curve 1 (Fig. 2) demonstrates such a potential dependence of R of Cu in 1 M H₂SO₄ which was used as a supporting electrolyte for Cu/Cu²⁺-deposition experiments. It is necessary to underline that curve 1 was quasi-reversible, i.e. any potential shift towards negative or positive direction resulted in fast (during 1 - 3 min) response of R-values, which then remained stable for a long time at each potential value. There is no oxide film on Cu in this acid solution, but water and sulfate anion adsorption occurs causing the R increase at positive potentials.

Addition of 0.1 - 0.3 M CuSO₄ to the solution strongly changed the polarization behavior of Cu (curves 2 and 3, Fig. 2), resulting in the realization of the reversible Cu/CuSO₄ electrode with high exchange current, about 1 mA/cm². At these conditions, it is more simple and profitable to study the initial stages of the electrochemical deposition Cu/Cu²⁺ using the galvanostatic polarization by cathodic current densities below 100 μ A/cm² and keeping in the mind that the charge density 350 μ C/cm² corresponds to one monolayer of bivalent metal electrodeposition. Fig. 3 shows the kinetics of changing of the R of Cu as a function of the cathodic polarization current in the electrolyte 1 M H₂SO₄ + 0.3 M CuSO₄ deaerated with

argon gas bubbling. In this electrochemical system at the open circuit potential there are two cathodic reactions - copper electroposition and the reduction of the remaining dissolved oxygen, but only one anodic reaction - electrochemical dissolution of copper. This results in a slow increase in time of R at the open circuit potential owing to anodic dissolution of the contacting crack walls, i.e. increasing of the distance between them. To equalize such a dissolution and to stabilize the R values it was necessary to apply a small cathodic current (as shown at the initial part A of the upper curve in Fig. 3). This cathodic current density is equal $7 \mu\text{A}/\text{cm}^2$ for the run reported in Fig. 3 and changed in other runs between 3 and $25 \mu\text{A}/\text{cm}^2$ depending upon the deaeration time.

After stabilization of the R values, the cathodic current was increased stepwise by $1 \mu\text{A}/\text{cm}^2$. This resulted in the decreasing of the R by 1 to 3 n Ω during the first 2 to 3 cycles of the specimen loading, i.e. during 10 to 15 s after increasing of the current. As it is shown in Fig. 3, this effect is reversible and well enough reproducible. Thus, the charge density 10 - $15 \mu\text{C}/\text{cm}^2$ corresponding to an average of about 0.03 - 0.05 monolayers may be considered as the sensitivity of the CER method to the electrodeposition of metals on the contacting surfaces.

The electrodeposition process takes place not only on the crack walls, but on all the rest surface of the sample, which is not covered by the protective varnish. Nevertheless, we may take into account only decreasing of the R and disregard the decreasing of the sample electric resistance owing to the electrodeposition on the flat sides of the sample until the thickness of the sample would increase for about $1 \mu\text{m}$, which corresponds to the charge density of about $1 \text{C}/\text{cm}^2$ (never reached in this work).

It is shown in Fig. 3 that both submonolayer Cu/Cu^{2+} electrodeposition and stripping of the deposited layer proceed very fast. It is interesting to note that it was not necessary to apply the anodic current for stripping, but it was enough to slightly diminish the cathodic current. The kinetics of the R decreasing as a function of the cathodic current density of Cu/Cu^{2+} electrodeposition is shown in Fig. 4. Being recounted into the charge units (or monolayers of coverage) all the experimental points from Fig. 4 can be represented by one S-shaped curve (Fig. 5), which actually characterizes the sensitivity of the CER method to the metal electrodeposition as a function of the thickness of the deposited layer. One can see that this sensitivity is very high for the first 0.1 - 30 monolayers, but becomes smaller and smaller with further copper electrodeposition in the region of 50 - 200 monolayers, which corresponds to the thickness of about 20 - 80 nm. This thickness is very small in comparison with the average crack opening (2 - $3 \mu\text{m}$) at the minimum load of the cyclic loading of the sample. The contacting crack walls are the fatigue fracture surfaces, which are not smooth. The distances between them at different points of the crack surface may vary from zero up to the average crack opening values according to some kind of the statistic distribution. This can be, for example, Gaussian type distribution. When in contact, between some parts of the contacting crack surfaces the remaining free distance is small enough for tunneling to occur. These areas are responsible to the sensitivity of the R to the adsorption of anions and/or submonolayer electrodeposition of metals^{5,6}. Probably only these areas are "actively operating", all the others having no noticeable input in the R.

The only reason for the R falling down during Cu/Cu^{2+} electrodeposition is decreasing of the distance between the contacting surfaces. It is not clear, why the CER-method has so high sensitivity to the very initial stages of this process, but decreasing of the sensitivity after deposition of 50 - 100 monolayers is probably connected with the decrease in the fraction

of the actively operating areas between contacting surfaces (smoothing of the surfaces). This proposition has the following experimental support. After 1800 s of the copper electro-deposition by the cathodic current $8 \mu\text{A}/\text{cm}^2$ the R sensitivity to electrodeposition became very low (curve 3, Fig. 4). At the time t^* indicated by an arrow the minimum load of the cycling loading of the sample was increased by 10 %. i.e. new actively operating areas were created. This immediately caused a sharp increase of the R sensitivity to the electrodeposition followed by its gradual falling down with time (curve 3', Fig. 4).

There are only two reactions, copper deposition and dissolution, which are able to change the R of the copper specimen in the deaerated $\text{H}_2\text{SO}_4 + \text{CuSO}_4$ solution at the polarization currents below exchange current of the Cu/CuSO_4 -electrode. The copper deposition in this electrochemical system always decreases the R of the specimen. Other systems like Ni/Cu^{2+} , Ag/Cu^{2+} , Ag/Pb^{2+} and Ag/Sn^{2+} are more complicated. To study the electrodeposition in such systems by the CER method it is necessary to use the potentiostatic polarization of the specimens and to take into account the specific electric resistances of the substrate and deposited metals. Let us consider the copper electrochemical deposition on silver as an example of the deposition of some metal on the other one having lower specific electric resistance. First of all the R-potential dependence was obtained for the substrate metal (silver) in the supporting electrolyte (0.5 M H_2SO_4) starting from high enough positive potentials (+0.4 V) and shifting the potential towards negative direction stepwise by 0.01 - 0.05 V after an exposure of 2 - 10 min at each potential value to reach quasiequilibrium values of the R (curve 1, Fig. 6). The most essential and important feature of this curve is gradual falling down of the R by any shift of the potential towards negative direction owing to decreasing of water and sulfate anions adsorption on silver^{5,6}.

Addition of 0.01 M CuSO_4 to the supporting electrolyte at starting potential (+0.4 V) had no remarkable effect on the R-potential behavior until the potential +0.25 V was reached (curve 2, Fig. 6). At this potential the R did not decrease (like it was before in the supporting electrolyte), but slightly increased which indicated the initial stage of copper electro-deposition. Submonolayer adsorption of the less electroconductive metal (copper) covers partly the contacting surfaces of the more electroconductive metal (silver) and has to increase its R, which was observed. The R growth became more pronounced by the following potential shifts to 0.24 and 0.23 V. At the potential 0.22 V the R started to increase again, but after 2 min it suddenly decreased. This indicated the bulk electrodeposition of copper on silver, which caused the decreasing of the distance between contacting surfaces like it was shown previously for Cu/Cu^{2+} electrodeposition (Figs. 3 and 4). By increase of CuSO_4 concentration the same R-potential behavior was observed at more negative potentials (curves 2 - 4, Fig. 6). Such an R-potential dependence was typical for all investigated cases of the electrochemical deposition of the less electroconductive metals on the more electroconductive metals.

The R-potential time dependencies like the curves in Fig. 6 were obtained for eight other systems $\text{Me}_1/\text{Me}_2^{n+}$ (listed in the Table 1) and then were recounted into the quasiequilibrium R-potential dependencies, some of which are shown in Figs. 7 and 8. Possibly this kind of the experimental data representation is more convenient and informative. For example, for the electrochemical deposition of cadmium on copper from the solution 0.5 M $\text{H}_2\text{SO}_4 + 0.75 \text{ M Na}_2\text{SO}_4 + 0.02 - 0.2 \text{ M CdSO}_4$ (Fig. 8) one can see, that the R-potential dependence for supporting electrolyte (curve 1) declines from these dependencies for cadmium containing electrolytes (curves 2 and 3) at much more positive potentials than equilibrium potentials (indicated by arrows) for corresponding cadmium-ion concentrations. This means that the

cadmium underpotential deposition on copper occurs in the investigated conditions. The cathodic polarization curves for copper in the supporting electrolyte and in cadmium containing electrolytes are nearly the same (curve 4) because the polarization current depends mainly upon hydrogen evolution.

If the potentials corresponding to the declination of the R-potential curves in the supporting (curve 1, Fig. 8) and cadmium containing (curves 2 and 3) electrolytes are the potentials of the cadmium electrodeposition on copper (E_{ED}), the underpotential ΔE may be accounted as a difference $\Delta E = E_{ED} - E_{ED}^0 = 0.27$ and 0.26 V for solutions with 0.02 and 0.2 M $CdSO_4$ respectively (E_{ED}^0 is the calculated equilibrium potential of the solution in question). The values $+\Delta E$ (underpotential) and $-\Delta E$ (overvoltage) of the metals electrodeposition obtained in this work by the CER-method and some available from literature data are listed in the Table 1. One can see, in the cases where comparison of the data is possible, that the CER-method provides underpotential electrodeposition values, which are slightly higher, but close to the published data. For Ni/Ni^{2+} electrodeposition a small overvoltage was measured, which increased twice owing to chlorine-ion addition into the electrolyte. Secondary parallel processes like hydrogen evolution and/or nitrate-ion reduction do not disturb the CER-method regarding the application for investigation of the very initial stages of the electrochemical deposition of metals. This method can be used in any electrolytes even at high temperatures and pressures⁵⁻⁷. It may be important, for example, for the investigation of the electrodeposition of metals from molten salts, where it is difficult or impossible to use other in situ methods.

Conclusions

1. We have demonstrated the possibility of an in situ CER-method application to study the very initial stages of the electrochemical deposition of metals. The underpotential values measured in this work are in good agreement with the published data.
2. The sensitivity of the CER method for Cu/Cu^{2+} electrodeposition in acid electrolytes is about 0.03 monolayers.
3. The secondary parallel processes like hydrogen evolution and/or nitrate reduction do not disturb the CER-method application for the electrodeposition processes.

References

1. D. M. Kolb, "Advances in Electrochemistry and Electrochemical Engineering", Eds. H. Gerisher, C. W. Tobias. Interscience, N.Y., 11 (1978): p. 125.
2. M. G. Chu, J. McBreen, G. Adzic, J. Electrochem. Soc., 128 11 (1981): p. 2281.
3. Fu-Ren F. Fan, A. J. Bard, J. Electrochem. Soc., 136 11 (1989): p. 3216.
4. M. P. Green, K. J. Hanson, R. Carr, I. Lindau, J. Electrochem. Soc., 137 11 (1990): p. 3493.
5. V. A. Marichev, Surface Science, 250 7 (1991): p. 220.
6. V. A. Marichev, Soviet Materials Science, 26 1 (1990): p. 8.

7. T. Saario, V. A. Marichev, H. Hänninen, Proceedings of the 12th Scandinavian Corrosion Congress and EUROCORR '92, Ed. P. J. Tunturi. Finncorr, 2 (1992): p. 169.

Table 1. $\Delta E = E_{ED} - E_{ED}^0$. Underpotential (+) and/or overpotential (-) deposition for investigated couples Me_1/Me_2^{n+} .

| Substrate Metal Cation | Electrolyte composition, pH | ΔE , V | | Ref. |
|------------------------------|------------------------------------------------------------------------------------------------------------------------------------|----------------|-----------|------|
| | | this work | published | |
| Cu/Sn ²⁺ | 1 M H ₂ SO ₄ + 0.1 M SnSO ₄ pH 0.5 | +0.15 | | |
| Cu/Zn ²⁺ | 2.5 M NaOH + 0.1 M ZnO pH 14.3 | +0.30 | +0.22 | [2] |
| Cu/Cr ³⁺ | 1 M NaCl + HCl + 0.1 M CrCl ₃ pH 1.5 | +0.32 | | |
| Cu/Cd ²⁺ | 0.5 M H ₂ SO ₄ + 0.75 M Na ₂ SO ₄ + 0.2 M CdSO ₄ pH 1 | +0.26 | +0.23 | [1] |
| Cu/Ni ²⁺ | 0.8 M Na ₂ SO ₄ + H ₃ BO ₃ + 0.6 M NiSO ₄ pH 4.5 | -0.13 | | |
| Ag/Cu ²⁺ | 0.5 M H ₂ SO ₄ + 0.3 M CuSO ₄ pH 1.2 | -0.01 | 0 | [1] |
| Ag/Pb ²⁺ | 0.1 M HNO ₃ + 0.1 M Pb(NO ₃) ₂ pH 2 | +0.17 | +0.16 | [1] |
| Ni/Ni ²⁺ | 0.5 M Na ₂ SO ₄ + H ₃ BO ₃ + 0.6 M NiSO ₄ pH 4.5 the same +0.1 M NaCl | -0.05 -0.10 | | |
| Ni/Cu ²⁺ | 1 M Na ₂ SO ₄ + H ₂ SO ₄ + 0.1 M CuSO ₄ pH 1.5 | -0.05 | | |

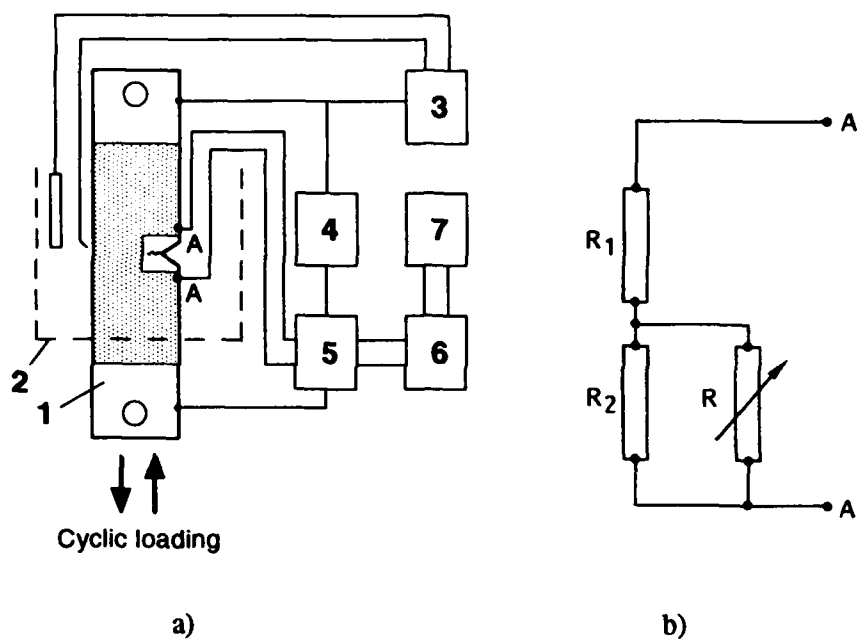


Figure 1. Scheme for measurement of the Contact Electric Resistance (CER) of the sample with a fatigue precrack (a). The electrical analog of the sample (b). (1) Sample, (2) electrochemical cell, (3) potentiostat, (4) direct current source, (5) double bridge, (6) amplifier, (7) recorder.

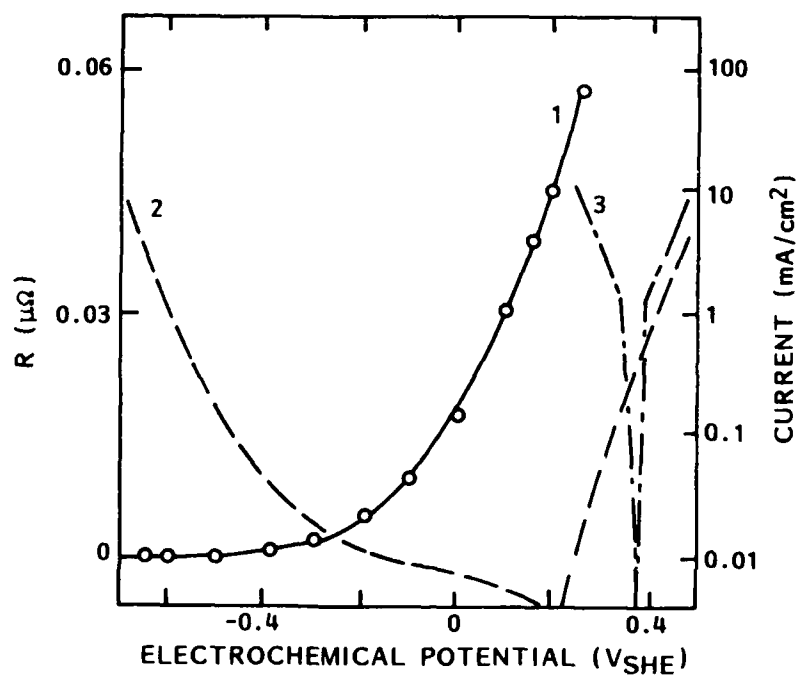


Figure 2. The potential dependence of the copper CER (R) in 1 M H₂SO₄ (1), polarization curve of copper in 1 M H₂SO₄ (2), polarization curve of copper in 1 M H₂SO₄ + 0.3 M CuSO₄.

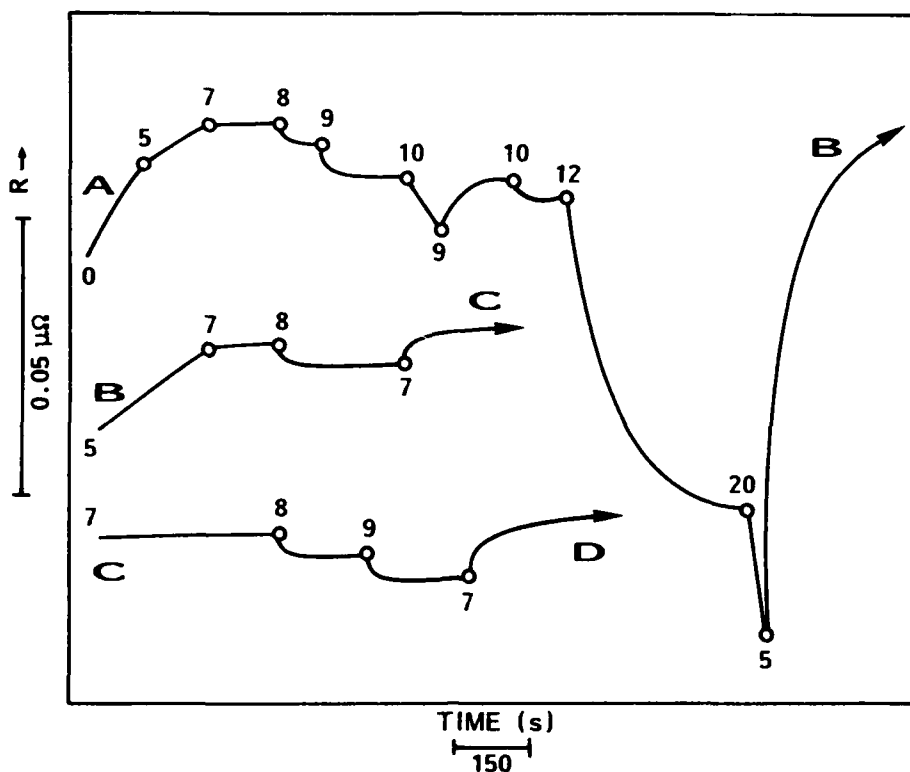


Figure 3. Kinetics of the R variations of copper during cathodic galvanostatic polarization in 1 M $\text{H}_2\text{SO}_4 + 0.3 \text{ M CuSO}_4$. Time sequence: A-B-C-D. The moments of current changes are indicated by point, near which the cathodic currents (μ/cm^2) are shown.

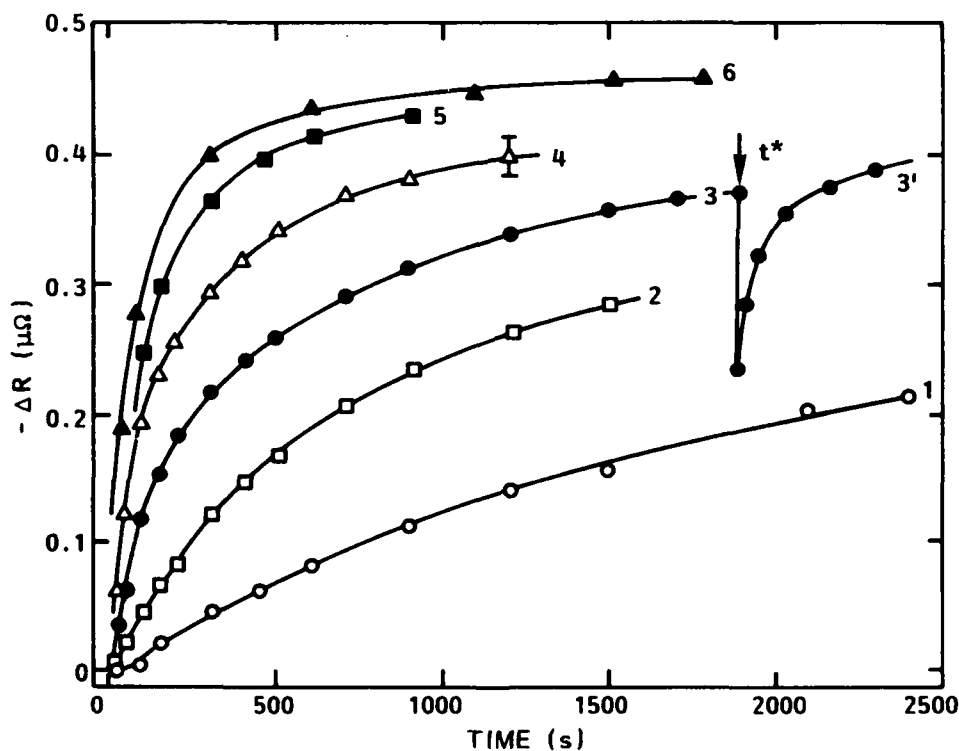


Figure 4. Decreasing of the CER of copper in 1M $\text{H}_2\text{SO}_4 + 0.3 \text{ M CuSO}_4$ as a function of time. Cathodic galvanostatic polarization by currents ($\mu\text{A}/\text{cm}^2$): (1) 1.5, (2) 3, (3) 8, (4) 18, (5) 35, (6) 80.

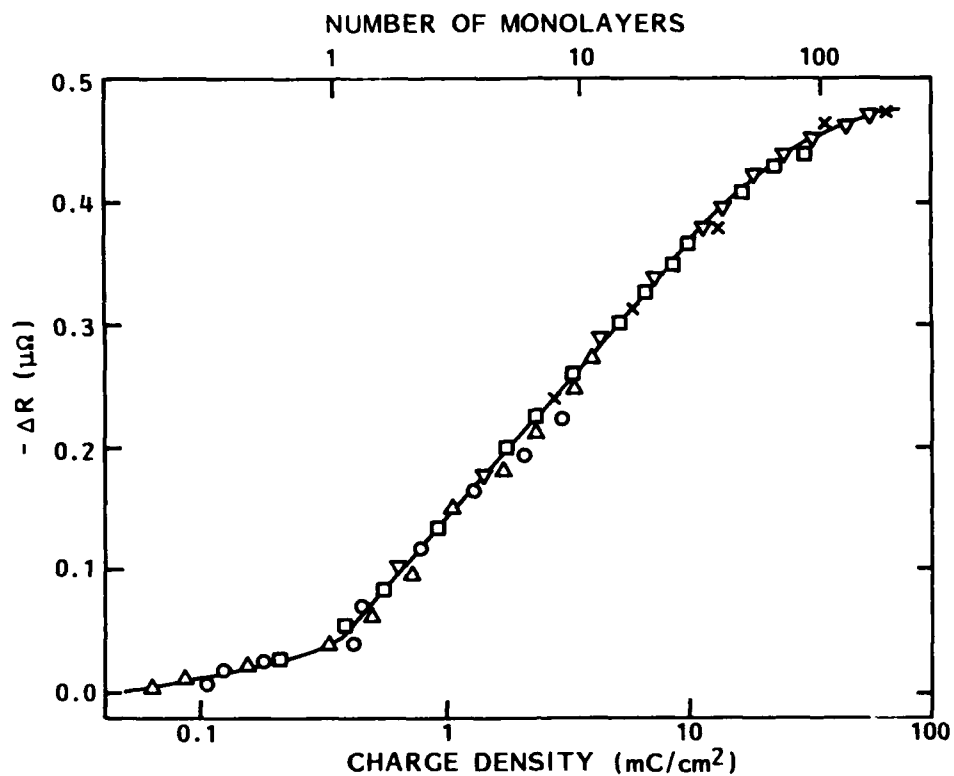


Figure 5. Decreasing of the R of copper in $1\text{M H}_2\text{SO}_4 + 0.3\text{ CuSO}_4$ as a function of the charge (Q) passed during the copper electrodeposition and/or quantity (N) of deposited monolayers. Different symbols correspond to the different cathodic current densities from 1.5 up to $80\ \mu\text{A}/\text{cm}^2$.

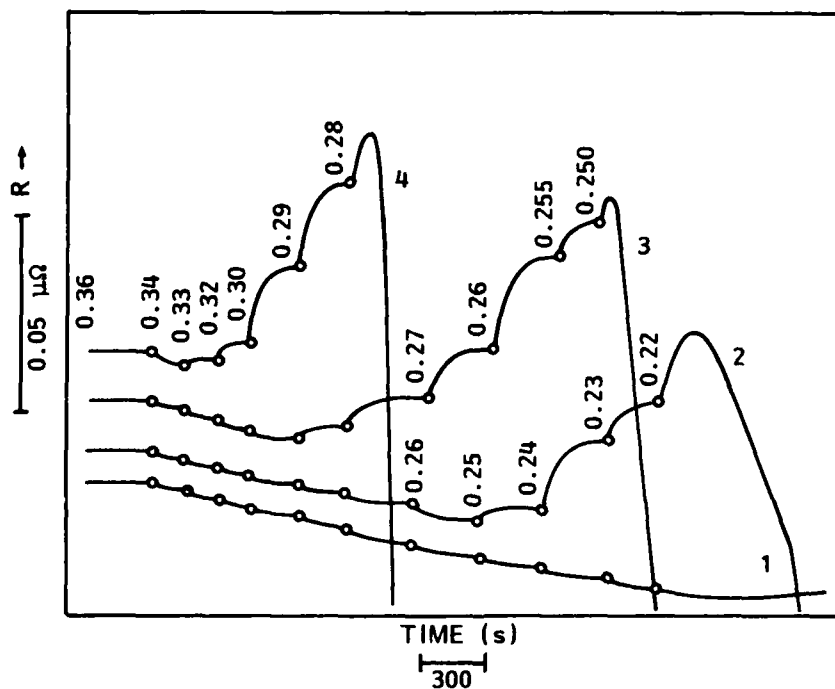


Figure 6. Kinetics of the R variations of silver during potentiostatic polarization in supporting electrolyte $0.5\text{ M H}_2\text{SO}_4$ with additions of CuSO_4 (M): (1) 0, (2) 0.01, (3) 0.1, (4) 0.4. The moments of the potential changes are indicated on the curves 1 - 4 by points, at which also the potential values are shown (V, SHE).

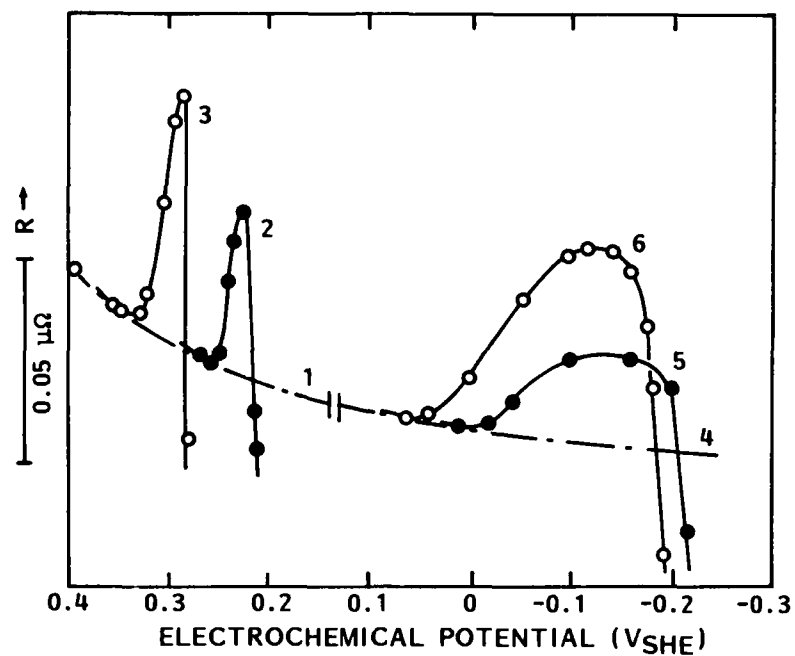


Figure 7. The potential dependence of the R of silver in 0.5 M H_2SO_4 with additions of CuSO_4 (M): (1) 0, (2) 0.01, (3) 0.4. The same in 0.1 M HNO_3 with additions of $\text{Pb}(\text{NO}_3)_2$ (M): (4) 0, (5) 0.01, (6) 0.1.

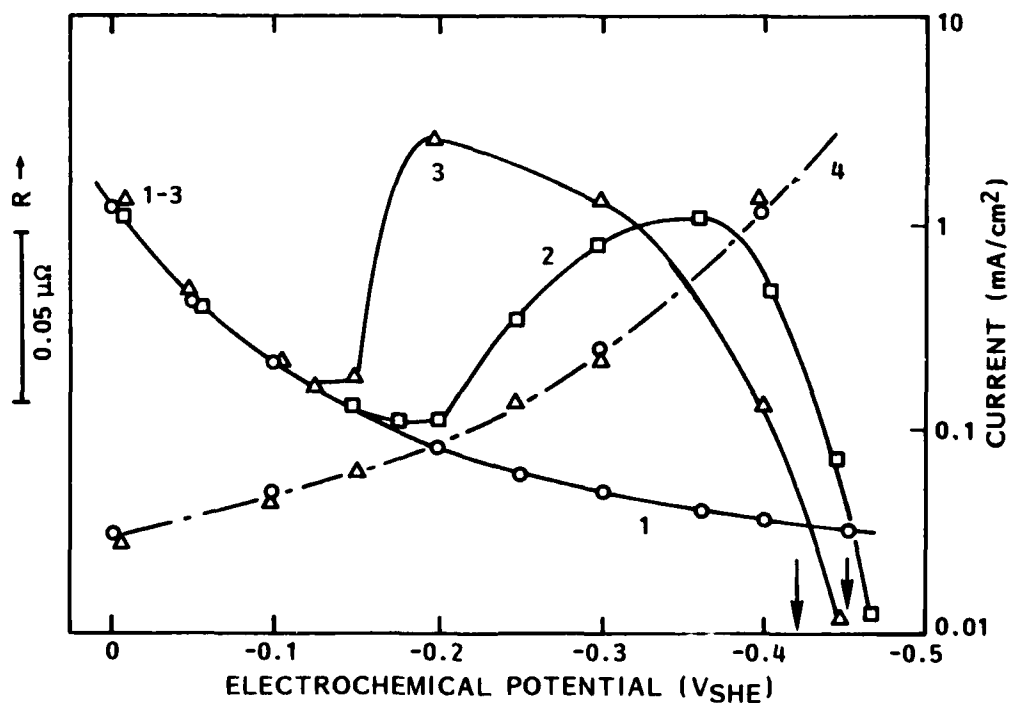


Figure 8. The potential dependence of the R of copper in 0.5 M $\text{H}_2\text{SO}_4 + 0.75$ M Na_2SO_4 with additions of CdSO_4 (M): (1) 0, (2) 0.02, (3) 0.2. Polarization curve for Cu in the solutions (1) and (3).

Corrosion Study of Polymer-on-Metal Systems Modified by Processing Conditions

Krassimir P. Nenov
MIT, Rm. 8-241
77 Massachusetts Ave.
Cambridge, MA 02139

Pradnya V. Nagarkar
MIT, Rm. 8-235
77 Massachusetts Ave.
Cambridge, MA 02139

D. B. Mitton
MIT, Rm. 8-235
77 Massachusetts Ave.
Cambridge, MA 02139

Ronald M. Latanision
MIT, Rm. 8-202
77 Massachusetts Ave.
Cambridge, MA 02139

Abstract

Capacitance measurements during dynamic electrolyte absorption were performed on 0.07-3.3 μm thick PMDA-ODA, BPDA-PPD and HFDA-APBP coatings on Cr-coated silicon wafers in 0.5 M NaCl. Subsequently, the specimens were monitored using electrochemical impedance spectroscopy and open-circuit potential measurements to follow the degradation of the coatings and to determine the time of failure of the polyimide/Cr interface.

The results showed that long-term capacitance increased approximately logarithmically with exposure time. Shortly before failure, sharp increases occurred in the capacitance and in the measured open-circuit potential. Those were immediately followed by the appearance of a second time-constant in the impedance spectra, an indication of an interfacial reaction.

The data showed that short-term capacitance measurements ($0 < t < 5000$ s) can be used to predict the long-term degradation trend and ultimately, the time-to-failure. In addition, capacitance measurements are sensitive to variations in the polyimide processing conditions and appear suitable for evaluation of electronic packaging materials.

Finally, capacitance data were processed to yield water and ionic diffusion coefficients. The following values for the diffusion coefficient of water in the coatings under immersion were measured at 21-23 °C: PMDA-ODA: $(2.53 \pm 0.43) \text{ E-9 cm}^2/\text{s}$; BPDA-PPD: $(2.75 \pm 0.15) \text{ E-10 cm}^2/\text{s}$; HFDA-APBP: $(1.26 \pm 0.20) \text{ E-10 cm}^2/\text{s}$. The values for PMDA-ODA and BPDA-PPD compare well with data in the literature. In general, dynamic capacitance measurements were found to represent a convenient alternative to gravimetric, bending beam, etc. methods for measurement of water diffusion coefficients in organic coatings. A major advantage is that the coatings are tested in their actual operating state, with no difference in the state of stress, cure conditions and other factors affecting the diffusional properties.

Introduction

Electronic packaging materials⁽¹⁾ and technology represent a major component of electronic product costs¹. Increasing circuit densities, sophisticated circuit technology and tougher reliability requirements continuously increase the role of packaging materials in the overall product performance. Development of new packaging materials continues at a fast pace, and there is a need for test procedures to evaluate various aspects of their performance.

Because of processing advantages and desirable technological and dielectric properties, polyimides have become materials of choice in the semiconductor industry. However, they possess the major disadvantage of being permeable to moisture and contaminants which over time contribute to the degradation of the chip performance and in some cases may limit the lifetime of the chip. Relative humidity, moisture entrapment during packaging, thermal cycling, contamination, potential bias, and galvanic coupling are among the major factors leading to corrosion failure at the polymer/metal interface^{2,3}.

The ultimate objective of this research project is to develop a procedure for life-time prediction of polymer/metal interfaces and quality control of electronic packaging materials in the semiconductor industry by means of accelerated testing. In the initial feasibility study, we attempt to correlate qualitatively the results from short term tests with those from long-term monitoring and with the time-to-failure of the interface. In addition, we used capacitance measurements to determine moisture and ionic diffusion coefficients in the coatings. The next stage will involve quantitative correlation of short and long-term results, and the construction of calibration relationships. Finally, provided that the technique is feasible, a multi-level interdigitated electrode structure will be considered for on-line testing in the industry.

This paper presents results from the feasibility study.

Experimental

I. Specimen and Test Cell Preparation

We tested three polyimide types that are presently used in the microelectronics industry: PMDA-ODA (DuPont PI2545), BPDA-PPD (DuPont PI2611) and HFDA-APBP (Amoco UD4212). In each case, the polyimide coatings were spin-cast onto a Cr-coated silicon wafer. Polyimide/Cr interfaces are very common in the industry due to the use of Cr as adhesion promoter. The 0.3 μm Cr layer was e-beam deposited on the 4" silicon wafer. The polyimide coating thicknesses ranged between 0.07 and 3.3 μm . Coatings thicker than 1 μm were spin-cast in two layers with an intermediate softbake step. This was done in part to ensure the absence of through-holes. Curing schedules were kept according to manufacturers' specifications. A Plexiglas[®] cylinder was affixed onto the coated substrate using epoxy. The Cr film represented the working electrode, and the circuit between the working and counter electrodes was completed through the coating and the electrolyte. The coating area exposed to electrolyte was typically 7.5 cm^2 . Four test cells were prepared from each wafer.

Testing was performed in an aqueous 0.5 M NaCl solution, at temperatures ranging between 21° and 23° C. Immersion testing was used because of the simplicity of control and also because it provided the necessary test acceleration. From published data, it can be inferred that results obtained in controlled RH environments can be linearly extrapolated to immersion conditions^{4,5}, indicating that no changes in corrosion and diffusion mechanisms take place as a result of immersion. Immersion tests avoid some problems associated with controlled RH tests,

(1) The term "electronic packaging materials" as referred to in this paper includes polymer applications for passivation, interlayer dielectrics, buffers, etc.

but the inability to produce static conditions between the electrolyte-free and fully saturated coating is a tradeoff, resulting in a more complicated dynamic absorption data analysis.

II. Test Equipment

The test setup consisted of a Solartron 1260 Impedance/Gain-Phase Analyser (FRA 1260) and an EG&G PAR 273 potentiostat. Data acquisition was computer-controlled via the GPIB bus using house software. Although the FRA 1260 can measure current directly, its limited current sensitivity and the large resistivity of the coating prevented such measurements. Therefore, the potentiostat was used to measure the cell current and maintain the cell at the equilibrium potential during EIS measurements.

III. Experimental Methods

Short-term testing consisted of capacitance measurements at a fixed frequency, typically 1000 Hz, starting upon immersion. A 20 mV rms sinusoidal amplitude⁽²⁾ was superimposed on the equilibrium dc potential. Typically, measurements lasted 5000 s, although in most cases 1000 s were sufficient to extract the necessary parameters. Initially, the coated substrate system can be represented by an RC-circuit with sufficient accuracy, the coating being equivalent to a parallel-plate capacitor with a finite resistivity. Due to the difference in relative magnitudes of the coating's resistance and capacitance, the capacitance can be calculated directly from the imaginary impedance component at the higher frequencies, with less than 0.1% error. Thus, the capacitance increase which is representative of the rate of ionic and water uptake can be monitored as a function of the time since immersion.

Long-term measurements included open-circuit potential (OCP) and electrochemical impedance spectroscopy (EIS) measurements. EIS spectra were acquired over a frequency range of 0.02 to 100,000 Hz. A 20 mV rms sinusoidal amplitude was used in each case. During EIS, the dc potential was maintained at the equilibrium open-circuit value.

Both the capacitance and the EIS measurements were verified on electrical components with capacitance and resistance values similar to those of the coatings, as estimated from the experimental data by means of Complex Nonlinear Least Squares Analysis (CNLS). The impedance responses of the equivalent electrical circuits were measured at several frequencies using an HP 4275A Multi-frequency Meter. These values were found identical to those obtained from the same circuits by means of a standalone FRA 1260 (3 V rms) and were considered exact. Thus, exact impedance spectra of the equivalent circuits over the entire frequency range were generated using the standalone FRA 1260 with a 3 V rms amplitude. Subsequently, the measurements were repeated using the actual experimental setup (FRA 1260 and potentiostat) and 20 mV rms amplitude. It was determined that the potentiostat introduced systematic errors, which even though small, lead to a relatively large (ca. 5-10 %) bias in the CNLS-regression estimates of the circuit parameters. The relative residuals spectra, calculated as

$$RZ_f = \frac{Z_f^{i,m} - Z_f^{i,e}}{Z_f^{i,m}} \quad \text{and} \quad RZ_f = \frac{Z_f^{ii,m} - Z_f^{ii,e}}{Z_f^{ii,m}} \quad (1)$$

where

RZ_f = relative residual in the real impedance component at frequency f ,

(2) The linearity condition $RT/F\delta$ establishes 20 mV as the maximum permissible amplitude under these particular conditions.

RZ_f'' = relative residual in the imaginary component at frequency f ,
 Z_f',m and Z_f'',m = measured real and imaginary impedance components, respectively,
 using the complete EIS setup (potentiostat and FRA) and 20 mV rms,
 Z_f',e and Z_f'',e = exact real and imaginary impedance components, respectively,
 measured using a standalone FRA and 3 V rms,

were found to remain fairly constant for capacitance and resistance values corresponding to a range of coating thicknesses. Finally, the residuals spectra were applied to the EIS data acquired from the actual coatings to correct for systematic errors.

Results and Discussion

Capacitance measurements during the initial electrolyte absorption provide a measure of the permeability of the coating to the electrolyte. Prediction of the lifetime of the metal/polymer interface from such measurements is possible provided that the interfacial reaction rate is governed by transport of reactants to and from the interface. Both the difference between the resistance of the polyimide-coated versus the bare Cr interface ($10^{11} \Omega\text{cm}^2$ vs. $10^6 \Omega\text{cm}^2$) in 0.5 M NaCl, as well as the evolution of the open-circuit potential indicate that this is indeed the case.

I. Open-Circuit Potential Evolution

Before testing, the test cells were stored in a desiccator for fixed periods of time. During the time of exposure of the coated substrates to the electrolyte the OCP generally exhibited a continuous increase, consistent with an interfacial reaction controlled by the flux of cathodic reactants. This flux increased over time due to coating degradation. In some cases, particularly during the testing of PMDA-ODA coatings, the potential rose sharply after several days to values comparable with the OCP of bare Cr in 0.5 M NaCl. The sharp rise coincided with the appearance of a second time constant in the EIS data and was interpreted as an indication of a major coating delamination, resulting in free access of electrolyte to the Cr surface. The absolute values and evolution trends of the open-circuit potentials of the three different polyimide/Cr systems are compared in Figure 2. Comparisons between potentials of PMDA-ODA and BPDA-PPD which have similar chemical compositions suggest that the transport rate through the coating is higher in the case of the former polyimide. Indeed, the normalized resistance⁽³⁾ of the water-saturated PMDA-ODA coatings was smaller than that of the BPDA-PPD coatings.

II. Capacitance Evolution

Typical data from capacitance measurements on PMDA-ODA coatings are shown in Figure 3. The logarithmic dependence of the normalized capacitance⁽⁴⁾ on the time since immersion which is evident from Figure 3 b was observed on all polyimide samples for $t > 200$ s.

(3) The normalized resistance was calculated as the product of the coating resistance times sample area over coating thickness and has dimensions of resistivity.

(4) The normalized capacitance was calculated as the coating capacitance divided by the sample area and the dielectric permittivity of vacuum ($\epsilon = 8.854 \times 10^{-14} \text{ F/cm}^2$) and multiplied by

Table 1, compiled assuming Fickian water and ionic diffusion with constant boundary conditions and constant diffusion coefficients, shows that a 3 μm PMDA-ODA coating becomes water-saturated within 100 s. Therefore, assuming insignificant swelling, the first slope (0-100 s) can be attributed to the combined water and ion uptake, while the second slope ($t > 200$ s) is governed entirely by ionic diffusion. The second slope is very nearly logarithmic for all three polymers, i.e. there is a linear dependence between the capacitance and the $\log(\text{time})$ for $t > 200$ s. Subtraction of the logarithmic trend from the capacitance data exposes the water absorption profile and allows the determination of the water diffusion coefficient (Figure 4). The plateau value in Figure 4 b corresponds to the dielectric constant of the pure, water-saturated coating. The average dielectric constants at 1000 Hz were equal to: PMDA-ODA/Cr: 3.85; BPDA-PPD: 3.29; HFDA-APBP: 3.01.

The diffusion coefficients cannot be extracted directly from the capacitance data unless additional assumptions are made, most importantly concerning the dependence of the relative permittivity on the diffusant's concentration. Assuming a linear relationship between the average dielectric permittivity and the average water concentration in the coating⁵:

$$\epsilon(t) = \epsilon_0 + b \bar{C}_w(x,t) \quad (2)$$

where

ϵ_0 = dielectric permittivity of the water-free coating,

b = constant,

and a Fickian diffusion process with a constant diffusion coefficient^{8,9}, the relationship for the coating capacitance as a function of time for $t > 4.66d^2/D_w$ becomes:

$$C(t) = C^\infty - b \frac{8}{\pi^2} (C_w^\infty - \bar{C}_w^0) \exp\left(-\frac{\pi^2 D_w t}{4d^2}\right) \quad (3)$$

where

C^∞ = capacitance of pure, water-saturated coating,

C_w^∞ = maximum water concentration in the coating,

\bar{C}_w^0 = initial average water concentration in the coating,

D_w = water diffusion coefficient,

d = coating thickness.

Regression of the capacitance data to (3) yielded following values for the diffusion coefficients: PMDA-ODA/Cr, PMDA-ODA/Pt (10 samples): $(2.53 \pm 0.43) \text{ E-}9 \text{ cm}^2/\text{s}$; BPDA-PPD/Cr (6 samples): $(2.75 \pm 0.15) \text{ E-}10 \text{ cm}^2/\text{s}$; HFDA-APBP/Cr (3 samples): $(1.26 \pm 0.20) \text{ E-}10 \text{ cm}^2/\text{s}$. Figure 5 shows typical plots of estimated (using (3)) versus measured capacitance. The regression quality was very good, except for slight deviation near saturation, attributable to water clustering¹⁰. The measured values for water diffusion in PMDA-ODA and BPDA-PPD are similar to values obtained by means of other, usually more complicated methods in controlled RH environments^{8,11}. The order of magnitude difference in diffusion coefficients between PMDA-ODA and BPDA-PPD which have similar chemical structures, has been attributed to water-affinity and ordering phenomena^{8,9,11} and will not be discussed further.

the coating thickness. It is a dimensionless quantity and corresponds to the dielectric permittivity (dielectric constant) of homogeneous bulk materials.

The relationship:

$$\epsilon(x,t) = \epsilon_0 + b C_w(x,t) \quad (4)$$

between the local water concentration and the local permittivity probably represents a better model than equation (2). Because of the water concentration profile during dynamic sorption, the coating can be represented approximately as a series of infinitesimal capacitors with dielectric permittivities dependent on the local water concentration. Hence, coating capacitance versus time becomes:

$$\frac{1}{C(t)} = \frac{1}{\epsilon_0} \int_{x=0}^{x=d} \frac{dx}{\epsilon(x,t)} \quad (5)$$

where the parameters have their usual significance.

Finally, inserting the solution to the second Fick's equation for diffusion with constant boundary conditions (no polymer swelling or relaxation) and constant diffusion coefficient into equations (4) and (5), the capacitance relationship becomes:

$$\frac{1}{C(t)} = \frac{1}{\epsilon_0} \int_{x=0}^{x=d} \frac{dx}{\epsilon_0 + b \left[C_w^{\infty} + 2(\bar{C}_w^0 - C_w^{\infty}) \sum_{n=0}^{\infty} \frac{(-1)^n}{(n+\frac{1}{2})\pi} \exp\left[-(n+\frac{1}{2})^2 \frac{\pi^2 D_w t}{d^2}\right] \cos\left[\frac{(n+\frac{1}{2})\pi x}{d}\right] \right]} \quad (6)$$

Equation (6) can be solved numerically, and the diffusion coefficients determined in this manner were found to correspond within 1% to those obtained using the previous simpler analysis. Therefore, the simpler equation (3) can be used to determine the diffusion coefficients with sufficient accuracy. The instantaneous water concentration in the coating can be determined from (2) with knowledge of constant b . The value of b can be obtained from combined capacitance and gravimetric or other measurements. Under the specific experimental conditions, we established the following relationship for BPDA-PPD to be:

$$\epsilon(t) = 2.94 + 0.238 \bar{C}_w(x,t) \quad (7)$$

The ionic diffusion process, characterized by a logarithmic capacitance-time dependence is non-Fickian. Therefore, additional measurements are required to extract the ionic diffusion coefficients. We are currently combining permeability (ion-selective electrodes) and capacitance measurements to obtain the concentration-permittivity relationships. This work will be described in a later article.

Experiments with BPDA-PPD and HFDA-APBA showed that in addition to their lower dielectric permittivities, these polyimides are more resistant to electrolyte diffusion than PMDA-ODA. The trends of normalized capacitance evolution for the three investigated polyimides are compared in Figure 6 where the capacitance curves have been shifted to allow easier comparison. In addition to the obvious difference in the slopes between PMDA-ODA and

the other two polyimides, the figure illustrates the above point that the short-term capacitance measurements correctly predict relative trends in the long-term behavior of the coating. Figure 7 shows the complete curve for the PMDA-ODA coating of Figure 6. There is an obvious change of the rate of increase of the normalized capacitance preceding delamination and failure.

Finally, it was possible to demonstrate that the dynamic capacitance method is sensitive to the morphology of the coating. Two identical PMDA-ODA/Cr samples were subjected to cure under different nitrogen flow conditions. Comparison of the Cr-oxide layers before and after cure by means of Auger spectroscopy showed no thickness changes in the case of the normal sample, while a significant oxide thickness increase resulted from curing in the reduced nitrogen flow. After the cure, both coatings appeared visually identical and IR spectroscopy showed no chemical differences between them. However, as illustrated by Figure 8 they behaved very differently upon exposure to the electrolyte, indicating that the cure under very low nitrogen flow had caused internal microporosity that lead to reduced resistance to electrolyte uptake.

II. Impedance Spectra

During the initial days of exposure to the electrolyte, the impedance spectra can be approximated by a single R-CPE⁽⁵⁾ parallel circuit using CNLS regression fitting. The quality of the regression fits decays progressively with exposure time, until at some point the above simple equivalent circuit becomes insufficient. In general, such behavior can be attributed to electrochemical processes developing at the polymer/metal interface. Due to the limited frequency range observable it was not possible to estimate the values of the new equivalent circuit parameters with confidence. Also, no visual changes were observed through the coating. Therefore, for the purposes of this study, the time of coating failure was defined as the time at which a single R-CPE circuit could no longer be used to model the impedance data.

As expected, the normalized coating capacitance and the resistance exhibited opposite trends. Due to the extremely large resistivity of the coating, regression estimates of the resistance were not as accurate as the estimates of the capacitance. Thus, the normalized capacitance gave a more reliable estimate of the state of the coating.

Table 2 contains a qualitative summary of the effects of some parameters on the test results of PMDA-ODA coatings. As seen from the table, the use of platinum instead of chromium films underneath the polyimide, as well as repeated cure under normal curing conditions resulted in longer time-to-failure. By contrast, the application of a significantly more positive (greater than OCP + 500 mV) dc bias during the initial capacitance measurements caused the lifetime of the coatings to decrease sharply. Finally, dessicator storage affected the initial values of the normalized resistance and capacitance but had no effect on their long-term trends and on the time-to-failure.

Most notably from Table 2, all factors causing an increase in the rate of degradation of the normalized capacitance also resulted in shorter time-to-failure. Moreover, high initial capacitance increase rates as measured between 200 and 5000 seconds after immersion correctly predicted faster long-term coating deterioration and ultimately shorter failure times. Therefore, at least in the case of PMDA-ODA, short-term capacitance measurements can be used to assess effects of processing parameters on the coating's lifetime.

Conclusions

In conclusion, the feasibility of qualitative life-time prediction for PMDA-ODA coatings from capacitance measurements during electrolyte absorption has been confirmed by this study. The procedure seems to be sensitive enough to detect variation in the processing conditions,

(5) CPE = Constant Phase Element⁷.

although additional experiments are necessary to define its precise scope of applications. Capacitance measurements can provide a tool for the evaluation of corrosion protective and diffusion properties of organic coatings, as well as for control of the integrity of packaging materials in the microelectronics industry.

Acknowledgement

The authors gratefully acknowledge funding and materials provided by the Electronics Packaging Program at MIT.

References:

1. D. P. Seraphim, R. Lasky, C. Li, ed., Principles of Electronic Packaging, (McGraw-Hill, 1989).
2. D. Wilson, et al., ed., Polyimides, (Blackie, 1990).
3. F. J. Belcourt, in Electronic Packaging and Corrosion in Microelectronics, M. E. Nicholson, ed., (ASM International, 1987), p. 71.
4. F. Bellucci, et al., J. Electrochem. Soc. 137, (1990) p. 1778.
5. D. Denton, et al., J. Electronic Matls. 14, (1985) p. 119.
6. J. R. MacDonald, ed., Impedance Spectroscopy, (John Wiley & Sons, 1987).
7. J. R. MacDonald, CNLS - Complex Nonlinear Immitance Fitting Program, (Chapel Hill 1990).
8. C. R. Moylan, M. E. Best, M. Ree, J. Polymer Science B 29, (1991) p. 87
9. K. Okomoto, et al., J. Polymer Science B 30, (1992), p. 1223
10. G. E. Zaikov, et al., Diffusion of Electrolytes in Polymers, (VSP Utrecht, 1988)
11. J.-H. Jou, et al., Polymer Journal 23, (1991), p. 1123

Table 1. Estimated characteristic times for diffusion of water, Na⁺ and Cl⁻ ions in PMDA-ODA coatings (Diffusion coefficients: water 2.0 E-9 cm²/s; ions 1.0 E-13 cm²/s).

| Coating Thickness (μm) | Time for water to reach the interface (s) | Time for water saturation (s) | Time for ions to reach the interface | Time for saturation with ions |
|------------------------|-------------------------------------------|-------------------------------|--------------------------------------|-------------------------------|
| 3 | 21 | 80 | 11.5 h | 18.6 days |
| 2.5 | 1.4 | 56 | 8.0 h | 12.9 days |
| 0.5 | 0.06 | 2.2 | 1151 s | 12.4 h |
| 0.1 | 0.002 | 0.09 | 46 s | 1780 s |
| 0.05 | 0.000 | 0.02 | 11.5 s | 4.45 s |

Table 2. Qualitative summary of results from PMDA-ODA (d=decrease, i=increase).

| EXPERIMENTAL PARAMETERS | Pt INSTEAD OF Cr | DESSICATOR STORAGE | REPEATED NORMAL | DC BIAS MORE POSITIVE |
|-----------------------------------------------------|------------------|--------------------|------------------------|-----------------------|
| SPECIMEN PARAMETERS | | | CUPE | |
| Initial normalized resistance | i (2x larger) | i (2x larger) | 0 | d |
| Normalized resistance decrease rate | d | i (till equal) | 0 | d |
| Initial normalized capacitance | d | 0 | 0 | d |
| Short-term (200<t<5000 s) capacitance increase rate | d | 0 | d | i |
| Long-term capacitance increase rate | d | 0 | d | i |
| CPE exponent decrease rate | d | 0 | 0 | i |
| Initial open-circuit potential | 0 | d | d | 0 |
| OCP increase rate | d | i (till equal) | i | d |
| Days to failure | i | 0 | i (on Cr) 0 (on Pt) | d |

Figure 3 a.

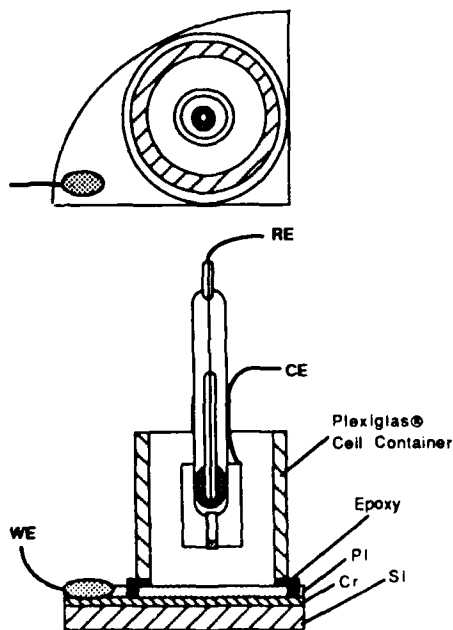


Figure 1. Test cell.

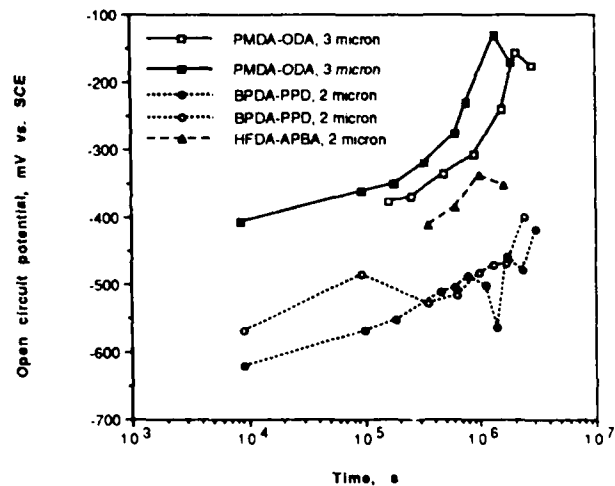


Figure 2. Open-circuit potentials as a function of exposure time.

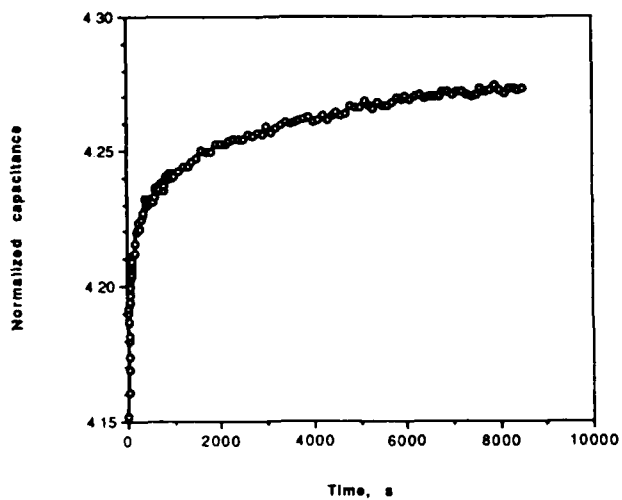


Figure 3 a. Linear plot of the normalized capacitance (dimensions of dielectric constant) vs time since immersion. PMDA-ODA on Cr, 2.8 μm thickness.

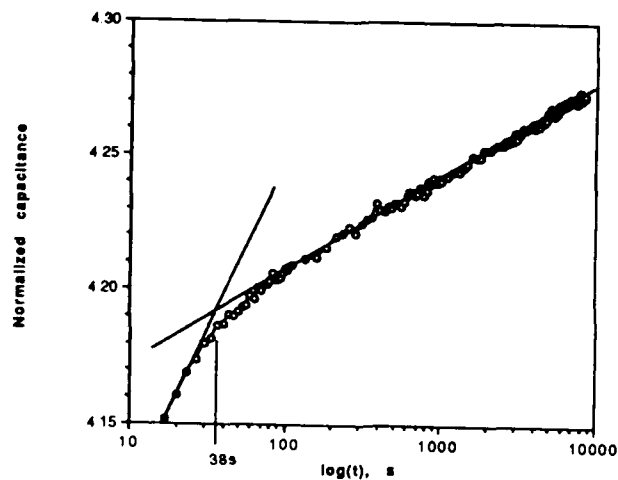


Figure 3 b. Logarithmic plot of the normalized capacitance for the coating from

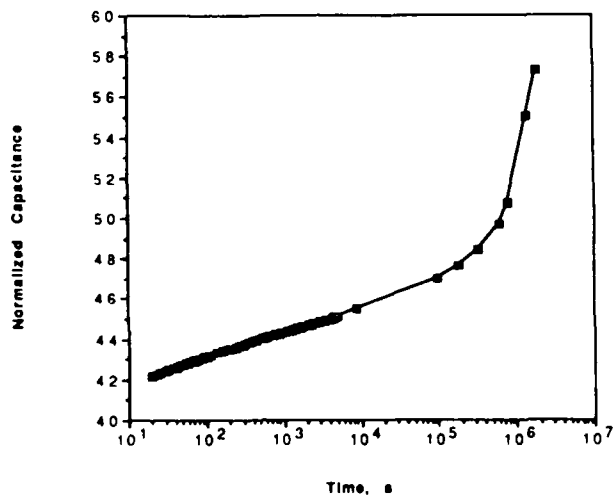


Figure 7. Complete (immersion to failure) plot of capacitance trend for the PMDA-ODA coating from Figure 6.

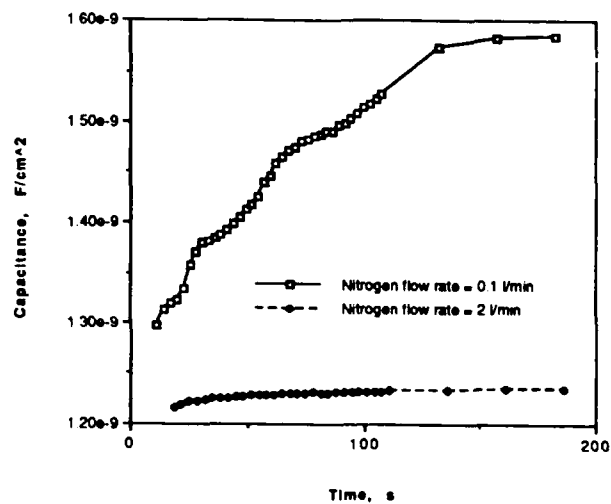
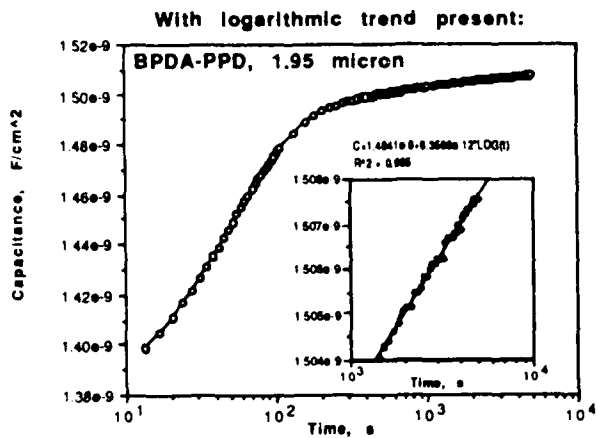


Figure 8. Comparison of the capacitance responses of two PMDA-ODA/Cr samples subjected to different cure conditions. Coating thickness was 2.7 μm .



Subtraction of the logarithmic trend reveals the underlying Fickian water diffusion process

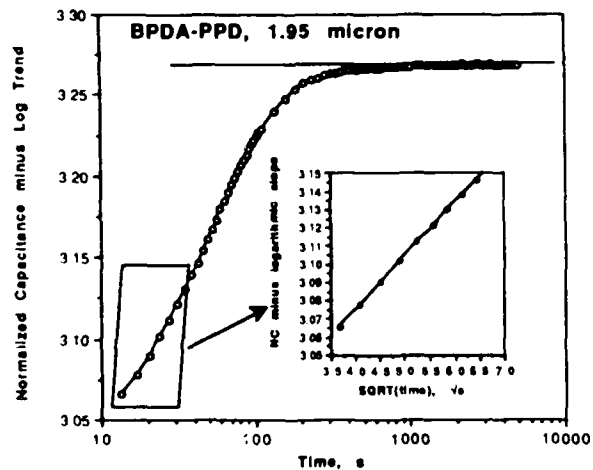


Figure 4. Subtraction of the logarithmic trend from the capacitance data reveals the underlying water-diffusion profile (BPDA-PPD/Cr, 1.95 μm).

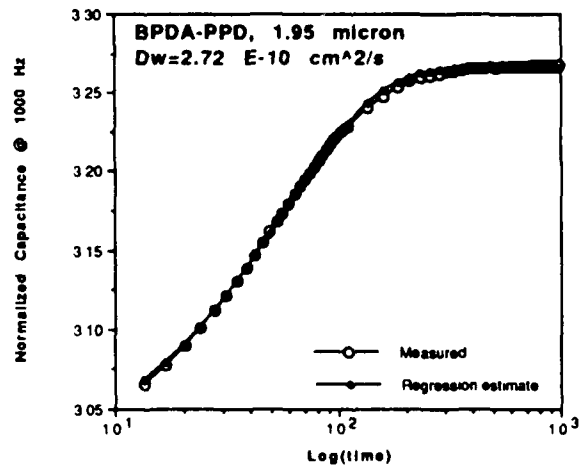


Figure 5. Regression to the capacitance data (logarithmic trend subtracted), using equation (3) (BPDA-PPD/Cr, 1.95 μm).

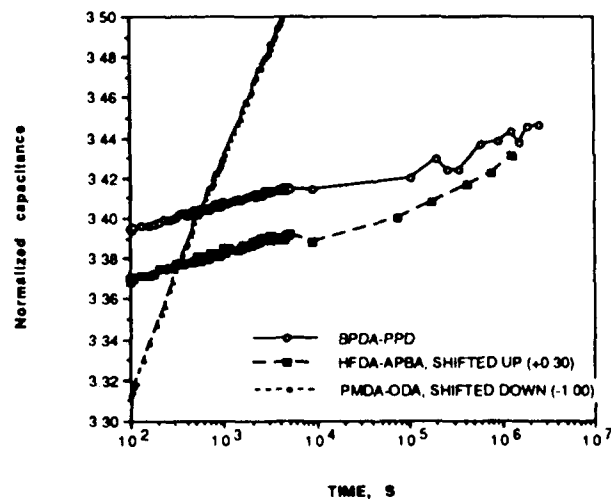


Figure 6. Comparison of normalized capacitance trends for PMDA-ODA, BPDA-PPD and HFDA-APBP coatings on Cr (Capacitance at 1000 Hz).

Quantitative Corrosion Testing Of EMI Materials For Aerospace Applications

Philip Lessner
Chomerics, Inc.
77 Dragon Court
Woburn, MA 01888-4014

Abstract

EMI shielding requirements for electronic systems are becoming increasingly demanding in military and commercial aerospace systems. This has led to increased use of conductive gaskets, sealants, and coatings ("conductive materials"). Such materials are used to provide a low impedance interface between mating joints in electronic enclosures and to enhance the shielding effectiveness of aircraft structures. The conductive materials often incorporate silver, silver-plated metals, copper, nickel, monel, or other metals. The electronic enclosures and structural components are typically made from aluminum alloys. When exposed to a corrosive environment, the conductive material and aluminum enclosure can form a galvanic couple. This results in corrosion of the aluminum because it is less noble than the conductive interface material. Depending on the type of conductive material, it too may deteriorate in the corrosive environment. Shielding effectiveness can degrade because of this conductivity loss or due to the buildup of non-conductive corrosion products between the conductive material and the mating flange.

When shielding is required in highly corrosive environments (e.g., salt spray), interface design and materials selection assume a high level of importance. Conductive elastomer shielding gaskets are usually chosen because of their good environmental sealing ability. Conductive elastomers are made from an elastomer binder filled with small conductive particles or fibers. These fillers can be silver, silver-plated cores, nickel, or carbon. Laboratory and field data have shown that the different filler types have a wide range of galvanic compatibility with aluminum in corrosive environments. The earlier data has been primarily qualitative. This paper describes the development of a quantitative test for measuring conductive elastomer galvanic compatibility (corrosivity) and electrical stability.

All the common conductive elastomer types were tested. There was almost a 200-fold difference in corrosivity between the least corrosive (silver-plated aluminum filled fluorosilicone) and the most corrosive (carbon-filled expanded polytetrafluoroethylene) gaskets. Significant differences were found among the silver-plated fillers depending on the core material. Differences in corrosivity and electrical stability were found between silver-plated aluminum filled fluorosilicones from different suppliers. Nickel-filled elastomers were found to be less corrosive than pure silver-filled elastomers, but were significantly more corrosive than the best silver-plated aluminum filled materials. Some of the nickel-filled materials were electrically unstable. The behavior of these systems is explained in terms of their corrosion chemistry.

Introduction

Electromagnetic Interference

Electromagnetic interference (EMI) is caused by the interaction of electromagnetic energy

with the circuitry of an electronic device. Electromagnetic fields are present in the everyday environment due to, for example, radio, TV, and cellular telephone transmissions, and emissions from personal computers and microwave ovens. In commercial aviation, high power transmitters and radars generate high electromagnetic field strengths. Military applications produce electromagnetic fields from these sources at even higher field strengths.

Due to the increasing use of sensitive digital circuits and higher clock speeds, protection of electronic equipment against EMI is becoming an increasing concern. In the aerospace market, the use of fly-by-wire aircraft has led to proposed regulations for protection of aircraft against HIRF (High Intensity Radiated Fields)¹. Recent incidents have highlighted the sensitivity of electronic flight controls to EMI².

One method of protecting electronic equipment consists of surrounding the device with a highly conducting metal enclosure. This "Faraday Cage" stops the penetration of electromagnetic energy. The enclosure is usually fabricated from a metal (such as aluminum, steel, or magnesium) or a metal-coated plastic. The enclosure can also be formed from part of a larger structure such as an aircraft skin. This approach is effective for preventing emissions from a device as well as protecting susceptible equipment from the ambient electromagnetic environment.

In real enclosures, openings need to be provided for covers, access panels, passage of signal cables, vents, etc. Leakage of electromagnetic energy through these joints causes a degradation in the shielding effectiveness⁽¹⁾ of the enclosure. Leakage occurs because the mechanical mismatch at these joints increases the contact impedance and creates air gaps through which electromagnetic energy can penetrate .

Conductive Shielding Gaskets

Conductive gaskets improve the shielding effectiveness of a "leaky" enclosure by decreasing the contact impedance at a mating joint and by filling the gap with a conductive material. Because they help decrease contact resistance, gaskets are also used to help dissipate the effects of a lightning strike, in some aircraft applications.

Conductive gaskets are fabricated from several different types of metals and elastomers. These (composite) materials are chosen for their mechanical properties and low electrical resistance. Typical metals include silver, silver-plated cores (e.g., copper, aluminum), nickel, carbon, monel, tin-plated steel, and Be-Cu. Conductive gaskets are available in several forms. The simplest gaskets are conformable metals such as monel mesh, tin-plated steel spiral, or Be-Cu "fingers". The metal can be formed around an elastomer core. Another type of gasket uses metal wires embedded in an elastomer and oriented perpendicular to the mating flange surfaces. Conductive elastomers are used when high shielding effectiveness and good environmental sealing ability are needed. They consist of small (ca. 30 to 150 μm) metal particles or fibers in an elastomer matrix.

⁽¹⁾ Shielding effectiveness (SE) = $20 \cdot \log(E_i/E_t)$ where E_i and E_t are the incident and transmitted electromagnetic fields. A higher SE means a greater attenuation of the electromagnetic radiation.

Corrosion Of Shielded Systems

Electronic systems and aircraft skin can be exposed to corrosive environments. These corrosive environments can range from mild (humid) to severe (salt spray plus pollutant gases). When exposed to corrosive environments, corrosion can occur between the conductive gasket and metal enclosure. A galvanic couple occurs if three conditions are present: electrolyte, dissimilar metals, and an electronic path. The corrosive environment provides the electrolyte. In almost all cases, the gasket metal is different from the enclosure metal it mates against. The good electronic path between the conductive gasket and enclosure material is required for low contact impedance and good electromagnetic shielding .

The formation of a galvanic couple results in corrosion of the enclosure material because it is less noble than the gasket material. However, depending on the type of conductive gasket, it too may deteriorate in a corrosive environment. Shielding effectiveness can degrade because of the conductivity loss or due to the buildup of nonconductive corrosion products between the conductive gasket and the mating flange.

The foregoing discussion points to three aspects of conductive gasket "corrosion resistance." The primary aspect is the corrosivity of the gasket towards the enclosure (i.e., galvanic compatibility). The second aspect is the ability of the conductive gasket to act as an environmental seal and prevent electrolyte from penetrating between itself and the mating surface. The third aspect is the ability of the conductive gasket to maintain the shielding integrity of the enclosure.

Corrosion of the gasket-enclosure system can be minimized by selection of the most compatible materials, good design practices, or optimally both. In a corrosive environment, conductive elastomers are usually chosen because of their good environmental sealing ability and high shielding effectiveness. Within the conductive elastomer family several types of filler materials are available. Selection of the most galvanically compatible filler is one of the keys to a successful corrosion resistant design.

Corrosion Testing

Previous work to evaluate the corrosion resistance of conductive elastomers has mainly relied on a visual determination of the corrosivity and sealing ability of the elastomer^{3,4}. These visual assessments have sometimes been supplemented by pitting depth measurements⁵. Sometimes, information is given about the condition (electrical, physical) of the conductive elastomer. The configuration of the conductive elastomer-flange joint, the exposure times in salt fog and the orientation of the specimen in the salt fog chamber have varied among the different investigations. These factors, combined with the qualitative or semi-quantitative nature of the results, has led to difficulty in comparing the corrosion resistance of different conductive elastomers. Attempts to correlate conductive elastomer corrosivity with the galvanic series have failed because of the composite nature of the gasket systems.

The objective of our work is to establish methods for the quantitative measurement of conductive elastomer-flange compatibility. The goal is to establish a series of tests useful to both the corrosion engineer and the EMC systems engineer. Two test methods were developed. One test method yields a quantitative scale of conductive elastomer corrosivity and a quantitative measure of DC electrical degradation of the conductive elastomer. In this method, aluminum was

selected as the flange material because of its widespread use in the electronics and aerospace industry. Aluminum weight loss was selected as a measure of aluminum corrosion, and volume resistivity of the conductive elastomer was selected as a measure of conductive elastomer electrical stability. The results of this test method are discussed in detail in this paper.

The second test measures the degradation of shielding effectiveness of a complete conductive elastomer-flange system. The shielding effectiveness measurements are made at radio and microwave frequencies. Development and results of that test are reported elsewhere⁶.

Experimental Methods

Circular die cut samples of the conductive elastomers were compressed against 6061-T6 aluminum alloy coupons (with a MIL-C-5541, Class 3 conversion coating) using the fixture shown in Figure 1. The aluminum alloy coupon was weighed and the conductive elastomer thickness and electrical resistance were determined before assembly, and the initial volume resistivity was calculated. Each fixture was bolted to a tray held at a 75° angle to the horizontal; this allowed for solution drainage. The fixtures were exposed to neutral (ASTM B117) salt fog in a Singleton Model 22 chamber. All samples were exposed for 168 hours.

After exposure, the fixtures were disassembled. The aluminum alloy coupon was cleaned for 15 minutes in concentrated nitric acid, rinsed, dried for 1 hour at 100°C, allowed to cool in a desiccator, and then reweighed. Aluminum weight loss (removal) was calculated from the difference between the initial and final weights. The electrical resistance and the thickness of the conductive elastomer were redetermined, and the final volume resistivity was calculated.

Details of the dimensions of the test pieces and the equipment used for measuring electrical resistance are available⁷.

Results

Elastomers Filled With Silver and Silver-Plated Cores

Figure 2 shows the average weight loss for 6061-T6 aluminum after contact with silicone and fluorosilicone elastomers filled with pure silver (Ag), silver-plated copper (Ag-Cu), silver-plated nickel (Ag-Ni), silver-plated glass (Ag-glass), and silver-plated aluminum (Ag-Al-1). An unfilled (non-conductive) silicone elastomer is included for comparison. Conductive elastomers containing Ag and Ag-Cu fillers are the most corrosive. The Ag-Ni and Ag-glass filled materials are of intermediate corrosivity. The Ag-Al-1 filled material is the least corrosive, but still shows more corrosion than the non-conductive silicone. The difference in corrosivity between the Ag-Al-1 filled elastomer and the Ag-Ni and Ag-glass filled elastomers is about a factor of 50; the Ag-Al-1 filled elastomer is about 100 times less corrosive than the Ag and Ag-Cu filled elastomers.

Figure 3 shows the volume resistivity of the conductive elastomers before and after exposure to 168 hours of ASTM B117 salt fog. With the exception of the Ag-Cu filled silicone, all the conductive elastomers had volume resistivities after salt fog within the MIL-G-83528B limits⁸.

The low corrosivity of the Ag-Al-1 filled fluorosilicone material led us to look at Ag-Al filled fluorosilicones from several different manufacturers. Figure 4 shows the corrosivities of the materials. Ag-Al-1 is the least corrosive material (2.2 mg average weight loss). The Ag-Al-2 (3.3 mg),

Ag-Al-3 (3.7 mg), and Ag-Al-4 (4.6 mg) materials are of intermediate corrosivity, and the Ag-Al-5 and Ag-Al-6 materials are the most corrosive (7.5 and 10.3 mg). The range of corrosivities is about a factor of five.

Figure 5 shows the average volume resistivity of the elastomers samples before and after salt fog exposure. The Ag-Al-1, Ag-Al-4, Ag-Al-5, and Ag-Al-6 elastomers underwent little change in volume resistivity after salt fog exposure. The Ag-Al-3 elastomer showed an increase, but the final volume resistivity was still well within the initial MIL-G-83528B, Type D specification.

The Ag-Al-2 material had low initial volume resistivity, but the volume resistivity increased to over 14 mohm-cm after salt fog exposure. Figures 6a and b show the surface of one of the Ag-Al-1 samples and one of the Ag-Al-2 samples after salt fog exposure. The surface of the Ag-Al-2 elastomer has many blistered areas; blisters were found on all of the Ag-Al-2 samples after salt fog exposure. The sample had a distorted circular shape. There was no blistering or distortion of any of the Ag-Al-1 samples.

Elastomers Filled With Nickel, Nickel-Coated Graphite, and Carbon

Figure 7 shows the corrosivity of the nickel and carbon-filled conductive elastomers. The corrosivity of the Ag-Al-1 conductive elastomer is included for comparative purposes. The nickel fiber-filled silicone elastomer (NiF) is about 8 times as corrosive as Ag-Al-1. The pure nickel powder (NiP) and the 80 wt% nickel coated graphite powder-filled fluorosilicone elastomers (NiGr80) are about 3 times as corrosive as Ag-Al-1. The 60 wt% nickel coated graphite-filled fluorosilicone elastomer (NiGr60) is about 10 times as corrosive as Ag-Al-1. The carbon-containing expanded polytetrafluoroethylene (C/EPTFE) gasket is about 200 times as corrosive as Ag-Al-1.

Figure 8 shows the volume resistivity of the conductive elastomers measured before and after salt fog exposure. The volume resistivity of Ag-Al-1, the NiGr60, and C/EPTFE elastomers are essentially unchanged. The volume resistivities of NiF, NiP, and NiGr80 elastomers increase by a factor of 5 to 10 times after salt fog exposure.

Discussion

The corrosivities of the different filler types can be understood by considering the corrosion reactions taking place. In the presence of air and an electrolyte (in this case a salt solution), aluminum corrodes by an electrochemical process:



The aluminum species can be an oxide or a chloride. The anodic corrosion process is driven by electrochemical reduction of oxygen:



In the absence of a conductive gasket material, aluminum corrosion will occur because Reaction (2) occurs on one part of the aluminum while Reaction (1) occurs in an adjacent area. When a dissimilar conductive material is contacted with the aluminum, the rate of Reaction (2) can be accelerated; this leads to a greater rate of aluminum corrosion (Reaction (1)). This is what happens when a metal-filled elastomer contacts the aluminum. Reaction (2) occurs at a greater

rate on the edge of the gasket compared to the aluminum without the gasket present.

Figure 2 shows there is a significant difference observed in corrosivity among the different silver-plated cores. It is necessary to consider the corrosion properties of the core materials as well as the silver-plated surface.

The Ag-Cu powder filled material is the most corrosive under these conditions. Copper corrodes rapidly in a salt fog environment:



The silver shell around the copper core is porous and the underlying copper can corrode by Reaction (3). The corrosion of the copper accelerates the corrosion of the aluminum; the CuCl_2 produced in Reaction (3) can migrate onto the aluminum surface and redeposit by the reverse of Reaction (3):



Copper is also a good catalyst for oxygen reduction. These copper rich areas form "mini" cathodes where Reaction (2) is accelerated. This leads to increased corrosion of the aluminum.

The Ag-glass and Ag-Ni-filled materials are less corrosive than the pure Ag-filled material. Glass and nickel are "neutral" cores--they neither accelerate or diminish corrosion. Differences in corrosion rate compared to the pure silver material are due to the lower conductivity of these materials compared to pure Ag-filled material and the difference in morphology of the particles.

The Ag-Al containing materials are one to two orders of magnitude less corrosive than the other silver-containing materials. Aluminum is a "sacrificial" core. Reaction (2) drives corrosion of the aluminum core material which decreases the corrosion of the aluminum flange material. A key to successful utilization of a Ag-Al material is to balance the sacrificial nature of the aluminum core against the electrical stability of the conductive elastomer. Figure 5 shows that the Ag-Al-1 elastomer successfully does this; the Ag-Al-1 elastomer retains a volume resistivity within the maximum specifications, after salt fog exposure.

The instability of the silver-plated aluminum filler particles causes the electrical instability of the Ag-Al-2 material. The elastomer surface blisters due to corrosion of the particles. Figures 9a and 9b show the Ag-Al-2 filler particles before and after salt fog exposure. Cracking of the silver plating and particle expansion occurred. Figure 10a shows a higher magnification SEM photomicrograph of a Ag-Al-2 filler particle in an advanced stage of degradation. Energy dispersive X-Ray analysis (Figures 10b and 10c) shows that the silver plating became disbonded from the core, and large areas of aluminum were exposed.

The corrosivity and electrical stability results for the nickel and nickel coated graphite fillers are in agreement with previous work on galvanic corrosion. Mansfeld and Kenkel⁹ studied the galvanic corrosion of 6061 aluminum coupled to various metals. Nickel accelerated the corrosion rate of 6061 aluminum by a factor of more than 50 times compared to uncoupled aluminum. The results reported in this paper confirm these literature results and show that nickel is not galvanically compatible with aluminum.

The NiGr60 elastomer was more corrosive towards aluminum than the NiGr80 elastomer. SEM photomicrographs (Figure 11a and 11b) of the two fillers reveals that there is only partial coverage of the graphite base by nickel for the 60 wt% nickel coated graphite filler, but the 80 wt% nickel coating completely encapsulates the graphite. Graphite is known to be galvanically incompatible with aluminum. Bellucci¹⁰ found graphite fiber composites to be galvanically incompatible with Al; the corrosion rate of Al was accelerated by an order of magnitude compared to the uncoupled case. The 60 wt% nickel coated graphite filler is less compatible with aluminum than the 80 wt% nickel coated graphite filler because of the larger area of graphite exposed, and the C/EPTFE gasket was found to be extremely corrosive towards aluminum.

The NiF, NiP, and NiGr80 elastomers are electrically unstable in salt fog. Nickel is not a noble metal and will undergo some corrosion in a salt fog environment. The NiGr60 and C/EPTFE elastomers were electrically stable.

Conclusions

A quantitative corrosion test has been developed to measure the corrosivity of conductive elastomer shielding gaskets toward aluminum alloys. This test also measures the electrical stability of the conductive elastomer.

The results demonstrate that there is a significant difference in corrosivity among the different filler types. There was almost a 200-fold difference in corrosivity between the least corrosive (silver-plated aluminum filled fluorosilicone) and the most corrosive (carbon-filled expanded polytetrafluoroethylene) gaskets. Significant differences were found among the silver-plated fillers depending on the core. Differences in corrosivity and electrical stability were found between silver-plated aluminum filled fluorosilicones from different suppliers. Nickel-filled elastomers were found to be less corrosive than pure silver-filled elastomers, but were significantly more corrosive than the best silver-plated aluminum filled materials. Some of the nickel-filled materials were electrically unstable. These results indicate that both the core and the plating material must be considered when determining galvanic compatibility. A straightforward application of the galvanic series is not applicable because of the composite nature of these materials and the corrosion results reported here should be used in lieu of the standard galvanic series.

Acknowledgements

Tom Clement performed the SEM and energy dispersive X-Ray analyses. David Greenwood, Russell Lucia, and Li-Mei Huang assisted in obtaining the corrosivity and electrical stability data.

References

1. SAE AE-4R Committee, Proposed HIRF Standards.
2. "Hazardous Music," *Time*, February 15, 1993, p. 13.
3. E. Carlson and W.S.V. Tzeng, "Design of Corrosion Resistant EMI Joints," CORROSION/86, Paper No. 3. (Houston, TX: National Association of Corrosion Engineers, 1986).

4. R. Hansen and H. Choudhary, "Evaluation of EMI Seals For Corrosive Environments," Item 1991, (West Conshohocken, PA: R+B Enterprises, 1991), p. 196.
5. W.W. Lin, J.J. Reilly, H.J. Lee, and R.J. Brown, "Preliminary Corrosion Study of EMI Gaskets For Avionic Systems," Report No. NADC-87020-60, (Warminster, PA: Naval Air Development Center, September 1987).
6. P. Lessner and D. Inman, "Quantitative Measurement of the Degradation of EMI Shielding and Mating Flange Materials After Environmental Exposure," Paper No. 921019, (Dallas, TX: IEEE International Symposium on Electromagnetic Compatibility, 1993).
7. Philip Lessner, "Test Method For Assessing Galvanic Corrosion Caused By Conductive Elastomers," CHO-TM100, (Woburn, MA: Chomerics, Inc., May 1992).
8. MIL-G-83528B, "Gasketing Material, Conductive Shielding Gasket, Electronic, Elastomer, EMI/RFI, General Specifications For,"
9. F. Mansfeld and J.V. Kenkel, "Laboratory Studies of Galvanic Corrosion of Aluminum Alloys," in Galvanic and Pitting Corrosion-Field and Laboratory Studies, ASTM STP 576, (Philadelphia, PA: American Society for Testing and Materials, 1976), pp. 20-47.
10. F. Bellucci, "Galvanic Corrosion Between Non-Metallic Composites and Metals: I. Effect of Metal and of Temperature," *Corrosion*, **47** (1991): p. 808.

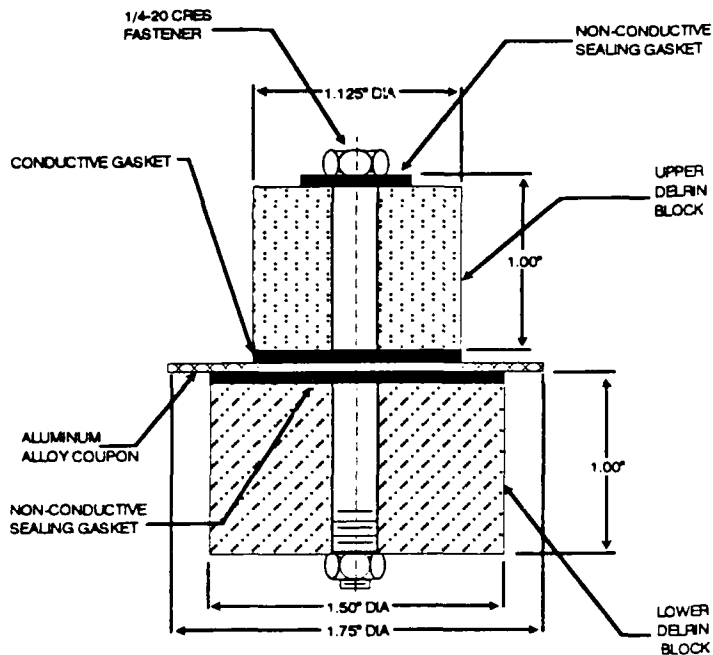


Figure 1 Test Fixture For Holding Aluminum Coupon and Conductive Elastomer in Contact During Environmental Exposure.

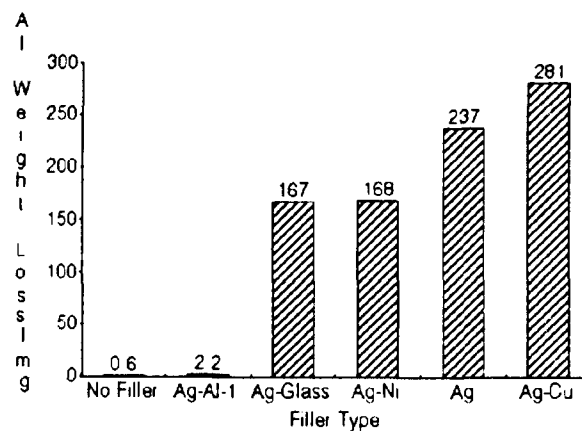


Figure 2 Avg. Weight Loss of 6061-T6 Al Coupons in Contact With (Fluoro)silicone Elastomers Filled With Silver and Silver-Plated Cores After 168 Hours Salt Fog Exposure.

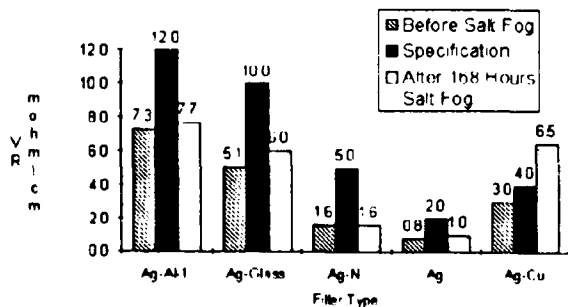


Figure 3 Volume Resistivity of Silicone and Fluorosilicone Elastomers Containing Silver and Silver-Plated Cores Before and After 168 Hours of ASTM B117 Salt Fog Exposure.

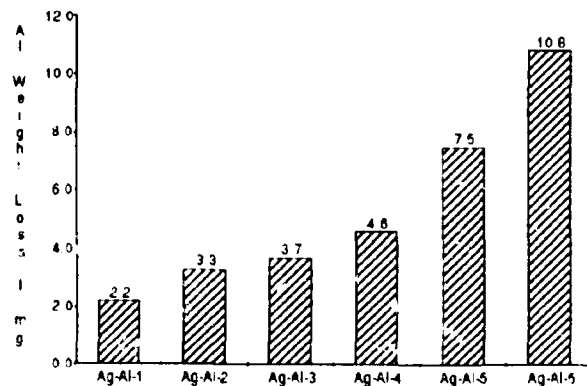


Figure 4 Weight Loss of 6061-T6 Aluminum Coupons in Contact with Silver-Plated Aluminum-Filled Fluorosilicone Conductive Elastomers After 168 Hours of ASTM B117 Salt Fog Exposure.

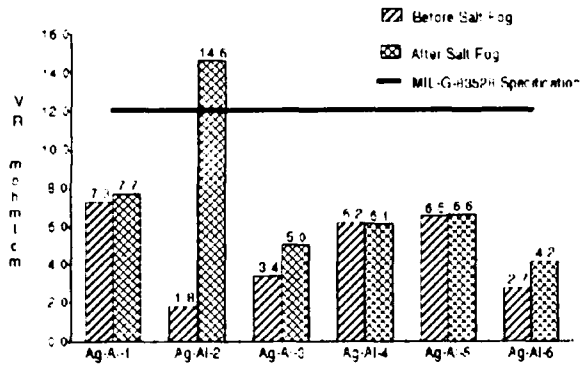


Figure 5 Volume Resistivity of Silver-Aluminum-Filled Fluorosilicones Before and After 168 Hours of ASTM B117 Salt Fog.



Figure 6a Surface of Ag-AI-1 After 168 Hours ASTM B117 Salt Fog Exposure.

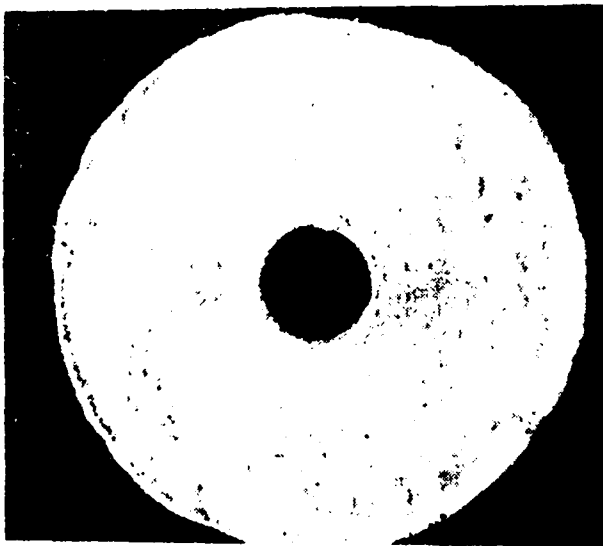


Figure 6b Surface of Ag-AI-2 After 168 Hours of ASTM B117 Salt Fog Exposure.

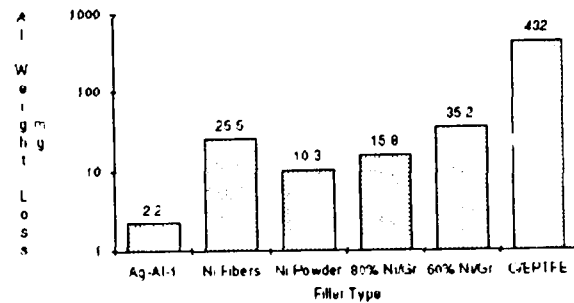


Figure 7 Weight Loss of 6061-T6 Al Coupons in Contact With Nickel and Carbon-Filled Elastomers After 168 Hours of ASTM B117 Salt Fog.

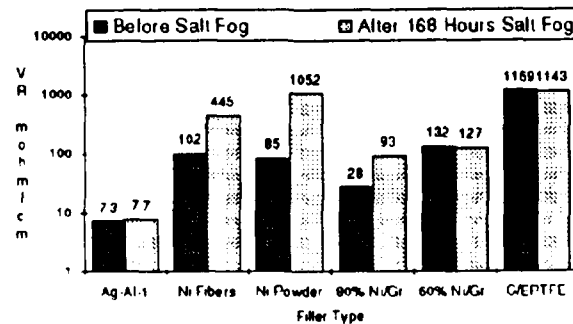
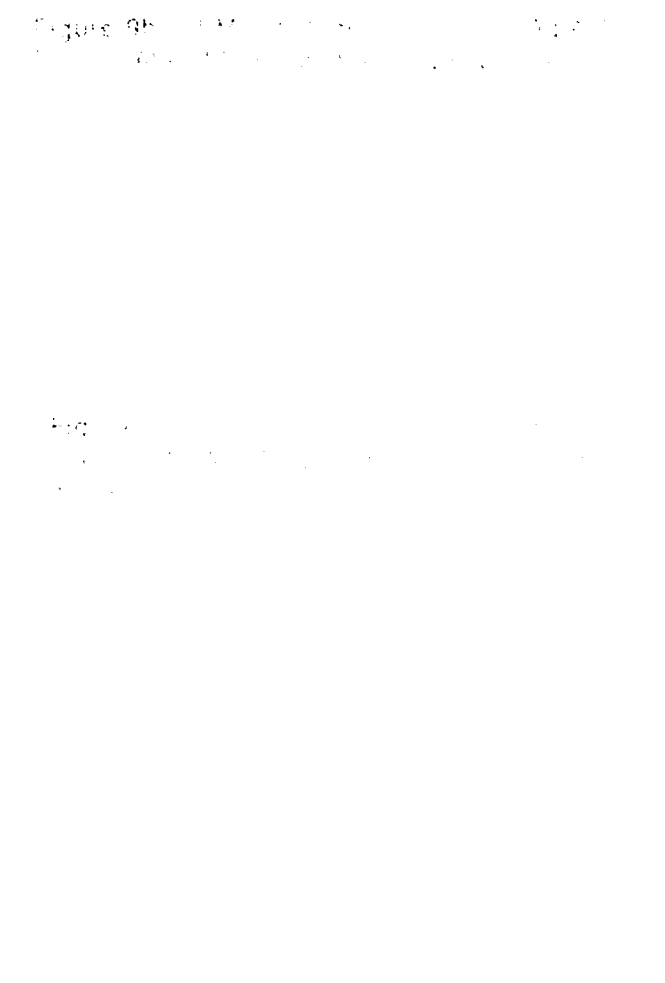
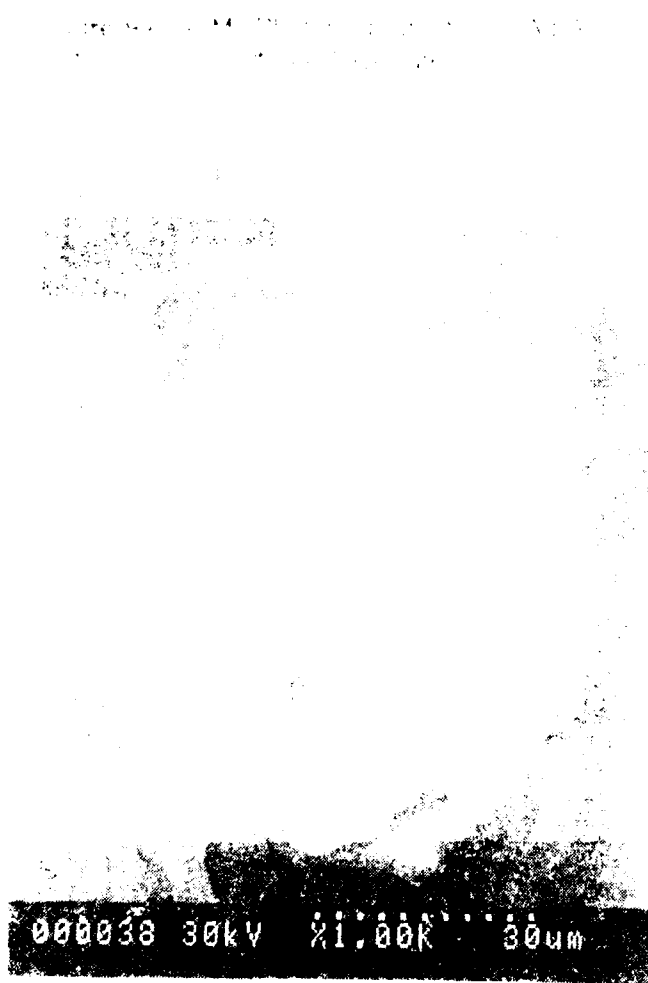
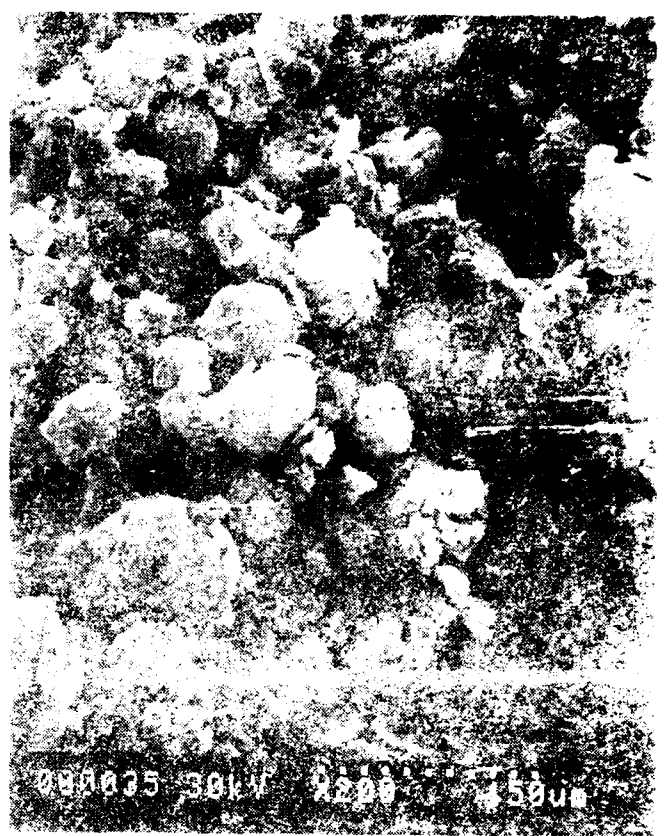


Figure 8 Volume Resistivity of Nickel and Carbon-Filled Elastomers Before and After 168 Hours of ASTM B117 Salt Fog



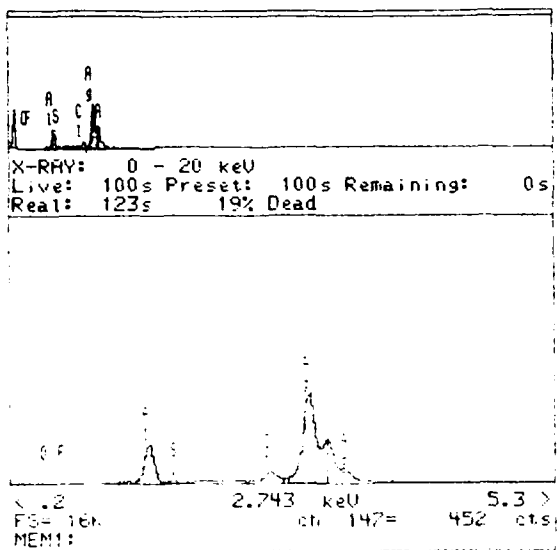


Figure 10b Energy Dispersive X-Ray Analysis of Area "A" of Figure 10a

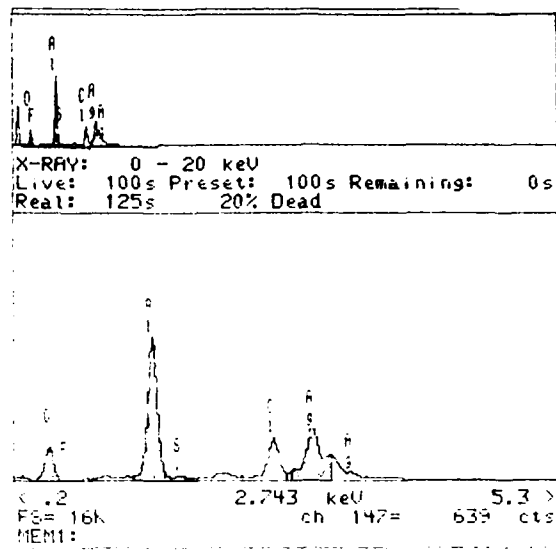


Figure 10c Energy Dispersive X-Ray Analysis of Area "B" of Figure 10a.



Figure 11a SEM Photomicrograph of 80 wt% Nickel-Coated Graphite Filler.



Figure 11b SEM Photomicrograph of 60 wt% Nickel-Coated Graphite Filler.

Corrosion of Electronics: Effect of Ionic Particulates

R. P. Frankenthal
AT&T Bell laboratories
Murray Hill, NJ 07974

R. E. Lobnig
AT&T Bell Laboratories
Murray Hill, NJ 07974

D. J. Siconolfi
AT&T Bell Laboratories
Murray Hill, NJ 07974

J. D. Sinclair
AT&T Bell Laboratories
Murray Hill, NJ 07974

Abstract

The reliability of electronic components, devices, and assemblies is strongly influenced by their use environment and, in particular, by the contaminants that are present. Ionic particles are ubiquitous in the environment. The absorption of moisture by the particles creates an electrolyte solution that leads to corrosion and, on electronic devices in the presence of an applied voltage, it results in leakage currents and electrolytic corrosion. Few studies have been reported on the effect of ionic dust particles on the corrosion of electronic metals and devices.

Methods are needed to generate and characterize submicron-sized ionic dust particles, to deposit them on metal coupons or small test substrates, and to evaluate their interaction with these surfaces at elevated temperatures and relative humidities. We describe the techniques (a) for generating high concentrations of submicron-sized particles, (b) for characterizing the composition of these particles, (c) for characterizing the concentration and size distribution of the particles, and (d) for depositing the particles onto the substrate metal or device to be studied.

We then describe a fundamental study of the corrosion of copper by submicron-sized $(\text{NH}_4)_2\text{SO}_4$ particles at various relative humidities. The results demonstrate that submicron ammonium sulfate particles, which are a major constituent of urban atmospheric dust, are an important factor in the formation of patina on copper.

Introduction

Particles are a ubiquitous component of the environments in which we live and work. The mass concentration of airborne particles in indoor electronic equipment environments¹⁻³ is frequently in the same range as the concentration of corrosive inorganic gases, e.g., SO_2 and NO_x .⁴ Yet research on atmospheric corrosion and on the degradation of electronic materials and assemblies has frequently been carried out without considering the potential effects of corrosive, water-soluble, ionic submicron-sized particles, which constitute the bulk of particulates transferred indoors from the outdoor environment.

Experience with failures in recent years has demonstrated the importance of particle effects. The increasing power density brought on by shrinking feature sizes in electronic devices requires that enhanced cooling be provided to equipment cabinets. This cooling is frequently accomplished using forced-air. As air velocity across surfaces increases, particle deposition velocity also increases.

An important characteristic of ionic particles with respect to reliability of electronics is their critical relative humidity (CRH). The CRHs at room temperature of some major constituents of urban environments are: NH_4HSO_4 – approximately 40%; $(\text{NH}_4)_2\text{SO}_4$ – 80%; NH_4NO_3 – 61%.⁵⁻⁸ In contrast, the effective CRH for most clean metal surfaces, as originally described by Vernon,⁹ is 70-80%. Ionic compounds dissolved in adsorbed water increase the conductivity of the water film. This leads to corrosion of metals and, on devices with an applied voltage, to leakage currents between metal conductors across the surface of insulating substrates and electrolytic corrosion.

We present here an overview of our research involving submicron-sized salt particles.^{10,11} The ability to generate and characterize submicron-sized particles representative of atmospheric pollutants, e.g., $(\text{NH}_4)_2\text{SO}_4$, and to deposit them on metal coupons or small test substrates is essential for conducting laboratory studies. Methods that have been developed for these processes are described. Then, results from an on-going investigation of the effect of $(\text{NH}_4)_2\text{SO}_4$ particles on the corrosion of copper are presented. The results clearly demonstrate that ammonium sulfate particles are an important factor in the formation of patina on copper.

Generation, Characterization, and Deposition of Submicron Salt Particles

Fundamental studies of the role of particles in corrosion processes are rare. We are conducting such studies under well-defined conditions of particle composition, purity, and size distribution. Stringent care has been taken to exclude all other contaminants or, when this is not feasible, to rigorously identify all contaminants and measure their concentrations. Techniques have been developed to (1) generate submicron-sized salt particles, (2) characterize their size distribution and concentration in the carrier gas, (3) determine the concentration and size distribution of any impurity particles that may be

present in the stream of salt particles, and (4) deposit the salt particles on the surface to be studied.

Particle Generation

Particles are generated^{10,11} at a constant rate from a salt solution by means of an atomizer that is fed by a mechanically driven syringe pump. The aerosol droplets are dried by a stream of hot nitrogen. Residual moisture is removed in a diffusion dryer. Any electrical charge on the particles is neutralized by a Kr-85 aerosol charge neutralizer, which brings the particles to a Boltzmann equilibrium.

Particle Characterization

Particle size distribution and concentration are characterized¹⁰ by laser light scattering: All particles $>0.014 \mu\text{m}$ were counted with a condensation nucleus counter, while all particles $>0.2 \mu\text{m}$ were sized and counted with laser particle counters that cover various size ranges; also particles from 0.09 to $3 \mu\text{m}$ were sized and counted with a laser aerosol spectrometer that resolves and counts particles in sixteen size channels. X-ray diffraction (XRD), Auger electron spectroscopy (AES), scanning electron microscopy (SEM), energy dispersive X-ray elemental analysis (EDX), and optical microscopy were used for characterizing the particles and their interactions with surfaces.

Impurity Characterization

Residual particles in the high-purity N_2 , which atomizes the solution and dries the aerosol, were characterized by laser light scattering as described above. Over a seven hour period, 221 measurements were recorded of which 196 were zero.¹² The counts that were recorded averaged $60 \text{ particles}/\text{m}^3$. The resistivity of the water used to make the salt solutions was $>16 \text{ Mohm}$. The concentration of residual particles $>0.05 \mu\text{m}$ in the water, as measured with a liquid particle sensor, was negligibly small, especially when compared to the concentration of particles generated from dissolved matter when the water was atomized.¹² The concentration of residual dissolved matter and fine ($<0.05 \mu\text{m}$) particle contamination in the water ranged from 2×10^{-9} to $8 \times 10^{-8} \text{ g}/\text{cm}^3$, as determined with a TOC (total organic carbon) analyzer and from the concentration and size distribution of particles generated by atomization of the water. It should be noted that the number of particles formed by the atomization process is independent of the concentration of contaminants; however, the size of the particles changes as the one-third power of the concentration.

Particle Deposition

$(\text{NH}_4)_2\text{SO}_4$ particles, 0.01 to 1 μm in diameter, were generated with a total concentration of $10^9/\text{m}^3$ of N_2 . Particles this small have little inertia and tend to follow the flow of the gas stream around solids. Consequently, deposition of particles from the gas stream is extremely slow and inefficient. To accelerate deposition, two methods have been used. The first method is thermophoretic deposition. The stream emerging from the particle generation system is heated, e.g., to 80°C , and the laminar flow emanating from the deposition apparatus is disturbed by the introduction of many protrusions into the stream's path. Since particles are thermophoretically attracted to a colder surface, deposition takes place on copper cooled to 0°C . This technique gives a uniform deposit over a large area but does not separate particles by size. The second method is deposition by cascade impaction.¹³⁻¹⁵ The impactor used in this study separates the particles into four size fractions, the smallest being 0.05-0.15 μm , and the largest being $>1.5 \mu\text{m}$. Impaction gives a nonuniform deposit of particles, with the deposit pattern being a function of the impactor design.

Effect of Submicron-sized $(\text{NH}_4)_2\text{SO}_4$ Particles on the Corrosion of Cu

The effect of $(\text{NH}_4)_2\text{SO}_4$ particles ($<1 \mu\text{m}$ in diameter) on the corrosion of copper is being investigated in air at 100°C and relative humidities of 65, 75, and 88%.¹¹ The CRH for $(\text{NH}_4)_2\text{SO}_4$ is 75% at 100°C . Particle deposition was by cascade impaction. Two size fractions were studied: 0.5–1.5 μm and 0.05–0.15 μm . No effect of particle size was observed. The oxidation time for all experiments was 120 hours.

Corrosion below the critical relative humidity (65% RH)

The presence of $(\text{NH}_4)_2\text{SO}_4$ particles on the copper has little effect on its corrosion. The original salt pattern is still observed by eye and in the SEM after 5 days at 100°C . XRD shows no change in the composition of the salt. The only corrosion product is Cu_2O . The oxide thickness is the same on copper with the particles as on a control coupon. The oxide grows by a solid-state process.

Corrosion at the critical relative humidity (75% RH)

With moderate amounts (10-400 $\mu\text{g}/\text{cm}^2$) of $(\text{NH}_4)_2\text{SO}_4$, the areas initially covered by particles are still clearly defined after oxidation. But, the particles are not present. Instead a bluish-green corrosion product, identified by XRD as brochantite, $\text{Cu}_4(\text{SO}_4)(\text{OH})_6$, has formed. Brochantite is a common component of copper patina. In areas that had not been covered by ammonium sulfate, a film of Cu_2O , the same thickness as on the control, is observed. With less than 10 $\mu\text{g}/\text{cm}^2$ of $(\text{NH}_4)_2\text{SO}_4$, little corrosion product is visible; only in the vicinity of the originally deposited salt particles are the interference colors different from the control. With more than

ca. 400 $\mu\text{g}/\text{cm}^2$ of $(\text{NH}_4)_2\text{SO}_4$, the corrosion product is so voluminous that the original pattern of the salt deposit is not visible. The corrosion product in this case is antlerite, $\text{Cu}_3(\text{SO}_4)(\text{OH})_4$, another common component of copper patina. At 75% RH, the salt particles absorb sufficient water to form a saturated electrolyte that reacts with the copper. However, the amount absorbed is not sufficient for the solution to spread beyond the region of the initial salt deposits. Consequently, the reaction between electrolyte and copper is localized, as are the corrosion products. The corrosion mechanism is discussed below.

Corrosion above the critical relative humidity (88% RH)

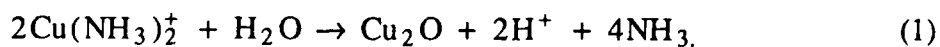
The same results are observed for all experiments independent of the amount of $(\text{NH}_4)_2\text{SO}_4$ deposited. A dark gray, dense, crystalline layer of corrosion product, which is several microns in thickness and has been identified by XRD as Cu_2O , covers the entire surface, only a fraction of which initially was coated with $(\text{NH}_4)_2\text{SO}_4$. By contrast, the oxide film on the control exhibits interference colors, indicative of a much thinner film. A dark green crystalline corrosion product is scattered randomly over the oxide layer at sites that are not related to the sites of salt deposition. These crystallites have been identified by XRD as antlerite, $\text{Cu}_3(\text{SO}_4)(\text{OH})_4$. In addition to the thick oxide layer that covers the whole surface, localized pitting is seen in metallographic cross section. The pits are filled with Cu_2O .

Sufficient water is absorbed at 88% RH to form a solution of $(\text{NH}_4)_2\text{SO}_4$ that covers the entire copper surface. Since the oxide is too thick to have been formed by a solid-state process at 100°C, sufficient copper must corrode at this RH to cause precipitation of both the oxide and antlerite from the electrolyte solution.

Corrosion mechanism for RH \geq 75%

The proposed corrosion mechanism for RH \geq 75% is as follows:¹¹ At the CRH, $(\text{NH}_4)_2\text{SO}_4$ absorbs water to form a saturated solution, 3.8 mol $(\text{NH}_4)_2\text{SO}_4$ in 1000 g solution.¹⁶ At 88%, sufficient water is absorbed at equilibrium to dissolve all the salt and form a solution that contains 2.5 mol $(\text{NH}_4)_2\text{SO}_4$ in 1000 g solution.¹⁷

Under all conditions, Cu_2O forms. Most likely, NH_3 , in equilibrium with NH_4^+ , reacts with Cu to form $\text{Cu}(\text{NH}_3)_2^+$. Under the given experimental conditions, the cuprous ammonia complex is more stable than any of the cupric ammonia complexes. The complex then reacts with H_2O to precipitate Cu_2O



This reaction, as well as the dissociation of NH_4^+ to form NH_3 and H^+ , leads to a decrease in pH. At the same time, the excess NH_3 slowly evaporates.

In acidic SO_4^- solution, Cu^+ disproportionates to Cu^{2+} and Cu^0 . Also, the cuprous ammonia complex is oxidized by O_2 in the air to a cupric ammonia complex. With decreasing NH_3 due to its evaporation, the electrolyte solution contains mainly acidic CuSO_4 , which has a CRH of 94% at 100°C . Consequently, at 75% and 88% RH H_2O will evaporate from a CuSO_4 solution. When the solubility product of brochantite or antlerite is exceeded, precipitation occurs. Brochantite is stable over the pH range 3.5-6.5, while antlerite is stable over the pH range 2.8-3.5.^{18 (1)} At 88% RH, sufficient Cu_2O is formed by Reaction 1 to lower the pH into the stability range for antlerite. At 75% RH, a sufficient amount of Cu_2O to lower the pH into stability range for antlerite will form only when more than $400 \mu\text{g}/\text{cm}^2$ of $(\text{NH}_4)_2\text{SO}_4$ is on copper. For lesser quantities, the formation of Cu_2O is only sufficient to lower the pH into the stability range of brochantite.

Summary

After noting the importance of particulate contamination to the corrosion and reliability of electronic materials and devices, recently developed techniques to aid in the study of these effects were described. Results were presented from a study of the effect of submicron-sized $(\text{NH}_4)_2\text{SO}_4$ particles on the corrosion of copper at 100°C and relative humidities of 65%, 75%, and 88%. A mechanism that accounts for the formation of Cu_2O , antlerite, and brochantite under the different experimental conditions was described.

Lastly, it is noted that both antlerite and brochantite are found in the naturally formed patina on copper. The present work clearly demonstrates that ammonium sulfate particles, which are a major constituent of urban dust, are an important factor in the formation of patina on copper.

(1) This stability range is at 20°C . The range at 100°C is not known.

References

1. J. D. Sinclair, *J. Electrochem. Soc.*, **135**, (1988): p. 89C.
2. J. D. Sinclair, L. A. Psota-Kelty, C. J. Weschler, and H. C. Shields, *Atmos. Environ.*, **24A**, (1990): p. 627.
3. J. D. Sinclair, L. A. Psota-Kelty, G. A. Peins, and A. O. Ibidunni, *Atmos. Environ.*, **26A**, (1992): p. 871.
4. R. B. Comizzoli, R. P. Frankenthal, P. C. Milner, and J. D. Sinclair, *Science*, **234**, (1986): p. 340.
5. R. C. Weast and M. J. Astle, "CRC Handbook of Chemistry and Physics", 59th Edition, (Palm Beach, FL: CRC Press, 1978), p. E46.
6. I. N. Tang, *J. Aerosol Sci.*, **7**, (1976): p. 361.
7. R. J. Charlson, D. S. Covert, T. V. Larson, and A. P. Waggoner, *Atmos. Environ.*, **12**, (1978): p. 39.
8. A. S. Wexler and J. H. Seinfeld, *Atmos. Environ.*, **25A**, (1991): p. 2731.
9. W. H. J. Vernon, *Trans. Faraday Soc.*, **31**, (1935): p. 1668.
10. R. P. Frankenthal, R. E. Lobnig, D. J. Siconolfi, and J. D. Sinclair, *J. Vac. Sci. Technol.*, in press.
11. R. E. Lobnig, R. P. Frankenthal, D. J. Siconolfi, and J. D. Sinclair, in "Corrosion and Reliability of Electronic Materials and Devices", J. D. Sinclair, Ed., (Pennington, NJ: The Electrochemical Society, NJ, 1993), p. 336; *J. Electrochem. Soc.*, submitted for publication.
12. D. J. Siconolfi, R. P. Frankenthal, and J. D. Sinclair in "Cleaning Technology in Semiconductor Device Manufacturing", R. Ruzyllo and R. E. Novak, Eds., (Pennington, NJ: The Electrochemical Society, 1992), p. 34.
13. P. C. Reist, "Introduction to Aerosol Science", (New York, NY: MacMillan Pub. Co., 1984), Chapter 7.
14. S. K. Friedlander, "Smoke, Dust, and Haze", (New York, NY: J. Wiley & Sons, 1977), p. 162.
15. W. B. Smith and J. D. McCain, in "Air Pollution Control", Part III, W. Strauss, Ed., (New York, NY: Wiley-Interscience, 1978), p. 138.
16. W. F. Linke, "Solubilities of Inorganic and Metal Organic Compounds", Vol. 1, (Washington, DC: American Chemical Society, 1965), p. 755.
17. G. Tammann, *Mem. Acad. Petersb.*, **35**, (1887): p. 84.
18. M. Pourbaix, *J. Electrochem. Soc.*, **123**, (1976): p. 25C.

ACCELERATED GASEOUS CORROSION TESTING

Rudolf Schubert
Bellcore,
Room 3X215
PO Box 7040
Red Bank, NJ 07701-7040

ABSTRACT

Multiple, low level, pollutant gas corrosion testing is fraught with difficulties, each of which has a unique solution. Challenges include depleted pollutants, air velocity control, system spatial uniformity, *in situ* dynamic corrosion monitoring, and system reproducibility. ASTM Committee B04.07 has written five standards to calibrate, monitor, and control flowing mixed gas chambers. These are standards on using mass gain to calibrate a chamber; using quartz crystal microbalances and electronic resistance monitors for dynamic, *in situ* monitoring; coulometric reduction of exposed metal coupons for corrosion product analysis at the end of the exposure; and a complete procedure for the actual exposure from startup to shutdown. Funding is being obtained to introduce these techniques to selected laboratories where there is interest in learning all the details of the technique or interest in participating in an inter-laboratory study. This paper describes usage of the standards and solicits additional laboratories to participate in the study.

I. Introduction

Virtually all surfaces corrode over time; the rate of corrosion depending on the material surface and the nature of the corrodant. For electronic equipment the corrodant is usually in the form of a gaseous pollutant, e.g., hydrogen sulfide, nitrogen dioxide, etc., although some of the materials used in manufacture can also leave behind a corrodant, e.g., soldering flux. All materials and components used in electronics are subject to corrosion, but the electrical contacts are most vulnerable for two reasons. They are not sealed from the atmosphere with a corrosion inhibiting material, and minute amounts of foreign, non conducting materials on the contact surface are sufficient to increase the junction contact resistance. Even with electroplated noble metal surfaces, the small pores which may be present in the surface coating can be the source of base metal corrosion and the cause of increased contact resistance.

Corrosive gas testing standards have been used for decades^[1] to evaluate the susceptibility of electronics to corrosion failure mechanisms. This initial standard^[1] used only the single pollutant gas, sulfur dioxide, at a level of $25,000 \pm 5,000$ parts per billion (ppb). That corrosion test does not simulate the typical environment that electronic equipment is usually exposed to and the IEC has developed additional standards with two gases and lower concentrations.^[2] Although specific pollutants vary by location, time of day, time of year, and their concentrations vary on a continuous scale; an extensive study by Abbott^[3] has suggested that a simplified, limited set of tests of selected pollutant levels could

approximate many of the conditions. He approximated the corrosive environment into four classes of common pollutants occurring together at selected concentrations. The classes, pollutants and concentrations are listed in Table I. Other pollutants and conditions are also known to affect the type and rate of corrosion; however, to keep the tests less complex only three pollutant gases were specified. A review of mixed flowing gas (MFG) testing and an extensive bibliography has recently been completed by the ASTM^[4].

Due to the difficulty of measuring and controlling low concentrations of pollutant gases and the many other variables present in such a test, interlaboratory studies produced corrosion results with a mass gain and/or corrosion film thickness varying by a factor of 2-3. This paper discusses a new series of ASTM standards that are designed to avoid exposure and testing pitfalls and to reduce test variations. Several of these standards provide corrosion monitoring techniques, both *in situ*^[5],^[6] and on a time integrated basis.^[7],^[8] A parent standard^[9] specifies how known corrosion testing variables are to be handled and the sequence of events required to conduct the exposure.

II. Corrosion Variables and Test Chamber

II.1 Selected Variables.

It is well known that a number of variables affect the rate of corrosion. These variables include corrodant chemical species and concentration, synergistic effects between species, relative humidity, temperature, transport of the corrodant to the test surface, and test surface (chemical/elemental) species and surface morphology. Major known variables, their tolerances, and interferences are listed in Table II for topics discussed in ASTM B 827^[9].

Test temperature is easiest to control if the required temperature is above the laboratory temperature. Since these tests are an acceleration of corrosion rate, there seldom is a reason to choose a test temperature at or below laboratory temperature. Typically a five degree difference between test and laboratory is sufficient unless the apparatus being tested is in the operating mode and is producing more heat than is necessary to heat the exchanged air.

Corrosion rate and the thickness of the adsorbed water film increases nonlinearly with increasing relative humidity. Adsorbed water film thickness in angstroms versus the atmospheric dew point in °C is shown^[10] in Figure 1 for an atmosphere temperature of 30 °C. Relative humidity control is best achieved by continuous introduction of moisture and by employing monitors that have a minimum susceptibility to corrosion, e.g., platinum mirror dew point meters.

House compressed air is usually unacceptable as the air source unless a method to remove moisture, oils, particulates, and air pollutants is also used. These impurities must be reduced to well below the level desired in the test exposure and then, as desired, some contaminant can be added back into the atmosphere with

proper control.

Local air velocity and total system air exchange rate are critical factors in the corrosion process; both variables help determine the rate at which a pollutant species can be delivered to a test surface. In ASTM B 827^[9] the velocity is left to the discretion of the vendor-tester-purchaser relationship. Exchange rate is divided into two categories; Method HX, the high exchange rate, typically has greater than 60 exchanges per hour and Method LX, the low exchange rate, typically operates with 5 to 15 exchanges per hour. Due to the strong influence of these variables on the corrosion rate, multiple system test operation experience may show that these components of the Standard need revision in the future.

II.2 Test Chamber Considerations.

A typical chamber and associated equipment is shown in Figure 2.^[10] The example utilizes three pollutant gases, but any number could be used, depending on the test requirements. All of the components that are in contact with the test atmosphere, i.e., gas delivery system, chamber walls, and gas monitoring systems, must be made of non-reactive and low-adsorbing materials. Clearly, non-reactive system materials are needed to avoid depletions and minimize transients in the pollutant gas concentrations. Low-adsorption is required to reduce the history effects of adsorbed gases when changing pollutant gases or concentrations. Materials known to be acceptable include glasses, fluorocarbon resin based materials, and acrylic based plastic resin materials.

Although electronic equipment placed in forced air cooled equipment racks will show substantially more dirt and corrosion on the materials closest to the fans, all of the equipment is typically manufactured to the same specifications. Therefore, to achieve uniform testing, gas flow through the test chamber and around the test specimens must be uniform to assure similar fluxes of pollutant gases to each test surface. Point sources/sinks of the chamber atmosphere supply/exhaust make spatial uniformity difficult. They cause "hot spots" or "dead volumes" in the chamber, i.e., nonuniform exposure conditions over a test sample, and may not reflect the exposure environment found in real applications. This difficulty can be overcome by using distributed gas input/exhaust systems. An example of a distributed input/exhaust using a combination of both perforated tubing and a perforated baffle is illustrated in Figure 3.^[11] Utilization of fans within the working volume of a corrosion chamber can introduce a local "hot spot" where the exit stream of the fan impinges on test samples. Insertion of baffles around the fan exhaust can reduce the "hot spot" problem; however, chambers with in-chamber fans are not likely to meet the uniformity requirements of ASTM B 810^[7].

II.3 Pollutant and Corrosivity Monitors.

II.3.1 Pollutant Monitors. Several manufacturers sell specific gas pollutant monitors that are capable of measuring pollutant levels at the few ppb level. In general, those monitors that operate on detecting a specific characteristic of the

molecule being measured, e.g., chemiluminescence of ozone and NO, are more stable and have less interferences than those that simply measure a parameter of a class of molecules and extrapolate the results to a single pollutant species. Monitors which operate on a class of pollutants, e.g., electron transfer of detected halogenated species, are subject to positive interference by other similar gases and negative interference by reducing species. Chlorine concentration is difficult to measure due to these interferences. At present, commercial instruments for measuring chlorine (ppb) are only effective, under the best of conditions, at the beginning or end of an MFG test when all the other pollutant gases have been removed. Those monitors which have obtained EPA certification are typically more stable than uncertified instruments.

II.3.2 *In Situ* Corrosivity Monitors. Four standards^{[5],[7],[8],[6]} are available to monitor the corrosivity of a test. The method based on mass gain of a quartz crystal microbalance (QCM) and the method based on the resistance change of a thin metal wire can be used *in situ* and provide dynamic, real time corrosion results. Both types of sensors can be made with the metal of interest in the corrosion study. For example, if copper corrosion were of interest then the electrodes on the QCM would be made of copper. As the copper oxidizes or forms other compounds, the mass of the electrode increases and the resonant frequency of the QCM decreases; the frequency change of the crystal is the parameter that is measured. A plot of mass gain by QCMs with copper electrodes versus time in an MFG test chamber is shown in Figure 4.^[11] This figure is discussed further in the following section. The composition of the mass gain, e.g., oxides, chlorides, sulfides, nitrides, etc., must be determined by other analytic techniques.

II.3.3 Integrating Corrosivity Monitors. Two integrating technique standards^{[6],[7]} utilize metal coupons for the monitoring. They are based on either mass gain^[7] of the coupon or on coulometric reduction^[6] of the corrosion film after exposure. Mass gain data for three different metal coupons exposed to a ten day test at 30 °C, 70 % relative humidity, 10 ppb H₂S, 10 ppb Cl₂, 200 ppb NO₂, and 200 ppb SO₂ are shown in Table III. These data show the uniformity of the chamber, since the coupons of different metals were hung periodically around the chamber. The data also show the different responses of the three metals to the same pollutant conditions, as expected.

IV. Test Chamber Operation

IV.1 Start-up/Shut-down

It is desirable to minimize the concentration transients that occur when an exposure is started or stopped. These occur when changing the pollutant flow, opening and closing the chamber, or loading the test samples (usually containing reactive surfaces) into the chamber. To minimize these transients, trial samples should be used to determine approximately what pollutant flow rates are needed to achieve the specified pollutant concentration. As mentioned in Section II.3.1, the chlorine

concentration must be determined prior to introduction of other interfering gases. This should also be checked again at the end of the exposure after other interfering gases have been removed. Once approximate flows have been determined on trial samples, correct flows can be fine tuned on the actual test specimens without encountering excessive transients.

IV.2 Chamber Sampling

In addition to avoiding transients, atmospheric composition in the chamber must be uniform, that is, upstream/downstream differences in pollutant concentration must be held to $< 15\%$ as per ASTM B 827, Section 7.3.^[9] Excessive loading or an insufficient number of air exchanges per hour can cause this condition to be violated, as discussed in the next section. To verify an acceptable concentration gradient across the working volume of the accelerated atmospheric corrosion chamber (AACC), pollutant gas monitoring should be performed both upstream and downstream of the working volume.

IV.3 Chamber Loading

Assume that a MFG test exposure requires a chlorine concentration of 10 ppb in the chamber atmosphere. If the exchange rate and air flow through the chamber are low, the insertion of one circuit pack with exposed metal surfaces may require that the input gas stream contain 15 ppb to maintain 10 ppb of chlorine in the chamber. Placement of a second pack in the chamber may require the input stream to contain 20 ppb of chlorine to maintain 10 ppb in the chamber. (The circuit pack above is figurative and could as well be 10 connectors and 20 connectors as an example.) This loading/flow problem causes severe discrepancies in the results of product exposure. The sample product near the inlet will be exposed to a concentration of 20 ppb Cl_2 whereas the product near the exhaust will only be exposed to 10 ppb. A factor of two in exposure severity is clearly outside of the ASTM B 827, Section 7.3^[9] requirement of $\pm 15\%$ across the chamber working volume.

An example will illustrate how the above problem can occur. Assume a 100 liter chamber ($\approx 4 \text{ ft}^3$) with 10 air exchanges per hour; this corresponds to 1000 liter of new air per hour. If the concentration of Cl_2 were 10 ppb in the new air, then 2.5×10^{17} Cl_2 molecules/hr would be introduced into the chamber. The mass of the corrosion film growing on the copper and zinc coupons listed in Table III corresponds to 7.5×10^{-6} grams/hour per coupon. If only 10% of this film is chlorine it corresponds to 1.3×10^{16} chlorine atoms per hour on each coupon. Thus the placement of only 10 coupons would reduce the available gaseous Cl_2 by 50% and cause nonuniform exposure across some sample surfaces. Thus, the air exchange rate of 10 times per hour in this example is unable to meet the calibration requirements of ASTM B 827.^[9] If the exchange rate were increased to 60 exchanges per hour, then only 14% of the available Cl_2 would be used with the above assumptions.

IV.4 Chamber Load Spacing

Figure 4 demonstrates that when one sample is placed directly upstream of a second sample, the second sample can have substantially reduced corrosion rates. Relative thickness of copper corrosion is plotted versus sample time in a three pollutant gas atmosphere. The four samples (curves 1 - 4) were placed uniformly around the corrosion chamber. After two hours a grid of five OFHC copper sheets, with a total surface area of 60 cm² and a footprint of 6.5 cm² was placed 0.5 cm above the copper sample labeled 1. At that time the corrosion rate of the copper 1 sample decreased and only increased after the grid was removed after 18 hours. Nonuniform corrosion rates can also be observed on one long sample, whose long axis is parallel to the air flow, rather than several short samples.) Samples should be placed side by side rather than upstream and downstream of each other. Preliminary measurements indicated that a spacing of 5 cm between test samples and between test samples and the chamber wall is sufficient to avoid the problem of one sample getting an adjacent sample's pollutant gases if the air velocity and exchange rates are at least as great as specified in ASTM B 827.^[9]

V. Interlaboratory Study

Additional interlaboratory studies are needed to verify that various test facilities can reproducibly and accurately conduct MFG tests at low concentration levels of pollutants. ASTM Subcommittee B 04.07, Electrical Contact Test Methods, is currently writing a proposal that is expected to be funded by the Institute of Standards Research (ISR) and participating laboratories. The ISR funding will cover the cost associated with the coupon samples, sample corrosion film analysis, corrosivity monitoring instruments, corrosivity monitoring devices, and other direct costs. Participating laboratories will fund chamber operating costs. Coupons and other types of samples of five metallic elements will be exposed and the resulting surface films will be analyzed by several different techniques. Participating laboratories are expected to provide the expertise needed to operate an AACC to a set of specified conditions. Each participating laboratory will be instructed and assisted in performing the exposure. For further information on how to participate in this study, please contact the author at (908)758-3185. A short course on MFG testing will be given at the Fall Meeting of the Electrochemical Society in New Orleans on October 24, 1993.

VI. Conclusions

Some of the pitfalls and difficulties that can produce erroneous results in low pollutant concentration level corrosive gas testing have been discussed. Solutions to these potential difficulties are also discussed. In general, if one adheres to the recently published series of ASTM standards on flowing mixed gas testing, reproducible results can be obtained. This will facilitate interlaboratory comparisons of test results.

REFERENCES

1. International Electrotechnical Commission, IEC Standard 68-2-42, Basic Environmental Testing Procedures, Test Kc: Sulphur Dioxide Test for Contacts and Connections, 1976.
2. International Electrotechnical Commission, IEC Technical Trend Document 68-2-60 TTD, Test Ke, Method C, Environmental Testing, Corrosion Tests in Artificial Atmosphere at Very Low Concentration of Polluting Gas(es), 1989.
3. W. H. Abbott, "The Development and Performance Characteristics of Flowing Mixed Gas Test Environments," IEEE Trans. CHMT, 11,1, 22(1988).
4. American Society for Testing and Materials, ASTM B-TBD, "Guide to Mixed Flowing Gas Tests for Electrical Contacts, Philadelphia, PA, 1993 and the references therein.
5. ASTM B808, "Standard Test Method for Monitoring of Atmospheric Corrosion Chambers by Quartz Crystal Microbalances," ASTM, Philadelphia, PA and the references therein.
6. ASTM B 826, "Standard Test Method for Corrosivity of MFG Environmental Tests by Electrical Resistance Monitoring," ASTM, Philadelphia, PA and the references therein.
7. ASTM B 810, "Standard Test Method for Calibration of Atmospheric Corrosion Test Chambers by Change in Mass of Copper Coupons," ASTM, Philadelphia, PA and the references therein.
8. ASTM B 825, "Standard Test Method for Coulometric Reduction of Surface Films on Metallic Test Samples," ASTM, Philadelphia, PA.
9. ASTM B 827, "Standard Practice for Conducting Mixed Flowing Gas Environmental Tests, ASTM, Philadelphia, PA.
10. R. Schubert, "A Second Generation Accelerated Atmospheric Corrosion Chamber," ASTM STP965, ASTM, Philadelphia, PA, 374(1988).
11. R. Schubert and G. G. Neuburger, "Rapid Determination of Corrosion Chamber Uniformity," J. Electrochem. Soc., 137,4, 1049(1990).

Table I. Pollutants and their concentrations used in the Battelle Classes and the corrosion mechanism expected.

| Battelle Class* | Pollutant Gas | Concentration (ppb) | Corrosion Mechanism |
|-----------------|------------------|---------------------|---------------------|
| Class I | H ₂ S | - | none |
| | Cl ₂ | - | visible |
| | NO ₂ | - | |
| Class II | H ₂ S | 10 | pore |
| | Cl ₂ | 10 | |
| | NO ₂ | 200 | |
| Class III | H ₂ S | 100 | pore and creep |
| | Cl ₂ | 20 | |
| | NO ₂ | 200 | |
| Class IV | H ₂ S | 200 | creep |
| | Cl ₂ | 50 | |
| | NO ₂ | 200 | |

* Temperature and Relative Humidity are also specified.

Table II. Test Variables, Tolerances, and Interferences.*

| Variable | Tolerance | Interference |
|------------------------------|-----------------------------------------------------|-------------------------------------------------------------------------------------------------------------------------------|
| Temperature | ± 0.5 °C | Internal hot spots |
| Relative Humidity | 1% | Detector corrosion Hot spots |
| Moisture Source | ASTM D 1193 Type I or better | Chlorine Hardness |
| Chamber Atmosphere | < 5 ppb Total Impurities | Humidity Pollutant gases Particulates |
| Pollutant Gases | ± 15 % or ± 3 ppb whichever larger | System Adsorption Carrier Gas Impurities Synergistic Effects Monitor Interferences System Leaks System History |
| Pollutant Monitors | EPA Limits | Other Gases |
| Pollutant Gradient | ± 15 % | System Overload Low Exchange Rate |
| Air Velocity Laminar Flow | ± 20 % | Turbulence Shielding |
| System Exchange Rate | Low or High | System Leaks |
| Corrosivity | Multiple Monitors As Specified | Cleaning Surface Morphology Physical position |
| Test Duration | ± 2 % or ± 2 hours | Work Schedules Holidays |
| Test Interruptions | < 5 % | Supply Replenishment Test Sample Measurement Startup and Shutdown |
| Samples | | Chemical Cleaning Structure |

* Detector calibration is not an interference although it is a common problem with all the variables and monitors.

Table III. Weight gain (μg) of nickel, copper, and zinc coupons with 10 cm^2 of surface area after ten days in a four gas test.

| | Copper | Nickel | Zinc |
|----------------|-------------|-------------|-------------|
| | 1830 | 2740 | 1790 |
| | 1830 | 2760 | 1830 |
| | 1880 | 3390 | 1700 |
| | 1740 | | 2120 |
| | 1790 | | 1660 |
| Average | 1813 | 2965 | 1820 |
| Range | $\pm 4.2\%$ | $\pm 7.6\%$ | $\pm 9.0\%$ |

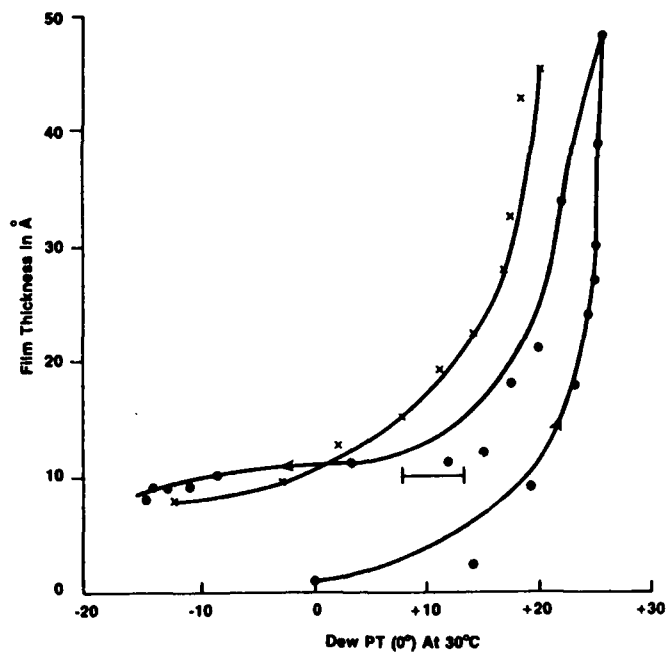


Figure 1. Adsorbed water film thickness versus the dew point of a $30\text{ }^\circ\text{C}$ ambient on quartz crystals with copper electrodes.

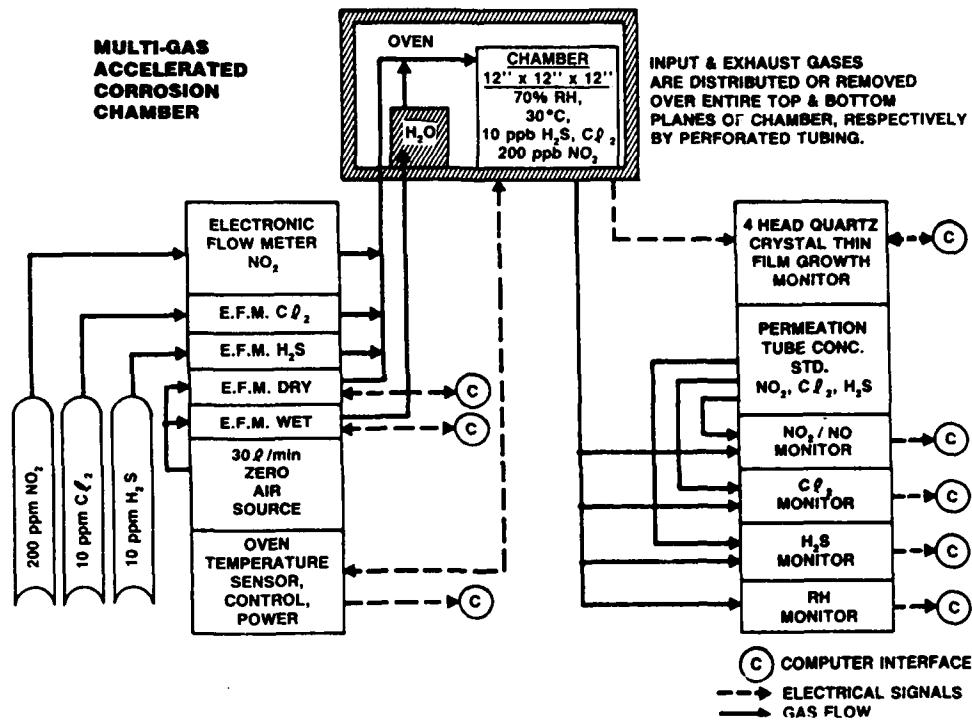


Figure 2. Schematic of a typical accelerated atmospheric corrosion chamber and associated equipment. The chamber size; corrosion conditions; and the number and type of pollutant sources can all be adapted to the specific test criteria.

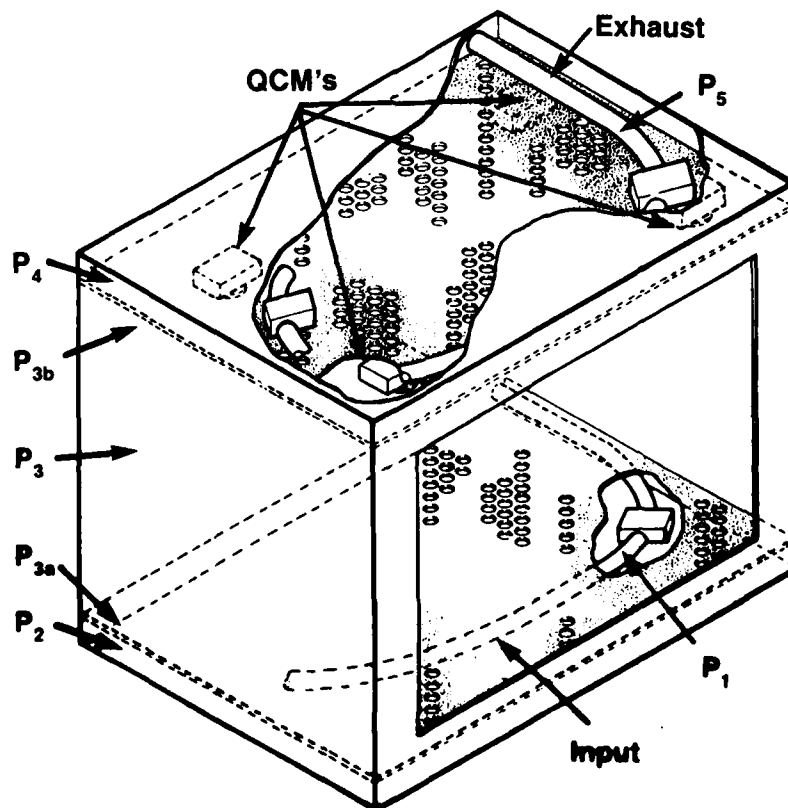


Figure 3. An example of a distributed input and exhaust system for a mixed flowing gas chamber.

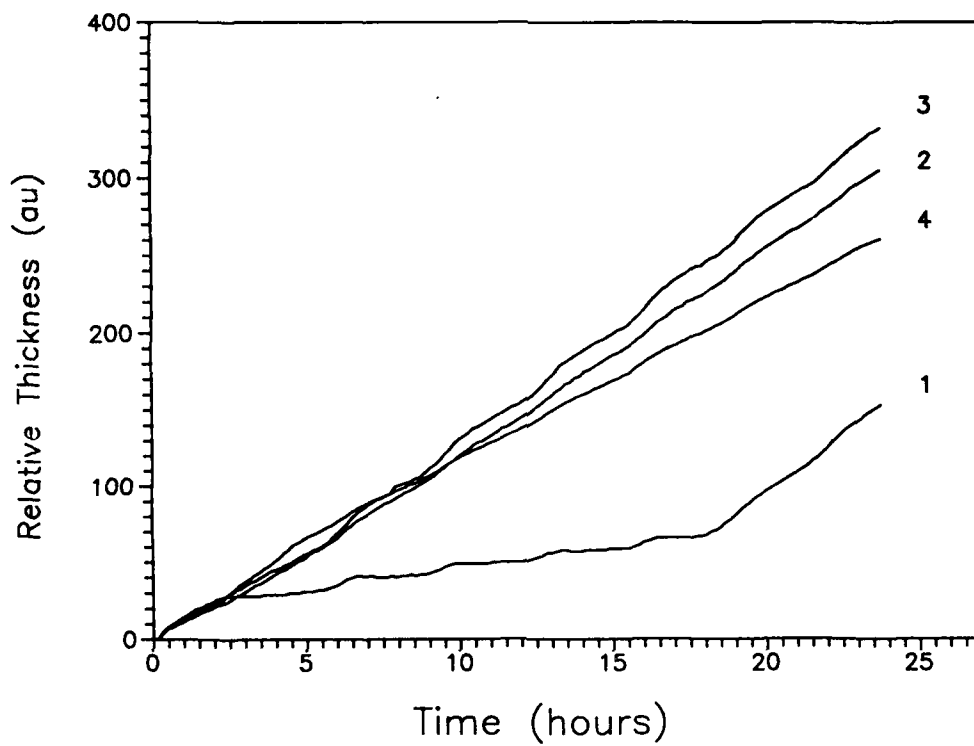


Figure 4. The relative thickness of copper electrodes on quartz crystals exposed to a corrosive atmosphere.

How to Formulate Corrosion Knowledge for Expert Systems

Tero Hakkarainen

VTT (Technical Research Centre of Finland)

P.O. Box 100

SF-02151 ESPOO, Finland

Tuulikki Hakkarainen

FINNCORR

P.O. Box 383

SF-02151 ESPOO, Finland

Abstract

Various possibilities of presenting, formulating and modeling corrosion knowledge to form a basis for expert systems are described and discussed. The main emphasis is put on semi-empirical models to completely cover the effects of all reasonable combinations of the variables considered. Also, various factors to be taken into account in the displays (queries, conclusions or information) presented to the users of the systems are discussed. The corrosion systems considered include stainless steels in aqueous solutions, various bimetallic combinations in contact with aqueous solutions and atmospheric exposure of metals and coatings.

Key terms: Expert system, corrosion, modeling.

Introduction

It is a common belief that to be useful expert systems on corrosion related problems must have access to large data bases containing reliably documented corrosion data. This is, however, not correct. For practical purposes, the information required from experts — or expert systems — is not data points from corrosion tables, but a somehow quantified indication whether harmful attack can be expected in a given application.

The corrosion resistance of a metal or alloy is not a simple material property that could be expressed as a single figure. Corrosion tables or equivalent data bases usually contain a limited number of data points for strictly defined environmental conditions. Data points corresponding to different values of a variable can be used to make conclusions applicable to a range of values for that variable.

For practical problems, however, factors not covered or not quantitatively treated by the data source may play a decisive role. A reliable estimation of the effects of such factors requires expertise in the field, i.e. a corrosion expert. The expert will make his or her decision on the basis of his experience, and possibly intuition, in a way that the result is consistent with the data available. This will result, hopefully, in a quantified estimate whether the solution under consideration is acceptable. A real expert should be able to give a useful answer for any relevant combination of the affecting variables, not only those found in databases or other comparable sources.

The expectations put on expert systems on corrosion are often unrealistic. e.g. quantitative estimates for corrosion rates or lifetimes. Truly quantitative dependencies are available for special cases only — and are normally not even needed. This is especially true for the localized modes of corrosion.

In estimating the possibility of corrosion attack, the information wanted usually is a "probability" of harmful attack to occur. In material selection problems, the question is whether a material will be "acceptable" for a given application. Also, a quantitative comparison of various alternatives may be desired. This may be accomplished by evaluating aspects of the "suitability" of the materials for the application and providing each material with a final "score", a number that can be used for comparison.

Some of the principles presented in this paper have been applied in expert system modules described in previous papers¹⁻⁴.

Corrosion Probabilities

Use of Transition Zones

When presenting corrosion related data, categories or regions with sharp boundaries are often used to characterize the effects of individual variables. This approach has its merits in presenting data in a compact form, like tables or figures. On the other hand, there is a disadvantage of having discontinuities at the border lines. This may lead to a critical difference in the results for combinations of variables close to each other, but separated by the border line.

If a solution is sought for a fixed combination of the values of the affecting factors, there may be no need to simultaneously see the solutions for other combinations. A single number or some other appropriate expression is all that is needed. This allows the use of calculations or approximations that result in continuous changes in the values of the property under consideration, rather than in categories with discontinuities at their boundaries.

Calculations resulting in continuous transition zones from "acceptable" to "unacceptable" solutions can easily be included in expert systems. Most corrosion experts probably apply the concept of such transition zones when making their recommendations — possibly without realizing it themselves and presumably without having fixed models for the calculations.

The main obstacle in trying to quantify the combined effect of individual variables and using transition zones is simply the lack of reliable documented data. A formulation of adequate models for calculation is a real challenge for a corrosion specialist. It requires a deep insight into the effects of various factors and a capability of identifying their relative significance. In most cases no absolute laws need to be determined, satisfactory empirical relations over limited ranges of values are sufficient.

Pitting of Stainless Steels

For chloride induced pitting of stainless steels, the basic variables are the chloride content of the solution and the temperature. When the temperature is increased, the minimum ("critical") chloride content required for pitting decreases. There may also exist a minimum temperature below which a given steel will not pit at any chloride concentration. Both the critical chloride content at a given temperature and the minimum temperature for pitting depend on the composition of the steel.

For a given steel, the critical chloride content for pitting at a given temperature may further depend on various factors, such as the presence or absence of oxidizing agents, the presence and amount of anions other than chloride, the pH of the solution, the flow rate of the solution, the possibility of formation of deposits on the steel surface, and the pretreatment of the steel surface.

In the following, an example is given how the effects of the various factors may be treated in a compact and systematic way. The default state may be chosen to be a neutral stagnant solution, with no other anions than chloride, dissolved oxygen as the sole oxidizing agent, and no deposits on the surface.

To start with, a simple equation relating the critical chloride content to the temperature could be a hyperbola

$$T = \frac{a}{C} + d \quad (1)$$

where T is the temperature, C is the chloride content, and a and d are constants. This equation fulfills the basic requirements: the temperature increases sharply when the chloride content approaches zero, and the chloride content increases sharply when the temperature decreases towards the value d . The shape of the curve may be adjusted more freely if a few more parameters are added:

$$T = \frac{a}{(C - b)^n} - k \cdot (C - b)^m + d \quad (2)$$

The constant b shifts the curve "horizontally" without changing its shape, the constant k allows a decrease of temperature below value d at increasing values of C , the constant n adjusts the "sharpness of bending" of the curve and the constant m determines its shape at high values of C .

Keeping in mind that the equation is used over limited ranges of T and C only, almost any reasonable empirical or deduced dependence between the critical chloride content and the temperature can be approximated, Figure 1. The values of the parameters a , b , k , d , n and m are specific for each steel and can be stored in a data base to be used for calculations by the expert system.

In the expert system, one may prefer to work with critical chloride contents at given temperatures. Even if the value of C at a given T is not easily solved in a closed form from equations like Equation (2), in an expert system it may be no problem to add an iterative loop to perform the calculation.

To include the effects of the other factors, the value of the critical chloride content " CI " calculated from Equation (2) can be modified to an "effective" critical chloride content CI_E in the case under consideration. The most straightforward way is to multiply or divide the value by appropriate numbers. These numbers may be or include parameters specific for each steel and may be a function of the temperature.

At this stage, a new question arises. The information for the evaluation of the values of these variables must be received from the user of the system. While the user should be able to provide values or estimates for the maximum temperature, the chloride content or the pH of the solution, it may not be reasonable to ask for numeric values for some other variables, like the oxidizing power of the environment or even the flow rate. Nevertheless, it is advisable to include a mechanism to treat also the effects of such factors on the basis of a continuous range concept. In the queries to the user, categories may still be used. For example, the flow rate may be characterized as "low", "intermediate" or "high" and the system may assign each of these a default value of the flow rate. An option may be provided to the user to give a definite value if it is known or can be estimated.

A possibility of deposit formation onto the steel surface deserves special attention. Because it involves a change of the nature of potential attack from "pitting type" to "crevice corrosion type", not only the value of the critical chloride content but also some of the parameters in Equation (2) may have to be

modified. A straightforward way to do this is to treat "underdeposit pitting" as a fully separate case from pitting on an open surface, with a complete set of parameters.

The presence of anions other than chloride in amounts of the same order as or greater than the amount of chloride ions usually tends to inhibit chloride induced pitting. One way to take this into account is to increase the calculated critical chloride content by an amount proportional to the amount of the other anions. Another way is, of course, to use for the environment an effective chloride content lower than the actual one.

Once the lower limit of the transition zone (the effective critical chloride content CIE) has been determined, a value can be assigned to the upper limit ($C2E$), e.g. by multiplying the value of the lower limit by an appropriate factor. This factor can again be different for different steels and may be made to depend on other variables, such as the temperature, the flow rate or the oxidizing power of the environment. Although the width of this type of a transition zone will be more or less arbitrary, it nevertheless can be very useful for the users of the expert system.

Within the transition range, the "probability" of corrosion increases from "negligible" to "certain", e.g. on a scale from 0 to 100. The change need not be linear. For example the following simple equation may be used to adjust its shape

$$P = \left(\frac{CE - CIE}{C2E - CIE} \right)^q \quad (3)$$

where P is the "probability number" for pitting, CE is the effective chloride content of the environment, CIE is the lower and $C2E$ is the upper limit of the transition zone and q is a constant. Some examples of curve shapes according to Equation (3) are shown in Figure 2.

The final evaluation of the "probability" of pitting will be done comparing the location of the effective chloride content of the environment to the transition zone.

Bimetallic Corrosion

To predict the "probability" of bimetallic ("galvanic") corrosion attack, a separate evaluation of the polarization behaviors of the two metals or alloys in the environment under consideration opens the possibility to include into the system various types of environments, the effects of several factors and a variety of metal combinations in a compact form. The basic question, of course, is whether the cathode is able to polarize the anode in a way that will result in enhanced possibility of attack.

First, it has to be deduced which one of the two dissimilar metals or alloys will act as the anode and which one as the cathode. This can be done by examining separately each environment or category of environments and assigning each metal or alloy an open circuit potential value in each environment. In a given environment, the anode will be the metal with the lower potential.

Next, the cathodic polarization behavior of the cathode and the anodic polarization behavior of the anode have to be characterized. Various possibilities have to be considered, Figure 3. The actual quantitative polarization curves for all relevant cases may not be available. As a first approximation, the basic types of polarization behavior may be characterized by simple descriptions like "strong uniform corrosion on anodic polarization", "passivity, no attack on anodic polarization" or "passive behavior,

pitting on anodic polarization". In this way, a limited number of categories will be obtained. Such information on each alloy and environment combination can be stored in a data base, e.g. as code numbers.

The difference between the open circuit potentials together with the characterization of the polarization behaviors serves as a basis for the judgement whether bimetallic corrosion will be expected. Additional factors to be taken into account are at least the relative areas of the anode and the cathode, but possibly also factors like the mode of wetting (continuous vs. intermittent), the presence of strong oxidizers and the flow rate of the solution.

The final result may be expressed as a "probability" of enhanced attack due to the galvanic contact of the two metals or alloys. A semi-quantitative form can be used, e.g. numbers or expressions on a scale divided into 10 categories of increasing intensity.

Suitability Numbers

Quantitative Comparison of Materials

In material selection problems, a quantitative measure for the relative performance of the candidate materials is needed. One possibility to arrive at such a quantity is to evaluate separately the suitabilities of the materials with respect to several aspects, and to combine these suitabilities to a final score for each material. In addition to corrosion resistance, factors like the ease of fabrication or a possibility to proper pretreatment procedures may easily be included. Information on cost and availability may also be added, but it has to be remembered that such information may become outdated much sooner than the purely technical aspects.

A practically continuous scale will be applied if the individual suitabilities are assigned a number from 0 to 100, and these are multiplied like probabilities: each number less than full 100 will decrease the result to a corresponding percentage. A suitability number value of 0 will cause the rejection of the material, regardless of the other values. A minimum value can be set for the final score for a material to be considered acceptable.

Material Selection for Atmospheric Exposure

When evaluating the corrosion resistance of a specific material in a specific atmospheric exposure, several interacting factors have to be considered, Figure 4. The admissible maximum service temperature (or a transition zone) may be higher for a dry surface than for a wet one. A water film on the surface is usually a prerequisite for any significant corrosion attack. The intensity of this attack is likely to increase with temperature within a temperature range where the temperature by itself would not put restrictions. Air impurities, e.g. sulphur dioxide or chloride, are normally expected to be harmful only when the surface is "wet". Also their effect is expected to increase when the temperature increases, and they may promote wetting of surfaces that would otherwise remain "dry".

The characterization of the "effective wetness" of the surface is a crucial element when evaluating the possibility of the environmental factors to cause harmful corrosion attack. A "time of wetness", expressed as a percentage of the total exposure time, could be a useful criterion if it can be estimated. In outdoor exposure with definite wetting periods through precipitation or condensation, this may be the

case. In indoor exposure, however, where occasional wetting may be possible e.g. through condensation or splashing, a "probability of wetting" or a "wetness number" may be more easily applied.

An estimate for the "effective" critical relative humidity can serve as a starting point. This value can then be modified, if necessary, to take into account a possible wetting of the surface due to external reasons. When evaluating the suitability number with respect to a specific variable, e.g. the sulfur dioxide content of the atmosphere, critical values of this "wetness number", between which the surface is considered to turn from "dry" to "wet", can be assigned each material. This approach enables the use of different criteria for surface wetting for the evaluation of the effects of the various variables. The transition may be made non-linear, e.g. using formulas like Equation (3). At a given effective wetness number of the environment, the suitability starts to decrease, again possibly in a non-linear way, as soon as the value of the environmental variable, e.g. sulfur dioxide content, exceeds a critical value. The suitability value may be made to remain on a non-zero level after the change is complete, Figure 5. The critical wetness numbers, the critical variable values, and the final suitability levels can, of course, be made temperature dependent.

The suitability of a specific material or coating for use under given environmental conditions can be evaluated separately with respect to the various variables, the effects of which are then combined. The information needed from the user of the expert system is the temperature, information necessary to deduce the effective wetness number for the environment, and estimates on the impurity levels in the atmosphere or in a solution that may form on the surface. For the suitability number with respect to the temperature, the transition zone may be dependent on the wetness number. For the effect of wetness (or humidity), the eventual transition zone may depend on the temperature. For sulfur dioxide, the transition zone depends on both the wetness number and the temperature. The effects of chloride and pH are expected to require the exceeding of critical wetness number values that may differ from each other and from that for e.g. sulfur dioxide. Again, all parameters needed in the calculations can be made specific to each material or coating and stored in a database.

Displays

The knowledge formulation bears a close relation to the presentation of knowledge on the screen. For example, the information used in calculations and the resulting criteria are normally readily available for presentation on the screen.

Care must be taken not to use similar expressions to describe alternative items on the same menu. The most common choice first on the menu (a "default" choice) may facilitate the use of the system. When the user is prompted to enter values of numerical variables, it may be helpful to indicate the permitted range. In some cases it may be advisable to provide default values for the user that can be either accepted or altered.

Although the layout of the displays to be seen on the screen is not a direct part of the knowledge formulation, some basic aspects may be emphasized also in this connection. For the user, the appearance of the displays can be even more important than the actual technical content of the system.

It is recommended to divide the screen in horizontal sections only, using the entire screen area. The natural direction of reading is from left to right, from up to down. If red and green are used on the same screen a possible red-green deficiency of the users should be taken into account. Colors always have an effect on each other, combinations of very strong colors can make the eyes tired. Complementary colors tend to produce afterimages.

Different types of displays (queries, explanatory information, intermediate conclusions, final conclusions) should be easy to recognize. The user should always be aware of the context the display belongs to. On equal displays, same type of information should be placed on the same location, a display of several pages (screens) may need page numbers. Necessary instructions of how to proceed or how to exit the session or the system should always be available on the screen. The information presented to the user should be restricted to the relevant. Additional information or explanations can be made available on request. The recommended maximum number of options on a menu is seven. Displays either too complicated or too simple may be equally frustrating for the user.

Conclusions

Through the inclusion of calculations, models and empirical dependencies into the mechanisms of reasoning when solving corrosion related problems, expert system technology offers a possibility to use the full competence of human corrosion experts.

By applying simple mathematical expressions, the corrosion knowledge of a human expert can be formulated to cover all relevant aspects or combinations of variables to obtain a quantified indication of e.g. the possibility of harmful corrosion attack or the relative suitabilities of various materials in a given application.

A feature common to the examples described is that the "knowledge" stored in the expert system is not "normal" corrosion data to be found in various corrosion tables or data bases, but mathematical formulas and parameters that allow the full spectrum of the expertise of the developer(s) of the system to be used.

References

1. T. Hakkarainen, L. I. Carpen, R.-L. T. Hakkarainen, "Microcomputer as Corrosion Expert - an Approach by Corrosion Specialists", CORROSION/88, paper no. 126, (Houston, TX: NACE 1988).
2. Tero Hakkarainen, Leena Carpen, Tuulikki Hakkarainen, "The Microcomputer as a Corrosion Expert", in "Corrosion Prevention in the Process Industries" (R.N. Parkins, Ed.), Proceedings of the First NACE International Symposium, November 8-11, 1988, Amsterdam, The Netherlands, (Houston, TX: National Association of Corrosion Engineers, 1990), p. 349.
3. T. J. Hakkarainen, P.J. Tunturi, R.-L. T. Hakkarainen, "Small Scale Expert Systems Relating to Corrosion Problems", CORROSION/90, paper no. 333, (Houston, TX: NACE, 1990).
4. T.J. Hakkarainen, L. I. Carpen, "Expert Systems on Corrosion - Experiences and Practical Aspects", CORROSION/92, paper no. 262, (Houston, TX: NACE 1992).

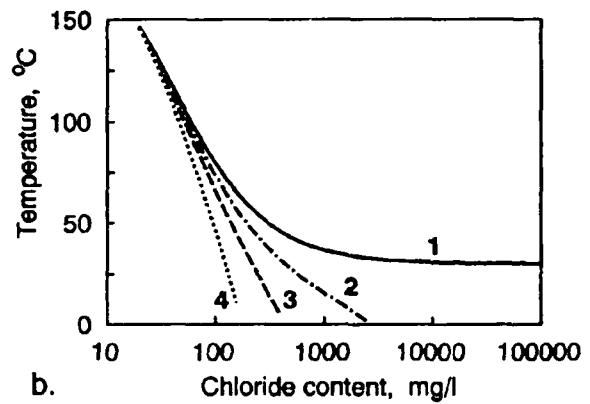
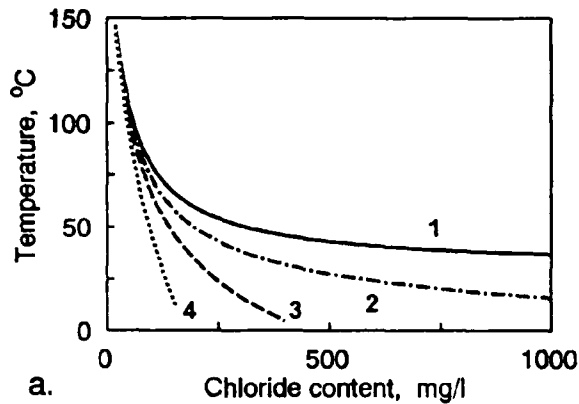


Figure 1. Examples of dependencies according to Equation (2) in linear (a) and semilogarithmic (b) presentation
 Curve 1: $a = 7\,000$, $b = -40$, $k = 10^{-6}$, $d = 30$, $n = 1.0$, $m = 1.0$
 Curve 2: $a = 6\,000$, $b = -40$, $k = 0.2$, $d = 20$, $n = 0.94$, $m = 0.60$
 Curve 3: $a = 4\,000$, $b = -40$, $k = 0.2$, $d = 0$, $n = 0.70$, $m = 0.80$
 Curve 4: $a = 3\,000$, $b = -40$, $k = 0.5$, $d = -5$, $n = 0.80$, $m = 0.90$

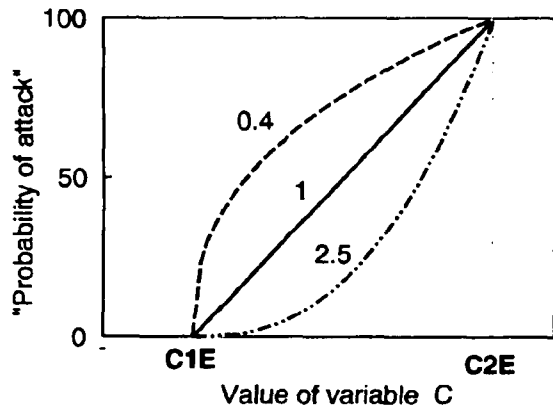


Figure 2. Examples of changes of probability in the transition zone according to Equation (3). The values of the parameter q are shown in the figure.

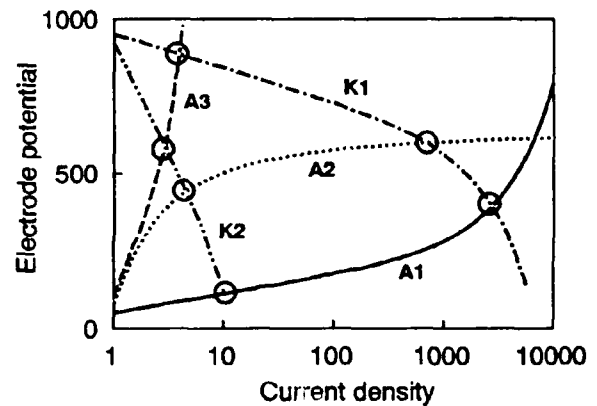


Figure 3. Examples of polarization behaviors of the anode and the cathode in bimetallic corrosion. A1: uniform corrosion, A2: pitting, A3: passivity, K1: strong cathodic reaction, K2: weak cathodic reaction.

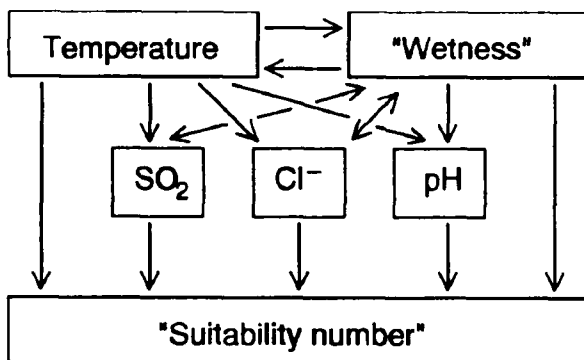


Figure 4. Interaction of variables affecting the performance of materials in atmospheric exposure.

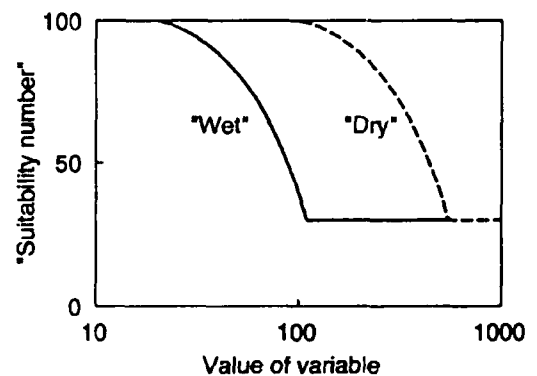


Figure 5. Example of transition zone for a suitability number, e.g. the effect of sulfur dioxide.

Transforming Computerized Information for its Integration into a Hyper Tutorial Environment

P.R. Roberge
Department of Chemistry and Chemical Engineering
Royal Military College
Kingston, Ontario
Canada, K7K 5L0

Abstract

The increasing availability of computerized information is making the topic of software accessibility and portability also increasingly important. While it has become possible to consult either shallow or very deep information systems at the touch of a few buttons, it remains difficult to move horizontally between these systems without going through series of menus and introductory screens. In the present paper, the general requirements for mainstream software portability were used as a model to establish the ideal format specialized software packages should possess for their seamless integration into a hyper tutorial environment. The architecture of the global system was designed to match an undergraduate course in corrosion engineering which would include an introduction to information processing of specialized data.

Most of the open ended programming environments which were evaluated for this task were found to be adequate for building friendly and universal user interfaces. The final choice of an ideal environment is still an unanswered question since the software linking standards are still being debated. Additionally the requirements for corrosion related information systems were evaluated for both their portability and their pertinence to such project.

Key terms: information processing, training, corrosion prevention, computer applications

Introduction

Societal aspect of corrosion damages

While the costs attributed to corrosion damages of all kinds (Table 1) have been estimated to be of the order of 4.2 % of North American gross national product (GNP), the responsibilities associated with these corrosion problems are sometimes quite diffuse. Major corporations, industries and government agencies have established groups and committees to look after corrosion related issues but in many cases the responsibilities are spread between the manufacturers or producers of systems and their users. Such a situation can easily breed negligence or ignorance which can be quite costly in terms of dollars and human lives.

A recent example of corrosion damages with shared responsibilities is the sewer explosion that killed over 200 people in Guadalajara¹, Mexico, in April 1992. Besides the fatalities, the series of blasts damaged 1,600 buildings and injured 1,500 people. Damage costs were estimated at \$75 millions. The sewer explosions have been traced to the installation of a water pipe by a contractor several years ago. The pipe was installed directly over a pipe line that corroded and leaked gasoline into the sewers. The Mexican attorney sought negligent homicide charges against four officials of Pemex, the government-owned oil company. Also cited were three representatives of the regional sewer system and the city's mayor.

Training and information processing as a solution to corrosion problems

Many universities offer an optional undergraduate course in corrosion engineering. Such a course is often offered by Metallurgical Engineering departments. Some universities also offer a graduate program in corrosion science and/or engineering. An excellent example of such a program is offered at the University of Manchester Institute of Science and Technology (UMIST) in the U.K., where more than 50 graduate students from many countries are enlisted and trained in all aspects of corrosion research and practices. But around the world, organizations and industries will always require a personnel trained in specific technical procedures for either inspecting for corrosion or for applying specific treatments to prevent corrosion.

The present worldwide wealth of information concerning corrosion problems and associated remedies is often invisible and difficult to access. Two types of intelligent information management technologies have recently gained the general confidence of both developers and users of these technologies and reached the main stream of computer goods. But these two technologies, database management systems (DBMSs) and expert systems (ESs), have had little interaction with each other. It is clear, however, that future decision-support systems will require both the problem-solving capabilities of ESs and the data-handling capabilities of DBMSs. A third technology, based on linking applications through icons and mouse actions, shows great promise as an information management tool since it can be used for consulting large amounts of varied information without having to digest series of menus and pages of reading material. The flexibility of hypertext and Windows™ environments allows materials engineers not only to consult built-in materials information, but also to access in an intuitive manner external databases, numerical programs or even ESs.

Graphical User Interface (GUI) Environments

Non linear writing and reading

During the early days of the telephone only a few people could afford the technology and only highly trained operators were qualified to operate the telephone. As telephone became an accepted part of life its proliferation forced the telephone industry to seek simpler and less operator intensive schemes. Eventually direct dialing became easy to use and openly available. Nowadays everyone has become an operator.

Similarly the portable computer has become an essential commodity among many other information processing goods and the computer industry has evolved from a very elitist market to a broad based general public market. As the proliferation of computers continues, the technologies that make computers more intuitive and easier to operate are being developed and new standards of graphical and manual interactions between computers and humans are set. GUIs such as Microsoft Windows™ are making the computer acceptable to a broader public and just as direct dialing allowed the general public to become its own operators, GUIs are now allowing the general public to become computer operators².

While the term hypertext was coined by Ted Nelson during the 1960s³, the concept itself can be traced back to Vannevar Bush's 1945 description of 'the memex'⁴. The first serious attempt to build a memex did not take place until 20 years after Bush's description. In 1968, Doug Engelbart, then at the Augmented Human Intellect Research Center (Stanford Research Institute), conducted a dramatic live demonstration of his Augment system during the Fall Joint Computer Conference where he worked collaboratively on a hypertext document with a colleague 500 miles

away⁵. Engelbart's system was centered on consoles which were sophisticated by the standards of these days. The consoles included television images and a variety of input devices such as Engelbart's best known invention, the mouse.

In the following years both interest and activity in hypertext have grown steadily. Some of the more important milestones have been described in the introductory paper of a special issue of Communications of the ACM⁶ which was devoted to hypertext as a form of electronic documentation or information management. An excellent survey of existing hypertext systems with a critical review of their strengths and weaknesses was published in 1987⁷. In this article the operational advantages of hypertext were described to be the following:

- ease of tracing references
- ease of creating new references
- hierarchical or non-hierarchical information structuring
- global and local views can be mixed effectively
- multiple functions customized documents
- modularity and consistency of information
- task staking

There are many ways in which associative linking or non-linear writing and reading can be used. Today hypertext links can be found in on-line help systems in a great variety of systems such as Microsoft WindowsTM, personal information managers, text retrieval systems, ESs and application generators.

Tools examined

Hypermedia development tools. Hypertext documents are highly interactive and can automatically take the user to the exact information requested regardless of the format or application. Two of eight hypertext development packages reviewed in a popular personal computer magazine⁸ were tested for their pertinence to the present project. The first system, HyperWriterTM from Ntergaid, was this magazine Editor's choice. It was said to have nearly every type of link available, from various kinds of text links to graphics, video and digitized sounds. This system was also described to be extremely attractive for its support of runtime versions, both for their price (free) and their navigational tools i.e. the ability to call a graphics map of links in the document, see a reading history, tag files and leave bookmarks.

The second hypertext development system tested, GuideTM by OWL International, was said to come close to the first in its functional richness. This Windows application was believed to have superior formatting capabilities and a very good control over graphics. It also had the advantage of being nested in Windows, which meant easy navigation between this software and other available Windows application packages.

Event and object oriented programming. Over the years software developers and researchers have used many different languages to come up with a better way of modeling real-world problems. Because these problems can be quite complex it helps to have methods for reducing the complexity of representing both data and the operations that can be used to process the data. This is what can be achieved best with object-oriented programming (OOP). OOP has been getting much attention lately. In fact, many programming language experts feel that in the 1990s OOP is going to have an impact similar to structured programming in the 1970s⁹.

The first environment evaluated for the construction of the tutorial system was the new edition of Borland's C++. With Borland C++ 3.1 it is possible to develop Windows 3.1 applications and benefit from the massive development effort behind such a mainstream tool. One of the best new features of Windows 3.1 is object linking and embedding (OLE) which allows the data from one application to be accessed directly by other applications. The second programming environment examined does not technically belong to the category of OOP software. Visual Basic™ 2.0 by Microsoft has been defined more correctly as an event oriented programming environment. Object orientation fundamentally implies that program methods can be created in full integration with the method by which the data will be addressed and utilized. But while Visual Basic cannot be classified as OOP, it really provides an environment which allows programming directly with objects and GUIs.

Processing Corrosion Information

Multidisciplinary nature of corrosion science and engineering

While the chemical reactions which occur on metals exposed to engineering environments have provided fascinating problems in physics, physical chemistry and even applied mathematics, the training for corrosion prevention is really focused on engineering systems and the environments in which they must function. The training of corrosion engineers and technicians should in principle be guided by the general requirements of increasing functionality of systems. But in practice each training program is inevitably colored by the familiarity of the instructor with a specific aspect of corrosion problems. In this perspective, the multidisciplinary nature of corrosion science and engineering is a serious challenge that is ideally met by employing a team of instructors. In many cases this is simply not possible. The following list of disciplines and their specific fields of applications in corrosion science and engineering summarizes the complexity of such a topic:

- Chemistry: organic coatings, water chemistry, inhibitors
- Electrochemistry: measurement techniques, fundamental processes
- Management: cost analysis, maintenance, liability & risk analysis, inspection scheduling
- Mechanical engineering: structural integrity, failure mechanisms
- Metallurgy: materials performance, selection and fabrication of materials
- Solid state physics: hot corrosion, inorganic coatings
- Surface science: surface modifications: laser, ion bombardment, microscopic techniques

In real life situations the multi domain expertise required to perform a simple task of cost and risk evaluation for specific corrosion prevention schemes is a good illustration of the need to cover all basic disciplines to a functional level in any good training program.

Multi linkage properties of hypermedia environments

Through the mouse and menu-based interface provided by the hypermedia systems, users can request diverse types of information coming from various sources, have a look at the information presented on the screen and quickly reach decisions concerning the progress of their queries. A hypermedia system can be built into an ultimate toolbox for software tools since it is potentially a unifying paradigm for areas of software application diversity. Some of the most famous expert systems (ESs) have not gone beyond the development stage because they could not be timely integrated in the workplace, they could not communicate smoothly with users. One of the main challenges faced by designers of such systems is the development of high grade user interfaces. Wide acceptance and use of any computer program presuppose a good interface and the task is not

necessarily easy. It is common knowledge amidst workers in the field¹⁰ that designing a good interface can consume up to one half of a project's development time. A few general observations have been made on which to base design requirements for user interfaces¹¹:

- No single interface can satisfy all categories of users, nor can it meet all the needs of a single user over time
- Any interface should be amenable to custom-tailoring by the end user
- Interfaces should be easy to understand and designed to avoid information overload
- An interface should be transparent and never leave the user in the dark

The hypertext technology is ideally suited to accomplish these demanding goals and facilitate the design of intuitive user interfaces for decision-support systems¹¹. While ESs are designed to solve specific problems, hypertext systems are built to convey information. These two objectives are flip sides of the same coin. Some of the inefficiencies of ESs can be overcome by integrating the features of hypertext and some of the weaknesses in hypertext systems can be overcome by using ESs.

Multi linkage properties of event and object programming environments

The high-level nature of objects provides numerous benefits. By combining procedures and data into objects the level of abstraction of programming tools can be greatly improved. Hidden inside each object are the methods and data structures needed to manipulate and process the object. The outside world talks to these objects by sending them what are commonly called messages. But the real power of objects is in the way they can be used to define other objects, a process called inheritance. Programmed objects have the following features⁹, they:

- are grouped into types called classes
- have internal data that define their current state
- support data hiding
- can inherit properties from other objects
- can communicate with other objects by passing messages

The object-oriented approach to programming is also based on the concepts of encapsulation and extensibility. OOP encapsulates in objects some data and programs to operate on the data. The notion of encapsulation has proven to be a natural and easy paradigm for various application environments such as GUIs. The extensibility concept refers to the ability to extend an existing system without introducing changes to it. OOP offers extensibility in two ways¹³: behavior extension and inheritance. The behavior of an object may be extended by simply including additional programs into it. The inheritance extension, on the other hand, allows the behavior and even the attributes of an object to be reused in the definition of more specialized objects.

Hyper Tutorial Systems

Three different development projects will serve to illustrate the hyper tutorial approach to training and information processing for corrosion control and prevention.

Failure Predictor

The development of an empirical model¹⁵ to evaluate the susceptibility of high strength aluminum alloys to SCC started as a master in engineering thesis project¹⁶. The first prototype was developed with an open ended approach (Fig. 1) to programming which included the usage of the HyperWriter™ system. In problems encountered in day to day failure analysis, incomplete

knowledge is common. This is not a major problem in itself since humans can function with this type of uncertainty. Human experts tend to make generalizations drawn from past experience and make predictions that cannot be absolutely confirmed by available evidences. Normal computational programs can not deal easily with this kind of uncertainty. They deal in straight forward calculations from known data to known conclusions using algorithms. In order to deal with uncertainty, probabilistic reasoning methods have been developed to allow ESs, for example, to incorporate incomplete data.

The measure of intensity of SCC was evaluated with an inverse probability theorem popularized by the 18th Century British Clergyman and mathematician, Thomas Bayes. This theorem is based on exact knowledge of the probabilities involved. But often the information can be more easily expressed as empirically derived rules or personal experiences that subjectively link effects to causes for given conditions. This type of probability is termed 'degree of belief'¹⁶ as it represents an estimate of the truth but is not itself verifiable.

The hypertext environments investigated¹⁷ all suffered from poor connectivity with the traditional algorithms that were required to perform various calculations. While such an environment simplified the construction of the user interface or the front end of the system, its maintenance was also complicated greatly by the need to switch between different environments. The structure and organization of the C++ OOP environment has thus since then been adopted to translate the scientific and practical knowledge of SCC intensity of metals. The concepts of encapsulation, abstraction, inheritance and polymorphism that describe the OOP environment will be used to describe the factors (Fig. 2) of SCC intensity. An example of transforming such knowledge of SCC intensity will be made with the information available, on high strength aluminum alloys, and which was organized during the development of the first prototype.

Coating Selector

Putting a barrier between a corrosive environment and the material to be protected is a fundamental method of corrosion control. It is, in fact, the most widely used method of protecting steel and other metals. The concept of adding coatings to surfaces is so ancient that its beginnings are lost in the mists of history. A common reason why protective coatings do not perform well is often because they have not been considered as systems. Most successful coating engineers approach a coatings project in much the same way that they approach any other engineering problem, beginning with the design of surfaces to be protected and ending with schedules for monitoring the completed work.

A global representation of the features which could be included in this hyper tutorial system is presented in Fig. 3. The generic information on coatings which are used for this prototype have been extracted from a well established document¹⁸. The system makes full use of the programming easiness provided for this kind of projects by Guide and the Windows environment. Tables have been constructed using the Excel™ database system which communicate to the hypertext environment through transparent Dynamic Data Exchange (DDE) links. The coatings tutorial is also linked to a fully operative commercial ES specialized in the selection of coatings (Coating Counsel™ by Counselware Inc.¹⁹). Coating Counsel is designed to select optimal coating systems for industrial maintenance applications. It can write complete Construction Specification Institute format specifications in a matter of minutes.

The hyper tutorial was constructed as a demonstration prototype with limited time and effort. The progress with commercial software since the prototype was developed (eighteen months ago), has

made its front end look archaic. This experience permitted to highlight the importance of defining the knowledge sources at the onset of a project and preserving the information gathered at that level in an easily maintained system such as a commercial database. While the front end looks archaic it still can be replaced quite easily if it is not too seriously glued to the information itself.

Aircraft Structural Information Services (ASIS)

The initial deliverable for this project is envisioned to be a working prototype that will have full capabilities with respect to data collection and production of reports. The ASIS project will deliver a system to store aircraft structural information in a database and have this database integrated and linked to the information system presently in usage. This structure will allow the capture of information through standard paper based corrosion reporting graphical forms and other electronic forms already used for structural information.

Additionally, the system will allow analysis of structural information in standard tabular or graphical formats plus digitized representations of damage mapping through grid cards for example. It is believed that ASIS will have a major impact on the Canadian Forces community. The ASIS working prototype is being constructed in Windows with Microsoft Visual Basic and its Professional Toolkit. The full development of ASIS should follow the successful demonstration of the capabilities of the prototype.

Conclusion

The ability to use words effectively in order to convey ideas and requests is one of the most important assets of modern society. The transition of the developed countries to the 'Information Society' has fueled a tremendous increase in the accumulated body of information. Hypermedia is a relatively new paradigm that forms the foundation of an effective training system and can enhance the rapidity of knowledge transfer processes.

While it is possible to construct systems with available hypertext development software systems, the connectivity to other computational tools commonly used in engineering creates a problem that could easily degenerate into maintainability problems. The rapid progress of Windows oriented software such as the new version of Borland C++ and Microsoft Visual Basic has rendered the use of prebuilt ES shells and hypertext environments somewhat obsolete. The excellent connectivity between Windows applications and high reliability of the environment itself have made multi linkage projects quite appealing even when resources are limited.

References

1. Materials Performance, 31 6 (1992): p. 10.
2. J. McCord, Windows Programmer's Guide to Borland C++ Tools, (SAMS Publishing, Carmel, IN, USA, 1992), p. xviii.
3. T.H. Nelson, "Getting it out of our systems," in Information Retrieval: A Critical Review, G. Schechter Ed., (Thompson Books, Washington, DC, 1967), p. 191.
4. V. Bush, "As we may think," Atlantic Monthly, 176 1 (July 1945): p. 101.
5. D.C. Engelbart and W.K. English, "A Research center for augmenting human intellect," in Proceedings of the 1968 Fall Joint Computer Conference, (Montvale, NJ, AFIPS Press, Fall 1968), p. 395.
6. J.B Smith and S.F. Weiss, "Hypertext," Communications of the ACM, 31 7 (1988): p. 816.
7. J. Conklin, "Hypertext: An introduction and survey," IEEE Computer, 2 9 (Sept 1987): p. 17.
8. H. Fersko-Weiss, "3D Reading with the Hypertext Edge," PC Magazine, May 28 (1991): p. 241.

9. K. Weiskamp and B. Flamig, *The Complete C++ Primer*. (Academic Press, N.Y., U.S.A., 1990), p. 28.
10. D.G. Bobrow, S. Mittal, S. and M.J. Stefilk, *Communications of the ACM*, 29 9 (1986): p. 880..
11. T. Barsalou, R. M. Chavez and G. Wiederhold, "Hypertext interfaces for decision-support systems: A case study," *Medinfo 89*, Proceedings of the sixth Conference on Medical Information, 1989, 126-130.
12. H.C. Arents, W.F.L. Bogaerts and A.S. Jovanovic, "Hypermedia Systems as Tools for Corrosion Analysis and Remaining Lifetime Assessment", *Life Prediction of Corrodible Structures*, Parkins, Ed., (National Association of Corrosion Engineers, Houston, TX, USA, 1992).
13. W. Kim, *Introduction to Object-Oriented Databases*, (The MIT Press, 1990), p. 9.
14. G.D. Bryson and P.R. Roberge, "Development of an empirical model for the Evaluation of Susceptibility to SCC" *Materials Performance: Sulphur and Energy*, (Canadian Institute of Metallurgy, Montreal, QC, 1992), p.247.
15. G.D. Bryson, "Material Analyst: an Expert System for the prediction of Material Maintenance" Master thesis, Royal Military College of Canada, Kingston, ON, 1992.
16. S.L. Tanimoto, *Elements of Artificial Intelligence - An Introduction Using LISP*. (Computer Science Press, Maryland, 1987), p 240.
17. P.R. Roberge, "The Hypermedia Technology as a Front End to Knowledge Processing Systems" Proceedings of the Fourth Symposium/Workshop on Applications of Expert Systems in DND, (Royal Military College of Canada, ON, 1992), p. 153.
18. C. G. Munger, *Corrosion Prevention by Protective Coatings*, (National Association of Corrosion Engineers, Houston, Texas, 1984).
19. S. Murray, "Coating Counsel: Automated Preparation of Painting Systems Specifications," *Counselware*, Montreal, Quebec, 1991.
20. *Economic Effects of Metallic Corrosion in the United States*, a report to the Congress by the National Bureau of Standards (NBS), U.S. Dept. Commerce, March 1978.

Table 1 Costs attributed to corrosion damages for North America in 1993^a.

| Category | Cost (B \$) | Avoidable^b (B \$) | Avoidable^b (% cost) |
|-------------------------------|------------------------|-----------------------------------------|-------------------------------------------|
| Energy industries | 184 | 3.8 | 2.1 |
| Electric utilities | 18.2 | 0.6 | 3.3 |
| Manufacturing industries | 38 | 1.1 | 2.9 |
| Infrastructures & governments | 49 | 12 | 24 |
| Private automobiles | 44 | 29 | 65 |
| Total | 333 | 46.5 | 14 |

^a adapted from²⁰.

^b avoidable by applying known prevention and control methods.

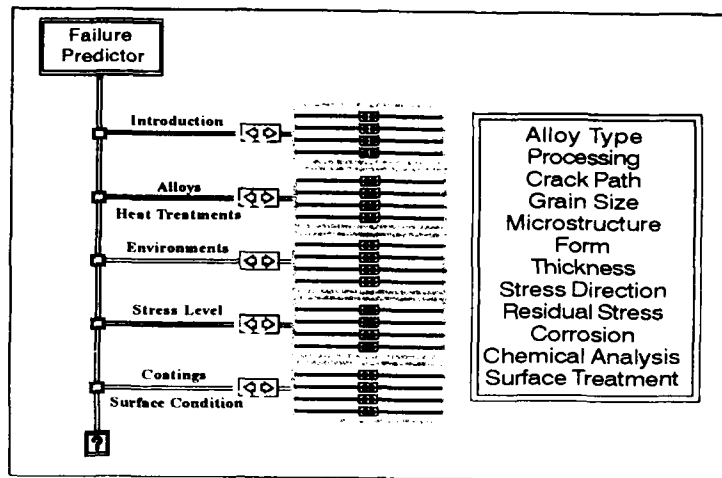


Fig. 1 General structure of Failure Predictor with links to main components of the KB.

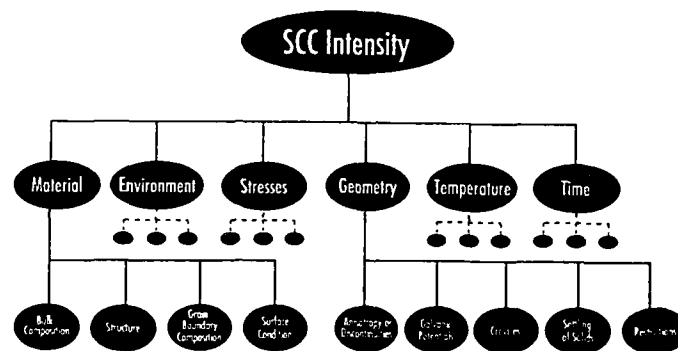


Fig. 2 Factors governing the SCC intensity of aluminum alloys.

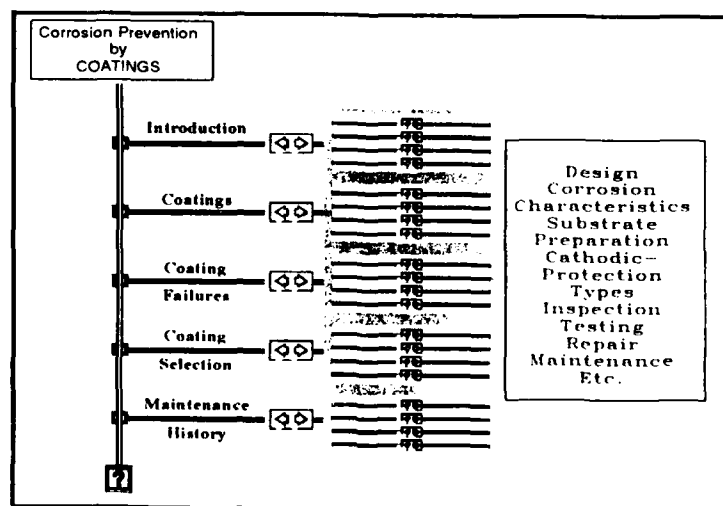


Fig. 3 General structure of Coating Instructor with links to main components of the KB.

Integrated Diagnostic System for Intelligent Processing of Field Inspection Data of Transmission Line Structures

Peter Mayer
Ontario Hydro Research Division
800 Kipling Avenue
Toronto, Ontario
Canada
M8Z 5S4

Stephen Moraes
Ontario Hydro Research Division
800 Kipling Avenue
Toronto, Ontario
Canada
M8Z 5S4

Abstract

Data obtained during the inspection of equipment is a vital source of information which is used by plant personnel to ensure safe, reliable and efficient operation. Processing of the data to yield information for routine decision making is a tedious, repetitive and time-consuming task. In spite of its nature, this task requires attention of an experienced expert to ensure efficient and effective application of existing knowledge.

Utilization of artificial intelligence technology can free the experts from this type of repetitive work and allow them to concentrate on the mitigation of non-routine equipment problems and the development of advanced knowledge.

In this work, an integrated system was developed to automate the process of routine decision making for maintenance of equipment. The system was successfully used to process data gathered during an inspection of electric power transmission superstructures to assess the extent of corrosion attack and make recommendations how to restore these to ensure their long-term, structural integrity. The details of the system and its implementation process will be discussed in detail.

Key terms: data acquisition, expert system, intelligent processing, integrated diagnostic system

1. Introduction

In recent years, the emphasis of the plant operators is on predictive/preventative maintenance to ensure reliable and safe operation. Breakdown maintenance is quickly becoming a thing of the past.

Ontario Hydro has approximately 45,000 galvanized steel (and coated steel pole) transmission line structures in the power system. The continued integrity of these structures is of critical importance to the reliability and safety of low cost electricity supply in Ontario. It will be an enormous task to maintain the performance of these structures over the next decade and beyond the year 2000. To minimize the impact of this effort on the resources of the Corporation, it is necessary to adopt a method of approach which balances both, short and long term costs of reliability and safety. A crucial element of this approach is a consistent application of the best available technological know-how on a corporation-wide basis. The purpose of the work described in this report is to increase the efficiency and effectiveness of this process resulting in significantly lower cost and overwhelmingly improved quality.

Due to the complexity of the task of maintaining transmission lines in a reliable and safe operating condition, the only way to achieve consistent application of up-to-date technological know-how is through the use of modern computer-based artificial intelligence techniques.

The first step toward this goal was the development of an integrated diagnostic system for transmission line structures in this program. The system is designed to electronically collect and process field inspection data using criteria developed by the Ontario Hydro to assess the condition of structures and recommend a plan of action to ensure reliability and safety.

The integrated diagnostic system consists of two main components: field inspection data collection system incorporating a hand-held device and an electronic data recording form, and automated expert system for processing of the data. Figure 1 illustrates schematically the intelligent data processing system used in this program.

Upon completion of the development, all elements of the diagnostic system were field tested and evaluated.

2. Field Inspection Data Collection System

It is advantageous, during field inspection, to record the data in a electronic form useable by the computer-based diagnostic system, instead of the traditional "pencil and paper" method. This electronic method improves the efficiency and reliability of data recording and the whole inspection process. At the same time, the electronic method has the flexibility and other advantages of the traditional method. Depending on sophistication of the technology, the field inspections can be made virtually "real time". At present, this is not needed, but the capability is there.

In this program, a hand held-device was used containing a specially developed field inspection form capable of recording the data into a file which can be electronically transferred to a microcomputer for intelligent processing using an expert system. Figure 1 illustrates schematically the hardware and data flow.

2.1. Electronic Data Collection Device

Review of various hand-held electronic devices indicated that Hewlett Packard HP95LX Palm Top PC with build-in Lotus 1-2-3 and MS-DOS satisfied all requirements of this developmental program. The requirements were:

- Easily programable to develop electronic form for field inspection data collection,
- Lotus 1-2-3 files can be used without modification by the data assessment expert system,
- Capability to exchange files between IBM compatible table-top PC,
- Sufficiently rugged for summer-time field inspections, and
- Inexpensive.

To date, field experience with this device indicates excellent performance and reliability. No hardware problems of any kind were encountered.

The connectivity pack, purchased with the device works very well, and files can be easily transferred from it to a table top PC and back. Continued use of this device is recommended for the future.

2.2. Field Inspection Data Recording Form

The form developed for use in the electronic data collection device is based on the "Steel Structure Inspection Form" developed by the Ontario Hydro (see Figure 2) for traditional "pencil and paper" method of data collection. This original form was expanded and modified to suit the requirements of the programming environment (Lotus 1-2-3) used in the electronic data collection device. The new form (see Figure 3) was carefully designed to prompt the user to record all necessary information about the structure to positively identify it, make condition assessment, and recommend appropriate remedial action if required.

The Lotus 1-2-3 software was used to create the data recording form during field inspections of the transmission line structures. Several versions of the form were developed with various degrees of detail. The form shown in Figure 3 is the simplest version which was used during the 1992 transmission line inspections.

A set of commands and instructions, called a macro, was developed to run the form on the electronic data collection device and perform the following functions:

- To access a blank form when needed,
- To allow the user to enter field inspection data and type comments as required,
- To save this information under any structure identification name or number, and
- To make any changes of the entered data and comments if necessary.

Field evaluation of the form showed that it is easy to use and is well suited for recording the field inspection data. The ability to make notes in the comments section was found to be a very useful feature.

3. Development of Expert System for Data Processing

The data collected during the field inspection must be processed to determine the condition of the line structures and recommend what action is required to ensure continued safe and reliable operation. Traditionally, this task is performed by an engineer, who applies his/her knowledge and available information. The effectiveness and efficiency of this process is determined by the level of the engineer's expertise and experience. Consequently, the results of field inspection data assessment may vary significantly, resulting in different conclusions and recommendations.

Through the development of computer-based expert system programs in this work, it was possible to eliminate the subjective component in the field inspection data processing. The developed programs can perform the task of data processing and:

- Provide consistent assessment of the line structures and recommendations for appropriate remedial action,
- Use always the same decision criteria and logic (standard decision-making),
- Request additional information if the data available are incomplete or insufficient (intelligent checklist),
- Give detailed justification why a certain recommendation was made and how it was reached (public thinking tool),
- Educate the user (transfer and preservation of knowledge), and
- Accept changes after checking for consistency with current knowledge (sharpening the expert).

Use of these expert systems in the future will enable the engineers to apply routinely the most up-to-date know-how and evaluate information more effectively and efficiently. This will result in significant quality improvements and lower costs.

3.1. Approach for Development of the Expert Systems

The expert system was built for automated processing of data recorded electronically using the hand-held data collection device.

Both expert systems are based on the heuristic and factual knowledge residing with the Ontario Hydro.

The expert system knowledge base was constructed around the decision criteria which were developed by the Ontario Hydro to recommend the appropriate action required to ensure safety and reliability of transmission line structures. This knowledge was used to create a decision tree structure incorporating the facts from technical literature, manufactures information, applicable standards, industry accepted codes of practice and heuristic components contributed by the experts at Ontario Hydro. Then, all the knowledge components were expressed in a form of IF-THEN rules using an expert system development package, EXSYS¹.

3.2. Expert System Development Package

EXSYS is a generalized expert system development package. An expert system is a type of artificial intelligence program that emulates the interaction a user might have with a human expert on a subject area. Expert systems developed with this package will ask user questions or request input data relevant to a subject. The user answers by selecting one or more answers from a list by entering a numeric value. The computer will continue to request for information until it has reached a conclusion. The conclusion may be the selection of a single recommendation or a list of possible recommendations arranged in order of likelihood. The computer can explain, in English, how it arrived at its conclusion and why.

Expert systems can be developed with this package for any problem that involves a selection from among a definable group of choices where the decision is based on logical rules. The rules can involve relative probabilities of a choice being correct. Any area where there is a person or group of persons that have special expertise needed by others is a potential area for EXSYS. Anything from identification of biological specimens, to automating complex regulations, to aiding customers in selecting from among a group of products, to automated user assistance is possible.

Expert systems deal with knowledge rather than data and the files they use are often referred to as knowledge bases. The rules that the program uses are IF-THEN type rules. A rule is made up of a list of IF conditions (normal English sentences or algebraic expressions) and a list of THEN conditions (more sentences) or statements about the probability of a particular choice being the appropriate solution to the problem. If the program determines that all of the IF conditions in a rule are true, it adds the rule's THEN conditions to what it knows to be true. The program determines what additional information it needs and how best to get this information. If possible, the program will derive information from other rules rather than asking the user. This ability to derive information allows the program to combine many small pieces of knowledge to arrive at logical conclusions about complex problems. The rule editor allows the rules to be easily modified, added or deleted.

The final goal of an expert system is to select the most appropriate recommendation based on the data input by the user. If more than one solution is possible, the program will provide a list of the possible recommendations arranged in order of probability.

3.3. Expert System Concept

Determining correctly the type and extent of line tower component damage is essential for making proper assessment of the structure condition and recommending plan of action to ensure safe and reliable operation. The component damage is defined as degradation leading to loss of load bearing capacity due to reduction of cross-section or physical deformation which would, if not remedied, lead to line tower failure.

In the conceptual design of the expert system, six broad classes of significant damage were considered:

- Protective (galvanizing or paint) coating degradation,
- Corrosion of tower material (sub-, and super-structure),
- Physical shape deformation,
- Missing components,
- Cracking of tower components, and
- Footing damage.

These represent all known routinely occurring damage processes and can be further categorized into 24 basic modes of damage which can independently or jointly bring a line tower to failure.

The expert system package was designed to make the assessment and recommendation based on the type and extent of damage. If the damage was minor, information on the aggressivity of the atmosphere at the tower location is also required to recommend the length and frequency of inspections.

The type and extent of line tower damage is determined during field inspection from:

- Detailed visual inspection information,
- Measuring cross-section loss of components,
- Measuring protective (galvanizing and paint) coating loss,
- Measuring structure-to-soil potential, and
- Measuring contamination on structure surfaces.

The expert system guide the automated enquiry to the most likely conclusion utilizing the build in knowledge organized into a decision tree structure. The source of information utilized by the expert system is a completed field inspection data recording form, shown in Figure 3, in an electronic form.

3.4. Example of Diagnostic Sessions with the Expert System

For the purpose of demonstrating diagnostic a session with the developed expert systems, a typical tower was chosen with some corrosion damage to the super-structure. The information entered into the electronic data collection device and stored under a structure number, e.g., DEMOSTR.WK1 was:

- Type of structure: lattice
- Type of environment at structure location: urban
- Atmospheric corrosivity at structure location: 5 (corrosion index)
- Surface coating: galvanized only
- Footing type: pad, pier or levelling concrete
- Corrosion of galvanized structure surface:
 - Surface colour: grey, yellow and red brown
 - Area of red brown colour: ~ 3%
- Total loss if cross-section due to corrosion: 0%
- Missing bolts: 0%
- Bent structural members: 0%
- Condition of concrete footings: damage free

Based on this information, the expert system perform the diagnosis.

The use of the developed automated expert system is exceedingly simple. The only thing to do, to perform a line tower diagnosis, is to type in the structure number at a prompt on the first screen:

SCREEN #1:

Input the structure number (e.g., ST8-109.WK1)

Enter: DEMOSTR.WK1

At this point, the expert system automatically accesses the Lotus 1-2-3 file number DEMOSTR.WK1, extracts the required information and then comes up with the diagnosis on the next screen:

SCREEN #2:

****RESULTS****

The footings are in good condition, but the structure must be painted. The protection of galvanizing has been lost and a number of structural members are corroding rapidly to such an extent that they must be painted with a protective coating to prevent further deterioration. Schedule painting of the whole structure within two years.

If necessary, the user can review and inspect all information the expert system utilized to make this assessment and recommendation.

4. Summary

An integrated diagnostic system for transmission line structures was developed. It was designed to electronically collect and process field inspection data to assess the condition of the structure and recommend a plan of action to ensure reliability and safety of the structures. The developed system consists of:

- Field inspection data collection system incorporating a hand-held device and an electronic data recording form, and
- Automated expert system for intelligent data processing.

Results of the field evaluation of the integrated diagnostic system are very encouraging. The system functions as designed and demonstrated incredible ease with which it can be used to make consistent diagnosis based on provided data. Electronic handling of data increases efficiency of the processing and reduces it to a fraction of time it would take to do it in a traditional way.

5. References

1. EXSYS is an Expert System Development Package, EXSYS Inc., P.O. Box 75158, Contr. Sta. 14, Albuquerque, NM 87194, U.S.A.

- TRANSMISSION LINE STRUCTURE
- INSPECTION FORM #1
- Fill all applicable (Y/M) entries!
- 1. STRUCTURE IDENTIFICATION INFO.
 - STRUCTURE #
 - LINE SECTION
 - LINE TITLE
 - CIRCUIT
 - REGION
 - SYSTEM PLAN #
 - YEAR OF CONSTRUCTION
 - INSPECT. DATE (DD/MM/YY)
 - 1.1 STRUCTURE TYPE (Y/M)
 - Lattice (Y/M)
 - Steel Pole (Y/M)
 - 1.2 TYPE OF ENVIRONMENT
 - At STRUCTURE LOCATION
 - Industrial OR (Y/M)
 - Urban (Y/M)
 - Rural (Y/M)
 - 1.3 ATMOSPHERIC CORROSIVITY
 - At STRUCTURE LOCATION
 - Corrosion Index (1 to 5)
 - 1.4 SURFACE COATING
 - Painted and/or
 - Galvanized only (Y/M)
 - Galvanized (Y/M)
 - 1.5 FOOTING TYPE (Y/M)
 - Grillage Steel (Y/M)
 - Augered Concrete OR (Y/M)
 - Pad & Pier OR (Y/M)
 - Levelling Concrete (Y/M)
 - 1.6 KNOWN PROBLEMS
 - Corrosion (Y/M)
 - Nuts & Bolts (Y/M)
 - Structural Members (Y/M)
 - Plates (Y/M)
 - Paint (Y/M)
 - Footings (Y/M)

- CRACKING OR CHALKING (t)
- 3.2 MEASURE REMAINING PAINT COATING
- Average thickness (mm)

- 4. EXTENT OF CORROSION AT RED BROWN AREAS
- 4.1 GENERAL ATTACK
 - (max. loss of x-sect. t)
 - (% of members with more than 10t loss x-section)
- 4.2 LOCALIZED ATTACK AREA
 - (max. loss of x-sect. t)
 - (% of members with more than 10t loss x-section)
- 4.3 CREVICE CORROSION
 - (max. pack-out in mm)
 - (% of pack-out cravices)
- 4.4 PITTING CORROSION
 - Density (f/dm2)
 - Max. depth (mm)
 - Max. x-sect. penetr. (t)
 - (% of members with more than 10t loss x-section)
- 4.5 INFOLIATION CORROSION
 - Max. loss of x-sect. (t)
 - (% of members with more than 10t loss x-section)
- 4.6 TOTAL X-SECTION t IS

5. CONDITION OF NUTS & BOLTS

- Grey bolts (t)
- Yellow brown bolts (t)
- Rusted (Red brown) bolts (t)
- Damaged bolts (t)
- 5.2 LOOSE (t)
- 5.3 MISSING (t)
- 6. CONDITION OF STRUCTURAL MEMBERS
- 6.1 MISSING (t)
- 6.2 BENT (t)
- 6.3 CRACKED
 - Max. thru x-section (t)
 - With more than 10t thru x-section

7. CONDITION OF CONNECTION PLATES

- 7.1 CORRODED
 - Max. area lost (t)
 - Plates with more than 10t area lost (t)
- 7.2 CRACKED
 - Max. thru x-section (t)

2. CORROSION OF GALVANIZED STRUCTURE SURFACE

- 2.1 SURFACE COLOUR/AREA
 - Grey, only (Y/M)
 - Grey & Yellow (Y/M)
 - Brown, only (Y/M)
 - Area (Yellow brown) (t)
 - Grey, Yellow and Red brown (Y/M)
 - Area (Red brown) (t)
- 2.2 MEASURE REMAINING GALVANIZING
 - Average thickness (mm)
- 3. CONDITION OF PAINTED SURFACE
 - 3.1 PAINTED SURFACE/AREA PEELING,

- Plates with more than 10t thru x-section (t)
- 7.3 TOTAL t NUTS & BOLTS
- 7.4 TOTAL t STRUCT. MEM

8. CONDITION OF FOOTINGS

- 8.1 CONCRETE
 - Cracked/crumbling (Y/M)
 - Rust stained (Y/M)
- 8.2 BURIED GRILLAGE STEEL
- 8.2.1 TYPE OF SOIL (Y/M)
 - Dry (Y/M)
 - Flooded (Y/M)
- 8.2.2 SOIL PH (Y/M)
- 8.2.3 SOIL RESIS. (ohm/m)
- 8.2.4 CORROSION LOCATION EXTENT
 - At grade level
 - Surface colour
 - Grey (Y/M)
 - Red brown (Y/M)
 - Yellow brown (Y/M)
 - Pitting corrosion (f/dm2)
 - (max. depth in mm)
 - (max. x-sect. penetr. t)
 - General corrosion (max. t thru x-section)
 - Cracked
 - (max. loss in x-sect. t)
 - One foot below grade
 - Surface colour
 - Grey (Y/M)
 - Yellow brown (Y/M)
 - Red brown (Y/M)
 - Pitting corrosion (f/dm2)
 - (max. depth in mm)
 - (max. x-sect. penetr. t)
 - General corrosion (max. t thru x-section)
 - Cracked
 - (max. loss in x-sect. t)

9. TOWER LEG POTENTIAL

- (IN SOIL) vs. Cu - Cu SULFATE
- Leg #1 (mV)
- Leg #2 (mV)
- Leg #3 (mV)
- Leg #4 (mV)
- 10. STRAY CURRENT IN TOWER LEGS
 - Current (amps)
 - Direction to ground (Y/M)

FIGURE 3
TRANSMISSION LINE STRUCTURE FIELD INSPECTION DATA
COLLECTION FORM BUILD INTO HAND HELD PALM-TOP COMPUTER

STEEL STRUCTURE INSPECTION FORM

DATE: _____
REGION: _____
CIRCUIT: _____
STRUCTURE NO: _____
STRUCTURE TYPE: _____
LINE SECTION: _____

LOCATION OF TOWER Industrial
 Urban
 Rural
FOOTING TYPE Grillage Steel
 Augered Concrete
 Pad & Pier
 Levelling Concrete

1. General Appearance of Structure- Colour

Gray. No Discolouration Anywhere

Yellow Brown 3% 5% 15% 25%
Red Brown 3% 5% 15% 25%

2. If there red brown areas check types of corrosion.

General Attack Where _____ Thickness _____
 Localized Attack Where _____ Thickness _____
 Crevice Corrosion Where _____
 Pitting Corrosion Where _____
 1 2 3 4 5
 Exfoliation Where _____
 Cracking Where _____

3. Severe corrosion of nuts and bolts
(nuts, bolts and threads showing metal loss,
sharp corners rounded, difficult to remove)

4. Nuts and bolts missing Where _____

5. Structural Members missing or bent Where _____

6. Concrete foundation cracked or crumbled

7. Painted Yes No

Paint peeling or cracked

0.1% 3% 33%

8. If red brown rust area not more than 5% measure galvanizing

FIGURE 2
TRANSMISSION LINE STRUCTURE FIELD INSPECTION
DATA COLLECTION FORM

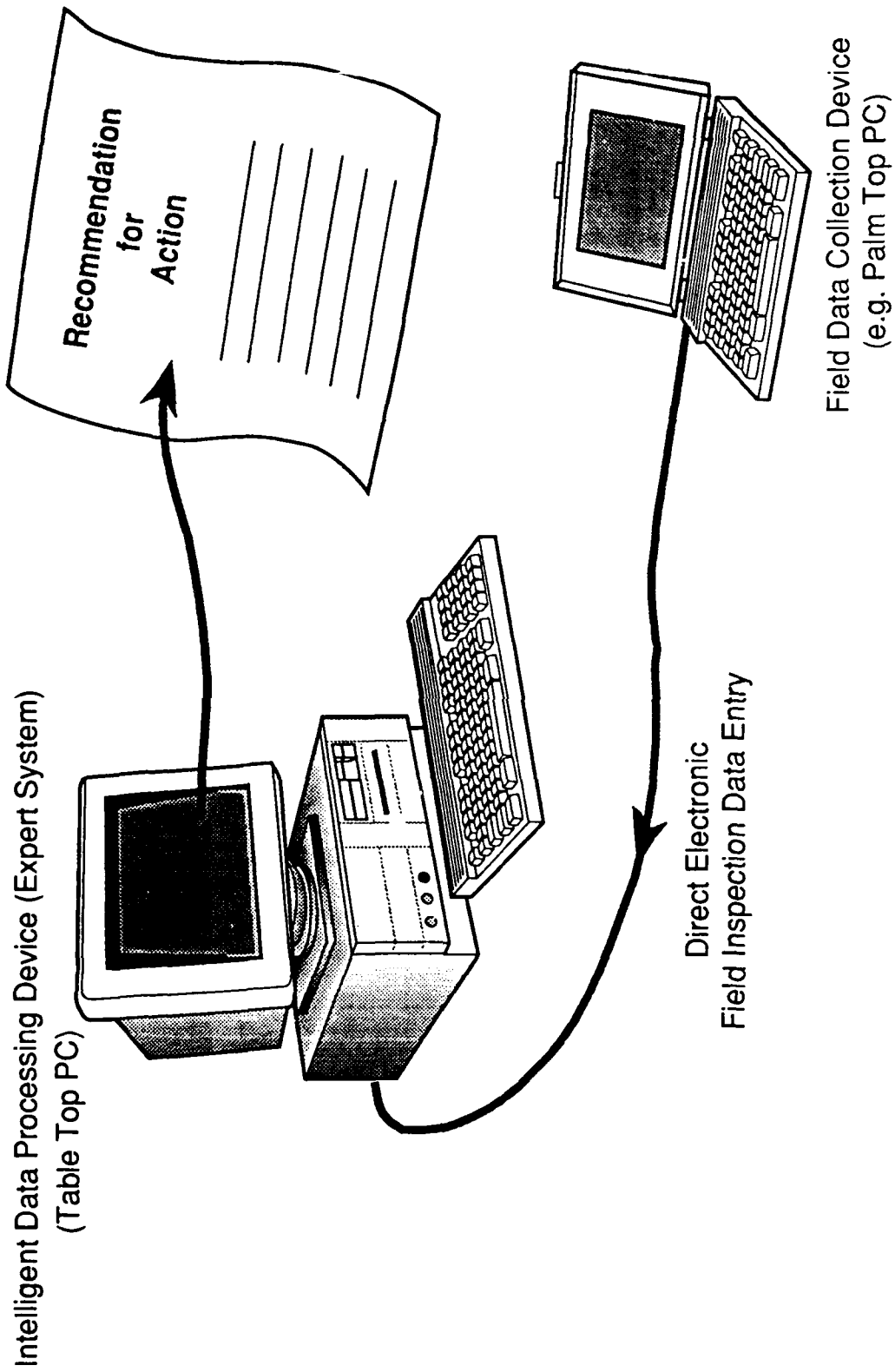


FIGURE 1
INTELLIGENT DATA PROCESSING
USING EXPERT SYSTEMS

Data Acquisition Update

Ronald A. Eberlein
Longview Inspection, Inc.
2411 S. Eastman Rd.
Longview, Texas 75602

Abstract

Paper No. 270, A DATA ACQUISITION SOLUTION, was presented at CORROSION 92. The paper described a complete Data Acquisition System. The system, software and hardware, was designed by users for users with the intent to make you interactive with your inspection program via a desktop PC and to eliminate the need for paper in the field.

The system is currently in use in several locations throughout the United States, in several different industries. This paper will briefly review the system and describe some applications and adaptations that have been made.

Introduction

The amount of data required for inspection programs has been and will continue to be on the increase. The only reasonable way to manage the data is in a computer program. This program has been written as a solution to finding a program that can be easily modified to handle individual wants and needs. This also allows modification to meet new code or government requirements as they arise.

The program can be modified and expanded to handle many different types of data. You are not limited to corrosion survey data. The program is designed for data acquisition only and therefore, it can be readily adapted to many different types of data acquisition problems.

The following are some case histories of corrosion programs currently underway which show the versatility and adaptive qualities of the program as well as how diversified industry is in its requirements for inspection programs. Some of the future applications that have been requested are also discussed.

Case #1

One of the first clients to utilize the software in-house did so to bring together information for pressure vessel and storage tank programs. The files containing U-1 Forms, Drawings, Inspection Reports and Inspection Procedures had become frayed and disorganized over the years with some of the information having found its way into filing cabinets in production and purchasing offices. Problems were also occurring as a result of having extra copies of old inspection reports circulating within the plant.

Rather than spending a great deal of time and money to get everything entered into the program right away, the inspection department simply began using the program to record inspections as they were completed on their normal schedule. A computer technician was assigned to handle AutoCad drawings and data input as necessary.

The sequence of events was as follows:

1. As a vessel is scheduled the file folder is pulled and a file opened in the software for that vessel.
2. Design data is entered in the Vessel Specification Screen and historical inspection data is entered into the Inspection Notebook.
3. A Standard Minimum Inspection Procedure is entered into the Procedure File
4. The procedure will be modified, where necessary, depending on the historical data and the vessel classification.
5. Minimum Allowable Thickness values and Flag values are entered into the data table.
6. The file is reviewed by the technician prior to performing the inspection.
7. As a part of the inspection the technician sketches the vessel and verifies nameplate and operating data.
8. Data is entered into the Data Table and Visual Inspection Notes are entered into the Inspection Notebook.
9. The Inspection Procedure is evaluated and modifications are documented as required by the inspection results.

This completes the Data Acquisition stage of the process. The data is then interfaced to other existing programs for analysis and archiving. Initially, information in the vessel file was also interfaced to another program that compared and updated information in the plant Mainframe System.

Discussion

The problem of locating the records necessary to begin a database is not uncommon. The records in this case were scattered between the Purchasing, Inspection, and Production Departments and gathering all the information took the cooperation of all three of these departments.

This company contracted the whole process to a 3rd party as they did not have the in-house resources to devote to the project. Other companies have had limited resources to contribute to the

process and have done so.

The addition of the Vessel Procedure Section was done quickly and has since been a standard offering in the software. It allows the user to plan logistics well in advance of the next inspection.

This case demonstrated the necessity that the file formats used in any program need to be common files, recognized by other computer programs. Much of the information included in these files is of use in areas other than inspection and should be made available to personnel who need it.

The idea of entering files at a normal pace rather than blitzing a project has saved the company time and money. It allows modifications to the program for changing technology and codes, and gives them a completion date for initial data entry.

This project is scheduled to be completed in 1996 and will consist of approximately 10,500 pressure vessels and storage tanks.

Case #2

The same basic path for vessels was followed due to the same types of problems as Case #1, however, there were some additional requirements.

1. Each vessel file had a photograph taken of it which was included in the vessel file as an Overview Image rather than drawing. Drawings were included in the section list beneath the Overview Image for each vessel.
2. A selection titled "Vessel Notebook" was added to each vessel file for input from production personnel as information pertinent to them for each vessel.
3. The software was placed on a network as "View Only" for distribution of information. The Vessel Notebook, however, could be accessed by production from the network.

Discussion

Many of the same problems that were solved in Case #1 were common in this case. They are problems common to many people. This is a case where the subject company wanted the Image capability used to a much greater extent. They believe in the "A picture is worth a thousand words" concept.

The networking of the information was not new but the solution to protecting the integrity of the data can have varied solutions. The solution used here was simply to offer "View Only" menus on the network with the exception of the "Vessel Notebook". Network

personnel are allowed to enter information into that section. The other common solution is to offer different levels of access when the system is logged into but that can become difficult when the software is networked so this seemed to be an easier more convenient method.

Case #3

This plants vessel program was assimilated into the software and he just continued with what he had been doing. While they had a good vessel program they were lacking in the area of piping.

1. Piping Systems were defined by process and applicable code.
2. Interplant pipelines were given their own overall directory as well as being included in each operating areas file. The entire route of the line was tracked using the Site and Sub-Site Maps.
3. The systems in each operating area were broken down in the Section List and data points added.
4. Additionally specific areas and fittings were designated in the Section List for more frequent inspection or for more specific inspection procedures.

Discussion

There are vast amounts of piping in any process plant and common pipelines between different processes pose special problems in the area of "Whom is responsible". Some of the current software programs in use require individual lines to have their own file and when multiple lines are used in a system, a multi-station loading facility, the number of files become difficult to track.

The interplant lines were traced through the entire plant on the Site Map. Individual sections were recorded on the Sub-Site Map and inspections were recorded in the Section List of that lines file. This allowed each area to be inspected where practical and the individual inspections updated the entire file for that line. This information was available to the entire plant via the network and individuals were able to change their inspection priorities as a result of someone else inspecting a few blocks away.

Being able to look at defined piping system consisting of more than one line in one file makes evaluation of the system much easier. The entire system may require inspection every 2 to 5 years but certain fittings or sections of the system may be subject to more frequent inspection or more extensive inspection using special techniques. These things were easily handled by using the Section List under the System Overview drawing. Again, each time an inspection is performed the whole file is updated.

The software uses "Grid Patterns" when the inspection point is an elbow or tee and asks how many readings you want to take around at an inspection point. This function is currently being modified to handle some proposed code requirements.

Additional Discussion

Common to all the files is the ability to use drawings and pictures at any point. One of the immediate benefits of this is the accuracy location of data points when the point is marked on an image of the immediate area. This capability also gives the user the option to use imagery to record damage or field changes to the equipment and accurately communicate that to personnel in other locations.

The piping drawings in one location were overlaid with a valve program and different materials of construction were color coded for the inspection program then used to reference a material evaluation R&D program from another department.

All the programs also have columns in the data tables for "Minimum" and "Flag" thickness. These are color coded for highlight purposes and are input when the initial file is created. They can be edited as conditions change.

We have been asked to create a program within the system to handle a vibration analysis program. The user is in a Plant Maintenance function and would like to have all his responsibilities documented in one software package.

The soon to be published API 570 has caused considerable concern among many people. We have been asked by many people to give the piping section expanded capabilities to address some of the items that are likely to be a part of the new standard and we are currently accepting input from any truly interested parties.

Conclusion

Computers and computer programs have become a way of life for all of us. There is simply no other efficient way of managing the vast amounts of data required in business today. At the same time this data must be easily accessible to many different people. Not everyone is a computer programmer nor do they have the time to become one so the programs must remain simple and easy to use.

Versatility has become essential in any program that is subject to change as often as a corrosion/erosion program. The technology available is changing as quickly as are the code requirements. Some states, even non-code states, are adopting as law certain codes to cover Pressure Vessels, Storage Tanks, and Piping Systems. These factors necessitate flexibility in a program to meet these

changing requirements. Additionally, the owner is still ultimately responsible for his equipment. Many owners exceed the requirements as dictated. There seems to be no hard and fast answer for any of us.

Communication of information is essential to the selection of any software program purchased today. Considerable time, effort, and money will go into establishing a data base for corrosion/erosion programs and every company should make maximum use of that information. Any software decision should include the ability of that software to communicate with other software programs and remain user compatible. The ideas are simple but are not always easy to accomplish.

CORROSION PREDICTION FROM LABORATORY TESTS USING ARTIFICIAL NEURAL NETWORKS

David C. Silverman
Monsanto Company
800 N. Lindbergh Blvd.
St. Louis, MO 63167

ABSTRACT

Artificial neural networks are computational systems which learn patterns between input and output information in the absence of a specific model. They then use the learned relationships to make predictions in new situations. Often, predictions are made from laboratory results by recognizing the pattern in the relationship among them in the absence of models. Artificial neural networks were trained to recognize the pattern in two such situations, the use of polarization scans to predict the possibility of localized and general corrosion and the use of a type of sequential immersion test for plastics and elastomers to predict if they would perform acceptably in service. Both neural networks were incorporated with an expert system to provide ease in data input, provide simple consistency checks, and make the final prediction once the pattern was recognized by the network. Examples are provided of each neural network/expert system.

Key terms: artificial neural network, corrosion, polarization tests, non-metallic materials, linings, plastics, elastomers, laboratory testing, sequential immersion test, expert system, crevice corrosion, localized corrosion, pitting, general corrosion, corrosion prediction

INTRODUCTION

One of the major functions of industrial laboratory corrosion testing is to provide information so that practical predictions can be made. Laboratory tests by their nature are usually accelerated tests. They tend to be simulations not actual duplications of the actual material-environment interaction. Very often the chemistry in industrial environments is at best only partially characterized. Limitations on the number of tests that can be run and the amount of time available to obtain the information that is needed mean that the prediction must often be made in the absence of complete characterization of the corrosion process. The corrosion expert often make the prediction by coupling the results of the laboratory tests with other experience with respect to behavior of the material in environments with similar components. A specific model of the corrosion process is usually absent. The thought process used to make the predictions may be similar to use of inductive reasoning. Predictions are made by recognizing the pattern of expected corrosion behavior that emerges by combining prior experience with the experimental results.

These observations suggest that the expertise and thought process used to make a prediction from a laboratory test might be captured in a computer-based system that is capable of recognizing patterns. Expert Systems are often used to capture expertise. However, such knowledge-based systems can be constructed only when the decisions are made using a well-defined structure of rules and deductive reasoning. The problem is that at least part of the interpretation of the experimental results and final decision is made in the absence of either rules or a specific model. This observation suggests that the computer simulation must be able to recognize patterns in the absence of a model. Such a system is the artificial neural network^{1,2}.

Artificial neural networks are computational systems that learn the pattern between a group of input observations (data) and a group of output observations (results). They can use that learned association to predict the appropriate outputs for input data not used in the training. No specific model is required

for relating the input to the output information. Pattern recognition is done in a manner analogous to inductive reasoning in which the relationship between inputs and outputs is generalized from a set of examples. These characteristics are consistent with those needed to relate experimental results to field predictions in the absence of complete information.

These observations led to a project to determine if artificial neural networks could be developed to capture the patterns (expertise) used by the corrosion practitioner to make practical predictions from laboratory tests. Networks were developed for two test procedures, use of cyclic polarization scans to determine the propensity of alloys to undergo localized corrosion and use of a type of "sequential immersion test" to determine if a non-metallic material plastic or elastomer can withstand an environment, usually as used as a lining. Each of the neural networks was incorporated within an expert system. The emphasis of this paper is not on the development of the networks but on how the artificial neural networks so developed can be used to aid in relating test results to field predictions. The results strongly suggest that this technology, shows promise of being able to recognize the pattern that ties the laboratory results to the field predictions. Then, incorporation within an expert system provides an easy way to incorporate the "rules" that are used, at least loosely, to translate the pattern into a prediction.

INPUTS AND OUTPUTS FOR ARTIFICIAL NEURAL NETWORK

Artificial neural networks were developed and trained for capturing the patterns between test results and field predictions for electrochemical polarization scans and the sequential immersion test. The two tests were chosen because they have been used extensively enough so that a reasonably substantial data base is available that can provide examples of both the laboratory results and the related field observations. Such a data base is necessary so that the neural network can "learn" the pattern during the supervised learning so that it can generalize to new situations¹².

The type of data extracted from the experimental results and actual observations used as input and output pairs for training the two networks are shown in Tables 1 and 2. They are explained and justified in detail elsewhere³⁴ and summarized below. This information was derived by paying very close attention to what characteristic experimental data are used for each test to make a prediction. Wherever possible, the actual behavior of the material in the environment was used as the output.

Polarization scans are usually used to screen alloys for their propensity to undergo localized corrosion. Figures 1a - 1d are four idealized polarization scans showing how the characteristics used by the network might appear on different types of scans. The relationship among the "repassivation" or "protection" potential, the pitting potential, and the corrosion potential are often used to make assumptions about the possibility of localized corrosion⁵. The presence or absence of a hysteresis between the forward and reverse portions of the scan is mentally recorded because if the experiment is run properly³⁶, a large hysteresis tends to be accompanied by a higher propensity for localized corrosion. The "anodic nose" is the name often given to the characteristic in which the current suddenly decreases. It changes from increasing with increasing potential to remaining constant at a low value. It usually indicates that a potential exists above which the oxidation state of the surface changes and the alloy goes from an "active" or higher corrosion rate state to a "passive" or lower corrosion rate state. The term "passive current" is meant to be a measure of the current that would occur at the corrosion potential. The modifier "passive" has been used because most of the interest is in alloys which exhibit little corrosion. The ability to estimate the appropriate current density comes directly from the experience of the practitioner. The potential at which the current changes from anodic to cathodic voltages during the reverse portion of the scan is assumed to be the potential of the anodic-to-cathodic transition. It tends to show if a passive film is established at the corrosion potential.

From these input variables are derived the qualitative conclusions of the ability of the alloy to withstand crevice corrosion and pitting and if general corrosion might be important.

In the "sequential immersion test", a sample of the non-metallic material is immersed in the fluid with periodic removal for weighing. The term "sequential" comes from this periodic removal for weighing followed by reinsertion of the sample. There are restrictions on the size and shape^{4,7}. After a certain time period, the sample is dried in air at the same temperature as the immersion, again with periodic weighing. Weight (mass) fraction change is plotted versus time. If the samples have one dimension much smaller than the other two and the area of the larger surface is unchanged among samples, diffusion is unidirectional and the plot provides a measure of the relative rate of diffusion into and out of the sample during exposure⁷. Figures 2a and 2b show "typical" plots.

The weight (mass) fraction uptake after the soaking provides a measure of the difference between the amount of the material migrating into the sample and the amount of material migrating out of the sample during exposure. The (mass) fraction change upon drying provides a similar measure of the amount of material (e.g. oils or plasticizer) lost during soaking. The larger these numbers, the worse the performance. The final curvature of each portion of the curve accounts for the fact that the exposure times may not be long enough for equilibrium to be reached and migration would still continue. The change in hardness is a mechanical property, large changes in which can signify attack. The final two variables are the signs of the changes in weight fractions. The output was kept simple, "acceptable" or "unacceptable" because of the qualitative nature of the test. No experience as yet exists to predict actual lifetimes from this experiment.

ARTIFICIAL NEURAL NETWORK/EXPERT SYSTEM

Complete descriptions of the set-up and training of the artificial neural networks and their incorporation in the expert system are given in detail elsewhere^{3,4}. The neural network architecture is the feed-forward, back-propagation network^{1,2,8}. The software package NeuralWare Professional IIPlusTM was used to train the network⁹. The sigmoid was used as the transfer function for training the polarization scan network and the hyperbolic tangent was used as the transfer function for training the sequential immersion test network. Two types of neural networks were combined for the polarization scans. One had all three outputs and two hidden nodes in one network. the other was a set of three neural networks, each with one output for each type of corrosion and one hidden node³. The neural network for the sequential immersion test had four hidden nodes and one output⁴. The neural networks were incorporated within their own expert system for each experimental procedure. The program V-P Expert¹⁰ was used as the shell. Figure 3 shows a schematic diagram of the information flow. The expert system enables simple consistency checks to be made and provides an efficient way to input data to the network from the user and to incorporate the results from the network into rules by which the numerical results are transformed into predictions.

Interpretation of the numerical output from the neural network are as follows. For the polarization scans, output > 0.8 means that the type of corrosion causing that output is likely, 0.2 < output < 0.8 means that a risk exists and a closer examination is needed, output < 0.2 means that the type of corrosion causing the output is unlikely to occur. The outputs from the single output and triple output neural networks are combined so by the expert system so that the most conservative prediction is used³ if a disagreement exists. Such disagreement might occur in the borderline region. For the sequential immersion test, output > 0.8 means acceptable behavior is expected, 0.2 < output < 0.8 means that the expectation is for marginal behavior and closer examination is needed, and output < 0.2 means that behavior would be unacceptable. No attempt was made to assign probabilities to these numbers, e.g. an output of 0.7 has a 70% chance of being successful¹¹.

APPLICATION TO PREDICTIONS FOR THE TWO NETWORKS

Use of the neural network/expert systems described above provide several advantages to the corrosion practitioner with respect to making predictions from laboratory data. They can serve as a check on interpretation by the expert. They help to insure that the predictions made from the experimental results are consistent with previous predictions for similar applications. They can aid in interpretation of results that might be influenced by noise or be in the borderline region between different types of behavior. When used by a less experienced person, they enable that individual to have access to expertise for interpreting experimental data in the absence of the expert. Neural networks are described to be robust in that they can capture the features so as to generalize even in the presence of noisy data². Following are examples for each network to show how the neural network/expert system can be utilized in practical corrosion studies.

Application to Polarization Scans

A vessel with soft natural rubber had a history of problems associated with the lining. After attempts to use other linings failed, the decision was made to use an alloy replacement. The question was which alloy to use. The process environment is an aqueous, acidic mixture with a pH of 4.5 and a chloride concentration lying between 2000 and 3000 ppm by weight. An excursion to pH of 3.5 may occur. The process temperature is 40°C (313K). Both polarization scans run in the laboratory and coupon immersion tests run in the process vessel were used to screen alloys¹². Though this example is "after-the-fact", it does provide one way that the artificial neural network might be applied.

The appropriate way to use this system is after the polarization scans are run and prior to the immersion tests. The goal would be to help to insure that the immersion tests, being of much longer duration, contain appropriate candidates. Ultimately, one would want to use the expert system to aid in choosing the material of construction directly from the polarization scan without the immersion test. However, from a practical standpoint, in view of the newness of the technology, such usage is premature. Therefore, the procedure would be to use this technology for preliminary guidance both for the longer immersion test and, as importantly, for any initial economic evaluation of alternative alloys that are promising candidates.

Figures 4 through 6 show the polarization scans for type 316ss (S31600), alloy 20 (N08020), and alloy 825 (N08825) at a pH of 4.5. Alloy 276 (N10276) was also evaluated but is not included in this discussion. A complete description of the experimental procedure is given elsewhere¹². The neural network/expert system is used once these polarization scans are generated. Table 3 lists the input values to and output values from the neural network for the three polarization scans. The headings of "single" and "triple" correspond to the two types of neural networks that are combined in the expert system³. Upon comparing between the outputs from the two networks, the expert system uses the most conservative value for each prediction. Table 4 shows the interpretation of the neural network and the observation from the coupon exposures to the liquid phase. There is excellent agreement. Also, no attack was predicted or observed for Alloy 825 exposed at a pH of 3.5. The conclusion would be that use of Alloy 825 should result in no attack of the vessel. There would be some risk of attack when using Alloy 20.

The prediction of borderline crevice corrosion for Alloy 20 was made because one of the outputs for crevice corrosion was between 0.2 and 0.8. When the input protection potential was changed from 0.15 V to 0.17 V, the outputs for crevice corrosion changed from 0.279 and 0.151 to 0.170 and 0.064 for each of the networks. The prediction changed from "border-line crevice corrosion" to "no attack". There are several conclusions. The propensity for crevice corrosion for Alloy 20 must be very close to the boundary between attack and no attack. At the boundary, differentiation between two cases becomes more difficult¹² for a neural network and the predictions must be used cautiously. The 89 cases used for training might not have been adequate to guarantee generalization. Some

memorization of the input data might have occurred. Predicting the required number of exemplars to prevent memorization is difficult¹². Lastly, the expert system is not expected to be 100% correct as no expert is 100% correct. Experience has indicated that this system is correct about 85% to 90% of the time³. Therefore, though the expert system can provide guidance and help to insure that interpretations are consistent with prior knowledge, coupon immersion tests or another independent experiment should be used for confirmation. Note that the final decision was to build the tank from Alloy 825 with Alloy C276 weld overlay on critical flange face gasket surfaces. The vessel has been in service for about 5 years. Vessel inspections and coupon monitoring have revealed no problems with the vessel.

Application to Non-metallic Material Evaluation

Prediction of degradation non-metallic materials in waste streams from laboratory tests is difficult because of the poor characterization of such streams coupled with the tested solutions usually being a "snapshot" of a changing situation. The problem was to predict the performance of lining and gasket materials in one such environment. Periodic replacement was required for gaskets made from EPDM (ethylene propylene dimonomer). One goal was to find an alternative to this gasket material. In addition, lining materials were to be evaluated for placement under some proposed containment vessels. Such linings had to be able to prevent leaching of any material. Three potential linings, high density polyethylene from two suppliers and a chlorinated, sulfonated polyethylene (CSMP) from a third were examined. Sequential immersion tests were run for the materials in as-caught samples at 49°C (the highest expected ambient temperature). Figures 7 and 8 show the mass change (as weight fraction) versus time for the two cases. Tables 5 and 6 show the values of the inputs to and outputs from the artificial neural network.

The output of the neural network shown in Table 5 agrees with the observation that EPDM would degrade in the environment. The expert system predicted that performance would be unacceptable. A perfluorinated elastomer was found to be an acceptable alternative. The agreement between field observation and network prediction for the first sample gives confidence to the prediction for the second sample. As far as the prediction for the linings, high density polyethylene is predicted to be acceptable in this service. The other lining is not. Normally, a decision of which lining to use would have been derived from the results shown in Figure 8. The neural network helps the corrosion practitioner to insure that the conclusion is consistent with other predictions made from this qualitative test for other systems. In this case, an alternative was found for the tanks and the system was not built.

During testing, this network was found to be about 80 to 85% correct⁴ in its qualitative predictions. No attempt was made to incorporate an expected lifetime prediction or a probability of failure for either material. The belief is that the sequential immersion test as now practiced is too qualitative to make a more quantitative decision from the results. Ultimately, data such as that shown in Tables V and VI might be used to estimate an average diffusion and sorption coefficient⁷. However, such calculations are premature because the methodology for decoupling the diffusion into and out of the lining into separate relationships is unclear.

Note that the output values in Table 6 sent to the expert system lie above 1 and below 0 even though the target is 0 or 1. The reason has to do with how the NeuralWare software does training. During training, scaling was done so that the actual output values (0 or 1) were scaled linearly to lie between -0.8 and +0.8 as outputs from the hyperbolic tangent transfer function. The network then adjusted the weights so that calculated and actual values of the output from the output node matched each other as closely as possible (-0.8 or +0.8 being the targets). During testing or use in which the inputs were not part of the training set, the output from the transfer function in the output node can be greater than 0.8 or less than -0.8 (+1 or -1 being the upper or lower bounds of the hyperbolic tangent). Scaling linearly between the output from the transfer

function and the real world would then result in the recorded output as sent to the expert system being greater than 1 or less than 0^o. This behavior was not found for the sigmoid used in the first neural network (see Table 3) because the output from the output node and the actual output were set at identical values so no scaling was needed³.

CONCLUSIONS

1. Artificial Neural networks can be powerful aids to the corrosion practitioner who is attempting to project laboratory results into field predictions. The results for the two laboratory techniques described in this paper demonstrate the feasibility of this technology to serve as such an aid. One caution is that enough data must be available for training so that the completed network can generalize to new situations.
2. Such networks provide a check that the prediction is consistent with those made previously. This check allows predictions to be made more confidently in the absence of a specific model for the corrosion process.
3. Incorporation of the neural network within an expert system is one way of making data entry and interpretation of the results "friendly" to the user and utilize rules often known once the pattern has been recognized.

REFERENCES

1. J. E. Dayhoff, Neural Network Architectures - An Introduction, Van Nostrand Reinhold, New York, 1990.
2. J. A. Freeman and D. M. Skapura, Neural Networks: Algorithms, Applications, and Programming Techniques, Addison Wesley Publishing House, Reading, MA, 1991.
3. E. M. Rosen and D. C. Silverman, Corrosion, **48**, 9(1992): p. 734.
4. D. C. Silverman, "Artificial Neural Network to Predict Degradation of Non-metallic Lining Materials from Laboratory Tests", to be presented at CORROSION/94, Baltimore, MD., February 28 - March 4, 1994.
5. ASTM Standard G61-86, "Standard Test Method for Conducting Cyclic Potentiodynamic Polarization Measurements for Localized Corrosion Susceptibility of Iron-, Nickel-, or Cobalt Based Alloys", Annual Book of ASTM Standards, Vol. 03.02, 1990.
6. D. C. Silverman, "Electrochemical Techniques-Simple Tests for Complex Predictions in the Chemical Process Industries", Corrosion Reviews, **10**, (1,2)1992: p. 31.
7. E. M. Rosen and D. C. Silverman, Corrosion, **46**, 11(1990): p. 945.
8. Rumelhart, D. E., Hinton, G. E., and Williams, R. J., "Learning Internal Representation by Error Propagation", in Parallel Distributed Processing: Explorations in the Microstructure of Cognition (D. E. Rumelhart and J. L. McClelland ed.), Vol. 1, p. 318, The MIT Press, Cambridge, MA, 1986.

9. NeuralWorks Professional IIPlus™, NeuralWare, Inc., Pittsburgh, 1990.
10. VP-Expert, Paperback Software, Version 2.0, 1988.
11. H. M. G. Smets and W. F. L. Bogaerts, Corrosion, **48**, (1)1992; p. 618.
12. R. E. McGuire and D. C. Silverman, Corrosion, **47**, 11(1991); p. 895.

TABLE 1

Data Inputs for Neural Network for Polarization Scans

| <u>Input Parameter</u> | <u>Value of Feature</u> |
|--------------------------------------------|--------------------------------------------|
| Repassivation Potential | $E_{\text{prot}} - E_{\text{corr}}$ |
| Pitting Potential | $E_{\text{pit}} - E_{\text{corr}}$ |
| Hysteresis | +1 = Positive 0 = None -1 = Negative |
| Anodic Nose | +1 = Yes 0 = No |
| Passive Current Density | $\mu\text{amp}/\text{cm}^2$ |
| Potential At Anodic-to-Cathodic Transition | $E_{\text{a-c}} - E_{\text{corr}}$ |
| | |
| <u>Output Parameter</u> | <u>Value of Feature</u> |
| Crevice Corrosion Predicted | +1 = Yes 0 = No |
| Pitting Predicted | +1 = Yes 0 = No |
| Should General Corrosion Be Considered | +1 = Yes 0 = No |

TABLE 2**Variables for Artificial Neural Network for Sequential Immersion Test**

| <u>Input Parameter</u> | <u>Value of Feature</u> |
|------------------------------------------------|--------------------------------|
| Soak Fractional Change | -1 to 1 |
| Dry Fractional Change | -1 to 1 |
| Final Curvature of Soak Cycle | Increasing = 1 Leveling = 0 |
| Final Curvature of Dry Cycle | Decreasing = 1 Leveling = 0 |
| Hardness Change | Actual Value |
| Sign of Final Soak Weight Minus Initial Weight | Positive = 1 Negative = 0 |
| Sign of Final Dry Weight Minus Initial Weight | Positive = 1 Negative = 0 |
| <u>Output Parameter</u> | <u>Value of Feature</u> |
| Rating | Good = 1 Bad = 0 |

TABLE 3**Inputs to and Outputs from Neural Network for pH=4.5, 40°C**

| <u>Input Parameter</u> | <u>316ss</u> | <u>Alloy 20</u> | <u>Alloy 825</u> | | | |
|-------------------------------------------------------------------------|---------------|-----------------|------------------|---------------|------------------|---------------|
| $E_{\text{pot}} - E_{\text{corr}}$ (Volt) | 0.0 | 0.15 | 0.4 | | | |
| $E_{\text{pit}} - E_{\text{corr}}$ (Volt) | 0.28 | 10* | 10* | | | |
| Hysteresis | Negative | Negative | Positive | | | |
| Anodic Nose | No | No | No | | | |
| Passive Current Density ($\mu\text{amp}/\text{cm}^2$) | 0.1 | 0.1 | 0.1 | | | |
| Anodic-to-Cathodic Transition $E_{\text{a-c}} - E_{\text{corr}}$ (Volt) | 0.0 | -0.1 | 0.0 | | | |
| <u>Output</u> | <u>316ss</u> | | <u>Alloy 20</u> | | <u>Alloy 825</u> | |
| | <u>Single</u> | <u>Triple</u> | <u>Single</u> | <u>Triple</u> | <u>Single</u> | <u>Triple</u> |
| Crevice Corrosion | 0.999 | 0.999 | 0.279 | 0.150 | 0.021 | 0.004 |
| Pitting | 0.053 | 0.053 | 0.042 | 0.00 | 0.042 | 0.00 |
| General Corrosion | 0.039 | 0.00 | 0.039 | 0.00 | 0.044 | 0.00 |

*If there is no pitting potential, then the value of 10 is used. This large value is a numerical approximation to a non-measurable pitting potential.

TABLE 4**Prediction vs. Results for In-plant Immersion Test**

| <u>Alloy/ Environment</u> | <u>Neural Network/ Expert System</u> | <u>Observed Corrosion Exposed Coupons</u> |
|-------------------------------|------------------------------------------|------------------------------------------------------------------|
| 316ss pH=4.5 | crevice corrosion likely to occur | crevice corrosion under TFE washer, no general corrosion |
| Alloy 20 pH=4.5 | border-line risk of crevice corrosion | less corrosion under TFE washer than above, no general corrosion |
| Alloy 825 pH=4.5 | no attack predicted | no attack observed |

TABLE 5**Variables for Artificial Neural Network for Gasket Evaluation**

| <u>Input Parameter</u> | <u>EPDM</u> | <u>PF Elastomer</u> |
|---------------------------------------------------|-------------|---------------------|
| Soak Fractional Change | 0.014 | 0.015 |
| Dry Fractional Change | -0.020 | 0.0014 |
| Final Curvature of Soak Cycle | Increasing | Increasing |
| Final Curvature of Dry Cycle | Decreasing | Leveling |
| Hardness Change | -10 | -1 |
| Sign of Final Soak Weight Minus Initial Weight | Positive | Positive |
| Sign of Final Dry Weight Minus Initial Weight | Negative | Positive |
| <u>Output Parameter</u> | 0.051 | 0.984 |

TABLE 6**Prediction vs. Results for the Sequential Immersion Test**

| <u>Input Parameter</u> | <u>HDPE-1</u> | <u>HDPE-2</u> | <u>CMSP</u> |
|---------------------------------------------------|---------------|---------------|-------------|
| Soak Fractional Change | 0.0120 | 0.013 | 0.22 |
| Dry Fractional Change | 0.0053 | 0.0068 | 0.021 |
| Final Curvature of Soak Cycle | Leveling | Leveling | Increasing |
| Final Curvature of Dry Cycle | Leveling | Leveling | Leveling |
| Hardness Change (Barcol 936) | 3 | 1 | 3 |
| Sign of Final Soak Weight Minus Initial Weight | Positive | Positive | Positive |
| Sign of Final Dry Weight Minus Initial Weight | Positive | Positive | Positive |
| <u>Output Parameter</u> | 1.05 | 1.03 | -0.12 |

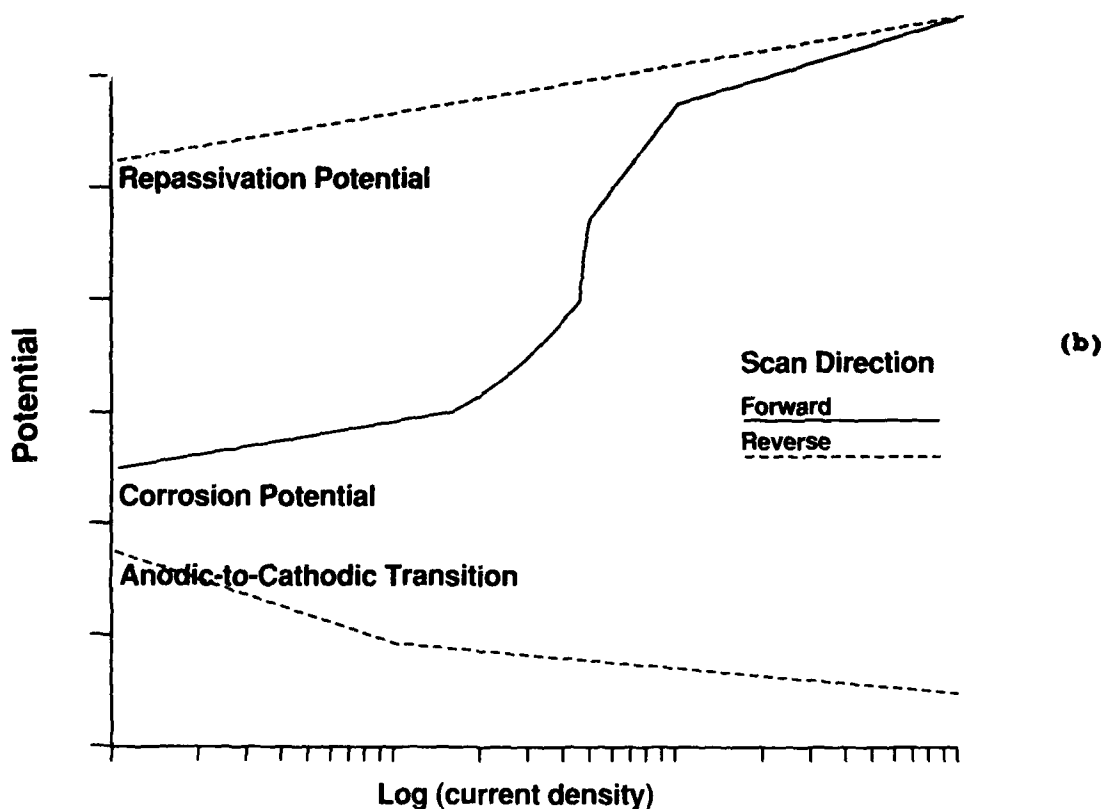
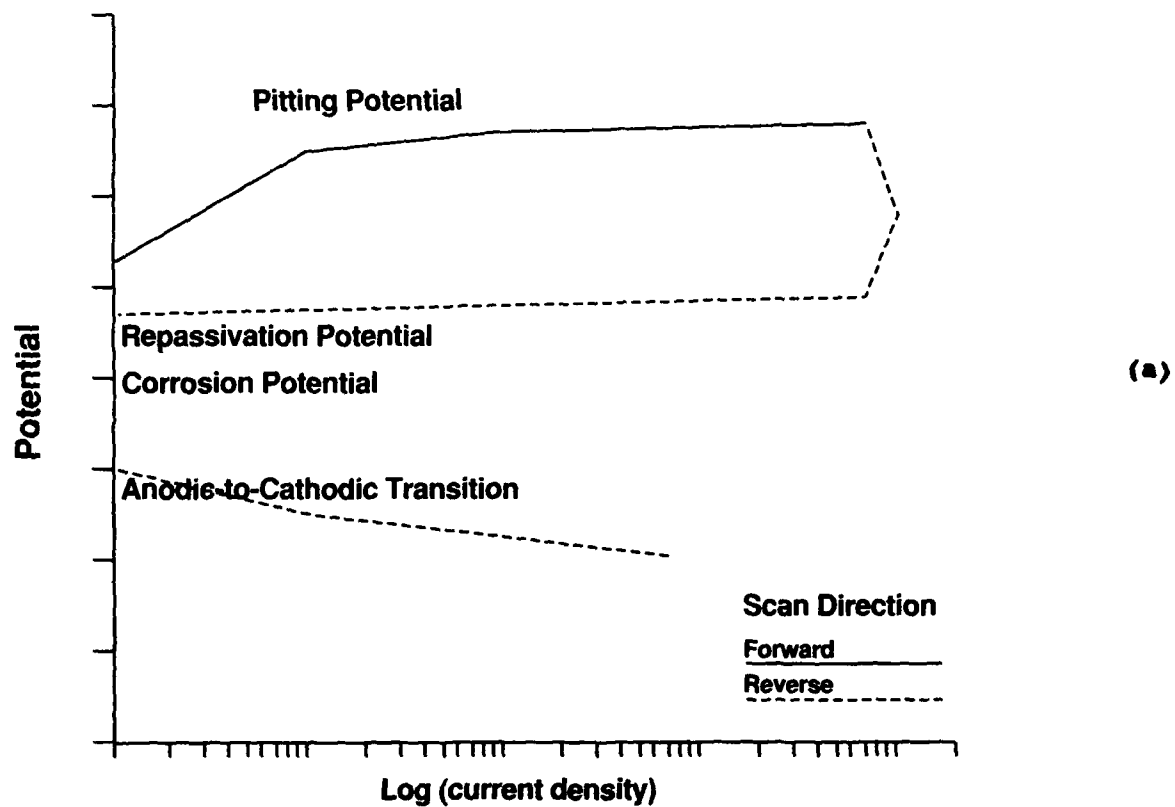


FIGURE 1. "Typical" polarization scans for (a) an alloy that might suffer localized corrosion with no general corrosion, (b) a completely passive alloy showing no corrosion.

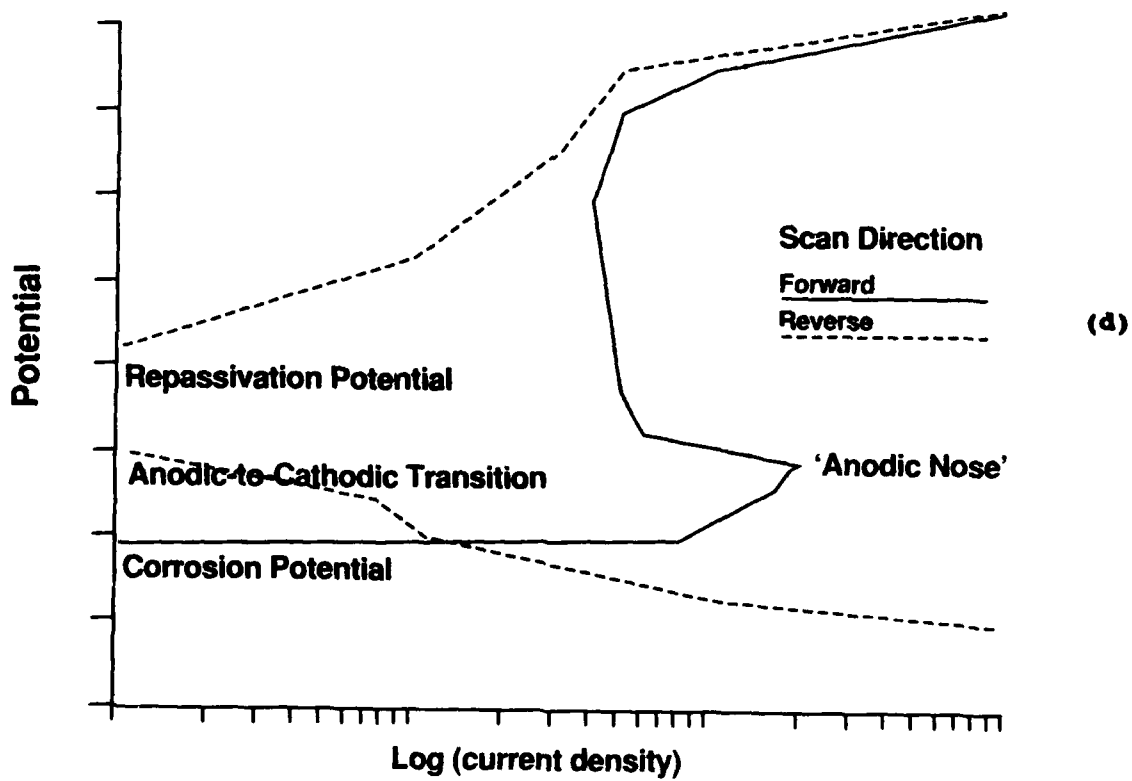
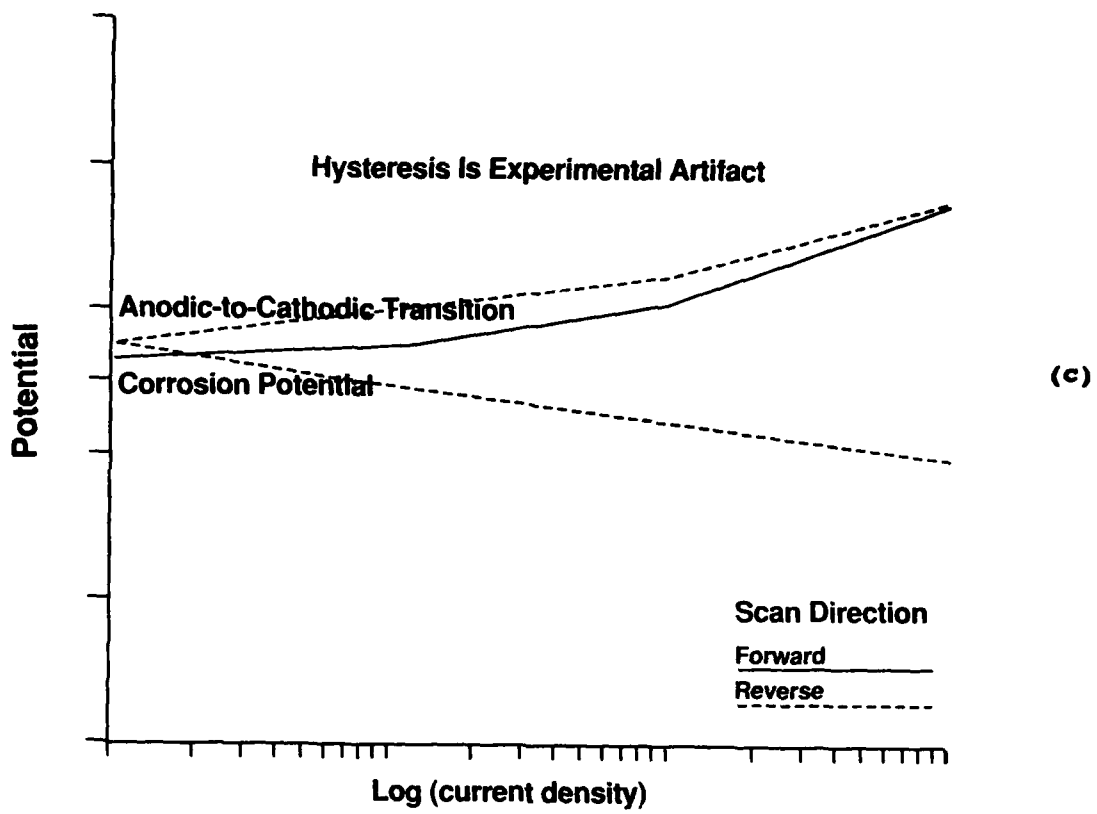


FIGURE 1. "Typical" polarization scans for (c) an alloy that might suffer rapid general corrosion, and (d) an alloy that has an "active-to-passive" transition with increasing potential.

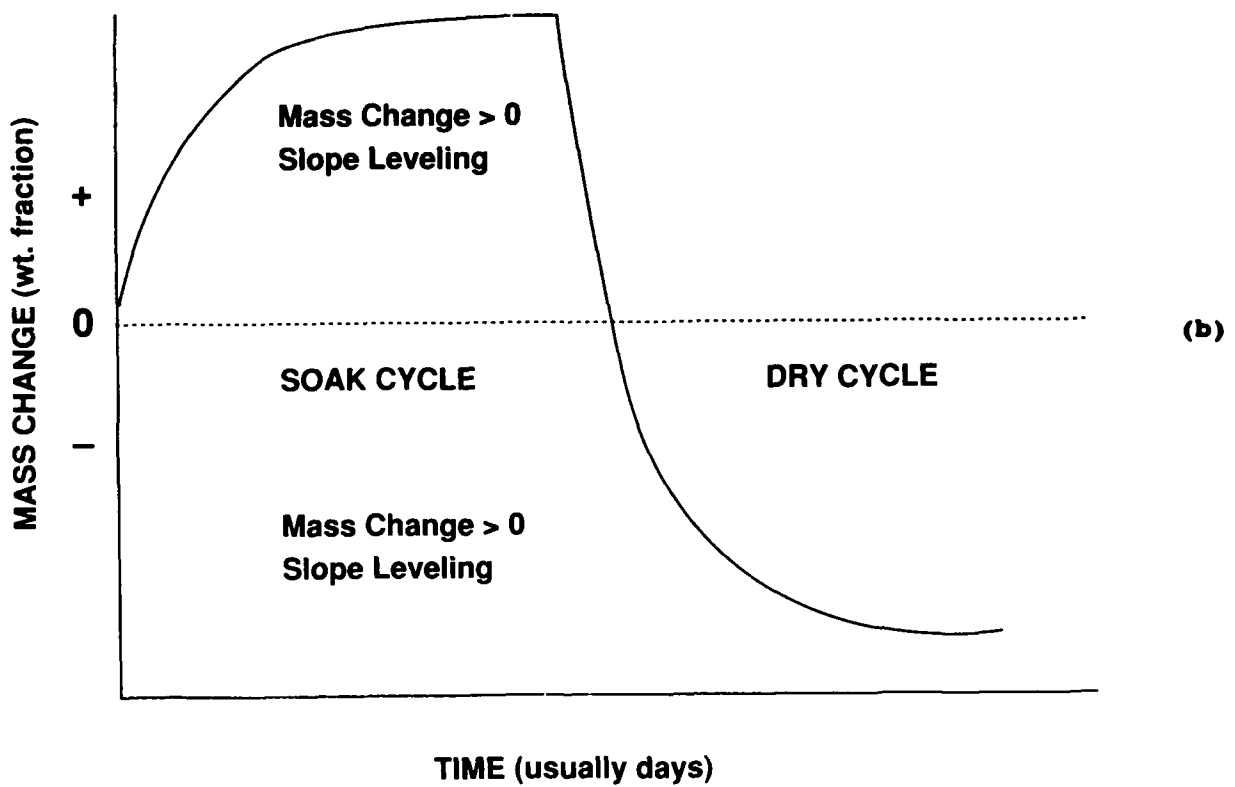
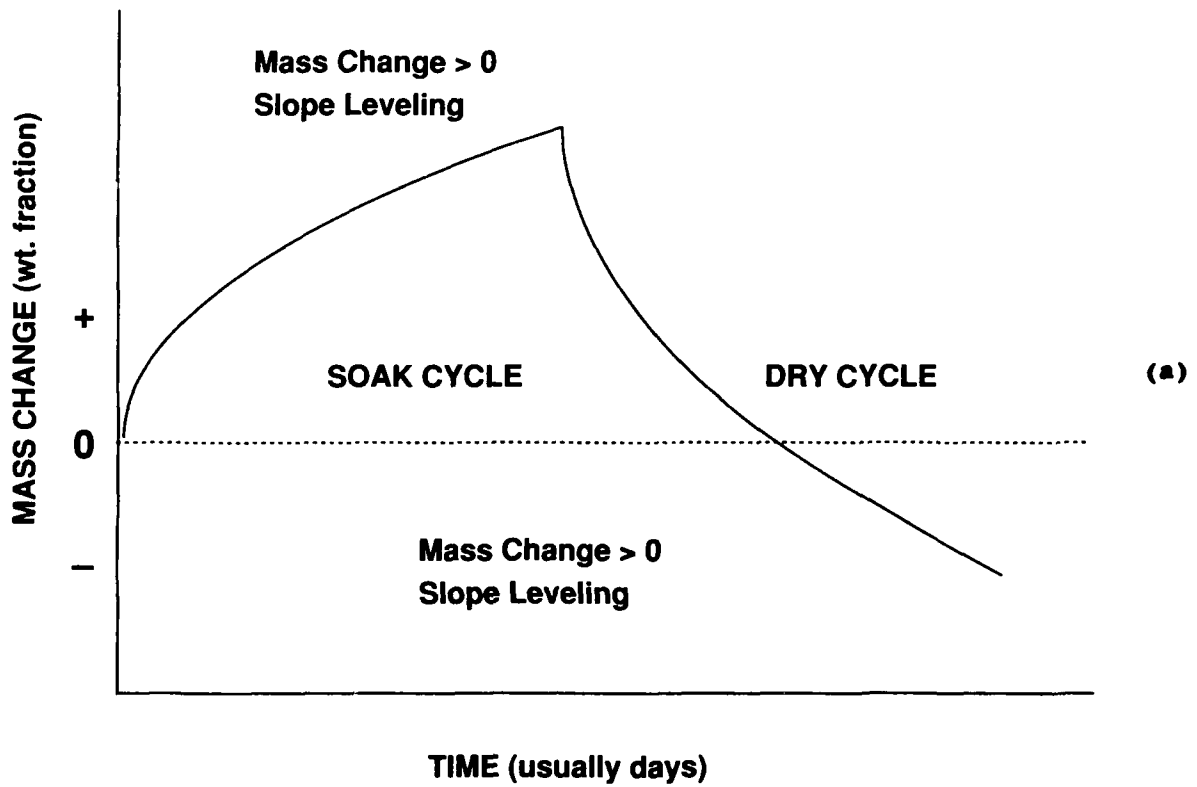


FIGURE 2. Examples of Sequential Immersion Test results for non-metallic materials showing (a) slow approach to saturation which could be large with leaching from the material during immersion and (b) rapid approach to saturation which could be high with some leaching from the material during immersion.

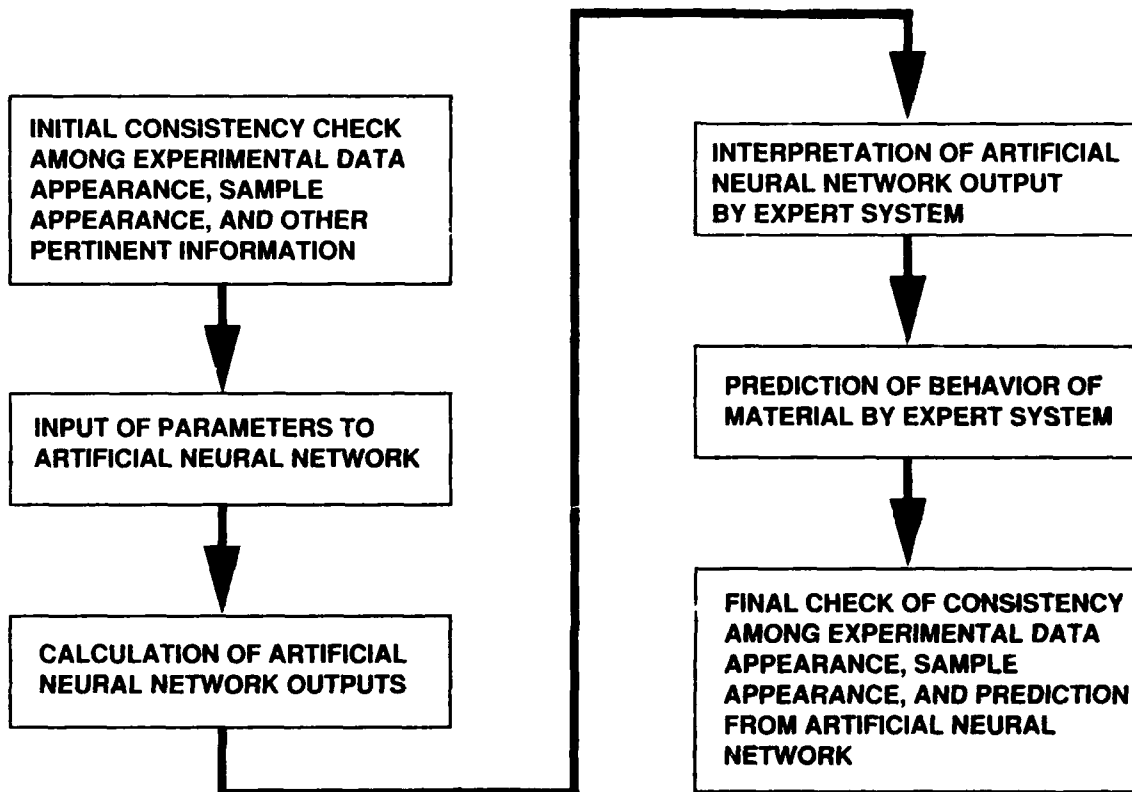


FIGURE 3. Structure of the information flow in the expert system with embedded artificial neural network.

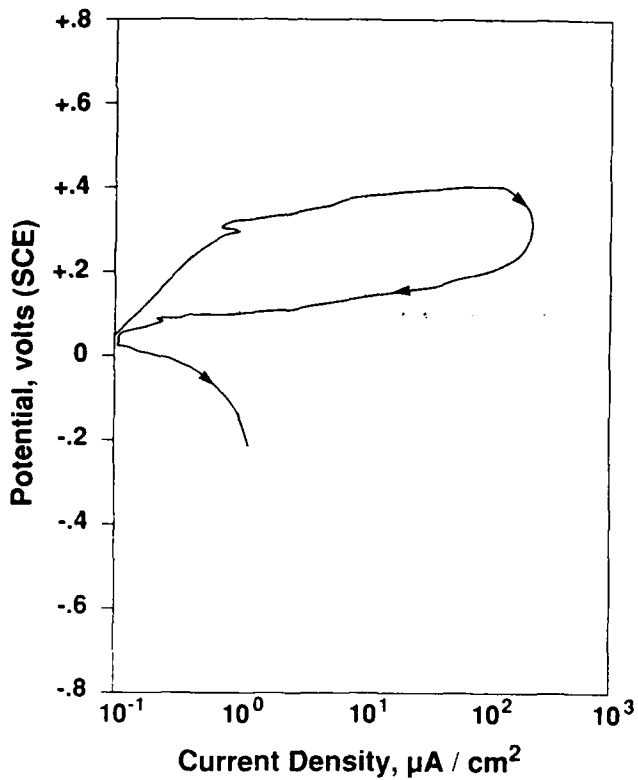


FIGURE 4. Polarization scan for 316 SS in process fluid at a pH of 4.5, 40°C (313K).

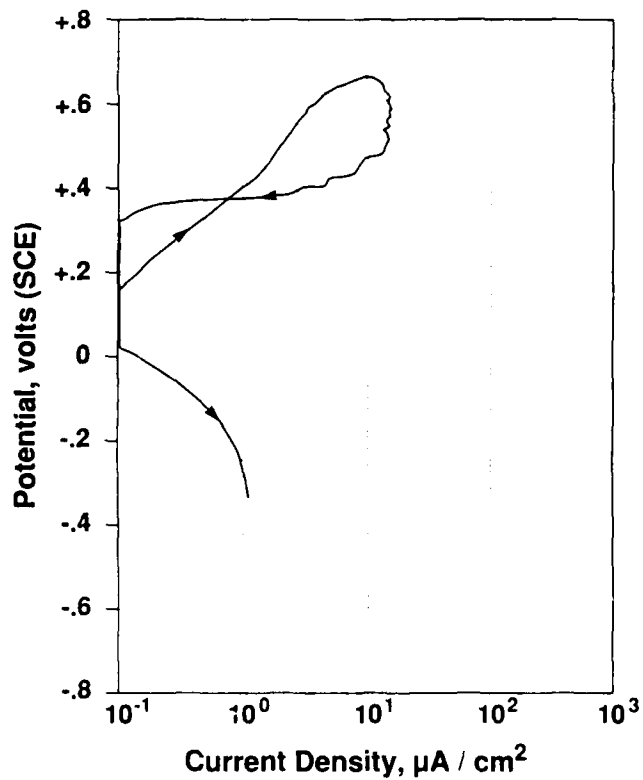


FIGURE 5. Polarization scan for Alloy 20Cb3 in process fluid at a pH of 4.5, 40°C (313K).

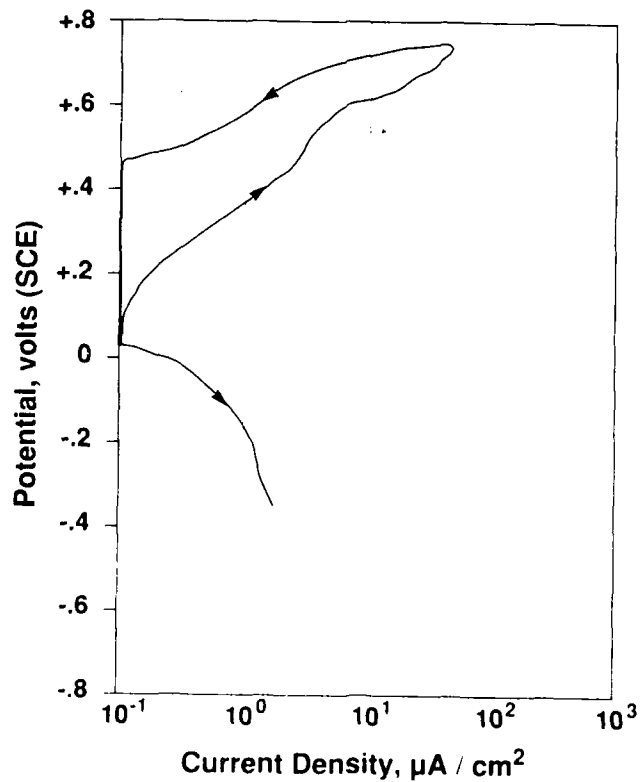


FIGURE 6. Polarization scan for Alloy 825 in process fluid at a pH of 4.5, 40°C (313K).

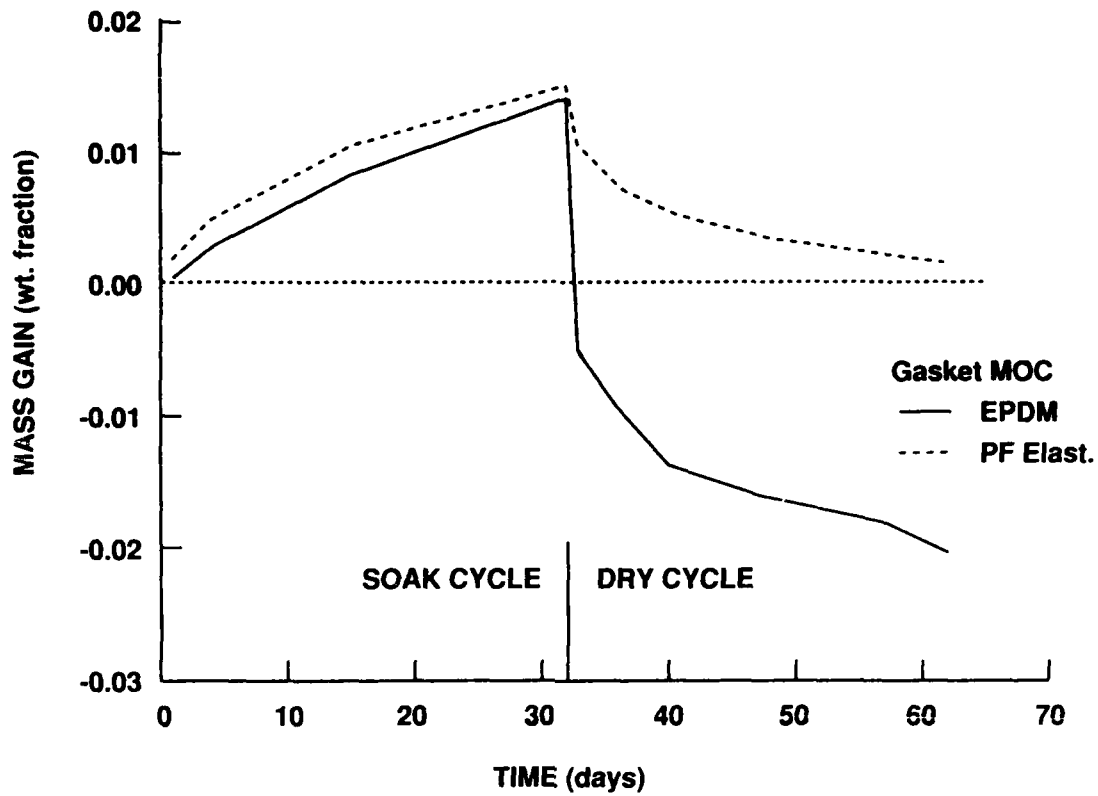


FIGURE 7. Mass fraction change versus time for gasket materials in process waste fluid at 49°C (322K).

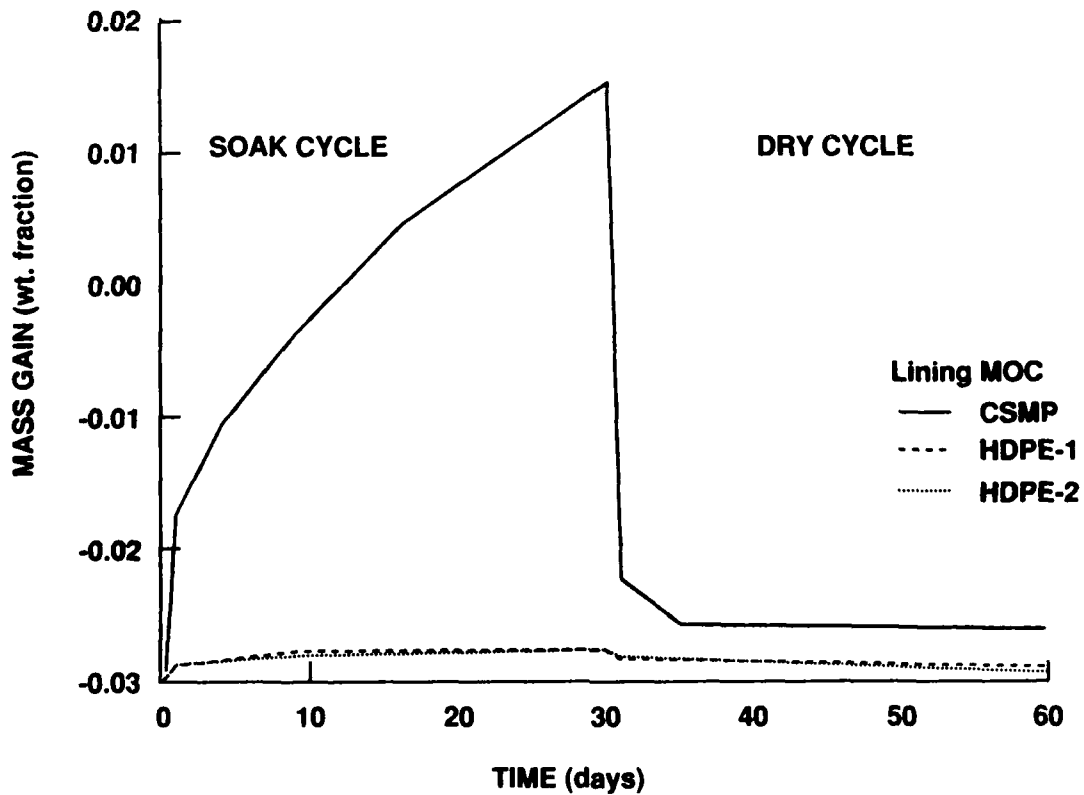


FIGURE 8. Mass fraction change versus time for lining materials in process waste fluid at 49°C (322K).

The Deterministic Prediction of Failure of Low Pressure Steam Turbine Disks

Chun Liu
Center for Advanced Materials
The Pennsylvania State University
University Park, PA 16802 USA

Digby D. Macdonald
Center for Advanced Materials
The Pennsylvania State University
University Park, PA 16802 USA

Abstract

Localized corrosion phenomena, including pitting corrosion, stress corrosion cracking, and corrosion fatigue, are the principal causes of corrosion-induced damage in electric power generating facilities and typically result in more than 50% of the unscheduled outages. Prediction of damage, so that repairs and inspections can be made during scheduled outages, could have an enormous impact on the economics of electric power generation. To date, prediction of corrosion damage has been made on the basis of empirical/statistical methods that have proven to be insufficiently robust and accurate to form the basis for the desired inspection/repair protocol. In this paper, we describe a deterministic method for predicting localized corrosion damage. We have used the method to illustrate how pitting corrosion initiates stress corrosion cracking (SCC) for low pressure steam turbine disks downstream of the Wilson line, where a thin condensed liquid layer exists on the steel disk surfaces. Our calculations show that the SCC initiation and propagation are sensitive to the oxygen content of the steam, the environment in the thin liquid condensed layer, and the stresses that the disk experiences in service.

Introduction

The progressive development of damage caused by the nucleation and growth of pits and stress corrosion cracks in various components in the heat transport circuits of light water (nuclear) reactors (LWRs) is recognized as a major contributor to unscheduled down time and hence to operating losses. The key issue is that damage forces unscheduled shutdowns, resulting in lost production and the need for the utility to purchase replacement power for its customers. If the development of damage can be predicted, then repairs could be made during scheduled shutdowns with a much lower impact on the economics of operation. Similarly, the economics of extending the operating lives of power reactors depends heavily on the prediction of corrosion damage that might occur in the future.

The extent of damage caused by localized corrosion, such as pitting and stress corrosion cracking, is best described in terms of the damage function¹, which is the histogram of the crack frequency (number of pits or cracks/unit area) versus pit or crack length, as shown schematically in Figure 1. In this scheme, we show three damage functions corresponding to different times of observation (t_1 , t_2 , t_3). Clearly, the lifetime of the component corresponds to the time required for the damage function to extend to a critical dimension, which is defined in purely engineering terms. In the case of stress corrosion cracking, the critical dimension might correspond to some physical length, such as the thickness of a pipe wall, or it may correspond to the length at which

the stress intensity (or some other fracture mechanics parameter) exceeds the value for fast (unstable) fracture (K_{IC}).

In this paper, we outline a deterministic approach for estimating the time for initiation and the kinetics of growth of cracks in reactor heat transport circuits. These techniques are then used to estimate times to failure (characterized by fast fracture) of reactor heat transport system components due to localized corrosion processes.

Why Deterministic Methods ?

Because of differences in design, materials of construction, and operating histories, each power plant (nuclear and fossil) is unique. As with living organisms, which are rendered prone to certain diseases because of inherent (genetic) defects and/or lifestyle factors, different types of power plants are more or less susceptible to different forms of corrosion-induced damage, which may range from being an operational nuisance to being fatal. However, the rate of development of damage is almost always a strong function of the history of operation, just as lifestyle greatly affects the onset of disease. It is the uniqueness of the relationship between the plant characteristics (design, materials, and operating history) and the rate at which damage develops that imposes a limit on the usefulness of statistically-based empirical methods, such as probabilistic analysis and extreme value statistics. The reason for this is simply that these empirical methods require an enormous amount of data and effort to characterize the damage and its dependence on system parameters, in order that reliable predictions can be made. This is particularly true for those regions of the heat transport circuit that are difficult to probe directly, such as the in-vessel regions of LWRs. In many cases, one essentially needs to know the answer (development of damage) in advance before predictions can be made. Clearly, in these cases, empirical methods are of marginal value.

The alternative approach is to devise mechanism-based, physico-chemical models for the development of damage, in much the same way that mechanics has been developed to describe statics and kinematics. In the limit, models of this type become entirely deterministic, in that future events (development of damage) can be determined from the present. In reality, because of the complex relationships that exist between the development of damage and the system parameters, we are unlikely to achieve pure determinism within the foreseeable future. Instead, an achievable goal appears to be models that are physically sound and realistic, but which contain unknown parameters that must be obtained by fitting the models to damage functions that have been measured under known conditions. However, it is important to note that this calibration procedure does not detract from the value of the model; but merely represents an indirect method of accessing various parameters. The critical requirement of any model is that it be realistically complex and that it obeys the natural laws of science. Otherwise, the model is non-deterministic, and any calibration of the model against experiment is empirical. These concepts are well developed in other branches of science and engineering (e.g. in mechanics and electrical engineering); however, they are only now being introduced into corrosion science and engineering.

As a case in point, consider the development of models for localized corrosion, such as pitting and stress corrosion cracking. Many models for these processes assume that the electrostatic potential at the crevice mouth is $\phi_s^m = -E_{corr}$, where E_{corr} is the corrosion potential of the steel in the environment. If this were the case, no current could flow from the crack to the external surfaces because of the lack of a potential gradient. Thus, if the cathodic process occurs on the external surfaces (which is generally the case in order to maintain occluded cell conditions), the models actually predict that localized corrosion cannot occur. These models are also fundamentally flawed because the fate of the current external to the crevice is not addressed.

This problem is probably best illustrated by considering an electrical equivalent circuit for a crack (Figure 2). Elementary circuit theory stipulates that the current (crevice growth rate) can only be determined if all of the voltages and resistances are specified. In essence, then, the problem of modeling an active crevice involves solving the potential dividing circuit for ϕ_c^m (Figure 2). To our knowledge, the only model that attempts to treat this problem in a quantitative manner, is the coupled environment fracture model (CEFM) that was developed several years ago to describe stress corrosion cracking of sensitized Type 304 stainless steel recirculation piping in boiling water reactors (BWRs)². Recognizing that the problem of specifying the electrostatic potential at the crack mouth is basically electrical in nature, the governing equation that must be satisfied is the conservation of charge, and any model that does not invoke this condition cannot be deterministic.

The Deterministic Prediction of Damage

The algorithm that has been developed in this program estimates the SCC initiation and failure times in a deterministic manner. Because stress corrosion cracking in steam components frequently initiates from pits, the module that estimates the SCC initiation time is a pit growth module. By specifying a critical dimension for SCC initiation, the pit growth module predicts the time at which the pit length reach that dimension. The module that estimates the crack growth rate and hence the failure time is in essence, the CEFM. By defining a critical dimension at which fast fracture (failure) occurs, the module predicts the time at which the crack reaches the critical size. The total time from pit initiation to fast fracture is defined as the service life of the component (low pressure steam turbine disk). The algorithm begins with the specification of the environment, including temperature, system composition, and various hydrodynamic parameters, if necessary. This information is then used in a series of modules to estimate various corrosion and electrochemical parameters, culminating in the calculation of the crack length and stress intensity as a function of time, from which the service life is estimated.

The Chemistry Module (CM). The chemistry module is designed to estimate the pH of the fluid in contact with the metal, as well as other parameters (e.g. oxygen concentration in the liquid at a liquid/gas interface). The module employs an equilibrium model, along with mass balance and charge balance constraints, and computes ion activity coefficients using the extended Debye-Huckel theory. The current module was designed to describe the chemistry of thin liquid films on metal surfaces, such as those that exist on the surfaces of low pressure steam turbines downstream of the Wilson line or on steam surface condensers. In each case, we assume that the liquid film is in equilibrium with the ambient environment, so that equilibrium calculations are applicable.

The Mixed Potential Module (MPM). The mixed potential module (MPM), which is based on the Wagner-Traud hypothesis³ for free corrosion processes, was developed to calculate the corrosion potentials of alloys in corrosive environments. The theory outlined here is essentially identical to that developed by Macdonald et al for calculating corrosion potentials for stainless steel components in the heat transport circuits of Boiling Water Reactors (BWRs)⁴⁻⁵. The theory is based on the physical condition that charge must be conserved in the system.

Because electrochemical reactions transfer charge across a metal/solution interface at a rate measured by the partial currents, charge conservation demands that

$$\sum_{j=1} i_{R/O,j}(E) + i_{\text{corr}}(E) = 0 \quad (1)$$

where $i_{R/O,j}$ is the partial current density due to the j -th redox couple in the system, and i_{corr} is the corrosion current density of the substrate. The currents are written as functions of the

potential E to emphasize the fact that the partial currents depend on the potential drop across the metal/solution interface. Indeed the solution to Eq.1 provides the quantity that we seek (the corrosion potential). Note that in deriving Eq.1, we assume that the surface of the alloy is equally accessible to all reactions in the system.

Calculated corrosion potentials for low pressure steam turbine disks are given in Figure 3 as a function of oxygen concentration and environmental variables in the condensed liquid phase. Oxygen reduction is the only cathodic reaction incorporated in the present considerations because it is believed to be the principal corrodent in steam turbine environments. It is predicted that oxygen in the steam has a significant influence on the corrosion potential, particularly at higher oxygen concentrations. Dependence of the corrosion potential on the composition of the condensed liquid phase is also demonstrated. However, at the extremely low oxygen concentrations normally present in turbine steam, the influence of the impurities in condensed liquid layer on the corrosion potential is predicted to be minimal (Figure 3).

The Coupled Environment Pit Growth and SCC Module. The Coupled Environment Pit Growth and SCC Module combines coupled environment models for calculating pit and crack growth rates. The pit growth module calculates the time at which an individual pit grows to a critical dimension, such that $K_I > K_{ISCC}$, and hence the pit transitions into a crack. The fracture module then calculates the crack propagation rate by incorporating appropriate mechanical parameters into the equations that describe events at the crack tip. This module was developed because a review of the available theoretical models for crack propagation indicated that only one of them could provide a deterministic prediction of the crack propagation rate. The problem is that most models for pitting and stress corrosion cracking fail to address the fate of the current that exits the crevice mouth, and which must be consumed by some cathodic reaction(s) on the external surfaces. In a previous study, Macdonald et al ² recognized this problem in developing their coupled environment fracture model (CEFM) for stress corrosion cracking in sensitized stainless steels in nuclear-reactor heat transport circuits. In that case, for high-resistivity water of the type employed in boiling water reactor heat transport circuits, it is theoretically predicted that the rate of crack growth is controlled by processes that occur in the external environment (e.g., oxygen reduction and ionic conduction), rather than by those that take place in the confine of the crack. Subsequently, although separately, workers at the Argonne National Laboratory ⁶ found experimentally that the kinetics of the crack growth in sensitized Type 304 stainless steel in high-temperature water are controlled by the rate of cathodic reactions that occur on the external surfaces and consume electrons released at the crack tip.

In light of the above, we selected a modified form of the CEFM as the most viable theory for estimating pit growth and crack propagation rates. This modified model incorporates a single algorithm to estimate the pit growth rate for $K_I < K_{ISCC}$ and the crack growth rate for $K_{ISCC} < K_I < K_{IC}$, where K_{ISCC} and K_{IC} are the critical stress intensities for slow crack growth and unstable (fast) fracture, respectively. This module also differs from the CEFM in that the thin electrolyte film that exists on the steel surface is modeled as an electrical transmission line of cylindrical geometry, rather than by solving Laplace's equation to obtain the net cathodic current consumed on the external surface.

A typical crevice on the metal surface in contact with a thin electrolyte film is shown in Figure 4. The crevice grows by the dissolution of metal occurring at the crevice tip. The principle of the transmission line approach is shown in Figure 5, which yields the following equation for the distribution of the electrostatic potential (ϕ_s) in the external environment.

$$\frac{d^2\phi_s}{dr^2} + \frac{1}{R} \frac{d\phi_s}{dr} - \frac{\rho}{hZ_s} \phi_s = 0 \quad (2)$$

where ρ is the resistivity ($\Omega \cdot \text{cm}$) of the solution, $R = \frac{\rho}{2\pi hr}$, is the resistance per unit length (Ω/cm) of the external solution, Z_s is the specific impedance ($\Omega \cdot \text{cm}^2$) of the external surface, h is the electrolyte film thickness, and r is the radial distance from the center of the cylindrical crevice. Note that Z_s is a function of distance, ($Z_s(r) = -(\phi_s - \phi_m) i_N^c$, where i_N^c is the net cathodic current density). The value of $Z_s(r)$ was determined iteratively when solving Eq. 2. We use the finite difference method to solve Eq. 2 for $\phi_s(r)$.

The distribution of the electrostatic potential within the crevice confine is obtained by solving the Laplace's equation, assuming that the the environment within the crevice confine is electrically neutral,

$$\nabla^2 \phi = 0 \quad (3)$$

The solution to Laplace's equation (Eq.3) yields the following expression assuming that the potential variation in the radial direction is negligible compared to that in the longitudinal direction:

$$\phi_s(z) = (\phi_s^0 - \phi_s^{-L}) \frac{z}{L} + \phi_s^0 \quad (4)$$

where ϕ_s^{-L} is the electrochemical potential at the crevice tip, and L is the pit depth. We also apply the Butler-Volmer equation to the electrodisolution reaction occurring at the crevice bottom to yield the electrochemical potential at the crevice tip as

$$\phi_s^{-L} = \phi_s^{00} + b_a \ln\left(\frac{i_0^0 A_t}{I_0}\right) \quad (5)$$

where ϕ_s^{00} is the (negative of the) standard electrochemical potential for the dissolution of the metal outside the crevice, i_0^0 is the standard exchange current density, b_a is the anodic Tafel constant for metal dissolution, and A_t is the effective active surface at the crevice tip, defined as follows,

$$A_t = \frac{2A_0}{\left(\frac{t_f}{t_0}\right)^{1/2}} + A_{pit} \quad (6)$$

where A_{pit} is the active area for pitting corrosion, $2A_0 / \left(\frac{t_f}{t_0}\right)^{1/2}$ is the equivalent area for crack propagation, t_0 is a constant, and t_f is the period of fracture of the passive film. A justification of Eq. 6 will be published at a later date.

The fracture frequency of the passive film is simply equal to the inverse of fracture period, or,

$$f_r = 1/t_f \quad (7)$$

where, as before ^{2,7}

$$f_r = 4.11 \times 10^{-11} K_I^4 (s^{-1}) \quad (8)$$

The stress intensity is calculated as

$$K_I = \sigma \sqrt{\pi L} \quad (9)$$

where σ is the applied stresses, and L is the length of the crack. For $K_I \leq K_{ISCC}$, the crevice develops by pitting corrosion, but when $K_I = K_{ISCC}$, a stress corrosion cracking initiates. The crack then propagates over $K_{ISCC} \leq K_I \leq K_{IC}$ by environmental-assisted fracture, but when $K_I \geq K_{IC}$ the crack leads to fast fracture (failure). Figure 6 illustrates the stages of development of a pit into a crack that results in fast fracture as the stress intensity reaches the critical value of K_{IC} .

Discussion

General Features

The model for coupled pitting corrosion and intergranular stress corrosion cracking developed in this work differs from previous models in a number of important aspects. The principal innovation is coupling of the internal and external environments explicitly through the conservation of charge, which must be satisfied by any electro-physico-chemical system. The model recognizes that pit or crack growth is determined by processes occurring both in the internal (crevice) environment and in the external environment. The processes taking place in the external environment include the reduction of oxygen, which consumes the positive current exiting the crevice mouth, and the ionic conduction through the external solution. In recognition of the fact that SCC is initiated by pitting corrosion, a single model is employed to describe propagation of the crevice for $K_I < K_{ISCC}$ (pitting) and $K_{ISCC} < K_I < K_{IC}$ (SCC). Accordingly, the model reveals the effects of mechanical properties (through stress intensity) on the crack growth rate, because increasing stress intensity raises the strain rate at the crack tip and hence increases the frequency of rupture of the passive film.

The Effect of Oxygen Concentration

The predicted effect of oxygen on the corrosion potential for the steel is presented in Figure 3. The data show a sharp increase in the corrosion potential as the oxygen in the electrolyte film increases from 1 ppb to 1 ppm, especially in the case that the electrolyte film is highly acidic. The principal role of oxygen in the external environment is to consume the positive current exiting crevice tip. Higher oxygen concentration in the external environment shortens the SCC initiation time and ultimately the failure time (Figure 14). However, the calculation indicates that the increase in oxygen concentration from 1 ppb to 1 ppm reduces the SCC initiation and the failure time (fast fracture) by a factor of only 2 to 3, suggesting that the control of oxygen is not the prime factor in extending the life of a turbine disk.

The Distribution of Potential Within the Crevice

The predicted variations in the electrostatic potential in the solution along the crevice is shown in Figure 7. The electrostatic potential distribution within the crevice varies with time as the crevice develops from a pit into a crack. During pitting stage, at a time = 4.59×10^5 s, the potential

increases by only 20 mV from the crevice mouth to the crevice tip for a crevice length of 6.0×10^{-3} cm. On the other hand, for a time of 5.25×10^6 s, after the pit has developed into a crack, we calculate that the potential increases more than 300 mV from the crevice mouth to the crevice tip. The crack length in this instance is equal to 0.536 cm. The potential and concentration gradients in the crack are the driving forces for the ionic current resulting from the dissolution of the metal at the crevice tip. Higher potential and concentration gradients are associated with a higher crevice growth rate.

The Distribution of pH Within the Crevice

The pH distribution in the crevice is illustrated in Figure 8. Acidification within the crevice is predicted during both the SCC initiation and propagation stages. The extent of acidification of a stress corrosion crack is a matter of great controversy, largely because of the difficulty of measuring pH in the confined space. Our calculation indicates that the extent of acidification, as reflected by $\Delta\text{pH} = \text{pH}(\text{crevice tip}) - \text{pH}(\text{crevice mouth})$ increases sharply as the crevice develops from a pit into a crack.

The Distribution of Species Concentration Within the Crevice

Distributions of various species down the crevice are shown for the cases of pit growth and the crack propagation, in Figures 9 and 10, respectively. The environment within the pit confine is predicted to be enriched in chloride ion to compensate the positive charge injected into the crevice by dissolution of the metal at the crack tip. The concentration profiles for the major species in the crevice are predicted to be flat near the crevice tip but are found to decrease substantially near the crevice mouth and eventually approach the concentrations in the external environment.

The Distribution of Potential in the External Environment

The distribution of the electrostatic potential in the external environment is presented in Figure 11. The calculation indicates that the electrostatic potential increases rapidly near the crevice mouth. At a time $= 4.59 \times 10^5$ s, during pitting stage, the increase in potential at the crevice mouth of 420 mV is predicted for a crevice of length equal to 6.0×10^{-3} cm. However, at a time of 5.25×10^6 s, after the pit develops into a crack, the increase in potential is calculated to be 610 mV for a crack length of 0.536 cm is predicted. In both cases, the potential drop occurs principally within a distance about 50 times the crevice radius. The rise in the potential in the external environment is the driving force for throwing the ionic current from the crevice mouth to the external surface.

The Distribution of Anodic and Cathodic Currents in the External Environment

The calculated distributions of the anodic and cathodic currents across the external surface are given in Figures 12 and 13. It is found that a small area exists around the crevice that is cathodically protected, where the anodic current is equal to zero. The radius of the cathodically protected area is about 25 times the radius of the crevice in the SCC initiation stage and about 50 times the radius of the crevice in the SCC propagation stage. The increase in the electrostatic potential in the solution gives rise to a net cathodic current, which, when integrated radially from the crevice, is equal to the positive current exiting the crevice mouth. At a sufficiently large distance from the crevice, the electrostatic potential equals the negative of the free corrosion

potential. At this point, the cathodic current equals the anodic current, resulting in the total current being equal to zero.

Failure in Low Pressure Steam Turbines

The calculated effect of oxygen concentration in the external environment on the SCC initiation and failure times (resulting from fast fracture) is illustrated in Figure 14. As stated earlier, the role of oxygen in the external environment is to consume the current exiting the crevice mouth, and we predict that higher oxygen concentrations shorten the time for both SCC initiation and failure, hence resulting in a short service life. Our calculation indicates that an increase in the oxygen concentration from 1 ppb to 1 ppm results in a decrease of the failure time by a factor of only 2 to 3.

The predicted effects of conductivity and of pH in the external environment (by varying the concentration of NaCl and HCl) on the SCC initiation time and failure are given in Figures 15 and 16. It is shown that the conductivity of the external environment has a strong effect on the SCC initiation and failure time. Increasing the concentrations of NaCl and HCl by a factor of 10^5 decreases the failure time at 450 K from ~ 100 years to a little more than one year.

The calculated effect of stresses (applied and residual) on the SCC initiation and failure times is presented in Figure 17. Because the stress determines the critical crack length and because higher stresses result in higher crack growth rates, it is not surprising that our calculations indicate that stress has a great impact on the the SCC initiation and failure times. It is predicted that reducing the stresses by a factor of 3, from 300 MPa to 100 MPa, leads to an increase in the time for SCC initiation and failure by as much as an order of magnitude.

Summary and Conclusions

The crack growth rates calculated in this work ($\sim 1.5 \times 10^{-7}$ cm/s, Figure 6) compare well with those reported in the literature (typically $1-2 \times 10^{-7}$ cm/s⁸), even though no particular attempt was made to reproduce the experimental data. Importantly, our calculations indicate that provided concentrated electrolyte solutions are prevented from forming at the disk surface, failure is unlikely to occur within a 40 year design life, even if the oxygen level is allowed to rise to the 0.1-1 ppm level in the condensate. This may explain the successful operation of many fossil plants worldwide on high oxygen water treatment without significant incidents of LP turbine failure. However, we predict that if concentrated electrolytes are allowed to form on the disks due to the transitioning of the Wilson line, rapid failure could result. Finally, our calculations predict that stress is a significant factor in determining the total failure time, and that a reduction in stress by a factor of three will increase the failure time by a factor of almost ten. This is principally the result of an increase in the critical crack length for the onset of fast fracture, because the crack growth rate is predicted to be only weakly-dependent on the stress intensity factor once a pit has transformed into a crack.

Acknowledgments

The authors gratefully acknowledge the support of this work by the US Department of Energy / Basic Energy Sciences through Grant No. DE-DG03-84ER45164.

References

1. D. D. Macdonald and M. Urquidi-Macdonald, "The Corrosion Damage Functions, Interface Between Science and Engineering," 1992 Whitney Award Address, NACE, Nashville, TN, submitted to Corrosion (1992).

2. D. D. Macdonald and M. Urquidi-Macdonald, *Corros. Sci.*, 32, 51 (1991).
3. C. Wagner and W. Traud, *Z. Electrochem.*, 44, 391 (1938).
4. D. D. Macdonald, *Corrosion* 48, 194 (1992).
5. D. D. Macdonald, Proc. 5th Int. Symp. Environ. Degrad. Mat. Nucl. Power Systs. - Water Reactors, Monterey, CA, August, 1991, (NACE, Houston, TX).
6. W. J. Shack, T. F. Kassner, J. Y. Park, W. E. Ruther, and W. K. Soppet, "*Environmentally Assisted Cracking in Light Water Reactors*," Argonne National Laboratory Report to the U.S. Nuclear Regulatory Commission, ANL-89/40, NUREG/CR-4667, Vol. 7 (March 1990).
7. F. P. Ford and M. J. Silverman, *Corrosion*, 36, 597, (1980).
8. J. Y. Liu, E. E. Lai, C. C. Su and H. C. Lai, Proc. 5th Int. Symp. Environ. Degrad. Mat. Nucl. Power Systs. - Water Reactors, Monterey, CA, August, 1991, (NACE, Houston, TX).

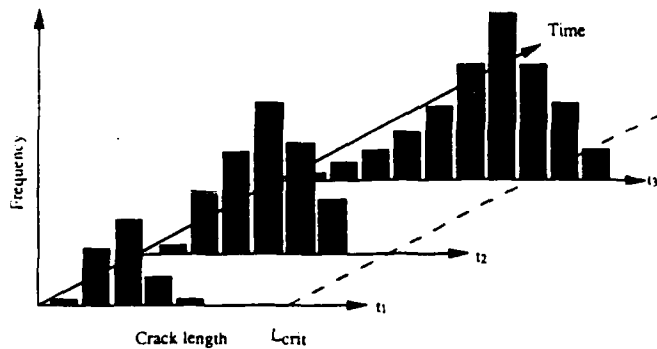


FIGURE 1 Schematic damage functions for three exposure times (t_1 , t_2 , t_3). The broken line represents a critical dimension (L_{crit}) defined in engineering terms (e.g. pipe wall thickness, corrosion allowance, or crack length for the onset of fast fracture).

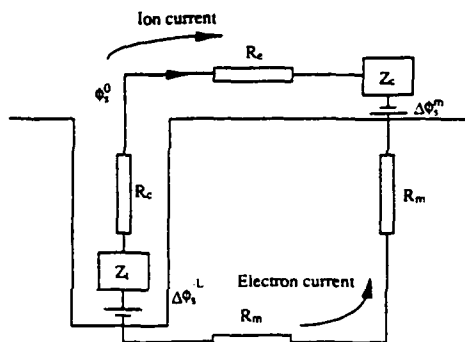


FIGURE 2 Simplified electrical analog for localized corrosion. R_c = resistance of solution in the crevice, R_e = resistance of external solution, R_m = metal resistance, Z_c = impedance at crevice tip (Voltage drop = $\Delta\phi_c^L$), Z_c = impedance due to the cathodic reaction on the external surfaces (Voltage drop = $\Delta\phi_s^m$), ϕ_s^L = electrostatic potential at the crevice mouth.

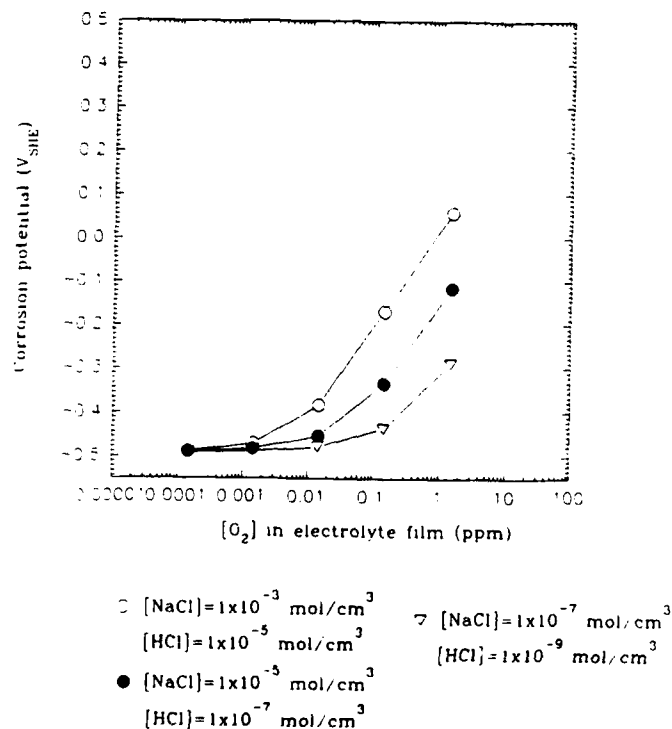


FIGURE 3 The corrosion potential of steel as a function of the oxygen concentration and of the impurities (NaCl and HCl) in the thin electrolyte film ($T=453\text{K}$, $h=1.0 \times 10^{-3} \text{ cm}$)

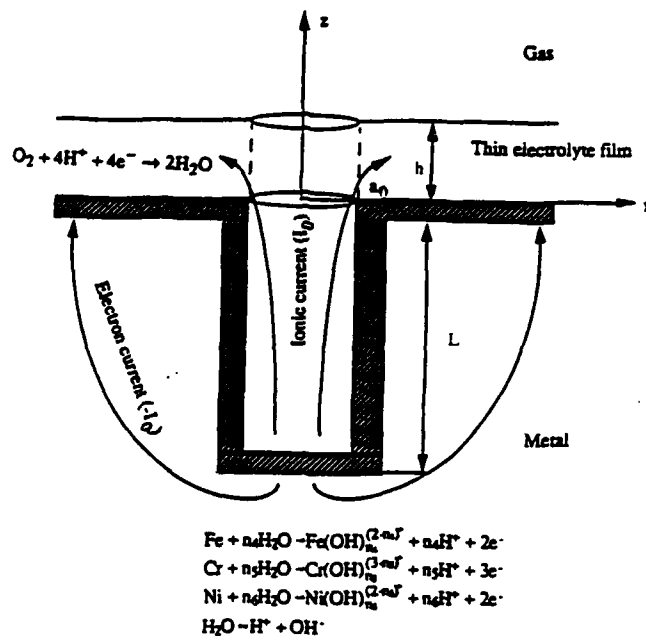
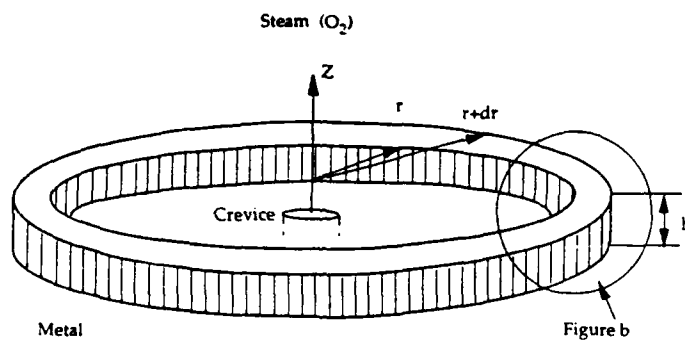
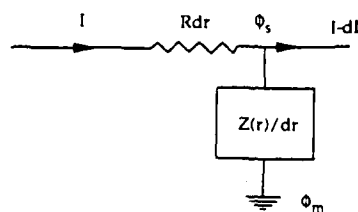


FIGURE 4 Schematic of a crevice on the surface of a disk in a low pressure steam turbine.



(a) Element of electrolyte film on the metal surface



(b) Element of transmission line for calculating current and potential distributions radially from the crevice mouth

FIGURE 5 Transmission line model for thin electrolyte film on the metal surface

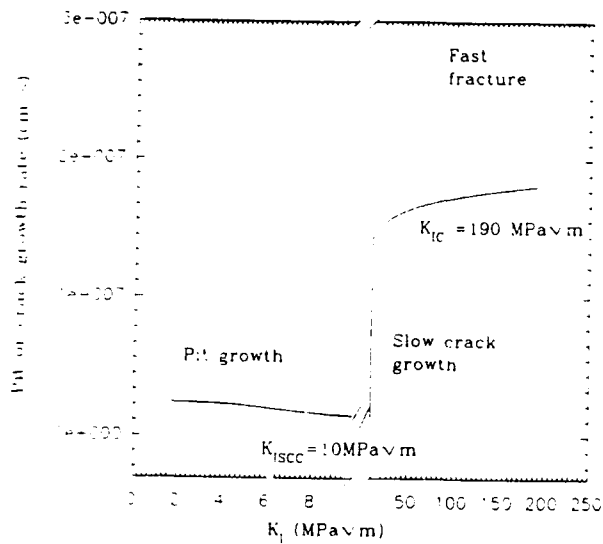


FIGURE 6 Stages of development of a pit into a crack, ultimately resulting in fast fracture, presented as a plot of growth rate versus stress intensity ($T=453\text{K}$, $[\text{NaCl}]=1.0 \times 10^{-3} \text{ mol/cm}^3$, $[\text{HCl}]=1.0 \times 10^{-10} \text{ mol/cm}^3$, $[\text{O}_2]=1.0 \text{ ppm}$, $\sigma=3.0 \times 10^2 \text{ MPa}$, $h=1.0 \times 10^{-3} \text{ cm}$, $a_0=5.0 \times 10^{-5} \text{ cm}$, $L_0=1.0 \times 10^{-3} \text{ cm}$)

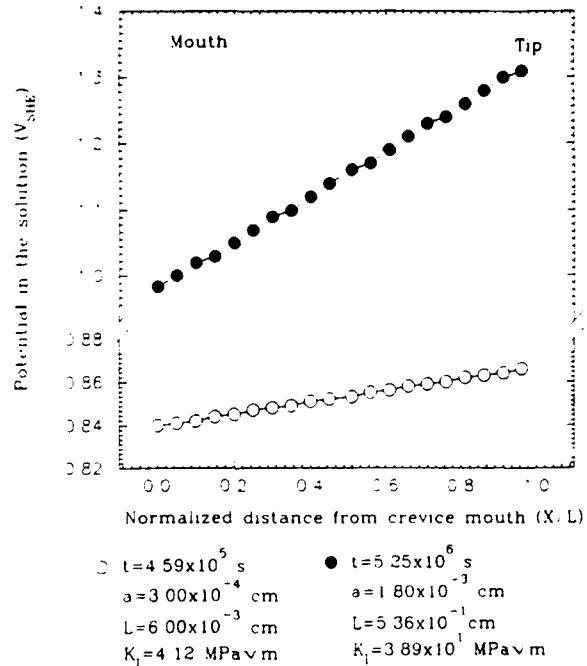


FIGURE 7 Calculated potential versus normalized distance down the crevice during pit growth and during crack growth. (○ at time= $4.59 \times 10^5 \text{ s}$, $K_I < K_{I,SCC}$, pit growth, ● at time= $5.25 \times 10^6 \text{ s}$, $K_I > K_{I,SCC}$, crack growth $T=453\text{K}$, $[\text{NaCl}]=10^{-3} \text{ mol/cm}^3$, $[\text{HCl}]=10^{-10} \text{ mol/cm}^3$, $[\text{O}_2]=1.0 \text{ ppm}$, $\sigma=3.0 \times 10^2 \text{ MPa}$, $h=1.0 \times 10^{-3} \text{ cm}$, $a_0=5.0 \times 10^{-5} \text{ cm}$, $L_0=1.0 \times 10^{-3} \text{ cm}$)

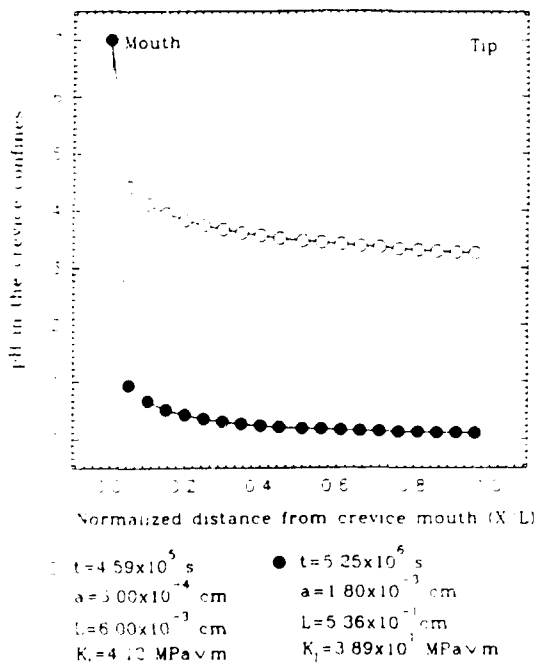


FIGURE 8 Calculated pH versus normalized distance down the crevice during pit growth and during crack growth (○ at time= $4.59 \times 10^5 \text{ s}$, $K_I < K_{I,SCC}$, pit growth, ● at time= $5.25 \times 10^6 \text{ s}$, $K_I > K_{I,SCC}$, crack growth $T=453\text{K}$, $[\text{NaCl}]=10^{-3} \text{ mol/cm}^3$, $[\text{HCl}]=10^{-10} \text{ mol/cm}^3$, $[\text{O}_2]=1.0 \text{ ppm}$, $\sigma=3.0 \times 10^2 \text{ MPa}$, $h=1.0 \times 10^{-3} \text{ cm}$, $a_0=5.0 \times 10^{-5} \text{ cm}$, $L_0=1.0 \times 10^{-3} \text{ cm}$)

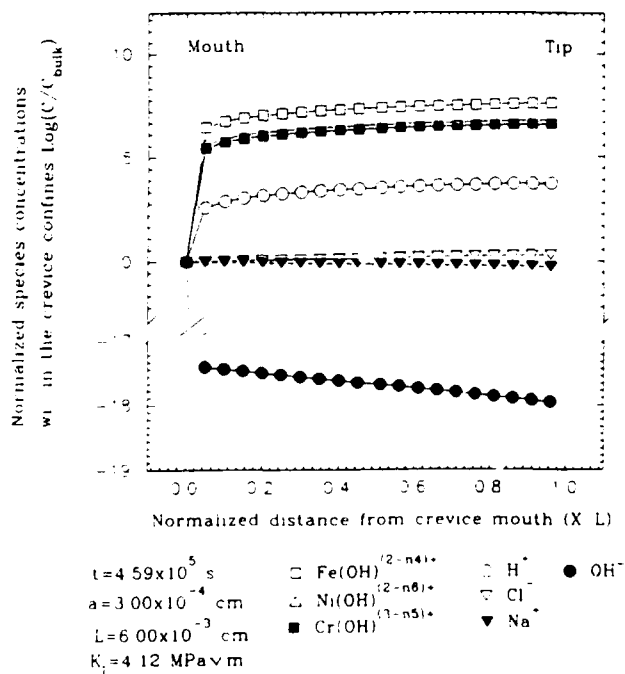


FIGURE 9 Calculated normalized species concentrations versus normalized distance down the crevice during pit growth (Time= $4.59 \times 10^5 \text{ s}$, $K_I < K_{I,SCC}$, $T=453\text{K}$, $[\text{NaCl}]=10^{-3} \text{ mol/cm}^3$, $[\text{HCl}]=10^{-10} \text{ mol/cm}^3$, $[\text{O}_2]=1.0 \text{ ppm}$, $\sigma=3.0 \times 10^2 \text{ MPa}$, $h=1.0 \times 10^{-3} \text{ cm}$, $a_0=5.0 \times 10^{-5} \text{ cm}$, $L_0=1.0 \times 10^{-3} \text{ cm}$)

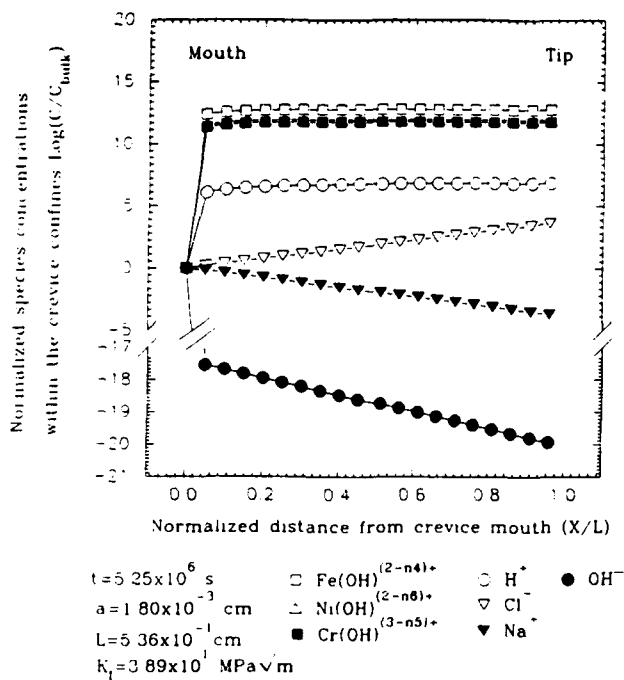


FIGURE 10 Calculated normalized species concentrations versus normalized distance down the crevice during crack growth. (Time = 5.25×10^6 s, $K_I > K_{I,SCC}$, $T = 453$ K, $[NaCl] = 10^{-3}$ mol/cm³, $[HCl] = 10^{-10}$ mol/cm³, $[O_2] = 1.0$ ppm, $\sigma = 3.0 \times 10^2$ MPa, $h = 1.0 \times 10^{-3}$ cm, $a_0 = 5.0 \times 10^{-5}$ cm, $L_0 = 1.0 \times 10^{-3}$ cm)

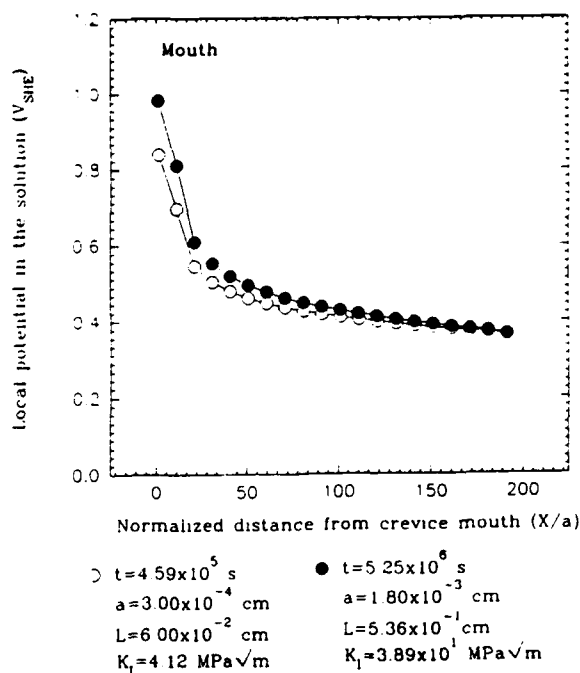


FIGURE 11 Calculated potential versus normalized distance across the external surface from the pit edge during pit growth and during crack growth (○ at time = 4.59×10^5 s, $K_I < K_{I,SCC}$, pit growth, ● at time = 5.25×10^6 s, $K_I > K_{I,SCC}$, crack growth $T = 453$ K, $[NaCl] = 10^{-3}$ mol/cm³, $[HCl] = 10^{-10}$ mol/cm³, $[O_2] = 1.0$ ppm, $\sigma = 3.0 \times 10^2$ MPa, $h = 1.0 \times 10^{-3}$ cm, $a_0 = 5.0 \times 10^{-5}$ cm, $L_0 = 1.0 \times 10^{-3}$ cm)

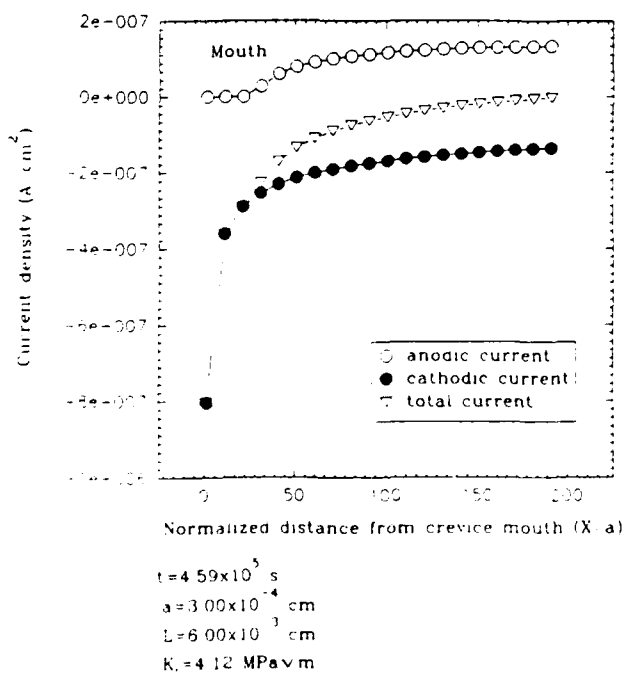


FIGURE 12 Calculated current versus normalized distance across the external surface from the pit edge during pit growth (Time = 4.59×10^5 s, $K_I < K_{I,SCC}$, $T = 453$ K, $[NaCl] = 10^{-3}$ mol/cm³, $[HCl] = 10^{-10}$ mol/cm³, $[O_2] = 1.0$ ppm, $\sigma = 3.0 \times 10^2$ MPa, $h = 1.0 \times 10^{-3}$ cm, $a_0 = 5.0 \times 10^{-5}$ cm, $L_0 = 1.0 \times 10^{-3}$ cm)

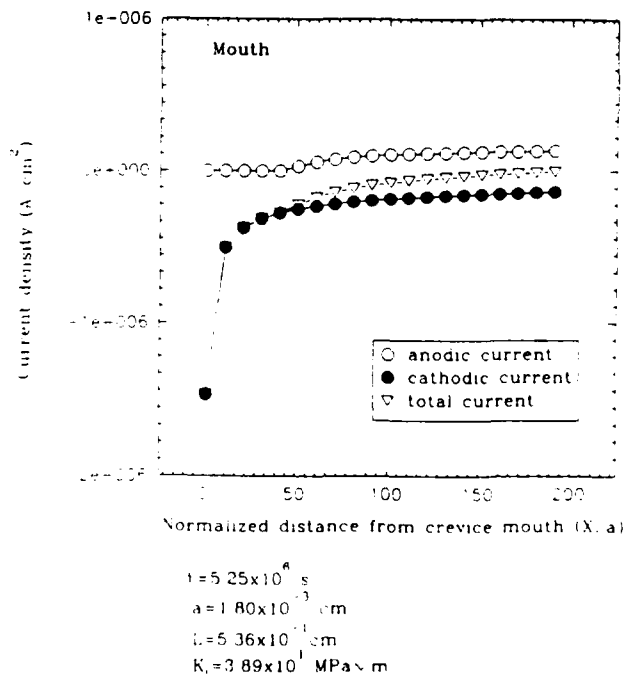


FIGURE 13 Calculated current versus normalized distance across the external surface from the pit edge during crack growth (Time = 5.25×10^6 s, $K_I > K_{I,SCC}$, $T = 453$ K, $[NaCl] = 10^{-3}$ mol/cm³, $[HCl] = 10^{-10}$ mol/cm³, $[O_2] = 1.0$ ppm, $\sigma = 3.0 \times 10^2$ MPa, $h = 1.0 \times 10^{-3}$ cm, $a_0 = 5.0 \times 10^{-5}$ cm, $L_0 = 1.0 \times 10^{-3}$ cm)

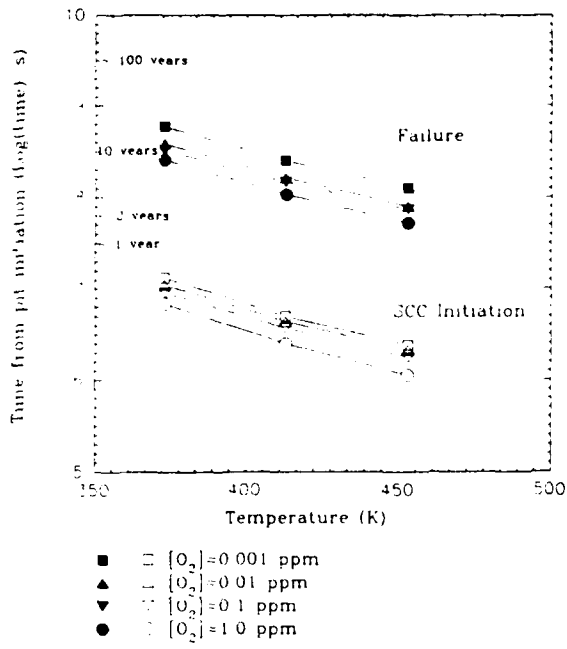


FIGURE 14 Calculated crack initiation ($K_I \rightarrow K_{I,SCC}$) and failure ($K_I \rightarrow K_{I,C}$) times for a low pressure steam turbine disk as a function of temperature and oxygen concentration ($[NaCl]=10^{-3} \text{ mol/cm}^3$, $[HCl]=10^{-5} \text{ mol/cm}^3$, $\sigma=300 \text{ MPa}$, $h=1.0 \times 10^{-3} \text{ cm}$, $a_0=5.0 \times 10^{-5} \text{ cm}$, $L_0=1.0 \times 10^{-3} \text{ cm}$, $K_{I,SCC}=10 \text{ MPa}\sqrt{\text{m}}$, $K_{I,C}=190 \text{ MPa}\sqrt{\text{m}}$)

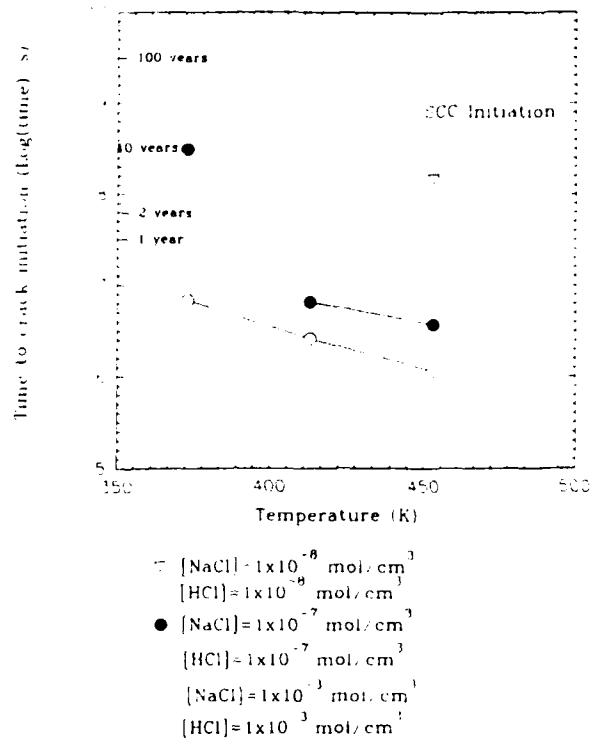


FIGURE 15 Calculated crack initiation ($K_I \rightarrow K_{I,SCC}$) time for a low pressure steam turbine disk as a function of temperature and electrolyte composition ($[O_2]=1.0 \text{ ppm}$, $\sigma=3.0 \times 10^2 \text{ MPa}$, $h=1.0 \times 10^{-3} \text{ cm}$, $a_0=5.0 \times 10^{-5} \text{ cm}$, $L_0=1.0 \times 10^{-3} \text{ cm}$, $K_{I,SCC}=10 \text{ MPa}\sqrt{\text{m}}$, $K_{I,C}=190 \text{ MPa}\sqrt{\text{m}}$)

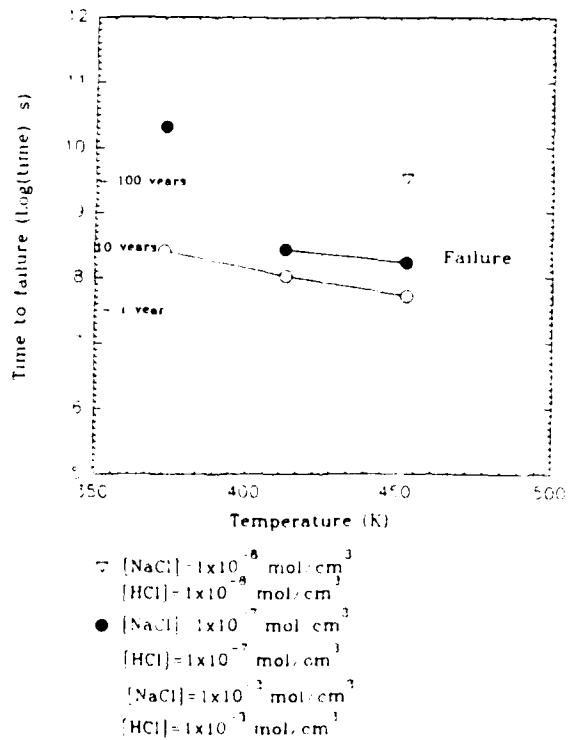


FIGURE 16 Calculated failure ($K_I \rightarrow K_{I,C}$) time for a low pressure steam turbine disk as a function of temperature and electrolyte composition ($[O_2]=1.0 \text{ ppm}$, $\sigma=3.0 \times 10^2 \text{ MPa}$, $h=1.0 \times 10^{-3} \text{ cm}$, $a_0=5.0 \times 10^{-5} \text{ cm}$, $L_0=1.0 \times 10^{-3} \text{ cm}$, $K_{I,SCC}=10 \text{ MPa}\sqrt{\text{m}}$, $K_{I,C}=190 \text{ MPa}\sqrt{\text{m}}$)

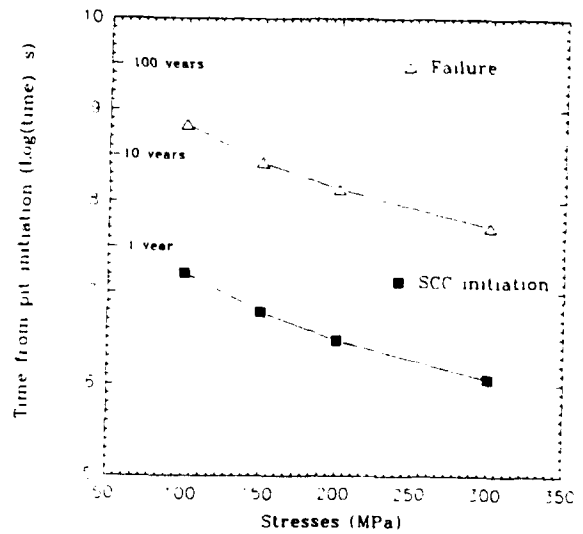


FIGURE 17 Calculated crack initiation ($K_I \rightarrow K_{I,SCC}$) and failure ($K_I \rightarrow K_{I,C}$) times for a low pressure steam turbine disk as a function of stress ($T=453 \text{ K}$, $[O_2]=1.0 \text{ ppm}$, $[NaCl]=10^{-3} \text{ mol/cm}^3$, $[HCl]=10^{-5} \text{ mol/cm}^3$, $h=1.0 \times 10^{-3} \text{ cm}$, $a_0=5.0 \times 10^{-5} \text{ cm}$, $L_0=1.0 \times 10^{-3} \text{ cm}$)

Prediction of Pitting Damage Functions For Condensing Heat Exchangers

Digby D. Macdonald
Center for Advanced Materials
The Pennsylvania State University
University Park, PA 16802 USA

Chun Liu
Center for Advanced Materials
The Pennsylvania State University
University Park, PA 16802 USA

Mirna Urquidi-Macdonald
Department of Engineering Science and Mechanics
The Pennsylvania State University
University Park, PA 16802 USA

Abstract

Pitting corrosion is a form of extremely localized attack resulting in rapid penetration into a metal substrate, and is one of the most destructive and insidious forms of corrosion that occurs in industrial systems. Traditionally, the damage function, i.e., the number of pits versus the pit depth, is measured experimentally, and the development of damage is described using empirical models. In general, the empirical models are successful because the distribution functions employed display great mathematical flexibility, but they require a significant database to achieve reliability. In fact, they are only really successful when the answer is known in advance. In this study, we developed a deterministic method for predicting localized corrosion damage functions for condensing heat exchangers. The method incorporates calculations for the composition of the condensed environment and the electrochemical corrosion potential of the alloy, and includes mechanistic treatments of the nucleation and the growth of pits. The role of the important environmental parameters are identified, such as the chloride concentration and the partial pressure of oxygen. Good agreement is observed between the predicted damage functions and the experimental data.

Introduction

The National Appliance Energy Conservation Act of 1987 requires that by 1992 all gas furnaces with heat output greater than 45,000 BTU/hour must be more than 78% efficient. These efficiencies can be achieved only by using condensing or near-condensing heat exchangers. Heat exchangers in which a liquid phase comes in contact with the metal surface are very susceptible to corrosion because of the presence of chloride in the condensate from the exhaust which results in various forms of localized attack (including pitting corrosion, stress corrosion cracking, and intergranular attack), depending on the alloy used for fabricating the tubes. Extensive corrosion testing carried out by Battelle Columbus Laboratories¹ on more than thirty potential tube materials has shown that only Alloys C-276 and AL29-4C, and plastic-coated galvanized steel, are immune to corrosion damage in condensing heat exchanger environments. However, the sensitivity of the cost of a furnace to the chosen tube material is such that it is desirable to reduce the cost of the condenser substantially (by about 50%), which can only be achieved by employing cheaper (but less corrosion-resistant) tube alloys. Thus, selection of the most cost-effective alloy for a specified design life under a given set of operating conditions (duty cycle,

combustion parameters, and condensate chemistry - chloride concentration, pH, etc.) requires methods for predicting the extent of corrosion damage to the heat exchanger.

In this paper, we outline a deterministic method for predicting the damage function for pitting corrosion in condensing heat exchangers. This method is considered to be potentially superior to empirical (including stochastic and probabilistic) techniques, because it is mechanistically-based and hence provides analytical relationships between the damage function (number of pits versus pit depth presented in the form of histogram²) and the damaging variables (chloride concentration, combustion parameters, etc.). Accordingly, deterministic methods are expected to be more efficient at using databases, because a lesser need exists to establish the damage function/damaging variable relationships empirically.

From our point of view, any deterministic model must account for the fact that localized corrosion involves nucleation and growth phenomena which occur sequentially for a single site, but that tend to occur in parallel for an ensemble of pits. Furthermore, the model must account for the experimental observation that the parameters that characterize the breakdown event are distributed, due to the fact that the population of sites on any real surface is not homogeneous. Outlined below is one model that satisfies these (and many other) conditions related to the nucleation and growth of damage resulting from localized corrosion. While the model may not be complete (or even correct), it is deterministic, in that the distribution function and the relationships between the model parameters and the damage function are analytic. In illustrating this technology, we have chosen to discuss the prediction of the damage function for pitting corrosion, because this form of attack is almost ubiquitous in condensing heat exchangers. Furthermore, pitting corrosion displays most of the features of all forms of localized attack, including an induction time and the autocatalytic development of the damage.

The algorithm developed in this study to estimate the damage functions for condensing heat exchanger contains five modules as outlined in Figure 1. Also indicated are the parameters that are propagated from one module to the next. The output of the algorithm can be specified in three forms:

- (1) For a specified probability of failure, the algorithm estimates the damage function as a function of exposure time and computes the number of pits with lengths exceeding the condenser wall thickness to predict the *service life*.
- (2) For a specified probability of failure and design life, the algorithm calculates the *wall thickness* to ensure acceptable performance.
- (3) For a specified wall thickness and design life, the algorithm calculates the *failure probability*.

Below we describe the various modules in this algorithm; however, due to the limited space available, we outline only the principles of these modules.

The Condensed Chemistry Module (CCM)

The composition of the flue gas will differ from burner to burner. With this in mind, we developed a generalized condensate model for the condensate environment. This model assumes the flue gas to be a mixture of CO, CO₂, H₂S, NO, NO₂, SO₂, SO₃, and H₂O. The relative proportions of these components may vary widely from furnace to furnace, depending on the nature of the ambient air, the air/gas ratio, and on the impurities of the gas. The goal of the Condensate Chemistry Module is to calculate the pH and the composition of the condensate on

the condenser surface. The pH is a key parameter in controlling the rates of pit nucleation and pit growth. The concentrations of species in the liquid layer determine the ionic conductivity of the solution, which has great impact on the pit growth rate. The module employs an equilibrium model along with mass balance and charge balance constraints, and computes ion activity coefficients using the extended Debye-Huckel theory. We assume that the condensed liquid film is in equilibrium with the ambient environment, so that equilibrium calculations are applicable. Details of this module are described in the literature.³

A typical gas-fired heat exchanger is schematically shown in Figure 2a.⁴ The temperature ranges from approximately 308 K in the cold end to 353 K in the hot end, depending on the design of the heat exchanger. Typical values of the pH and chloride concentration in these different zones are given in Figure 2b.⁴ It is shown that the condensed liquid phase is enriched in chloride in the hot end to the extent of approximately 150 ppm. Acidification of the condensed thin liquid layer is also found, in that pH values as low as 2.7 and 3.3 are found at the hot end and the cold end, respectively. In Figure 2c we present the computed pH for a typical composition of the flue gas and the chloride content of the condensate. Our calculation shows a variation in pH from 2.93 to 3.32 from the hot end down to the cold end. Recognizing the wide range of operating conditions and designs of condensing heat exchangers, it is concluded that good agreement is observed between the experimental data and theoretical prediction.

The Mixed Potential Module (MPM)

The mixed potential module (MPM), which is based on the Wagner-Traud hypothesis⁵ for free corrosion processes, was developed to calculate the corrosion potentials of alloys in corrosive environments. The theory outlined here is essentially identical to that developed by Macdonald et al for calculating corrosion potentials for stainless steel components in the heat transport circuits of Boiling Water Reactors (BWRs).⁶⁻⁷ The theory is based on the physical condition that charge must be conserved in the system.

Because electrochemical reactions transfer charge across a metal/solution interface at a rate measured by the partial currents, charge conservation demands that

$$\sum_{j=1} i_{R/O,j}(E) + i_{\text{corr}}(E) = 0 \quad (1)$$

where $i_{R/O,j}$ is the partial current density due to the j -th redox couple in the system, and i_{corr} is the corrosion current density of the substrate. The currents are written as functions of the potential E to emphasize the fact that the partial currents depend on the potential drop across the metal/solution interface. Indeed, the solution to Eq. (1) provides the quantity that we seek (the corrosion potential). Note that in deriving Eq. (1), we assume that the surface of the alloy is equally accessible to all reactions in the system.

Experimental polarization curves and kinetic data for the reduction of oxygen on Alloy AL29-4C were used as input to the Mixed Potential Module. The module then calculates the corrosion potential of the alloy under the service condition, as shown in Figure 3. The calculation indicates that if the solution is saturated with oxygen, the corrosion potential is only weakly dependent upon the temperature. However, as the partial pressure of oxygen is reduced to 10^{-4} atm, as in the case of an operating condensing heat exchanger, the corrosion potential varies from -290 mV to -460 mV as the temperature increases from 300 to 370 K.

The Pit Nucleation Module (PNM)

As a result of an intensive effort over the past decade to develop an understanding of the breakdown of passive films, we have derived theoretical distribution functions for passivity breakdown that are in good agreement with experiments.⁸⁻¹¹ We derived these distribution functions from our point defect model for the growth and breakdown of passive films, by assuming that breakdown occurs when a critical concentration of cation vacancies accumulates locally at the metal/passive-film interface, such that decohesion occurs between the barrier layer and the metal substrate. Subsequently, localized dissolution and/or mechanical instability leads to rupture of the film.⁸ We further assumed that the breakdown sites are normally distributed with respect to the diffusivity of cation vacancies within the film.⁹⁻¹¹ The full derivation of these distribution functions can be found in the literature.⁸⁻¹¹

From the point defect model,⁸ the breakdown voltage and the induction time for a single pit nucleation site on the surface are given by

$$V_c = \frac{4.606 RT}{\chi \alpha F} \log \left[\frac{J_m}{J^o \hat{u}^{-\chi/2}} \right] - \frac{2.303 RT}{\alpha F} \log(a_x) \quad (2)$$

and

$$t_{ind} = \xi' \left[\exp \left(\frac{\chi \alpha F \Delta V}{2RT} \right) - 1 \right]^{-1} + \tau \quad (3)$$

respectively, where χ is the film stoichiometry ($MO_{\chi/2}$), α is the dependence of the potential drop across the film/solution interface on applied voltage, a_x is the activity of halide ion in the solution, τ is a relaxation time ($\tau \sim 0$), $\Delta V = V - V_c$, V is the applied voltage (or the corrosion potential under open circuit conditions).

$$J^o = \hat{a} D \quad (4)$$

and

$$\hat{a} = \chi K \left[\frac{N_v}{\Omega} \right]^{1+\frac{\chi}{2}} \exp \left[-\Delta G_v^o / RT \right] \quad (5)$$

The parameters u and J_m are defined in the original derivation.⁸

Assuming that the breakdown sites are normally distributed in terms of the cation vacancy diffusivity,

$$\frac{dN}{dD} = \frac{1}{\sqrt{2\pi}\sigma_D} \exp \left[-\frac{(D-\bar{D})^2}{2\sigma_D^2} \right] \quad (6)$$

where \bar{D} is the mean diffusivity and σ_D is the standard deviation, the point defect model yields the following expressions for the distributions in the breakdown voltage and induction time⁹⁻¹¹:

$$\frac{dN}{dV_c} = -\frac{\hat{\gamma} D}{\sqrt{2\pi}\sigma_D} \cdot e^{-(D-\bar{D})^2/2\sigma_D^2} \quad (7)$$

and

$$\frac{dN}{dt_{ind}} = \left[\frac{\xi u^{z/2}}{\sqrt{2\pi} \sigma_D \hat{a}} \right] e^{-(D-\bar{D})^2 / 2\sigma_D^2} \cdot \frac{e^{-\hat{\gamma}}}{a_x^{z/2} (t_{ind} - \tau)^2} \quad (8)$$

where

$$\hat{\gamma} = \chi F \alpha / 2RT \quad (9)$$

Eqs. (7) and (8) contain four important system parameters; \bar{D} and σ_D which describe the transport properties of cation vacancies in the passive film, and α and β which appear in the expression for the dependence of the potential drop across the film/solution interface on applied voltage and pH

$$\phi_{f/s} = \alpha V + \beta_{pH} + \phi_{f/s}^0 \quad (10)$$

All four parameters can be determined by independent experiment: \bar{D} from electrochemical impedance spectroscopy, σ_D from passivity breakdown induction time measurements,⁸ and α and β from film growth data, much of which exists in the literature. Accordingly, Eqs. (7) and (8) represent analytical distribution functions for the nucleation of pitting attack, provide that the assumptions in the model hold. Our previous work⁹⁻¹¹ has demonstrated the quantitative nature of these expressions for representing experimental distribution in V_c and t_{ind} , for those cases where sufficient experimental data are available for analysis.

The Pit Growth Module (PGM)

The pit growth module computes the pit growth rate of an individual pit. Figure 4 shows schematically a typical pit that develops on the surface of a metal in contact with a thin liquid layer. The module developed in this study calculates the pit growth rate for a pit of cylindrical geometry. Details of the theoretical approach can be found in the literature^{12,13}, except that we develop a transmission line analog of the external environment from which the distributions in the electrostatic potential and the current in the external environment, as a function of distance away from the pit, can be estimated.

The principle of the transmission line approach is shown in Figure 5, which yields the following equations for the distributions in the electrostatic potential (ϕ_s) and the current in the external environment

$$\frac{d^2 \phi_s}{dr^2} + \frac{1}{r} \frac{d\phi_s}{dr} - \frac{\rho}{hZ_s} \phi_s = 0 \quad (11)$$

$$\frac{d^2 I}{dr^2} - \frac{1}{r} \frac{dI}{dr} - \frac{\rho}{hZ_s} I = 0 \quad (12)$$

where ρ is the resistivity ($\Omega \cdot \text{cm}$) of the solution, Z_s is the specific impedance ($\Omega \cdot \text{cm}^2$) of the external surface, h is the electrolyte film thickness, and r is the radial distance from the center of the cylindrical pit. Note that Z_s is a function of distance, ($Z_s(r) = -(\phi_s - \phi_m) / i_N^c$, where i_N^c is the net cathodic current density). The value of $Z_s(r)$ was determined iteratively when solving Eq. (11) by substituting for the net current density the following expression

$$i_N^c = \frac{e^{-(\phi_s - \phi_s^*)/b_a} - e^{(\phi_s - \phi_s^*)/b_c}}{\frac{1}{i_0} + \frac{1}{i_{l,f}} e^{-(\phi_s - \phi_s^*)/b_a} - \frac{1}{i_{l,r}} e^{(\phi_s - \phi_s^*)/b_c}} + i_p(\phi_s) \quad (13)$$

where the first term on the right hand side is the generalized Butler-Volmer equation for the oxygen electrode reduction



and the second is the polarization current of the substrate, both of which are function of the potential difference across the interface. The parameters ϕ_s^* , i_0 , $i_{l,f}$, $i_{l,r}$, b_a and b_c in Eq. (13) are the (negative) of the equilibrium potential for Reaction (14), i_0 is the exchange current density, $i_{l,f}$ and $i_{l,r}$ are the limiting current densities for Reaction (14) in the forward and reverse directions, respectively, and b_a and b_c are the corresponding Tafel constants. Note that the signs of the exponents in the first term in Eq. (13) are opposite to those normally defined, because we have written the current in terms of the electrostatic potential in the solution with respect to the metal. We use the finite difference method to solve Eqs. (11) and (12) for $\phi_s(r)$ and $i_c(r)$, respectively.

The distribution of the electrostatic potential within the pit is obtained by solving Laplace's equation, assuming that the environment within the pit confine is electrically neutral,

$$\nabla^2 \phi = 0 \quad (15)$$

The solution to Laplace's equation (Eq. (15)) yields the following expression, assuming that the potential variation in the radial direction is negligible compared to that in the longitudinal direction,

$$\phi_s(z) = (\phi_s^0 - \phi_s^{-L}) \frac{z}{L} + \phi_s^0 \quad (16)$$

where ϕ_s^{-L} is the electrochemical potential at the pit tip, L is the pit depth, and z is a negative quantity. We also apply the Butler-Volmer equation to the electrodisolution reaction occurring at the pit bottom to yield the electrochemical potential at the pit tip as^{6, 14}

$$\phi_s^{-L} = \phi_s^{00} + b_a \ln\left(\frac{i_0 A}{I_0}\right) \quad (17)$$

where ϕ_s^{00} is the (negative of the) standard electrochemical potential for the dissolution of the metal, i_0^0 is the standard exchange current density, b_a is the anodic Tafel constant for metal dissolution, and A_t is the effective active surface at the pit tip. The model outlined above is a variant of the Coupled Environment Fracture Model (CEFM) that we developed some time ago¹⁵ for describing crack growth in stainless steel piping in nuclear power reactor heat transport circuits. Thus, following out previous work,¹⁵ Eqs. (11), (12), (16) and (17) are solved for the unknowns $\phi_s(r)$, $i_c(r)$, and I_0 , such that charge conservation, expressed as

$$I_0 + \int_S i_c^N dS = 0 \quad (18)$$

is obeyed, where I_0 is the (positive) current exiting the pit mouth and dS is an increment of the external surface ($dS=2\pi r dr$). Because the cathodic current due to oxygen reduction predominates on the external surface, the second term on the left side of Eq. (18) is negative. Once I_0 is known, then pit growth rate is calculated using Faraday's law:

$$\frac{dL}{dt} = \frac{\bar{M}I_0}{2\rho_m \bar{Z}FA} \quad (19)$$

where ρ_m is the density of metal (g/cm^3), \bar{M} is the composition-averaged atomic weight of the alloy, and \bar{Z} is the composition-weighted oxidation state of the metal dissolving at the pit tip. Finally, the pit length is calculated as a function of time using the recursive formula:

$$L(t) = L(t-1) + \frac{dL}{dt} \Delta t \quad (20)$$

where $L(t-1)$ is the depth of the pit calculated from the previous time ($t-1$), and Δt is the increment in time.

The Damage Function Module (DFM)

By combining Eqs. (8) and (20), for a fixed density of potential breakdown sites (N_0 , number/cm²), it is possible to estimate the pitting damage function. Thus, if one observes the system at time t_{obs} , then the number of pits that nucleate over the time increment Δt at t_{ind} is ΔN , as determined from Eq. (8). However, these pits will have grown to a depth $L(t)$, as given by Eq. (20), at the time the system is examined. By moving the increment Δt from $t=\tau$ to $t=t_{\text{obs}}$, we then generate the damage function in the form of the number of pits versus the depth of the pits. If this procedure is repeated for different observation times, a family of damage functions is generated that extends to greater depth with increasing t_{obs} .

By specifying the surface area of interest, it is possible to define the service life as the time taken for one or more pit to grow to the critical length, which in this case corresponds to the wall thickness of the condensing heat exchanger. The number of pits whose the length exceeds the critical dimension is simply calculated as

$$N|_{L \geq L_{\text{crit}}} = S \sum_{L_{\text{crit}}}^{L_{\text{max}}} N(L) \cdot \Delta L \quad (21)$$

where $N(L)$ is the density of pits per unit surface area and per unit increment in pit length (number/cm³) in the damage function, S is the surface area of interest (cm²), L is the pit length, ΔL is the increment of the pit length in the damage function, and L_{crit} is the critical dimension. The service life is simply the time at which $N|_{L \geq L_{\text{crit}}} = 1$.

Discussion

The procedure outlined above for estimating damage functions for localized corrosion is currently being developed to explore the impact of corrosion on condensing heat exchangers in domestic and industrial gas-fired furnaces. The practical problem lies in selecting the most cost-effective alloys for the condensing stages of heat exchangers, because of the highly competitive nature of the furnace manufacturing business. Consequently, little room exists for "over-

designing" furnaces by employing highly-alloyed and costly materials for fabricating the condensing sections. Therefore, selection of materials with adequate pitting resistance, and of acceptable cost, is of prime concern to furnace manufacturers and users, alike. It is evident, then, that the design and materials specifications for condensing heat exchangers would greatly benefit from the development of a deterministic method for predicting localized corrosion damage functions. This, in turn, could reduce the cost of the alloy by decreasing the required database, through the availability of deterministic relationships between the damage function and important environmental variables (including pH, $[Cl^-]$, gas composition).

In this study, we present predictions of the model in comparison with experimental damage functions measured on Type 304L SS by G. Stickford, B. Hindin and A. K. Agrawal of The Battelle Columbus Laboratories. For the experimental data, the damage functions are measured on condensing heat exchanger tubes after a given number of cycles, at the hot end (temperature ranging from 326 to 353 K) and at the cold end (temperature ranging from 308 to 326 K). Each cycle consists of 240 s with burner on and 480 s with burner off, which represent the "dry" and "wet" conditions, respectively. It was shown in a previous study,⁴ that no significant difference exists in the damage functions between the hot end and the cold end; the damage functions are therefore plotted without distinguishing between the hot ends and cold ends. Based on this experimental finding, the model is constrained to the case where the surface is covered at all times by a condensing liquid phase (wet condition). However, we choose the appropriate temperature at the hot end to calculate the damage functions in order to avoid "under-estimating" the damage.

The experimental data reported by Battelle were measured at 3 levels of chloride concentration (3, 26, and 225 ppm) on a number of different candidate alloys. We present in this study only the damage functions for Type 304L SS, as shown in Figures 6, 7, and 8, as a function of chloride concentration. Not surprisingly, fewer pits are observed at the lower chloride concentration (3 ppm, Figure 6). At higher chloride levels (26, 225 ppm), the number of pits increases substantially (Figures 7, 8) and leads to perforation of the wall in shorter times, hence reducing the service life. However, the experimental data show some inconsistencies, which are due to the fact that different tubes are used to determine the damage functions in each case. The chemical composition, the metallurgical history, and the surface state may vary from tube to tube.

Because, the kinetics of the cathodic oxygen reaction on Alloy AL29-4C are considered to be essentially identical to those on Type 304L SS, the parameters for AL29-4C are chosen for calculating the corrosion potential that is used in estimating the damage functions (Table 1). Calculated damage functions are presented in Figures 9 through 12 for chloride levels of 3, 10, 26 and 225 ppm. The calculations clearly indicate the progressive nature of the nucleation and growth of pits on the alloy surface. It is predicted that at lower chloride concentration (3 ppm), fewer pits exist on the surface of the steel, while at higher chloride concentrations (26 to 225 ppm), the number of pits increases substantially, leading to the majority of the pits perforating the wall thickness in a short period of time.

The predicted service life is presented as a function of chloride concentration in Figure 13, in comparison with the experimental data. The calculations indicate that the service life of a condensing heat exchanger is highly sensitive to the chloride level in the condensate, especially at the lower chloride concentration (3 ppm). The principal effect of increasing chloride is to accelerate pit nucleation, so that, in the limit of very high chloride concentration, (~ 100 ppm) in the condensate, the failure time is dominated by pit growth. Because the pit growth rate is dominated by the conductivity of the external environment (the condensate film), for any given pH and oxygen concentration, and because the conductivity is dominated by non-chloride species, the failure time thus becomes constant at sufficiently high chloride levels. This corresponds to the situation where the entire service life is determined by the time required for

the pits that nucleate on initial exposure of the alloy to condensate, to grow through the condenser wall. Noting that the service life for the case shown in Figure 13 is calculated to decrease from 1.55×10^8 s (4.92 years) for a chloride concentration of 3 ppm to 2.34×10^7 s (0.74 year) for a chloride concentration of 225 ppm, it is evident that the time required of an active pit to perforate the wall is about 3/4 of a year, corresponding to an average pit growth rate of 0.7 mm/year. Clearly, then, the increase in the service life on lowering the chloride concentration is due almost entirely to an increase in the initiation time, and it would seem that substantial service lives for this alloy can only be obtained if nucleation becomes the dominant phase in the development of damage. Finally, we note that due to the fact that different tubes are used in determining the damage functions, the experimental data are rather scattered. In recognition of this observation, relatively good agreement is claimed between the experimental data and the theoretical prediction.

The influence of the oxygen partial pressure on the development of damage functions has been calculated, and is shown in Figure 14. The calculations indicate that oxygen has a great impact on the service life of heat exchangers. This is because oxygen, in the condensed liquid phase on the external surface, consumes the positive current associated with the pit tip dissolution process, thereby driving the growth of the pit. It is found that, by decreasing the partial pressure of oxygen from 10^{-4} atm to 10^{-8} atm, the service life of a heat exchanger having the characteristics assumed in this work could be extended from 3.02×10^7 s (1 year) to 1.05×10^9 s (approximately 30 years).

Summary and Conclusions

A deterministic model has been developed to predict the damage functions for condensing heat exchangers in gas-fired furnaces. The model incorporates calculations for the condensed chemistry environment, the electrochemical corrosion potential of the alloy, and mechanistic treatments of the nucleation and the growth of pits.

The model predicts that the chloride concentration in the condensed liquid layer has great impact on the service life of the condensing heat exchanger, particularly at low chloride concentrations. At high chloride concentrations, the service life of the condensing heat exchanger is predicted to be relatively independent of the chloride concentration, corresponding to the dominance of pit growth in determining the failure time. The service life for the condensing heat exchanger with Type 304L SS tubes is predicted to decrease from 1.55×10^8 s (4.92 years) for a chloride concentration of 3 ppm to 2.34×10^7 s (0.742 year) for a chloride concentration of 225 ppm.

The model predicts that the service life of the condensing heat exchanger also depends strongly on the oxygen content in the flue gas; by decreasing the partial pressure of oxygen from 10^{-4} atm to 10^{-8} atm, the service life of the condensed heat exchanger can be extended from 3.02×10^7 s (1 year) to 1.05×10^9 s (approximately 30 years).

Recognizing the scattered nature of the experimental data, we conclude that the algorithm developed in this work provides estimates of the service life that are in good agreement with the available experimental data, even though, no a priori fit of the experimental data to the model was made.

Acknowledgments

The authors gratefully acknowledge the support of this work by the Gas Research Institute (GRI) through Contract No. 5090-260-1969, and G. Stickford, B. Hindin, and A. K. Agrawal at The

Battelle Columbus Laboratories for supporting the experimental damage functions used in this study.

References

1. R. Razgaitis, J. H. Payer, S. G. Talbet, B. Hindin, E. L. White, D. W. Locklin, R. A. Cudnik, and G. H. Stickford, "*Condensing Heat Exchanger Systems for Residential/Commercial Furnaces and Boilers*," Phase II, Battelle Report to DOE/BNL, BNL Report No. 51943, Oct. 1985.
2. D. D. Macdonald and M. Urquidi-Macdonald, "*The Corrosion Damage Functions, Interface Between Science and Engineering*," 1992 Whitney Award Address, NACE, Nashville, TN, submitted to Corrosion (1992).
3. D. D. Macdonald, M. Urquidi-Macdonald, S. D. Bhakta, N. Khalil and H. Yashiro, "*Development of Analytical Methods for Predicting Damage Functions for Pitting Corrosion in Condensing Heat Exchangers*," Final report, GRI No 5090-260-1969, Jan. 1992.
4. G. H. Stickford, B. Hindin, S. G. Talbert, A. K. Agrawal, M. J. Murphy, R. Razgaitis, J. H. Payer, R. A. Cudnik, and D. W. Locklin, "*Technology Development for Corrosion-Resistant Condensing Heat Exchanger*," Final Report to the Gas Research Institute, GRI-85/0282 (October 1985) NTIS PB86-172038.
5. C. Wagner and W. Traud, *Z. Electrochem.*, 44, 391 (1938).
6. D. D. Macdonald, *Corrosion* 48, 194 (1992).
7. D. D. Macdonald, Proc. 5th Int. Symp. Environ. Degrad. Mat. Nucl. Power Systs. - Water Reactors, Monterey, CA, August, 1991, (NACE, Houston, TX).
8. L. F. Lin, C. Y. Chao, and D. D. Macdonald, *J. Electrochem. Soc.*, 128, 1194 (1981).
9. D. D. Macdonald and M. Urquidi-Macdonald, *Electrochim. Acta*, 31, 1079 (1986).
10. D. D. Macdonald and M. Urquidi-Macdonald, *J. Electrochem. Soc.*, 134, 41 (1987).
11. D. D. Macdonald and M. Urquidi-Macdonald, *J. Electrochem. Soc.*, 136, 961 (1989).
12. D. D. Macdonald, M. Urquidi-Macdonald, Chun Liu, S. Bhakta, N. Khalil and H. Yashiro, Proc. Int. Gas Res. Conf., Nov. 92, Orlando, FL, USA.
13. D. D. Macdonald, M. Urquidi-Macdonald and Chun Liu, CORROSION 93, Paper # 173, Mar. 1993, New Orleans, LA, USA.
14. F. P. Ford and M. Silverman, *Corrosion*, 36, 597, (1980).
15. D. D. Macdonald and M. Urquidi-Macdonald, *Corros. Sci.*, 32, 51 (1991).

Table 1. VALUES FOR PARAMETERS USED IN CALCULATING DAMAGE FUNCTIONS

| PARAMETER | VALUE | UNITS |
|--------------------------------------------------------------------|-----------------------|------------------------------|
| χ (Passive film stoichiometry) | 3 | |
| Ω (Mole volume of passive film) | 30 | cm ³ /gm cation |
| ΔG_{A-1}^0 (Gibbs energy of Cl ⁻ absorption) | -60 | kJ/mol |
| $\phi_{f/s}^0$ (Constant) | -0.375 | V |
| ΔG_s^0 (Gibbs energy of cation vacancy formation) | 20 | kJ/mol |
| τ (Relaxation time) | 0 | s |
| ϵ (Electric field strength) | 1×10^6 | V/cm |
| α (Constant) | 0.25 | |
| β (Constant) | -0.001 | V |
| ξ (Critical areal concentration of vacancies) | 1×10^{16} | No/cm ² |
| J_m (Vacancy flux in metal phase) | 0.12×10^7 | Vacancies/cm ² .s |
| \bar{D} (Standard deviation in cation vacancy diffusivity) | 1.0×10^{-18} | cm ² /s |
| σ_D (Standard deviation in cation vacancy diffusivity) | $0.5\bar{D}$ | cm ² /s |

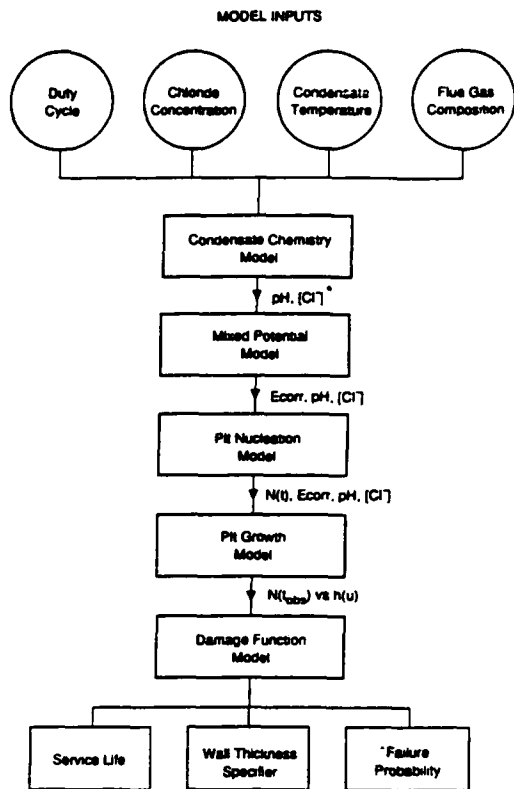


FIGURE 1. Structure of the algorithm for the prediction of damage function (* Parameters propagated from one model to the next).

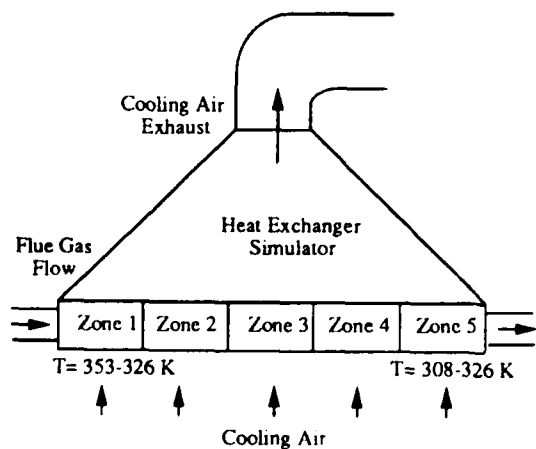


FIGURE 2a. Scheme of a typical heat exchanger in a gas-fired furnace⁴.

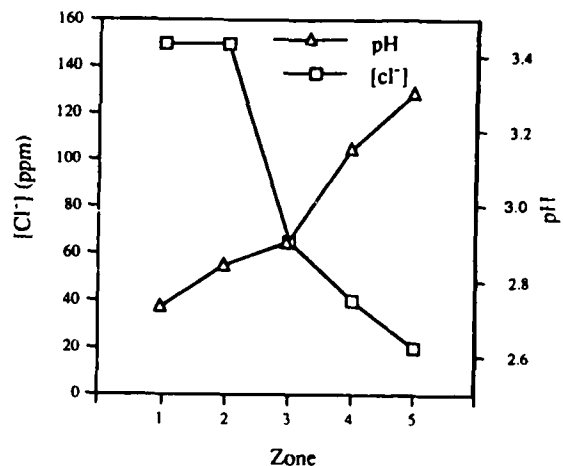


FIGURE 2b. Characteristics of flue-gas condensate from different zones⁴.

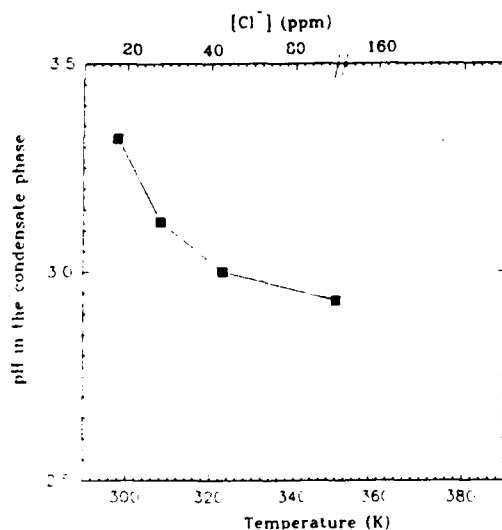


FIGURE 2c. Calculated pH in the condensate as a function of temperature and chloride concentration ($P_{CO}=2.60 \times 10^{-5}$ atm, $P_{CO_2}=6.80 \times 10^{-2}$ atm, $P_{SO_2}=9.37 \times 10^{-9}$ atm, $P_{SO_3}=2.00 \times 10^{-9}$ atm, $P_{H_2S}=1.20 \times 10^{-4}$ atm, $P_{NO}=1.74 \times 10^{-8}$ atm, $P_{NO_2}=2.67 \times 10^{-8}$ atm, $P_{O_2}=1.00 \times 10^{-4}$ atm).

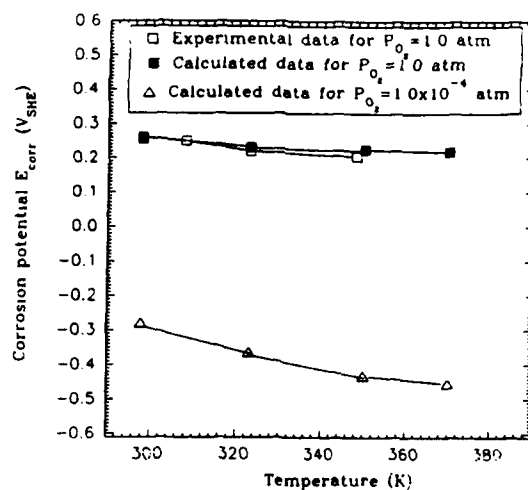


FIGURE 3. Calculated and measured corrosion potential as a function of temperature and partial pressure of oxygen for alloy Al29-4C (The solution composition for the experimental measurement: $[HCl]=200$ ppm, $[HF]=40$ ppm, $[H_2SO_4]=20$ ppm, $P_{CO}=2.60 \times 10^{-5}$ atm, $P_{CO_2}=6.80 \times 10^{-2}$ atm, $P_{SO_2}=9.37 \times 10^{-9}$ atm, $P_{SO_3}=2.00 \times 10^{-9}$ atm, $P_{H_2S}=1.20 \times 10^{-4}$ atm, $P_{NO}=1.74 \times 10^{-8}$ atm, $P_{NO_2}=2.67 \times 10^{-8}$ atm).

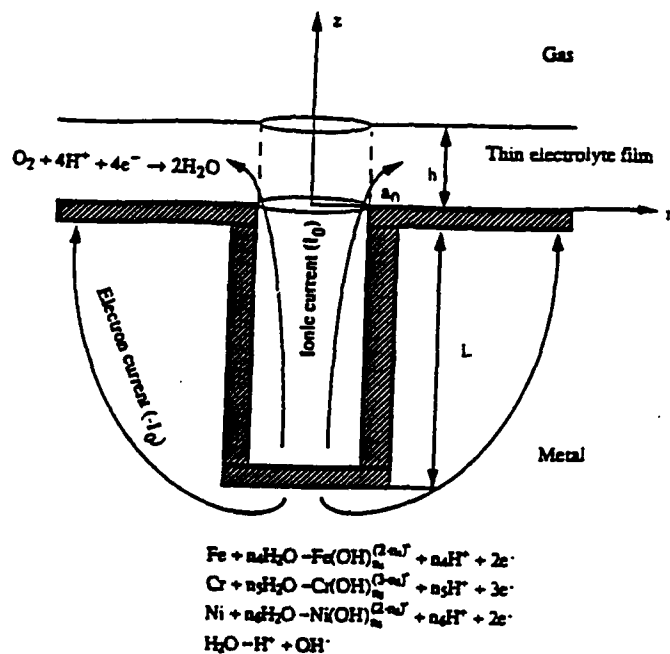


FIGURE 4. Schematic of a pit on the surface of condensing heat exchanger.

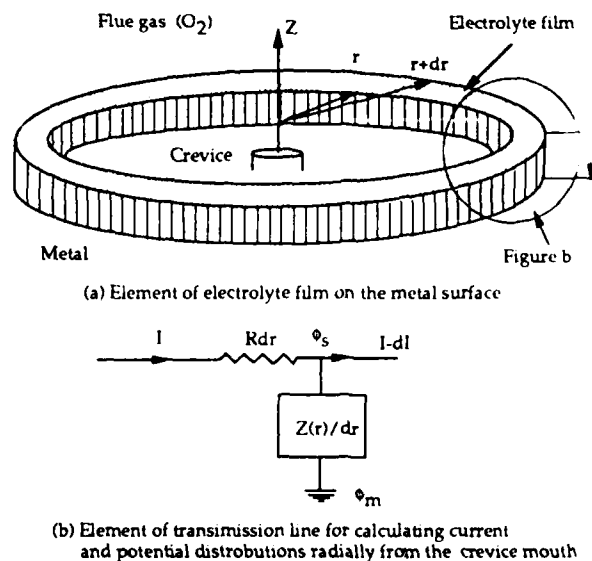


FIGURE 5. Transmission line model for thin electrolyte film on the metal surface.

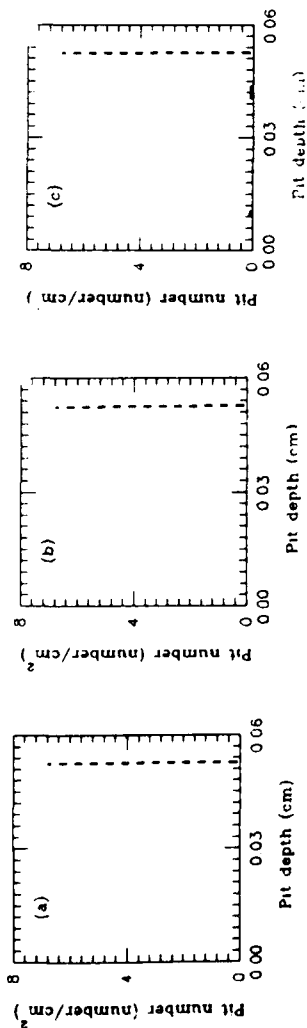


FIGURE 6. Measured pitting damage functions for Type 304L SS heat exchanger tubes under condensing conditions. ($[Cl^-]=3$ ppm, temperature ranging from 308 to 353 K, pit counting interval= 2.54×10^{-3} cm. a) $T_{obs}=4.32 \times 10^6$ s; b) $T_{obs}=8.63 \times 10^6$ s; c) $T_{obs}=1.73 \times 10^7$ s; tube thickness= 5.34×10^{-2} cm, as indicated by the dashed line).

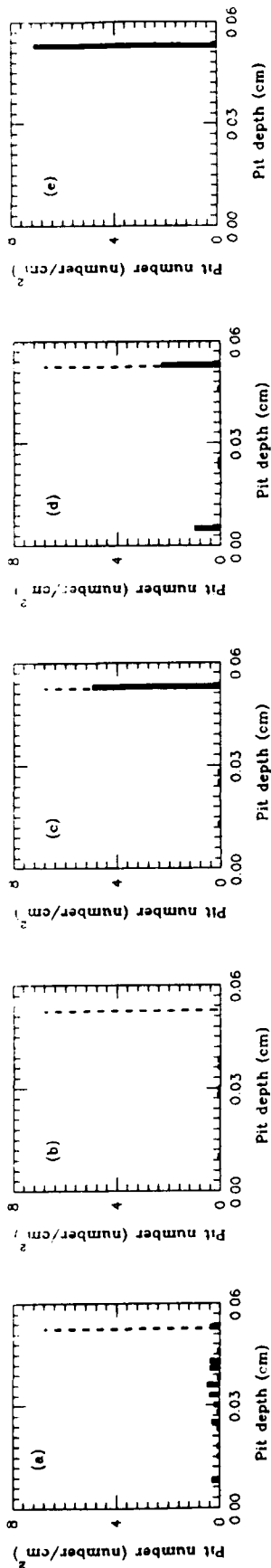


FIGURE 7. Measured pitting damage functions for Type 304L SS heat exchanger tubes under condensing conditions. ($[Cl^-]=26$ ppm, temperature ranging from 308 to 353 K, pit counting interval= 2.54×10^{-3} cm. a) $T_{obs}=4.32 \times 10^6$ s; b) $T_{obs}=8.63 \times 10^6$ s; c) $T_{obs}=1.73 \times 10^7$ s; d) $T_{obs}=3.46 \times 10^7$ s; e) $T_{obs}=5.18 \times 10^7$ s; tube thickness= 5.34×10^{-2} cm, as indicated by the dashed line).

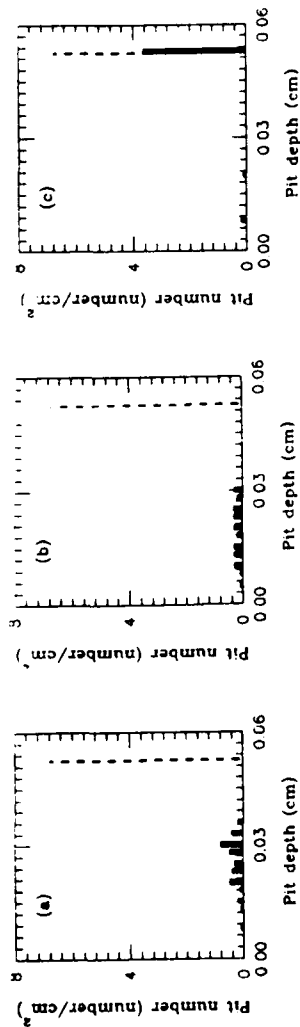


FIGURE 8. Measured pitting damage functions for Type 304L SS heat exchanger tubes under condensing conditions. ($[Cl^-]=225$ ppm, temperature ranging from 308 to 353 K, pit counting interval= 2.54×10^{-3} cm. a) $T_{obs}=4.32 \times 10^6$ s; b) $T_{obs}=8.63 \times 10^6$ s; c) $T_{obs}=1.73 \times 10^7$ s; tube thickness= 5.34×10^{-2} cm, as indicated by the dashed line).

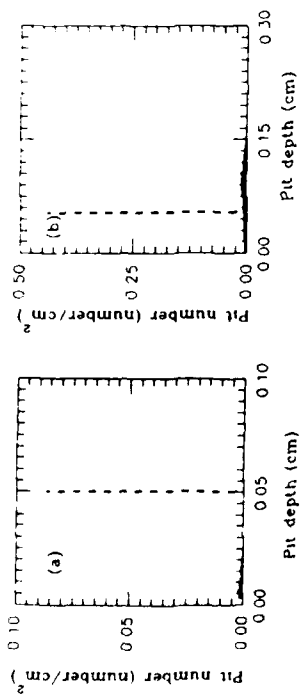


FIGURE 9.

Calculated pitting damage functions for Type 304L SS heat exchanger tubes under condensing conditions.

($[Cl^-]=3$ ppm, temperature=350 K, $P_{CO}=2.60 \times 10^{-5}$ atm, $P_{CO_2}=6.80 \times 10^{-2}$ atm, $P_{SO_2}=9.37 \times 10^{-9}$ atm, $P_{SO_3}=2.00 \times 10^{-9}$ atm, $P_{H_2S}=1.20 \times 10^{-4}$ atm, $P_{NO}=1.74 \times 10^{-8}$ atm, $P_{NO_2}=2.67 \times 10^{-8}$ atm, $P_{O_2}=1.00 \times 10^{-4}$ atm, pit radius 1.00×10^{-4} cm, initial pit depth 1.00×10^{-3} cm, pit counting interval= 2.54×10^{-3} cm., a) $T_{obs}=6.30 \times 10^7$ s; b) $T_{obs}=1.58 \times 10^8$ s; tube thickness= 5.34×10^{-2} cm, as indicated by the dashed line).

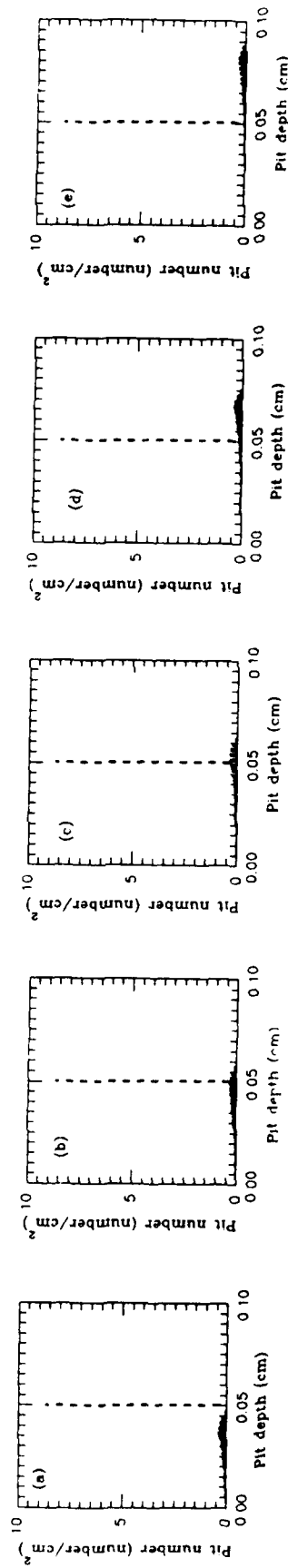


FIGURE 10.

Calculated pitting damage functions for Type 304L SS heat exchanger tubes under condensing conditions.

($[Cl^-]=10$ ppm, temperature=350 K, $P_{CO}=2.60 \times 10^{-5}$ atm, $P_{CO_2}=6.80 \times 10^{-2}$ atm, $P_{SO_2}=9.37 \times 10^{-9}$ atm, $P_{SO_3}=2.00 \times 10^{-9}$ atm, $P_{H_2S}=1.20 \times 10^{-4}$ atm, $P_{NO}=1.74 \times 10^{-8}$ atm, $P_{NO_2}=2.67 \times 10^{-8}$ atm, $P_{O_2}=1.00 \times 10^{-4}$ atm, pit radius 1.00×10^{-4} cm, initial pit depth 1.00×10^{-3} cm, pit counting interval= 2.54×10^{-3} cm., a) $T_{obs}=3.15 \times 10^7$ s; b) $T_{obs}=4.10 \times 10^7$ s; c) $T_{obs}=4.41 \times 10^7$ s; d) $T_{obs}=5.36 \times 10^7$ s; e) $T_{obs}=5.34 \times 10^{-2}$ cm, as indicated by the dashed line).

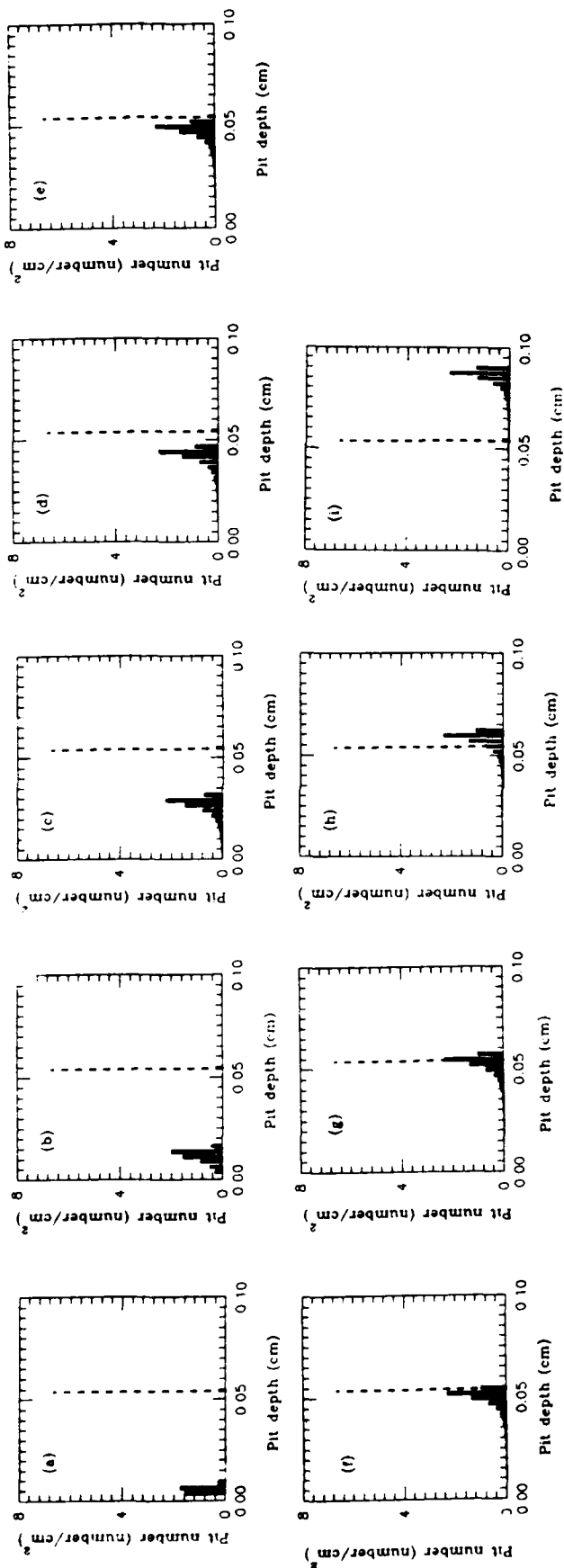


FIGURE 11. Calculated pitting damage functions for Type 304L SS heat exchanger tubes under condensing conditions.

([Cl⁻]=26 ppm, temperature=350 K, P_{CO}=2.60x10⁻⁵ atm, P_{CO₂}=6.80x10⁻² atm, P_{SO₂}=9.37x10⁻⁹ atm, P_{SO₃}=2.00x10⁻⁹ atm, P_{H₂S}=1.20x10⁻⁴ atm, P_{NO}=1.74x10⁻⁸ atm, P_{NO₂}=2.67x10⁻⁸ atm, P_{O₂}=1.00x10⁻⁴ atm, pit radius

1.00x10⁻⁴ cm, initial pit depth 1.00x10⁻³ cm, pit counting interval=2.54x10⁻³ cm., a) T_{obs}=4.32x10⁶ s; b)

T_{obs}=8.63x10⁶ s; c) T_{obs}=1.73x10⁷ s; d) T_{obs}=2.52x10⁷ s; e) T_{obs}=2.84x10⁷ s; f) T_{obs}=2.99x10⁷ s; g)

T_{obs}=3.15x10⁷ s; h) T_{obs}=3.46x10⁷ s; i) T_{obs}=5.19x10⁷ s; tube thickness=5.34x10⁻² cm, as indicated by the dashed line).

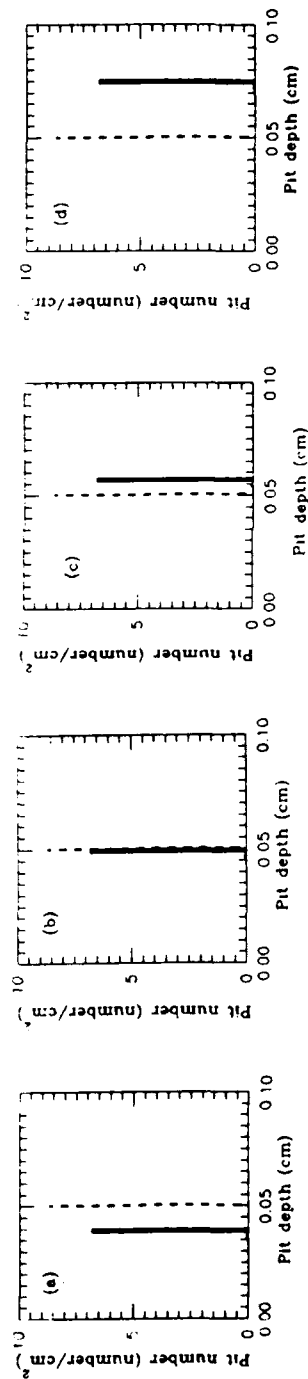


FIGURE 12. Calculated pitting damage functions for Type 304L SS heat exchanger tubes under condensing conditions.

([Cl⁻]=225ppm, temperature=350 K, P_{CO}=2.60x10⁻⁵ atm, P_{CO₂}=6.80x10⁻² atm, P_{SO₂}=9.37x10⁻⁹ atm,

P_{SO₃}=2.00x10⁻⁹ atm, P_{H₂S}=1.20x10⁻⁴ atm, P_{NO}=1.74x10⁻⁸ atm, P_{NO₂}=2.67x10⁻⁸ atm, P_{O₂}=1.00x10⁻⁴ atm, pit radius

1.00x10⁻⁴ cm, initial pit depth 1.00x10⁻³ cm, pit counting interval=2.54x10⁻³ cm., a) T_{obs}=1.58x10⁷ s; b)

T_{obs}=2.21x10⁷ s; c) T_{obs}=2.52x10⁷ s; d) T_{obs}=3.15x10⁷ s; tube thickness=5.34x10⁻² cm, as indicated by the dashed line).

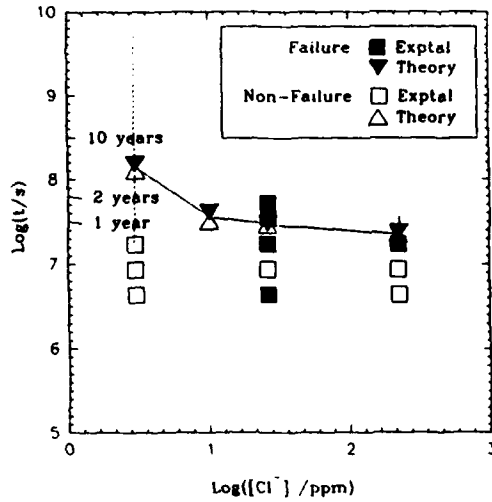


FIGURE 13. The measured and calculated service life for for Type 304 SS heat exchanger tubes as a function of the chloride concentration (parameters are identical to that for FIGUREs 6-8 for experimental data and FIGUREs 9-12 for calculation, respectively).

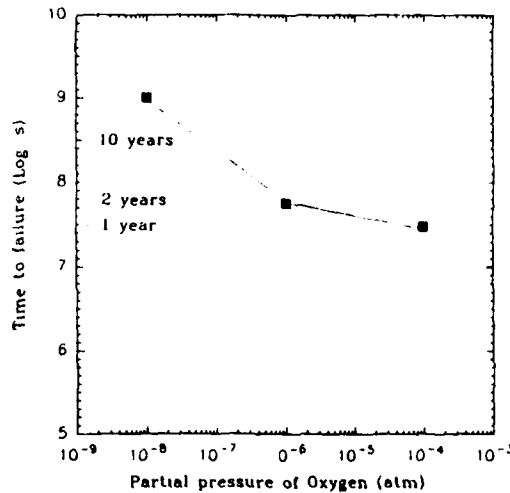


FIGURE 14. The calculated service life for for Type 304L SS heat exchanger tubes as a function of the partial pressure of oxygen (temperature=350 K, $P_{CO}=2.60 \times 10^{-5}$ atm, $P_{CO_2}=6.80 \times 10^{-2}$ atm, $P_{SO_2}=9.37 \times 10^{-9}$ atm, $P_{SO_3}=2.00 \times 10^{-9}$ atm, $P_{H_2S}=1.20 \times 10^{-4}$ atm, $P_{NO}=1.74 \times 10^{-8}$ atm, $P_{NO_2}=2.67 \times 10^{-8}$ atm).

An estimation of maintenance costs related to corrosion
in Brazilian electric power system

A. Marinho Jr
Light Serviços de Eletricidade S.A.
Divisão de Ensaio
Rua Bergamo 320 Triagem
20911-000 Rio de Janeiro RJ Brasil

Abstract

Maintenance costs related to corrosion in Brazilian electric power system were estimated. The study was carried out by the materials testing laboratory of Light Serviços de Eletricidade S.A., an electric power company operating in Rio de Janeiro. The results obtained were based on previous studies: First, a detailed internal survey was undertaken by the lab, and the mean annual cost of corrosion in the company was calculated. The part of the results concerning maintenance was extrapolated to the entire Brazilian electric system. Second, it was considered an evaluation of maintenance costs carried out by a working group of the electric energy national coordination committee. About 10% of the total maintenance costs in the electric power utilities was attributed to corrosion. Finally, an assessment based on a provisional calculation of national corrosion costs was utilized for the purpose of this study. Basically, it was considered the participation of the electric power industry in the GNP. The analysis of data from studies above mentioned led to some conclusions. For example, the major corrosion costs appears to be associated with maintenance of transmission towers, substations and power plants components. The mean annual costs were estimated ranging from US\$ 75 to 100 million. It was found that only by using the technology at hand in the electric power utilities, it is possible to save about 20% of expenditures related to corrosion.

Introduction

Maintenance represents a major cost in the electric power industry. A significant part of maintenance cost is related to corrosion prevention and control. In modern industry decisions are based almost exclusively on economic considerations and corrosion is, basically, an economic problem.

Brazilian electric power system has an installed capacity of about 51,000 MW, mainly from hydroelectric plants. There is a transmission system of about 150,000 Km in alternate current up to 750 kV and 1,600 Km in direct current at 600 kV.

More than 33 million consumers are served, from rural to industrial areas, using aerial, underground or mixed distribution networks. The entire electric power system, considered as an integrated grouping of power plants, substations and transmission lines is, on the average, 25 years old. There are exceptions, some utilities having still older equipments in operation. Fortunately, aging of equipments and facilities is a world-wide preoccupation. In addition, manufacturers and research centres efforts in R&D provides evidence that a reduction in maintenance costs can be achieved through the proper execution of an efficient predictive maintenance program².

Brasilian electric power system experiences all types of corrosion problems. In generation, transmission and distribution areas there are atmospheric corrosion of above ground metallic structures and soil-ground water corrosion of buried structures.

In generation, about 95% of power plants in operation are hydroelectric. The principal problems are related to metallic structures, immersed or not, general piping, pumps and turbines. In hydroelectric plants, major maintenance costs related to corrosion are associated with painting, metallic coatings and cathodic protection. There are also a few thermal power plants, coal and oil-fired, and only one PWR 626 MW nuclear. They present the classical corrosion problems in the water steam and fire sides of boiler tubes. Maintenance corrosion costs are associated with water treatment and use of inhibitors.

In transmission, towers, lines and hardware are exposed to atmospheric attack in some regions. Towers are constructed of galvanized steel and those installed in aggressive atmospheres are maintained by anticorrosion painting, which extends considerably the tower's life. Major maintenance costs related to corrosion in electric power utilities are associated with anticorrosion painting of transmission towers and other structures of galvanized steel.

In distribution, corrosion problems are similar to those of transmission area, involving galvanized steel hardware and underground cables, but maintenance practices are quite different. All components presenting corrosive attack are replaced by new ones. Zinc consumption to galvanize new hardware in the company's workshops is an important item of corrosion costs in distribution.

This paper presents estimations of maintenance costs related to corrosion in brasilian electric power system, based on different approaches. First, an extrapolation of the values obtained for corrosion costs in an internal survey carried out

years ago by the materials testing laboratory of Light Serviços de Eletricidade. Second, it was considered an evaluation of maintenance costs carried out by a working group of the Brazilian electric energy coordination committee (GCOI). Finally, an assessment based on a provisional calculation of national corrosion costs was utilized for the purpose of this study, considering the participation of the electric power industry in the Gross National Product. All the costs cited in this text are expressed in US dollar as of December 1992.

Light's survey on corrosion costs

In general, electric power utilities, like many other industrial sectors, do not have overall figures on corrosion costs. They are limited to localized calculations, usually in anticorrosion protection designing.

Light Serviços de Eletricidade S.A. is an electric power utility operating in Rio de Janeiro. Its concession area of 11,000 sq.Km corresponds to 25% of Rio de Janeiro state's surface. It attends to about 2,700,000 consumers in 29 cities and has 158,000 Km of distribution lines, comprising 145,000 of aerial and 13,000 Km of underground cables. Its installed capacity is 4,476 MVA, being 2,516 MVA of aerial and 1,960 MVA of underground networks.

Until 1980, the company's area of concession comprised Rio de Janeiro and São Paulo states. This area included 33% of the total number of Brazilian consumers. In 1977 the company distributed 44% of the electric energy available in the country.

From 1976 to 1978 Light's materials testing laboratory carried out a survey on corrosion costs in the company, involving generation, transmission and distribution. The results obtained were presented in a previously published paper³. More recently, the study was reviewed taking into account current prices and the values are summarized in Table 1.

From data showed in Table 1, it was possible to obtain some interesting informations: When the survey was undertaken, Light's generation capacity was 2,100 MW, 1,630 being provided by hydroelectric plants and 470 provided by one oil-fired unit. This gives \$ 412 / MW for maintenance costs related to corrosion in generation.

In transmission lines, there were about 15,000 towers in the company, 5,100 being in aggressive regions. Around 500 towers were painted yearly, not only by our own personnel but also by contractors, giving an annual painting cost of \$ 5,880 per

tower. This cost refers to totally painted towers, comprising surface preparation, one application of a primer, one of intermediate paint and two applications of finish paints. This gives a mean annual cost of \$ 1,180 /application/tower. Considering a typical 138 kV tower having a 300 sq.m surface, one finds around \$ 4 / sq.m / application.

In distribution, Light's substations capacity was 16,505 MVA. Painting of metallic structures, traveling cranes, insulating oil tanks, transformers, circuit breakers and other components led to expenditures showed in Table 1, giving a mean annual cost of \$ 49 / MVA. Costs cited in Table 1 for underground cable represents the replacement of only 1 Km of underground lead-covered cables, giving \$ 158,000 / Km.

Only with the expenditures showed in Table 1, it was found a corrosion cost of at least \$ 5.4 million each year in Light Serviços de Eletricidade, around \$ 4.8 million being exclusively maintenance costs. Considering the limitations of the survey, it was possible to conclude that the costs were underestimated. In fact, the study did not consider, for example, indirect costs. Further calculations led to values up to \$ 8 million for the total annual corrosion costs in the company, so maintenance costs related to corrosion are around 60% of the overall costs.

As a consequence of the study, the company improved specialized training programs on corrosion, installed a corrosion control laboratory and increased the standardization of anti-corrosive products. This improved the performance of the maintenance teams and the results showed, in the last 10 years, that only by using the technology at hand, it was possible to save around 20% of the expenditures of maintenance related to corrosion.

Estimation via Light's survey

The ratio of the installed capacity of Brazilian electric power system to that of Light Serviços de Eletricidade was 16:1 at the time of survey. Extrapolating the Light's figures to the entire Brazilian electric system, one finds around \$ 77 million / year for the maintenance costs related to corrosion in the Brazilian electric power system.

Estimation via overall maintenance costs

In the USA for example, 50% of maintenance costs in generation of electricity and 10% of maintenance costs in transmission, distribution and miscellaneous are due to corrosion. In Brazil, the majority of power plants are hydroelectric and therefore the corrosion factor in

maintenance costs in generation was estimated in 10%. Overall maintenance costs in Brazilian electric power system are about \$ 750 million / year⁵, so it was found \$ 75 million / year for maintenance costs related to corrosion.

Estimation via GNP's constant

A number of assessments of national corrosion costs have been carried out in several industrial nations⁴. In the United States, it was estimated as 4.0% of the Gross National Product (GNP). In the United Kingdom, 3.5% and in German Federal Republic and Australia, 3%. Corrosion costs in industrial nations appears to be an approximately constant percentage of GNP, around 3%.

Brazilian GNP in 1992 was about \$ 332 billion. One estimates that the entire electric system contributes to the GNP in 2%. Considering Brazilian corrosion costs as 2.5% of GNP it was found about \$ 8.3 billion/year for Brazilian corrosion costs and about US\$166 million/year for corrosion costs in the Brazilian electric system⁶. As cited before in the case of Light's survey, at least 60% of the overall corrosion costs are maintenance expenditures. Assuming that this percentage remains valid for all other utilities, one estimates \$ 100 million / year for maintenance costs related to corrosion in the entire Brazilian electric power system.

Conclusions

Using different approaches it was possible to estimate maintenance costs related to corrosion in the Brazilian electric power system, which ranges from \$ 75 to \$ 100 million / year, as summarized in Table 2.

The major item of maintenance costs related to corrosion in electric power utilities is anti-corrosion painting of galvanized steel transmission towers.

According to results obtained by Light Serviços de Eletricidade, a saving of about 20% of maintenance costs related to corrosion can be achieved only by using the technology at hand.

References

1. NACE, "Direct Calculation of Economic Appraisals of Corrosion Control Measures" Standard RP-02-72(Foreword), Houston, Texas, USA, 1972

2. Maquire, M., "Predictive Maintenance: What does it do?", Electrical World, June 1992, pp 11-12.
3. Marinho Jr, A. and Sampaio, E. G., "Corrosion Costs in an Electric Power Company", 8th International Congress on Metallic Corrosion, Mainz, Federal Republic of Germany, Sept. 1981.
4. NBS Report, "Economic Effects of Metallic Corrosion in the United States - Part 1", NBS Special Publication 511-1, Washington, D.C., 1978.
5. GCOI-SCM, "Envelhecimento do Sistema Elétrico, estudo interno do Sub-Comitê de Manutenção do Grupo Coordenador para Operação Interligada", Seminário do SCM, Vitória, ES, Brasil, 1987.
6. Marinho Jr, A., "Considerações sobre custos de corrosão no Setor Elétrico", Colóquio sobre corrosão em Linhas de Transmissão, CEPTEL, Rio de Janeiro, março de 1990.

TABLE 1 - Summary of corrosion costs in Light Serviços de Eletricidade (see ref.2) - (US\$ / year)

| | |
|--------------------------------|-----------|
| GENERATION | |
| Anti-corrosion painting | 750,000 |
| Inhibitors | 115,000 |
| TRANSMISSION | |
| Anti-corrosion painting | 2 940,000 |
| Hardware replacement | 60,000 |
| DISTRIBUTION | |
| Anti-corrosion painting | 810,000 |
| Hardware replacement | 300,000 |
| Underground cables replacement | 158,000 |
| MISCELLANEOUS | |
| Materials storage: | |
| Losses by rusting | 16,000 |
| Zinc for galvanizing | 248,000 |
| Workshops and transport | |
| Repairs by painting | 33,000 |
| TOTAL | 5,430,000 |

TABLE 2 - Maintenance costs related to corrosion in Brazilian electric power system - (US\$ million / year)

| | |
|-------------------------------|-----|
| Via Light's survey | 77 |
| Via overall maintenance costs | 75 |
| Via GNP's constant | 100 |

**Numeric Model for Hydrogen Embrittlement Prediction for Structures Cathodically Protected
in Marin Environment**

**Jean-François Regnier
Alcatel Fibres
35 rue Jaurès
BP 115
95874 Bezons Cedex
FRANCE**

**Dominique Festy
IFREMER
Centre de Brest
BP 70
29280 Plouzane
FRANCE**

Abstract

Stress corrosion and hydrogen embrittlement have been studied for structures cathodically protected in marin environment.

A numeric model, based on finite elements method, has been developped for crack growth prediction.

Key terms : stress corrosion, hydrogen embrittlement, modellization, life prediction

D) Introduction

Different elements as stress corrosion in marine environment, crack propagation or hydrogen embrittlement can lead metallic structures to serious problems when they're exposed to these phenomena.

Life prediction with experimental characterization would need too many experiments, due to the complexity of the responsible factors of these phenomena and the interdependence of these factors. On the other hand, approach with model considering stresses and hydrogen diffusion could be a good solution for crack propagation determination.

II) Modellization Hypothesis

Model principle is based on the following hypothesis :

- hydrogen penetration depends on the environmental parameters (temperature, pH, pressure, potential,...),
- hydrogen diffusion coefficient and solubility depend on stresses in material,
- due to K_{Ic} dependence on hydrogen concentration, for material with initial crack length and stresses, there is a hydrogen concentration threshold leading to crack length increasing

III) Model principle

Model is based on finite elements method using, with ADINA software, allowing mechanical and thermal solutions determination.

The figure 1 describes the principle with all calculating steps :

- geometric definition (initial crack length, sizes, ...)
- mechanical calculation step, leading to stresses determination
- diffusion coefficients definition in accordance with mechanical results
- thermal step with hydrogen diffusion determination, and so on until finding the time necessary for crack length increasing.

IV) Results

Figures 2 shows results obtained with 42CD4 steels study, with following experimental conditions:

- material : steel 42CD4
- $E=2.1$ GPa
- $\sigma_e= 1510$ MPa
- Static load : 2000 daN
- Hydrogen concentration on external surface : $0.2 \text{ cm}^3 \text{ H}_2 / \text{cm}^3 \text{ Fe}$
- Hydrogen diffusion coefficient ($\sigma = 0$) : $4 \cdot 10E-6 \text{ cm}^2\text{s}^{-1}$
- Hydrogen diffusion coefficient (σ) = $4 \cdot 10E-6 * (1 + \sigma/20)$

Results presented in figures 2 and 3 give us examples for initial definition, mechanical stresses definition, and hydrogen concentration at several times.

V) Conclusion

The results presented in figures 2 and 3 illustrate the method principle. With only a few experiments giving us the characteristic parameters, as diffusion coefficient versus stresses, and with the knowledges about K_{Ic} variations versus hydrogen concentration, it's possible with this model to determine the crack length variation and so the life prediction for the structure.

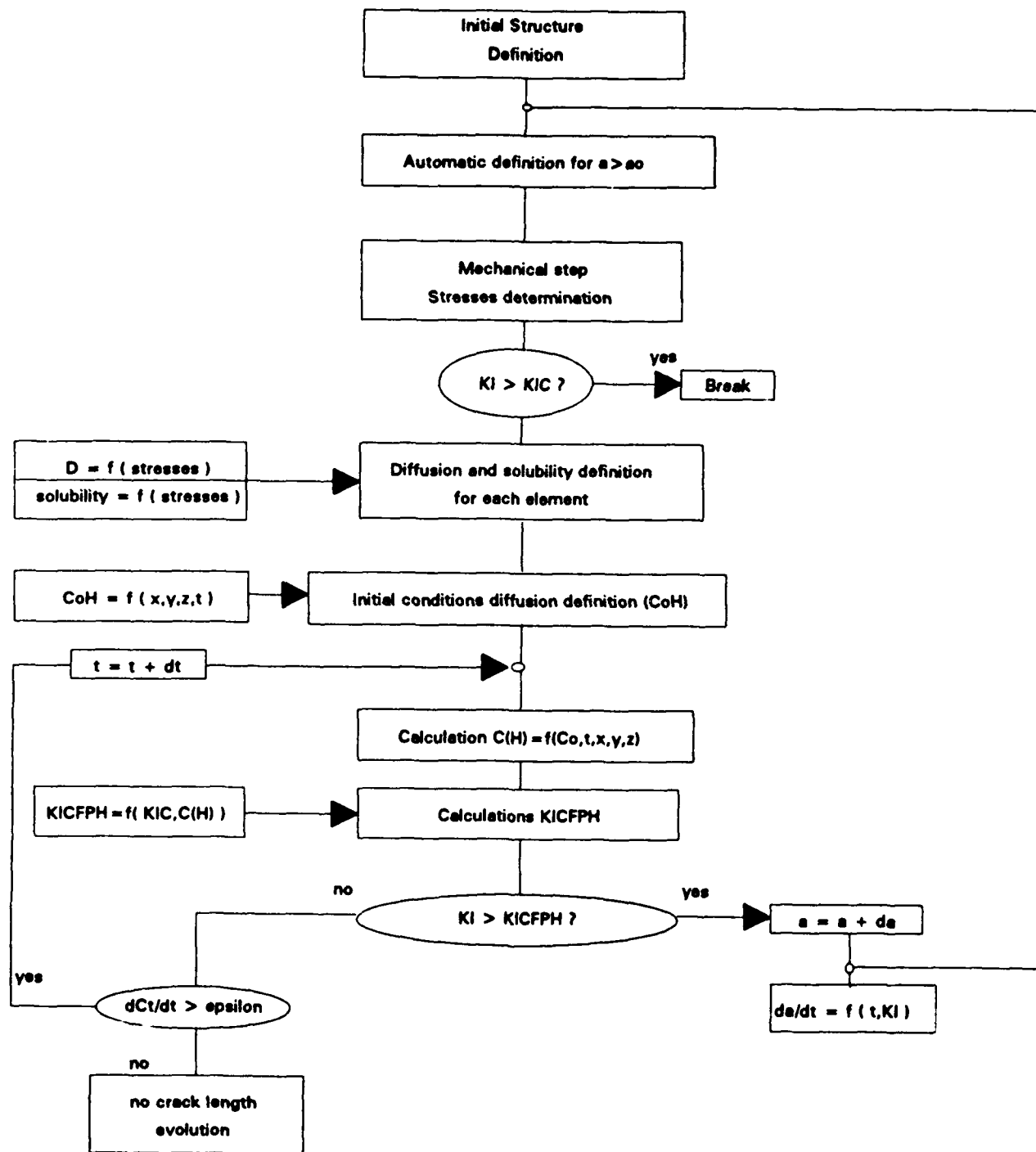
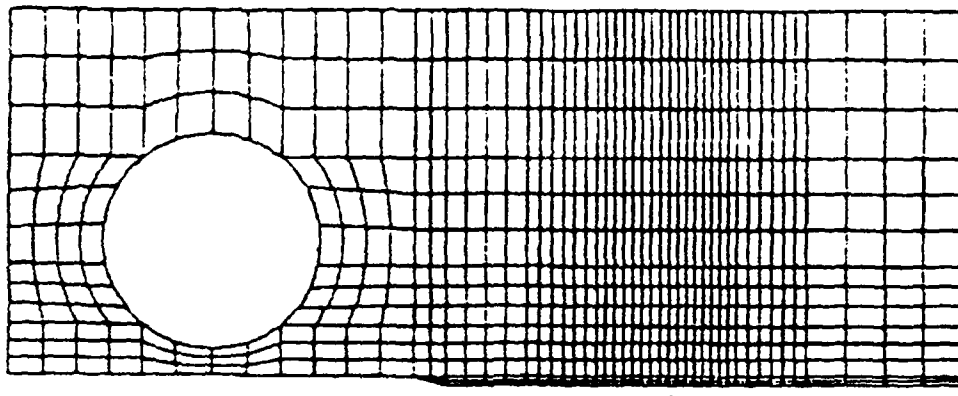
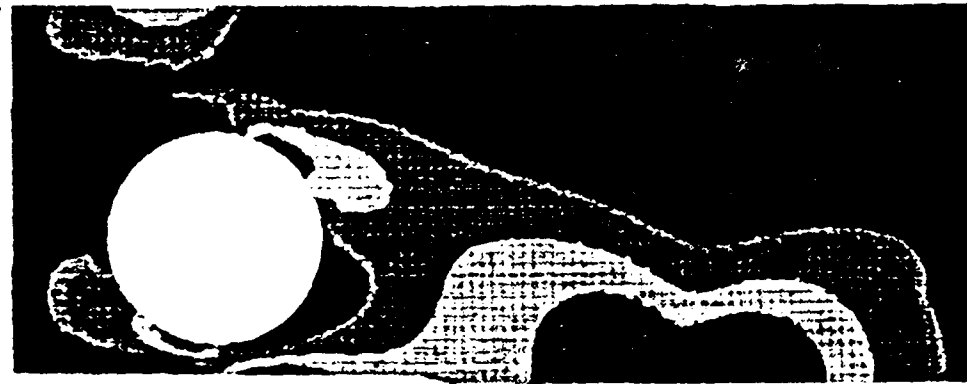


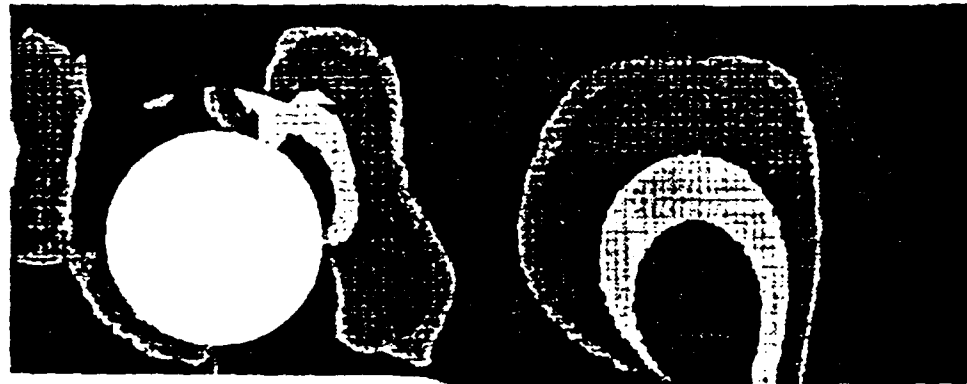
Figure 1 : Modelization principle



▲
crack extremity



▲



▲



▲

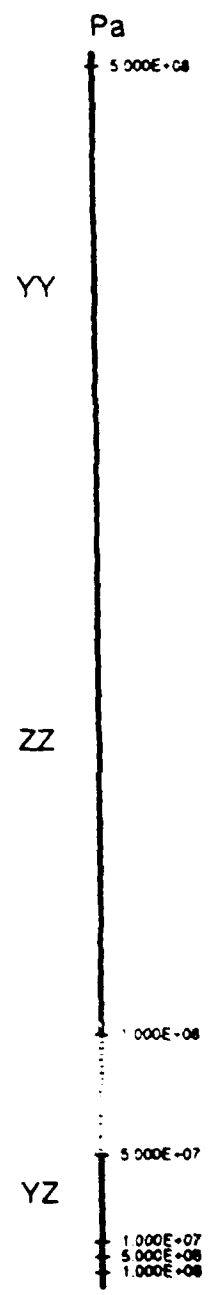


Figure 2 : Results obtained with 42CD4 steel.
Initial Definition and Stresses YY, ZZ, YZ views

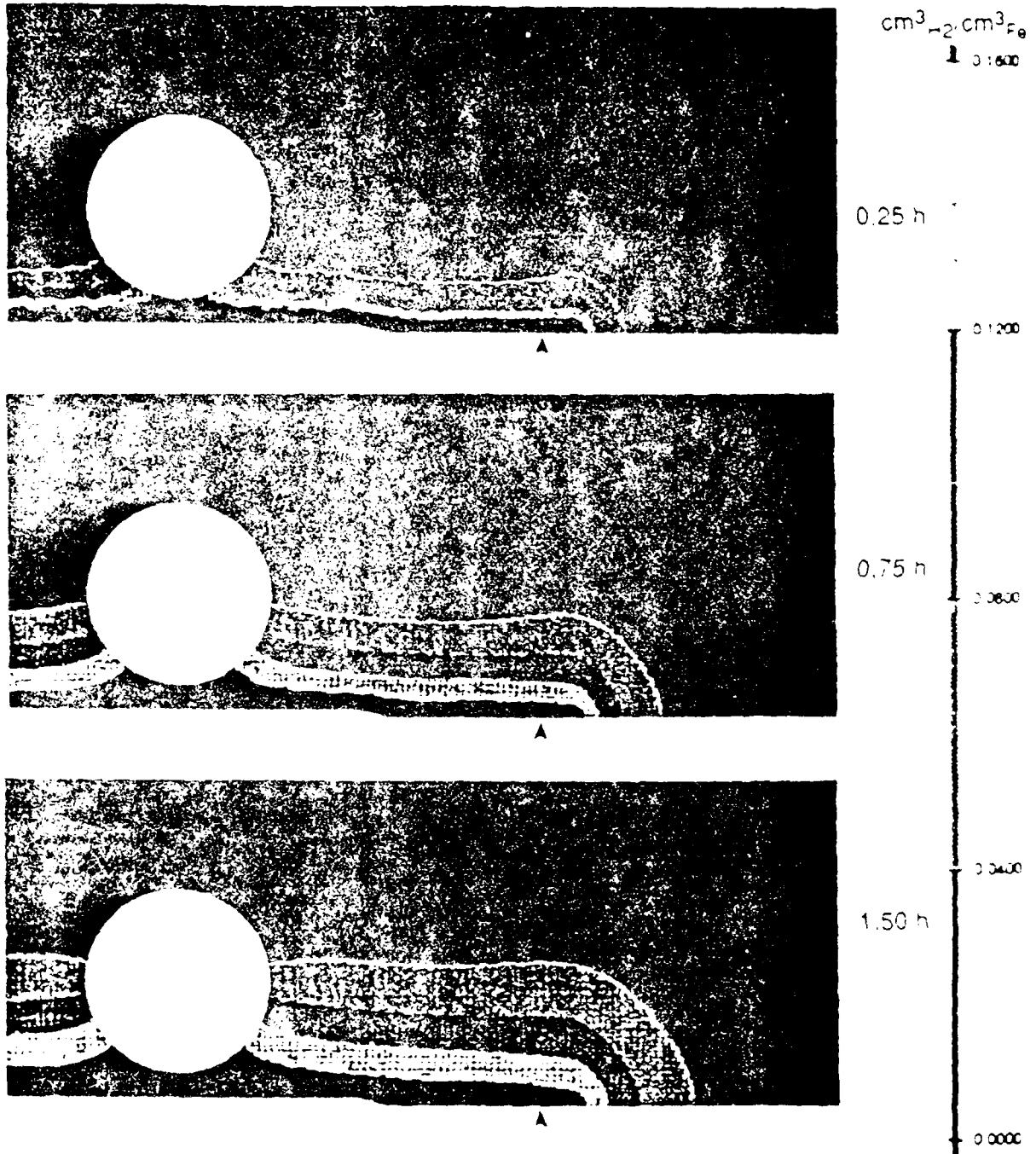


Figure 3. Results obtained with steel 42CD4
 Hydrogen concentration views at several times

Use of Fuzzy Logic As a Decision Making Tool in the Rehabilitation of Concrete Bridge Structures

Moavin Islam
Philip D. Simon
CC Technologies Inc
2704, Sawbury Blvd
Columbus OH 43235

Abstract

Fuzzy logic is a concept derived from the branch of mathematical theory of fuzzy sets. It permits the mathematical representation of imprecise or uncertain information. Unlike traditional computer logic that recognizes statements as only 'true' or 'false', fuzzy logic is capable of expressing linguistic terms such as 'tall', 'warm', 'active', 'nearby', 'unlikely' and so on. Fuzzy logic provides a powerful means of representing real-world events that are inherently imprecise in nature. In general, fuzzy logic when applied to computers, allows them to emulate the approximation of the human reasoning process, quantify imprecise information, make decisions based on vague and incomplete data, yet arrive at *definite conclusions*.

The present paper shows how the concepts of fuzzy logic can be effectively applied in the decision making process when trying to prioritize rehabilitation of bridge structures. The method utilizes objective (quantitative data) and subjective (judgement and experience) information to complete the decision making process.

Key terms: Fuzzy logic, bridge structures

Introduction

Fuzzy logic is a powerful, yet straightforward problem-solving technique with widespread applicability, especially in the areas of control and decision making. The term 'fuzzy logic' was first coined by Lotfi Zadeh, a Russian-born mathematician at the University of California at Berkeley who published his concepts in 1965¹. Since then a large number of books and research papers have been published and continue to be published²⁻¹¹. Fuzzy logic is derived from the branch of mathematical theory called fuzzy sets. In general, it is most useful in handling problems not easily definable by practical mathematical models. Much of its power relies on its ability to draw conclusions and generate responses based on vague, ambiguous, qualitative, incomplete, or imprecise information. In this respect, fuzzy-based systems have a reasoning ability similar to that

of humans which allows them to quantify imprecise information, make decisions based on vague and incomplete data, yet arrive at definite conclusions. In conventional logic a decision tree is used to determine the outcome and the data value to be used at each decision point enroute to the final result is set prior to applying the logic to a specific case. However, conventional logic is bi-valent. That means that each decision point is answered with a yes or no or in the case of computers a 0 or 1. Fuzzy logic allows degrees or gradations of a decision value between yes and no or 0 and 1. The gradations are still preset conditions, however they allow judgment and experience to enter into the decision process.

Fuzzy logic is being utilized for diverse applications such as consumer appliances (dishwashers, camcorders, vacuum cleaners, television, washing machines etc), subway trains, elevators, anti-lock brakes systems and even managing stock market portfolios. The present paper shows how the concepts of fuzzy logic can be effectively used in the decision making process when trying to prioritize replacement or rehabilitation of bridge structures.

Application of Fuzzy Logic Concepts to Bridge Structures

There are close to 600,000 bridges on the roads and highways in the USA. Severe deterioration of a large number of these structures for a variety of reasons is a major source of concern for the different states. The rehabilitation of the structures require prioritization for which the states rely on their team of *bridge inspectors*. During a bridge inspection, information collected and perceived by the inspector can be divided into objective and subjective parts. The objective portion involves measurable information on characteristics such as crack width, scaling depth, percent delamination etc. at specific locations, whereas the subjective portion involves the wisdom and the experience of the inspector, who must evaluate the severity of the deficiencies and their combined impact on the overall structural integrity. Although the importance of the subjective information is recognized, the present inspection procedure does not have the capability to incorporate systematically the subjective information into the rating process.

Fuzzy logic allows verbal descriptions to be assigned to numerical characteristics. A membership value is assigned to the appropriate verbal description for each characteristic. When the numerical characteristic is not clearly in a specific verbal range, the membership value is weighted between two adjacent verbal descriptions. In a way probability is combined with conventional logic in fuzzy logic. The relative importance of each characteristic is predetermined as well as its range of values. These graded and weighted values are then combined to give an overall verbal and numerical description in a specific case. The resultant numerical value can also be used to rank several specific cases. For example, the relative deterioration condition of a number of concrete bridges structures can be ranked for the prioritization of rehabilitation or replacement strategies. For this purpose, a number of characteristics of the structure have to be taken into consideration which can be assigned quantitative values as well as verbal descriptions.

These characteristics may include : cracking, delamination, spalling, scaling, chloride content, corrosion of the rebar etc. One of the primary advantages of fuzzy logic is that a decision or ranking can be made without data on each and every characteristic in all cases.

It should be noted that when computing the overall condition of the structure, not all the characteristics may have the same degree of influence on its integrity. Hence a relative importance (RI) rating, a number between 0.0 and 1.0, has to be assigned to each characteristic to reflect its influence on the overall structural integrity. For example, a small RI value would be assigned to the characteristic that is relatively unimportant while for 'important' characteristics, the RI values would be nearly equal to 1. The RI values for the different characteristics is normally arrived at through a consensus of expert opinion. The value may differ from one group of experts to another. The example below will illustrate further the application of fuzzy logic to bridge structures.

Illustrative Example

Table 1 shows the different characteristics, the range of values and the RI rating for each characteristic to be used in the illustrative example. Specific values from Table 1 can then be input into a spread sheet like Excel or Lotus 123 to compute a membership table and a resultant condition rating for a specific structure. The first step, however, is to generate raw membership values for each of the characteristics being considered which is best done graphically and is shown later.

The raw membership values are entered into the spreadsheet which then computes the 'raw' membership table. The corrected membership table is obtained by multiplying each raw membership entry with the corresponding RI coefficient (cf. Table 1). At the same time the spreadsheet also computes the "Sum" and "Union" of flaws which result in a rating for that bridge based on the combined effect of all flaws. The combined numerical rating ranges used in this example are 1=very poor, 2=poor, 3=fair, 4=good and 5=very good. In addition to ranking several bridges for prioritization of action the rating range can be used to categorize an individual bridge condition according to the verbal descriptions above.

As an example assume a bridge with the following condition data characteristics of :

| | |
|--------------------------|---------------|
| Crack (CR) width | 0.027 inches |
| Scaling (SC) depth | 0.1 inch |
| Spalling (SP) width | 4.5 inches |
| Delamination (DE) | 60 % |
| Chlorides (CL) | 1.9 lbs/cu.yd |
| Cover (CV) | 1.5 inches |
| Half Cell Potential (HC) | -330 mV |
| Rate of Corrosion (RC) | 9 mA/sq.ft |

As mentioned above the raw membership functions for the various characteristics are first calculated graphically as shown in Figures 1 - 8. Next, the raw membership table (Table 2) is generated on the spread sheet by entering the raw membership values from Figures 1 - 8. The final step is to compute the corrected membership table (Table 3) by multiplying with the RI coefficients which also yields the "Sum" and "Union" of flaws together with an overall rating for the structure based on the combined effect of all flaws.

The "Union" and "Sum of Flaws" provide an indication of the boundaries of the membership values in a specific condition category (for example 0.855=union and 0.965=sum for the Fair category). The union indicates the maximum degree that any given flaw effects that condition category. The sum is an indication of the combined effect of all the flaws on that verbally defined condition category. If an individual membership value is defined as μ then the union (maximum) is easily calculated. For example, the union of the Fair category above would be:

$$\mu_{uf} = \text{Max}[\mu_f(\text{CR}), \mu_f(\text{SC}), \mu_f(\text{SP}), \mu_f(\text{DE}), \mu_f(\text{CL}), \mu_f(\text{CV}), \mu_f(\text{HC}), \mu_f(\text{RC})]$$

In this case;

$$\begin{aligned} \mu_f(\text{CR}) &= 0, & \mu_f(\text{SC}) &= 0, & \mu_f(\text{SP}) &= 0.45, & \mu_f(\text{DE}) &= 0, & \mu_f(\text{CL}) &= 0, & \mu_f(\text{CV}) &= 0.56, \\ \mu_f(\text{HC}) &= 0.86, & \mu_f(\text{RC}) &= 0 \end{aligned}$$

Therefore, the membership value for the Fair condition Union (μ_{uf}) would be:

$$\mu_{uf} = \text{Max}[0, 0, 0.45, 0, 0, 0.56, 0.86, 0] = 0.86$$

The combined effect membership value (μ_{sf}) of all flaws on the Fair condition category is defined as :

$$\begin{aligned} \mu_{sf} &= 1 - [1 - \mu_{sf}(\text{CR})] \times [1 - \mu_{sf}(\text{SC})] \times [1 - \mu_{sf}(\text{SP})] \times [1 - \mu_{sf}(\text{DE})] \times [1 - \mu_{sf}(\text{CL})] \times [1 - \mu_{sf}(\text{CV})] \\ &\quad \times [1 - \mu_{sf}(\text{HC})] \times [1 - \mu_{sf}(\text{RC})] \end{aligned}$$

In this case :

$$\begin{aligned} \mu_{sf} &= 1 - [1 - 0] \times [1 - 0] \times [1 - 0.45] \times [1 - 0] \times [1 - 0] \times [1 - 0.56] \times [1 - 0.86] \times [1 - 0] \\ &= 1 - 1 \times 1 \times 0.55 \times 1 \times 1 \times 0.44 \times 0.14 \times 1 \\ &= 0.965 \end{aligned}$$

The upper and lower bounds of the union and sum of flaw membership values can be used to determine the overall condition category considering the effects of all flaws. This is done by drawing or visualizing a condition classification histogram. In this histogram each classification or category is modeled as a four sided polygon of equal width, with

one side representing the union and the other the sum of flaws membership value. The area and moment of each category is calculated and combined to determine the overall condition category which most represents the combined effects of all flaws. For the example shown above this histogram would be as shown in Figure 9.

The weighted mean of the above membership is the total area divided by the total moment. For this example the calculations would be:

$$\begin{aligned} \text{Total Area} = & [\mu_{uvg} + 0.5x(\mu_{svg}-\mu_{uvg})] + [\mu_{ug} + 0.5x(\mu_{sg}-\mu_{ug})] \\ & + [\mu_{uf} + 0.5x(\mu_{sf}-\mu_{uf})] + [\mu_{up} + 0.5x(\mu_{sp}-\mu_{up})] \\ & + [\mu_{uvp} + 0.5x(\mu_{svp}-\mu_{uvp})] \end{aligned}$$

For this example:

| | |
|--------------------|---------------------|
| $\mu_{uvg} = 0.8$ | $\mu_{svg} = 0.8$ |
| $\mu_{ug} = 0.45$ | $\mu_{sg} = 0.6$ |
| $\mu_{uf} = 0.855$ | $\mu_{sf} = 0.965$ |
| $\mu_{up} = 0.563$ | $\mu_{sp} = 0.763$ |
| $\mu_{uvp} = 0.9$ | $\mu_{svp} = 0.974$ |

Therefore, the total area calculation would be:

$$\begin{aligned} \text{Total Area} &= [0.8+0.5x(0.8-0.8)] + [0.45+0.5x(0.6-.45)] + \\ & [0.855+0.5x(0.965-0.855)] + [0.563+0.5x(0.763-.563)] + \\ & [0.9+0.5x(0.974-0.9)] \\ &= (0.8) + [0.45+0.5x(0.15)] + [0.855+0.5x(0.11)] + [0.563+0.5x(0.2)] \\ & + [0.9+0.5x(0.074)] \\ &= 0.8+0.45+0.075+0.855+0.055+0.563+0.1+0.9+0.037 \\ &= 3.84 \end{aligned}$$

$$\begin{aligned} \text{Total Moment} &= 1x\mu_{uvg} + 1.17x[0.5x(\mu_{svg}-\mu_{uvg})] + 2x\mu_{ug} + 2.17x[0.5x(\mu_{sg}-\mu_{ug})] + \\ & 3x\mu_{uf} + 3.17x[0.5x(\mu_{sf}-\mu_{uf})] + 4x\mu_{up} + 4.17x[0.5x(\mu_{sp}-\mu_{up})] + \\ & 5\mu_{uvp} + 5.17x[0.5x(\mu_{svp}-\mu_{uvp})] \end{aligned}$$

$$\begin{aligned}
&= 0.8 + 1.17 \times 0.5 \times (0.8 - 0.8) + 2 \times 0.45 + 2.17 \times 0.5 \times (0.6 - 0.45) + 3 + 0.855 + 3.17 \times 0.5 \times (0.965 - 0.855) + 4 \times 0.563 + 4.17 \times 0.5 \times (0.763 - 0.563) + 5 \times 0.9 + 5.17 \times 0.5 \times (0.974 - 0.9) \\
&= 0.8 + 2 \times 0.45 + 2.17 \times 0.5 \times (0.15) + 3 \times 0.855 + 3.17 \times 0.5 \times (0.11) + 4 \times 0.563 + 4.17 \times 0.5 \times (0.2) + 5 \times 0.9 + 5.17 \times 0.5 \times (0.074) \\
&= 0.8 + 0.95 + 0.1628 + 2.56 + 0.1744 + 2.252 + 0.417 + 4.5 + 0.1913 \\
&= 11.97
\end{aligned}$$

Mean = Total Moment/Total Area

$$\begin{aligned}
&= 11.97/3.84 \\
&= 3.12
\end{aligned}$$

This provides a combined flaw condition rating of Fair on the scale of:

1 = very poor; 2 = poor; 3 = fair; 4 = good; and 5 = very good.

A similar exercise may be carried out for a large number of bridge structures and a rating obtained in each case. It may be mentioned here that the spreadsheet shown in Table 3 needs to be set up only once. For calculating the rating numbers, only the characteristic values need to be entered into the table and the rest is taken care off by the spreadsheet. Additionally, it is not required to enter values for each and every characteristic. Based on the rating number, a prioritization scheme may be adopted for rehabilitation of the structures.

Conclusions

The procedure for rating bridge structures for purposes of rehabilitation requires a careful evaluation of several complex factors. Such evaluation is often based on the personal judgement, intuition as well as the experience of each bridge inspector. As a result different inspectors may asses a given bridge differently. Fuzzy logic offers a logical assessment procedure capable of incorporating both objective knowledge and subjective judgement.

A number of factors such as cracking, scaling, spalling, delaminations etc., are known to effect the overall condition of bridge structures. Because of imprecise knowledge concerning the severity of the factors, linguistic instead of numerical rating variables are used to describe their condition.

Successful application of the fuzzy logic concepts to bridge structures depends on the development of adequate membership functions. The membership functions presented in the this paper are based on information from the literature and structural analysis. Membership functions can also be developed on the basis of expert opinion.

References

1. L.otfi A. Zadeh, "Fuzzy Sets. Information and Control. Vol.8", (Academic Press, New York, 1965), p.338
2. A. Kaufmann, "Theory of Fuzzy Sets", (Academic Press, New York, 1975)
3. C.V. Negoita, D.A. Ralescu, "Application of Fuzzy Sets to System Analysis", (Halstead Press, New York, 1975)
4. M. Gupta, G. Sardis, B. Gaines, Eds., "Fuzzy Automata and Decision Processes" (North-Holland, Amsterdam, 1977)
5. D. Dubois, H. Padre, "Fuzzy Sets and Systems", (Academic Press, New York, 1980).
6. C.V. Negoita, "Fuzzy Systems", (Abacus Press, Tunbridge Wells, England, 1981)
7. J.L.A. Chameau, A, Altschaeffl, H.L. Michael, J.T.P. Yao, Journal of Man-Machine Studies, 24(1983): P.9
8. M.D. Bowman, G.E. Nordmark, J.T.P. Yao, International Journal of Approximate Reasoning, 1(1987): p.197
9. A.B. Tee, M.D. Bowman, K.C. Sinha, Transportation Research Record, 1184 (1989): p.22
10. J.M. Sibigroth, AI Expert, April (1992): p.25
11. G. Viot, Dr. Dobb's Journal, February (1993): p.40

Table 1. List of Characteristics for Bridge Structures with Value Ranges and Relative Importance Coefficients

| Characteristic | Value Ranges | Relative Importance Coefficient* |
|----------------------|----------------------|----------------------------------|
| Crack Width | 0.001 - 0.040 inches | 0.75 |
| Depth of Scaling | 0.10 - 2.0 inches | 0.80 |
| Width of Spalling | 0.10 - 12.0 inches | 0.90 |
| Percent Delamination | 0 - 100 % | 0.90 |
| Chloride Content | 0 - 10 lbs/ cu.yd | 0.60 |
| Concrete Cover | 0 - 5 inches | 0.85 |
| Half Cell Potential | 0 - -650 mV vs CSE | 0.95 |
| Rate of Corrosion | 0 - 12 mA/sq.ft | 0.60 |

*1.0 = Important; 0.1 = Relatively Unimportant

Table 2. Raw Membership Table Based on Values Obtained from Figures 1 - 8

| | Very Good | Good | Fair | Poor | Very Poor |
|-----------|-----------|------|------|------|-----------|
| Cracks | 0 | 0 | 0 | 0.75 | 0.25 |
| Scaling | 1 | 0 | 0 | 0 | 0 |
| Spalling | 0 | 0.5 | 0.5 | 0 | 0 |
| Delams | 0 | 0 | 0 | 0 | 1 |
| Chloride | 0 | 0 | 0 | 0 | 1 |
| Cover | 0 | 0.34 | 0.66 | 0 | 0 |
| Half Cell | 0 | 0 | 0.9 | 0.1 | 0 |
| Corr.Rate | 0 | 0 | 0 | 0.67 | 0.33 |

Table 3. Corrected Membership Table After Multiplying with RI Coefficient

| | Very Good | Good | Fair | Poor | Very Poor |
|------------------------------|-----------|------|-------|-----------------|-----------|
| Cracks | 0 | 0 | 0 | 0.56 | 0.19 |
| Scaling | 0.80 | 0 | 0 | 0 | 0 |
| Spalling | 0 | 0.45 | 0.45 | 0 | 0 |
| Delams | 0 | 0 | 0 | 0 | 0.9 |
| Chloride | 0 | 0 | 0 | 0 | 0.6 |
| Cover | 0 | 0.29 | 0.56 | 0 | 0 |
| Half Cell | 0 | 0 | 0.86 | 0.1 | 0 |
| Corr. Rate | 0 | 0 | 0 | 0.4 | 0.2 |
| | | | | | |
| Union (Max) | 0.8 | 0.45 | 0.855 | 0.5625 | 0.9 |
| Sum of Flaws | 0.8 | 0.6 | 0.965 | 0.763 | 0.974 |
| | | | | | |
| Combined Effect of All Flaws | | | 3.12 | = Rating Number | |

Example Membership Values
 For Crack Width 0.027 in
 poor - 0.75 very poor - 0.25

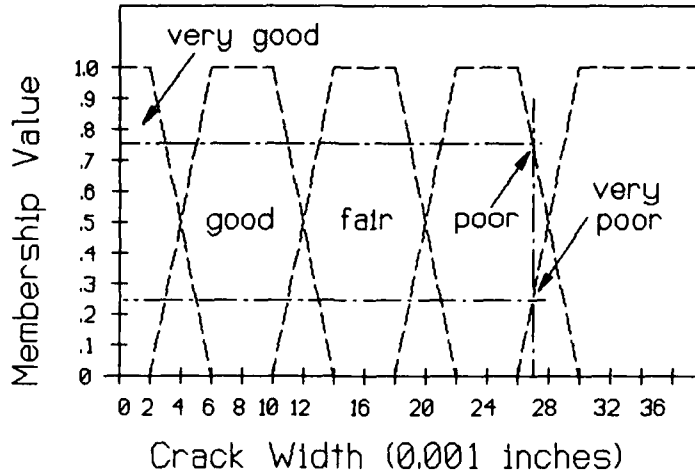


Figure 1. Determination of Raw Membership Value for Crack Width

Example membership value
 For depth of scaling 0.1 inch
 Very Good - 1

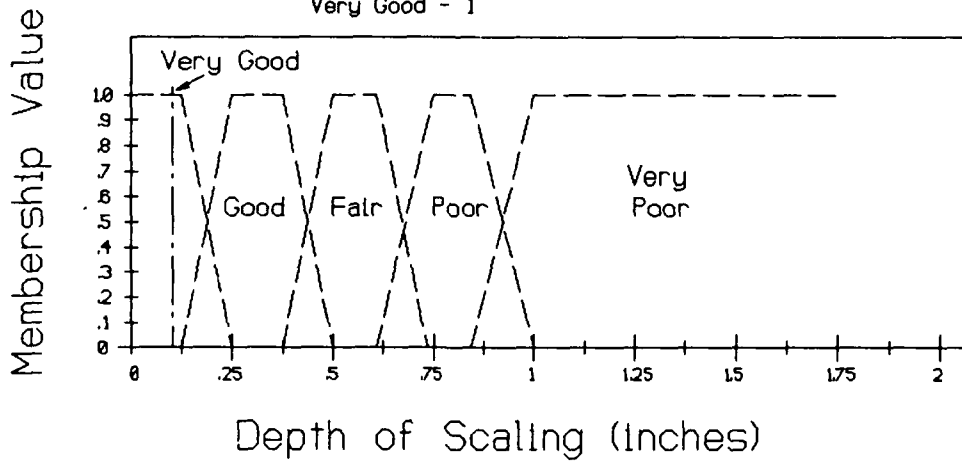


Figure 2. Determination of Raw Membership Value for Depth of Scaling

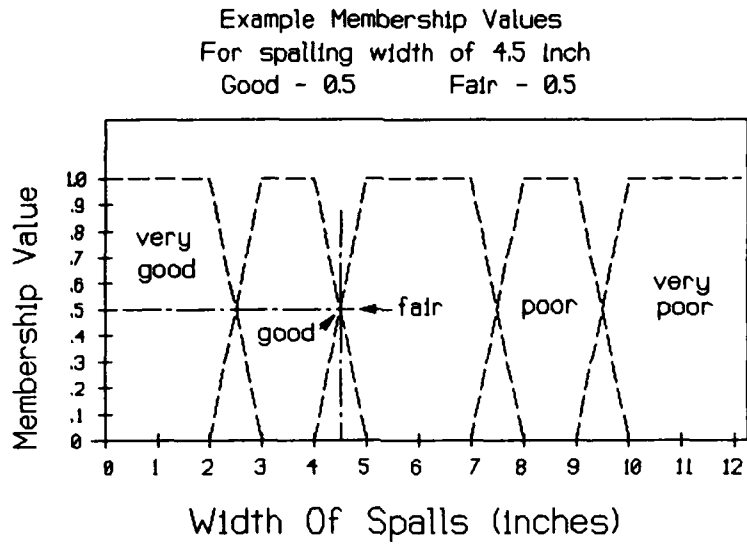


Figure 3. Determination of Raw Membership Value for Width of Spalling

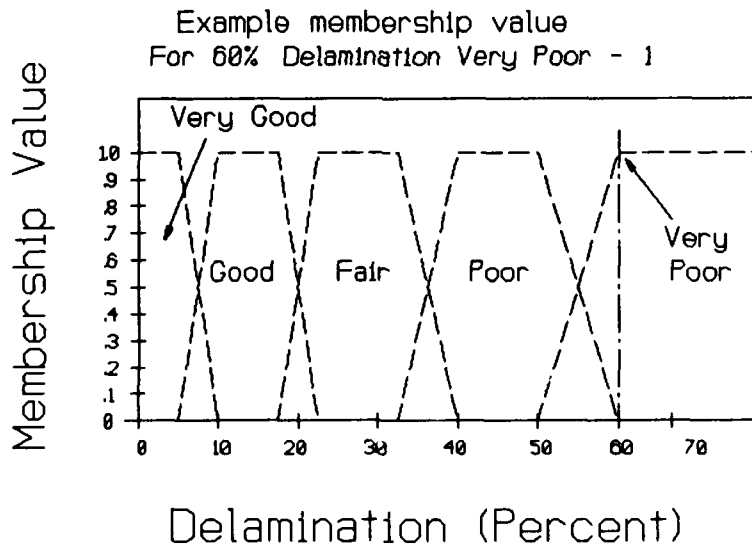


Figure 4. Determination of Raw Membership Value for Percent Delamination

Example Membership Value
 For Chloride content of 1.9 lbs/cuyd
 Very poor - 1.0

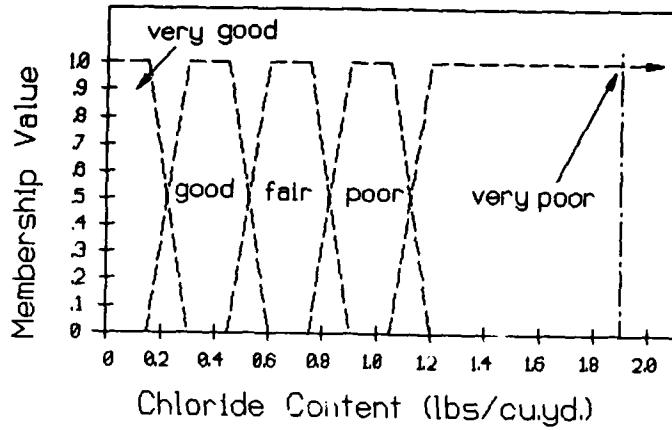


Figure 5. Determination of Raw Membership Value for Chloride Content

Example Membership Values
 For concrete cover of 2.17 inches
 Fair - 0.66 Good - 0.34

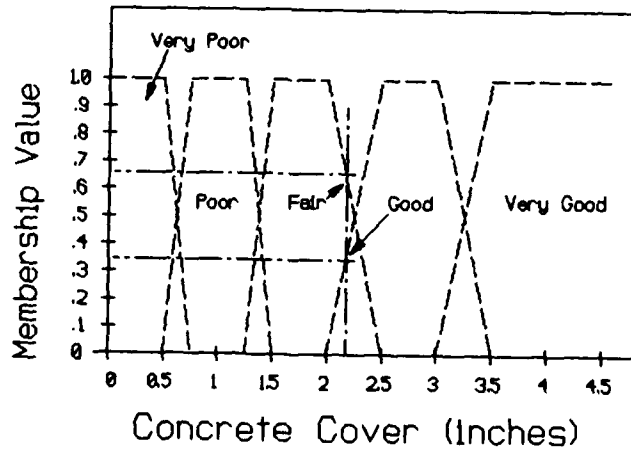


Figure 6. Determination of Raw Membership Value Depth of Concrete Cover

Example Membership Values
 For half cell potential -330 mV
 Fair - 0.9 Poor - 0.1

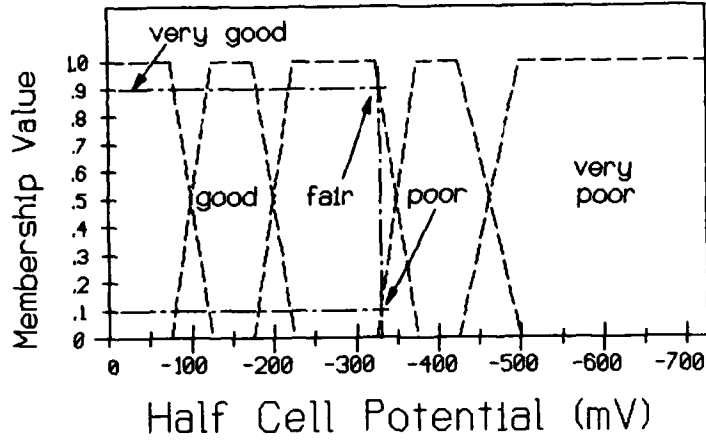


Figure 7. Determination of Raw Membership Values for Half Cell Potential

Example Membership Values
 For rate of corrosion of 9 mA/sqft
 Poor - 0.67 Very Poor - 0.33

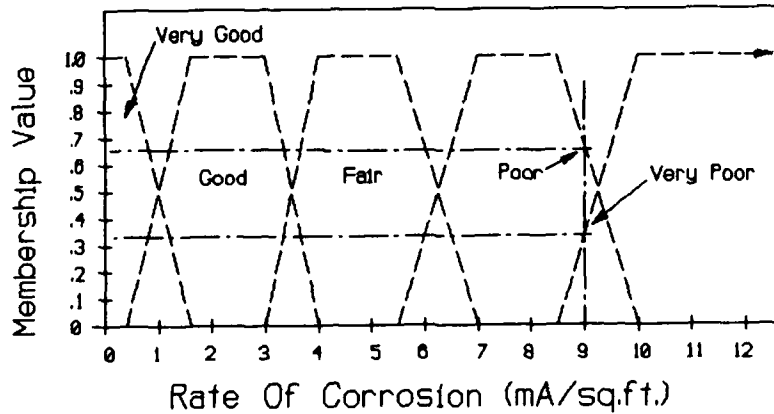
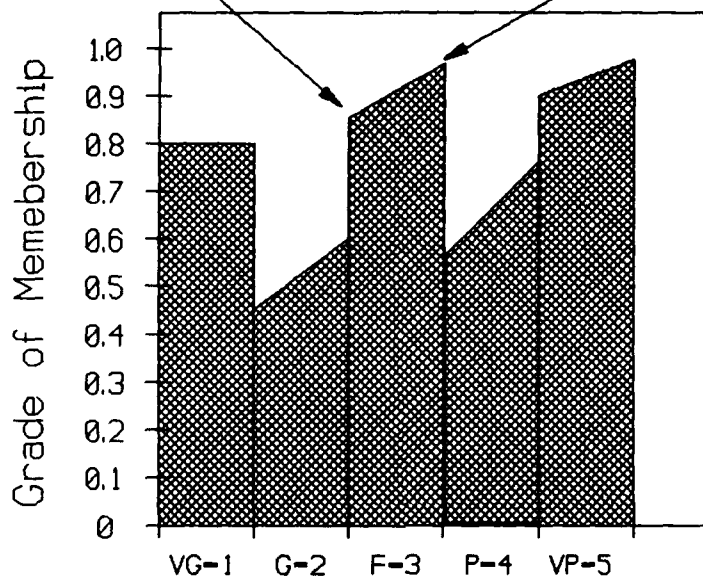


Figure 8. Determination of Raw Membership Values for Rate of Corrosion Measurements

Union for Fair Category Sum of Flaws for Fair Category



Histogram of Membership Values

Figure 9. Histogram of Membership Values

The System Analysis Of A National Scale Refining Equipment Corrosion Database

Yanhong Luo
Equipment Research Institute
Luoyang Petrochemical Engineering Corporation, SINOPEC
P.O. Box 063
Luoyang, Henan
471003 P.R. China

Abstract

Based on the synthetic analysis of a large number of corrosive factors and consideration for different customers' demands, the representative corrosion factors are optimized to form the elements of the database; relational data structure has been built up; normalised result is tested by set operation, which avoid the redundancy while the structure is reasonable; a hierarchical system architecture is applied to develop the functions for look-up, tabulation, drafting, analysis and forecast.

Key terms: corrosion, refining equipment, database, system analysis, structure design

Introduction

As the information era has come, more and more information occur in various fields of science. Information need to be processed, which include data collecting, recording, classifying, sequencing, storing, computing, transmitting, tabulation, drafting etc. This will makes significant information resources be used effectively. The database management system, as a speedy developing software, is a novel technique which make the data processing be managed scientifically. Today, database technique has become the necessary way in data processing. The Corrosion Database for Refining Equipment (CDRE for short) is initiated under such situation.

Definition Of The Objective Functions

CDRE orients to whole petrochemical engineering industry in China, it not only provides the decision-makers with macro-information and micro-information for surveying and judging but also provides the engineers and designers in corrosion circle for studying and analyzing, so that suitable measures will be taken. Although corrosion of refining equipment can be influenced by many factors^(1,2), taking too detailed corrosion factors into account is not available. Based on the synthetic analysis of a large number of factors and consideration for decision-makers, engineers or designers' different demands, the representative corrosion factors should be optimized to form the elements of the database which can reflect:

- A. The corrosive conditions when various crude oil are refined.
- B. The corrosion and protection on certain location of refining equipment in different corrosion surroundings.
- C. The corrosion and protection in different corrosion surroundings.

The realizations of above three functions can not only be independent but also become relative or infiltrated.

Structure Design

The structure design of a database contains data structure design and system structure design. The successful design of a database structure should have the following advantages: minimal redundant information, less error rate, enough flexibility, friendly user' interface, convenient programing and running. This is one of the most difficult tasks in database design^(a).

A. Data structure

Relational data structure is built up in CDRE. As an optimised result of corrosion factors, the fourteen data items that have no overlapping attributes form the following set:

Z- {Equipment, Location, Materials, Corrosion rate, Refining plant, Year, Crude oil, Salt(mg/l), Sulphur(%), Acid value(mg KOH/g), Nitrogen(%), Corrosion surroundings, Corrosion media, Temperature(K)}(1)

In the normalization process, four aspects are considered as follows:

1. Objective-facing. According to different objective-facing, the set Z is disintergrated into crude oil relationship set Z1, equipment relationship set Z2 and corrosion relationship set Z3:

Z1- {Crude oil flag, Crude oil, Salt(mg/l), Sulphur(%), Acid value(mg KOH/g), Nitrogen(%)}(2)

Z2- {Equipment flag, Equipment, Location, Materials, Corrosion rate, Refining plant, Year}(3)

Z3- {Corrosion surroundings flag, Corrosion surroundings, Corrosion media, Temperature(K)}(4)

2. Repetitive field treatment. To avoid parallel information repetition, the data that have such possibility are separated to father-and-son files connected by conjunction words. For example, a refining plant contains several sets of equipment, therefore, several repetitive plant fields would occur in a number of records of the equipment. To avoid the above redundancy, the refining plant and equipment are placed in two files which can be connected with each other if necessary.

3. Prevention of the disintergrate keyword dependence. Slave fields should rely on an intergrated keyword expression. Otherwise, if you put equipment and corrosion surroundings in one file, the index expression consists of both equipment flag and surroundings flag. However, the equipment information field rely on the equipment flag in the keyword instead of corrosion surroundings flag in keyword, thus, each piece of corrosion information must be input to equipment information. This will increase the number of data and the searching time. The problem can be solved by putting equipment information and corrosion surroundings information in two files which can be connected

with each other by conjunction words if necessary.

4. Transmission dependence treatment. In each file, all slave fields only rely on keywords rather than other fields.

After normalization, the data structure consists of six files:

R1-{Crude oil flag, Crude oil, Salt(mg/l), Surlphur(%), Acid value(mg KOH/g), Nitrogen(%)}(5)

R2-{Crude oil flag, Refining plant}(6)

R3-{Equipment flag, equipment, Year, Crude oil flag}(7)

R4-{Equipment flag, Location flag, Location, Materials, Corrosion rate}(8)

R5-{Corrosion surroundings flag, Corrosion media, Temperature(K), Location flag}(9)

R6-{Corrosion surroundings flag, Corrosion surroundings}(10)

Obvioualy,

$Z = \{(R1 \cup R2 \cup R3 \cup R4 \cup R5 \cup R6) - (R1 \cap R2) - (R2 \cap R3) - (R3 \cap R4) - (R4 \cap R5) - (R5 \cap R6)\}$ (11)

The equation (11) proves that these files are lossless joint, which is very important to the design of database structure. it guarantees any concrete relationship in original set be restored by its projection of disintegrated files through natural joint calculus^[4]. The design diagram of the data structure is shown in Fig. 1.

B. System structure

The system architecture design should realize the following objectives:

1. The easier way will be provided to users who would be able to get the necessary information without having the knowledge of file structure^[6].

2. Besides keywords, refining plant, years, corrosion media, materials or location can be indexed.

3. Corrosion principle can be described in chart.

It is corollary that as the corrosion records of refining equipment change annually, data can be easily updated, added, modified and deleted without affecting existing program.

A hierachical architecture is applied to the CDRE' system. Function modules are adopted to realize all the functions. Multi-funtions in one module and several function modules are

arranged in tree structures, which are scheduled through master control module. Main menus to select six major functions are provided by master control module. The system architecture is shown in Fig. 2.

The characteristics of the module structure lie in independence of each module, which is beneficial to separately programming and function modifying of individual modules and also convenient to later function modification and extension. Besides, on-line help module provides users with detailed function introductions, operating description and error signals.

Conclusion

Based on the synthetic analysis of a large number of corrosion factors for refining equipment, the key factors have been optimized to build up an effective database structure, which has minimal redundancy in data structure, less error rate, more flexibility and friendly users' interface. That lays the excellent foundation for programming and running.

References

1. Institute of Chemical Machinery (Ministry of Chemical Industry) : Corrosion and Anti-Corrosion Manual, Chemical Industry Publishing House, Beijing (1988)
2. Beijing Design Institute (SINOPEC) : Refining Plant Heating Furnace Design Manual (Section Four), Hydrocarbon Press, Beijing (1986)
3. Zhou Su : dBASE IV Design, Tianjing Scientific Publishing House, Tianjing (1990), p.437
4. Zheng Ruozhong : Database Principles and Methods, Hunan Scientific Publishing House, Changsha (1983), p.175
5. Gio Wiederhold : Database Design, McGraw-Hill Book Company, New York (1983), p.450

Acknowledgment

I thank especially Xingzhong Lin and Jingling Xiao (senior engineers), Liqun Xiao and Weimin Lu (engineers) for their reviews and corrections.

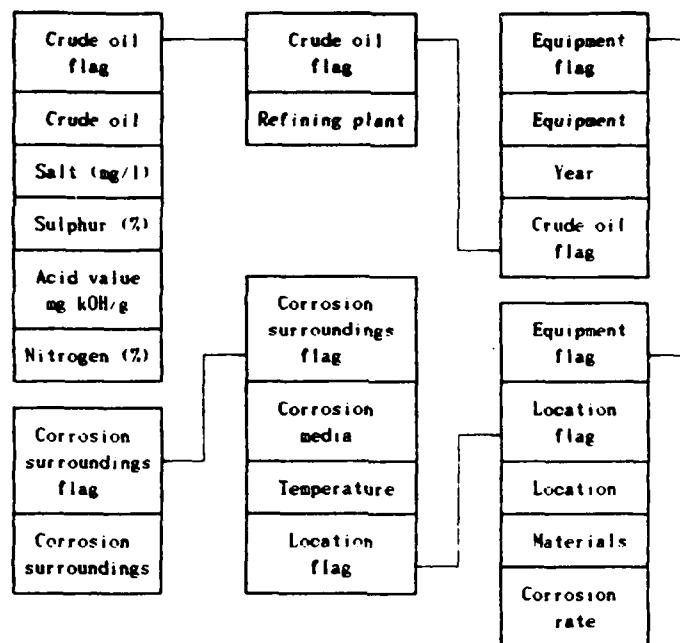


Fig. 1 Data structure

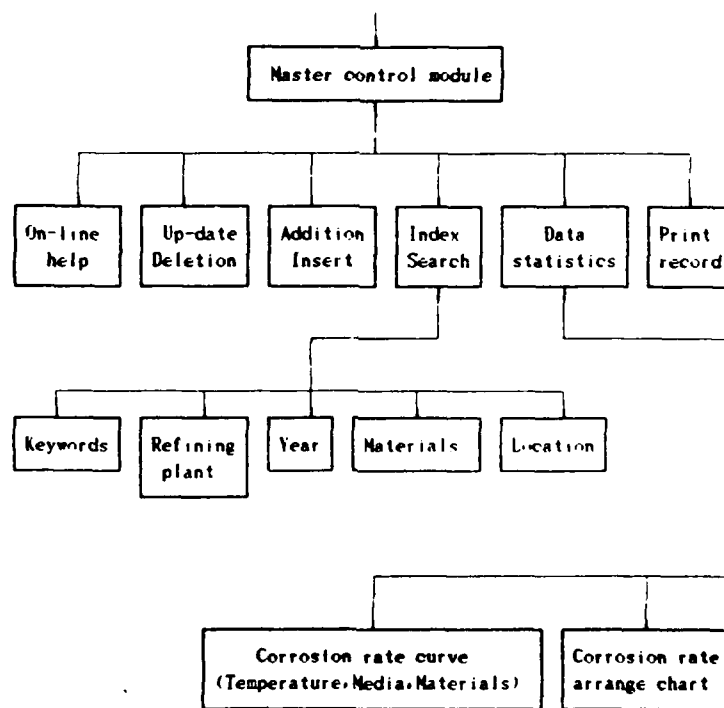


Fig. 2 System architecture

Interpretation of Electrochemical Impedance Data for Damaged Automotive Paint Films

Carlos Diaz, Mirna Urquidi-Macdonald, and Digby D. Macdonald
The Pennsylvania State University
Center for Advanced Materials
517 Deike Building
University Park, PA 16802

A.C. Ramamurthy
BASF Corporation
Southfield, MI

Wim J. van Ooij and Ashok Sabata
Armco Research and Technology
Middletown, OH

Mats Ström and Gunnar Ström
AB Volvo
Gothenburg, Sweden

Abstract

In this paper, we outline the use of Electrochemical Impedance Spectroscopy (EIS) in characterizing damage to painted automotive panels, in which the damage has been nucleated by particle impact. We illustrate the use of the Kramers-Kronig transforms in validating the impedance data, and we identify common sources of error. Using EIS data obtained from a test program, we show how the impedance data are identified and analyzed. For the latter, we use electrical transmission line models that simulate the extension of corrosion damage beneath the paint film as disbonding occurs between the phosphate layer and the galvanized coating. The transmission line model possesses cylindrical geometry, and the model parameters are estimated by using multivariate fitting (optimization) algorithms operating on an impedance data set that covers a wide range of frequency. By using these procedures, we establish correlations between the type and extent of damage, environmental parameters, and properties of the paint and substrate.

Key terms: electrochemical impedance, automotive paint films

Introduction

The durability of coatings is a key issue in maintaining corrosion protection in automobiles, particularly in those exposed to corrosive environments. The coatings must not only be capable of withstanding chemical attack by deleterious species in the environment (e.g. road salt, acid rain), but they must also resist impact damage of the type that may result in perforation of the paint and hence in the nucleation of localized corrosion. Over the past few years, extensive test programs have been carried out (e.g. by BASF/Armco/Volvo) with the goal of identifying those structural, morphological, and chemical factors that render coatings (paints) resistant to damage. Electrochemical impedance spectroscopy (EIS) is now being employed as an analytical tool for characterizing the type and extent of damage, so that it ultimately may not only be used as a quality control probe, but it may also yield fundamental information on the nucleation and development of the damage.

EIS measures the electrochemical transfer function by superimposing a small amplitude alternating voltage or current across the metal/coating/test solution interphase and by then measuring the steady-state alternating response (current or voltage, respectively). Because the perturbation and response are vector quantities, the ratio (known as the admittance or impedance

for controlled voltage or current, respectively) contains both phase and amplitude information. Provided that the system conforms to the constraints of linear systems theory (LST), which can be demonstrated by using the Kramers-Kronig transforms, the impedance (or admittance) data can be interpreted in terms of passive electrical analogs composed of resistors, capacitors, and inductors.

In this paper, we will outline the use of EIS to characterize damage to painted automotive panels in which the damage has been nucleated by particle impact. We will illustrate the use of the Kramers-Kronig transforms in validating the impedance data, and we will identify common sources of error. Using EIS data obtained on panels from the test program, we will show how the impedance data are obtained and interpreted. For the latter, we use an electrical transmission line model that simulates the extension of corrosion damage beneath the paint film as disbonding occurs between the phosphate layer and the galvanized coating.

Description of the Experimental Data Sets

The samples used for this study were commercial quality sheets of galvanized steel covered with a layer of polycrystalline phosphate. A coating of a commercial paint was applied on top of the phosphate layer, following standard industrial procedures for the manufacture of auto bodies. As is now widely used in this kind of study, artificial defects were generated on the samples, by drilling very small holes through the coatings (zinc and paint—see, for example, Ref. 1). It is assumed that the defect compromises the paint and zinc layers, but does not penetrate the steel, which remains intact. The samples were exposed in a climate test chamber², as part of an extensive study on the effect of structural, morphological and environmental factors on the corrosion in auto bodies^{3,4}. The complete test involves a 12 week period, in which the samples were exposed to periodic changes in the environment. Every week the samples were extracted from the chamber temporarily for the EIS measurements. These measurements were made with a standard experimental setup, in which the sample is both the working electrode and the bottom wall of the cell. A SCE was used as reference, placed 1 cm above the sample, and a H₂SO₄ solution was used as the electrolyte. The frequencies used span the range from 0.01Hz to 100kHz. In this way, 12 data sets, one corresponding to each week of the test, were obtained for each sample. A sample of the experimental data sets is shown in Figure 1.

Validation of Experimental Data

Proof that the system conforms to the constraints of Linear Systems Theory (LST) is essential before any attempt can be made to interpret the impedance data in terms of passive electrical analogs composed of resistors, capacitors, inductors, and diffusion-related elements. These kinds of electrical circuit models are commonly used in the literature to analyze EIS data for painted metals⁵, although seldom, if ever, are the data demonstrated to conform to LST. Validation of the experimental data can be carried out by means of the Kramers-Kronig (KK) transformations^{6,7} provided that the real and imaginary components of the impedance span a wide enough frequency range. These well-known integral relations state that the real and imaginary components of the impedance are not independent quantities. Instead, if the experimental data span a wide enough frequency range, one component of the complex impedance can be determined from the other by integrating over frequency on either side of the frequency of transform. The use of these relations requires knowledge of the impedance as a function of frequency for at least two orders in magnitude of frequency above and below the frequency of transform.

We have carried out the KK transformations on the present experimental data sets, and our results show, in general, good agreement between the experimental values and the values calculated from the transformation relations over most of the frequency range. The deviation of

the calculated values with respect to the experimental data increases at lower frequencies, as can be seen in Figure 2, which is a typical result. The deviation at low frequencies is most probably due to instability resulting in a slow drift with time of the electrochemical properties of the system, such that the properties of the system may change significantly over the data acquisition time (inverse of the frequency).

Transmission Line Model

A problem that frequently arises when measuring electrochemical properties of systems of the type considered here is due to the asymmetrical geometry. This produces a "transmission line" effect, that has been considered by several authors in relation to other experimental situations⁸. This effect appears when the electrochemically active surface of the metal is not uniformly accessible to the monitoring signal. More specifically, the penetration length of the signal applied at the monitoring point (which, in our case, is the external border of the defect) depends on the frequency of the perturbation.

To account for this feature, we have developed a transmission line model for the system that employs radial symmetry. This is based on the well-known fact that the corrosion process in this system, which principally affects the zinc layer, propagates radially from the defect site. Also, we consider that it is extremely important in the present work to recognize that the geometrical parameters may change with time of exposure to the corrosive environment. A transmission line model can help to interpretate the results, not only in terms of the intrinsic impedance of the metal/solution interface, but also in terms of the particular electrode geometry, both of which may depend on the time of exposure.

For the development of the model, we considered a metallic electrode, composed of a sheet of steel, coated with a layer of zinc. On top of the zinc layer there is a coating of paint, which is considered to be an insulator. The sample has an artificial defect, which is cylindrical, with a given radius, r_0 , and the defect reaches the steel surface but does not penetrate into the substrate. We also suppose that the system has suffered some degree of corrosion, which produced dissolution of the zinc layer and resulted in delamination of the paint to form a characteristic blister. The cavity under the blister is assumed to be disk-shaped, of radius r_b and of a constant thickness δ (r -independent). A diagram of the geometry of the model is shown in Figure 3 and details of the cross section are shown in Figure 4.

We assume that the potential of the metal phase is constant, while the potential in the solution phase is r -dependent, $V(r)$. By applying Ohm's and Kirchoff's laws to any circular ring in the disk-shaped cavity, of internal radius r and external radius $r+dr$, we obtain the following equations for the potential $V(r)$ and the current $i(r)$

$$\frac{dV(r)}{dr} = - \frac{R_s}{2\pi r \delta} i(r) \quad (1)$$

$$\frac{di(r)}{dr} = - \frac{2\pi r}{Z_i} V(r) \quad (2)$$

where R_s is the solution resistivity and Z_i is the impedance of the metal/solution interphase. By differentiation and rearrangement of both equations, we obtain

$$\frac{d^2V(r)}{dr^2} = - \frac{1}{r} \frac{dV(r)}{dr} + \alpha V(r) \quad (3)$$

$$\frac{d^2 i(r)}{dr^2} = -\frac{1}{r} \frac{di(r)}{dr} + \alpha i(r) \quad (4)$$

where $\alpha = Rs/Zi\delta$. By making the transformation $x = r\alpha^{1/2}$, these equations take the form

$$f''(x) = -\frac{1}{x} f'(x) + f(x) \quad (5)$$

where f is either V or i . This equation corresponds to the modified Bessel equation, and its solutions are given by

$$f(x) = A I_0(x) + B K_0(x) \quad (6)$$

where $I_0(x)$ and $K_0(x)$ are the modified Bessel functions of zero-order. The integration constants A and B are given by the boundary conditions that apply to the potential and current:

$$I(x_0) = I_{\text{applied}} \quad I(x_b) = 0 \quad (7)$$

$$\left. \frac{dV(x)}{dx} \right|_{x=x_0} = -I(x_0) \frac{\rho}{2\pi x_0 \delta} \quad \left. \frac{dV(x)}{dx} \right|_{x=x_b} = 0 \quad (8)$$

where x_0 and x_b are the values of x corresponding to r_0 and r_b , respectively. The total impedance of the metal surface under the blister, is then given by

$$Z_T = \left. \frac{V(x)}{I(x)} \right|_{x=x_0} \quad (9)$$

By applying the boundary conditions to the solutions and replacing in the last equation, we obtain

$$Z_T = -\frac{Rs}{2\pi x_0 \delta} \frac{I_0(x_0) K_1(x_b) + I_1(x_b) K_0(x_0)}{I_1(x_0) K_1(x_b) - I_1(x_b) K_1(x_0)} \quad (10)$$

where I_1 and K_1 are the modified Bessel functions of first order. To obtain the measured impedance, we must add to this expression:

1. The resistance of the solution between the sample and the reference electrode; this term is given by the resistivity of the solution times the distance between the working and reference electrode;
2. The capacitance generated by the intact paint, which is proportional to the relative dielectric constant and the exposed surface area of intact coating, and is inversely proportional to the thickness; the proportionality constant being the permittivity of the space. Because the impedance of the coating is inversely proportional to frequency, its effect on the impedance of the interphase is expected to be more visible at higher frequencies.

General Results

We have carried out numerous calculations using the model outlined above to obtain the parameter values that best reproduce the experimental data sets, by using different electrical circuit analogs for the interfacial impedance (Z_i in Figure 4). We have also evaluated various analogs that describe the cathodic and anodic processes contained within the interfacial impedance function.

The average of the determined values for the cavity thickness was 2.2×10^{-5} cm, and was found to be almost constant with time, with a very low dispersion between the different data sets. This value is lower than expected, being about 5 times smaller than the zinc layer thickness. This difference might be due to the fact that the quotient between the solution resistivity R_s and the cavity thickness δ behaves as only one parameter in the model. We have kept constant the value of the solution resistivity (estimated from the composition of the electrolyte solution used for the measurements); accordingly, the low value for the cavity thickness possible reflects the fact that the solution resistivity in the cavity is much larger than the value for the electrolyte solution used in the impedance measurements. Also, previous surface studies on similar samples³ have shown that the cavity appears to fill with corrosion products, thereby, decreasing the effective free space occupied by the solution.

The values determined for the cavity radius are shown as a function of time in Figure 5. The radius of the cavity grows rapidly during the initial stages of exposure to the corrosive environment, but after about 6 weeks, the cavity shows little further growth. This is expected, because the periphery scales directly with the radius so that if the current exiting the defect changed only slowly with time, the current density for zinc corrosion should vary inversely with r . Furthermore, increasing radius results in a substantial increase in the resistance in the crevice, which will have the effect of progressively depressing the current exiting the defect with time.

The capacitance of the paint coating is found to be very low, with an average value of 5.0×10^{-9} Fcm⁻² and is found to not change with time. This low value may be an indication that the paint does not absorb water in significant quantities over the time of the exposure experiments.

The values of the parameters that determine the interfacial impedance could not be determined as accurately as those discussed above. From the several models used for this part of the analysis, we have chosen one that accounts for separate contributions from the anodic and cathodic processes. We attempted to use serial combinations of polarization resistances (R) and diffusional impedances (W) for these two processes, with the analog for each partial process being connected in parallel with the double layer capacitance (C_{dl}). A diagram of this arrangement is shown in Figure 6. The diffusional (Warburg) components of the interfacial impedance were expressed in the form

$$W_i = R_{W2} \cdot \text{th}(j\omega\tau_i)^{1/2} / (j\omega)^{1/2} \quad (11)$$

where "th" signifies the hyperbolic tangent function, $j = \sqrt{-1}$, and τ_i is a relaxation time. Equation (11) corresponds to diffusion over a finite length⁹. Provided that $\omega\tau_i$ is sufficiently small, Equation (11) converts to the semi-infinite Warburg expression.

$$W_i = \sigma_i / \omega^{1/2} - j \sigma_i / \omega^{1/2} \quad (12)$$

where $\sigma_i = \sqrt{2} \cdot R_{W2}$. Both Equations (11) and (12) were used in these simulations and, for exposure periods up to ten weeks, no significant difference resulted from using either form.

However, for the last two exposure periods, the finite-length expression for W_1 (Equation (11)) provided a significantly better fit than did the expression (Equation (12)) for semi-infinite diffusion. Because the radius of the crevice increases with exposure time, the transition from semi-infinite to finite-length diffusion conditions cannot be associated with the change in the crevice dimension. A more likely explanation is that the transition arises from the accumulation of corrosion products within the crevice.

The results of several calculations and optimizations with this model have shown that it is difficult to determine significant values for one of the diffusional impedances, particularly the one directly connected to the lower polarization resistance. The average values found were $R_1 = 91 \text{ k}\Omega$, $R_2 = 430 \text{ k}\Omega$, $W_2 = 204 \text{ k}\Omega$, $\tau_{W2} = 3.6 \text{ s}$, $C_{dl} = 1.4 \text{ }\mu\text{F}\cdot\text{cm}^2$. The most important result stemming from these parameters is that their values do not show any systematic dependence on time after the second week of exposure, although in some cases the standard deviations are very large.

Discussion

In general, we can see that the model is able to reproduce the general characteristics of the experimental impedance data by changing only the parameters that define the electrode geometry, while keeping the interfacial impedance related parameters almost time-independent (Figure 7). *This is an important finding, because it demonstrates that the changes observed in the measured impedance are due almost entirely to dimensional (geometrical) changes, and not to variations in the specific electrochemical properties inside the crevice.* In turn, this finding suggests that the crevice reaches a steady state with respect to the specific interfacial parameters soon after rupture of the paint film.

The model can be extended to account for more fine details of the system. One feature that should be addressed is that the cavity under the blister is not completely full of electrolyte solution but, instead, it may contain large quantities of corrosion products, in the form of a porous phase of precipitated zinc compounds. Also, the corrosion products can be electrochemically inactive (as $\text{Zn}(\text{OH})_2/\text{Zn}(\text{OH})_2\cdot\text{ZnCl}_2$) or active (as ZnO , which may be an active cathode). Another improvement in the model may involve relaxing the assumption that the cavity is disk-shaped and is of constant thickness. Furthermore, the model may be extended by assuming an explicit spatial separation between the cathodic and anodic areas. Some of these features are being investigated in order to explore how readily they might be incorporated into the model.

Still, the problem remains of how to best consider the impedance of the metal/solution interphase. In this study, we explored simulations that assume a simple equivalent electrical circuits for the impedance functions for complex electrochemical reaction mechanisms. A more satisfactory approach would be to use a hybrid model, in which the geometrical properties of the system are accounted for in terms of a transmission line of cylindrical geometry (as employed in this paper) and the interfacial impedances are described in terms of reaction models. The reaction models would include charge transfer processes at the electrode surface coupled with chemical reactions in the electrolyte and in precipitated reaction product phases, and with the mass transport of reactants and products to and from the metal surface. Perhaps the most efficient way of incorporating these models is to use the formalism of the "schemes of squares"¹⁰. We believe that this procedure will yield a flexible way to develop more physically-realistic models of the complex electrochemical processes that lead to the development of damage. We are presently incorporating these methods into the blister impedance simulation software.

Acknowledgments

The authors gratefully acknowledge the support of this work by the BASF Corporation through a Grant-in-Aid to The Pennsylvania State University.

References

1. F.M. Geenen, J.H.W. de Wit and E.P.M. van Westing, *Prog. Org. Coat.* **18** (1990) 299.
2. M. Ström, G. Ström, W.J. van Ooij, A. Sabata, R.A. Edwards and A.C. Ramamurthy, *SAE Tech. Paper Series No. 912282* (1991).
3. W.J. van Ooij, A. Sabata, D. Loison, T. Jossic and J.C. Charbonier, *J. Adhesion Sci. Technol.* **3** (1989) 1; *idem*, **3** (1989) 79.
4. W.J. van Ooij and A. Sabata, *Scand. J. Metallurgy* **21** (1992) 32.
5. G.W. Walter, D.N. Nguyen and M.A.D. Madurasinghe, *Electrochim. Acta* **37** (1992) 245.
6. M. Urquidi-Macdonald, S. Real and D.D. Macdonald, *J. Electrochem. Soc.* **133** (1986) 2018.
7. M. Urquidi-Macdonald, S. Real and D.D. Macdonald, *Electrochim. Acta* **35** (1990) 1559.
8. D.D. Macdonald, M. Urquidi-Macdonald, R.C. Rocha-Filho and Y. El-Tantawy, *Corrosion* **47** (1991) 330.
9. J.R. Macdonald (Ed.), *Impedance Spectroscopy*, John Wiley & Sons, New York, NY 1987.
10. M. Seralathan and S.K. Rangarajan, *J. Electroanal. Chem.*, **191** (1985) 209; *idem*, **109** (1985) 229; *idem*; **109** (1985) 237.

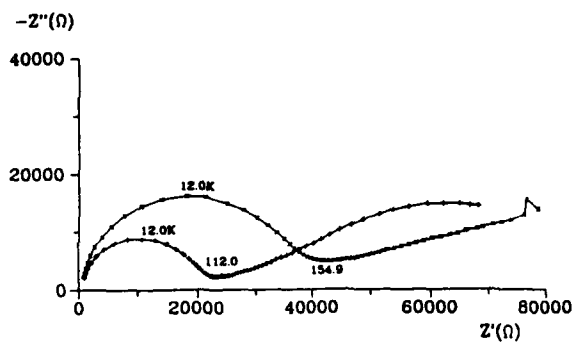


Figure 1. A sample of the experimental data obtained for the painted metals. The two impedance spectra shown correspond to the 6th (x) and the 12th (+) week of the test, for the same sample. The numbers superimposed are the frequencies, in Hz, of the maximum and minimum of each curve.

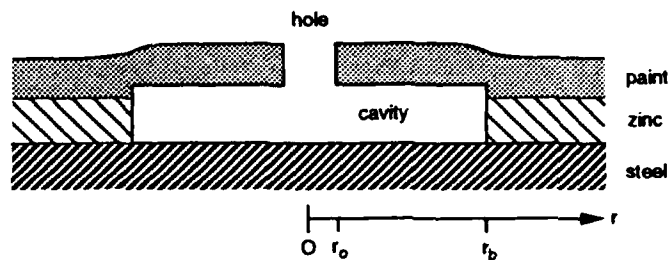


Figure 3. Schematic of the cross section of the sample at the position of the defect, showing the steel substrate, the zinc and the paint layers, and the cavity formed by zinc dissolution.

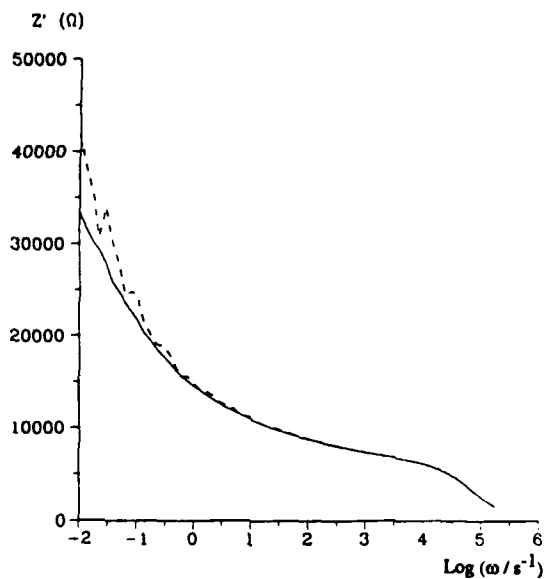


Figure 2. Imaginary axis-to-real axis Kramers-Kronig transform of one of the data sets for the third week of the test. The continuous line represents the experimental points while the broken line represents the calculated points.

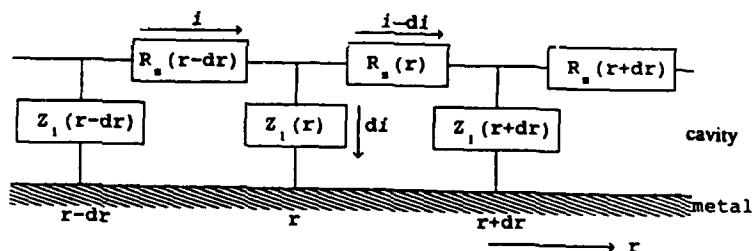


Figure 4. Detail of the radial transmission line model used to analyze the corrosion process under a blister on painted steel. R_s is the resistance of an element dr in the cavity, which is given by $R_s(r) = (\rho_s/2\pi r\delta) \cdot dr$, where ρ_s is the resistivity of the solution (in $\Omega \text{ cm}$) and δ is the thickness of the cavity under the blister (in cm). Z_i is the specific impedance of the interphase metal/solution (in $\Omega \text{ cm}^2$).

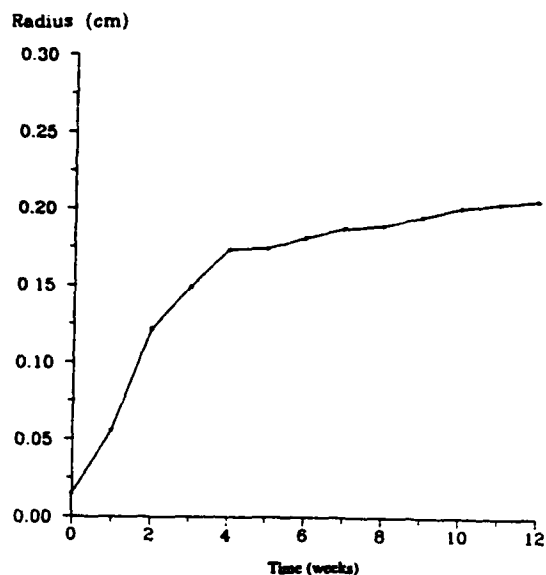


Figure 5. Cavity radius for the radial transmission line as a function of the exposure time.

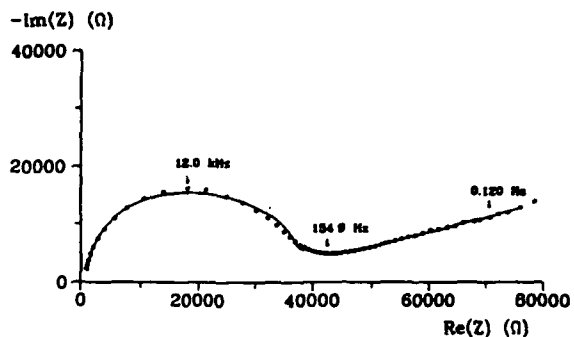


Figure 7. Comparison of experimental (*) and fitted (—) values for a data set corresponding to week number 6. Some frequency values are shown. The computed values were obtained with the following parameter values: $r_0=0.015\text{cm}$, $r_b=0.181\text{cm}$, $\delta=2.23\times 10^{-5}\text{cm}$, $C_{\text{paint}}=5.0\times 10^{-9}\text{Fcm}^2$, $R_1=95.3\text{k}\Omega$, $R_2=423.6\text{k}\Omega$, $R_{W2}=256.3\text{k}\Omega$, $\tau_{W2}=3.6\text{s}$, and $C_{dl}=1.3\times 10^{-6}\text{Fcm}^2$.

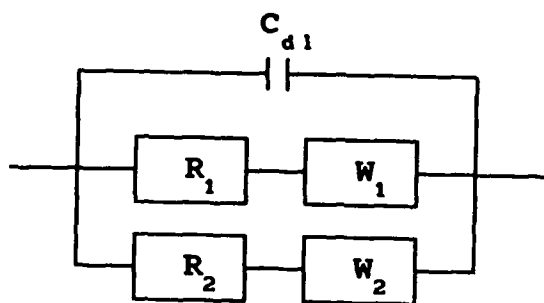


Figure 6. Electrical circuit analog for the impedance of the interphase metal/solution.

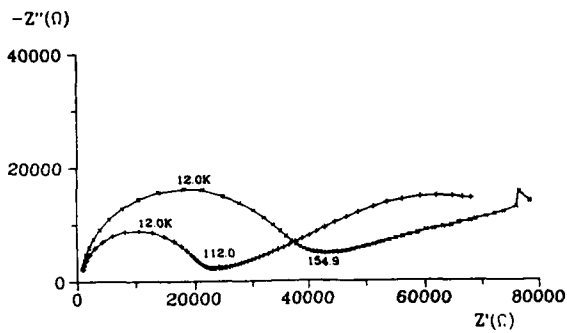


Figure 1. A sample of the experimental data obtained for the painted metals. The two impedance spectra shown correspond to the 6th (x) and the 12th (+) week of the test, for the same sample. The numbers superimposed are the frequencies, in Hz, of the maximum and minimum of each curve.

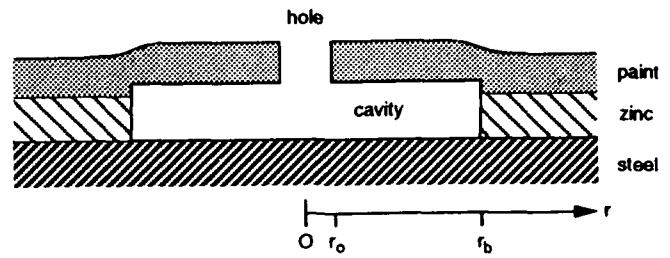


Figure 3. Schematic of the cross section of the sample at the position of the defect, showing the steel substrate, the zinc and the paint layers, and the cavity formed by zinc dissolution.

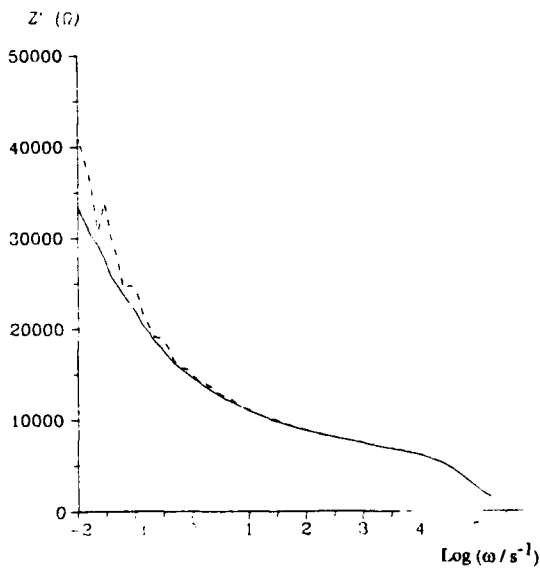


Figure 2. Imaginary axis-to-real axis Kramers-Kronig transform of one of the data sets for the third week of the test. The continuous line represents the experimental points while the broken line represents the calculated points.

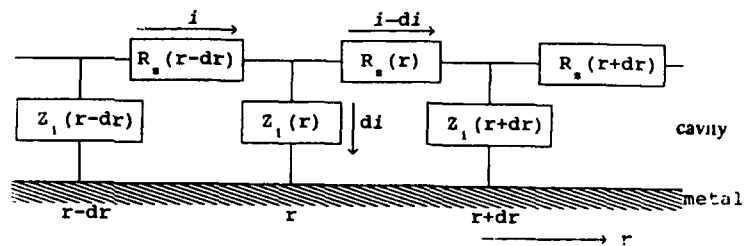


Figure 4. Detail of the radial transmission line model used to analyze the corrosion process under a blister on painted steel. R_s is the resistance of an element dr in the cavity, which is given by $R_s(r) = (\rho_s/2\pi r\delta) \cdot dr$, where ρ_s is the resistivity of the solution (in $\Omega \text{ cm}$) and δ is the thickness of the cavity under the blister (in cm). Z_i is the specific impedance of the interphase metal/solution (in $\Omega \text{ cm}^2$).

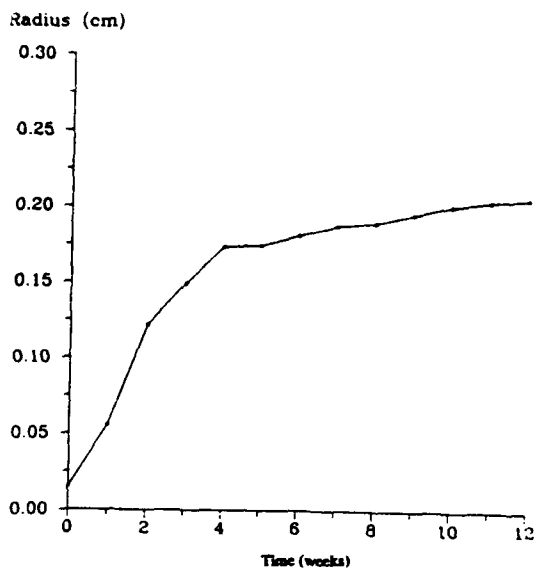


Figure 5. Cavity radius for the radial transmission line as a function of the exposure time.

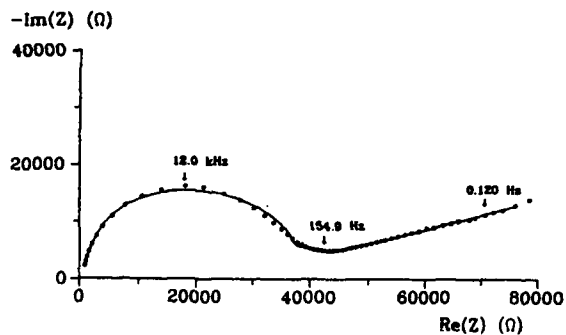


Figure 7. Comparison of experimental (*) and fitted (—) values for a data set corresponding to week number 6. Some frequency values are shown. The computed values were obtained with the following parameter values: $r_0=0.015\text{cm}$, $r_b=0.181\text{cm}$, $\delta=2.23\times 10^{-5}\text{cm}$, $C_{\text{paint}}=5.0\times 10^{-9}\text{Fcm}^2$, $R_1=95.3\text{k}\Omega$, $R_2=423.6\text{k}\Omega$, $R_{W2}=256.3\text{k}\Omega$, $\tau_{W2}=3.6\text{s}$, and $C_{dl}=1.3\times 10^{-6}\text{Fcm}^2$.

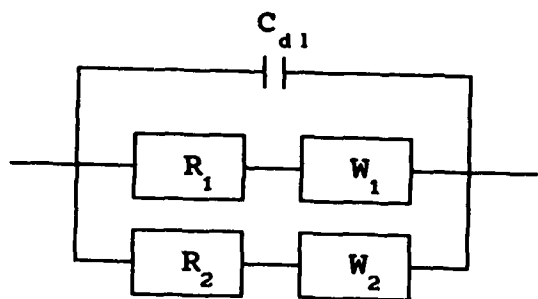


Figure 6. Electrical circuit analog for the impedance of the interphase metal/solution.

A Test of the Reliability of Mathematically Modeling Corrosion

J. Peter Ault, Jr.
Ocean City Research Corporation
Tennessee Avenue and Beach Thorofare
Ocean City, New Jersey USA

John J. Meany, Jr.
Bismarck, Inc.
PO Box 1006
Ocean City, New Jersey USA

Abstract

Engineers increasingly solve corrosion control design problems and analyze corrosion processes using mathematical models, particularly finite element-type models. Often this approach becomes complicated and its basis obscure. A pragmatic corrosion engineer may wonder if such approaches constitute window dressing and image projection rather than a straightforward and understandable engineering approach.

The present paper compares finite element modeling predictions to the results of a controlled laboratory full scale test. The finite element model supposedly predicted the expected life for the anodic alloy tubing where tubing of two different alloys connected with internal flowing seawater. The full scale test results show that the mathematical model didn't consider either the effects of time and environmental variables or pitting corrosion.

The laboratory test results show that neither the measurement of galvanic current nor the mathematical model calculation forms a basis for estimating of the magnitude of the most important type of corrosion of 70/30 CuNi tubing. The laboratory tests identified pitting corrosion as most important. The deepest pit was not immediately adjacent to the Inconel 625 tubing as most mathematical models predict. For the particular tubing configuration tested, turbulence-induced corrosion caused more damage than that relating to the Inconel 625-70/30 CuNi couple. Thus, in-service mismatches between Inconel 625 and 70/30 CuNi tubing may be of more concern about corrosion of the CuNi tubing than galvanic effects.

The laboratory testing results comprised physical examination of specimens exposed to flowing seawater for six months with the continuous monitoring of the more significant environmental variables. The comparison of modeling predictions and actual tubing corrosion places suspicion upon the mathematical model. It appears that the model provides reasonable "order of magnitude" estimation of galvanic current flow. The model neither accurately predicted long term current distribution nor the magnitude of pitting corrosion. This raises a very pertinent question -- "If a mathematical model can't reliably handle simple galvanic corrosion, how reliable are such models when applied to more complex situations?"

Introduction

OCRC obtained a computer program which had been used to calculate the expected galvanic corrosion rate of 70/30 CuNi alloy piping when coupled to Inconel 625 piping. D.J. Astley developed the technical approach that formed the basis for the program. His paper is entitled, "A Method for Calculating the Extent of Galvanic Corrosion and Cathodic Protection in Metal Tubes Assuming Unidirectional Current

Flow," (Corrosion Science Vol. 23, No. 8, pp 801-832, 1983). The technique described by the paper applies Ohm's and Kirchoff's laws to the piping geometry. It assumes: 1) unidirectional current flow down the length of the pipe; 2) the electrode (metal surface) corrosion potential against a standard electrode varies linearly down the pipe in direct proportion to the local current flow; and 3) the decrease in current flow down the pipe is the result of current flow to the tube wall resulting in local polarization. Tube wall polarization behavior is approximated by a linear polarization resistance term. The present report presents the results of limited testing conducted with the objective of validating the model through the comparison of the results of laboratory test results with those of the model.

Experimental Approach

Figure 1 shows the general arrangement of the testing facility. The unfiltered seawater supply fed into the test run through a Monel-body pressure regulator. This comprised the only metallic element in the seawater supply system. Approximately 30 feet of plastic piping intervened between the regulator and the upstream end of the test pipe run. Adjustment of the pressure regulator set point assured a continuous flow through the test pipe at a velocity of approximately 11 fps. A thermowell upstream of the test piping provided for the measurement of flowing seawater temperature.

Figure 2 shows the layout of the test run itself. The run consists of about 16.2 feet of 70/30 CuNi tubing and about 20 feet of Inconel 625 tubing, both with nominal internal diameters of 0.75 inch. The actual measured inside diameter of the 70/30 pipe approximated 0.90 inch; the Inconel 625 approximated 0.85 inch. Figure 2 shows the segment lengths and their arrangement for both alloys.

Figure 3 shows the method followed for joining the tubing segments, the electrical connections and the provision of capillaries for measurement of segment potentials to a reference electrode. The segments were placed on a tight fitting teflon rod, spaced approximately 0.1 inch apart. A thin glass capillary tube was placed between the two segments, perpendicular to the tubing axis surrounded by a 1/4-inch PVC pipe nipple. Two AWG #12 copper wires were soldered at each end of all segments, providing for electrical contact with the segments. A form was placed around the entire assembly which was then filled with Scotchcast resin. This encapsulation prevented seawater leakage and assured electrical isolation between segments.

Shrink sleeves were installed on four inches of each end of the longer segments. Those segments were then joined using plastic tubing couplings. A 1/4-inch PVC coupling was tapped into the sleeve and a valve placed on the end of the nipple. An adapter allowed connection of a small diameter plastic capillary tube to the downstream end of the valve. Cracking of the valve, allowing slow leakage, and inversion of the downstream end of the capillary in a glass beaker allowed for measurement of the potential of the segments to a reference electrode.

Seawater was introduced into the tubing upon completion of its assembly. Adjustment of the pressure regulator provided for a reasonably constant flow rate through the tubing at a flow velocity of about 11 feet per second. All segments were then short circuited to adjacent segments, except for the joint between the 12-inch Inconel 625 segment and the 0.5-inch 70/30 segment. This condition continued for about two weeks, allowing for reasonable stabilization of potentials.

Precision shunt resistors then installed between all adjacent segments allowed for the measurement of current interchange between segments and the calculation of the values of current interchange between the segment and the flowing seawater. Precision digital voltmeters, Fluke Model 805A, provided

instantaneous measurements of these parameters. Continuous monitoring of current interchange between 70/30 CuNi segments and between the 70/30 CuNi 0.5-inch segment and the 12-inch Inconel 625 segment was performed with recording strip charts in the earlier part of the test run. Later, a personal computer (IBM PC) and an analog to digital board monitored the more important environmental variables, including flowing seawater temperature, resistivity, and turbidity. The following sensors/transmitters were used:

| | |
|----------------------|---------------------------------------------------|
| Seawater Temperature | Cole Parmer Digisense, Model 2186 |
| Seawater Resistivity | Foxboro 870EC Transmitter Foxboro 871EC Sensor |
| Turbidity | Turner Model 40 Nephelometer |

An Omnidata "Easy Logger" monitored the potentials across the shunt resistors of the 70/30 CuNi segments for the majority of the test run.

Results and Discussion

Physical Inspection

Figure 4 shows the results of the post test physical inspection of the 70/30 CuNi tubing. The plotted data indicates the deepest pit found in each segment of this tubing. The figure does not show the deepest pit on the entire tubing length. One pit, located about 0.125 inch downstream of the seawater inlet to the tubing, nearly penetrated the .0825-inch tubing wall, indicating a pitting rate of about 161 mils per year. Visual inspection suggested that high turbulence intensity caused this pit. The upstream end of the 70/30 tubing did not mate closely with the adjoining pipe section, there being a transition from CuNi pipe to PVC pipe.

The deepest pit in the region nearest the Inconel 625 tubing was located approximately 8.7 inches upstream of the Inconel. This is near the downstream end of the 5-inch segment. No evidence of typical turbulence-related corrosion was evident.

Figure 5 shows a 20X cross section of the internal surface of the segment immediately adjacent to the Inconel 625 tubing. The slight taper on the right end of the section resulted from reaming of the tubing after cutting prior to the test. No gradual reduction of cross section exists as the finite element predictions suggest.

Current and Potential Monitoring

Galvanic current monitoring showed wide variations of current magnitudes and locations of current interchange between the tubing and seawater. Seawater temperature seemed the major factor affecting the galvanic current. Very frequently, however, variations in galvanic current did not relate to any single monitored environmental variable. The maximum corrosive effects of the galvanic current generally occurred within 12 tubing diameters of the point of connection between the two types of tubing. The maximum corrosive current density values did not exceed 10 microamps/cm² (\approx 10 mils/year corrosion). The magnitude of anodic current density, however, varied over a wide range. The location of the maximum anodic current density also varied. During the early part of the testing, maximum anodic current density generally occurred adjacent to the Inconel 625 tubing. Later, however, anodic

current density frequently occurred 4 inches or further from the Inconel 625 interface. As a practical matter, determination of the cumulative effects of anodic current at any location presents formidable data analysis problems.

Figure 6 shows the values of galvanic current between the two alloy pipes immediately after closing the circuit between the two tubing sections. A computer, with a one-second recording interval, recorded the plotted values.

Measurement of the internal resistance between the two tubing types shortly before circuit closure gave a value of 104.4 ohms. Figure 7 shows a potential profile obtained just before circuit closure. With the measured internal resistance and the open circuit potential between the two tubing types of 0.25 volt, the initial galvanic current value, prior to any polarization of either alloy, would be expected to be:

$$I_g = E_{oc}/R_{int} = 0.25/104.4 = 0.0024 \text{ amperes}$$

Figure 6 shows an initial current value of about 390×10^{-6} amperes, a considerably smaller value than that calculated from the internal resistance and open circuit potential. This indicates that polarization reduced the driving potential substantially during the first second after circuit closure. The figure also shows that the galvanic current did not reach a reasonably stable value until an elapsed time of about one hour after circuit closure.

Figure 8 shows the galvanic current together with the more important environmental variables over the first 24 hours after circuit closure. After the first five hours, the galvanic current varied within a relatively narrow limit, as did the environmental variables, except turbidity, which remained at a relatively high level.

Figure 9 shows potential profiles, one measured during the early part of the test period, the other near the end of the test period. The latter values fall in significantly more active ranges.

Figure 10 shows current profiles on the 70/30 CuNi pipe showing characteristics at four different times during the testing period. The average of the three recorded environmental variables follow:

| Test Period <u>hours</u> | Temperature <u>degrees C</u> | Resistivity <u>ohm-cm</u> | Turbidity <u>ju</u> |
|-----------------------------|---------------------------------|------------------------------|------------------------|
| 149 to 179 | 3.0 | 45.0 | 7.5 |
| 339 to 349 | 5.8 | 37.8 | 10.5 |
| 3984 to 4007 | 25.4 | 23.4 | 13.7 |
| 4152 to 4174 | 25.4 | 23.9 | 13.7 |

Note that the values of resistivity shown are those at flowing seawater temperature. Figure 11 shows typical resistivity-temperature relationships for three levels of chlorinity.

Figure 12 shows the density of current interchange between the tubing and the seawater flowing through it. The figure shows averages for the individual segments. The difference between the magnitudes of current densities between the two curves reflects changes that could not be predicted through passive circuit simulations (e.g., simple mathematical models). The higher current densities in the areas from

3.5 and 12.5 inches upstream of the Inconel 625 seem particularly interesting, seemingly correlating with the location of the deepest pits.

Figure 13 shows total galvanic current and seawater temperature over a 20-hour period midway in the test. Visually, a correlation between the two variables seems evident. Regression analysis showed a relationship as:

$$I_g = 163.2 + 9.41 * T$$

The correlation coefficient R^2 was 0.96, indicating a reasonably good correlation.

Figure 14 shows the total galvanic current together with the three recorded environmental variables over about a 24-hour period in the later part of the test. Visual inspection shows no identifiable correlation between the values of any single variable and the value of galvanic current flow. Also note that the above relationship between galvanic current and temperature would predict a current of about $400\mu A$ for this period -- significantly lower than the actual current.

Equivalent Circuit Simulations

General. Figure 6 and its previous discussion showed that conventional passive dc circuit analysis can only predict that current that will flow in a galvanic cell at the instant of half cell connection. The significant difference between galvanic current calculated from the open circuit potential and the internal resistance between the two half cells suggest that the initial predicted current flow causes activation polarization of one, or both, of the half cells. The longer term reduction of galvanic current, through the first three hours indicates that concentration polarization significantly affects the galvanic current magnitude. This complicates the true galvanic corrosion cell simulation through any type of fixed electrical analog that does not include time-dependent elements.

Evaluation of the applicability of mathematical models to the prediction of galvanic current values and the distribution of the alloy/electrolyte interchange of the current must first consider the nature of the alloy of concern. The 70/30 copper-nickel alloy typically corrodes in a pitting mode when exposed to relatively slow moving seawater. Many studies conducted by OCRC show that the deepest pits of 70/30 CuNi tubing exhibit an extreme value probability distribution. This means that the greater the length of tubing the deeper the deepest pit will be. A recent OCRC study, conducted under the same conditions as the galvanic corrosion study reported here, showed that a pit whose depth is 15 mils would be expected to be found if 1500 feet of 70/30 CuNi tubing of the same diameter was exposed. Since the length of tubing involved in the present test was only about 16 feet, the probability of finding a pit representing a pitting rate of 15 mils per year would be very unlikely. The location of such a pit near the point of connection to the Inconel 625 would be even more unlikely. It seems reasonable, therefore, to conclude that the galvanic current stimulated the deepest pit near the galvanic couple.

Present mathematical models predict corrosion (anodic) current densities. No studies to date validate any rigorous relationship between pitting corrosion depth and average anodic current density, particularly regarding an alloy with corrosion characteristics similar to those of 70/30 CuNi in flowing seawater. In addition, such models can not predict total corrosion over any period other than that immediately after the assumed polarization characteristics whose values the model uses. The models do not consider the time-dependent characteristics of polarization. The previous discussion illustrated rapid changes in polarization characteristics and extreme variability of environmental conditions that influence the

magnitude of galvanic current. In addition, the discussion showed that, at times, changes in the any individual environmental condition did not correlate with changes in galvanic current values. The mathematical models can predict the general magnitude of expected galvanic current. The model can suggest the degree of probability that the galvanic current will be of sufficient magnitude to affect the corrosion of the anodic half cell; prediction of pitting rates, however, falls beyond the scope of such models. Furthermore, less complex mathematical methods can yield the same general results.

The presently reported testing could not include the determination of any electrochemical characteristics whose determination required impressing significant current between the seawater and the pipe surface. Such action would have disturbed the naturally occurring corrosion phenomenon and invalidated the key element of the program, the physical measurement of the extent of corrosion after completion of the test. Fortunately, data is available from a similar test program previously conducted by OCRC using 70/30 CuNi tubing and flowing seawater. This program included periodic determination of polarization characteristics of the tubing.

Figure 15 shows the results of a determination of the anodic polarization characteristics of the 70/30 CuNi tubing after about 8 months exposure to seawater flowing at about 7 feet per second. The data, plotted in the conventional manner, has a log X-axis.

Figure 16 shows the same data plotted with a linear X-axis. Refer now to figure 9 which shows the tube potentials after two intervals of exposure to flowing seawater. The 288-hour curve shows that the 70/30 nearest the Inconel polarized to an active potential of about -0.08 volt. Now refer to figure 16 which shows that the 70/30, in reaching this potential, passes through different potential/current density relationships. Simplifying this situation, we can strike two straight lines through the curves. The first line, from the zero current density point to about 10 microamps/cm², exhibits a slope of about 1250 ohm-cm². The second slope, using the portion of the data above about 20 microamps/cm², gives a slope of about 13,000 ohm-cm². This would be the expected polarization resistance for those 70/30 CuNi areas closer than about 10 inches to the Inconel.

Now consider the polarization of that portion of the 70/30 tube more than about 10 inches upstream of the Inconel. This area polarized only to about -0.16 volt. This polarization would be in the 1250 ohm-cm² range only, as would that portion of the tube further from the Inconel. Any mathematical simulation that does not consider these differences could not yield accurate data.

Figure 17 shows the changes in polarization resistance throughout the course of the test run from which figures 15 and 16 were derived. A model that does not consider such changes could not yield accurate long-term results.

Another factor that must be considered is the validity of the substitution of passive resistors for the active voltages that exist in the real-life galvanic cell. Most mathematical simulations consider only the initial open circuit potential between the two half cells. They may use the initial half cell potentials to a reference electrode; the galvanic potential between the half cells being the difference between these two potentials. This presents another problem, since the formation of long-duration oxidation or reduction films inherently change the initially assumed open circuit potentials. This is evident in figure 9.

Mathematical Models

Computer Model Analysis. The computer program described in the *Introduction* was run using data gathered in the current effort. The open circuit potential difference was obtained from figure 6 -- about 0.25 volt. The tube dimensions are those actually tested. The polarization resistance value for the Inconel 625 was a commonly accepted value of 520,000 ohm-cm². The polarization resistance values for the 70/30 CuNi were obtained from the previous OCRC testing. Referring again to figure 16, the "average" polarization resistance for the 70/30 CuNi when the couple is under complete anodic control -- worst case for total current -- is about 4,200 ohm-cm². The least attenuation would occur in the situation where the 70/30 CuNi exhibits its highest polarization resistance; for this situation a value of 15,000 ohm-cm² was used for the analysis.

The results of the program runs for each condition were similar -- the results are controlled primarily by the high polarization resistance of the Inconel. In both cases the total predicted current was about 300 μ A which corresponds well with the initial measured currents in the range of 390 μ A. However, as discussed, this current rapidly decreased to about 75 μ A -- about 25% of that predicted. Using an arbitrary "effect" of less than 0.5 mpy as the extent of an effect of the galvanic couple, the models suggest that most of the current will attenuate within 8 to 10 inches. This is relatively good agreement with the observations in the actual test. The predicted galvanic corrosion rates do not agree with those measured. The prediction suggests that the corrosion will attenuate from the couple -- a phenomenon not observed. The maximum corrosion, in the form of pitting, occurred 8.7 inches downstream of the couple.

Tee-Section Analysis. An alternative method, mathematically more simple, for estimating the galvanic corrosion would be a Tee-section attenuation analysis, as shown in figure 18. Assume the length of each section as 10 centimeters. The resistance of the seawater path down tube would be, with a seawater resistivity of 25 ohm-cm, 60 ohms for each section. This would be the value of R_1 in figure 18. R_2 would be the interfacial ohmic resistance. Empirical considerations indicate an assumption of about 70 ohm-cm² would be reasonable for this value. R_3 would be the polarization resistance -- and values of 4,200 to 15,000 ohm-cm² can be used as before. Given the surface area of each segment, 4.1 cm², the complete interfacial resistance would be about 1040 to 3675 ohms. Since our test loop was about 170 inches long, we can assume 43 repetitive test sections of 10 cm each.

Figure 19 shows the attenuation of galvanic current based upon the two polarization resistance values discussed above. Obviously, the higher the assumed polarization resistance, the lesser the attenuation of galvanic current. If the likelihood exists that the galvanic current will accelerate the corrosion pitting rate, then the two curves suggest that, at the worst, one might be concerned about the region in which perhaps the first 50% of the galvanic current interchanges from alloy to seawater. With the larger polarization resistance, this would be the first 20 inches (20 pipe diameters) from the couple. For the lower polarization resistance this would be the first 18 inches -- no major difference between the two values, from a pragmatic standpoint. This agrees well with the measured values.

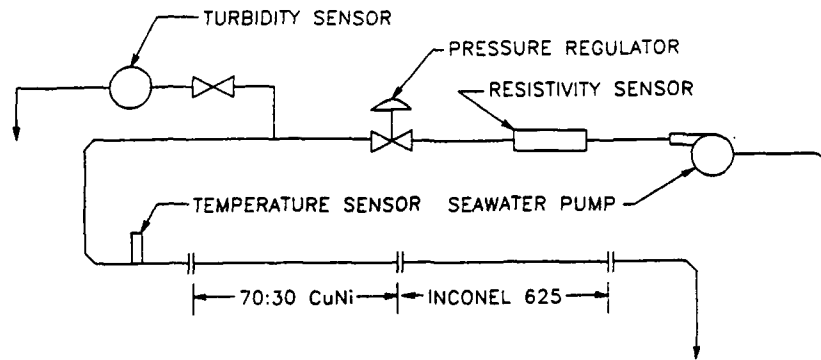
The next important factor focuses on a simple method for determination of a threshold value of total galvanic current that might be a concern as a corrosion accelerating factor on the anodic half cell (70/30 CuNi). The derivation of the actual critical galvanic current value falls beyond the scope of the present study. The polarization resistances of the two alloys of concern differ substantially. 520,000 ohm-cm² represents an accepted value for the Inconel alloy. Figure 20 shows the calculated input resistance value for 1-inch OD Inconel pipe, as a function of pipe length, based upon this polarization resistance value.

The curve derived from resistances calculated for four different lengths of Inconel 625 tubing, using classical mesh network calculations. Obviously, a very short length of Inconel tubing would polarize rapidly if connected to a rather long length of 70/30 tubing. The Inconel's polarization would keep the galvanic current flow to a low value with insignificant corrosion effects.

Using a similar technique to calculate the input resistance of the 70/30 CuNi section (i.e., 16.2 feet in length) used in the current test determines that the input resistance would range from 388 to 472 ohms for polarization resistance values from 4,200 to 15,000 ohm-cm². The Inconel test length was 20 feet. From figure 20 this results in an input resistance of 3,000 ohms. For an open circuit potential difference of 0.25 volt (as initially observed), the predicted current would be in the range of 72 to 74 μ A. This is very close to the measured current about 1 hour after the initiation of testing. Higher corrosion rates would have been expected with longer lengths of either Inconel or 70/30 CuNi.

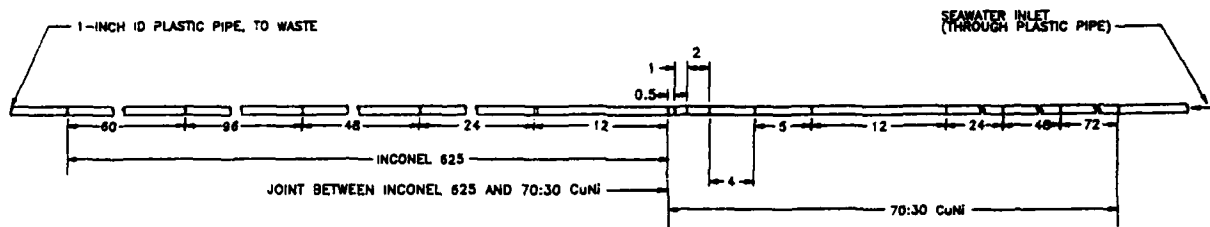
Conclusions

1. Pitting corrosion, the predominant form of corrosion for the alloy tested, does not necessarily follow the predicted attenuation as distance from the galvanic couple is increased. While the effects of the galvanic couple will attenuate with increasing distance, it is not unreasonable to expect that the maximum pitting rate will occur some distance from the actual couple. This precludes any meaningful life prediction from the mathematical model discussed in the *Introduction*.
2. Mathematical models can provide an estimate of the magnitude of galvanic current that would be expected to flow between segments of mixed metal seawater piping systems. These models can also suggest the extent or length of piping over which this current would attenuate.
3. The accuracy of these models is only as good as the data input to the models -- if the data input is not representative of the current electrochemical conditions, the model output is faulty. The present simple laboratory tests have shown that the electrochemical parameters can vary significantly during the lifetime of a structure. This also precludes meaningful life prediction from mathematical models.
4. The models are limited by their inability to accurately model the effects of current density on polarization resistance and the effect of time on polarization resistance. Also very important is the variation in EMF along the anodic or cathodic half-cell over time and distance from the couple. The current testing has shown that the EMF can vary over time and that it can vary along the length of each half-cell.
5. Given the variation in actual electrochemical parameters, the output of any model should be reviewed carefully. Extreme sophistication in computational effort does not necessarily insure results any more meaningful than those that might be provided by much simpler models. Truly accurate models must consider time effects that can be chaotic, and thus very difficult, if not impossible, to quantify. Often simple estimates are as accurate and meaningful as complex analysis.



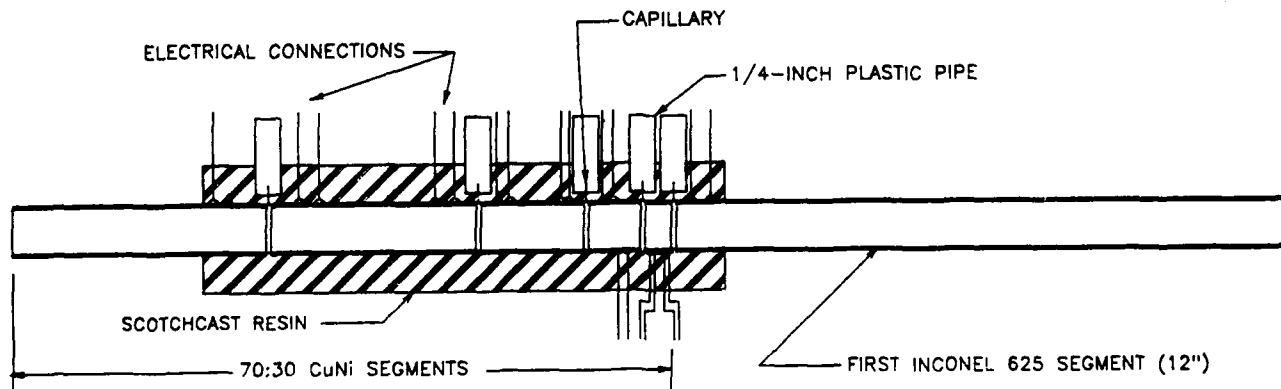
GENERAL ARRANGEMENT
GALVANIC COUPLE TESTING

Figure 1



GENERAL ARRANGEMENT
GALVANIC COUPLE TEST PIPING

Figure 2



SEGMENT ASSEMBLY METHOD

Figure 3

**INCONEL 625-70/30 CuNi COUPLE
MAXIMUM PIT DEPTHS**

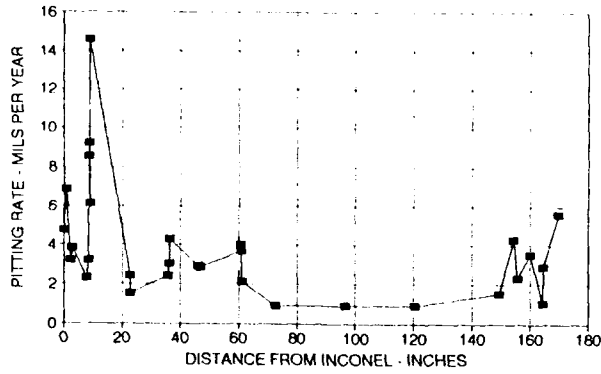
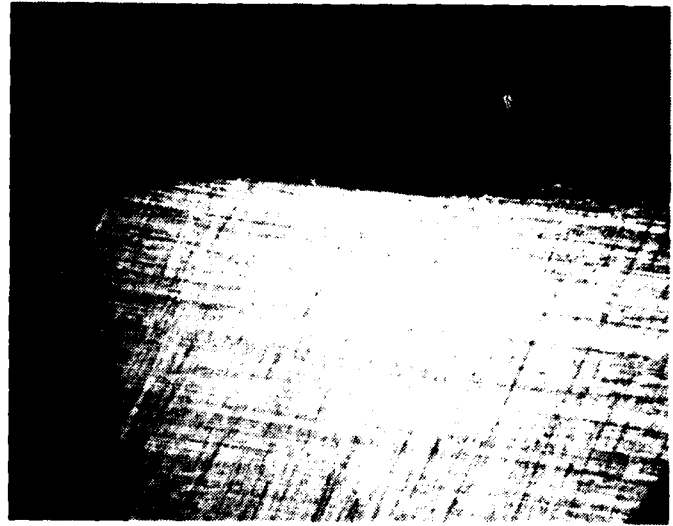


Figure 4



Internal Surface of 70/30 CuNi Tubing Nearest the Inconel 625 (20X magnification).

Figure 5

**INCONEL 625 - 70:30 CuNi COUPLE
TOTAL GALVANIC CURRENT AT START-UP**

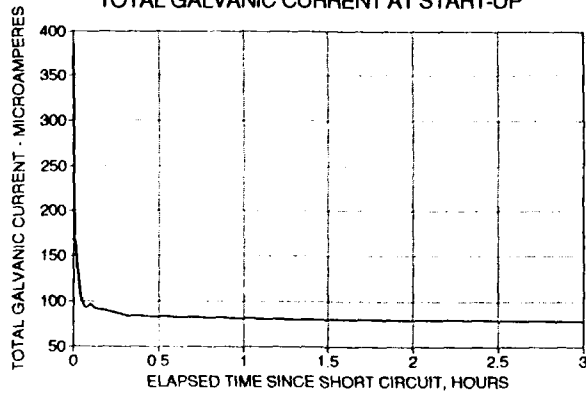


Figure 6

**INCONEL 625/70-30 CuNi COUPLE
OPEN CIRCUIT POTENTIALS, 1/27/92**

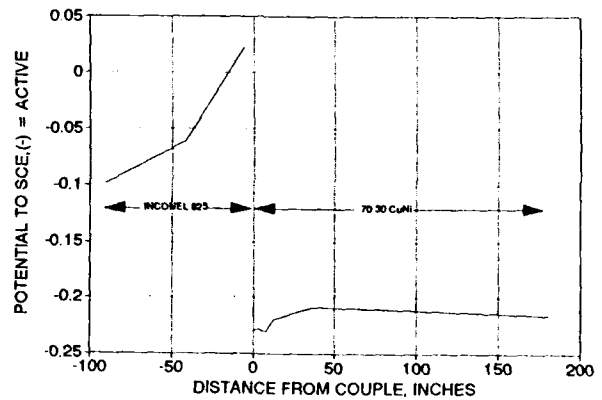


Figure 7

**INCONEL 625 - 70:30 CuNi COUPLE
TOTAL GALVANIC CURRENT AT START-UP**

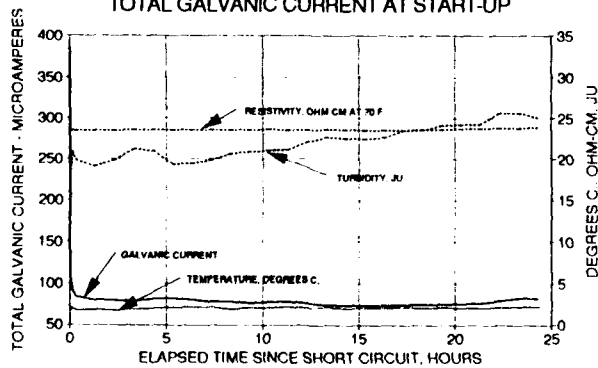


Figure 8

**INCONEL 625 - 70:30 CuNi COUPLE
POTENTIAL PROFILE**

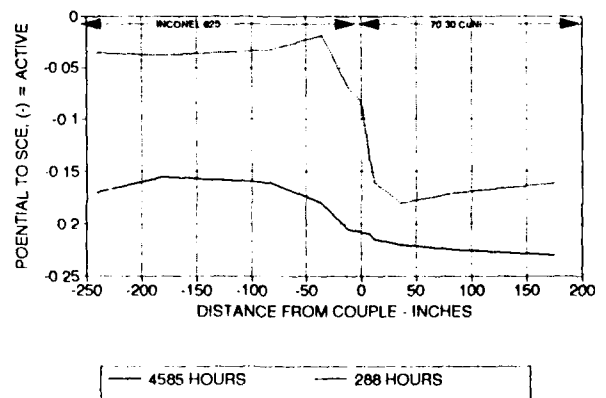


Figure 9

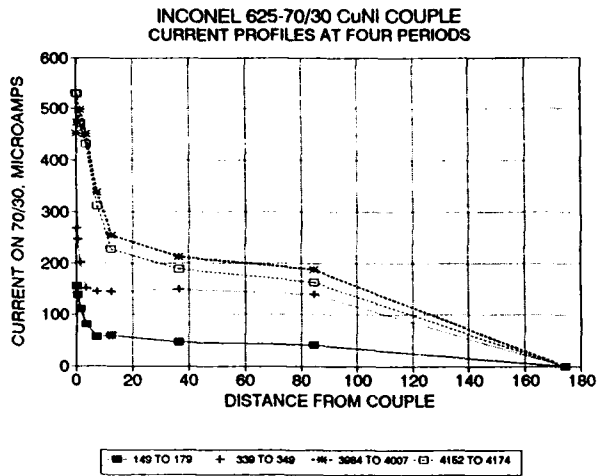


Figure 10

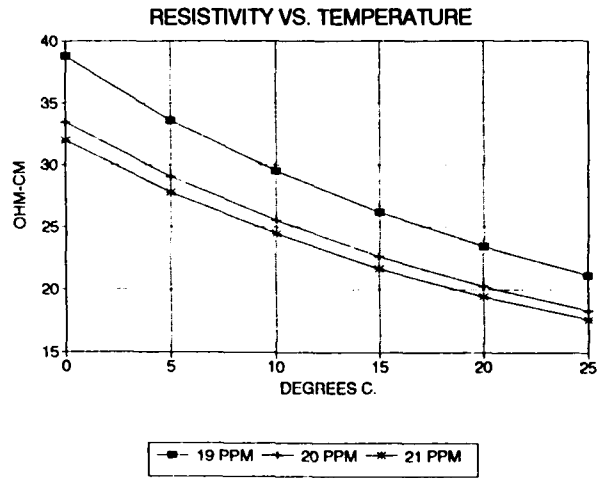


Figure 11

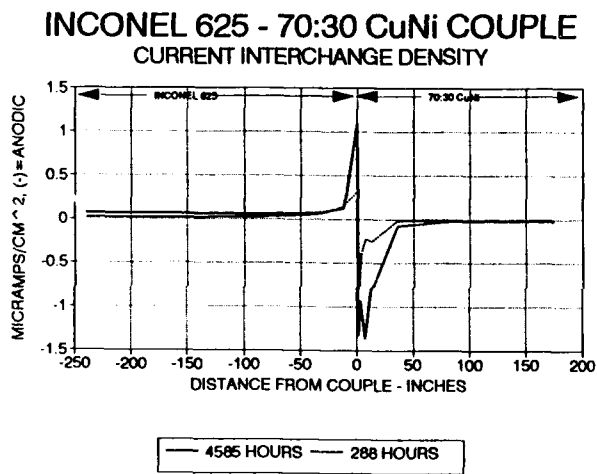


Figure 12

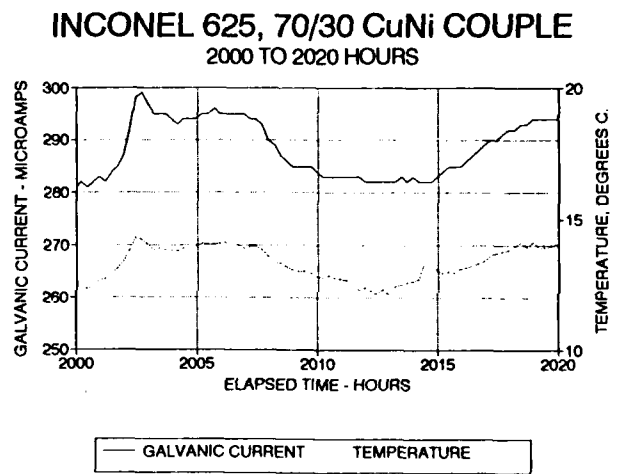


Figure 13

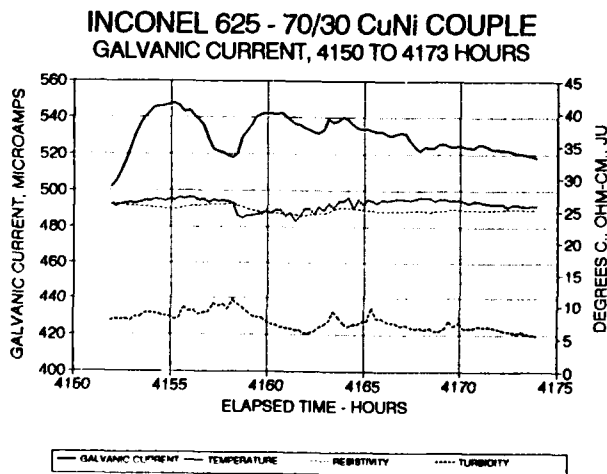


Figure 14

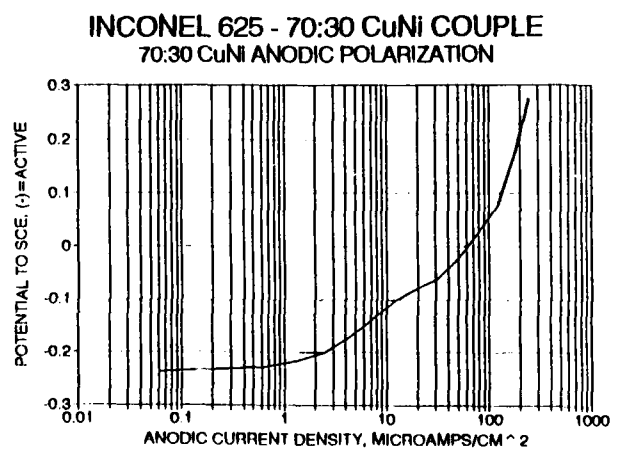


Figure 15

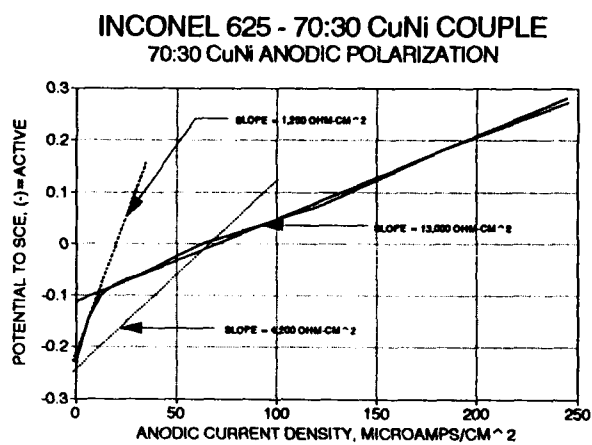


Figure 16

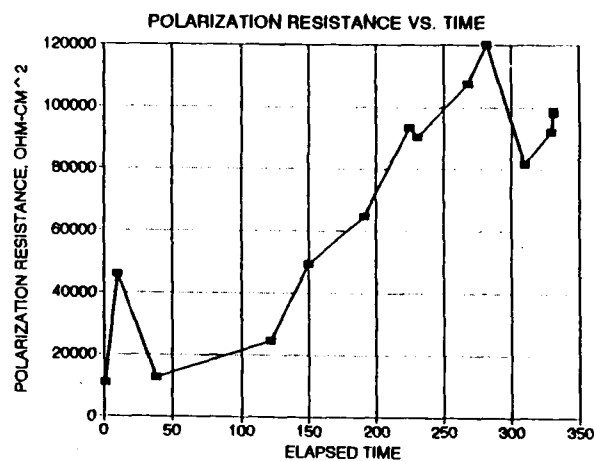


Figure 17

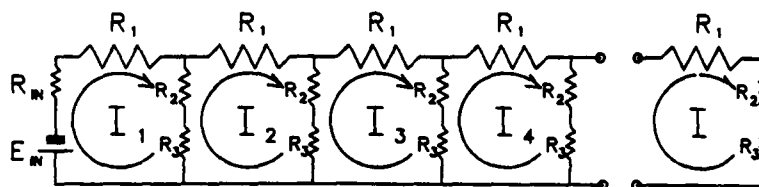


Figure 18

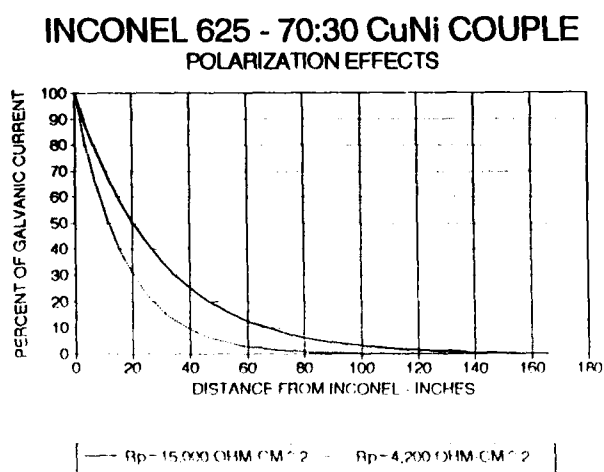


Figure 19

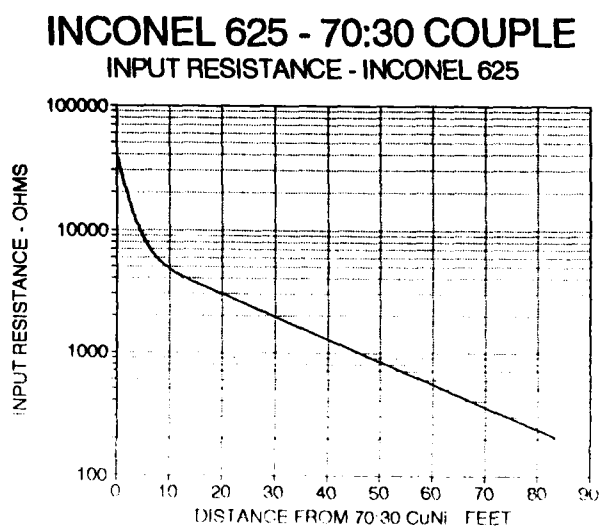


Figure 20